

C18
~~SECRET~~
(NASA-SP-391) OPERATIONAL APPLICATIONS OF
SATELLITE SNOWCOVER OBSERVATIONS (NASA)
430 p HC CSCL 08L

OPERATIONAL APPLICATIONS OF SATELLITE SNOWCOVER OBSERVATIONS

N76-16561
THRU
N76-16590
Unclass
08506

G1/43

A workshop held in
SOUTH LAKE TAHOE, CALIFORNIA
August 18-20, 1975



NATIONAL AERONAUTICS AND SPACE ADMINISTRATION

REPRODUCED BY
NATIONAL TECHNICAL
INFORMATION SERVICE
U.S. DEPARTMENT OF COMMERCE
SPRINGFIELD, VA. 22161

OPERATIONAL APPLICATIONS OF SATELLITE SNOWCOVER OBSERVATIONS

The proceedings of a workshop held August 18-20, 1975
at the Waystation, South Lake Tahoe, California

Edited by
ALBERT RANGO

Sponsored by
The National Aeronautics and Space Administration
and
The University of Nevada, Reno

Prepared at Goddard Space Flight Center



Scientific and Technical Information Office 1975
NATIONAL AERONAUTICS AND SPACE ADMINISTRATION
Washington, D.C.

The requirement for the use of the International System of Units (SI) has been waived for this document under the authority of NPD 2220.4, paragraph 5.d.

For sale by the National Technical Information Service
Springfield, Virginia 22161

FOREWORD

Recent progress in extracting meaningful snow information from satellite data led to the institution of a NASA Applications Systems Verification Test (ASVT) on Operational Applications of Satellite Snowcover Observations. Nine operational water management agencies in the Western United States are participating in this ASVT in cooperation with NASA. The Workshop on Operational Applications of Satellite Snowcover Observations at the Waystation in South Lake Tahoe, California, August 18-20, 1975, was held primarily to bring the various cooperating agencies together for an information exchange of analysis techniques, results, and problem solving. Including participants outside the ASVT, attendance at the workshop totaled one hundred. Many discussions between operational water management personnel and remote sensing specialists resulted in regard to the use of remotely sensed snowpack information for improving snowmelt-runoff forecasts.

Twenty-eight scientific papers were presented over two days covering the photointerpretation and digital techniques used in analyzing LANDSAT and NOAA satellite data, the use of snowcover observations in streamflow forecasting, and new advances in extraction of snowpack parameters, other than snow extent, employing a variety of remote sensors. An additional day-long working session provided the participants with a chance to examine and try the various techniques used for obtaining snowcovered area and an opportunity to discuss the snow mapping ASVT activities with the various investigators. Presentation session chairmen were A. Rango, NASA/Goddard Space Flight Center, Greenbelt, Maryland; D. R. Wiesnet, NOAA/National Environmental Satellite Service, Suitland, Maryland; A. J. Brown, California Department of Water Resources, Sacramento, California; and J. N. Washichek, USDA/Soil Conservation Service, Denver, Colorado. V. V. Salomonson, NASA/Goddard Space Flight Center, Greenbelt, Maryland chaired the working session on August 20, 1975. M. Cutler of the General University Extension, University of Nevada, Reno was the Program Coordinator of the Workshop.

The papers published in these proceedings are in the same order as presented at the Workshop. In order to expedite the publication of the proceedings, papers were prepared in camera ready format. Each author assumes full responsibility for the content of his paper.

Albert Rango
Workshop Director
NASA/Goddard Space Flight Center



**WORKSHOP ON OPERATIONAL APPLICATIONS
OF SATELLITE SNOWCOVER OBSERVATIONS**

TABLE OF CONTENTS

<u>Paper No.</u>		<u>Page</u>
1	An Overview of the Applications Systems Verification Test on Snowcover Mapping, A. Rango, Goddard Space Flight Center	1 D1
2	Operational Applications of Satellite Snowcover Observa- tions and LANDSAT Data Collection Systems Operations in Central Arizona, Herbert H. Schumann, U.S. Geological Survey	13 D2
3	The Application of Hydrometeorological Data Obtained By Remote Sensing Techniques for Multipurpose Reservoir Operations, W. L. Warskow, T. T. Wilson, Jr., and K. Kirdar, Salt River Project.	29 D3
4	Interpretation of Snowcover from Satellite Imagery for Use in Water Supply Forecasts in the Sierra Nevada, A. J. Brown, Snow Surveys Branch; Department of Water Resources; J. F. Hannaford, Sierra Hydrotech	39 D4
5	Operational Applications of Satellite Snowcover Observa- tions in Rio Grande Drainage of Colorado, Jack N. Washicheck and Tony Mikesell, USDA-Soil Conservation Service	53 D5
6	Operational Application of Satellite Snowcover Observa- tions - Northwest United States, Fred A. Limpert, Bonneville Power Administration	71 D6
7	The Operational Program of Satellite Snowcover Ob- servations at NOAA/NESS, Stanley R. Schneider, NOAA/NESS	87 D7

<u>Paper No.</u>		<u>Page</u>
8	Use of Areal Snow Cover Measurements from ERTS-1 Imagery in Snowmelt-Runoff Relationships in Arizona, J. S. Aul and P. F. Ffolliott, University of Arizona	103 D8
9	Utilization of LANDSAT Monitoring Capabilities for Snowcover Depletion Analysis, A. G. Thompson, WRRI, University of Wyoming	113 D7
10	Operational Use of LANDSAT Imagery for the Estima- tion of Snow Areal Extent, Edwin F. Katibah, Remote Sensing Research Program, University of California	129 DIV
11	Operational Applications of NOAA-VHRR Imagery in Alaska, R. D. Seifert, R. F. Carlson, D. L. Kane, Institute of Water Resources, University of Alaska	143 D11
12	Employment of Satellite Snowcover Observations for Improving Seasonal Runoff Estimates, A. Rango and V. V. Salomonson, NASA/Goddard Space Flight Center, and J. L. Foster, Geology Department/University of Maryland	157 D12
13	Applications of Satellite Snow Cover in Computerized Short-Term Streamflow Forecasting, C. F. Leaf, Fort Collins, Colorado	175 D13
14	Sierra Nevada Snow Melt from SMS-2, Laurence C. Breaker, NOAA National Environmental Satellite Service; Michael C. McMillan, NOAA National Environmental Satellite Service	187 D14
15	Synopsis of Current Satellite Snow Mapping Techniques, with Emphasis on the Application of Near-Infrared Data, James C. Barnes and Michael D. Smallwood, Environ- mental Research & Technology, Inc.	199 D15
16	Comparison of Different Methods for Estimating Snow- cover in Forested, Mountainous Basins Using LANDSAT (ERTS) Images, M. J. Meier, U.S. Geological Survey; W. E. Evans, Stanford Research Institute	215 D16

<u>Paper No.</u>		<u>Page</u>
17	Approaches to Digital Snow Mapping with LANDSAT-1 Data, K. I. Itten, Department of Geography, University of Zurich	235 D17
18	An All Digital Approach to Snow Areal Mapping and Snow Modeling, V. Ralph Algazi and Minsoo Suk, University of California	249 D18
19	Digital Snow Mapping Technique Using LANDSAT Data and General Electric Image 100 System, William C. Dallam, General Electric Company; James Foster, Geology Department, University of Maryland	259 D19
20	Snow Cover Monitoring by Machine Processing of Multitemporal LANDSAT MSS Data, S. G. Luther, L. A. Bartolucci and R. M. Hoffer, Laboratory for Applications of Remote Sensing, Purdue University. . .	279 D20
21	Snowcover Mapping by Machine Processing of SKYLAB and LANDSAT MSS Data, L. A. Bartolucci, R. M. Hoffer and S. G. Luther, Laboratory for Applications of Remote Sensing, Purdue University	295 D21
22	A Progress Report on Estimating Snow Depth Using VHRR Data from NOAA Environmental Satellites, D. F. McGinnis, Jr., National Environmental Satellite Service, NOAA	313 D22
23	A Comparison of Operational and LANDSAT-Aided Snow Water Content Estimation Systems, James M. Sharp, Social Sciences Group; Randall W. Thomas, Remote Sensing Research Program, University of California	325 D23
24	Red and Near-Infrared Spectral Reflectance of Snow, Harold W. O'Brien and Richard H. Munis, U.S. Army Cold Regions Research and Engineering Laboratory	345 D24
25	Remote Sensing of Snowpack Density Using Shortwave Radiation, Michael C. McMillan, NOAA, National Environmental Satellite Service; James L. Smith, USDA Forest Service	361 D25

Paper
No.

Page

26	Snow Wetness Measurements for Melt Forecasting, William I. Linlor, Ames Research Center; Fred D. Clapp, Consultant, University of California; Mark F. Meier, U.S. Geological Survey, USDI; James L. Smith, U.S. Forest Service USDA	375 D26
27	Microwave Emission from Dry and Wet Snow, T. C. Chang and P. Gloersen, Goddard Space Flight Center	399 D27
28	Application of Bayesian Decision Theory to Airborne Gamma Snow Measurement, Vernon C. Bissell, National Weather Service, River Forecast Center . . .	409 D28
29	Summary of the Operational Applications of Satellite Snowcover Observations Working Session — August 20, 1975, V. V. Salomonson and A. Rango, NASA/Goddard Space Flight Center	421 D29

**AN OVERVIEW OF THE APPLICATIONS SYSTEMS VERIFICATION TEST
ON SNOWCOVER MAPPING**

A. Rango, *Goddard Space Flight Center, Greenbelt, Maryland*

ABSTRACT

The capability of the LANDSAT and NOAA satellites to accurately measure snowcovered area on various size watersheds has been demonstrated by a number of investigators. Additionally, recent research has shown a highly significant statistical relationship between satellite-derived snowcovered area at the beginning of the snowmelt period and seasonal runoff. The decision was made, therefore, to test the results of several satellite snowcovered area studies in an Applications Systems Verification Test (ASVT) Program where quasi-operational evaluations of total technical capability are performed. The objective of these ASVT's is to provide all the information necessary for a potential user to make effective decisions concerning the implementation of the new remote sensing technology in an operational applications system. The ongoing Operational Applications of Satellite Snowcover Observations (OASSO) Project became part of the ASVT Program in July 1975, and is described in this paper. In cooperation with various operational water management agencies in Arizona, California, Colorado, and Oregon, the OASSO Project is scheduled for completion in September 1978.

INTRODUCTION

The capability of the LANDSAT and NOAA satellites to accurately measure snowcovered area on various size watersheds on a repetitive basis has been demonstrated in several research projects sponsored by NASA, NOAA, and other agencies. Other research (Leaf, 1971 and Rango, Salomonson, and Foster, 1975) has provided an indication that snowcovered area, provided either by aerial or satellite surveys, can be employed as an additional parameter in the prediction of snowmelt-derived runoff. Because of positive research results in both snow mapping and runoff correlations, the decision was made to operationally test the use of remotely sensed snowcovered area for improving snowmelt runoff forecasts in an Applications Systems Verification Test (ASVT) Program where quasi-operational evaluations of total technical capability are performed.

NASA ASVT's result from exploratory investigations in the research program that have shown promising conclusions. As a result, when an ASVT is undertaken, most necessary supporting research has already been completed. An ASVT is an integrated test of the capability of a remote sensing based system to accomplish a specific applications objective on an operational basis. To accomplish this, ASVT's directly involve the user community, provide a user oriented assessment of the system and provide in summary form the information necessary for a potential user to make effective decisions concerning the implementation of the technology in an operational framework. Mandatory products from an ASVT are a documented methodology suitable for widespread distribution, a comprehensive user evaluation of the systems accuracy and reliability, and a complete cost-benefit relationship study.

The Operational Applications of Satellite Snowcover Observations (OASSO) project was initiated in July 1974 and formally became a part of the NASA ASVT Program in July 1975. Through December 1975, existing satellite data collected since 1973 will be analyzed. It is planned that analysis of real time satellite data will begin during the 1976 snowmelt season. Being conducted in cooperation with nine operational water management agencies in the Western United States, the OASSO project is scheduled for completion in 1978.

GENERAL OBJECTIVES

The OASSO project has the following general objectives.

1. Map snowlines, areal snowcover, and associated changes in snowcover using satellite data for the 1973, 1974 and 1975 snow seasons in four separate Western U.S. study areas in order to evaluate the usefulness of the data had they been available in near real-time.
2. Map snowcover changes through FY 78 in each of the study areas in a near real-time mode (data to user \leq 72 hours) so that the data base can be extended to a total of at least five years.
3. Compare and evaluate satellite-derived snow mapping products with reference to products from conventionally-derived snow data.
4. Develop or modify methods in an operational framework over the study period that will allow incorporation of satellite derived snowpack observations into the prediction of snowmelt-derived streamflow for specific areas.

5. Produce a documented methodology and cost/benefit analysis sufficient for user organizations to make Go/No Go decisions concerning the use of this satellite-assisted snowmelt runoff methodology in their operational responsibilities.

PROJECT ORGANIZATION

Day to day management of the OASSO project is conducted at NASA's Goddard Space Flight Center (GSFC) in coordination with the Earth Resources Program Office and NASA/Headquarters. The satellite snow investigations are carried out at four Western United States study centers located in Arizona, California, Colorado, and the Northwest as shown in Figure 1. NOAA's National Environmental Satellite Service (NESS) is also participating in OASSO by supplying operational NOAA satellite data and supporting analysis work.

Each of the four study areas in the West have operational agency personnel working in cooperation with remote sensing specialists to adapt the existing technology to water supply forecasting needs. Table 1 lists the Arizona Snow ASVT organization and responsibilities and Figure 2 locates the Arizona study watersheds. Similarly Tables 2, 3, and 4 list the Snow ASVT organization and responsibilities for California, Colorado, and the Northwest respectively, while Figures 3, 4, and 5 locate the study

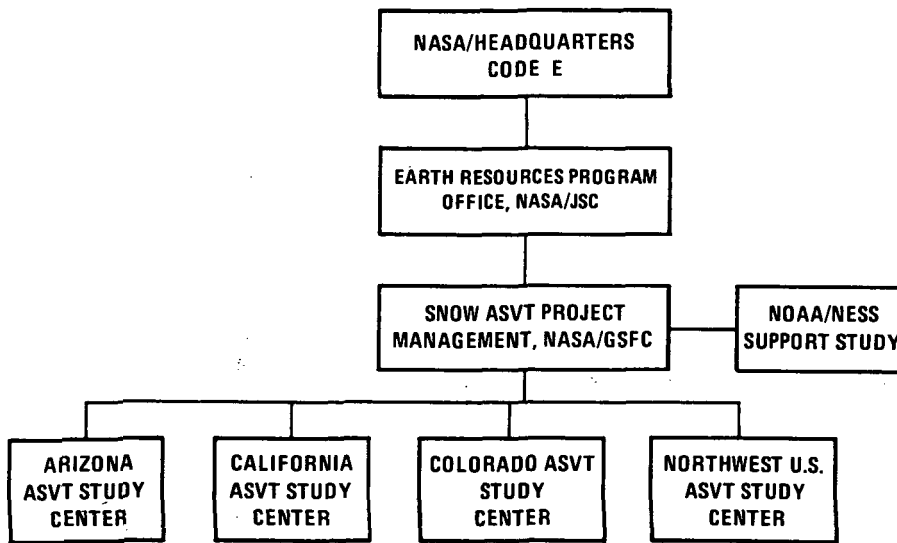


Fig. 1—Snow ASVT project management structure

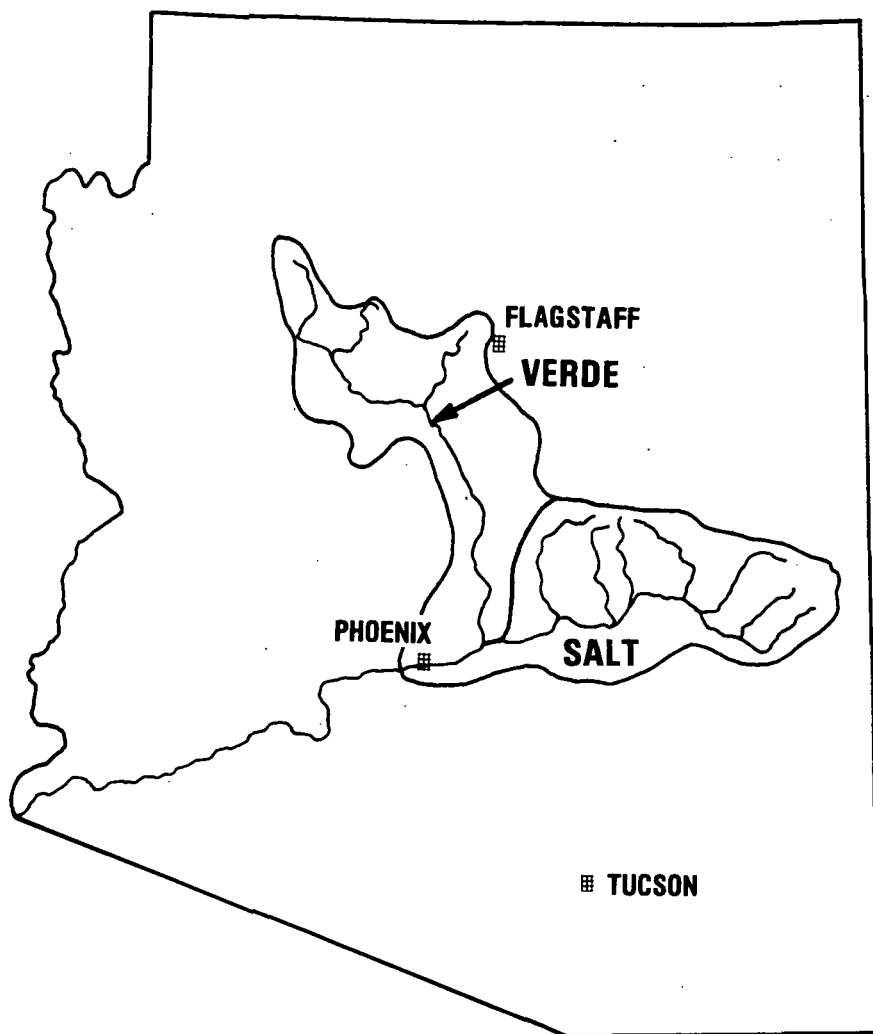


Fig. 2—Arizona snow ASVT study watersheds

watersheds for the same areas. The organization and responsibilities in the NOAA/NESS support study are shown in Table 5.

STUDY AREA ACTIVITIES

In Arizona LANDSAT and NOAA imagery, LANDSAT data collection system relayed data, and aircraft flights are being used as a total system for improving short term and seasonal forecasts to benefit Salt River Project operations. In particular the Arizona investigators are interested

Table 1

Arizona Snow ASVT Organization and Responsibilities

A. Project Coordinator	Mr. Herbert H. Schumann USGS, WRD Phoenix, Arizona
B. Operational Agency Cooperators	Mr. William Warskow, Watershed Specialist, Watershed Division Mr. Ted Wilson, Lead Engineer, Water Resource Operations Salt River Project Phoenix, Arizona
C. Remote Sensing Specialist	Mr. Herbert H. Schumann, USGS
D. Study Watersheds	Salt River Verde River
E. Applications of Data	Reservoir Regulation (for power, irrigation, water supply, and flood control in order of priority) Short Duration Runoff Forecasting

in substituting satellite snowcover measurements for many of their conventional low altitude aircraft surveys, and at the same time using satellite information to identify critical snowmelt situations where it would be advantageous to fly an aircraft mission.

One of the principal goals for all the study areas is to use satellite information to reduce existing streamflow forecast error. In California, the Department of Water Resources is focusing on using the satellite data for updating forecasts after April 1 through the end of the snowmelt season. Procedural forecast errors would thus be treated rather than the early season, weather-variability errors. Additionally, California is particularly interested in using satellite snowcover data to obtain additional snowpack knowledge from ever increasing restricted-access wilderness areas and other remote regions.

In the attempt to reduce forecast errors, historical records are being analyzed and correlated to conventional watershed and snowpack

Table 2

California Snow ASVT Organization and Responsibilities

A. Project Coordinator	Mr. A. J. Brown, Chief Snow Surveys Branch California Department of Water Resources Sacramento, California
B. Operational Agency Cooperators	Snow Surveys Branch California Department of Water Resources Sacramento, California
C. Remote Sensing Specialist	Mr. Barry Brown, California Department of Water Resources
D. Study Watersheds	Feather River Upper Sacramento River San Joaquin River Kings River Kern River Kaweah River Tule River
E. Applications of Data	Supply various California Snow Survey Cooperators with Seasonal Runoff Forecasts. Irrigation Power Generation Flood Control

measurements. It is hoped that with five years of satellite data as a base, meaningful snowcovered area indices could be used in normal regression approaches to streamflow forecasting. Additionally, various numerical watershed models are being employed with the snowcovered area estimates in Colorado and the Northwest to attempt to improve shorter duration runoff forecasts. The Streamflow Simulation and Reservoir Regulation (SSARR) model used by the Columbia River Forecasting Service, as an example, requires the input of snowcovered area for generating daily streamflows. Satellite snowcover data will be input to the SSARR model for studying possible improvements in streamflow forecasts for past and current years resulting from use of actual data as opposed to model

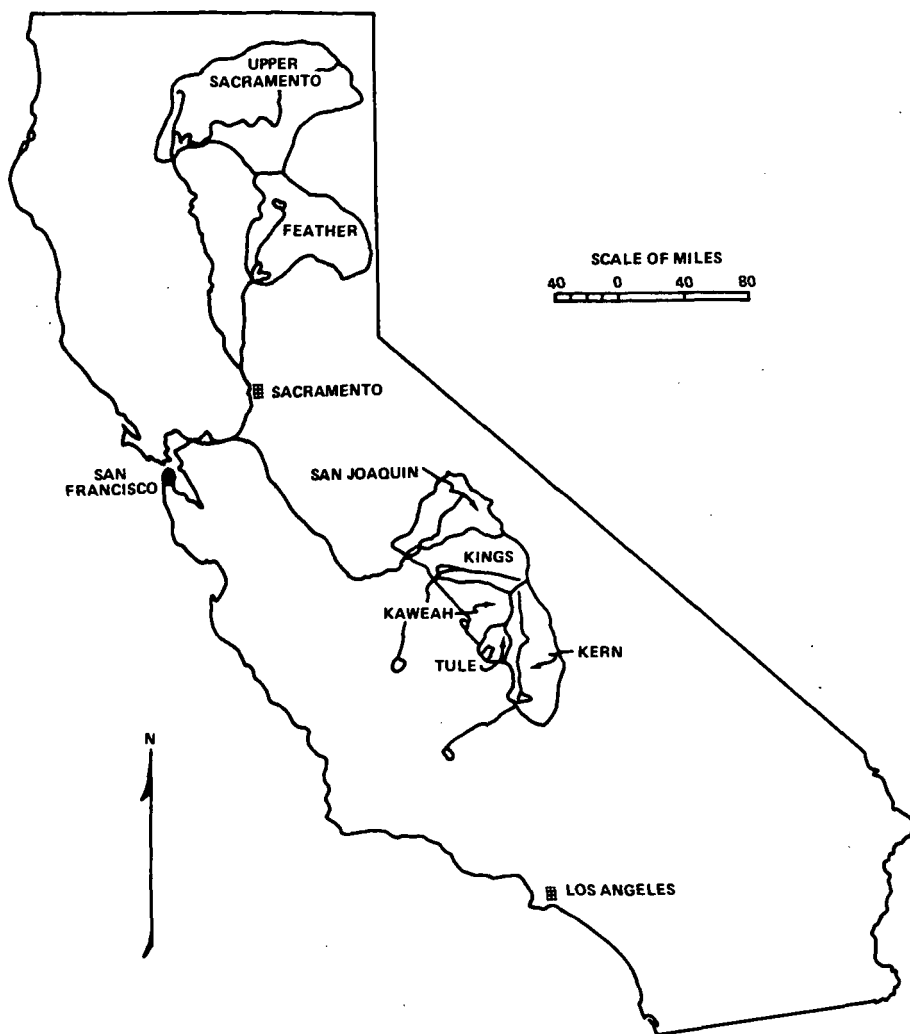


Fig. 3—California snow ASVT study watersheds

calculated snowcovered area. The utility of the remotely sensed data for the various models being tested will be assessed and documented.

At the end of the OASSO project the user agencies will evaluate the utility of the satellite data in light of their own unique requirements and comment upon possible continuing application of the data. Recommendations will also be made for changes and improvements necessary to make the data more applicable to operational functions. The required cost-benefit study will produce results regarding the worth of using satellite

Table 3

Colorado Snow ASVT Organization and Responsibilities

A. Project Coordinator	Mr. Jack Washichek Snow Survey Supervisor Soil Conservation Service Denver, Colorado
B. Operational Agency Cooperators	Mr. Jack Washichek Soil Conservation Service Dr. Jerry Danielson, Deputy - State Engineer Colorado Division of Water Resources Mr. Bob Hansen U.S. Bureau of Reclamation
C. Remote Sensing Specialist	Mr. Bob Hansen, USBR
D. Study Watersheds	Rio Grande River Above Del Norte Conejos River Above Mogote Culebra River Above San Luis San Juan River Above Carracus Arkansas River Above Salida
E. Applications of Data	Better Flow Forecasts on the Rio Grande River so that the State of Colorado can Better Regulate Reservoir Releases of Water to the State of New Mexico as Required by Law. Reservoir Regulation for Irrigation and Power . Requirements.

snowcover data for operational purposes based upon the results obtained in each of the four study centers. Documentation and dissemination of the results from the OASSO project for informational purposes will include widespread distribution of handbooks, workshop proceedings volumes, final reports, and scientific papers.

Table 4

Northwest Snow ASVT Organization and Responsibilities

A. Project Coordinator	Mr. Fred A. Limpert, Head Hydrology Section Bonneville Power Administrator Portland, Oregon
B. Operational Agency Cooperators	Columbia River Forecast- ing Service, (CRFS) Portland, Oregon CRFS is composed of: 1) Bonneville Power Administration 2) U.S. Army Corps of Engineers 3) NOAA/National Weather Service
C. Remote Sensing Specialist	Dr. Mark Meier, USGS
D. Study Watersheds	Boise River North Santiam River Snake River Kootenai River Clearwater River Flathead River
E. Applications of Data	Power Generation Flood Control

SUMMARY

As a result of promising conclusions derived in several remote sensing snowcover studies, an Application Systems Verification Test (ASVT) has been initiated in the Western United States to evaluate under operational conditions the overall utility of satellite snowcover observations for streamflow forecasts. A total of six federal agencies and three state agencies are cooperating in four regions centered in Arizona, California, Colorado, and Oregon. These agencies are employing earth resources satellite data, data collection system relayed information, aircraft flights, conventional ground information, and regression and

Table 5
NOAA/NESS Snow ASVT Support Study

A. Study Coordinator	Mr. Russ Koffler, Chief Environmental Products Group NOAA/NESS Washington, D.C.
B. Operational Agency Cooperator	Mr. Jack Bottoms, Manager NOAA/NESS Satellite Field Services Station Redwood City, California
C. Remote Sensing Specialists	Mr. Don Weisnet Dr. David McGinnis NOAA/NESS Environmental Sciences Group Mr. Stan Schneider NOAA/NESS Environmental Products Group
D. Operational Services	Support in the Form of Im- agery for Each of the ASVT Study Watersheds from the Satellite Field Services Sta- tion and Supplemental Snow- cover Analyses for Several other Rivers in the West. Snowcover Values are sent by Teletype to NWS River Forecast Centers.
E. Research Study	Investigate Effect of Vegeta- tion, Tree Lines, and Moun- tainous Terrain on Snow Map- ping. Digital Enhancements of Snow/Terrain Interfaces. Examination of Sources of Snow Mapping Errors.

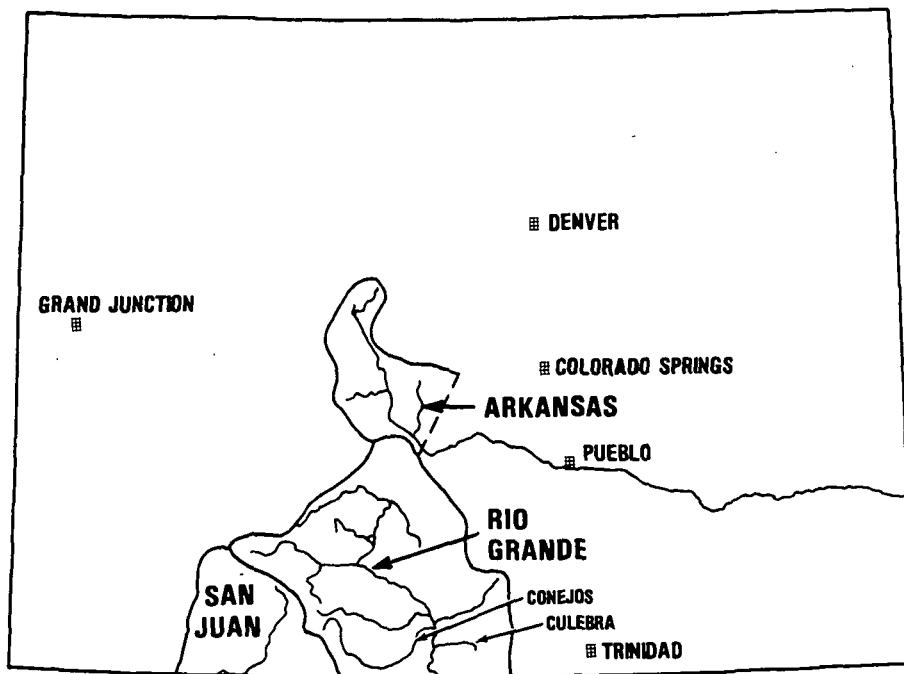


Fig. 4—Colorado snow ASVT study watersheds

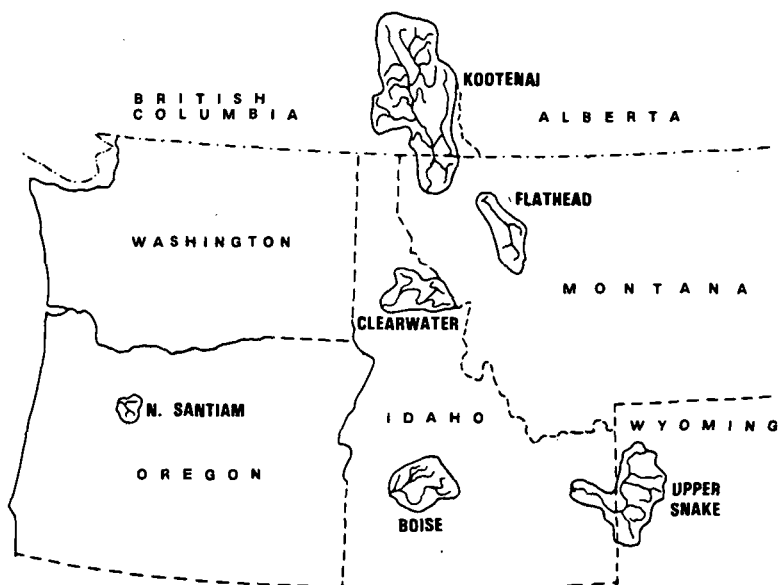


Fig. 5—Northwest snow ASVT study watersheds

numerical streamflow prediction models in an attempt to quantitatively determine the usefulness of the timely remotely sensed information. At the conclusion of the ASVT, handbooks, workshop proceedings, final reports, and scientific papers produced in conjunction with this project will be disseminated so that all interested parties may evaluate the overall results and assessments of the application of satellite snowcover observations.

REFERENCES

- Leaf, C. L., Areal snow cover and disposition of snowmelt runoff in Central Colorado, USDA Forest Service Research Paper RM-66, 19 pp., Forest Service, Rocky Mountain Forest and Range Experiment Station, Fort Collins, Colorado, 1971.
- Rango, A., V. V. Salomonson, and J. L. Foster, Seasonal Streamflow Estimation Employing Satellite Snowcover Observations, Document X-913-75-26, 27 pp., National Aeronautics and Space Administration, Goddard Space Flight Center, Greenbelt, Maryland, 1975.

OPERATIONAL APPLICATIONS OF SATELLITE SNOWCOVER OBSERVATIONS AND LANDSAT DATA COLLECTION SYSTEMS OPERATIONS IN CENTRAL ARIZONA

Herbert H. Schumann, *U.S. Geological Survey, Phoenix, AZ*

ABSTRACT

Repetitive LANDSAT and NOAA-4 satellite imagery together with aerial surveys are being evaluated to develop an operational capability for mapping snowcover distributions on the Salt-Verde watershed of central Arizona. Satellite telemetry is also being used for near-real time relay of hydrologic data to aid in the management and operation of reservoirs on the Salt and Verde Rivers.

Aerial reconnaissance flights were conducted to collect information on the depth and distribution of snowcover to provide ground truth for use in the analysis of the satellite imagery. A technique for rapid and economical determination of snow depths, using oblique aerial photography of snow markers, has been developed.

The LANDSAT Data Collection System (DCS) is being used to relay hydrologic data from earth-based sensors located at remote and relatively inaccessible sites. The LANDSAT telemetry system is being used to relay information from streamflow and snow-monitoring installations located in the upper parts of the Salt-Verde watershed.

INTRODUCTION

The inability to accurately measure and monitor moisture conditions over large remote areas often presents serious land and water-management problems in Arizona and other semi-arid regions. The lack of timely information about moisture conditions in central Arizona including precipitation, snow-water content, rates of snowmelt, and resultant volumes of runoff presents vexing water-management problems related

to multiple-use reservoir operations that have resulted in millions of dollars of downstream property damage and loss of life.

The Salt-Verde River watershed includes approximately 13,000 square miles (34,000 square kilometres) of central Arizona, ranges from 1,325 to 12,670 feet (400 to 3,900 metres) above mean sea level, and receives from 10 to 25 inches (25 to 65 centimetres) of annual precipitation (fig. 1). The highly variable runoff from the Salt and Verde Rivers is regulated by six reservoirs that have a combined storage capacity of approximately 2 million acre-feet (2.5 cubic kilometres) (fig. 2). These reservoirs are operated by the Salt River Project to furnish hydroelectric power and municipal, industrial, and irrigation water to more than 1 million people and 250,000 acres (1,200 hectares) of land in the Salt River Valley near Phoenix, Arizona (fig. 1).

OBJECTIVES

The Arizona Test Site is one of four test sites included in the NASA Applications Systems Verification Test (ASVT) on Snow mapping. The principal objectives of this investigation are (1) to evaluate repetitive satellite imagery together with aerial surveys in an attempt to develop an operational capability in Arizona for using satellite imagery for mapping snowcover distributions, (2) to develop techniques and procedures for systematic monitoring of snowcover and moisture conditions using remote-sensor methods including repetitive satellite and aerial observations together with the use of the LANDSAT Data Collection System to relay ground-truth data, and (3) to develop or modify methods that will allow incorporation of satellite observations of snowpack into operational procedures used by the Salt River Project for predicting both short-term and seasonal snowmelt-derived runoff.

AERIAL OBSERVATIONS

Snowcover Distributions

Aerial observation of snowcover distributions can provide valuable information during periods of cloud cover that preclude satellite snowcover observations.

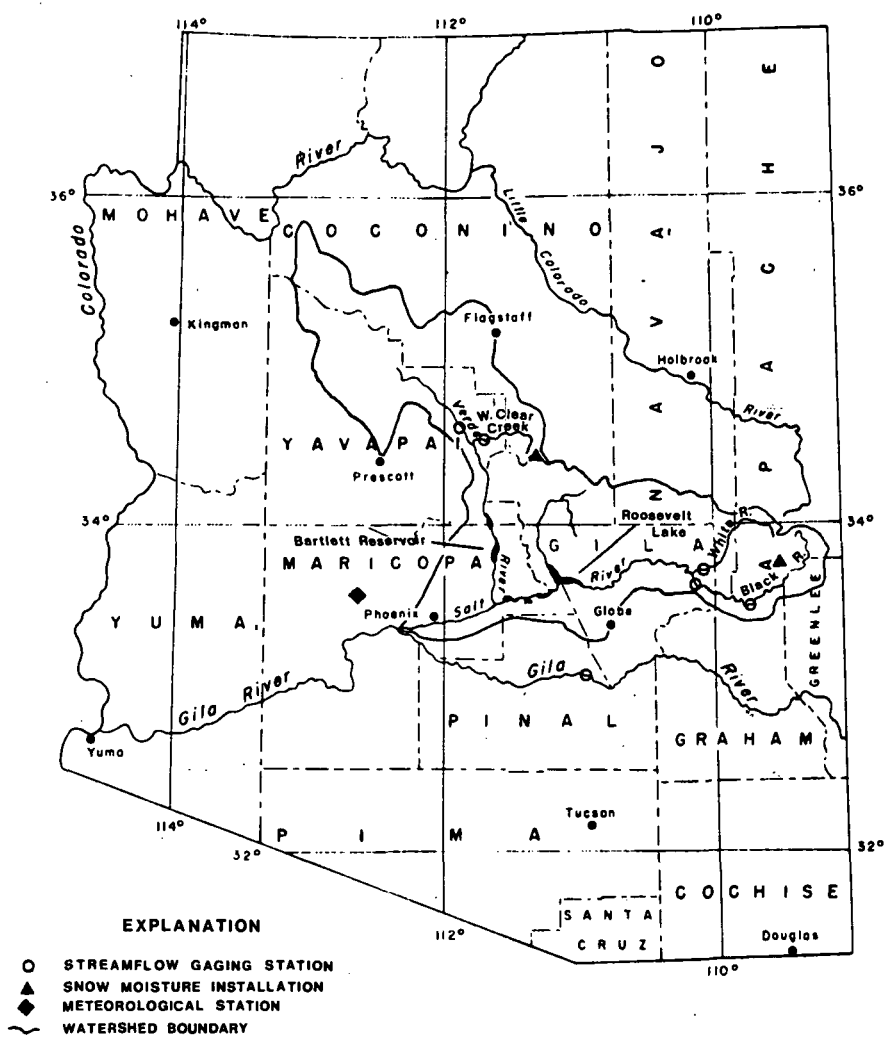


Fig. 1-Location of LANDSAT Data Collection Platforms and Salt and Verde watersheds, Arizona

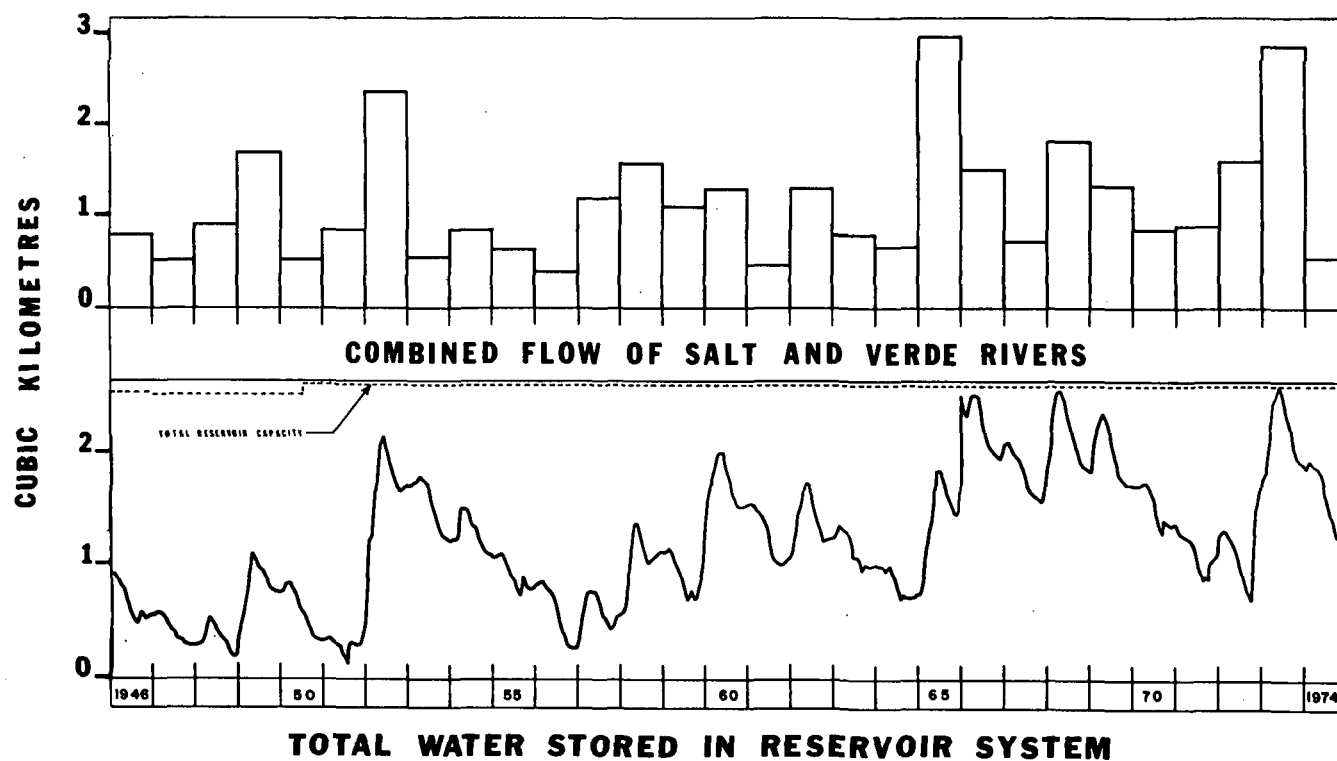


Fig. 2-Combined flow of Salt and Verde Rivers and total water stored in reservoir system

During the spring of 1975 eight aerial reconnaissance flights, averaging 4 to 6 hours in duration, were flown over the Salt-Verde watershed to collect information on the depth and distribution of snowcover and to train additional aerial observers. Maps of snowcover distributions were prepared during these flights using visual mapping techniques and a 1:1,000,000-scale LANDSAT-I image map of Arizona (fig. 3).

Snowcover distributions, as mapped by inexperienced aerial observers, were more generalized and tended to show lesser amounts of snowcover than snowcover distributions observed on LANDSAT imagery. However, snowcover distributions mapped by experienced observers were in close agreement with the snowcover distributions shown on the LANDSAT imagery. Similar results were observed when Barnes compared snowcover distributions observed on 1972-73 LANDSAT-I imagery with snowcover distributions on the Salt-Verde watershed mapped by the Salt River Project using visual mapping techniques (1). Barnes found an average difference of 7 percent between the two mapping techniques (table 1). However, when the aerial observations were made on or within 1 day of the data of the LANDSAT-I imagery, differences as small as 2 percent were observed.

Rapid snowmelt at elevations below 7,000 feet (2,100 metres) above mean sea level cause large and rapid changes in the snowcover on the Salt-Verde watershed. The snowcover on the Upper Tonto Creek watershed decreased from 70 percent to 5 percent between February 18 and 27, 1975, as shown on LANDSAT imagery (fig. 5).

Aerial Observations of Snow Depths

Surface wind speeds, estimated to be as great as 50 knots per hour, over the mountains of central Arizona produced rough air conditions during the spring of 1975 that often prevented low-level observation of snow markers and natural features such as logs and fences used to estimate snow depths. Oblique aerial photography of aerial snow markers on the upper Salt River watershed was attempted to obtain the desired snow-depth information.

After considerable experimentation, a technique was developed for obtaining economical, high resolution, aerial photography of the snow markers from safe altitudes above the

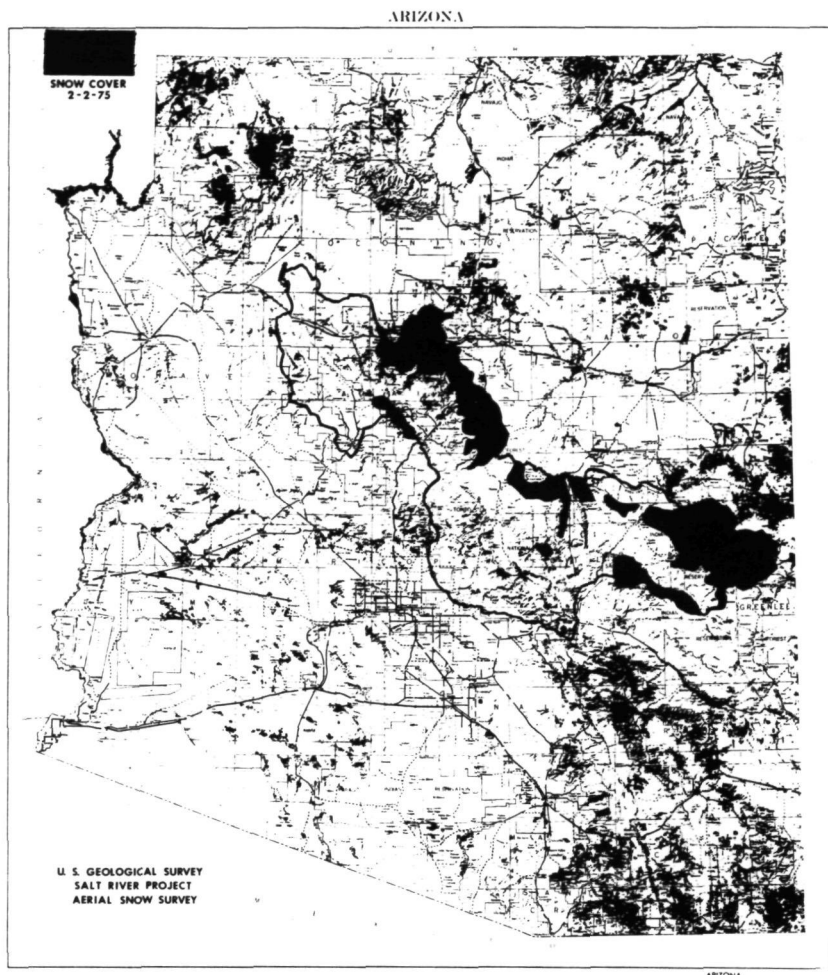


Fig. 3-Snow cover on Salt-Verde Watershed, Arizona

Table 1. --Comparison between snowcover mapped from ERTS imagery
and aerial snow surveys for Salt-Verde watershed, Arizona 1972-73

Case	Date of ERTS imagery	Date of aerial snow survey	Interval between ERTS and aerial observations (days)	Percent of area snow covered		
				ERTS	Aerial	Difference
1	21 Nov.	14 Nov.	7	19	33	14
2	11 Jan.	12 Jan.	2	19	26	7
3	01 Feb.	02 Feb.	1	22	29	7
4	18-19 Feb.	15 Feb.	3-4	39	48	9
5	26 Mar.	26 Mar.	0	51	53	2
6	13 April	12 April	1	25	27	2
7	02 May	27 April	5	25	36	11
MEAN DIFFERENCE FOR ALL 7 CASES						7

Data from Barnes, Bowley and Simmes, 1974

terrain (500 feet or 150 metres). Several types of cameras and telephoto lenses of various focal lengths were evaluated. The combination of a motorized 35-mm camera fitted with a 500-mm focal-length lens, and Kodak High Speed Ektachrome color film was found to consistently provide the scale and quality of photography required. The use of a motorized camera allowed the acquisition of multiple images of the snow markers during a single imaging pass by the aircraft.

The processed film was mounted in slide mounts for interpretation using standard 35-mm film projection equipment. Knowing the dimensions of the aerial snow markers (including the total height, width of the bars, and the spacing between adjacent bars) it was possible to easily and quickly determine the snow depth with an estimated accuracy of ± 3 inches (± 7.5 mm) from photography taken at as much as 1,000 feet (305 metres) above the terrain.

The use of high-speed color film was found to significantly facilitate the interpretation of aerial snow markers photographed under cloudy or overcast conditions. Examples of oblique aerial photography of a 9-foot (2.7 metre) simulated aerial snow marker, using the previously described camera system, are shown in figure 4. The shadow of the aerial snow marker is often more easily evaluated than the vertical marker itself. The shadow of the marker can be observed with the least distortion when photographed directly toward the sun (fig. 4B).

One major advantage of this technique for determination of snow depths is that it utilizes only standard and readily available photographic and projection equipment. Another advantage is that it provides a low-cost permanent photographic record of the snow markers that can be evaluated in the office as opposed to attempting to read the snow markers visually from low-flying light aircraft over mountainous terrain — often under less than ideal flying conditions.

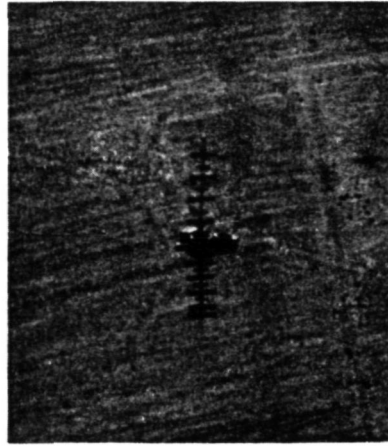
SATELLITE OBSERVATIONS

LANDSAT Imagery

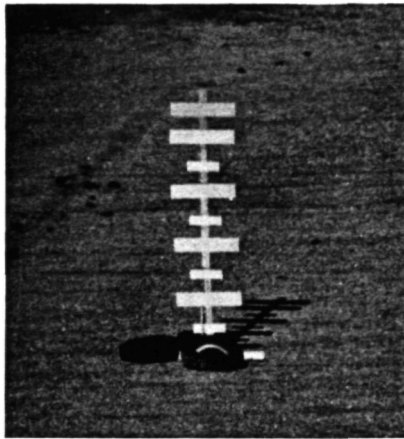
Film positive copies of 1:1,000,000-scale LANDSAT Band 5 (0.6-0.7 μ m) imagery are essentially orthographic and provide sufficient detail for operational mapping of snowcover



A. from 1000 feet



B. from 500 feet



C. from 200 feet

Fig. 4-Oblique aerial photography of simulated aerial snow marker

21
 REPRODUCIBILITY OF THE
 ORIGINAL PAGE IS POOR

distributions and changes in snowcover distributions on the Salt-Verde watershed of central Arizona (fig. 5). Using visual interpretation techniques, an experienced analyst can accurately map snowcover distributions over the entire 13,000 square miles (34,000 square kilometres) of the Salt-Verde watershed from the LANDSAT imagery in less than 2 hours. Approximately 5 hours of flight time and 1 to 2 hours of map preparation are required to map the same area using aerial reconnaissance techniques.

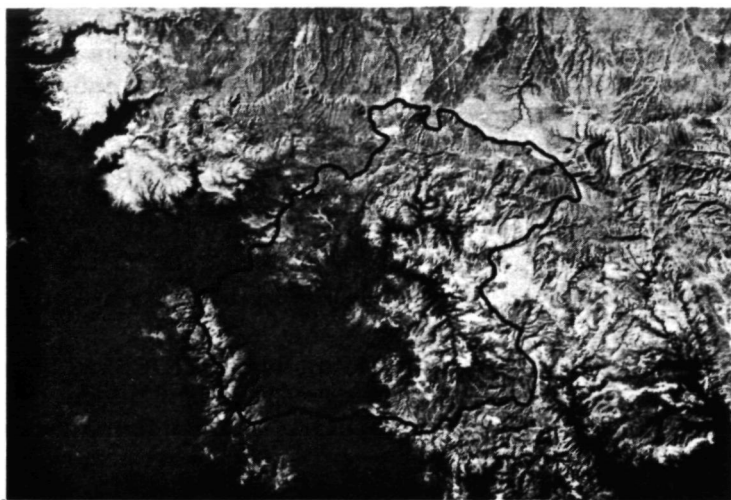
The use of density-slicing techniques, together with appropriate watershed masks, allows rapid determination of the percentage of snowcover on individual watersheds and sub-watersheds of particular interest for runoff forecasts. Color additive viewing of the multispectral LANDSAT imagery greatly facilitates the determination of snowcover distributions on the small, but densely forested, upper parts of the Salt-Verde watershed.

The single factor that has precluded operational utilization of LANDSAT imagery for snowcover mapping in central Arizona is the 4-week processing and shipping delay between the time of acquisition of the imagery by the satellite and its receipt in Arizona. Satellite imagery, to be used for operational prediction of short-term, snowmelt-derived runoff in central Arizona, must be received in Arizona within 48-72 hours after acquisition by the satellite.

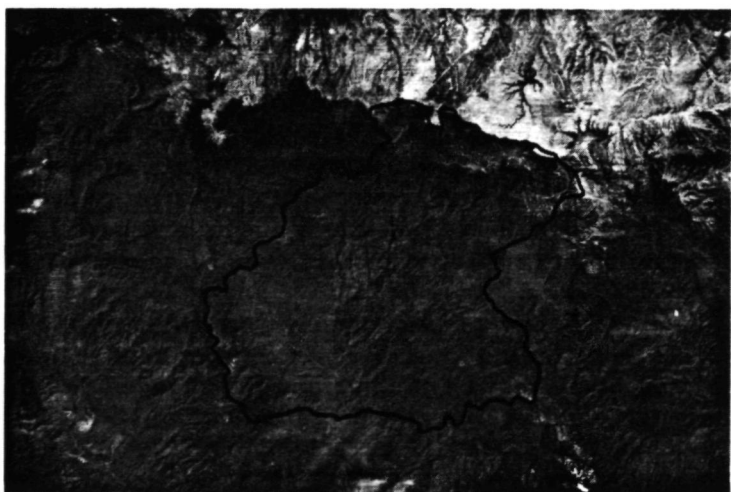
Meteorological Satellite Imagery

Sample copies of the NOAA Very High Resolution Radiometer (VHRR) visible band (0.6-0.7 μm) and SMS/GOES (0.55-0.75 μm) satellite imagery over Arizona were received from the NOAA National Environmental Satellite Field Services Station in Redwood City, California, during the spring of 1975.

The high-polar-orbital NOAA satellite imagery and, to a lesser degree, the geostationary SMS/GOES imagery contain considerable distortion and are much more difficult to fit to planimetric maps than the nearly orthographic LANDSAT imagery. The resolution of both types of meteorological satellite imagery is reported to be 1 kilometre at nadir and is much lower than that of the LANDSAT imagery. However, the meteorological satellite imagery does cover very large areas — the entire Salt-Verde watershed and adjacent areas



LANDSAT II 2027-17213-5 February 18, 1975



LANDSAT I 1949-17170-5 February 27, 1975

Fig. 5-Snow cover changes on Upper Tonto Creek watershed

REPRODUCIBILITY OF THE
ORIGINAL PAGE IS POOR

are covered on a single image. Because meteorological satellite imagery is available on a daily basis, it is potentially of significant value for operational monitoring of snowcover over the Salt-Verde watershed where large changes in snowcover occur within very short periods. Wiesnet and McGinnis (1973) described the successful use of NOAA VHRR together with LANDSAT-I imagery for snow mapping in the American River Basin, California (3).

LANDSAT DATA COLLECTION SYSTEM OPERATIONS

The LANDSAT Data Collection System (DCS) is being used to relay streamflow and snow-water equivalent information from six remote sites in central Arizona in support of the operational snowcover mapping on the Salt-Verde watershed (fig. 1). The LANDSAT-DCS provides the capability to collect data transmitted from earth-based environmental sensors by means of Data Collection Platforms (DCP's) and to relay these data to ground-receiving sites located at Goldstone, California, and at Greenbelt, Maryland.

The DCP's will accept inputs from as many as eight different environmental sensors in analog, serial digital, or parallel digital form. Eight channels of analog data, or eight 8-bit parallel digital words, or 64 serial digital bits can be input to a single DCP. Each analog input requires the use of one 8-bit word and the analog input voltage range is 0 to +5 volts DC. Any combination of analog inputs and parallel digital inputs, resulting in a total of 64 bits, can be accepted.

The DCP's operate continuously and transmit a 38-millisecond burst of data, each 90 or 180 seconds, containing the platform identification number and the encoded 64 bits of data from the eight sensor channels. When the LANDSAT satellite is in mutual view of a transmitting DCP and one of the ground-receiving sites the satellite relays the DCP transmission to the ground-receive site through an on-board receiver/transmitter. The LANDSAT satellite has no on-board DCS data storage capability and acts as a real-time relay. According to the system design the satellite should be in mutual view of at least one ground-receiving site and a DCP located almost anywhere in North America during at least two orbits per day. In Arizona DCS data have been received during two to six orbits per day depending on local site conditions. The DCS data handling and data products are described in detail in the

The data flow from the ground sensor through the DCS and back to the Arizona user is shown diagrammatically in figure 6. DCP-equipped streamflow gages and a snow-water equivalent measurement site are shown in figures 7 and 8, respectively.

During the spring of 1973, the Salt River Project used near-real time hydrologic data furnished by microwave and LANDSAT-DCS telemetry to successfully predict the volume of runoff into their reservoir system and by prudent water management prevented flooding in the Phoenix metropolitan area. This was accomplished although the record snowfalls on the watersheds of central Arizona produced the greatest volumes of runoff recorded in recent years (2).

The data collection system associated with the operational SMS/GOES geostationary satellites offers increased data transmission capacity and will operate in either a self-timed or in an interrogate mode. Several new convertible data collection platforms, capable of transmitting to either LANDSAT or SMS/GOES satellites, have been purchased. Field testing of these units in central Arizona is scheduled for the fall of 1975.

SUMMARY AND CONCLUSIONS

Aerial observation of snowcover distributions has the significant advantage of providing the required information during periods of cloud cover that preclude satellite snowcover observations. Aerial reconnaissance flights also allow visual and photographic estimates of snow depths. For these reasons, aerial reconnaissance flights will continue to provide a valuable hydrologic tool and will provide complimentary data to satellite snowcover observations on the Salt-Verde watershed.

The feasibility of using satellite telemetry to furnish near-real time hydrologic data for use by water-management agencies in Arizona has been successfully demonstrated by the LANDSAT data collection system. The SMS/GOES data collection system offers an increased data handling capacity and will soon be field tested in Arizona.

The LANDSAT imagery at a scale of 1:1,000,000 is

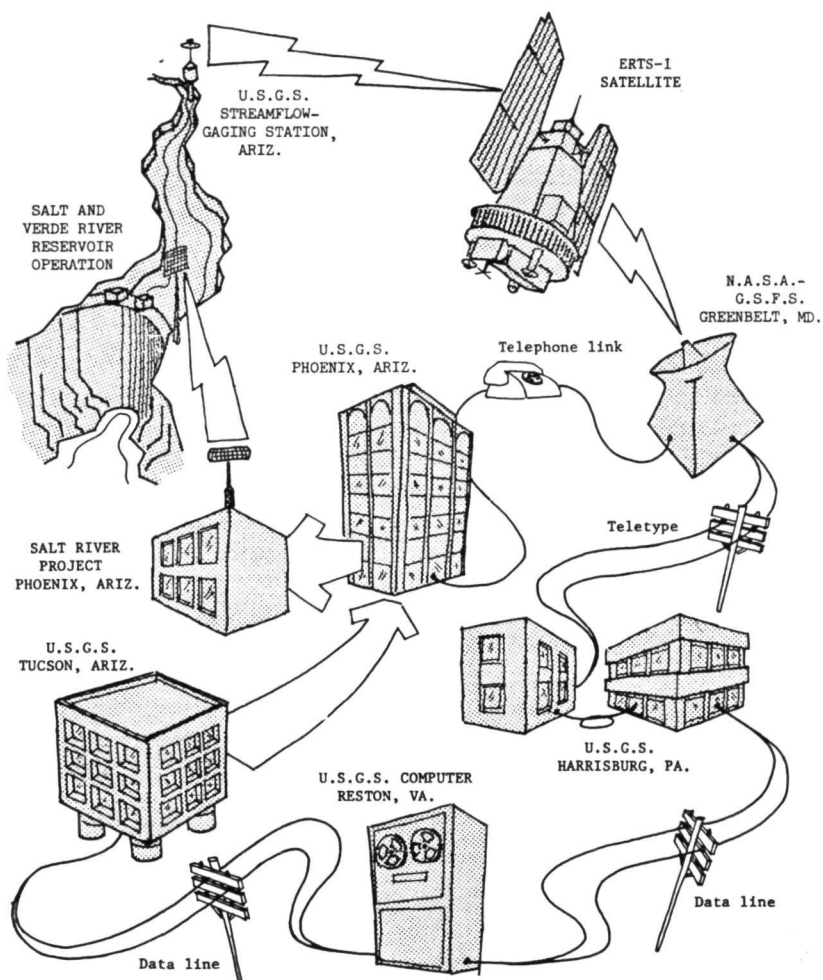


Fig. 6-LANDSAT Data Collection System operations in Arizona

REPRODUCIBILITY OF THE
ORIGINAL PAGE IS POOR



Fig. 7-White River streamflow gage near Ft. Apache, Arizona
equipped with LANDSAT Data Collection Platform

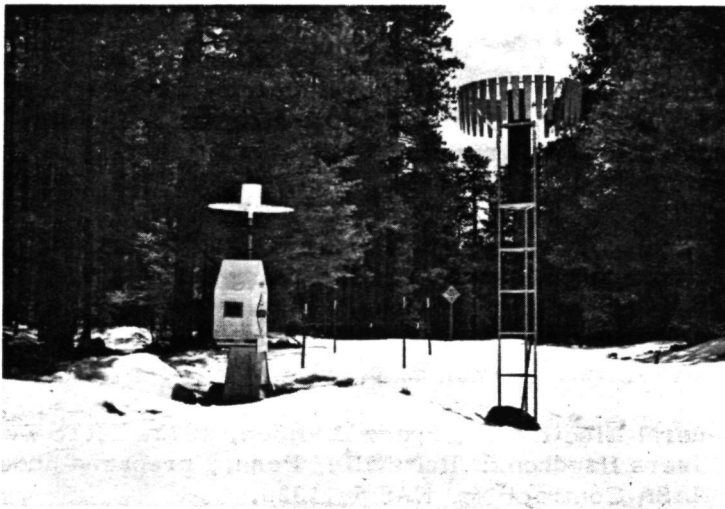


Fig. 8-Snow-water equivalent measurement site at Baker Butte,
Arizona equipped with LANDSAT Data Collection Platform

relatively free of image distortion and provides sufficient resolution for operational snowcover mapping in central Arizona. However, the development of new procedures for rapid processing and delivery of the imagery, within 48-72 hours after acquisition by the satellite, will be required to allow operational utilization of the LANDSAT imagery for snowcover mapping.

The small irregular scale and relatively low resolution of NOAA VHRR and SMS/GOES meteorological satellite imagery cause it to be much more difficult to use than LANDSAT imagery for operational snowcover mapping in Arizona. However, because the meteorologic satellite imagery is available on a daily basis, it may be of significant value for monitoring the rapid changes in snowcover observed in central Arizona.

REFERENCES

1. Barnes, J. C., Bowley, C. J., and Simmes, D. A., 1974, The Application of ERTS Imagery to Mapping Snowcover in the Western United States, Final Report under Contract NAS 5-21803, Environmental Research and Technology, Inc., Concord, MA, 77 pp.
2. Schumann, Herbert H., 1974, Hydrologic Applications of ERTS-1 Data Collection System in central Arizona: in Proceedings of Third Earth Resources Technology Satellite-1 Symposium, NASA, vol. 1, sec. B, p. 1213-1223.
3. Wiesnet, D. R., and McGinnis, D. F., Jr., 1974, Snow-Extent Mapping and Lake Ice Using ERTS-1 MSS Together with NOAA-2 VHRR: in Proceedings of Third Earth Resources Technology Satellite-1 Symposium, NASA, vol. 1, sec. B, p. 995-1008.
4. General Electric Co. Space Division, 1972, ERTS Data Users Handbook: Beltsville, Penn., prepared under NASA Contract No. NAS 5-11320.

THE APPLICATION OF HYDROMETEOROLOGICAL DATA OBTAINED BY REMOTE SENSING TECHNIQUES FOR MULTIPURPOSE RESERVOIR OPERATIONS

W. L. Warskow, T. T. Wilson, Jr., and K. Kirdar, *Salt River Project, Phoenix, Arizona*

ABSTRACT

Watershed snowpack and streamflow data obtained and transmitted by (ERTS) satellite has been used in the operational and water management decisions in the Salt River Project. Located in central Arizona, the Project provides water and electric power for the more than 1.1 million residents of the Salt River Valley. The water supply source is a 33,670 square kilometre (13,000 square mile) watershed and 250 deep well pumps. Six storage reservoirs, four of which have hydroelectric capability, located on two river systems have a storage capacity of over 246,600 hectare-metres (2,000,000 AF.). Information from the watershed during the normal runoff period of December to May and more especially during critical periods of high runoff and minimum reservoir storage capacity is necessary for the reservoir operation regimen. Extent of the snowpack, depth of snow, and the condition of the pack has been observed and reported by an observer in aerial flights over the watershed. Snow density, air temperature, accumulated precipitation and streamflow quantities have been relayed by satellite data collection stations. These data, along with bi-weekly snow surveys have been the bases for runoff volume forecasts and for the development of the reservoir operations plan. The application of snow mapping techniques from satellite imagery which can provide frequent definition of the areal extent of watershed snow cover holds good potential for improved accuracy of the volume forecasts as well as providing needed information for the day to day critical operational decisions.

INTRODUCTION

Water for municipal, industrial, and agricultural use in the Salt River Valley of Central Arizona is provided, in large part, by the Salt River Project. The 1.1 million people and 101,175 hectare (250,000 acre) urban and agricultural area requires annually about 148,000 hectare-metres (1,200,000 acre feet) of water from the Project, water that is diverted from the surface supply or pumped from the groundwater basin.

THE SALT RIVER PROJECT SYSTEM

Surface Water

The surface water originates from precipitation falling on a 33,670 square kilometre (13,000 square mile) watershed which ranges in elevation from about 400 metres (1300 feet) to almost 3870 metres (12,700 feet). Three separate major drainage basins, the Salt, Tonto, and Verde, comprise the watershed, and runoff from these basins flows into six reservoirs on the Salt and Verde rivers. About 75% of the mean annual runoff, 1913-1974, from the three streams results from winter cyclonic and frontal storm systems which occur during the December - May runoff season. Much of the precipitation from these storms falls as snow. The snow that is deposited above the 2135 metre (7000 foot) elevation normally remains until the spring snowmelt period of March, April and May. About 90% of the total watershed lies below 2135 metres (7000 feet) and the snow that falls on this area, down to as low as 760 metres (2500 feet) is ephemeral in nature and subject to very rapid melt induced by either subsequent rainfall or sharp increases in temperature. Because of the large areal extent of this portion of the watershed and the instability of the snowpack, very high runoff volumes can be experienced in relatively short periods of time creating major flooding potentials if reservoir storage is high.

Groundwater

The groundwater supply for the Project is pumped from the alluvial aquifers of the Salt River Valley within the Project's water service area. Two hundred fifty-five deep well pumps, which are located throughout the water transmission and distribution system, can develop 35 to 40% of the annual water requirement. Operation of these pumps is normally minimized in order to conserve both groundwater and energy; their use is supplemental to the surface water supply.

Reservoir System

The Salt River Project has six dams which create a reservoir storage capacity of 255,485 hectare-metres (2,072,050 acre feet). Four of the six dams are located on the Salt River and two on the Verde River. Theodore Roosevelt dam and lake is the largest of the six providing just over 65% of the total water storage capacity. Each of the four dams in the Salt system are equipped for hydro-electric power generation with a total capacity of 248,000 KW; two of the dams have reversible pump turbines providing a water pump-back capability. The two dams on the Verde River have reservoirs with a combined capacity of 39,175 hectare-metres (317,715 acre feet). This is used for short term or temporary storage of water and the system does not have hydrogeneration capability.

The water management objectives of the Salt River Project are (1) have sufficient quantities of water available from either surface or groundwater sources or both to meet the demands for municipal, industrial and agricultural use in the Salt River Valley; (2) provide reservoir carryover 123,300 to 160,290 hectare-metres (1.0 to 1.3 million acre feet) at the end of each year to insure sufficient surface supply for two years hence; (3) maximize hydroelectric generation during the high power demand summer months; (4) to the extent possible, minimize pumping (5) use Verde system storage to supplement outflow from the Salt system so that release of water on the Salt other than for power generation is not necessary; (6) reduce Verde system storage to 10-15% of capacity by the first of December each year; (7) during periods of high runoff and maximum storage, limit necessary controlled spillway releases to flows that would result in minimal flood damage to property along the Salt River channel through the Valley area and maximize power generation and agricultural water use; (8) end the December-May runoff period with reservoir system full.

A Project Reservoir Operating Plan is formulated during the latter part of each year to meet these objectives. This plan is under constant review during the ensuing year and modification or adjustment is made periodically to meet the prevailing conditions of demand, runoff, and storage. Operational criteria that must be considered includes: (a) the total monthly demand for water, (b) the amount of groundwater pumping that is required; this is a function of the amount of storage and the prospects for runoff as well as the availability and cost of energy for pumping; (c) the amount of surface water demand; (d) the reservoir system or systems from which the surface water should be withdrawn, whether the Salt, the Verde or both in order to accomplish objectives 3, 5, and 6; (e) runoff quantities forecasted or expected in each of the reservoir systems for the month.

Runoff Forecasting

The present method for forecasting seasonal runoff at the Salt River Project is based on the multiple regression analysis theory. It is also known as the Index Forecast Method. Briefly, this method involves correlations of historical runoff records with indices of important determinants of runoff for the area. The use of this method provides seasonal volumetric runoff forecasts utilizing bi-weekly snow survey information from mid-January to April 1st. The method was developed in Arizona in 1961 as the result of a research effort between the Soil Conservation Service and the University of Arizona (Cluff, 1961). The present updated and improved runoff forecast equations were obtained during 1967 by Project personnel (Wilson, 1970). Present runoff forecasting is done cooperatively by Soil Conservation Service and the Salt River Project personnel. The two main drawbacks of the present

method are: (1) the method relies strongly on averages, therefore it fails to accommodate abnormal snow or weather conditions. (2) the seasonal volumetric runoff information may not always be adequate for the critical reservoir operation decisions.

The present goal is to develop short range runoff forecast techniques and monitor the effects of the major storms on the reservoir system. While the Project has no legal responsibility for flood control, it feels obligated as a good neighbor to try to minimize the potential for flooding through the Salt River Valley while at the same time meeting its legal responsibility to its shareholders to maximize reservoir storage. To maintain the delicate balance required, more information than that provided by established data collection sites is needed. Few snow survey sites exist in the ephemeral snow zone. Information on areal extent, depth, and condition of the snowpack over large areas in this snow zone is required if the flood hazard was to be adequately monitored. Snowcourses, aerial snow markers, soil moisture stations and snowpillows are all point samples and do not provide all the information needed for the lower-elevation snowpack. A technique for estimating snow depths and mapping snowpack areal extent and percent coverage has been developed by the Project (Warskow, 1975).

AERIAL SNOWMAPPING TECHNIQUE

Mapping

During the years 1965-68, maps of the Salt-Verde snowpack were drawn at a scale of approximately 1:3,000,000 from notes taken during each watershed flight. The snowline depicted on these early maps was generalized - primarily on the basis of elevation. Direct enroute mapping was first attempted in 1969 using the 1:1,000,000 Arizona aeronautical chart. This proved so successful that a copy of the Salt-Verde portion of the chart was mounted permanently on a 28 by 43 centimetre (11 by 17 inch) lap-board. Superimposed over this base map was a removable mylar overlay showing the watershed boundary, elevation by 305 metre (1,000 feet) increments, towns, and the major drainage systems.

The shaded relief on the Arizona aeronautical chart very accurately depicts watershed topography, enabling the aerial observer to map the snowpack with considerable precision. The edge of the pack is traced on the mylar overlay with a colored pencil as the flight progresses over the watershed. Ocular estimates of the percent of the ground covered with snow are made and recorded marginally. Snow depths are recorded in a similar manner.

Estimating Snow Depths

Highway right-of-way and range fences were originally used to obtain aerial estimates of snowpack depth. The aerial observer's knowledge of fence heights and strand placement coupled with

a simple observation of how many strands remained above the snow and an estimate of the distance between the top of the snow and the lowest exposed strand permitted fairly accurate estimates (+ 5.0-7.5 centimetres; + 2-3 inches) of snow depth. By using fence shadows, estimates with similar accuracy could be obtained from a height of 305 to 460 metres (1,000 to 1,500 feet) above ground.

Early observations indicated that surface rock, vegetation and cull logs might be useful yardsticks. Utilizing a knowledge of the variations in these features over the Salt-Verde watershed, a technique to estimate snow depths was developed.

The volcanically-derived soils underlying most of the juniper vegetation zone on the Salt-Verde watershed are covered with dark rocks of varying size. These contrast sharply with the white of snow. With a familiarity of their size (height above soil line), it becomes relatively easy to estimate depths from the air. For example, a "powdered sugar" appearance with numerous dark "freckles" indicates depths of less than 2.5 centimetres (1.0 inches). As snow depth increases, fewer rocks are visible and the snow takes on a "wet, lumpy cotton" look. By the time snow depth reaches 15 centimetres (6 inches) the sides of individual rocks are no longer visible and their presence is indicated only by mounds "softly" outlining them.

At this stage, it becomes necessary to transfer the reference point to other features. Grass stems are a good indicator for depths of 15 to 20 centimetres (6 to 8 inches). Half-shrubs are useful for depths of 15 to 30 centimetres (6 to 12 inches). Depths greater than 30 centimetres (12 inches) require the use of logs or some other indicator.

The widespread occurrence of logs in Arizona forests makes them one of the most useful references available for estimating snow depths. A knowledge of the relative sizes of logs in each area is, however, required for accuracy.

The visibility of the underedge and sides of the log, presence or absence of snow bridging between its top and sides and the form of the snow mound over the log are all used to determine the depth of the snow relative to the log's diameter. If the snow is less than half the log's diameter, its curved underedge will be visible. If one-quarter or less, significant shadow can usually be seen depending on the log's orientation to the sun.

Bridging between the snowcap on top of the log and the snow on the ground occurs at depths between fifty and sixty-five percent of log diameter depending on the wetness of the snow. At depths greater than two-thirds log diameter, the sharp outline of the log under the snow begins to soften to the point it almost disappears at depths equal to or slightly greater than the log's diameter. A very flat mound revealing the log's presence may sometimes occur up to depths of fifteen to twenty-five percent greater than the log's diameter depending on other factors such as wind and snow wetness. The upper limits for using this method in Arizona is about 107 centimetres (42 inches). Depths greater than this require the use of man-made aerial snowmarkers.

Estimating Snowpack Condition and Runoff Stage

Relative condition of the snowpack can also be observed and mapped aerially. The presence of ice can usually be detected by a dull sheen at or just below the surface of the snow. Pack discoloration, striation and deformation can all be used to detect the imminence of snowmelt. The presence of ongoing melt can be determined from the brilliant, mirror-like reflectance of the sun through small holes in the pack. Relative river stage can also be determined by an aerial observer. A rising stage is indicated by heavy sediment loads and lack of fresh high water marks. Wet sandbars, presence of bank seepage, fresh high water marks and clearer water generally indicate flow recession.

Accuracy

The quality of snowpack information obtained by the method described is directly affected by the experience of the observer, his physical condition during the flight, the time spent at altitude without supplementary oxygen, the quality of existing light conditions, and the depth of snow relative to the depth indicators being used. Under good to fair conditions, experienced aerial observers have been able to consistently estimate snow depths within +5.0 centimetres (+2.0 inches) of the depths reported independently by various ground observers. For operational purposes, this variation is more than acceptable.

Barnes (1974), independently comparing the Project's snow-maps for seven dates in 1972-73 with snow maps compiled from imagery obtained in the 0.6-0.7 μ m spectral band by the ERTS-1 satellite, reports a mean areal difference of only seven percent between the two mapping methods. Snow melt or deposition occurring between the date of a low level reconnaissance flight and the date of the comparable satellite image plus approximation of the snowline by the aircraft observer for areas not directly overflowed account for most of the differences between the satellite and aircraft maps. Other differences arise due to the aerial observer's ability to map shallow, partial snow cover which may not at times be visible on the satellite imagery. The difference between the two mapping methods dropped to two percent when the low level maps were produced from direct overflights conducted on or near the same day the satellite passed overhead.

USE OF SATELLITE INFORMATION

Data Collection

Streamflow data is telemetered to Project offices from six upstream gaging stations. In the past, problems with ice detuning the antennas on the mountain top repeaters has made data unavailable when it was most needed during critical runoff events. System performance has been improved with the installation of better equipment but is still not perfectly reliable.

In 1973, data from an ERTS-1 DCP located on the Verde River at Camp Verde was relayed to Project offices by NASA several times a day when the Project's communication link with the site failed. Installation of another ERTS-1 DCP on the Black River the same year and at several other sites, including two snowpillows and meteorological data sites, since has permitted acquisition of data from remote watershed areas without the necessity of installing additional, high-priced, mountain-top repeaters. This information plus streamflow data received via the Project's telemetry system and via ERTS-1 has been successfully used as a guide for making adjustments in reservoir outflows during critical runoff periods. Snowmelt runoff may take from a few hours to one or two days to reach the nearest Project early-warning gaging station. Early detection of major runoff events when Project reservoirs were at or near capacity has permitted additional time for orderly releases through Project hydroelectric generators and into the canal system for use by Project shareholders. Release of the same volume of water over a shorter period of time would have required the use of spillway gates with attendant tailrace damage, loss of power revenues and wasting of the water down river. When reservoir releases are already in progress, early detection of flow recession becomes important. The early knowledge provided by the aerial flights and satellite telemetry that the snowmelt supporting a runoff event was almost ended has permitted earlier termination or reduction in reservoir releases than would have been possible when stream gages were the only source of data. By utilizing the flight and satellite information, the amount of water that would otherwise have been wasted down river was materially reduced.

Snow Maps

Because the hydrologic diversity and the transient characteristics of the snow pack in the Salt-Verde watershed, snow maps could become an important integral part of the general evaluation for the reservoirs operational decisions. The results of investigation (Barnes, 1974) indicate that ERTS imagery has substantial practical application for snow mapping.

The current application of snow mapping techniques from satellite imagery is in the initial stage at the Salt River Project. But based on the experiences in the application of the hydrometeorological data obtained by remote sensing techniques it can confidently be stated that the use of satellite snow maps is highly promising at the Project. Timely, accurate, and dependable information of areal extent of watershed snow cover could be invaluable for critical reservoir operational decisions.

A limited study was undertaken by the Project personnel on a set of snow maps prepared from NOAA imagery by the Environmental Products Group for the 1974-75 snow season of Salt and Verde basins. These maps have been prepared on an operational basis and the snow cover was expressed in percent of the total watershed area by S. R. Schneider of NOAA.

An attempt was made to analyze the Salt River Basin snow cover percentage. Using the basin's hypsometric curve, a snow line was determined from the percent of snow cover. The snow melt area was computed for each specific melt time and the average elevation was calculated for the area. Due to the lack of the average snow density (water content) at the computed average melt elevation, potential snow melt volume could not be computed. If the water content were available then the potential melt volume could be computed. Then a basin yield factor could also be determined from the gaged versus computed potential runoff.

The basin yield factor could be very valuable for monitoring and also for predicting the inflow from major storms. Availability of this information can be used to develop short range forecasting and storm monitoring techniques which are needed for timely reservoir operational decisions.

It is the authors' opinion that satellite snow maps can be used at the Salt River Project as a direct input to streamflow synthesis models and also in the regression analysis method for computing seasonal runoff. Frequent snowmaps obtained in real time would contribute positively to stream flow forecasting accuracy, which has direct impact on the Water Resource Operations Department's ability to meet the Project's water management objectives.

CONCLUSION

The existence of distinct snow zones on the Salt and Verde River watersheds became evident early in the Project's aerial snow survey flights. Subsequent observations made on snow accumulations, depths, and melt characteristics were used to identify and map areas having similar snowpack characteristics. Snow zone characteristics and size coupled with ground and flight information on existing soil moisture and snowpack conditions have been used for empirical calculations of maximum potential streamflow, timing of runoff from individual watersheds, and the total amount of reservoir inflow anticipated for the season. It is anticipated that the availability of repetitive imagery and telemetered snowpack data from the LANDSAT, NOAA AND GOES satellites will make it possible to develop this same information quantitatively within the next few years. Operational applications will require that both the imagery and telemetered data be available to the user in real time.

Accurate and timely long and short range runoff forecasts are essential tools for reservoir operations and for estimating the quantity of water available for an adequate and assured water supply for the Salt River Project and Central Arizona.

References Cited

- Barnes, James C., Clinton J. Bowley, and David A. Simmes. 1974. The Application of ERTS Imagery to Mapping Snow Cover in the Western United States. Environmental Research and Technology, Inc., Lexington, Massachusetts.
- Cluff, C. B. 1961. Seasonal Streamflow Forecasting for Central Highlands, Arizona, Masters Thesis. University of Arizona, Tucson, Arizona.
- Warskow, W. 1975. Aerial Snowpack Mapping. Hydrology and Water Resources in Arizona and the Southwest. Vol. 5.
- Wilson, T., Jr. and Edib Kirdar. 1970. Use of Runoff Forecasting in Reservoir Operations, Journal of the Irrigation and Drainage Division, ASCE, Vol. 96, No. IR 3, Proc. Paper 7541.

INTERPRETATION OF SNOWCOVER FROM SATELLITE IMAGERY FOR
USE IN WATER SUPPLY FORECASTS IN THE SIERRA NEVADA

A. J. Brown, *Snow Surveys Branch, California; Department of Water Resources, Sacramento, California;* J. F. Hannaford, *Sierra Hydrotech, Placerville, California*

ABSTRACT

The California ASVT test area is composed of two study areas; one in Northern California covering the Upper Sacramento and Feather River Basins, and the other covering the Southern Sierra Basins of the San Joaquin, Kings, Kaweah, Tule, and Kern Rivers. The paper describes the experiences of reducing snowcover from satellite imagery; the accuracy of present water supply forecast schemes; and the potential operational advantages of introducing snowcover into the forecast procedures.

INTRODUCTION

The National Aeronautics and Space Administration is investigating application of satellite imagery to interpretation of snowcover in the western United States, including California's Sierra Nevada. The objective of the overall investigation is application of data on areal extent of snowcover to operational water supply forecasts. NASA has contracted with the California Department of Water Resources to explore potential application of snowcover data from satellite imagery to the Department's hydrologic forecasting responsibilities. The Department of Water Resources has contracted with Sierra Hydrotech, a consulting firm in Placerville, California, for technical assistance in developing procedures for data reduction and in investigating applications of satellite data on snowcover to hydrology.

The objective of this paper is to outline plans and goals of the California investigation and to report upon progress made in achieving these goals over the past year.

Preceding page blank

BACKGROUND

The Sierra Nevada and the southern portion of the Cascade Range supply California's fertile San Joaquin and Sacramento Valleys with water for agricultural, municipal, and industrial use. Portions of this water supply are exported via the California State Water Project for use in Southern California. The average water-year runoff of Sierra streams tributary to the San Joaquin Valley and Tulare Lake Basin is approximately 9 million acre-feet, while the average water-year runoff of Sierra and Southern Cascade streams tributary to the Sacramento Valley is approximately 15 million acre-feet. In southern Sierra streams where elevations range up to 14,000 feet, as much as 75 percent of the average annual runoff occurs during the April-July snowmelt season. In the northern Sierra streams where elevations are much lower, only about 40 to 50 percent of the average annual runoff occurs during the snowmelt season.

It is interesting to note that the first program of formalized snow water content measurements was initiated here in the Lake Tahoe Basin by Dr. James E. Church, University of Nevada. As early as 1910 Dr. Church made measurements of snowpack water content with a snow sampling tube, similar to that used today, with the objective of predicting the annual rise of Lake Tahoe as a means of resolving certain water rights problems in the Truckee River Basin.

The importance of water in the Central Valley of California has long generated a keen interest by water managers in methods of predicting the volume of the seasonal water crop and the time-distribution of runoff for operational planning. Although water supply forecasts have been utilized since well before the turn of the century, the State of California coordinated the early diverse interests through initiation of the California Cooperative Snow Survey Program in 1929. The legislature mandated in that year that an annual and seasonal projection of the State's snowmelt water crop be made. The program of snow measurement and water supply forecasting has been conducted continuously by the State and its cooperators for 45 years.

The high degree of development and use of water in California's Central Valley has required development of sophisticated techniques for predicting volume and

time-distribution of runoff for water management purposes. Water management problems in certain areas require continual surveillance of streamflow and updating of forecasts during the runoff season to provide for management decisions as the season progresses. Forecast technology has advanced to the degree that application of new data types may possibly generate only limited improvement in forecast accuracy, particularly early in the season when forecast error is highly dependent upon the precipitation which occurs after the date of forecast. Development of new data types, such as snowcover from satellite imagery, will not eliminate the necessity or advisability of collecting data on precipitation, snowpack water content, and rates of snowpack accumulation and melt in the foreseeable future.

INVESTIGATION

The objectives of the California ASVT investigation and the location of the study areas are described in the next two sections.

Objectives

The technical objectives of the California ASVT may be grouped as (1) reduction and interpretation of basic snowcover data, and (2) operational application of snowcover to water supply forecasting. It should be pointed out that development of sophisticated techniques for snowcover reduction is not part of the first objective. The purpose of the snowcover reduction phase is merely to quickly learn how to obtain data required later during the operational applications phase of the study. Once the applicability of snow covered area from satellite imagery to the State's hydrologic responsibilities has been determined, then techniques for reduction and interpretation of imagery for operational purposes can be finalized.

The most important objective of the investigation is the determination of the applicability of snow covered area from satellite imagery to water supply forecasting in general, but more specifically the updating of forecasts as the melt season progresses and the estimation of potential rates of melt and corresponding stream discharge. Initial investigation suggests that adequate data on snow covered area may prove of more value in estimating melt rate and updating forecasts than in preparation of early season water supply forecasts.

Study Area

The study area, comprising 38 major basins and sub-basins is actually two study areas covering a wide variety of topographic, climatologic, and hydrologic conditions. The first study area covers the Sacramento River above Shasta Dam and the Feather River above Oroville Dam and includes 24 major basins and sub-basins within and adjacent to these two watersheds. The other area is composed of five southern Sierra streams, the San Joaquin, Kings, Kaweah, Tule and Kern River Basins, and includes 14 major basins and sub-basins for which data is being reduced. Plate 1 shows the location of these study areas.

DATA REDUCTION AND INTERPRETATION

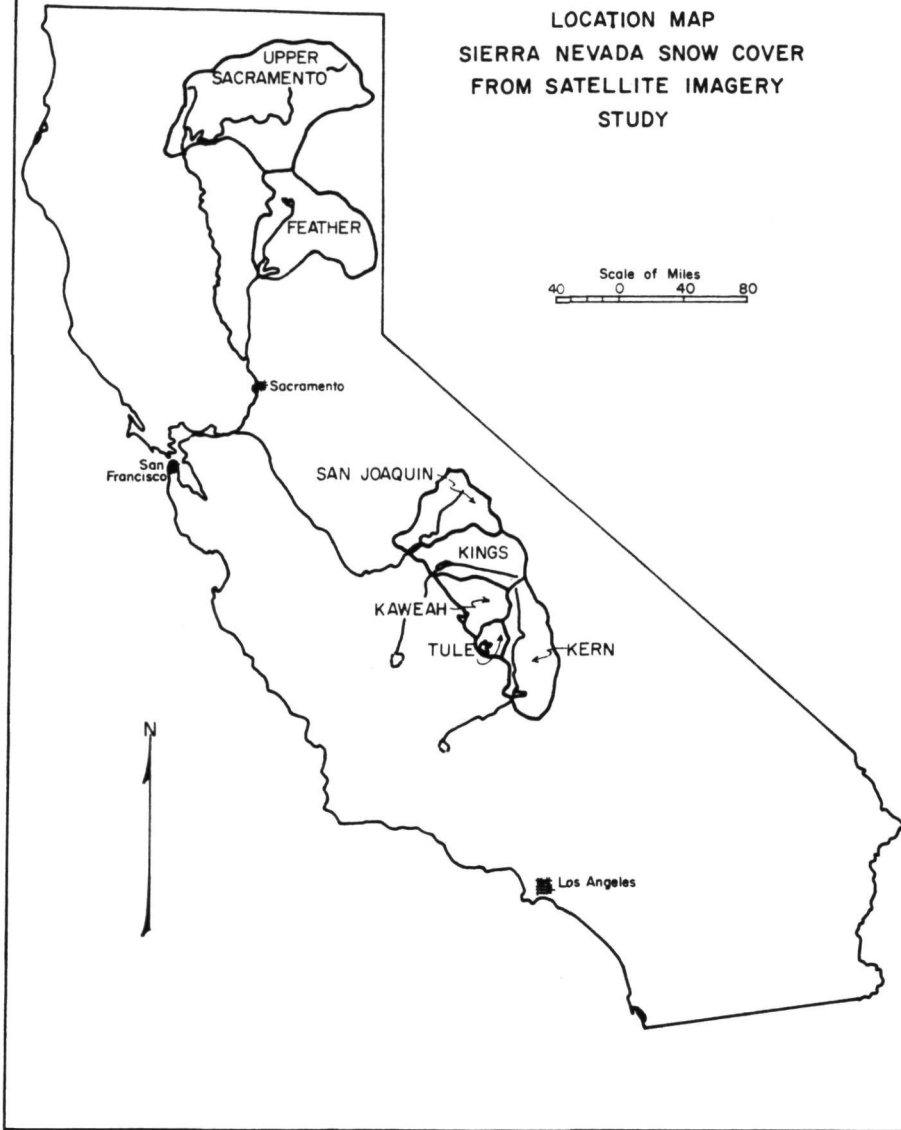
Techniques for reduction and interpretation of snow covered area from satellite imagery were reviewed (ref. "Handbook of Techniques for Satellite Snow Mapping", December 1974 by James C. Barnes and Clinton J. Bowley) and adapted to conditions found in the northern and southern project areas. Different techniques and the work of different technicians have been compared to investigate reproducibility of results. Most of the actual data reduction has been restricted to the 1:1 million LANDSAT imagery to develop the necessary technical skills required for interpretation of the lower resolution, smaller scale (1:3.5 million and 1:10 million) NOAA imagery. The more detailed LANDSAT imagery is available only on an 18 or nine-day cycle, while the lower resolution NOAA imagery is potentially available daily. It is hoped that the more detailed LANDSAT data may be used as a means of checking and calibrating the lower resolution NOAA data to permit more detailed investigation of change in snowpack area with time.

LANDSAT Imagery

LANDSAT imagery for 1972-73 and 1973-74 for 38 basins and sub-basins within and adjacent to the areas of investigation has been reduced to (a) maps of snow covered area, (b) area of snowcover in square miles, and (c) equivalent snow line elevation. LANDSAT images have been interpreted at the 1:1 million scale by direct overlay and, for investigation of reliability of results, they have also been interpreted at a scale of 1:500,000 using the Zoom Transfer Scope. Comparative results have not been examined at this time.

LOCATION MAP
SIERRA NEVADA SNOW COVER
FROM SATELLITE IMAGERY
STUDY

Scale of Miles
40 0 40 80



Estimates of snow covered area from a relatively large number of basins and sub-basins in each study area are being made simultaneously. In some cases, cloud cover, missing imagery, or other factors may contribute to loss of data from a specific basin or portion of the study area on any given day. Basins vary in size from 38 square miles to 6,400 square miles. The approach permits crosschecking between adjacent and nearby basins which will provide for a means of estimating snowcover conditions even when portions of a given project area may be obscured by clouds.

The following table summarizes LANDSAT imagery which has been reduced at this time.

Project Area	No. of Basins and Sub-Basins	No. of Days of Record Reduced
Northern	24	29
Southern	14	39

At the present time, it is impossible to reduce "current" data within a strictly operational time frame. LANDSAT imagery is being received about three weeks to a month after it is originally taken. Although it is recognized that the program is not intended to provide operational data at this time, it should be pointed out that satellite imagery should be received in Sacramento within three days of the satellite pass to be of optimum operational value in projecting melt rates and updating water supply forecasts. Time required for reduction and interpretation of satellite imagery, even utilizing the hand techniques currently employed, should not pose an operational problem in reducing data from the 20 major snowmelt watersheds in California.

NOAA Imagery

Additional work has been done in study of techniques for reducing the lower resolution NOAA imagery. Difficulty has been encountered in obtaining consistent results, a problem which was somewhat anticipated due to the small size of many sub-basins. Although snow lines are very apparent in certain exposed areas, particularly where great elevation changes exist, it is often difficult to interpret area of snowcover in heavy timber. Enhancement and enlargement techniques currently being investigated offer encouragement that the NOAA imagery may become more helpful.

WATER SUPPLY FORECASTING

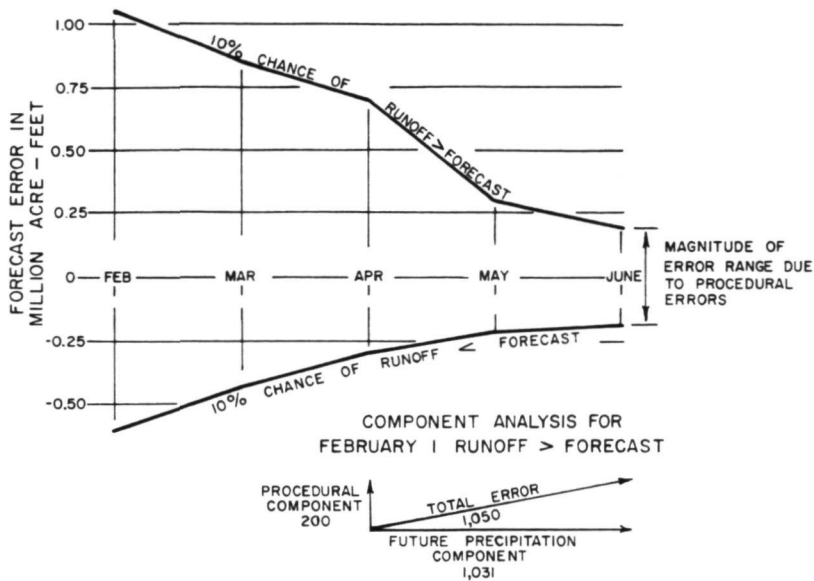
Water supply forecasts prepared by the California Cooperative Snow Surveys Program relate snowmelt season runoff to indexes of basin wetness and water stored as snowpack within the basin as reflected by measurements of precipitation, snowpack water content, and other hydrologic parameters. Since the days of Dr. Church, water supply forecasts have been based upon indexes of snow water volumes in basins. No operational water supply forecast has ever successfully attempted to measure the snow water volume. Thus errors (and consequently an opportunity for improvement) in water supply forecasts are related to indexing capability and not necessarily to accuracy of volumetric measurement. It is hoped that satellite imagery can provide supplemental data on snowcover which will result in improved indexing of the snowpack contribution to runoff.

Forecast Errors

Most April-July water supply forecasts procedures currently in use by DWR have been developed to the point that procedural error, or error in the snowpack-precipitation-runoff relationships, should give calculated April-July runoff values having standard errors smaller than 10 to 15 percent of observed runoff values. However, precipitation subsequent to the date of forecast is a major factor in forecast error. To illustrate the magnitude of this factor, April-July runoff forecast error funnel diagrams for the Feather River inflow to Lake Oroville and the San Joaquin River inflow to Millerton Lake (Friant) are presented on Plate 2. The June 1 error represents the basic forecast scheme error or that error which remains after all forecast parameters have been identified. The increases in error ranges that occur with earlier forecast dates are due only to uncertainty in future weather conditions.

To summarize the existing forecast error situation for each basin in the study area, the following tabulation of April 1 forecast and procedural error is presented.

FEATHER RIVER ABOVE LAKE OROVILLE
APRIL - JULY RUNOFF
80 % RANGE FORECAST
ERROR DIAGRAM



SAN JOAQUIN RIVER ABOVE MILLERTON LAKE
APRIL-JULY RUNOFF
80% RANGE FORECAST
ERROR DIAGRAM

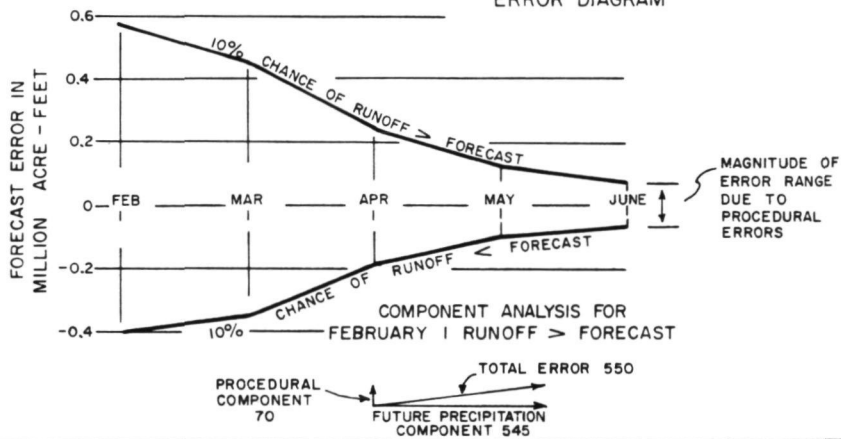


PLATE 2

80 Percent Error Range^{1/}
in Percent of Average
April-July Runoff
April Forecast
Forecast
Procedure

Forecast Point	Forecast	Forecast Procedure
Sacramento inflow to Shasta	56.4	24.8
Feather inflow to Oroville	53.7	20.4
San Joaquin inflow to Friant	31.9	12.0
Kings inflow to Pine Flat	34.4	12.0
Kaweah inflow to Terminus	33.2	15.5
Tule inflow to Success	42.4	34.0
Kern inflow to Isabella	52.5	28.6

^{1/} This range is the sum of positive and negative errors. For example, the April 1 San Joaquin 80 percent error range shown on Plate 2 is from -180,000 acre-feet to +240,000 acre-feet for a total error range of 430,000 acre-feet. $430,000 \text{ acre-feet} \div 1,193,000 \text{ acre-feet} = 31.9\%$. (1,193,000 acre-feet is the average April-July flow of the San Joaquin.)

The above tabulation indicates that the greatest forecast procedural or scheme error exists in the Sacramento, Feather, Tule and Kern forecasts. Thus, it is expected that these basins are the ones which could benefit most from incorporation of snow line location data into a forecast. Such a conclusion is logical because these basins are the ones which have the greatest variability in snow line location.

Operational Applications

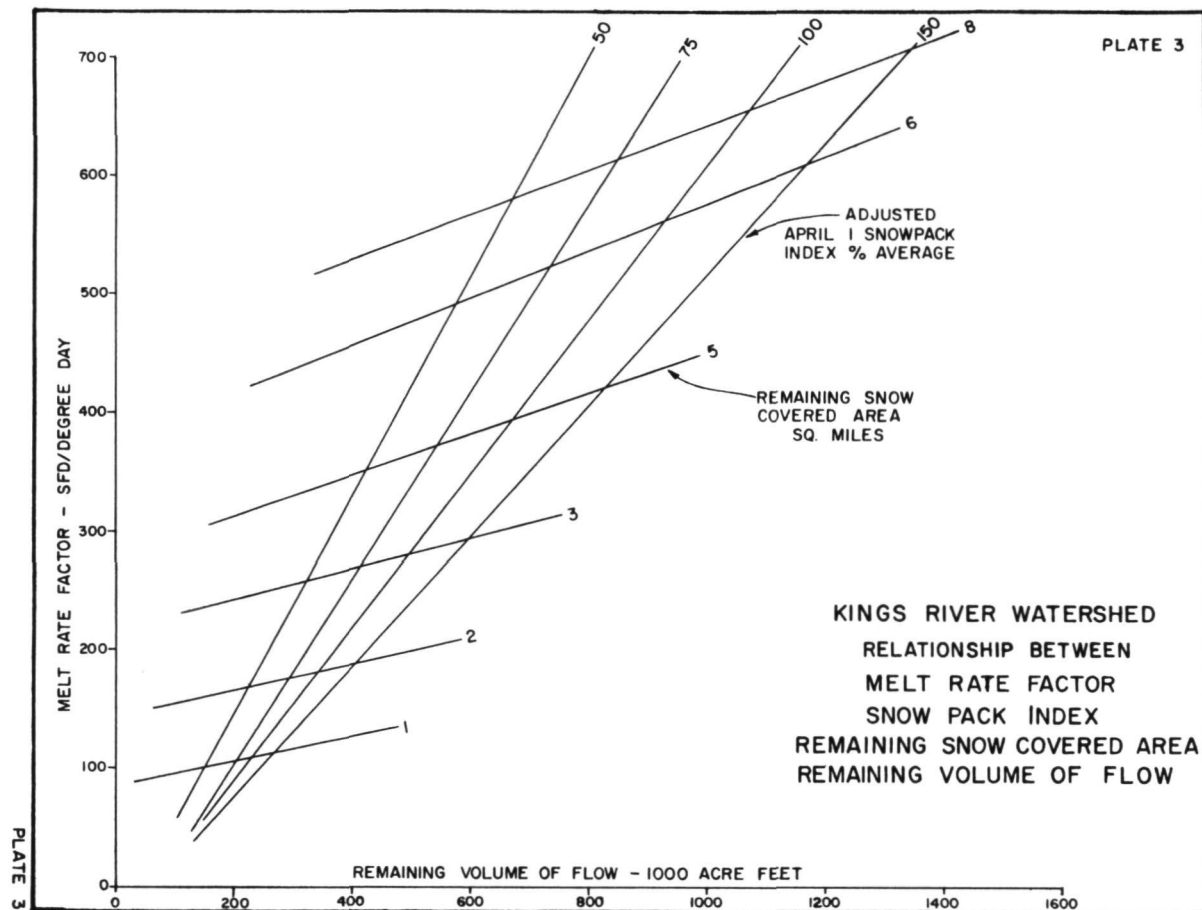
Preliminary work has been undertaken to investigate the potential benefits obtainable through observation of areal snowcover and hydrologic modeling as related to updating of late season runoff projections. The Corps of Engineers has obtained estimates of the extent of areal snowcover in the Kings River Basin by aircraft observation and mapping for over twenty years. Records consist of periodic observations and estimates of the area of snowpack cover during the period of spring snowmelt, generally from early May until the remaining area of snowcover becomes less than 100 square miles in this 1,500 square mile watershed. These observations of snowpack areal extent have been plotted against time to obtain a recession of the snow covered area on a year-by-year basis.

Preliminary analysis indicates that a correlation exists between observed melt rate, remaining area of snowcover, the April 1 measurement of snowpack water

content adjusted for subsequent precipitation, and the remaining volume of snowmelt runoff after the date of observation. The characteristics of this relationship are delineated in Plate 3. Even though techniques in current use appear quite effective in relating observed melt rate to remaining volume of runoff for southern Sierra watersheds, refinement of the technique through detailed daily or periodic observation of snow covered area could provide additional reliability and confidence.

Watersheds in the southern Sierra are characterized by a high correlation between snow line elevation and area of snowcover, at least through a major part of the snowmelt season. However, in the northern Sierra, topography and precipitation characteristics of the watersheds lead to a situation in which the area of snowcover may be more variable, both from season to season and from date to date within a given snowmelt season. Although no investigation has yet been made of relationships which may exist between melt rate, snowcover, and remaining runoff in northern Sierra basins, if such relationships can be established they would be effective tools in updating runoff projections as the snowmelt season progresses. Further investigation of the relationship between snow covered area and other factors, such as rate of change of water content at snow sensor sites, could provide effective parameters for updating water supply forecasts and estimating future runoff rates.

Updating Forecasts--The degree of forecast accuracy in many cases is not so critical early in the snowmelt season when precipitation after the date of forecast represents the major portion of forecast error and there is still ample time for adjustment of water management plans. However, as the snowmelt season progresses from mid-May through early July, procedural error remains the same in terms of acre-feet and the amount of water represented by this error may become critical in the operation of a water project. In the southern Sierra, the critical period is generally from mid-May through mid-June when snowmelt runoff rates are highest and reservoirs are nearing capacity. In the northern Sierra, these critical dates normally occur earlier in the snowmelt season. Procedures for updating forecasts as the snowmelt season progresses are of great value to water managers who must make important decisions regarding reservoir filling, reduction of spills, flood releases and the requirements of water users.



Hydrologic Models--The Department of Water Resources operates hydrologic models on the Kings and San Joaquin Rivers which simulate daily snowmelt runoff through evaluation of snowpack quantity, temperature, and other factors relating to runoff. An important feature of these models is that the quantity of runoff remaining as snowpack can be assessed and predictions of remaining flow revised as the snowmelt season progresses. Hydrologic modeling techniques permit updating forecasts of remaining flow with a much higher degree of accuracy than would be possible utilizing only conventional water supply forecasting techniques.

FUTURE PLANS

Work will continue on reduction of LANDSAT imagery to expand the file of historic data. Additional investigation and reduction of the lower resolution NOAA imagery will be pursued, with particular emphasis on the period of snowmelt (April through July). It is anticipated that sufficient data will soon be available to permit more detailed investigation of application of snow covered area to projections of water supply and melt rate.

The capability of reducing snowcover for satellite imagery is being developed now within the staff of the Snow Surveys Branch, which will establish the necessary skill at the operational level. The Department's water supply forecasters will become involved in testing the extent to which the addition of snowcover to the procedures improves the water supply forecast. They will be aided in this effort by assistance and advice from Sierra Hydrotech.

CONCLUSIONS

The following conclusions have been reached with regard to data reduction and interpretation, although they must be considered preliminary at this time due to the limited amount of work which has been accomplished.

1. When working with 1:1 million scale imagery a reasonably accurate snow line can be drawn for the southern Sierra Nevada basins by using a direct overlay.
2. The Sacramento and Feather basins have been more difficult to analyze using direct overlays because
 - imagery has given poorer coverage,
 - cloud cover is more frequent,

- vegetation hides more snow,
 - geologic conditions (lava flows) cause confusion in interpretation,
 - sun angle is lower,
 - topography is more erratic and does not provide an easily identified elevation change, and
 - the relationship between elevation and snowcover is less consistent than in the southern Sierra Nevada.
3. The promise of snow covered area definition providing improvement in water supply forecasts is greater for the Feather and Sacramento basins because the snowcover area differs greatly from year to year.
 4. Use of NOAA 1:10 million imagery has presented many problems, particularly in the northern Sierra. Image quality does not allow large magnification using a Zoom Transfer Scope and distortion is very bad.
 5. Use of NOAA 1:3.5 million imagery may be practical once more experience has been obtained.

OPERATIONAL APPLICATIONS OF SATELLITE SNOWCOVER
OBSERVATIONS IN RIO GRANDE DRAINAGE OF COLORADO

Jack N. Washicheck and Tony Mikesell, *USDA-Soil Conservation Service, Denver, Colorado*

ABSTRACT

It is hoped that snowcover as determined from satellite pictures can be used in streamflow forecasting. An improvement in forecasting is an improvement in management.

Various mapping techniques were tried and evaluated. There were many problems encountered such as distinguishing clouds from snow and snow under trees.

A partial solution to some of the problems involves ground reconnaissance and low air flights. Some problems go unanswered.

Snow areas, cloud cover and total areas were planimetered after transferring imagery by use of zoom transfer scope. These determinations were then compared to areas determined by use of a density slicer. Considerable adjustment is required for these two values to compare.

NOAA pictures were also utilized in the evaluation.

Forest cover is one of the parameters used in the modeling process. The determination of this percentage is being explored.

Introduction

In the past 5 years, the Western States in general and Colorado in particular have experienced phenomenal growth. There have been unprecedented demands and competition for the limited water resources available in this arid region. The demands come not only from within the state of Colorado but also from other states that want more and more of the waters of the interstate streams. Since the waters of these streams are apportioned among the states, it becomes imperative that accurate forecast models be developed. This would allow the maximum delivery of water to Colorado users and still permit the delivery of water to satisfy out-of-state obligations. The problem is nowhere more apparent than in the Rio Grande Basin where predictions of total annual and seasonal runoff must be made as early as March 1. Many other water users such as municipalities, power companies, ranchers, and farmers also need the information as soon as possible. These

people use the first available forecasts in their planning and then use future forecasts to update plans. This use terminates for the farmer when his crops are planted but continues for others until end of snowmelt. About 80 percent of the water supplies of the West come from melting snow so accurate forecasts are extremely important. Total snow cover may prove to be a vital parameter in the forecasting model.

Objectives

The project discussed in this paper was undertaken to determine if satellite imagery could be used to improve forecasts and, hence, to improve management.

Secondary aspects of the project include applying LANDSAT imagery to associated land use problems that bear on runoff yield and water demand and monitoring various aspects of land use.

Procedure

It was decided to use two different investigating teams and to divide areas of responsibility.

First team, consisting of the Soil Conservation Service and the U.S. Bureau of Reclamation, would be responsible for the overall program and for obtaining imagery, ascertaining what data to collect, and determining the best methods to acquire the data.

Second team, under leadership of the Colorado Division of Water Resources, would provide the technical staff needed to develop the predictive models for runoff forecasting.

Mr. Charles Leaf of M.W. Bittinger and Associates, Inc., a water and land resources consultant firm, would assist this team.

It was decided to use three large basins in Colorado in the analysis (Map #1): Rio Grande, Arkansas, and San Juan Basins.

Rio Grande Basin

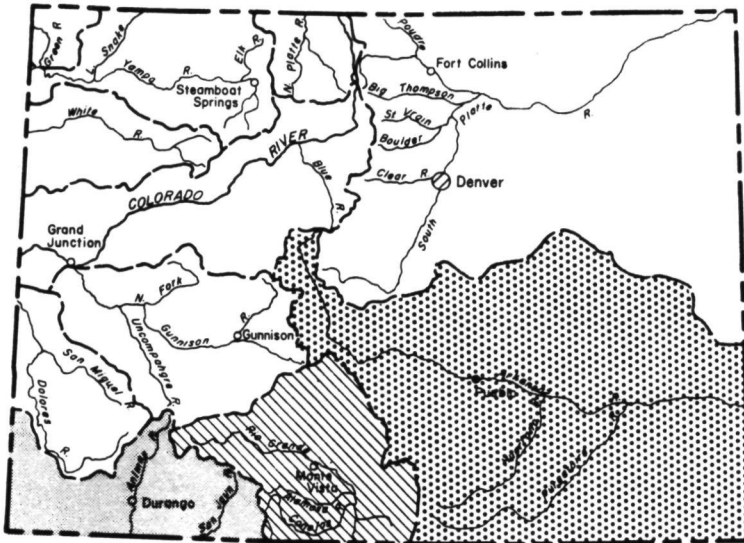
The primary target is the Rio Grande Basin (Map #2). The entire basin is being studied with the improvement of forecast accuracy as the prime objective. This area provides irrigation water to Colorado's San Luis Valley as well as to the area along the river throughout its course in New Mexico, Texas, and Mexico. The river is administered under the Rio Grande Compact between the three states as well as by an international agreement between the United States and Mexico. Extreme accuracy in estimating runoff is required to satisfy these objectives.

The Rio Grande Basin is being studied by using three sub-basins (Map #3): the mainstem of the Rio Grande above Del Norte, the Conejos River above Mogote, and the Culebra River above San Luis. These basins are being studied to determine if forecasts can be improved on smaller basins: Conejos, 730 square kilometers (282 square miles), and Culebra, 570 square kilometers




MAJOR BASINS BEING ANALYZED IN

COLORADO

20 0 20 40 60
SCALE IN MILES



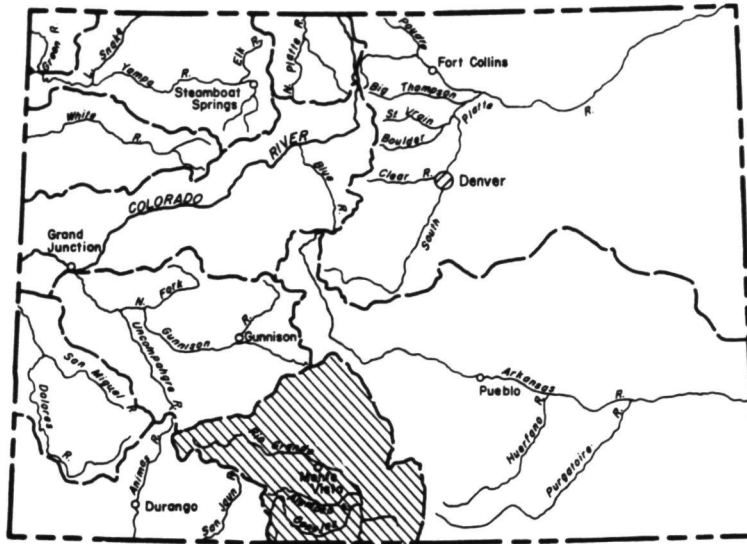
MAP #1

-  SAN JUAN DRAINAGE
-  RIO GRANDE DRAINAGE
-  ARKANSAS DRAINAGE

REPRODUCIBILITY OF THE
ORIGINAL PAGE IS POOR

COLORADO

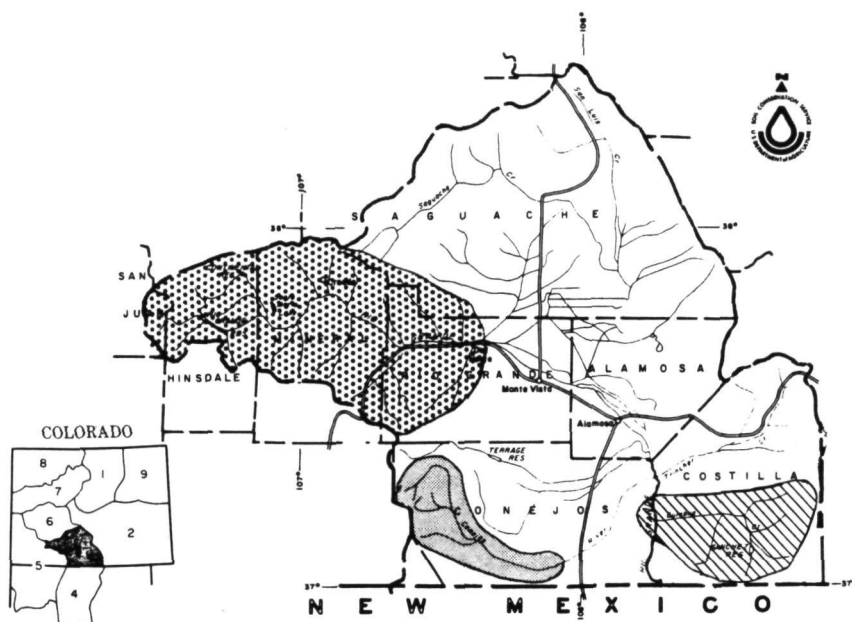
20 0 20 40 60
SCALE IN MILES






MAP #2

 PRIMARY AREA BEING ANALYZED

THREE SUB-BASINS IN RIO GRANDE ARE BEING STUDIED



MAP #3

-  RIO GRANDE ABOVE DEL NORTE
-  CONEJOS ABOVE MOGOTE
-  CULEBRA ABOVE SAN LUIS

(220 square miles); as well as larger basins: Rio Grande, 3,419 square kilometers (1,320 square miles).

Conejos River Drainage

It was decided to concentrate the first efforts on the Conejos River Drainage (Figure 1). This is a small drainage of fairly high elevation (Figure 2), with an average of 1.5 meters (5 feet) of snow at medium elevations. This 730-square-kilometer (282-square-mile) area produces an average 246.6 hectometers³ (200,000 acre-feet) of water annually.

The Conejos Basin contains mostly uplands with the river splitting the basin. Much of the drainage is 3,048 meters (10,000 feet) or more above sea level. There is very little irrigation and no diversions above the gaging station at Mogote. Platoro Reservoir is near the headwaters and is used to regulate flows.

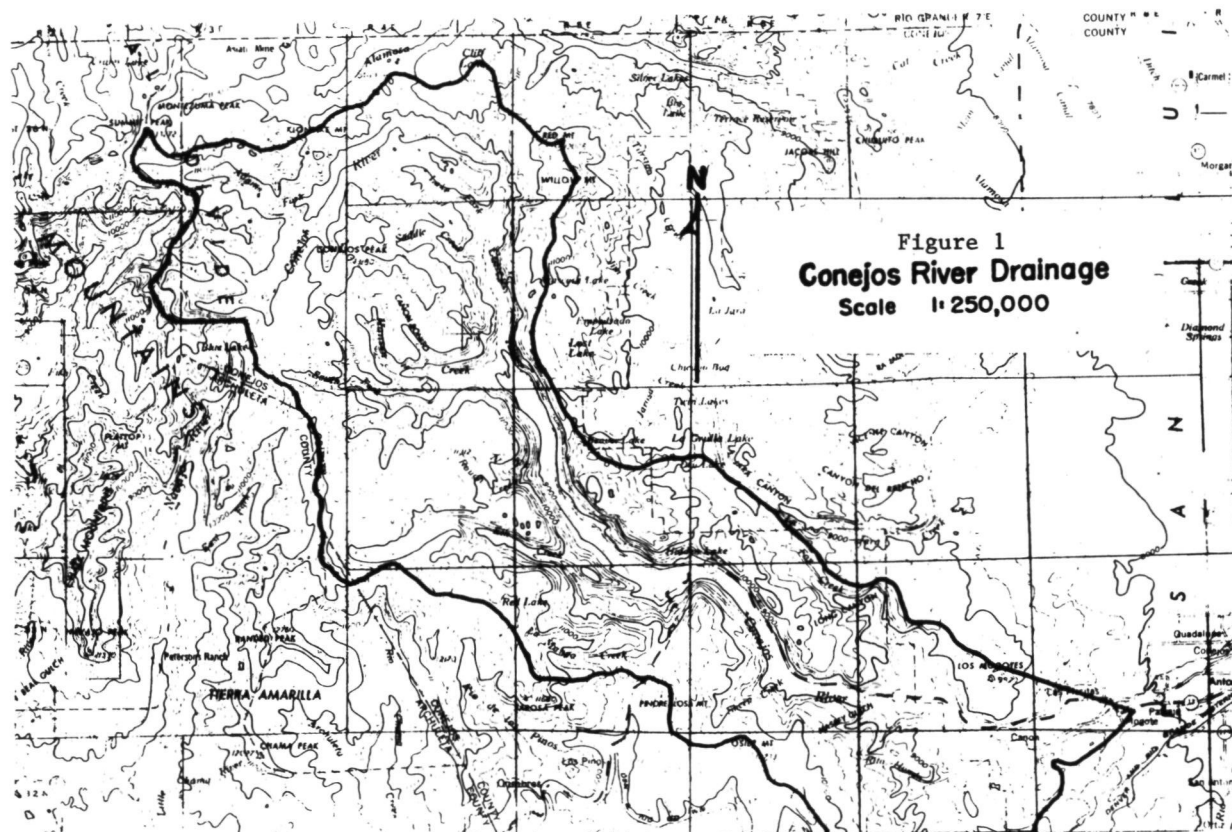
Waters from the river provide irrigation for acreage in the San Luis Valley in Colorado and areas along its course in New Mexico. Without irrigation water, the valley is of little commercial value. It is covered by low sage and rabbitbrush. Several subdevelopments have sprung up in the valley. Where water is available, high-value truck crops such as lettuce, onions, and potatoes are grown.

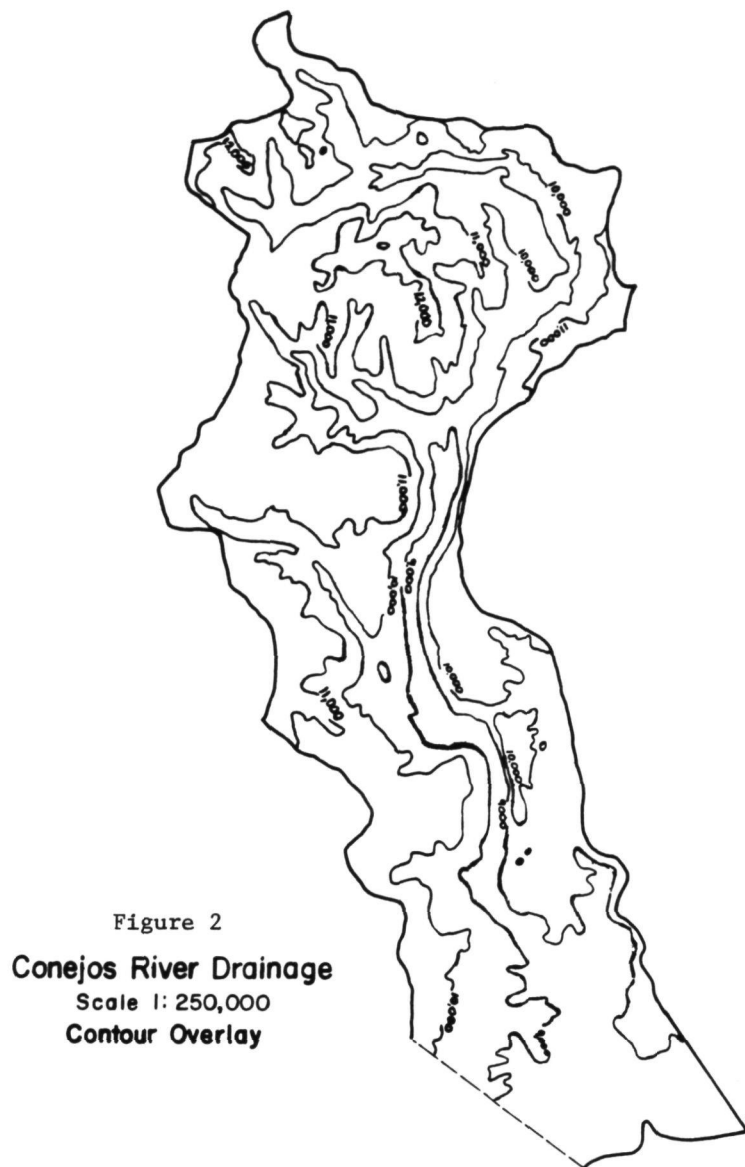
This paper deals primarily with snow mapping in this drainage and covers our progress to date.

LANDSAT Images

LANDSAT 1 and 2 satellite images provide the bulk of information in our snow mapping operation. These 1:1,000,000 scale images have sufficient detail to allow an overlay to be made in a 1:250,000 scale which is our standard reference size. The finished 1:250,000 scale overlay is large enough to identify the snow area and small enough to be useful with the necessary optical equipment. The enlargements from the satellite images are made as overlays. All overlays are prepared using the Bausch and Lomb* zoom transfer scope. This instrument allows one to view simultaneously the satellite image and a drawing surface. Consistent orientation of the drainage boundaries is accomplished by aligning stream courses with a boundary overlay showing streams. This enables us to compare them with each other and with the U.S. Geological Survey (USGS) map at a scale of 1,250,000.

*Trade names are used solely to provide specific information. Mention of a trade name does not constitute a guarantee of the product by the U.S. Department of Agriculture nor does it imply an endorsement by the Department over comparable products that are not named.





In addition to overlays, a data color system is used to evaluate images. This instrument measures the amount of light transmitted through black-and-white satellite image transparency. The light intensity is broken into 12 discrete levels and displayed in 12 colors on a color monitor. Any color or combination of colors can be measured as a percentage of the area viewed. To make this area measurement meaningful, the areas outside the Conejos Drainage are masked. To accomplish this masking, an overlay is made by optically reducing the boundary of the Conejos with the zoom transfer scope. Great care must be taken in making the overlay because the pen width used in drawing is several hundredths of an inch thick and on the image one hundredth of an inch is approximately a tenth of a mile. Caution is required in orienting the overlay too, because the same errors are generated here.

In 1973, 33 satellite images were made available to us. Of these, 6 were of the Conejos Drainage and of the 6, 2 were usable for mapping. This figure reflects the normally heavy cloud cover in the San Juan Mountains. When snow covers the entire area no usable data is provided for our modeling and forecast procedures, so these passes are of little value.

In 1974, 22 images were received. Figure 3 indicates images received. Six of the images covered the Conejos and, again, only 2 were usable. This situation seems to have greatly improved with the addition of LANDSAT-2. With double the number of images available, more complete data in 1975 seems a certainty.

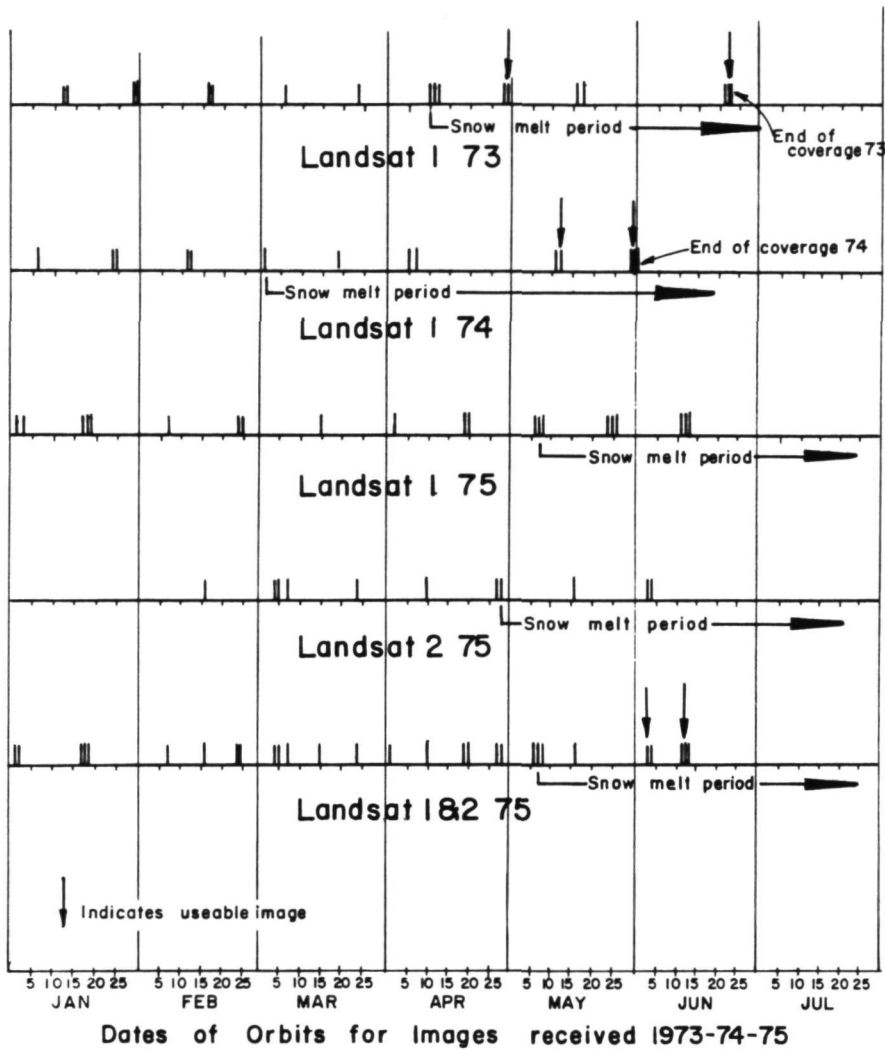
Figure 4 indicates the elapsed time during 1975 from the date each LANDSAT picture was taken until we received the imagery. The maximum time required was 53 days; and minimum, 14. Average period was 29 days. We do not know if any special rush period was tried or if this was routine. When and if the data is to be used operationally, a much shorter transmission period would be desirable.

Problems of Snow Mapping

Problems arise in differentiating snow from various rock and ground areas. Other problems occur if forest cover pattern is very complex. Many of these problems have been relieved by using medium-altitude aerial photography and low-level oblique aerial photos. The medium-altitude photos were obtained through the Colorado State Planning Office. The state has a number of medium-elevation photos made by the Hurd Company to aid in land use planning, and these were made available to us. The low-level oblique photos were shot by Robert Hansen, Head, Remote Sensing and Engineering Physics Section of the U.S. Bureau of Reclamation, on a flight in a U.S.B.R. plane. The flight was made to coincide with the June 3 satellite pass. The flights were close enough in time to allow us to gain more information as to the snow cover under trees. This flight was made by several members of the

Figure 3

USEABLE IMAGERY BY YEARS



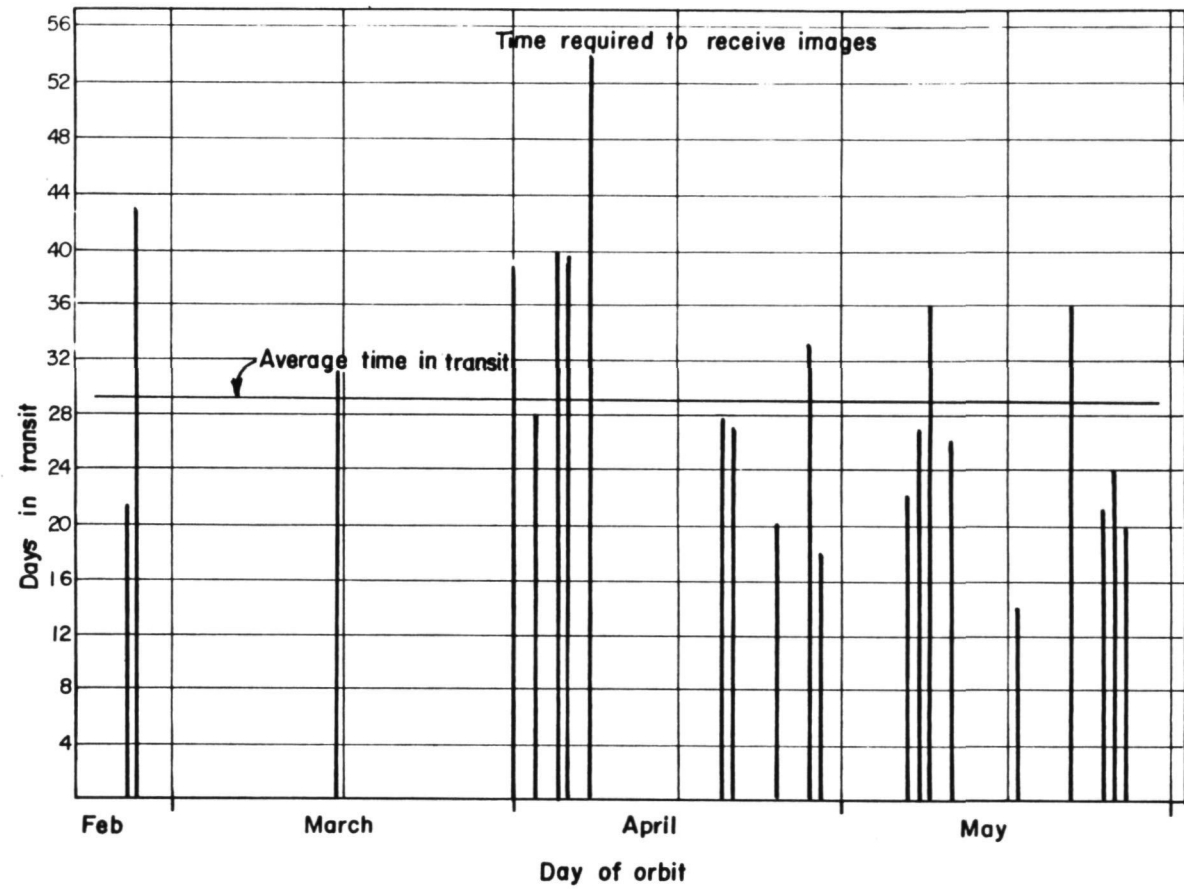


Figure 4

investigating team. This provides not only pictures to be used in later analysis, but gives one a feel for the area one cannot achieve in the office.

In the Platoro Reservoir area in the northern Conejos Drainage are several large areas of bare rock and soil. Also, some areas have extremely intricate snow patterns making differentiation between tree cover and melt patterns difficult. These areas are easily confused with snow, but by using the oblique photos these areas are quickly identified and disregarded in future snow mapping. Once identified these areas present no problems. This type of familiarity seems to provide very necessary information. Figure 5 shows the June 3 satellite imagery. This imagery is almost cloud-free so that the corresponding medium-elevation plane flight coincides extremely well.

The area near Cumbres Pass is one of our problem areas with heavy patterning. By using the Hurd aerial photos to determine tree cover and by using our small plane photos to determine snow patterns and amount of snow under trees, we can more accurately map snow cover from past and future images.

Comparison of Results

A difference in results is obtained between the visual overlays and the data color measurements. In two comparisons definite snow cover was 140 square kilometers (40.2 square miles) on the visual overlay and 137 square kilometers (53 square miles) on the data color image on the first set. On the second, the images indicated 159 square kilometers (61.4 square miles) on the overlay and 184 square kilometers (71 square miles) on the data color. These relations are 75 and 86 percent respectively.

When investigating probable or debatable snow areas we find a consistently greater area in the data color measurement than visual planimetering. This is to be expected as the density slicer uses all areas while with some experience, manual planimetering can eliminate some areas.

Future comparisons will be made to determine if these percentages will remain. If so, the density slicer could be used and an index established for use in our modeling procedures.

Forest Cover Evaluation

One of the parameters in the modeling program is the percentage of forest cover. Mr. Leaf, our modeler, divided the Conejos River Basin into ten watershed sub-units (Figure 6). These units are homogeneous in respect to slope, elevation, and aspect. Leaf will cover the modeling program more thoroughly in a later paper.

Mapping of tree cover was tried in two ways. In one method the tree cover outlines were traced from Hurd aerial photos. These tracings were photographically reduced to the 1:250,000

Figure 5
June 3 Satellite Imagery



REPRODUCIBILITY OF THE
ORIGINAL PAGE IS POOR

scale. The transparent reductions were assembled into a mosaic of the drainage. The forest areas were then planimetered and percentage of cover computed.

The other method was a mapping procedure using the zoom transfer scope and some summer images. This method was very similar to snow mapping. Using the zoom transfer scope, the intense lighting necessary for mapping washed out most detail from the low-contrast summer image. To correct this problem, photographs of the image were taken using a view camera and polaroid technical film. Great care was taken to ensure that the scale of the photo was exactly the same as the satellite image. By varying the length of exposure and time of development, a higher contrast and higher density photo was obtained. Forest cover was traced as in snow mapping and again planimetered. Percentage of forest cover was computed for each watershed sub-unit (Figure 7).

Both methods were evaluated. The overlays indicated a great deal of distortion was present in the edges of the Hurd photos. Although forested patches are easily identified and plotted, the distortion of the sides cannot be corrected.

We feel that the satellite images provide the best data; however, the Hurd photos provide good spot checks.

NOAA Images

In addition to LANDSAT images, NOAA weather satellite images have been used in various areas as supplemental data. Unfortunately, two problems have stopped us from using NOAA images more extensively. First there is a lack of land features in our area that are definite enough to allow us to orientate the drainage areas in the 1:5,000,000 NOAA scale. The other problem is severe distortion of the drainages as shown on the photographs. The areas in which we have the most interest appear very near the edge of the image.

Future Plans

Our plans are to continue our mapping on the other drainage areas in the basin. At this time it would seem that mapping of the snow cover can be accomplished. We are now trying to find the most simple and expeditious method of obtaining this data.

Conclusion

There is no substitute for experience. By looking at the satellite imagery, crossing the area by foot or car, personally observing from a plane, and viewing medium-elevation photos, one gains a knowledge of the area that is invaluable. Whether this can be accomplished in all areas of interest is debatable. Possibly new ideas to accomplish the mapping mission will be forthcoming from these experiences.

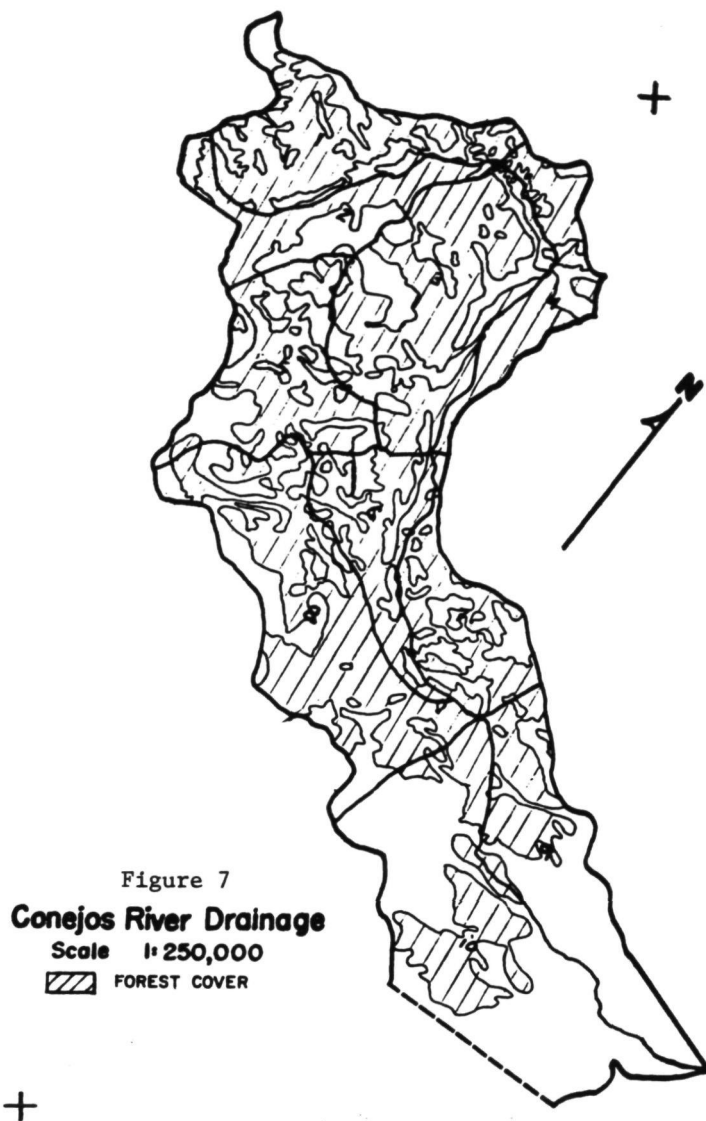


Figure 7
Conejos River Drainage
Scale 1:250,000
[Hatched Box] FOREST COVER

We are sure that total snow cover can be used as a variable in the forecast formula. How much it will improve forecasts is still unknown due to limited data. Whether the data will be available when needed is also a problem. With the addition of LANDSAT-2, our chances for cloud-free pictures are doubled, so we have high hopes.

Only time, experience, and education will tell.

OPERATIONAL APPLICATION OF SATELLITE SNOWCOVER
OBSERVATIONS - NORTHWEST UNITED STATES

Fred A. Limpert, *Bonneville Power Administration, Head, Hydrology Section*

ABSTRACT

A demonstration project has been undertaken in the Pacific Northwest to determine the applicability of satellite snowcover observations for operational use in three test areas of the Columbia River Basin.

INTRODUCTION

Operational application of satellite snowcover observations in the Northwestern United States is one of several demonstration projects sponsored by the National Aeronautics and Space Administration's Goddard Space Flight Center. A contract was entered into between NASA and the Bonneville Power Administration and the North Pacific Division, Corps of Engineers. BPA is the primary contracting agency with Dr. Mark Meier of the Geological Survey acting as the technical field advisor. This contract implements a study using satellite data for determining snowcover area which is a prime factor in forecasting runoff for flood control and power operation.

APPLICATION

More than 80 percent of the electric energy produced in the Pacific Northwest comes from hydroelectric power generation. As of December 31, 1974, there are 159 hydroelectric plants which generate over 21 million kilowatts and 39 thermal plants which generate 3.6 million kilowatts. An additional 8.6 million kilowatts of hydro is under construction with another 5.0 million authorized or licensed. There are 2.4 million kilowatts of thermal under construction and 8.6 million kilowatts licensed. Existing, under construction, and authorized or licensed hydro plants total 34.6 million kilowatts and thermal plants 14.6 million kilowatts.

The hydro-based system in the Pacific Northwest makes this area second to none as a producer of hydroelectric power. The hydroelectric projects of the region have been undertaken by private utilities, public agencies, municipalities, and the United States Federal Government. These developments take into consideration all of the multipurpose uses such as power, flood control, irrigation, recreation, pollution control, and navigation.

Although considerable development has been undertaken by all participating agencies, the larger multipurpose developments have been constructed by the Corps of Engineers and the Bureau of Reclamation. Nearly all of the economically feasible hydro sites have been developed and thermal power plants will be needed more and more to meet the ever growing power load of the area. Eventually thermal will carry the base load with hydro providing the peak power requirements. There are still some feasible flood control sites in the area. Under all of these conditions, an accurate forecast of volume runoff for proper scheduling of the river operation to meet all of the multipurpose project uses is of paramount importance, Figure 1.

The Columbia River Basin contains more than 668,200 km² (258,000 mi²), almost twice the size of California. The Basin contains most of Washington, Oregon, and Idaho; that part of Montana west of the Rocky Mountains; small areas of Wyoming, Utah, and Nevada; and the southeastern part of British Columbia.

The Columbia River is second only to the Mississippi in average runoff for rivers in the United States. The average annual precipitation over the Basin is about 71 cm (28 in). Of this amount, 30.5 cm (12 in) is returned to the atmosphere by evapotranspiration and 2.54 cm (1 in) of the amount withdrawn for beneficial use is consumed leaving 38 cm (15 in) for runoff. This amount is equivalent to 228 billion m³ (185 million acre-feet) of water annually or a flow of 7220 m³ per second (255,000 cubic feet per second). Average flows for key power points in the Basin are shown in Table 1.

Flow records of the Columbia River at The Dalles, Oregon, cover a period of over 96 years. During this time, the flows have ranged from a low of 991.1 m³/s (35,000 ft³/s) on January 12, 1937, to a high of 35,112.9 m³/s (1,240,000 ft³/s) on June 6, 1894. The high flow is about six times the long-term average of 5493.5 m³/s (194,000 ft³/s) at The Dalles and the low flow is about one-sixth the average.

Storage projects in the Basin are used to regulate the streamflow runoff. There are 25.5 billion m³ (20.7 million acre-feet) of storage in Federal reservoirs, 5.8 billion m³ (4.7 million acre-feet) in non-Federal reservoirs, and 19.1 billion m³ (15.5 million acre-feet) in the reservoirs in the Canadian portion of the Basin. Thus, usable storage capacity for power projects existing, under construction, and authorized or licensed totals about 50.4 billion m³ (41 million acre-feet). Optimal storage in the Basin is estimated to be somewhat in excess of 61.7 billion m³ (50 million acre-feet). The ratio of runoff to storage available provides a measure of the usability of the water available. A comparison of the Columbia, the Colorado, and the Missouri project storage capacities is shown in Table 2. From these figures it can be seen that the capacity of the Colorado and Missouri projects are several times the average annual runoff. Conversely, the reservoir storage capacity in the Columbia River system is about one-quarter the average runoff. The low ratio of reservoir capacity to average runoff in the Columbia system can produce large amounts

MAJOR POWER PROJECTS OF THE PACIFIC NORTHWEST

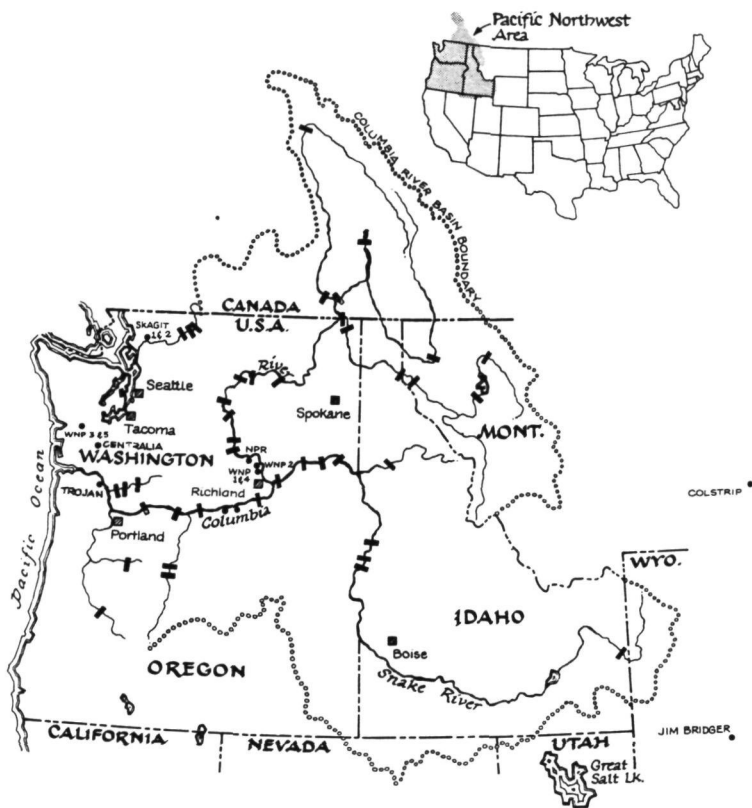


Figure 1

TABLE 1 Average Flow for Period July 1928, Through June 1968,
Adjusted to 1970 Level of Development

Project	Annual Runoff Million Acre-Feet	kcfs	Project	Annual Runoff Million Acre-Feet	kcfs
<u>MOUTH OF COLUMBIA RIVER</u>	185.0	255.0	<u>N. F. CLEARWATER RIVER</u>		
Bonneville	132.8	183.3	Dworshak	4.1	5.6
The Dalles	128.9	177.9	<u>M. F. CLEARWATER RIVER</u>		
John Day	124.9	172.4	Penny Cliffs	4.9	6.7
McNary	123.0	169.8	<u>GRAND RONDE RIVER</u>		
Ben Franklin	85.9	118.5	Wenaha	2.1	2.9
Priest Rapids	85.8	118.4	<u>SALMON RIVER</u>		
Wanapum	85.7	118.3	Lower Canyon	7.8	10.8
Rock Island	85.6	118.2	Freedom	7.7	10.6
Rocky Reach	83.1	114.7	Crevice	7.0	9.7
Wells	81.5	112.5	<u>CHELAN RIVER</u>		
Chief Joseph	78.2	108.0	Chelan	1.4	2.0
Grand Coulee	78.0	107.7	<u>SPOKANE RIVER</u>		
Murphy Creek	51.4	70.9	Long Lake	5.7	7.8
Hugh Keenleyside	29.0	40.2	Nine Mile	5.2	7.2
Revelstoke Canyon	20.9	28.8	Monroe Street	4.9	6.7
Downie Creek	18.7	25.8	Post Falls	4.5	6.2
Mica	14.9	20.5	<u>PEND OREILLE RIVER</u>		
Calamity Curve	4.7	6.5	Waneta	20.1	27.8
Luxor	1.4	1.9	Boundary	19.4	26.8
<u>DESCHUTES RIVER</u>			Box Canyon	18.8	26.0
Pelton	3.1	4.3	Albani Falls	18.3	25.3
<u>SNAKE RIVER</u>			Cabinet Gorge	15.8	21.8
Ice Harbor	34.6	47.7	Noxon Rapids	14.1	19.4
Lower Monumental	34.6	47.7	Thompson Falls	14.3	19.8
Little Goose	34.2	47.2	<u>FLATHEAD RIVER</u>		
Lower Granite	34.1	47.1	Buffalo Rapids No. 4	8.5	11.8
Asotin	23.1	31.9	Kerr	8.0	11.5
China Gardens	20.6	28.5			
Appaloosa	12.4	17.1			
Oxbow	12.0	16.5			
<u>SNAKE RIVER TRIBUTARIES</u>					
<u>CLEARWATER RIVER</u>					
Lenore	10.2	14.1			

REPRODUCIBILITY OF THE
ORIGINAL PAGE IS POOR

TABLE 1 Average Flow for Period July 1928, Through June 1968,
Adjusted to 1970 Level of Development
(continued)

Project	Annual Runoff		Project	Annual Runoff	
	Million Acre-Feet	kcfs		Million Acre-Feet	kcfs
<u>S. F. FLATHEAD RIVER</u>			<u>MCKENZIE RIVER</u>		
Hungry Horse	2.5	3.5	Walterville	3.3	4.5
<u>KOOTENAI RIVER</u>			Leaburg	3.1	4.3
Brilliant	22.2	30.6	<u>S. F. MCKENZIE RIVER</u>		
Corra Linn	20.0	27.6	Cougar	0.6	0.8
Katka	10.2	14.1	<u>M. F. WILLAMETTE RIVER</u>		
Kootenai Falls	9.0	12.4	Lookout Point	2.1	2.9
Libby	8.2	11.3	Hills Creek	0.8	1.1
Bull River	4.4	6.1	<u>COWLITZ RIVER</u>		
<u>DUNCAN RIVER</u>			Mayfield	4.4	6.1
Duncan Reservoir	2.5	3.5	Mossyrock	3.7	5.1
<u>WILLAMETTE RIVER</u>			<u>LEWIS RIVER</u>		
Sullivan	22.2	30.6	Ariel	3.5	4.8
<u>CLACKAMAS RIVER</u>			Yale	2.8	3.9
North Fork	2.0	2.7	Swift No. 2	2.1	2.9
<u>OAK GROVE FORK</u>			<u>BAKER RIVER</u>		
Oak Grove	0.4	0.5	Lower Baker	1.9	2.6
Timothy Meadows	0.7	0.1	Upper Baker	1.4	2.0
<u>NORTH SANTIAM RIVER</u>			<u>SKAGIT RIVER</u>		
Detroit	1.5	2.1	Gorge	3.3	4.5
<u>SOUTH SANTIAM RIVER</u>			Diablo	3.0	4.1
Foster	1.8	2.5	Ross	2.5	3.4
<u>MIDDLE SANTIAM RIVER</u>			<u>NISQUALLY RIVER</u>		
Green Peter	1.2	1.6	La Grande	1.0	1.4
			<u>SKOKOMISH RIVER</u>		
			Cushman Nol 2	0.6	0.8

BPA - Branch of Power Resources
April 22, 1975

REPRODUCIBILITY OF THE
ORIGINAL PAGE IS POOR

TABLE 2 Flow and Storage - Columbia, Colorado and Missouri Rivers

	Storage Capacity Billion m ³ <u>1/</u>	Annual Runoff Billion m ³ <u>1/</u>			Headwater Elevation meters <u>2/</u>	Drainage Area Billion m ² <u>3/</u>
		<u>Average</u>	<u>Maximum</u>	<u>Minimum</u>		
Columbia	50.6 (41)	228.2 (185)	315.8 (256)	149.3 (121)	807.7 (2.65)	668.2 (258)
Colorado	66.6 (54)	17.3 (14)	27.1 (22)	4.9 (4)	2652.0 (8.70)	626.8 (242)
Missouri	92.5 (75)	29.6 (24)	45.6 (37)	13.6 (11)	2134.0 (7.00)	1364.9 (527)

1/ Figures in () are x 10⁶ acre-feet.

2/ Figures in () are mean sea level in feet x 10³.

3/ Figures in () are miles² x 10³.

of secondary energy. This low storage to runoff ratio and the large difference in average and maximum streamflow at The Dalles, Oregon, shows the need for accurate volume runoff forecasting and optimum use of storage for flood regulation.

The National Weather Service (NWS), the Corps of Engineers, North Pacific Division (USCE, NPD), and the Bonneville Power Administration (BPA) are cooperatives in the Columbia River Forecasting Service (CRFS). The overall goal of the CRFS is to pool certain resources of the agencies in the interest of improving streamflow forecasting methods, to provide uniform forecasts, and to increase the efficiency of operation.

Daily operational runoff forecasts for streams in the Pacific Northwest are made using the Streamflow Synthesis and Reservoir Regulation (SSARR) computer model. The program description and user manual along with associated publications referenced in the manual provide detailed background on the development of the model and how it is used for operational river forecasting and river management activities (1).

One of the major factors in runoff in the Columbia River Basin is snowmelt. Snowmelt calculation with the SSARR model is made by the temperature index method or by the use of the generalized snowmelt equation for a partly forested area. At the present time we are using the temperature index method for day-to-day forecasts. In general, the snowmelt equation is not used for daily operational forecasts because of the lack of real time energy budget data.

Snowmelt runoff in inches is determined for the snow area using the temperature index method:

$$m = (T_A - T_b) R \left[\frac{PH}{24} \right]$$

where

m = Snowmelt runoff in inches of water over the snowcover area.

T_A = Period temperature at the median elevation of the melting snowpack.

T_b = Base temperature ($^{\circ}F$), specified as a constant for a watershed.

R = Melt rate, specified to the computer, or given as a function of accumulated runoff, in inches of water per degree day.

PH = Period length in hours.

Values used for the base temperature and the melt rates can be adjusted to either minimum, mean, or maximum daily temperature daily temperature data. Melt rates can be specified for each day of the run to conform to the natural variability encountered during the melt season.

Two methods are available to evaluate snowmelt from a watershed. The basin method evaluates the snow-covered area runoff relationships using a snowcover depletion function. The other method divides the watershed into elevation bands with each band

being examined separately with respect to snow accumulation and melt. Studies are now underway to evaluate this second method for some of the sub-basins in the region.

Snowcover observations in the United States portion of the Basin are made by the Corps of Engineers personnel in small aircraft flying at a low altitude. Similar flights are made in the Canadian portion of the Basin by the British Columbia Hydro and Power Authority. Observations of this type are made by experienced personnel and must, of necessity, be subjective. Two to four flights are generally made each season for each area depending upon the type of season and flying conditions. In the United States portion of the Basin, flights generally occur in April, May, and June and in the Canadian portion in May and June. Though quite effective, these flights may present a safety problem and are relatively expensive.

The satellite data collection program provided an excellent opportunity for testing aerial snowcover observations as an alternate to such determination by small aircraft. BPA and the Corps of Engineers formulated a proposal to the National Aeronautics and Space Administration/Goddard Space Flight Center (NASA/GSFC) to study snowcover observations which would hopefully improve forecasting procedures.

The primary contracting agency was BPA. A Memorandum of Understanding was signed to cover contractual work for one year by BPA and the Corps of Engineers for NASA/GSFC. Work included: (1) the mapping of snowcover in three candidate areas for the 1973 and 1974 spring melt seasons, (2) input of snowcover information in the SSARR model for reconstitution of the temporal distribution of the spring melt runoff, and (3) compare results with reconstitutions made with the conventional data for the past two seasons.

The basins studied are: the Boise River above Lucky Peak Dam, drainage area 7254 km² (2800 mi²); North Santiam River above Detroit Dam, drainage area 1132 km² (437 mi²); and the upper Snake River above Palisades Dam, drainage area 13,489 km² (5208 mi²). These three basins were chosen initially because of some associated work being done by Dr. Mark Meier of the Geological Survey on the Santiam Basin, reconstitution work already done by the Corps of Engineers and the National Weather Service on the Boise and Snake River Basins, and because it was expected that adequate satellite imagery would be available. Satellite data for 1975 is being examined now to determine adequate cloud-free coverage over the Flathead River above Hungry Horse Dam, the Kootenai River above Libby Dam, and the North Fork of the Clearwater River above Dworshak Dam, Figure 2.

Imagery from the Earth Resources Satellite, LANDSAT-1, was assembled for the 1972-73 and 1973-74 snowmelt season. This imagery was processed under a subcontract with Stanford Research Institute (SRI) utilizing its Electronic Image Analysis Console (ESIAC) to determine the percentage of snowcover area (2). The SRI ESIAC greatly expands the capability of the human analysts, particularly their ability to effectively use time-sequence, multispectral imagery and provide objective and repeatable mea-

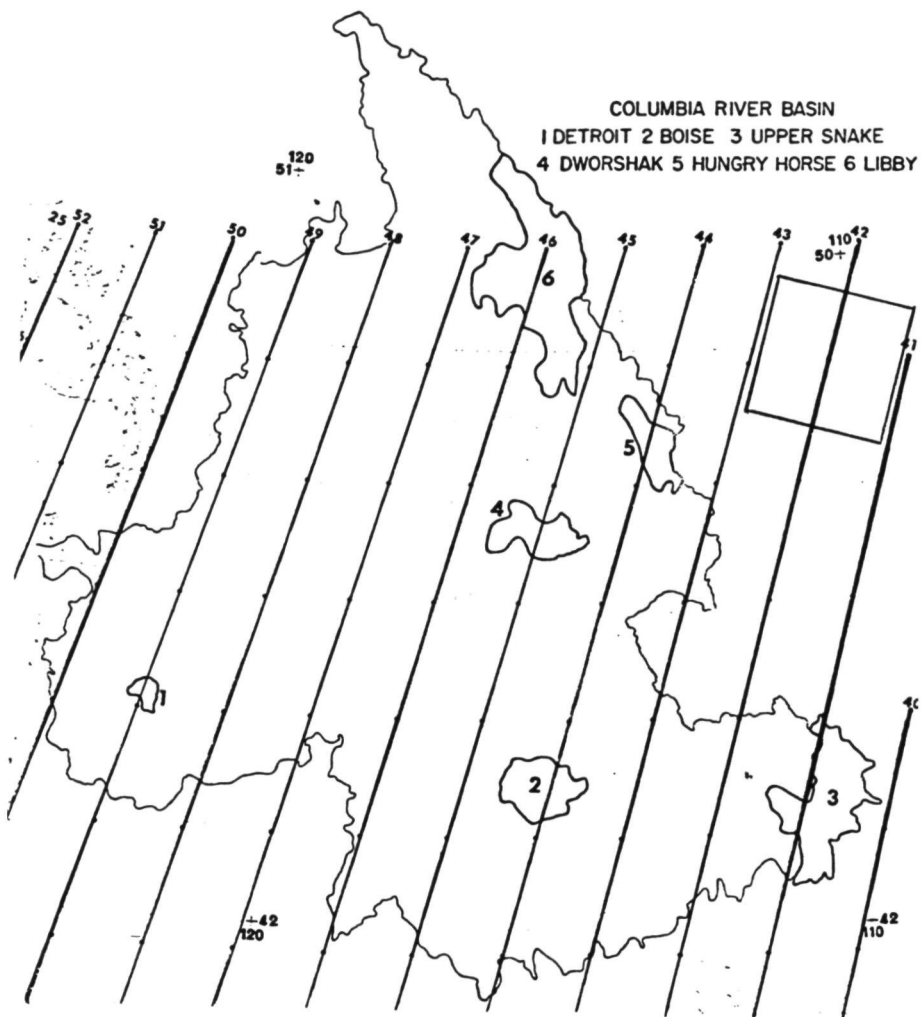


FIGURE 2

LANDSAT Orbital Tracks Over Test Basins
Using Canadian Numbering System

surements. It also provides a bridge between manual photo interpretation and machine processing. SRI presented three main options, in ascending order of cost and degree of refinement, for analyzing the imagery: manual photo interpretation, ESIAC classification from one spectral band, and advanced ESIAC analysis using two spectral bands and use of variable area, above threshold elevation masks to establish localized snowline elevations and to predict shadow regions. The second option using ESIAC classification from one spectral band (MSS-5) was chosen.

The satellite orbital tracks using the Canadian numbering system and the frame coverage is shown on Figure 2. One LANDSAT frame will generally cover the North Santiam Basin, and this basin was used to develop detailed procedures. About two frames are needed to cover the Boise Basin and from two to four frames are required for the Upper Snake Basin.

Snowcover area was determined from a program that combines an objective classification using single-band (MSS-5) radiance thresholding with subjective editing using elevation contours and other reference data as a guide. LANDSAT imagery was scaled to the ESIAC TV screen, about 55 x 40 km or 0.5° by 0.5° longitude and latitude. This scaling approximately matched the display resolution to the LANDSAT imagery resolution. This magnification required one TV view for the North Santiam Basin, four views for the Boise Basin and eleven views for the Upper Snake Basin. A binary basin outline map and a Universal Transverse Mercator (UTM) grid in 2.5 km x 2.5 km boxes were superimposed over each view. All of these data were specially registered to each other during the entry process.

Registered color, time-lapse sequences were created for each basin. A mask of the snowcover area was generated for each view based on radiance thresholding, localized threshold adjustments, and superimposed elevation contours with final editing when necessary. The masks were documented by photography, by numerical pixel count of the total area, and by a digital array depicting tenths of snowcover for each 2.5 x 2.5 km cell. The cell-by-cell numerical documentation provides a convenient means for machine recording and manipulating the data, comparing with other methods of determining snowcover, and, more importantly, for use with advanced modeling techniques such as elevation bands as mentioned earlier.

Final results of the work on the measurement of snowcover from satellite imagery are not as yet available. Very adequate data were obtained for the North Santiam Basin; however, this basin was chosen primarily for the work being done by Dr. Mark Meier to test snowcover area methods. The North Santiam Basin is a coastal basin and the runoff is, for the most part, during the winter season from rain. Thus, it is not included as a primary snow runoff basin in the SSARR model. Data for the North Santiam Basin is shown in Table 3.

The Upper Snake Basin snowcover is shown in Table 4. During 1973, because of persistent cloud cover, LANDSAT-1 images were usable for only three dates, 29 March, 22 May, and 9 June. More-

TABLE 3 N. Santiam Basin Snow CoverageBasin Area = 1146 km²

Average Elevation ~ 3900 ft MSL

Date	% of Basin Area Covered by Usable Imagery	Snow Coverage	
		Area (km ²)	% of Basin Area*
<u>1973</u>			
6 January	100	858.4	74.9
11 February	100	891.4	77.8
6 April	100	519.1	45.3
24 April	100	475.6	41.5
12 May	100	205.1	17.9
<u>1974</u>			
1 January	100	975.2	85.1
6 February	100	1002.8	87.5
24 February	100	1080.7	94.3
12 June	100	405.7	35.4
30 June	100	190.2	16.6

*Derived by dividing the measured snow area within the basin by the viewable area within the basin.

TABLE 4 Upper Snake Basin Snow Coverage

Basin Area = 13,339.6 km² Average Elevation ~ 8000 ft MSL

Date	% of Basin Area Covered by Usable Imagery	Snow Coverage		
		Area (km ²)	% of Basin Area*	
			LANDSAT	SSARR
<u>1973</u>				
29 March	96.9	11888.0	92.0	100
22 May	95.0	5128.4	40.5	33
9 June	94.9	1738.8	13.7	19
<u>1974</u>				
22 June	96.8	1942.2	15.3	

*Derived by dividing the measured snow area within the basin by the viewable area within the basin.

over, no aircraft snow flights were made in 1973 as this was a very low year for precipitation and runoff. Agreement between the SSARR depleted data using the temperature index and the LANDSAT data are fair. The large gap between 29 March and 22 May misses the high runoff which started in mid-May and peaked on 22 May. In 1974 only one usable image was available for 22 June. This was much too late in the season and efforts are being made to secure additional coverage from overlapping imagery to the east that would cover most of the basin.

The Boise Basin snowcover is shown in Table 5. Again, there were no aircraft snow flights in 1973 but the SSARR depleted coverage shows good agreement with LANDSAT-1 data particularly during the runoff period. Of particular interest are the data for 1974. Very good agreement is evident between the satellite and SSARR data except for 14 April where the SSARR data shows 57 percent and the satellite data 74.1 percent coverage. The probable cause of this disagreement was a thin skin of new snow that fell on 12 April. This new snow extended below the 4000 foot elevation and showed up on the satellite; but, because of its transitory nature, provided little in the way of runoff.

Comparison of the actual hydrograph and the reconstitution of satellite and SSARR data for runoff from the Boise Basin is shown on Figure 3. As can be seen, the correlation is very good.

It is still too early to draw any definite conclusions on the use of satellite data for determining area of snowcover in this region; particularly with the large number of cloud-covered days, the problem of determining the snowline in forested areas, and the lack of high resolution with the Synchronous Meteorological Satellite (SMS) data. The addition of new satellites this past year and future improvement in resolution should materially improve satellite data. Yet to be tested is the turn around time in getting the satellite data from the receiver sites to the user for real-time application. Nonetheless, what we have seen to date shows that satellite determination of snow coverage is a promising adjunct to our current methods. Continuation of our project, particularly with the deep snowpack and late runoff experienced in 1975, should provide us with much added information. We are much indebted to NASA/GSFC for supporting this valuable project.

REFERENCES

- (1) U.S. Army Engineer Division, North Pacific, 1975: Program Description and User Manual for SSARR Model Streamflow Synthesis and Reservoir Regulation, Program 724-K5-G0010, Portland, OR., 188 pp.
- (2) Wiegman, E. J., Wm. E. Evans, R. Hadfield, 1975: Measurement of Snow Coverage From Satellite Imagery During 1973 and 1974 Melt Season: N. Santiam, Boise, and Upper Snake Basins, Draft of Final Report under BPA-SRI Contract No. 53442, Stanford Research Institute, Menlo Park, CA., 63 pp.

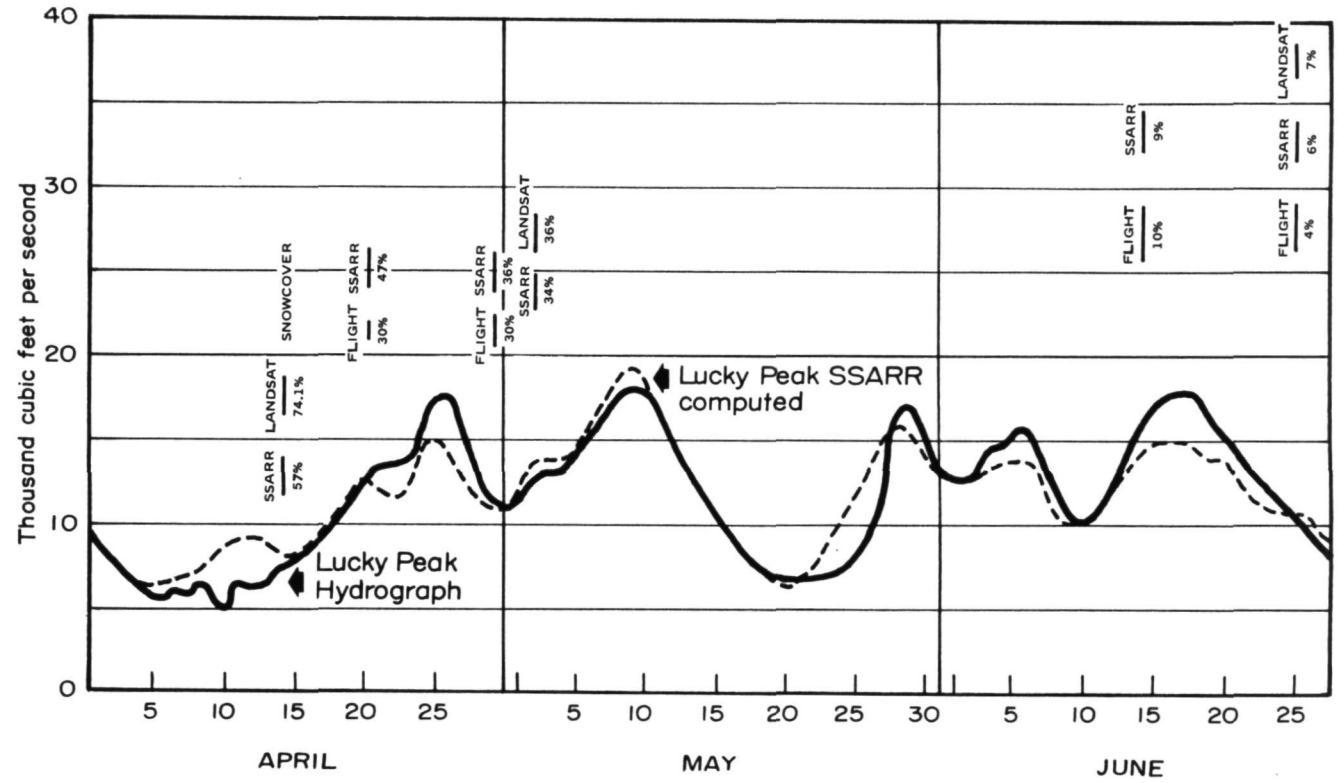
TABLE 5 Boise Basin Snow CoverageBasin Area = 7254 km²

Average Elevation ~ 6000 ft MSL

Date	% of Basin Area Covered by Usable Imagery	Snow Coverage		
		Area (km ²)	% of Basin Area*	
			LANDSAT	SSARR
<u>1973</u>				
19 April	100	4750.4	65.5	54
7 May	100	2270.4	31.3	32
12 June	100	594.0	8.2	6
30 June	100	278.6	3.7	2
<u>1974</u>				
14 April	100	5377.0	74.1	57
2 May	100	2609.5	36.0	34
25 June	100	504.5	7.0	6

*Derived by dividing the measured snow area within the basin by the viewable area within the basin.

Figure 3 : Boise Basin above Lucky Peak Dam , Hydrograph and
SSARR Computed Flows



THE OPERATIONAL PROGRAM OF SATELLITE SNOWCOVER OBSERVATIONS AT NOAA/NESS

Stanley R. Schneider, NOAA/NESS, Washington, D. C. 20233

ABSTRACT

The operational river basin snow mapping program at NESS is described with emphasis on quality control techniques and results for the 1974-1975 snow season.

INTRODUCTION

NOAA's National Environmental Satellite Service (NESS) has been producing satellite derived areal snow cover maps for selected river basins during the past three snow seasons. This project began in the Spring of 1973 with four basins originally targeted for study. The basins were selected so as to provide a variety of topographic, spatial and climatological characteristics (Wiesnet and McGinnis, 1973). The subject areas included the American River basin in California, the Willamette River basin in Oregon, the Red River of the North basin in North Dakota and Minnesota, and two sub-basins of the Genesee River in New York. An increase in manpower resources and the procurement of an electronic planimeter has enabled NESS to expand this successful program. Operational coverage is now being provided for 18 basins in the United States as well as several in Canada.

SATELLITE IMAGERY

The satellite imagery currently being used for snow mapping at NESS is from NOAA-4, a polar orbiting satellite that is the third in a series of improved TIROS operational satellites; the first, NOAA-2, was launched on October 15, 1972. The imaging system relevant to snow mapping on board NOAA-4 is the Very High Resolution Radiometer (VHRR). It provides daily coverage over the United States in the visible portion of the spectrum ($0.6 - 0.7 \mu\text{m}$) and twice daily coverage in the thermal infrared ($10.5 - 12.5 \mu\text{m}$). Spatial resolution for both the visible and the infrared data is one kilometer at nadir.

METHODOLOGY

Snow maps are produced by first registering a VHRR image to a hydrologic basin map. A Bausch and Lomb Zoom Transfer Scope is

utilized for this purpose. The snow line seen on the image is then traced onto the basin map.

The percentage of snow cover for the basin is determined through use of either a manual or an electronic planimeter. To use the manual planimeter, the area covered by snow is first measured and then divided by the total basin area. The manual planimeter works best for basins in which there is a single continuous snow line. In basins where there are isolated peaks and valleys, such as the Cascade Range, each snow area must be measured separately and then added together, thus compounding operator error.

Measurements can be made with great speed using an electronic planimeter. However, the operator is obligated to shade in the snow map and prepare a basin silhouette or "mask" before using the electronic planimeter.

THE CURRENT SNOW MAPPING PROGRAM

Snow cover measurements are taken whenever the subject area is cloud free and are generally transmitted within 30 hours of a satellite pass to serve as input to computer run-off models. Measurements are being made for eighteen river basins in the United States, ranging in size from 2541 km² for the Genesee River above Portageville, New York to 104,120 km² for the Red River of the North above Emerson, Manitoba (see Table I).

The primary users of these areal snow extent data are the National Weather Service River Forecast Centers (RFC). Twelve River Forecast Centers provide river stage forecasts and flood warnings for most of the United States. Each RFC is served by one or more River District Offices (RDO). These River District Offices maintain stream gauges in their geographic areas of responsibility, relaying data to the RFC. Areal snow cover percentages determined by NESS are being sent to the Hartford, Harrisburg, Kansas City, Salt Lake City, Sacramento and Portland RFC, as well as the Phoenix RDO.

River basins have been added to the snow mapping program upon request of the NWS, Office of Hydrology. As can be seen from Table I, half the basins being analyzed for snow cover are located within the states of Oregon and Idaho. These basins are all a part of the Columbia River drainage system and have proved to be areas in which snowmelt is a critical factor in regard to water supply forecasting and flooding. In fact, rapid snowmelt in the Salmon, Clearwater and Payette basins caused extreme flooding in Idaho during June, 1974.

In addition to those listed in Table 1, a number of basins located in densely wooded areas are being mapped by NESS in a joint effort with agencies of the Canadian Government as part of

TABLE 1
BASINS FOR 1974-1975 OPERATIONAL MAPPING

<u>RIVER BASIN</u>	<u>LOCATION</u>	<u>DRAINAGE AREA IN km²</u>	<u>RFC</u>
Red River of the North (Above Emerson, Manitoba)	Dakotas-Minnesota Manitoba	104,120	Kansas City
Souris River (Above Westhope, N.D.)	North Dakota Saskatchewan	43,771	Kansas City
Willamette	Oregon	26,159	Portland
Deschutes	Oregon	27,195	Portland
John Day	Oregon	19,632	Portland
Umatilla	Oregon	5,931	Portland
Salmon (Above Whitebird, Idaho)	Idaho	35,095	Portland
Clearwater (Above Peck, Idaho)	Idaho	20,824	Portland
Weiser	Idaho	3,781	Portland
Payette (Above Emmett, Idaho)	Idaho	6,941	Portland
Boise (Above Lucky Peak, Idaho)	Idaho	6,941	Portland
American (Above Folsom)	California	5,601	Sacramento
Genesee (Above Portageville, N.Y.)	New York	2,541	Hartford
Genesee (Below Portageville, N.Y.)	New York	3,812	Hartford
Chemung	New York- Pennsylvania	6,721	Harrisburg
Salt	Arizona	16,141	Salt Lake City
Verde	Arizona	17,094	Salt Lake City
San Juan	Colorado-Utah- Arizona-New Mexico	65,273	Salt Lake City

a World Meteorological Organization program of snow studies by satellite. These include four sub-basins of the Winnipeg River, the upper Columbia River and the St. John River basin in Maine and New Brunswick.

RESULTS FOR THE 1974-1975 SNOW SEASON

Approximately 440 snow cover measurements were transmitted by NESS to RFCs between November 1, 1974 and June 30, 1975. A monthly breakdown is provided in Table II. All maps and measurements were determined by the NESS/Environmental Products Group (EPG) except for the American River basin which was turned over to meteorologists of the NESS/Synoptic Analysis Section (SAS) on January 11, 1975. As many as 16 basins were mapped on a single day, at a rate of less than one half man-hour per basin. Since basins were mapped whenever cloud free, the number of measurements for an area depended mainly on weather conditions. Other factors that affected the quantity of data were basin latitude, elevation and drainage area.

Northeast

The amount of data retrieved for the Genesee and Chemung Rivers was limited due to poor weather conditions in the Lake Ontario region and the long periods during which the basins were 100 percent snow covered (no snow maps were made in such cases). None the less, a combined total of 28 snow cover measurements were determined for the three basins during the 1974-1975 snow season.

Snow maps for the St. John River basin were made at a 1:2,500,000 scale, segregated into about 50 sub-basins through use of a transparent plastic overlay, and then transmitted to the New Brunswick Department of the Environment over XEROX 400 Telecopier. The following data were determined:

St. John River Basin (Areal Snowcover Percentages)

22 April 1975	100 Percent Snow Covered
1 May 1975	71 Percent Snow Covered
10 May 1975	35 Percent Snow Covered
14 May 1975	21 Percent Snow Covered
17 May 1975	15 Percent Snow Covered
25 May 1975	Snow Free

TABLE II

NUMBER OF SNOW COVER MEASUREMENTS
November 1, 1974 - June 30, 1975

River Basin	November	December	January	February	March	April	May	June	TOTALS
Red River of the North	2	1	2	0	4	2	Snow Free	Snow Free	11
Souris River	0	0	0	1	2	0	Snow Free	Snow Free	3
Willamette	0	4	3	2	6	4	6	2	27
Deschutes	0	4	2	2	2	3	6	3	22
John Day	0	3	2	5	7	3	6	3	29
Umatilla	0	2	3	5	3	2	3	0	18
Salmon	2	1	0	0	2	3	4	6	18
Clearwater	0	3	0	0	1	2	3	4	13
Weiser	1	2	0	1	4	3	7	5	23
Payette	1	3	0	1	4	3	7	7	26
Boise	1	2	1	1	4	3	7	8	27
American	4	6	11	8	6	8	12	10	65
Lower Genesee	2	0	1	2	2	3	Snow Free	Snow Free	10
Upper Genesee	2	0	0	0	2	4	Snow Free	Snow Free	8
Chemung	2	0	0	2	2	4	Snow Free	Snow Free	10
Salt	3	4	8	9	6	9	4		43
Verde	3	5	8	10	8	6	Snow Free	Snow Free	40
San Juan	6	7	5	10	4	8	5	3	48
TOTALS	29	47	46	59	69	70	70	51	441

Midwest

As in the Northeast, the paucity of data for the Souris, Red River of the North and Winnipeg basins was largely due to inclement weather and long periods of total snow cover. In fact, the Souris basin was 100 percent snow covered from the last week of December 1974 until the third week in February 1975. A substantial decrease in snow cover was then recorded for the Souris; from 89 percent on February 27 to 42 percent on March 18. However, heavy snow storms in late March completely blanketed the area again; the basin was observed as being 100 percent snow covered as late as April 10. Unfortunately, poor weather conditions prevented any opportunity of monitoring the subsequent melt from satellite imagery. By the time the Souris could next be seen, which was on April 21, the area was almost completely snow free. The drastic decrease in snow cover during this 10 day period was closely paralleled in the Red River of the North basin. Results for the four sub-basins of the Winnipeg River were particularly disappointing. Due to excess cloud cover and rapid melt, only one snow map could be made.

Southwest

Weather conditions in the Southwest were ideal for snow mapping. A large quantity of data for the Salt, Verde and San Juan rivers were worked up; a total of 131 snow maps for the three basins combined. Maximum (1975) areal snow cover for the Salt-Verde basins was observed on February 18 with a reading of 70 percent for the Salt basin and 57 percent for the Verde basin. The San Juan River basin was totally blanketed on several occasions during the winter but this was a temporary phenomenon owing to rapid melt at lower elevations in the basin. In one case, 19000 km² of snowcover were observed to melt off within 24 hours. Snow in the Verde River basin was almost totally gone by the end of April 1975 but remained in the headwater region of the Salt for another few weeks. Snow in the San Juan Mountains persisted into July 1975.

Sierra Nevadas-California

Generally clear California weather and the relatively small size of the drainage area being studied (5601 km²) allowed for 65 measurements to be made of the American River basin during this past snow season. The snow pack in the Sierras built up very slowly between November 1974 and January 1975. However, heavy snow storms commencing early in February caused a steep increase in areal snow cover. The American River basin was determined to be 59 percent snow covered on February 11; the highest figure obtained for the basin in three seasons of monitoring by NESS (the previous high had been 49 percent). In fact, basin snow cover remained over 50 percent during much of March and April, reflecting a heavy snow year in the Sierras.



Figure 1a. VHRR image of Idaho on May 10, 1975. Wallowa Mts. are at (A), Salmon R. at (B), Weiser R. basin at (C), Payette R. (D), Boise R. at (E) and Craters of the Moon at (F).



Figure 1b. VHRR image of Idaho on May 5, 1974.

Pacific Northwest-Idaho

The Weiser, Payette, Boise, Salmon and Clearwater River basins were totally snow covered during much of the past winter. Snowmelt in these basins began later in March and ended in July. The 1974-1975 snow season was particularly heavy. Figures 1a and 1b clearly show more extensive snow cover in Idaho on May 10, 1975 than there was on May 5, 1974. Areal snow cover percentages for these dates are given below:

	Weiser	Payette	Boise	Salmon
May 5, 1974	16%	49%	35%	50%
May 10, 1975	26%	73%	68%	82%

Pacific Northwest-Oregon

The number of snow cover measurements for the Willamette, Deschutes, John Day and the Umatilla basins (96) was surprisingly high considering the generally wet weather in Oregon. The maximum snow cover in the Willamette was 47 percent as determined on December 23, 1974 while the Deschutes, John Day and the Umatilla basins were observed as being totally snow covered for a short time in January 1975. Snow in these basins was mostly gone by the second week in June, with the exception of several glacial peaks in the Cascades.

Rapid winter snowmelt in the Oregon basins has been observed on VHRR imagery. Figures 2a and 2b show the Willamette, Deschutes and the John Day River basins on February 7 and February 10, 1974. The snow maps derived from these images are depicted in Figures 2c and 2d. The fog that is labeled on the VHRR image for February 10 is a common feature in the Willamette River valley and makes snow mapping in that basin difficult.

QUALITY CONTROL

Quality Control is an important part of the NESS snow mapping program. Snow maps derived from the VHRR imagery are compared to those produced from alternate satellite sensors (LANDSAT MSS and GOES VISSR) as well as to data obtained from aerial surveys and ground observations. Computer enhanced VHRR imagery have been useful in locating basin snow lines.

Ground Observations

Data from ground observations is regularly obtained for many of the study basins. The two satellite maps in Figure 3 depict snowcover conditions in the Red River of the North basin for April 9 and April 16, 1974. Note the decrease in snowcover during

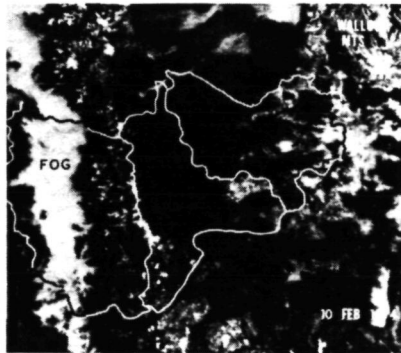
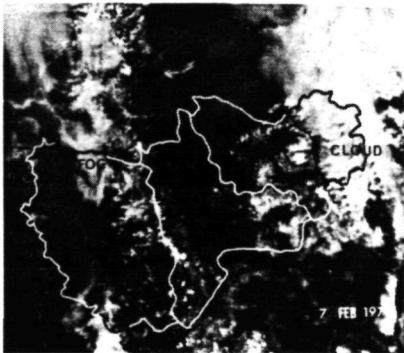


Figure 2a. VHRR image showing Oregon on February 7, 1974. Willamette River basin is on the left, Deschutes in the middle and John Day on the right.

Figure 2b. VHRR image showing Oregon on February 10, 1974.

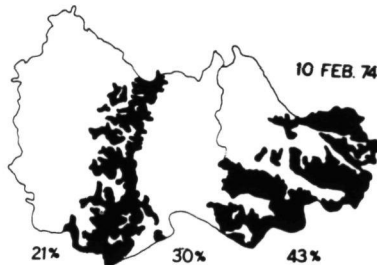
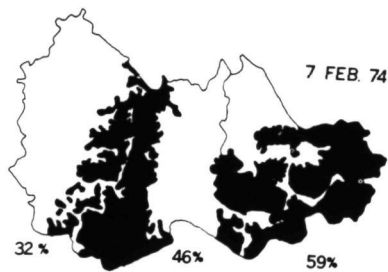


Figure 2c. Snow maps derived from the February 7th imagery (black areas are snow covered).

Figure 2d. Snow maps derived from the February 10th imagery.

REPRODUCIBILITY OF THE
ORIGINAL PAGE IS POOR

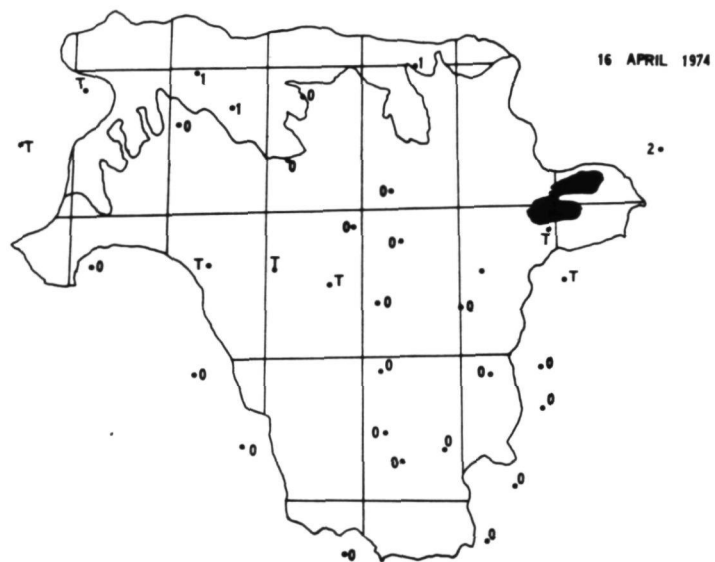
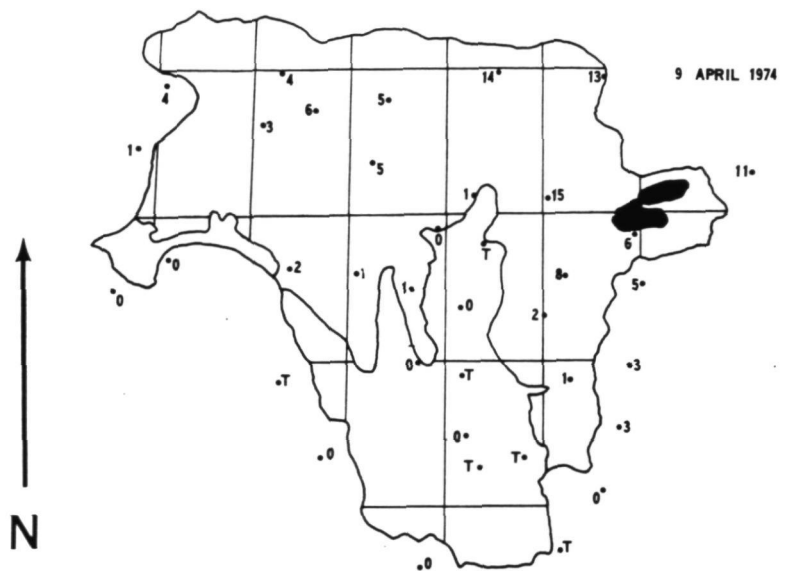


Figure 3. Snowcover maps for the Red River of the North above Emerson, Manitoba. The features in black are the Upper and Lower Red Lakes.

this one week period. The point measurements obtained from NOAA's Environmental Data Service (EDS) match well with the snow line location determined from the VHRR imagery.

Aerial Surveys

Satellite snow maps have been favorably compared with aerial survey data in the past (Barnes and Bowley, 1970; Barnes and Bowley, 1974). Aerial survey data for this past season have been provided to NESS by the Salt River project and the British Columbia Hydro and Power Authority. Figure 4 shows an aerial survey map of the Salt-Verde River basin together with a VHRR derived snow map. The two maps are in general agreement but there are differences as to location, extent and presence of several snow covered areas. These differences may have been caused by the 24 hour gap between data collection, the small scale of the VHRR imagery, snow on the northern slopes being obscured in the imagery by a low sun angle, the lack of reflectance of shallow "mottled" snow areas and finally, the differing judgements of aerial surveyor and satellite image interpreter.

LANDSAT and GOES

The additional spatial, temporal and spectral coverage provided by the sensor systems on board LANDSAT and GOES (Geostationary Operational Environmental Satellite) has been a boon to the NESS snow mapping program.

Highly detailed (80-meter ground resolution) can be obtained in four spectral bands from the Multispectral Scanner (MSS) on board the LANDSAT satellite. Owing to this high resolution, snow maps derived from the MSS-5 (0.6 - 0.7 μ m) data have been used at NESS as a "calibration standard" for those derived from VHRR data (Wiesnet and McGinnis, 1973).

Unfortunately, the LANDSAT imagery has certain limitations when used operationally. These limitations include the satellite's 18 day revisit period (reduced to nine days with the addition of LANDSAT-2) and the limited geographic area covered in a LANDSAT image frame. The latter makes snow mapping difficult in basins larger than 34,000 km² (Wiesnet and McGinnis, 1973). For such large basins frames from more than one satellite pass (taken one day apart) would have to be used together to assure complete geographic coverage. However, dynamic changes in weather conditions and areal snow cover can preclude the use of LANDSAT data in this manner.

Geostationary satellites occupy a position in space that is fixed relative to the ground. The NESS operates two such satellites, GOES-1 and GOES-2. They are currently stationed over the equator at 75°W and 115°W longitude respectively. Imaging capability is provided by the Visible and Infrared Spin Scan Radio-

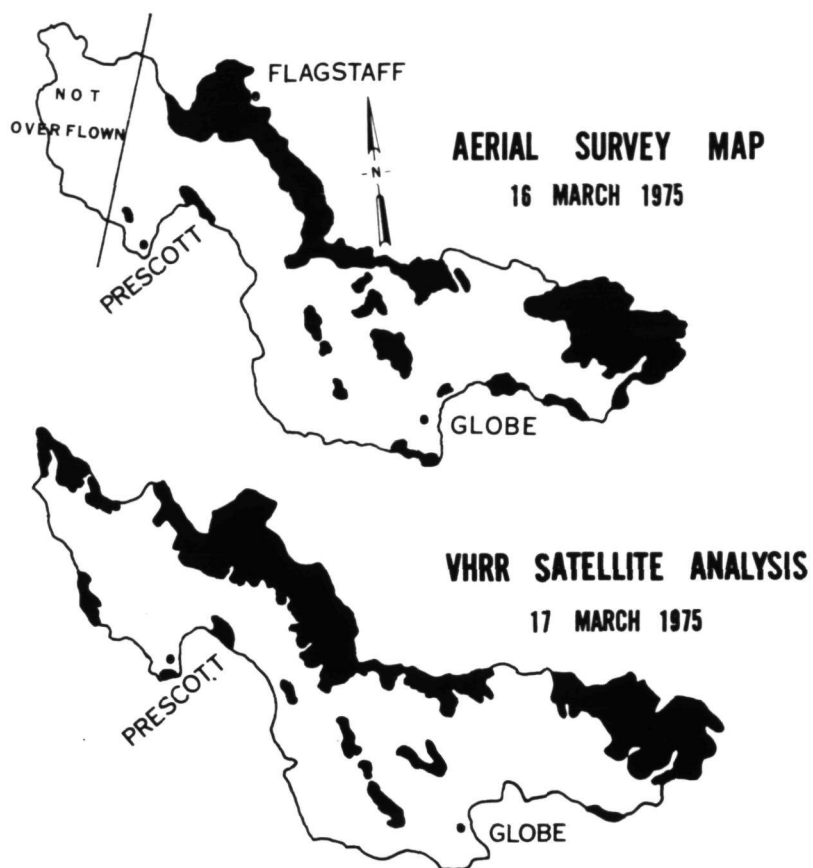


Figure 4. Comparison of Aerial Survey Map and VHRR Satellite Analysis for the Salt-Verde River basins. Areas in black are snow covered.

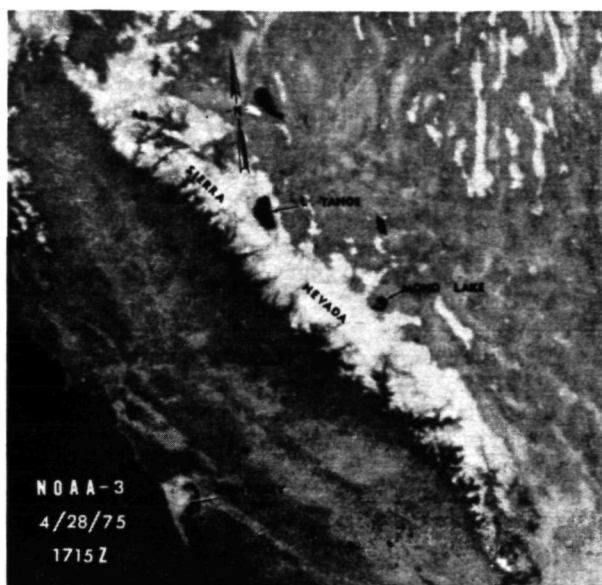


Figure 5a. VHRR image of the Sierra Nevadas.

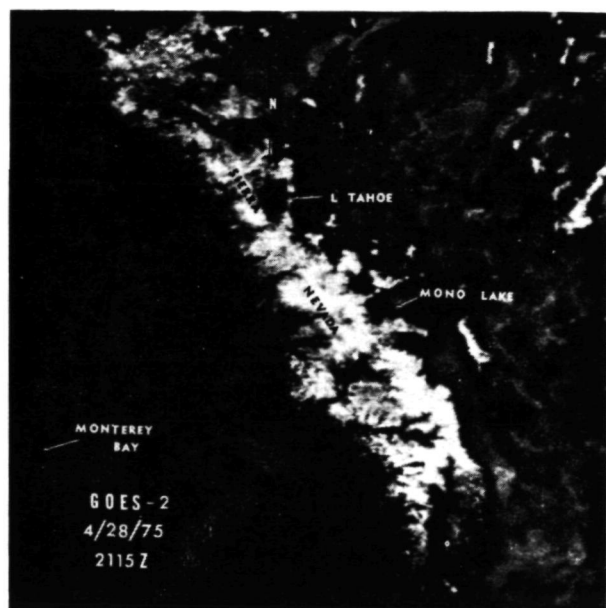


Figure 5b. VISSR image of the Sierra Nevadas.

meter (VISSR) which can sense in both the visible (0.55 - 0.75 μ m) and thermal infrared (10.5 to 12.6 μ m) portions of the spectrum. The imagery is available at several resolutions (Bristor, 1975), with the optimum resolution for the visible data being 1 kilometer. Coverage may be as frequent as every half hour.

Figures 5a and 5b depict the Sierra Nevada Mountains as viewed by NOAA-3 and GOES-2 on April 28, 1975. As can be seen, the fog in Monterey Bay has dissipated and there has been a build-up of cumulus clouds in the intervening 4 hours. The "squashed" appearance of features on the VISSR image is due to the oblique receiving angle afforded by GOES-2.

The usefulness of GOES data for snow mapping is currently being evaluated at NESS. Preliminary results show that snow maps of the American River basin (39°N) prepared using VISSR imagery, differ from those derived from VHRR data by an average of 3.25 percent of basin snow cover (ten cases have been studied thus far). The Salmon River basin in Idaho will also be studied to determine the amount of degradation in VISSR imagery for basins in more northern latitudes.

Computer Enhancements

With the aid of computers, VHRR digital tape data can be enhanced to bring out desired ground features, (i.e. snow lines). However, the time involved in computer handling precludes the use of such data for real-time analysis.

FINAL COMMENTS

Several additional basins are scheduled to be added to the mapping program during the 1975 through 1976 snow season. A number of basins are also being consigned to the NESS/Synoptic Analysis Section where four teams of meteorologists, working on rotating shift, will be able to transmit areal snow cover data to users within 8 hours of a satellite pass, instead of the present 30.

Complete sets of snow maps for this past season are available for the basins listed in Table 1 from the NESS/Environmental Products Group (EPG). Members of the hydrologic community are invited to contact EPG to arrange for possible transmission of areal snow cover percentages and/or maps on a continuing basis.

ACKNOWLEDGEMENTS

I would like to express appreciation to Mr. P. S. Neal and Mr. R. M. Barazotto for their help in preparation of illustrations and to Mrs. Mary Young for typescript preparation.

REFERENCES

- Barnes, J. C., and Bowley, C. J., The Use of Environmental Satellite Data for Mapping Snow-Extent Decrease in the Western United States, Final Report, Contract No. E-252-69(N), Allied Associates, Inc., Concord, Mass., 1970, 105 pp.
- Barnes, J. C., and Bowley C. J., Handbook of Techniques for Satellite Snow Mapping, ERT Document No. 0407-A Environmental Research and Technology, Inc., Concord, Mass., 1974, 95 pp.
- Bristor, C. L., Central Processing and Analysis of Geostationary Satellite Data, NOAA Technical Memorandum NESS 64, U.S. Department of Commerce, Washington, D. C., March 1975, 155 pp.
- Environmental Data Service, Climatological Data Minnesota, Climatological Data North Dakota, Vol. 80, No. 4 and Vol. 83 No.4, National Climatic Center, NOAA, U. S. Department of Commerce, Asheville, N. C., April, 1974.
- National Weather Service, River Forecasts Provided by the National Weather Service, Vol. 1, U. S. Department of Commerce, National Oceanic and Atmospheric Administration, Rockville, Md., 1972, 62 pp.
- Schwalb, A., Modified Version of the Improved TIROS Operational Satellite (ITOS D-G) NOAA Technical Memorandum NESS 35, U. S. Department of Commerce, Washington, D. C., April 1972, 48 pp.
- Wiesnet, D. R., The Role of Satellites in Snow and Ice Measurements, NOAA Technical Memorandum NESS 58, U. S. Department of Commerce, Washington, D. C., August 1974, 12 pp.
- Wiesnet, D. R. and McGinnis, D. F., Snow-Extent Mapping and Lake Ice Studies using ERTS-1 MSS together with NOAA-2 VHRR, Third Earth Resources Technology Satellite-1 Symposium, December 10-14, 1973, Goddard Space Flight Center, Washington, D. C., pp. 995-1009
- U. S. Department of the Interior, Geological Survey, Water Resources Review for June 1974, Water Resources Review, U. S. Geological Survey, Reston, Va., July 1974, 14 pp.

USE OF AREAL SNOW COVER MEASUREMENTS FROM ERTS-1 IMAGERY
IN SNOWMELT-RUNOFF RELATIONSHIPS IN ARIZONA

J. S. Aul and P. F. Ffolliott, *University of Arizona, Tucson, Arizona*

ABSTRACT

An analysis of methods of interpreting ERTS-1 imagery to measure areal snow cover and the relationship of areal snow cover and runoff were among the objectives in this study of use of ERTS-1 imagery for forecasting snowmelt-runoff relationships.

INTRODUCTION

The increase in demand for water in the Southwest, coupled with the construction of multipurpose reservoirs to control and regulate snowmelt runoff, requires accurate streamflow forecasting. Forecasts are needed to determine allowable releases from reservoirs for power, irrigation, municipal use, recreation, pollution abatement, and flood control.

Areal snow cover measurements may be an especially valuable input to streamflow forecasting in Arizona. For example, snowmelt runoff accounts for two-thirds of the mean annual streamflow from the Salt-Verde Watershed (Warskow 1971). The Arizona snowpack is shallow and intermittent in contrast to most Rocky Mountain states. However, because of the nature of the snowpack, measures of snowpack depletion may have a high correlation with the volume of snowmelt runoff.

The Earth Resources Technology Satellites (ERTS) have shown potential use in determining areal snow cover (Barnes et al. 1974, Meier 1973). ERTS (now referred to as LANDSAT) has the advantage of offering small scale photography while maintaining high resolution. Each scan by ERTS views a swath 180 kilometers wide, and features greater than 70 meters in diameter can be detected on the imagery (Rango et al. 1974). Furthermore, ERTS operates continuously and, with two satellites currently in orbit, scans are repeated every nine days. With the availability of ERTS imagery, flights for photographing or reconnaissance of a snowpack need not be commissioned, assuming ERTS proves satisfactory in monitoring changes in areal snow cover.

Preceding page blank

DESCRIPTION OF THE STUDY

An exploratory study was conducted to determine whether ERTS-1 imagery could be used to monitor changes in areal snow cover for use in developing snow cover-runoff relationships in east-central Arizona. ERTS-1 imagery was selected for study because this was the imagery available for the time period analyzed. The objectives of the study were to:

1. ascertain the availability of quality ERTS-1 imagery to monitor changes in areal snow cover;
2. determine whether ERTS-1 imagery could be interpreted for areal snow cover by employing manual or semi-manual methods of interpretation;
3. compare estimates of areal snow cover obtained from ERTS-1 imagery with estimates derived from low-altitude aerial snow surveys; and
4. determine whether a relationship exists between measures of areal snow cover and subsequent runoff during the snowpack depletion period.

Study Area

The Black River Watershed above the Black River Pumping Station, an area of 1,450 square kilometers, was chosen as the study area. This watershed ranges in altitude from 1,745 meters at the Black River Pumping Station to 3,533 meters at the top of Mt. Baldy and, therefore, receives relatively heavy snowfalls during the winter. The Black River is the major contributor to the Salt River, which is an integral part of the reservoir system that provides water to Phoenix and central Arizona. Seasonal flow from the Black River Watershed averages over 125 million cubic meters per year.

Vegetation on the Black River Watershed is primarily montane-conifer forest, with smaller areas in the spruce-fir, mountain meadow, and pinyon-juniper types. The watershed is almost totally basaltic in respect to geologic formation. Soils have igneous materials, almost exclusively, as parent material.

Interpretation of ERTS-1 Imagery for Areal Snow Cover

The ERTS-1 satellite was launched on July 23, 1972, into a near-polar, sun-synchronous orbit at an altitude of 910 kilometers. The orbital configuration provides day-to-day sidelpap of the viewing swaths of 14 percent at the equator to more than 80 percent at high latitudes. ERTS-1 data are gathered and relayed in a digital format which may then be processed into imagery.

ERTS-1 imagery, in both 245 millimeter and 70 millimeter

formats, was the data source for this study. The imagery was obtained from the Western Aerial Photography Laboratory, Division of the Agricultural Stabilization and Conservation Service, Salt Lake City, Utah. Specific imagery used was in the red band (0.6-0.7 Mm) because previous studies have indicated that snow cover can be most easily detected in this band (Barnes and Bowley 1973, Evans 1974, Rango et al. 1974).

The time period analyzed was November 1, 1972, to June 12, 1973. A near record snowpack accumulated in Arizona during this period, with estimates of snowpack water equivalent 300 percent above normal on the Salt River Watershed in early April (Barnes et al. 1974). It was felt that a heavy snow year would provide the most ERTS snow cover data.

An overlay was developed for interpretation of the imagery. The scale of the 245 millimeter positive transparencies is 1:1,000,000 and, to interpret this imagery for snow cover, the Black River Watershed boundary had to be known. Therefore, the boundary was delineated on a 1:250,000 scale U.S. Geological Survey topographic map and reduced to a 1:1,000,000 scale through a photographic process. Shading film was laid over the outline of the watershed and cut with a fine razor knife along the boundary. The shading film was then removed and, by photographing the watershed, a 1:1,000,000 scale overlay was developed, with the watershed area being transparent and areas beyond opaque. The river channel on the overlay was opaque to facilitate location of the overlay on the ERTS-1 imagery.

Snow covered areas were determined on the imagery by comparison of the brightness level on the watershed with the edge of the snowpack. If areas within the watershed appeared brighter than areas just beyond the edge of the snowpack, they were judged snow covered. When not obliterating view of the snowpack, clouds were differentiated from snow by pattern recognition, shadows, recognition of terrestrial features, and pattern stability.

Four methods were used in the interpretation of areal snow cover on the ERTS-1 imagery. The first method employed was a simple dot grid. A dot grid, with dots approximately 0.1 millimeter in diameter and with a density of 50 dots per square centimeter, was developed through a photographic reduction process. Black and white positive transparencies with a 245 millimeter format were viewed on a light table, with the watershed overlay used to delineate the watershed on the imagery. A dissecting microscope at 7X power was used for dot counting because the microscope, at this power, made viewing of the dots easier and still allowed the observer to see patterns on the watershed. A total number of dots over the entire watershed was determined by randomly dropping the dot grid on the watershed overlay and counting the number of dots. This process was repeated ten times to derive a mean total of dots. Percent of snow cover was found by randomly dropping the dot grid on the imagery covered by the watershed overlay, counting the number of

dots landing on snow covered area, and dividing by the total number of dots on the watershed. This process was repeated three times to obtain a mean percent of snow cover.

A second method of interpretation utilized a grid of squares, six millimeters per side, drawn on a sheet of clear mylar. Black and white positive transparencies with a 245 millimeter format were viewed on a light table. The squares grid was placed over the watershed located on the imagery by the overlay. The grid was located in the same position with respect to the overlay each time it was used. Percent of snow covered area was determined by estimating the amount of snow cover in a full or partial square to the nearest twenty percent, multiplying that estimate of snow cover by the area of that full or partial square, and dividing by the total area of the watershed.

A third method employed a planimeter for interpretation of snow cover. Planimetry snow cover directly from 1:1,000,000 scale imagery was difficult. Therefore, it was necessary to transfer the imagery to a larger scale. To accomplish this transfer, 70 millimeter negative transparencies of the watershed area were used to make 35 millimeter positive slides. The slides were projected to a 1:250,000 scale base map of the watershed, and the projector was moved until the stream channels of the imagery and the base map coincided. Boundaries of snow covered areas were traced onto the watershed base map and planimetry to determine the snow covered area. Percent of snow cover was found by dividing the snow covered area by the total area of the watershed at a 1:250,000 scale.

Finally, a fourth method of interpretation utilized a densitometer. Black and white positive transparencies with a 245 millimeter format were viewed on a light table with the watershed overlay blocking out all areas outside the watershed. A camera above the light table viewed the imagery and projected it to a television screen, where it was zeroed-in and brought to full scale. In viewing an image, the densitometer splits the shades of gray on the imagery into twelve discrete levels and, by flipping a switch on the densitometer, the image on the screen goes from black and white to false color. Using this switch, the densitometer can be calibrated to a particular image with the objective, in this case, of making a given set of false colors occupy the snow covered area. When a given set of false colors occupied what the interpreter considered to be snow covered, switches above those false colors were flipped to the percent scale, and the densitometer gave area of snow cover as a percent of the total area of the watershed projected on the screen.

Analyses of Interpretations of ERTS-1 Imagery

To analyze whether ERTS-1 imagery could be interpreted for areal snow cover, analyses were made on the basis of

estimates of areal snow cover by one observer and on estimates of areal snow cover by four observers.

Areal snow cover estimates were made by one observer, using all four methods of interpretation. Measurements of areal snow cover were made within a one week period. After a set of measurements was completed, a week was allowed to pass before again analyzing the imagery. This process was repeated three times. A split plot analysis of variance was used to test for differences.

Areal snow cover estimates were also made by four observers using the dot and squares grid methods of interpretation. All observers were instructed to interpret snow covered areas by the methods previously described. The dot and squares grid methods were selected for interpretation because these were the methods that were judged to be most readily available to those who may use areal snow cover data. A split plot analysis of variance was again used to test for differences.

Comparison of ERTS-1 and Snow Survey Data

Low-altitude aerial snow surveys were frequently flown by the Salt River Project throughout the 1972-73 snow season because of the near record snowpack and the transient characteristics of the snowpack on the Salt-Verde Watershed. To provide a basis for comparison with ERTS imagery, areal snow cover obtained from the snow surveys was mapped on a 1:1,000,000 scale base map of the Salt-Verde Watershed. Percent of areal snow cover on the Black River Watershed was obtained from the snow survey maps by orienting the watershed overlay on the snow survey map, planimetering the snow covered area, and dividing by the total area of the watershed.

Developing Relationship Between Snow Cover and Runoff

Measures of areal snow cover and runoff subsequent to a date of snow cover measurement needed to be determined before it could be ascertained whether a relationship existed between areal snow cover and subsequent runoff during the snowpack depletion period. A single value of areal snow cover for each date of imagery interpreted was obtained by taking a mean of values from all methods of interpretation judged to be feasible for measuring areal snow cover. Runoff subsequent to each date that snow cover was measured was determined by accumulating daily runoff records through June 12, 1973. This date was arbitrarily chosen as the termination date because: the hydrograph was approaching base flow, suggesting that no significant amounts of snowmelt runoff were occurring; examination of imagery on June 5, 1973, indicated little snow cover remained on the watershed; and heavy rainstorm occurred over the watershed on June 13 and 14, so runoff after that storm would be largely from rainfall rather than snowmelt.

The snowpack depletion period was arbitrarily chosen when the general trend of the data appeared to indicate a decrease in snow covered area over the watershed.

RESULTS AND DISCUSSIONS

Arizona has more days suitable for aerial photography than any other state (Avery 1968). Also, the sidelap of viewing swaths of ERTS-1 and the position of the Black River Watershed in the viewing swaths allowed coverage of the watershed on two consecutive days for each sweep of the region by the satellite. However, despite these advantages, only imagery from seven of 13 possible two day periods could be interpreted for snow cover, with clouds obscuring all, or significant portions, of the watershed on the remaining photo periods.

All scans from November 1, 1972, to May 19, 1973, that could be interpreted were evaluated in determining the feasibility of using ERTS-1 imagery for areal snow cover interpretation. The June 5, 1973, scan was not used in evaluating the use of ERTS-1 imagery for snow cover interpretation because of the lack of a sizeable snowpack on that date. However, this scan was used in attempting to develop snow cover-runoff relationships.

Interpretation of ERTS-1 Imagery

Significant differences ($\alpha = 0.05$) were detected among the four methods of interpretation by one observer for six dates throughout the 1972-73 snow season. A multiple range test was used to determine which methods differed (Table 1). Based on this test, it was concluded that no single method can be considered unfeasible because none of the results from a given method of interpretation were unreasonable in relation to results obtained by the other methods.

Table 1. -- DIFFERENCES AMONG FOUR METHODS OF SNOW COVER INTERPRETATION BY ONE OBSERVER FOR SIX DATES THROUGHOUT 1972-73 SNOW SEASON.

Densitometer	Dot Grid	Squares Grid	Projection-Planimeter
-- percent areal snow cover --			
69	71	72	74

Note: line under means indicates not significantly different ($\alpha = 0.05$).

Each method of interpretation has advantages and disadvantages. The squares grid method required approximately 25 minutes per date of imagery and only a light table for interpretation. The dot grid method yielded results in the same amount of time as the squares grid method but required a microscope, in addition to a light table, for interpretation. The planimeter method yields a map of areal snow cover but required approximately 45 minutes per date of imagery for interpretation; also, a "Zoom Transfer Scope" is needed if more accuracy is needed than can be obtained from the available imagery. Finally, the densitometer method yields an estimate of snow cover in the least amount of time, approximately 15 minutes per date of imagery, but requires a high initial investment and may yield less precise values than the other methods.

No difference in estimates of snow cover in time was discerned among the methods of interpretation on the basis of one observer. This lack of difference would indicate that, once an observer has guidelines in mind as to which areas to consider snow covered, these measures can be reliably repeated at a later time.

Significant differences ($\alpha = 0.05$) were noted among observers and between methods when four observers used the dot and squares grid methods to determine percent of areal snow cover. The differences among observers indicated that individuals have different interpretations of snow covered areas despite following the same guidelines for interpretation.

The results of the tests among the four observers indicated that interpretation of snow cover from ERTS-1 imagery was not necessarily a matter of distinguishing black from white. Specific problems encountered were: the imagery often varied in density and contrast within and among the dates of interpretation; differing types and densities of vegetation frequently caused snow covered areas to appear in differing shades of gray; patchiness of snow cover created problems in deciding whether an area was snow covered; poor illumination due to shadowing effects resulted in misinterpretations of snow covered areas; and, in addition to totally preventing interpretation, clouds also created problems on dates when cloud cover was not severe enough to prevent interpretation.

Comparison of ERTS-1 and Snow Survey Data

On the basis of a paired t -test, no difference ($\alpha = 0.05$) was found between estimates of percent snow cover obtained from a mean of values from all four methods of interpretation of ERTS-1 imagery and from low-altitude aerial snow surveys. These results are in accordance with those from a study designed to compare measures of snow cover from ERTS-1 imagery and from low-altitude aerial snow surveys over the entire Salt-Verde Watershed (Barnes *et al.* 1972). These results would indicate that an experienced observer familiar with a particular watershed could obtain comparable measures of snow cover extent from ERTS

imagery and aerial reconnaissance.

Barnes et al. (1974) noted that more detail can be mapped from ERTS-1 imagery than from low-altitude aerial reconnaissance. Results of this study also showed snow cover being mapped in more detail from ERTS-1 imagery than from snow surveys. However, this does not necessarily imply that greater accuracy can be obtained in mapping snow cover from ERTS imagery. The lack of detail on low-altitude snow survey maps may simply be a function of the time the observers chose to spend mapping rather than an inability to map in detail.

Relationship Between Snow Cover and Runoff

To determine whether a relationship exists between areal snow cover and subsequent runoff, it was first necessary to select the beginning of the snowpack depletion period. The general trend of the snow cover data appeared to indicate a decline in snow covered area beginning on February 18, 1973. Therefore, this date was arbitrarily chosen as the beginning of the snowpack depletion period.

A significant linear relationship ($\alpha = 0.05$) was determined to exist between areal snow cover and subsequent runoff during the snowpack depletion period, based on four observations of areal snow cover from ERTS-1 imagery. The relationship is:

$$\hat{Y} = 5.2(10^5) + 2.7(10^5) X$$

where \hat{Y} = subsequent runoff in cubic meters;

X = areal snow cover in square kilometers.

The coefficient of determination (r^2) was 0.995.

As mentioned earlier, measures of snow cover from ERTS-1 imagery and from low-altitude aerial snow surveys were similar. Therefore, data from the two sources were combined to assess what effect an increased amount of snow cover data would have on the regression analysis. The general trend of the combined snow cover data appeared to indicate a decline in areal snow cover beginning on February 15, 1973, the data arbitrarily chosen as the beginning of the snowpack depletion period.

A significant linear relationship was also found to exist between areal snow cover and subsequent runoff during the snowpack depletion period, based on nine combined observations of areal snow cover from ERTS-1 imagery and low-altitude aerial snow surveys.

The above-mentioned regressions, which do not differ significantly from each other, indicated that a highly significant relationship existed between the tested variables. Therefore, the increased amount of areal snow cover data available from the two sources did not change the results of the regression based on data from ERTS-1 imagery alone.

The results of the regression relationships appear encouraging for using measures of areal snow cover obtained

from ERTS-1 imagery for snowmelt runoff forecasting, especially residual volume forecasting. However, the analysis should be viewed with some restraint. The limited amount of source data might not have accurately monitored changes in areal snow cover. Temperature variations in Arizona cause the snowpack to advance and recede many times throughout the winter. For example, measures of areal snow cover from ERTS-1 imagery indicate a peak in extent of areal snow cover in February or March, but snow course measurements of water equivalent throughout the Salt-Verde Watershed indicated that the peak seasonal snowpack occurred in early April (Barnes et al. 1974). It is possible that measures of areal snow cover from ERTS-1 imagery may have been too infrequent to detect the peak accumulation.

Another possible limitation of the data was that it represented a year with a near record snowfall. Therefore, the regressions between areal snow cover and subsequent runoff may have been influenced by the unusual nature of the winter, possibly limiting their overall usefulness.

A technical difficulty encountered in use of ERTS-1 imagery was the time necessary to obtain the imagery. A minimum wait of two weeks was common after an order was submitted. If attempts were made to use ERTS imagery in real-time monitoring changes in areal snow cover, this delay would have to be overcome.

SUMMARY

1. Nearly one-half of the scans of ERTS-1 imagery analyzed over the study period were obscured by cloud cover, which may preclude dependence on satellite imagery, by itself, for monitoring snow cover depletion in Arizona.

2. Differences among observers in estimating areal snow cover suggests difficulty in using ERTS imagery for this purpose unless an observer is familiar with the area.

3. None of the methods of interpretation employed to measure areal snow cover could be ruled unusable, with the method to be used dependent on the investment to be made, the level of precision desired, and whether a map of snow cover extent is wanted.

4. Estimates of areal snow cover from ERTS-1 imagery were similar to comparable estimates obtained by low-altitude aerial reconnaissance.

5. A significant relationship between snow cover and subsequent runoff during the snowpack depletion period for the year of study suggests that measures of areal snow cover obtained from ERTS imagery may become a valuable tool in forecasting snowmelt runoff in Arizona.

LITERATURE CITED

- Avery, T. Eugene. 1968. Interpretation of aerial photography. Burgess Publishing Co., Minneapolis, Minnesota, 324 p.
- Barnes, James C., and Slinton J. Bowley. 1973. Use of ERTS data for mapping snow cover in the western United States. Symposium on Significant Results Obtained from the ERTS-1, NASA-Goddard Space Flight Center, NASA SP-327, pp. 855-862.
- Barnes, James C., Clinton J. Bowley, and David A. Simmes. 1974. The application of ERTS imagery to mapping snow cover in the western United States. ERTS Type III Final Report, January 1974, NASA-LR-137223, National Technical Information Services E74-10400, 80 p.
- Evans, W. E. 1974. Progress in measuring snow cover from ERTS imagery. Proceedings, Western Snow Conference 42: 37-45.
- Meier, M. F. 1973. Evaluation of ERTS imagery for mapping and detection of changes of snow cover on land and on glaciers. Symposium on Significant Results Obtained from the ERTS-1, NASA-Goddard Space Flight Center, NASA SP-327, pp. 863-878.
- Rango, A., D. F. McGinnis, V. V. Salomonson, and D. R. Wiesnet. 1974. New dimensions in satellite hydrology. U.S. National Committee for the International Hydrological Decade 30: 703-711.
- Warskow, William L. 1971. Remote sensing as a watershed management tool on the Salt-Verde Watershed. Proceedings, ARETS Symposium 2: 100-108.

**UTILIZATION OF LANDSAT MONITORING CAPABILITIES FOR
SNOWCOVER DEPLETION ANALYSIS**

A. G. Thompson, *WRRI, University of Wyoming, Laramie, Wyoming*

ABSTRACT

LANDSAT images for three snowmelt seasons have been utilized to map and analyze snowcover depletion on a small river basin in southeastern Wyoming. Results indicate that snowcover-runoff curves established from repetitive LANDSAT coverage may be used in conjunction with streamflow data to provide low-cost seasonal runoff forecasts having a high degree of accuracy. Additionally, detectable variations within a snowpack might provide temporal estimates of peak flows.

INTRODUCTION

Runoff from melting snows provides most of the usable water supply for the Western United States; but unfortunately this runoff is not timed to meet the water requirements of crop production, hydroelectric power generation, or municipal needs (Garstka, Love, Goodell, 1958). The need to plan for expected water supply has led to runoff forecasting programs such as the snow survey administered by the Soil Conservation Service (SCS). The economic value of the SCS water supply forecasts has been estimated at between \$32 million and \$65 million per year accruing to agriculture alone (Nelson, 1969). While estimates of forecast value vary according to source, it is generally accepted that forecasts are necessary and worthwhile, particularly as competition for available water supplies increases.

Whether a particular runoff forecast procedure is based on some form of index method or rational method, all procedures have one thing in common: raw data are required and the costs of raw data are continually rising. Snow course measurements for the SCS in the states of Colorado, Montana, and Wyoming presently cost \$300-\$400 per snow course per year, and this figure is expected to rise as high as \$500 in the near future.

(U.S. Department of Agriculture, SCS, 1975). Any new forecasting procedure under consideration must cost less or no more than those now being used and provide accuracy as good as or better than that presently available. The LANDSAT satellites now provide information usable for forecasting procedures which may satisfy the requirements of cost and accuracy.

The value of knowledge concerning the areal extent of snowcover has been recognized for some time. The close relationship between snowcover depletion and accumulation for a given basin has been well documented (Leaf, 1971). The main problems confronting users of snowcover data have been the high cost of the data if aerial photography was used and the inaccurate data obtained from snowcover estimations (U.S. Army Corps of Engineers, 1960). The LANDSAT satellites provide snowcover information on a regular basis and at minimal cost. The purpose of this study was to examine the snowcover monitoring qualities of LANDSAT data with respect to runoff forecasting.

A small basin of 404 km^2 (156 mi^2) with substantial ground truth available was used as a test area. The study utilized LANDSAT data covering 3 snowmelt seasons. Study results indicated a poor relationship between snowcovered area at a given time and total runoff for the melt season in this basin. However, an excellent relationship was established between snowcover as a percentage of total basin area and the accumulated runoff to a given image date as a percentage of the total seasonal runoff. Additionally, analysis of variations of reflectance within the snowpacks indicated a relationship between these variations and climatological parameters which might be used in the temporal estimation of peak flows.

Results show that LANDSAT data is operationally useful from the standpoints of both economics and accuracy. LANDSAT data may aid in overcoming the high cost of data acquisition and data acquisition problems brought about by physical or legislated limitations.

STUDY BASIN AND DATA BASE

That portion of the Little Laramie River basin above the United States Geological Survey streamflow gage 06661000 near Filmore, Wyoming, comprises the test basin used for this study (Fig. 1). The basin lies on the east-facing slopes of the Medicine Bow Mountain Range in southeastern Wyoming, 64 km (40 mi) west of Laramie, Wyoming. This portion of the basin covers an area of 404 km^2 (156 mi^2) and rises from 2316 m (7600 ft) in elevation at the Filmore gage to

3659 m (12,005 ft) at the top of Medicine Bow Peak.
The general area-elevation of the basin is as follows:

<u>Elevation</u>	<u>Area</u>
3353 m (11,000 ft)	1%
3048 m (10,000 ft)	19%
2743 m (9000 ft)	55%
2438 m (8000 ft)	82%

Figure 2

Vegetation of the basin consists of prairie grasses and sagebrush on the valley floor and lower slopes with lodgepole pine and fir-spruce krumholz forest on the higher slopes and mountains. Low vegetation and scrub trees are characteristic of the alpine areas of the basin. The forest crown cover exceeds 70 percent only in scattered stands of lodgepole pine.

This particular basin was chosen as a test site because it is centrally located in the LANDSAT image track, because flow data for the Filmore gage are available for a continuous period of 38 years, and because the basin contains two sub-basins which act as hydrometeorological observatories for the Wyoming Water Resources Research Institute (WRRRI). The Nash Fork Creek and Libby Creek sub-basins contain 13 WRRRI hydrologic or meteorologic instrument stations (Fig. 2). Recorded data for solar radiation, temperature, precipitation, wind, and streamflow are available for some of the sites for a period of 8 years. Precipitation, solar radiation, and temperature data from the Little Brooklyn Lake instrument site at 3170 m (10,400 ft) elevation were used as base data for yearly comparisons.

This portion of the Little Laramie River basin is also the location of 5 SCS snow courses. Data are available for all 5 courses for a continuous period of 27 years. The average April 1 water equivalent of these 5 snow courses correlates with the flow totals at the Filmore gage with $R^2 = .79$.

Ground truth data were collected for the 1975 accumulation and early melt season at 5 WRRRI meteorologic instrument stations from 2560 m (8400 ft) to 3231 m (10,600 ft) elevation (Fig. 2). Readings of snow depth, water equivalent, and snowpack temperature were taken at each of the 5 sample sites. Photometer readings were also taken filtered for direct light and the approximate ranges for the 4 LANDSAT MSS bands. These data were collected from 18 Feb 75 to 13 May 75 concurrent with LANDSAT overflights or as close as weather, time, and the usual field problems permitted.

Positive 18.54 cm (7.3 in) x 18.54 cm

transparencies of all MSS bands were ordered for each scene that offered any possibility of interpretation of the snowcover for 1973, 1974, 1975. Of 27 scenes available for the snowmelt seasons, 15 scenes could be used to map snowcover. Several of these were marginal at best and could be used only with color enhancement and then only for total snowcover. It was hoped to attain a good number of scenes for the 1975 melt season as two satellites were imaging; but cloud conditions and image accession problems combined to limit the usable scenes to 5, of which 2 were marginal for snow mapping. Quality of the images received usually ranged between 5555 and 8888. Distortion of individual band images presented problems in only several instances and these were rectified with the aid of a zoom transfer scope.

METHODOLOGY AND EQUIPMENT

The snowcover was mapped for each usable MSS 5, MSS 7, 4-band color diazo composite, and in some cases an MSS 5 high-density black diazo. The mapping was done on a Bausch and Lomb ZT4 Zoom Transfer Scope at a scale of 1:250,000. Tonal and color variations within the snowcover were mapped in addition to total snowcover. The respective areas were measured with a K & E compensating polar planimeter with an average combined instrument and operator error of less than 1 percent. As a check on mapping accuracy, all snowcover scenes for 1973 were independently remapped after two months. Area measurements and snowpack shapes were found to be essentially the same for the two trials. Differences that were noted stemmed from increased experience in distinguishing clouds from snow.

Initially the color enhancement diazo process was used experimentally to facilitate mapping of snow-covered scenes which had cloud interference. Test composites showed that a false color infrared diazo composite had variations in the snowpack which took on a bluish tint and corresponded closely to tonal variations in MSS 5 and MSS 7 black and white transparencies. Trials were run on each band for color, exposure time, and developing of the diazo film to arrive at a combination that provided the desired image enhancement, not only for snow mapping but for general use of the composite. Once the desired colors, exposure times, and developing times were set, a color composite could be made which was standard enough to allow comparison from scene to scene and from season

to season. The final composite had MSS 4 as yellow, MSS 5 as red, and both MSS 6 and 7 as cyan. A 3-band composite leaving out MSS 6 undesirably reduced the apparent color variation within the snowpack.

Photometer readings were taken in order to examine reflection variation between bands during the melt season. A Science and Mechanics Model A-3 photometer was used with filter modifications filtered for:

MSS 4:	.48 μm -.59 μm
MSS 5:	.59 μm -.66 μm
MSS 6:	.70 μm -1.1 μm
MSS 7:	.83 μm -1.1 μm

For each reading of each band another reading was taken of an 18 percent grey scale card at the same time. The figure then used for analysis was the ratio of the grey scale photometer reading to the snow photometer reading for each filter. Use of the grey scale card provided a basis for reflectance comparison between bands, sites, and observations.

A Joyce-Loebl MKIIICS automatic recording microdensitometer and a Spatial Data Systems Model 401/704 Datacolor/Edge Enhancer System were also used for image analysis, but only quantitatively to this point due to time considerations and mechanical problems. Snowcovered areas delineated by the systems were comparable to those obtained by manual mapping; however, the same problems exist in differentiating between clouds and snow. Computer compatible tapes of LANDSAT scenes were not used for this study due to the cost of the tapes for a monitoring situation.

ANALYSIS AND RESULTS

Use of the snowcovered area of a basin as a forecasting index of total runoff does not appear promising based on this study. Table 1 shows the progression of snowcover depletion during the snowmelt seasons for which LANDSAT coverage was available. Actual snowcovered area for given dates in 1973 seem to approximate or exceed the area for similar dates in 1974, although the total April 1-July 31 runoff for 1973 was 716 m³/sec (25,300 cfs) as compared to 917 m³/sec (32,393 cfs) for 1974. Also, the snowcovered area is consistently higher for the 1975 season than for 1974, yet the respective April 1-July 31 flows for the 2 years are nearly equal, with 933 m³/sec (32,959 cfs) for 1975. This same relationship is also borne out by characteristic snow depletion-runoff curves derived

for the individual seasons. The relationship becomes even less in light of the fact that the hydrograph rise did not really begin until May 9 in 1975, as compared to April 15 for 1974 and April 20 of 1973.

Meaningful statistical analysis is not possible with only three data points, but it should be noted that the flows for 1974 and 1975 represent fairly normal flows compared to the seasonal average over 58 years of record of 863 m³/sec (30,478 cfs) and as such do not represent extremes which might account for error. The difference between flows and snowcover is not accounted for either in these seasons by late-season precipitation. The question also arises as to whether snowcover for such a small basin on a given index date would vary enough from year to year to suffice as an accurate runoff index. However, this is only one basin and significant yearly snowcover variations may be found in other basins, particularly larger basins (Rango, Salomonson, Foster, 1975).

Far more promising results for the use of LANDSAT snow mapping for total runoff forecasting were obtained in comparing basin snowcover percentages to accumulated runoff to dates of the LANDSAT scenes. For better comparison between yearly melt seasons, the parameters were made dimensionless with $X = \text{snowcover}/\text{total basin area}$ and $Y = \text{accumulated runoff}/\text{total April 1-July 31 runoff}$ (Table 1).

Nonlinear regression using MSS 5, MSS 7, and color-composite derived data established a semi-logarithmic relationship between the X and Y parameters. The color composite data realized the highest relationship, with $R^2 = .98$ using 11 data points and $\log_{10} Y = 2.03888 + (-.0156482)X$. Figure 3 shows the plotted composite data and the resultant curve on a standard graphic scale. Initially, all data derived from all scenes starting with the last scene showing 100 percent snowcover were used, with $R^2 = .91$. However, the 100 percent data points were dropped since they were not reflective of the last actual date of 100 percent snowcover and hence not indicative of accumulated runoff at the beginning of snowcover depletion.

Although the individual snowcover depletion curves vary considerably for each year, the dimensionless depletion-accumulation curve (Fig. 3) holds for each of the test years regardless of varying weather conditions, depth of snowpack, water equivalent of snowpack, and total runoff. Such close relationships as were found are consistent with the literature on snowcover depletion-runoff accumulation relationships and with a snowpack's position as a "thermometer" of

physical factors affecting the yearly melt cycle. The obvious implication of the dimensionless depletion-accumulation relationship is that if the snowcovered area can be accurately determined at any point during the melt season and if streamflow data are available, then the total expected runoff may be accurately forecast. Also, a short-term picture of the time distribution of runoff might be formulated by comparison to yearly hydrographs. Using the depletion curves derived from the dimensionless curve for 1973, 1974, 1975, the peak flow dates came at 47, 46, and 40 percent, respectively of the April 1-July 31 total runoff.

While the dimensionless curve established may be unique to a single basin, the availability of LANDSAT data makes the development of similar curves for any number of basins simple and relatively inexpensive. Also, the accuracy of LANDSAT data for areal measurements of the size of snowpacks is dependable (Barnes, Bowley, 1973). Further, LANDSAT provides a scale that is workable for small basins and rivers. Streamflow data can be obtained with relative ease from a gage that need not be located in the severe conditions of a snowpack area for use in conjunction with snowcover data. Table 2 shows color and tonal variations within the snowpacks mapped from MSS 5, MSS 7, and color composites as percentages of total snowcovered area. The areas mapped were analyzed to determine possible significance of the variations noted. It was felt these variations stemmed from (1) areas of melting snow detected in MSS 7; (2) differing reflectance characteristics of metamorphosed snow; or (3) scattering of light reflectance due to ground vegetation showing through shallow snow.

Nonlinear regression of these variation values against accumulated runoff percentages gave a lower R^2 ($= .62$), which was the highest for this series and attributable to the composite data.

In examining the first variation possibility, the photometer readings collected for 1975 were analyzed. If MSS 7 was detecting any areas of melting snow, a change in photometer readings for MSS 7 relative to the other filtered bands was hypothesized. Cloud problems prevented comparison of photometer readings to the LANDSAT data for the early melt season in May 1975. However, analysis of variance showed no significant difference for the MSS 7 reflectance for the sample data from the 5 sample sites. MSS 7 appears to be of little aid in direct measurement of areas of snowmelt. This is supported by the fact that the MSS 7 bandwidth is $.8 \mu\text{m}$ - $1.1 \mu\text{m}$, while the greatest decrease in reflectance of melting snow occurs between $1.1 \mu\text{m}$

and 1.3 μm (Weisnet, McGuinness, 1974).

Multiple regression of the variation data against accumulated average daily temperature from March 1 to scene date and accumulated precipitation from March 1 to scene date produced an $R^2 = .88$. Again this was the value from the composite data and was the highest. Solar radiation was not used in the multiple regression since instrument problems did not provide sufficient continuous data for the 3 melt seasons.

This relation suggests that the area of variation as mapped reflects accumulated heat supply and additions of precipitation, usually in the form of snow. Ground truth samples measured the changes in depth in the early melt season. By 13 May 75, ground vegetation was showing through the snow at the 2 lower sample sites. Also by this date, surface snow at the lower elevations had been thawed and refrozen and was generally frozen at the hour LANDSAT overflights were made. It was also noted at the sites that light spring snowstorms would cover the lower elevations and the metamorphosed snow. This fresh snow would remain past the hour of overflights. Also in the accumulation period of the snowpack for 1975, snow on the valley floor was usually light and vegetation showed through the snowcover. The area of the valley floor in the accumulation period scenes nearly always showed up as an area of color or tonal variation.

With such a small sample as 3 seasons for one basin, meaningful statistical conclusions are difficult to arrive at. However, the variation data do appear to evidence an inverse relationship to the time of the runoff hydrograph peak. The date of the runoff peak has varied over 39 years at the Filmore gage from May 12 to June 28 with the average time as June 6. Peak dates for the 1973, 1974, 1975 melt seasons were June 11, June 6, and June 16, respectively. Peaks having the highest flows are characteristic of the latter part of May.

Since a river's hydrograph is sensitive to heat requirements for the melting of a snowpack, it is felt the color and tonal variations as mapped reflect the melt cycle variations indirectly by depicting the depth changes near the outer limits of the receding snowpack. Further work is necessary, but these variations might be used in the estimation of peak flow dates and for more accurate forecasting of the time distribution of runoff.

CONCLUSIONS

1. Color composites of LANDSAT scenes provide the best all-round snow mapping capability, particularly for manual interpretation.
2. Prospects for use of snowcovered area as a sole index for total runoff from basins of the size used in this study do not appear favorable with any degree of acceptable accuracy based on the results of this study.
3. The use of dimensionless snowcover-runoff curves developed from LANDSAT imagery appears to be a viable method of obtaining low-cost forecasts of total runoff and short-term forecasts of time distribution of seasonal runoff within acceptable accuracy.
4. Mapping of color or tonal variations within receding snowpacks as an indirect measure of the snowpack melt cycle may lend itself to usable estimates of peak flow times and runoff distribution as additional LANDSAT data become available.
5. Analysis of changing snowcover characteristics provides indices of data parameters that are much more difficult and expensive to acquire on a monitoring basis than are LANDSAT images.
6. LANDSAT provides a scale and resolution of data that are necessary for work concerning smaller basins of the size used in this study.
7. The major drawback to operational use of LANDSAT data in runoff forecasting is the hands-on time required from data collection to user at the present time. However, as the operational value of LANDSAT type data becomes more and more apparent, distribution systems will undoubtedly increase in number and speed of delivery.

REFERENCES

- Barnes, J. C., and C. J. Browley, Mapping Snow Extent in the Salt-Verde Watershed and the Southern Sierra Nevadas Using ERTS Imagery, in Proceedings of the Third ERTS-1 Symposium, NASA Sp-351, Vol. 1, pp. 977-994, U.S. Government Printing Office, Washington, D.C., 1974.
- Garstka, W. U., L. D. Love, B. C. Goodell, Factors Affecting Snowmelt and Streamflow, 189 pp., USDI Bureau of Reclamation and USDA Forest Service, 1946-53 Cooperative Snow Investigations, U.S. Government Printing Office, Washington, D.C., 1958.
- Leaf, C. F., Areal Snow Cover and Disposition of Snowmelt Runoff in Central Colorado, USDA Forest Service Research Paper, RM-66, 19 pp., Rocky Mountain Forest and Range Experiment Station, Fort Collins, Colorado, 1971.
- Nelson, M. W., Social and Economic Impact of Snow Survey Data and Water Supply Forecasts, 7 pp., Idaho Snow Survey Supervisor, for presentation at the Western Snow Conference, Salt Lake City, Utah, April 15-17, 1969.
- Rango, A., V. V. Salomonson, and J. L. Foster, Seasonal Streamflow Estimation Employing Satellite Snow-cover Observations, NASA preprint X-913-75-26, 34 pp., Goddard Space Flight Center, Greenbelt, Maryland, 1975.
- U.S. Army Corps of Engineers, Runoff from Snowmelt, Engineering Manual 1110-2-14061, 413 pp., U.S. Government Printing Office, Washington, D.C., 1960.
- U.S. Department of Agriculture, Soil Conservation Service, Snow Survey Headquarters for Colorado, Montana, Wyoming, Telephone communication, 1975.
- Weisnet, D. R., and D. F. McGuiness, Snow Extent Mapping and Lake Ice Studies Using ERTS-1 MSS together with NOAA-2 VHRR, in Proceedings of the Third ERTS-1 Symposium, NASA Sp-351, Vol. 1, pp. 995-1009, U.S. Government Printing Office, Washington, D.C., 1974.

TABLE 1

1973, 1974, 1975 LANDSAT-derived snowcovered areas as percentages of total basin area for MSS 5, MSS 7, and color composites, and accumulated runoff as percentage of total runoff, April 1-July 31.

<u>Date</u>	<u>MSS 5</u> <u>%</u>	<u>MSS 7</u> <u>%</u>	<u>Color</u> <u>Composite</u> <u>%</u>	<u>Accumulated</u> <u>Runoff</u> <u>%</u>
12 APR 73	99	99	99	2
18 MAY 73	58	57	57	12
5 JUN 73	32	31	32	34
23 JUN 73	16	15	13	67
11 JUL 73	6	1	2	87
25 APR 74	100	100	100	3
31 MAY 74	30	28	30	34
18 JUN 74	21	18	18	67
6 JUL 74	7	2	6	88
2 APR 75	100	100	100	.2
17 MAY 75	77	77	77	7
4 JUN 75	57	50	48	18
13 JUN 75	42	39	39	33
22 JUN 75	29	30	24	52

TABLE 2

1973, 1974, 1975 LANDSAT-derived snowpack variations for MSS 5, MSS 7, and color composites as percentages of total snowcover area.

<u>Date</u>	<u>MSS 5 Grey Tone %</u>	<u>MSS 7 Grey Tone %</u>	<u>Composite Bluish Color %</u>
7 MAR 73	17	18	--
25 MAR 73	21	24	0
12 APR 73	19	24	58
18 MAY 73	59	59	63
5 JUN 73	41	35	86
23 JUN 73	56	56	100
11 JUL 73	83	100	100
25 APR 74	38	41	--
31 MAY 74	43	64	57
18 JUN 74	57	56	78
6 JUL 74	86	50	86
15 MAR 74	14	16	15
17 MAY 74	-- Clouds	-- Clouds	--
4 JUN 74	40	56	--
13 JUN 74	45	33	39

Figure 1

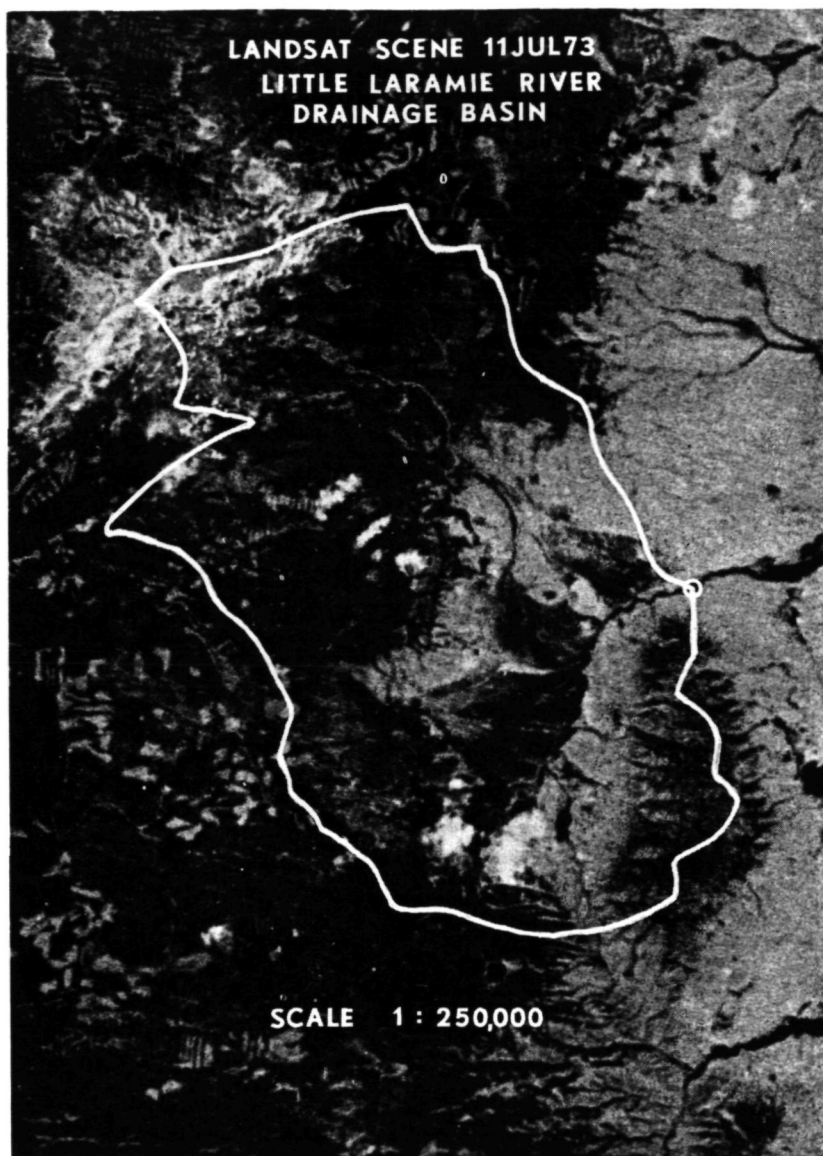
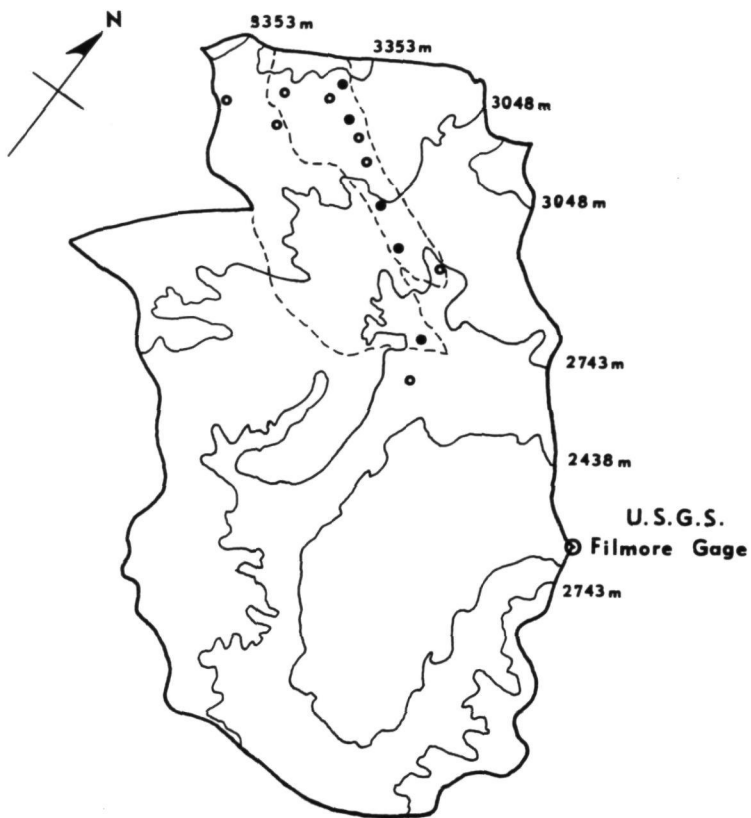


Figure 2



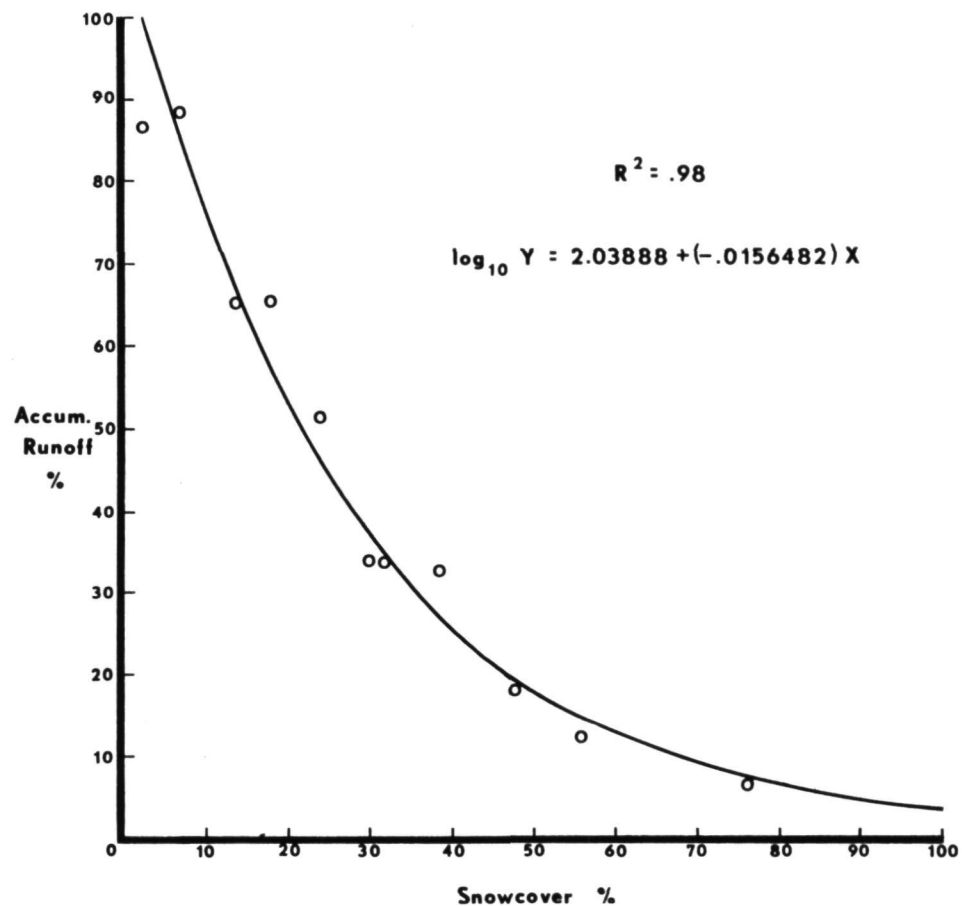
SCALE 1: 250,000

----- Libby Creek and Nash Fork
Creek Sub-basins

○ Hydrometeorological
Instrument Stations

● Sample Sites at
Instrument Stations

LITTLE LARAMIE RIVER
DRAINAGE BASIN



PLOTTED DATA
COMPOSITE SNOWCOVER
%
-V-
ACCUMULATED RUNOFF
%

OPERATIONAL USE OF LANDSAT IMAGERY FOR THE ESTIMATION
OF SNOW AREAL EXTENT

Edwin F. Katibah, *Remote Sensing Research Program, University of California, Berkeley, California*

ABSTRACT

Quantification of the surface area of snow covering watersheds can be a useful parameter in estimating snow water content for inclusion in water runoff prediction equations. This paper documents an operational manual interpretation technique which allows fast and accurate estimates to be made of the areal extent of snow parameter using LANDSAT-1 imagery. The analysis procedures and the statistical results are presented in this paper.

INTRODUCTION

One of the most easily detected of all resources from Earth orbiting satellites is snow. Investigators have proposed that relationships could be developed between snow-cover depletion and water runoff (Leaf, 1969) and in more specific terms, between snow-cover depletion and snow water content. Investigators have shown that areal extent of snow in specific vegetation, elevation and aspect relationships can be cost-effectively related to the actual snow water equivalent for a given area using snow survey data collection systems similar to those in use in many areas (Thomas, 1974; Thomas and Sharp, 1974). Since relationships such as the ones described above have been developed using areal extent of snow to provide the major portion of the information to be used in water runoff equations, techniques had to be developed which would provide fast, economical, and accurate estimation of this parameter. The following research deals with the development of techniques for estimation of snow areal extent.

Using conventional aerial photography as the data base for obtaining snow areal extent information would obviously prove extremely costly if this necessitated covering entire watersheds on a sequential basis. Satellite imagery, more specifically LANDSAT-1 satellite imagery, could provide the data base, relatively inexpensively and on a repetitive basis. In order to quantify areal extent of snow, techniques were developed which analyzed the imagery for areal extent of snow based on reflectance and such parameters as elevation, vegetation and aspect. The technique describes a relatively simple procedure which none-the-less

provides very solid quantitative results.

PROCEDURE

The estimation procedure described in the following pages is based upon analyses of imagery defined by artificial units (grids). This technique differs substantially from the snow mapping approach reported in the literature (Barnes and Bowley, 1969; Rango and Foster, 1975; Rango, Salomonson, and Foster, 1975-Wiesnet, 1974), where the snowpack boundary is delineated directly. The procedures developed allow the image analyst to make decisions in discrete units of the imagery as to the areal extent of snow based upon such factors as density and type of vegetative cover, elevation, aspect, actual reflectance of the snowpack, and by inference (i.e., by the presence of directly observable snowpack). These techniques also provide for the direct application of appropriate statistical methods for the estimation of the true areal extent of snow, as well as providing a means of determining the precision of that estimate.

LANDSAT-1 imagery in the form of simulated color infrared enhancements of bands 4, 5, and 7 was used for the interpretation procedures. These enhancements were made from individual 9-1/2 inch LANDSAT-1 black-and-white positive transparencies and combined using a technique developed at the Remote Sensing Research Program (Katibah, 1973). Consequently, enhanced imagery of just that portion of the LANDSAT-1 frame desired could be produced with excellent quality. Use of this technique also provided original enhancements directly on negative color film so that high quality reflection prints could be produced for interpretation purposes.

Snow Areal Extent Inventory

During the spring of 1973, the LANDSAT-1 satellite provided essentially cloud-free coverage of the Feather River Watershed on April 4, May 10, and May 28. On these (or at the most, two days thereafter) random transects were flown across the watershed using a 35 mm camera to acquire large scale aerial photography that could be used as an aid in determining the actual snow condition on the ground (i.e. "ground truth").

To estimate the areal extent of snow, the LANDSAT-1 images were gridded with image sample units (ISU's), each equaling 400 hectares (Figures 1, 2, 3, and 4). These image sample units were then transferred to the large scale photography where applicable. The image sample units on the large scale photography were coded as follows:

<u>Code</u>	<u>Snow Cover Class</u>	<u>Midpoints</u>
1	No Snow present within the ISU	0
2	0-20% of ISU covered by snow	.10
3	20-50% of ISU covered by snow	.35
4	50-98% of ISU covered by snow	.74
5	98-100% of ISU covered by snow	.99

The gridded LANDSAT-1 images were then interpreted, sample unit-by-sample unit, and coded using the following method to account for vegetation cover and density and to some degree, aspect, elevation and slope as they impact snow cover.

Scale matched simulated color infrared enhancement of LANDSAT-1 imagery were produced for April 4, 1973; May 10, 1973; May 28, 1973 and also for August 31, 1972 in reflection print form. The April and May dates represent the snowpack and were gridded, while the August 1972 date, representing a cloud-free summer image, was not gridded. The purpose of the August date was to provide a clear aerial view of actual ground relationships of vegetation/terrain features. The August date was superimposed with each of the snowpack dates using a mirror stereoscope. By blinking first one eye and then the other, the image analyst could observe what conditions actually occurred on the ground in the image sample unit he was interpreting for snowpack. Obviously this technique capitalizes on the human image analyst's ability to synthesize large amounts of pertinent data and quickly arrive at a decision.

The image analyst, using this technique, spent three hours training himself to interpret the LANDSAT-1 imagery. The April 4th date comprising 2218 image sample units was subsequently interpreted in nine hours, the May 10th date (2050 image sample units) in six hours, and the May 28th date (2013 image sample units) in three hours. The decrease in interpretation time can undoubtedly be related to the increasing experience of the analyst and the decreasing snowpack.

The LANDSAT-1 interpretation results were compared to the coded large scale photography where applicable. Tables I, II, and III summarize the interpretation test results. The sample unit-by-sample unit interpretation of the LANDSAT-1 image was then used to find the estimate for the areal extent of snow in the watershed. Totals for each of the individual snow cover classes were found and multiplied by 400 hectares, the area of each image sample unit on the ground. This gave the hectares for each class; these values were then multiplied by the appropriate snow cover class midpoints to give the total hectares of snow in each class. Finally, these totals were added to give the estimated areal extent of snow. See Table IV.

The areal extent of snow thus calculated was based solely upon the LANDSAT-1 interpretation results. To correct this estimate, the image sample units where snow areal extent "ground truth" was obtained (from large scale aerial photographs) were compared with the same image sample units on the LANDSAT-1 imagery. The relationship between the snow areal extent values on these corresponding LANDSAT-1 and "ground truth" sample units is the basis for the application of the ratio estimator statistical technique (Cochran, 1959). This technique not only provides a correction for the original interpretation estimate, but also allows for an estimate of the precision of this technique through the application of confidence intervals. The confidence intervals around the areal extent of snow estimates were calculated for four different levels of confidence 99%, 95%, 90% and 80% for comparative purposes. The confidence intervals are expressed in hectares (Table V).

It is desirable to check and see if the values in the snow cover class from the LANDSAT-1 image data come from the same statistical probability distribution as the values in the snow cover classes from the large scale photography data. If they come from the same distribution, it may be expected that our estimation procedure will provide good results. If there were also a way to lump snow cover classes to improve the indications that the two sets of values came from the same distribution, this would give some idea on how to improve the estimation procedure in the future. To perform such probability distribution likeness tests, a Chi-square statistic,

$$\chi^2 \sim \sum_{i=1}^k \frac{(O_i - E_i)^2}{E_i},$$

was used. The values in the snow cover classes from the large scale photo data were designated as the expected values (E_i), since they were assumed to be "ground truth". The values in the snow cover classes from the LANDSAT-1 image data were designated as the observed values (O_i). For each date a Chi-square test was run, using the data as recorded versus the data with snow cover classes 4 and 5 combined, to see if an improvement in class widths could be realized.

Results of the Snow Areal Extent Inventory

The results of this inventory are summarized in the following tables of interpretation results, statistical computations (including areal extent of snow estimates, variance of areal of snow estimate, population ratio estimator, etc.), confidence intervals and allowable errors found in the following pages.

Tables I, II, and III deal with April 4, May 10, and May 28 interpretation data respectively. Table IV deals with the results of the ratio estimator statistic on all three dates. Table V deals with the confidence intervals associated with the areal extent of snow estimates on all three dates.

Conclusion of Snow Areal Extent Inventory

Improvement in the snow areal extent inventory, as it is currently done is possible by increasing the sample size and by optimizing the image sample unit size.

The Student's-t statistic reaches its smallest value when the degrees of freedom (sample size minus one) are approximately 120. In subsequent inventories using this approach, each date for which large scale aerial photography is flown should have approximately this number of image sample units definable.

One of the items that should be investigated is the optimum size of the image sample unit. Several approaches are possible as well as a combination of all of them. For instance, image sample unit size may be plotted against interpretation time, variance, or variance times cost to determine the optimum image sample unit shape and size under those constraints.

The one improvement that by itself can substantially decrease the width of the confidence intervals is that of decreasing the sample variance. As already shown, the April 4 data had the smallest variance, the May 10 data had the next smallest and the May 28 data had the largest. The reason for this progressive increase in sample variance most likely can be attributed to the decrease in the snow pack over the three dates. The image analyst's ability to classify seems to be related to the proportion of snow cover; however, the majority of the variance may not be due to the analyst, but rather to a natural state of greater snow areal extent variability among sample units over an area defined as a watershed.

The Chi-square test indicated that on all dates the experimental set-up was adequate. Substantial improvements in matching the corresponding value distributions of the large scale photography data and the LANDSAT-1 image data were realized by lumping snow cover classes 4 and 5. This indicates that the analyst had difficulty in separating snow areal extent class 4 areas from class 5 areas. If the snow cover classes were to be redistributed (0-20%, 20-40%, 40-60%, 60-80%, 80-100% for example) the analyst might realize an improvement in his ability to classify snow cover conditions. Provided the analyst's ability to classify snow cover conditions did improve, then it would be expected that the sample variance for each set of interpretation results would go down, and consequently, the width of the confidence interval would decrease given constant sample sizes and confidence levels.

Conclusions and Recommendations

Although the nature of the data acquired by the LANDSAT-1 satellite lends itself directly to automatic computer analysis for areal extent of snow estimation, research in manual techniques can be justified by comparing the two methods of operation to one another on a cost-effective basis. Research is currently being carried out on both phases of snow areal extent estimation procedures and analyses will be conducted testing both automatic, manual and a combination of automatic and manual on a cost-effective basis.

Besides being justifiable on this basis, continued research utilizing manual techniques can provide analyses in certain circumstances where computer classification has not been sufficiently refined. Scattered cloud cover over snowpack may present some difficulty to present computer analysis; however, the human has little difficulty distinguishing the two as they appear on LANDSAT-1 imagery.

The inventory methods for areal extent of snow estimation described in this paper show great promise for providing fast, economical, and accurate inventories of snowpack extent. As it is refined, such as by optimizing image sample unit sizes and snow cover class width, estimates as to the true areal extent of snow should become more precise and should be made with greater confidence, all other factors being equal.

ACKNOWLEDGEMENTS

The research reported on in this paper was sponsored by NASA Grant NGL 05-003-404.

REFERENCES

- Barnes, J.C. and C.J. Bowley, 1969. Satellite Photography for Snow Surveillance in Western Mountains. In Proceedings of the 37th Annual Meeting of the Western Snow Conference. pp 34. Salt Lake City, Utah.
- Cochran, W.G., 1959. Sampling Techniques. John Wiley & Sons, Inc. New York, New York.
- Garstka, W.V., L.D. Love, B.C. Goodell, and F.A. Bertle, 1958. Factors Affecting Snowmelt and Streamflow. A Report on the 1946-53 Cooperative Snow Investigations At Fraser Experimental Forest, Fraser, Colorado. U.S. Government Printing Office.
- Katibah, E.F., 1973. A Simple Photographic Technique for Producing Color Composites from Black-and-White Multiband Imagery with Special Reference to ERTS-1. Information Note, Remote Sensing Research Program, Berkeley, California.
- Krumpe, P.F., 1973. A Regional Approach to Wildland Resource Distributional Analysis Utilizing High Altitude and Earth Orbital Imagery. In proceedings of the 39th Annual Meeting of the American Society of Photogrammetry. pp 336. Washington, D.C.
- Leaf, C.F., 1969. Aerial Photographs for Operational Streamflow Forecasting in the Colorado Rockies. In Proceedings of the 37th Annual Meeting of the Western Snow Conference. pp. 19. Salt Lake City, Utah.
- Rango, A., V.V. Salomonson, and J.L. Foster, 1975. Seasonal Streamflow Estimation Employing Satellite Snowcover Observations. Document X-913-75-26. pp. 34. Goddard Space Flight Center, Greenbelt, Maryland.
- Rango, A., and J.L. Foster, 1975. A Method for Improving the Location of the Snowline in Forested Areas Using Satellite Imagery. Document X-910-75-41. pp 8. Goddard Space Flight Center, Greenbelt, Maryland.
- Thomas, R.W., 1974. Approach to Remote Sensing-Aided Water Yield Estimation; Chapter 2(B), Section 2.100b; In An Integrated Study of Earth Resources in the State of California Using Remote Sensing Techniques; R.N. Colwell, Principal Investigator, Semi-annual Progress Report, NASA Grant NGL 05-003-404, December 1974, Space Sciences Laboratory, Series 16, Issue 2, University of California, Berkeley.

Thomas, R.W. and J.M. Sharp, 1974. A Comparative Cost-Effectiveness Analysis of Existing and LANDSAT-Aided Snow Water Content Estimation Systems; Chapter 6; In An Integrated Study of Earth Resources in the State of California Using Remote Sensing Techniques; R.N. Colwell, Principal Investigator, Semi-annual Progress Report, NASA Grant NGL 05-003-404, December 1974, Space Sciences Laboratory, Series 16, Issue 2, University of California, Berkeley.

Wiesnet, D.R., 1974. The Role of Satellites in Snow and Ice Measurements. In Advanced Concepts and Techniques in the Study of Snow and Ice Resources. pp 447. National Academy of Sciences. Monterey, California.

TABLE I

APRIL 4, 1973 LANDSAT-1
 AREAL EXTENT OF SNOW INTERPRETATION RESULTS
 (ALSO LISTING OF x_i 's AND y_i 's)

		Large Scale Photo Data				
		Snow Cover Classes				
		1	2	3	4	5
LANDSAT-1 Image Data	Snow Cover Classes	1	0 6	40 1		
		2	40 10		296 1	
		3	140 2	40 6	296 2	
		4		140 1	296 12	
		5			296 6	396 33

TABLE II
 May 10, 1973 LANDSAT-1
 AREAL EXTENT OF SNOW INTERPRETATION RESULTS
 (ALSO LISTING OF x_i 's AND y_i 's)

		Large Scale Photo Data				
		Snow Cover Classes				
		1	2	3	4	5
LANDSAT-1 Image Data	Snow Cover Classes	1	0 4	40 4		
		2	40 13	140 2		
		3	140 1	140 9	296 1	
		4		140 2	296 3	
		5			296 5	396 8

TABLE III

MAY 28, 1973 LANDSAT-1
AREAL EXTENT OF SNOW INTERPRETATION RESULTS
(ALSO LISTING OF x_i 's AND y_i 's)

Large Scale Photo Data					
Snow Cover Classes					
	1	2	3	4	5
	0	40			
1	0 3	0 4			
2	40 1	40 16	40 1	140	
3		40 2	140 9	140 3	296
4			140 2	296 4	296
5				396 4	296

	y_i
x_i	f

x_i = sample LANDSAT-1 estimate of the number of hectares of snow per cell by snow cover class = (snow cover class midpoint) (400 hectares).

y_i = sample large scale photo estimate of the number of hectares of snow per cell by snow cover class = (snow cover class midpoint) (400 hectares).

f = interpretation frequencies

TABLE IV

SUMMARY OF RESULTS
AREAL EXTENT OF SNOW ESTIMATION

		April 4, 1973	May 10, 1973	May 28, 1973
LANDSAT-1 estimate of the areal extent of snow	x	511,378	205,768	60,516
Estimate of the true areal extent of snow	\hat{Y}_R	501,355	195,644	57,847
Standard deviation of the areal extent of snow estimate	$\sqrt{V(Y_R)}$	12,776	14,526	17,126
Population ratio estimator	\hat{R}	.9804	.9509	.9559
Total number of acres inventories		879,642	813,014	798,340
Total number of image sample units inventories	N	2,218	2,050	2,013
Total number of image sample units sampled	n	80	52	49

TABLE V

CONFIDENCE INTERVAL AND ALLOWABLE ERROR STATEMENTS

AREAL EXTENT OF SNOW ESTIMATION

Level of confidence	April 4, 1973	May 10, 1973	May 28, 1973
	Confidence Interval	Confidence Interval	Confidence Interval
99%	$477,649 \leq Y_R \leq 545,107$	$166,897 \leq Y_R \leq 244,638$	$14,566 \leq Y_R \leq 106,466$
95%	$485,940 \leq Y_R \leq 536,816$	$176,601 \leq Y_R \leq 234,935$	$26,075 \leq Y_R \leq 94,958$
90%	$530,575 \leq Y_R \leq 532,651$	$181,423 \leq Y_R \leq 230,112$	$31,778 \leq Y_R \leq 89,242$
80%	$494,858 \leq Y_R \leq 527,898$	$186,899 \leq Y_R \leq 22,463$	$38,252 \leq Y_R \leq 82,781$



Figure I. April 4, 1973 LANDSAT-1 simulated color infrared enhancement. Image sample units (grids) = 400 hectares each.

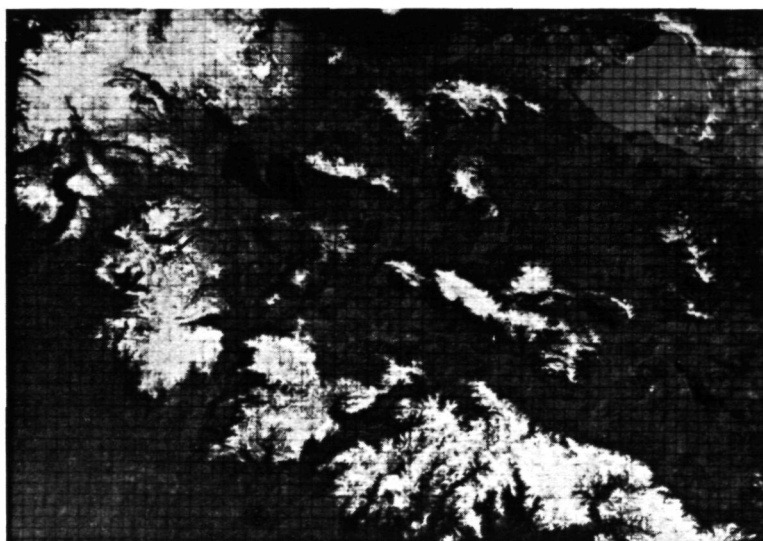


Figure II. May 10, 1973 LANDSAT-1 simulated color infrared enhancement. Image sample units (grids) = 400 hectares each.

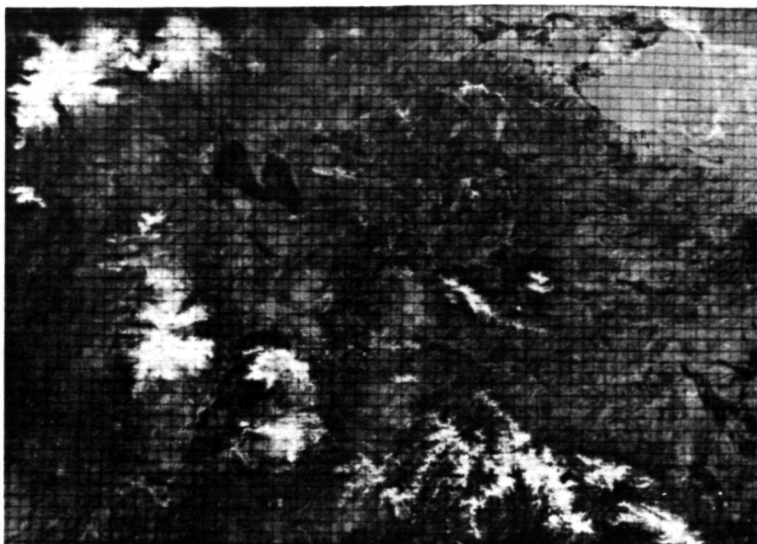


Figure III. May 28, 1973 LANDSAT-1 simulated color infrared enhancements. Image sample units (grids)= 400 hectares each.

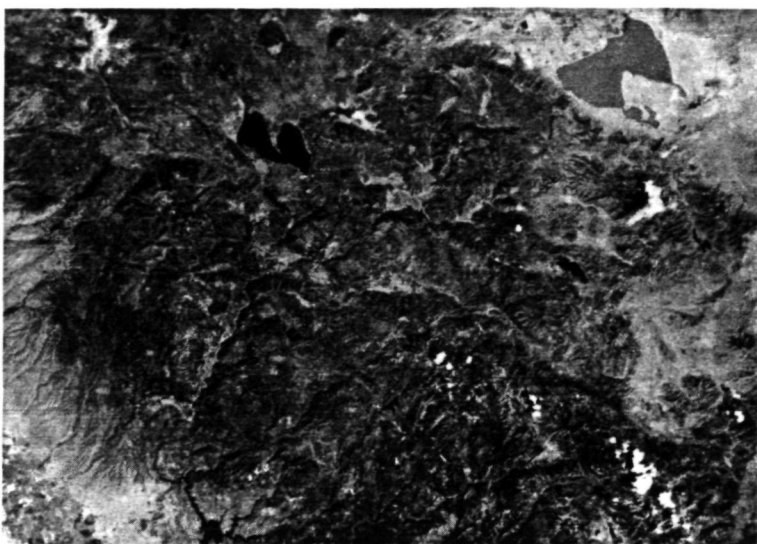


Figure IV. August 31, 1972 LANDSAT-1 simulated colored infrared enhancement. Cloud-free summer image.

REPRODUCIBILITY OF THE
ORIGINAL PAGE IS POOR

OPERATIONAL APPLICATIONS OF NOAA-VHRR IMAGERY IN ALASKA

R. D. Seifert, R. F. Carlson, D. L. Kane, *Institute of Water Resources, University of Alaska, Fairbanks, Alaska*

ABSTRACT

A discussion of near-real time operational applications of NOAA satellite enhanced thermal infrared imagery to snow monitoring for river flood forecasts, and a photographic overlay technique of imagery to enhance snowcover are presented. Ground truth comparisons show a thermal accuracy of $\pm 1^\circ\text{C}$ for detection of surface radiative temperatures. The application of NOAA imagery to flood mapping is also presented.

INTRODUCTION

In Alaska, snow is a fact of life for most of the state for at least 6 months of the year and, in the Arctic, it is present for 8 to 9 months. It is surprising, therefore, that more is not known about the snowcover at this stage of development. The facts are, however, that observation stations and snowcourses are sparse; the population is small; and what ground based data is present tends to be clustered around the larger population centers: Anchorage, Fairbanks, and Juneau. For this reason, the availability of daily synoptic NOAA - Very High Resolution Radiometer (VHRR) imagery was a welcome addition to the sparse data network of snowcover observations.

The NOAA series satellites are polar orbiting and sun-synchronous. The VHRR is only one of many sensors which are carried on board the satellite, but is the only one of interest for snow observations. Imagery is produced in the visible portion of the spectrum ($0.6 - 0.7 \mu\text{m}$) and in the thermal infrared ($10.5 - 12.5 \mu\text{m}$), hereinafter referred to as IR. Standard imagery is $1:8.5 \times 10^6$ scale and a single orbital pass can scan an area 1700 km wide and about 6000 km long. Consequently the entire state of Alaska can be monitored easily in two successive passes. No other satellite provides this frequency of coverage at Alaska's latitude. Resolution is 900 meters at nadir. The IR imagery can also be calibrated to display radiative surface temperatures to an accuracy of $\pm 1^\circ\text{C}$ (Barnes, *et al.*, 1974), and has been applied successfully to synoptic snowmelt monitoring.

Previous work on applications of NOAA-VHRR has centered mainly on snowmapping for water resource information or for scientific interest (Wiesnet, 1974; McGinnis, *et al.*, 1975; Rango, 1975; and Barnes, *et al.*, 1974; Barnes, *et al.*, 1974). Water contained in the snowpack is important as a source of summer water supplies for communities and irrigation and for aquifer recharge. Information obtained for these purposes can be integrated into timely resource allocation plans. In Alaska, however, applications of VHRR imagery are of a more expedient nature. Since few communities in Alaska rely on snowmelt information for water or irrigation, snowmapping is not usually necessary. Instead, snowmelt itself is the important factor because of the frequent flooding it causes. What is needed in Alaska is synoptic, near real-time imagery which clearly delineates the physical (thermal) state of the snowpack, allowing hydrologists to analyze the progress of snowmelt and the possibilities of flooding caused by rapid snowmelt and ice jams.

Since a data-link communication system exists between the U.S.W.S. Offices in Fairbanks, Anchorage, Juneau, and the data acquisition facility at Gilmore Creek (near Fairbanks), the ability to transmit imagery in near-real time is limited only by the necessity to calibrate an IR display. Calibration is necessary because of variability in the VHRR sensor on board the satellite. This problem was solved by programming the calibration functions on a small HP-65 calculator on site at Gilmore tracking station so that the necessary calibration time was only about twenty minutes. Consequently, calibrated IR displays could be sent to the Regional Hydrologist's Office in Anchorage and Fairbanks about two hours after they were acquired.

With snowmelt information as a first priority, an enhanced thermal IR display was felt to have the most value as an operational tool. The enhanced IR display was specially developed for hydrologic applications. Since the 0°C isotherm is the most significant feature during the spring snowmelt, this temperature was singled out for enhancement. After tests of a few display schemes, the following scheme was put into daily operational use:

I. Radiative temperatures from -20°C to just below freezing (-0.5°C) are displayed in an ascending gray scale. This means that any temperatures which are detected to be -20°C or colder are displayed as white, and temperatures intermediate between -20°C and -0.5°C are displayed in a shade of gray. The darker the grays, the warmer the temperatures, until at -0.5°C the display is black. This is essentially the same type of display used in a standard IR image, but the display has been adjusted to cover a much narrower band than usual (usually 185-315°K).

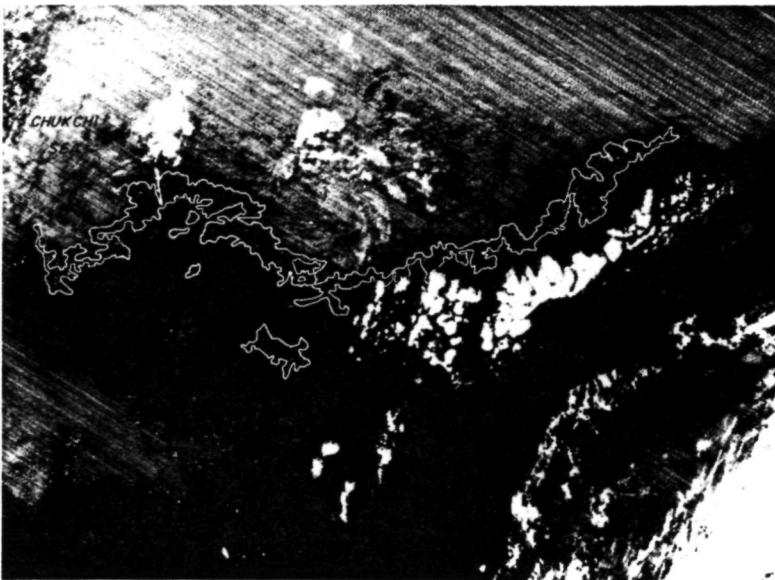
II. Next, the display was designed to enhance the areas at the freezing temperature by showing them as white. The abrupt change from black to white results in a clear depiction of the areas of melting and ripe snow. A range from 0 to +1°C is displayed as white, because if only 0°C is displayed as white the resolution of the satellite may not detect melting areas clearly, since the zone of melting snow may be very narrow or patchy, especially in mountainous areas. By displaying the 0°C to 1°C range as white, the display clearly shows the melting regions without adding much error. This is because surface temperatures rise rapidly once an area becomes snowfree, and the actual area which is snowfree and at 1°C is rather small. Essentially what results is a compromised, but very useful and informative snow-map. Melting snow can be seen in the imagery as a stippled white and black area instead of the expected continuous white region (Figure 1).

III. Finally, any areas with detected radiative temperatures equal to or greater than 2°C were displayed as black. This has two advantages; first it produces the same logical display as a visible image, since snowfree areas are always the darker areas in the visible band imagery. Secondly, it results in another abrupt change, this time from white to black to delineate those areas which are snowfree from those which are still at or just above the freezing temperature.

An example of this display scheme on June 4, 1975 is shown in Figure 1, along with the visible band image of the same general area, the Brooks Range and North Slope regions of Alaska. It should be pointed out that both images are always more useful and have more information content when used together. In the thermal IR, the sensor is essentially viewing a field of "glowing" objects and, since normal visual images are not analogous, orientation is extremely difficult using just the IR imagery. By comparing the visible with the IR, considerable additional information is gained. In the example for June 4 (Figure 1) the stippled white area (0 to +1°C) in the enhanced IR image clearly shows the area of melting snow lying in a band across the entire region with still frozen snow to the north and snowfree conditions to the south. A unique situation exists here also, since the snowfree areas are generally at a higher elevation than most of the remaining snowcover. Snowmelt on Alaska's North Slope initiates in the middle elevations (600-900 m) and proceeds in both directions, with the highest peaks and the lowest coastal areas the last to melt. When comparing this "band" of ripe and melting snow with the visible image, it is evident that it corresponds closely to the edge of the snowcover. A limitation of the IR imagery is also shown because the presence of low stratus cloud cover on the coastal plain obscures the snow cover in the IR. The visible imagery shows that a large, open, sea-ice lead is present off the northwest coast and the IR imagery shows that



a)



b)

JUNE 4, 1975 , ORBIT No.2519, NOAA -4-VHRR

a) Vis. Enlargement

b) Enhanced I.R. Enlargement

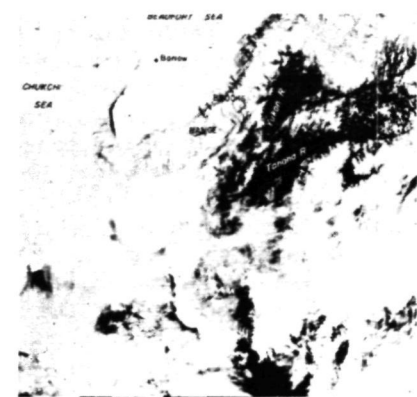
Figure 1

146
REPRODUCTION OF THE
ORIGINAL PAGE IS POOR

it is isothermal with the stratus cloud cover. Water can be seen flowing out over the shorefast sea ice (ice frozen to the shore) at the mouths of the Colville, Sagavanirktok, and Kuparuk Rivers. This is also a unique feature of Arctic rivers. It is due to the pattern of snowmelt and the presence of shorefast ice. Because the coastal plain and shorefast ice are still frozen and snow-covered when runoff begins to flow down the river channels, some of the water simply continues out over the channel ice and shorefast ice at the mouths, flooding large areas of the sea ice.

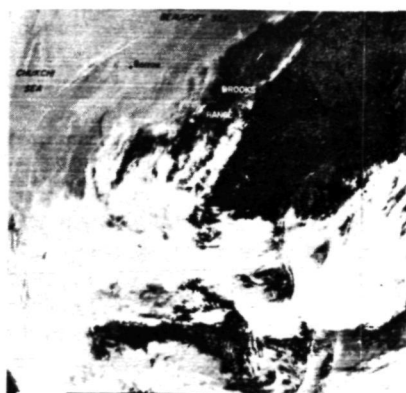
Fortunately, there were some extreme weather conditions this spring which permitted tests of the response of the enhanced imagery. On May 10 and 11, 1975, record high temperatures of 27°C (80°F) and 26°C (79°F) respectively, were recorded at the Fairbanks WSO and record high temperatures were experienced generally throughout the Tanana and Yukon Valleys. This was also the mid-point of the snowmelt period and consequently snowmelt was rapidly accelerated. Figure 2 shows a series of images, the visible and IR images from May 10, and the same images for May 13. A comparison of the enhanced IR images of both days shows some striking changes and discrepancies. In fact, the first impression is that the snow cover has increased, even though no precipitation fell during the four-day period. The weather on May 13 was generally cooler (10 - 15°C) and moderately strong winds (16 - 20 km/hr) were recorded at most of the interior Alaska weather stations. Interpretation is further confused in that comparisons of both days' visible images with the enhanced IR images shows discrepancies both days between indicated snow cover in each type of imagery.

The worst 1975 case of discrepancy of the imagery is presented here in order to show the dependence of interpretation on surface weather conditions. Under conditions of very high surface temperatures the imagery will indicate greater snowmelt than is actually present. This is probably the result of advection of warm air over the melting snow areas and the integrated thermal effect of warm air and emergent vegetation warmed by the air and sun over the remaining snow cover, causing it to appear "thermally snowfree." The opposite effect occurs on windy, lightly cloudy days, as air movement obliterates any surface heating and low light cloud cover lowers the radiative temperature. There may be other, subtler effects as well, but a theoretical analysis will not be attempted in this paper. The important point is that interpretation of the enhanced IR imagery must be tempered with the synoptic context of surface weather conditions and use of visible, standard IR, and enhanced IR imagery. This will enable an operational river forecaster to give his forecast with more confidence in lieu of the limitations inherent in the enhanced IR imagery.



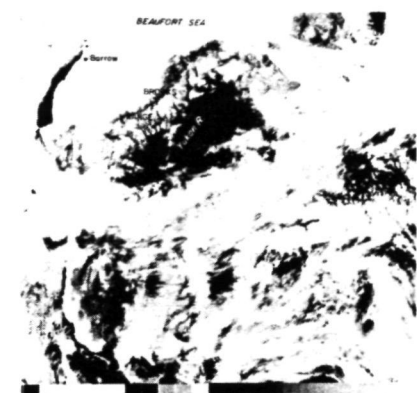
21:07:16 2206 V2F2276 10MAY75 N4 13S 01E

a) 10 MAY VIS.



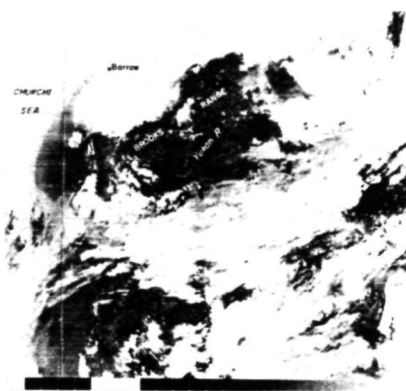
21:07:10 2206 12F2238 10MAY75 N4 13S 01E

10 MAY I.R.



133:20:03:01 2243 V2F2276 13MAY75 N4 12S

b) 13 MAY VIS.



GIL 133:20:02:56 2243 12F2238 13MAY75 N4 12

13 MAY I.R.

A COMPARISON OF THERMAL I.R. ENHANCEMENTS UNDER DIFFERENT SURFACE CONDITIONS:

- a) May 10, 1975, Record High Temperatures Which Induced Flood Warnings
- b) May 13, 1975, Strong Winds

Figure 2 - These examples show the possibility for errors in interpreting enhanced IR imagery if it is not used with the visible and standard IR images. Measurements of the snowfree areas centered around the Yukon River on the two days shown indicated 27% less snowfree area on 13 May than had been measured three days earlier.

REPRODUCIBILITY OF THE
ORIGINAL PAGE IS POOR

GROUND TRUTH TEST

A test of the imagery was made with ground truth water temperature measurements made in the Yukon River at various villages in the interior of Alaska. These measurements are taken by village residents with U.S.W.S. equipment. The comparisons are tabulated in Table 1.

TABLE 1

COMPARISONS OF SATELLITE VHRR-IR MEASUREMENTS
WITH YUKON RIVER WATER TEMPERATURE MEASUREMENTS

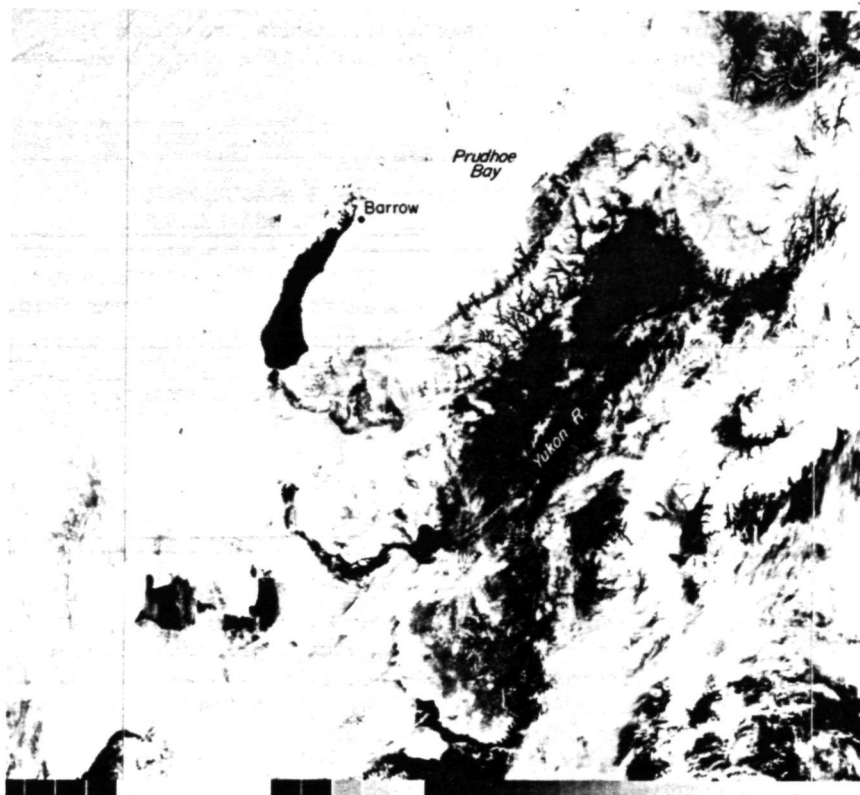
Location of River Temp. Meas.	Date	Thermal IR "Temp."	*Measured
		Measured From Enhanced VHRR Imagery	River Temp.
Beaver, Alaska	14 May	0-1°C	1.7°C
Eagle, Alaska	16 May	>2°C	2.2°C
Circle, Alaska	16 May	0-1°C	1.7°C
Beaver, Alaska	16 May	0-1°C	1.1°C
Beaver, Alaska	19 May	0-2°C	1.7°C
(Stippled & Black)			

*Courtesy of U.S.W.S. Regional Hydrologists Office.

The temperatures compare closely with a maximum difference of 0.7°C. This confirms the stated accuracy of NOAA thermal IR imagery of $\pm 1^\circ\text{C}$ (Barnes, *et al.*, 1974b). When temperatures rose above 2°C (36°F), the calibrated IR could no longer differentiate temperatures because the display scheme was designed to show all temperatures above 2°C as black.

ADDITIONAL APPLICATIONS

Another opportunity to provide snowcover information in a synoptic form is available through the technique of photographic combination of the visible and enhanced IR images. By overlaying one image negative on top of the other and aligning them, a print can be made of an entire frame of the imagery which enhances snow cover (Figures 3, 4, and 5). Since an IR enhancement is used, areas which are "thermally snowfree" will be displayed as black, similar to the visible imagery. Terrain shadowing effects can be somewhat eliminated by this technique because the IR temperatures will cause them to be displayed as white, i.e. snowcovered, when they might be displayed dark in the visible imagery. Because this process uses negatives, snow cover is always retained and enhanced in the image, because its image density in the enhanced IR will be greater than, for instance, the density of a corresponding shadowed area. This also means

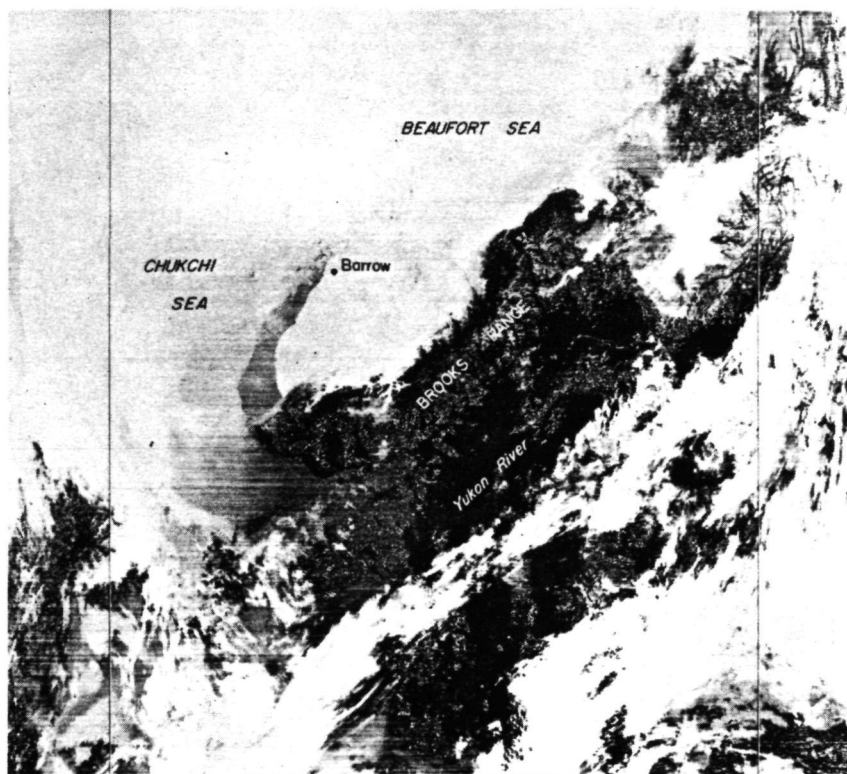


GIL 134:20:57:12 2256 V2F2276 14MAY75 N4 13S 04E

MAY 14, 1975

Figure 3 - An exceptionally clear day during the snow melt period, and nearly the entire state is visible. The negative of this standard visible band image was overlain on the negative of the enhanced IR image (Figure 4) to produce the print shown in Figure 5.

REPRODUCIBILITY OF THE
ORIGINAL PAGE IS POOR



GIL 134:20:57:06 2256 I2F2238 14MAY75 N4 13S 04E

MAY 14, 1975

Figure 4 - This enhanced IR image was used in producing the overlay print shown in Figure 5. Note the stippled white areas indicating melting or ripe snow. Nearly the entire Brooks Range is in this condition. The Yukon River is also visible because it is at or near the 0-1°C temperature range. A water temperature measurement at the village of Beaver was made this same day, and the measured temperature was 1.7°C.

REPRODUCIBILITY OF THE
ORIGINAL PAGE IS POOR



MAY 14, 1975, ORBIT No.2256

AN OVERLAY PRINT USING BOTH THE VISIBLE
IMAGE NEGATIVE & THE ENHANCED I.R. NEGATIVE

Figure 5 - This overlay technique enhances marginally snow
covered areas, and may eliminate some problems of shadowing
that often effects visible imagery.

REPRODUCIBILITY OF THE
ORIGINAL PAGE IS POOR

that marginally snowcovered (patchy) areas are enhanced, because they are more likely to be at the freezing temperature and thus displayed as white. Some shadowed areas may be displayed as dark in the enhanced IR as well because they are just below the freezing temperature. This problem could be remedied by expanding the enhanced IR display scheme to display a wider temperature range in white. This was not attempted in Alaska, however, because it would eliminate detection of "ripe" snow, which, in Alaska, is a more important factor. In snow surveys where detection of melting snow is not critical, this technique could prove very useful.

The overlay technique is not operational in real time because the images can only be produced photographically at present. This is not a limitation for water resource inventories however, and the possibility exists for daily or weekly snow cover overlay images which could be made available a day or two after initial acquisition.

Snowmelt runoff is responsible for many floods in Alaska and, during the river break-up, ice jams can cause rapid and unpredictable rises in water levels both when they form and again when they break. Two floods caused by ice jams were observed in the standard IR imagery and in the enhanced IR during the river breakup. Both were on the Yukon River and both flooded areas were greater than 2500 km². The first flood occurred near Holy Cross, Alaska, a Yukon River village, on May 24, 1975. It is depicted best on the regular IR imagery, and an enlargement showing the flooded area is shown in Figure 6. The flooded area was measured with a polar compensating planimeter and found to be 2590 km² ±5%. Just as a comparison, this is more than 5 times the surface area of Lake Tahoe. NOAA imagery provided the only areal measurement available for this flood.

A second flood caused by ice jams occurred May 29, 1975, in the Yukon Delta. The flooded area was also measured with a planimeter and found to be 2710 km² ±5%. A comparison of the mapping accuracy is pending in lieu of receipt of a LANDSAT image made of this area on the same date.

CONCLUDING REMARKS

NOAA VHRR imagery has demonstrated its utility for daily synoptic, near-real time snowmelt information. By using all the available VHRR imagery (visible, IR, and enhanced IR), reliable and timely supplemental river forecast information is available by 3 p.m. each day. Ground truth comparisons are very encouraging and more will be sought. A NOAA satellite field service station is to become operational in November of this year and tests and developments will continue as new data needs and uses evolve.

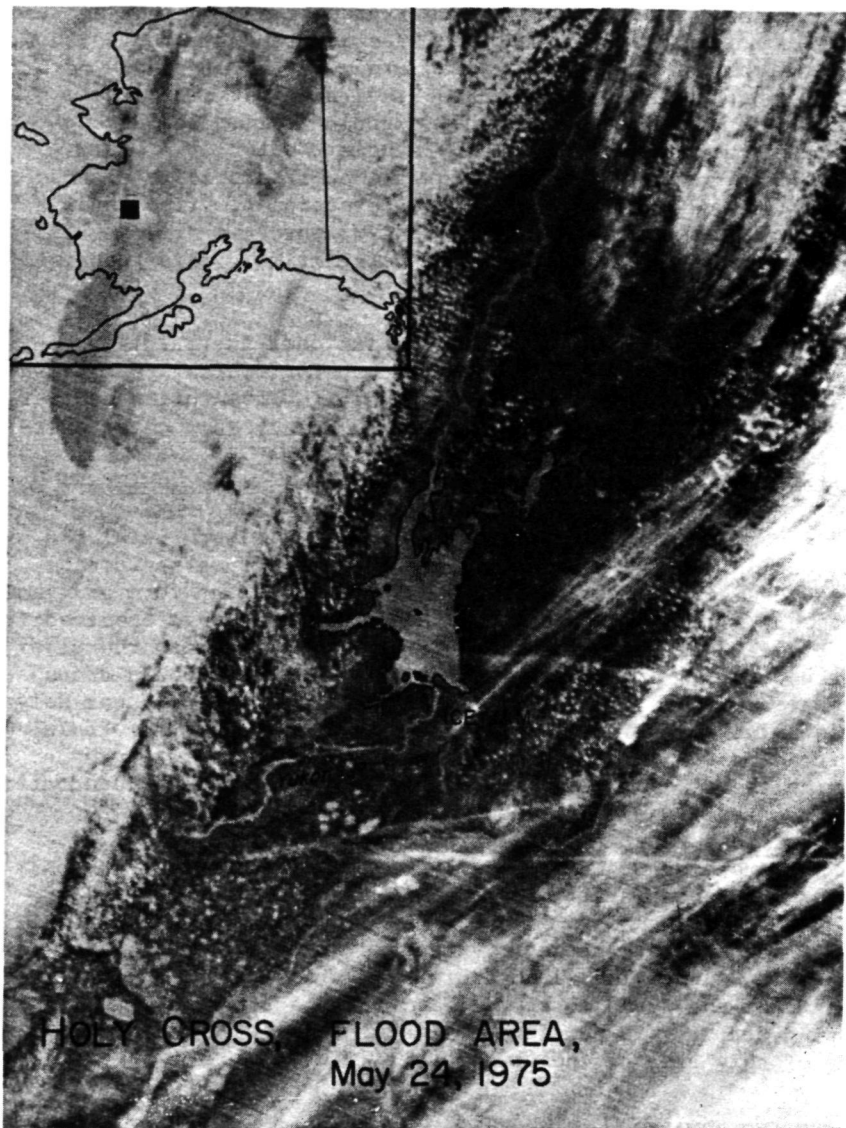


Figure 6 - An enlargement of a standard IR image demonstrating the ability of the VHRR to detect flooded areas. This flood was measured using a polar compensating planimeter and found to be 2590 km² in area. This is more than five times the surface area of Lake Tahoe (499 km²).

REPRODUCIBILITY OF THE
ORIGINAL PAGE IS POOR
154

ACKNOWLEDGEMENT

This work was accomplished under the Alaska Pilot Project grant from the National Oceanic and Atmospheric Administration (NOAA), National Environmental Satellite Service (NESS).

REFERENCES

- Barnes, J. C.; Bowley, C. L.; and Simmes, D. A. (1974). The application of ERTS Imagery to Mapping Snow Cover in the Western United States. NASA ERT Document 9407-F, NASA GSFC, Greenbelt, Md., January.
- Barnes, J. C.; Bowley, C. J.; Cogan, J. L. (1974). Snow Mapping Applications of Thermal Infrared Data. NOAA VHRR, NASA-ERT Doc. No. 0438-F, NASA-GSFC, Greenbelt, Md., November.
- Holmgren, B.; Benson, C.; and Weller, G. (1973). A Study of the Breakup on the Arctic Slope of Alaska by Ground, Air, and Satellite Observations. IN: *Climate of the Arctic, Proceedings of the 24th Alaska Science Conference*, Fairbanks, Alaska, Aug. 15-17, pp. 358-366.
- McGinnis, D. F.; Pritchard, J. A.; and Wiesnet, D. R. (1975). Snow Depth and Snow Extent Using VHRR Data from the NOAA-2 Satellite. NOAA Tech. Memo NESS 63, Dept. of Commerce, NOAA-NESS, Wash., D.C., February.
- Rango, A. (1975). Applications of Remote Sensing to Watershed Management. NASA-GSFC, Technical Info. Div. Code 250 GSFC, Greenbelt, Md. 20771.
- Wiesnet, D. R. (1974). The Role of Satellites in Snow and Ice Measurements. NOAA Tech. Memo 58, Dept. of Commerce, NOAA-NESS, Wash., D.C., August.

EMPLOYMENT OF SATELLITE SNOWCOVER OBSERVATIONS FOR IMPROVING SEASONAL RUNOFF ESTIMATES

A. Rango and V. V. Salomonson, *NASA/Goddard Space Flight Center, Greenbelt, Maryland*,
and J. L. Foster, *Geology Department/University of Maryland, College Park, Maryland*

ABSTRACT

Low resolution meteorological satellite and high resolution earth resources satellite data have been used to map snow-covered area over the upper Indus River and the Wind River Mountains of Wyoming, respectively. For the Indus River early Spring snowcovered area was extracted and related to April through June streamflow from 1967-1971 using a regression equation ($r^2 = 0.91$). Prediction of the April-June 1972 streamflow from the satellite data was within three percent of the actual total. Composited results from two years of data over seven Wind River Mountain watersheds indicated that LANDSAT-1 snowcover observations, separated on the basis of watershed elevation, could also be related to runoff in significant regression equations. It appears that earth resources satellite data will be useful in assisting in the prediction of seasonal streamflow for various water resources applications, non hazardous collection of snow data from restricted-access areas, and in hydrologic modeling of snowmelt runoff.

INTRODUCTION

The melting of the snowpack in the Spring is the source of greater than 50 percent of streamflow in most areas of the Western United States (Committee on Polar Research, 1970 and Rooney, 1969). For example, about 75 percent of the runoff in the Colorado River originates from snowmelt in key basins that represent only 13 percent of the contributing land area (U.S. Department of Interior, 1970). The early prediction of the amount of runoff to be derived from the snowpack allows more efficient utilization of the limited water supply for power generation, irrigation, flood control, domestic and industrial water supplies, and recreation. Historically, the Soil Conservation Service has prepared seasonal snowmelt runoff forecasts for western river basins that have been extremely useful for water management purposes. For the Western United States, error in seasonal runoff forecasts prepared on 1 April ranges from 7 to 40 percent, with an average of approximately 18 percent (U.S. Department of Interior, 1974).

These discrepancies are due to forecasting errors inherent in the procedures used and to errors resulting from variations in the weather after 1 April. The forecasting errors result from uncertainties in point measurements of snow water equivalent which are commonly used as indices of basinwide snowmelt runoff in prediction equations. The errors in predicted runoff tend to be largest in years of unusually heavy or light snowpack accumulation.

Observations of the areal extent of the snowpack has long been recognized as an important (but difficult to obtain) hydrologic parameter related to both the average snowpack water equivalent and the snowmelt-derived runoff. The U.S. Army Corps of Engineers (USACE) in the Northwest and the Salt River Project in Arizona have in the past flown low altitude missions in order to measure snowcover areal extent to aid in their runoff prediction responsibilities. The rate at which the snowcover depletes is an index which is inversely related to the snow water equivalent and the generated snowmelt runoff. As the snow leaves the low elevations of the watershed, the hydrograph begins to rise and continues to do so until the snowpack area reaches a critical value where meteorological snowmelt conditions cannot produce ever increasing amounts of runoff. The hydrograph then begins to recede until the remaining snowpack disappears and the runoff is maintained by baseflow. The slower the snowline retreats up the watershed to the elevation where the hydrograph starts a downward trend, the greater the resulting runoff volume and, usually, peak flow.

Although high resolution, temporal areal snowcover data are important, it has been difficult for various user agencies to obtain these data on a regular basis. As a consequence very few runoff prediction techniques are compatible with snowcovered area inputs. Since 1972, however, satellites possessing relatively high resolution sensors have been regularly observing snowcovered area. LANDSAT-1 (previously known as ERTS-1) has been providing 80 m resolution, multispectral visible and near infrared observations over a 185 km x 185 km area as often as once every 18 days since July 1972. LANDSAT-2 has been providing similar data since its launch in January 1975. The currently operating two satellite system effectively provides once every 9 day coverage over a given area. NOAA-2 (3 and 4) has provided daily visible and thermal infrared observations, but with a resolution of about 1 km. The work reported on here using small watersheds has used data from LANDSAT-1 only.

The purpose of this study was to examine the possibilities of seasonal streamflow estimation employing satellite snowcover observations, both from existing long term, low resolution meteorological satellite data and from the newly available high resolution multispectral satellite information. There are various reasons why satellite snowcover data, if proved effective, would be desired by water resources agencies in preference to aircraft or ground derived data. Fatal accidents have occurred during both ground-based and aerial snow surveys, and, as a result, the

safety factor would optimumly increase with unmanned space surveys. Wiesnet and McGinnis (1974) have shown that snow extent mapping is both six times faster from LANDSAT-1 imagery than from high altitude aerial photographic surveys, and that the cost of snow maps produced from LANDSAT-1 is about one-two hundredth the cost of the simplest maps made from aircraft surveys. In addition, the procedures for mapping snow-cover from space and its excellent comparison with conventionally derived snowcover maps have been documented by many investigators. Such techniques and results have been compiled in handbook form by Barnes and Bowley (1974). Ground-based snow observations are gradually being restricted in mountainous areas as a result of marked increases in wilderness areas developed under the 1964 Wilderness Act (Brown, 1974). Because these areas are continually increasing and accessibility to high alpine snowpack areas is continually decreasing, satellite observations may be the way to serve both the environmentalist's and the snow surveyor's objectives. Even in nonrestricted areas snow data are difficult to obtain from remote regions and often too few and perhaps unrepresentative samples are available. Remote sensing provides a reasonable way to monitor snow in these remote regions, and the data may even eventually be used to extrapolate conventional point data more effectively over entire watersheds. Finally, some watershed numerical models are beginning to require the input of the observed snowcovered area (U.S. Army Engineer Division, 1972). Satellite derived snowcover seems to be a logical source for satisfying such requirements in the future.

Even though it has been shown that snow extent can be accurately measured from LANDSAT-1 imagery (Barnes, Bowley, and Simmes, 1974), there has been some question about usefulness in terms of predicting snowpack yield or seasonal runoff in view of the fact that only the area covered by snow, and not snow depth or water equivalent, is observed. This is true of all visible, near infrared, or thermal infrared sensors, no matter what their resolutions. Only two years of snowcover versus runoff information exist for LANDSAT-1 (or NOAA-2), and this is generally not a sufficient number of observations to indicate the validity of any empirical statistical relationship that might appear to exist between snowcovered area and runoff. As a result, longer duration data than presently exists for LANDSAT-1 had to be obtained.

Using the Image Dissector Camera System on Nimbus 3 and 4, Salomonson and MacLeod (1972) mapped the areal extent of snowcover over the Indus River Basin in the Western Himalayas. The areal extent of snowcover for 1969 and 1970 was plotted so as to relate a decrease in the snowcover to an increase in the mean monthly runoff. The results by Salomonson and MacLeod (1972) indicated that some success might be achieved in predicting the seasonal runoff volume or the level of peak discharge if the snow areal extent and location of the snowline in late winter or early spring were monitored by satellite. Because several years of meteorological satellite data now exist, this research has been extended

to cover six years of snowcover versus runoff and to test whether an empirical relationship of statistical significance was evident. Additionally, LANDSAT-1 data have been used over seven watersheds in the Wind River Mountains of Wyoming to determine if any of the relations prevalent on the Indus River might similarly exist on relatively small watersheds.

STUDY AREAS AND DATA SOURCES

The Indus River Basin above Attock, Pakistan covers approximately 260,000 km² with elevations ranging from 305 m at the streamgage (IHD Station HD-23) to over 8,500 m in the Hindu Kush, Karakoram, and Himalayan Mountains. Portions of the basin are located in Pakistan, Afghanistan, India, and China. At the time of the study, no major diversions for water resources projects occurred above the streamgage thus making the recorded flow indicative of the snowmelt runoff. Watersheds this large without significant flow diversions do not exist in the United States. Streamflow data were received from the Pakistan Water and Power Development Authority from 1967-1972. The 4 km resolution Advanced Vidicon System on various ESSA satellites provided coverage for the years 1967-1972, and similar resolution Scanning Radiometer data from NOAA satellites are available for 1973 and 1974. One of the world's largest reservoirs, the Tarbela Dam, is being constructed 64 km above the gage at Attock and may affect flow measurements as early as 1973.

The Wind River Mountains are located in west central Wyoming and range in elevation from 2000-5000 m. Two major rivers rise out of the Wind River Range, namely, the Green and Wind Rivers, and flow diversions for irrigation are numerous; only in the extreme headwaters or on small tributary streams do relatively unimpaired records exist. Seven such small watersheds were selected ranging in area from 200 km² to 1200 km². Preliminary streamflow records for 1973 and 1974 were supplied by the U.S. Geological Survey for the seven streamgages. Eighty meter resolution LANDSAT-1 multispectral scanner data in the 0.5-0.6, 0.6-0.7, 0.7-0.8, and 0.8-1.1 μ m wavelength bands were available from July 1972 to the present. Additional data included high altitude U-2 color infrared photography over the watersheds in 1974 and U.S. Soil Conservation Service ground snow survey measurements for 1973 and 1974.

METHODS

Images over the Indus River Basin from April through July were selected from 35 mm microfilm rolls of available ESSA and NOAA satellite data. The data were scanned on a daily basis and approximately one clear image per week over the Indus Basin was selected and made into a 35 mm positive slide. The 35 mm slides were projected onto a 1:2,000,000 scale aeronautical chart of the basin and the scale of the image adjusted using a zoom lens to fit the chart. The amount of snowcover was then mapped

from the chart onto a transparent overlay and the percent of snowcovered area calculated with a planimeter. Due to a lack of detail on maps of this scale and the large size of the basin, the snowline altitude was not calculated for the Indus Basin.

The areal extent or percent of snowcover for the entire season can be plotted so as to relate a decrease in snowcover to an increase in weekly or monthly runoff. In order to better simulate a prediction situation, however, percent snowcover area from satellite images between 1-15 April of each year were averaged and plotted against the seasonal runoff occurring from 1 April to 30 June. A regression equation for the years 1967-1971 was developed initially. When the 1972 snowcover data was obtained, the regression equation was used to predict the seasonal streamflow. Subsequently, the 1972 snowcover and runoff data were incorporated into the regression relation.

LANDSAT-1 imagery was obtained for each pass over the Wind River Mountain watersheds for 1973 and 1974 in the standard photographic, single-band 1:1,000,000 scale positive transparency format. Generally, only the 0.6-0.7 and 0.8-1.1 μ m black and white transparencies were used for snowcover area extraction. The snow was mapped using the LANDSAT-1 transparencies, U.S. Geological Survey 1:250,000 scale topographic maps, and a zoom transfer scope. The zoom transfer scope with its mirrors, lenses, and scale adjustments allowed the 1:1,000,000 scale image to be superimposed optically onto the map so that drainage areas could be delineated and snowlines mapped at a scale of 1:250,000.

Once the snowline was located, the percent and area of snowcover within a given watershed was calculated with the aid of a planimeter. The snowline altitude, if desired, could be determined by using the Equivalent Snowline Altitude (ESA) method (Meier, 1973). The ESA method is based on an area-altitude function whereby for a given mountainous drainage basin, the percent of area above various elevation contours is planimetered and the percent of basin area is plotted against the corresponding elevation. Thus, when the percent of snowcovered area is measured, the elevation of the snowline can be obtained by referring to the ESA function for that particular basin.

Next, the average snowcover area depletion for all seven Wind River Mountain watersheds was plotted and graphically related to increasing runoff for 1973 and 1974 separately. Additionally, the same data were separated into two groups of watersheds based on mean elevation and replotted in the same way. Subsequently, the percent snowcovered area on 15 May in 1973 and 1974 for each watershed was plotted versus the 15 May-31 July seasonal runoff for the high elevation watersheds (6 data points) and the low elevation watersheds (8 data points). A regression analysis was performed on these two data sets assuming that the watersheds within each elevation group were very similar in all respects. Factors that could contribute to the total regression variance, however, were recognized as differences in watershed shape, percentage of forest cover, and mesoscale

meteorology and climatology. In order to account for variations in watershed size and subsequent runoff, the streamflow data were converted to discharge per unit area values.

LANDSAT-1 snow mapping was facilitated by examining false color composites employing 0.5-0.6, 0.6-0.7, and 0.8-1.1 μ m data taken during the summer so that forested and bare rock areas could be located and positioned. The 0.6-0.7 μ m band was used to obtain snowcover area measurements for the runoff relations, and snow extent measurements using the 0.8-1.1 μ m band were compared to the 0.6-0.7 μ m band area measurements in order to estimate areas of metamorphosed snow, i.e., snow either actively undergoing melt or snow that had been melting the previous day but was refrozen at the time of satellite over pass. Rationale for this assumption is provided by H. W. O'Brien and R. H. Munis (unpublished data, 1974). Finally, high resolution U-2 aircraft data for 1974 over three of the watersheds was areally compared to snowcover areas obtained from temporally similar LANDSAT-1 passes. It was felt that the U-2 information was the best alternative snowcovered area data source available for use in this study.

RESULTS AND DISCUSSION

Figure 1 presents an example of the annual variation in snowcover at the beginning of April over the Indus River Basin as observed from ESSA 9. Early April was chosen as the beginning of significant snowmelt and the index time for predicting the April-June seasonal runoff. Figure 1 shows that on 4 April 1969 the snowcover was heavy and covered 60 percent of the basin. Resulting seasonal runoff was about 29.6 million acre-feet ($3.65 \times 10^{10} \text{ m}^3$). On 3 April 1971, however, the snowcovered area was 44 percent and the subsequent seasonal runoff totalled approximately 25 million acre-feet ($3.08 \times 10^{10} \text{ m}^3$). The scenes shown in Figure 1 were indicative of the 2-3 scenes that were averaged between 1-15 April of 1967-1971, and the snowcover area mapping was easily accomplished.

The 1967-1971 average percent basin snowcover for 1-15 April was then plotted against the 1 April - 30 June corresponding measured runoff in acre-feet (m^3) and a straight line relationship was evident. A significant linear regression equation was derived using these points which took the form $R = (0.288S + 11.98) \times 10^6$ where R is the April to June yield in acre feet and S is the percent basin snowcovered. The coefficient of determination, r^2 , for this equation is 0.91 (significant at the one percent level) and the standard error was 5 percent of the mean seasonal yield. When the 1972 satellite snowcover data became available, the above regression equation was used to predict the April-June 1972 seasonal runoff. The satellite-measured 1-15 April average snowcover was 67.3 percent and the predicted April - June yield was 31.5 million acre-feet ($3.88 \times 10^{10} \text{ m}^3$). When the 1972 streamgauge records were obtained, the actual April-June yield was determined to be 32.3 million acre-feet

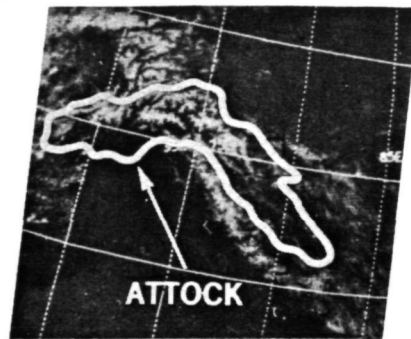
4 APRIL 1969



SNOWCOVERED AREA = 60%

APRIL—JUNE RUNOFF =
29,590,000 ACRE—FEET

3 APRIL 1971



SNOWCOVERED AREA = 44%

APRIL—JUNE RUNOFF =
24,990,000 ACRE—FEET

Fig. 1—ESSA 9 observations of the annual variation in snowcovered area at the beginning of snowmelt in the Indus River Basin above Attock, Pakistan.

($3.98 \times 10^{10} \text{ m}^3$). The difference between predicted and actual yield was only 0.86 million acre-feet ($1.06 \times 10^9 \text{ m}^3$) or within three percent of the actual seasonal yield. Figure 2 shows the 1967–1972 snowcover versus seasonal yield data plotted and a new regression line obtained by incorporating the 1972 data into the relation. The new equation is $R = (0.300S + 11.52) \times 10^6$ with r^2 being 0.92 (significant at the one percent level) and the standard error again equalling 5 percent of the mean seasonal yield.

These results indicate that even though snow depth or water equivalent are not directly measured, it appears that areal snow extent is an adequate index parameter for aiding in the prediction of seasonal runoff on a large data-sparse watershed. Because watersheds of this size and relatively undisturbed nature are not commonly found in areas such as the United States, the same kind of test was applied to several very small watersheds in Wyoming using the high resolution LANDSAT-1 data.

Figure 3 is a $0.6\text{--}0.7\mu\text{m}$ view of the Wind River Mountains taken in August 1972 which delineates the seven watersheds selected for analysis. The Green, Pine, East Fork, and Big Sandy watersheds are in the Colorado River Basin, whereas Bull Lake, Dinwoody, and Wind are in the Missouri River Basin. More importantly, for this analysis, Wind River, Green River, East Fork River, and Big Sandy River were grouped as low watersheds with mean elevations less than 3050 m. Bull Lake Creek, Dinwoody Creek, and Pine Creek all had mean elevations in excess of 3050 m and were grouped as high watersheds. The smallest watershed under study was Pine Creek (200 km^2) and the largest was Green River (1200 km^2).

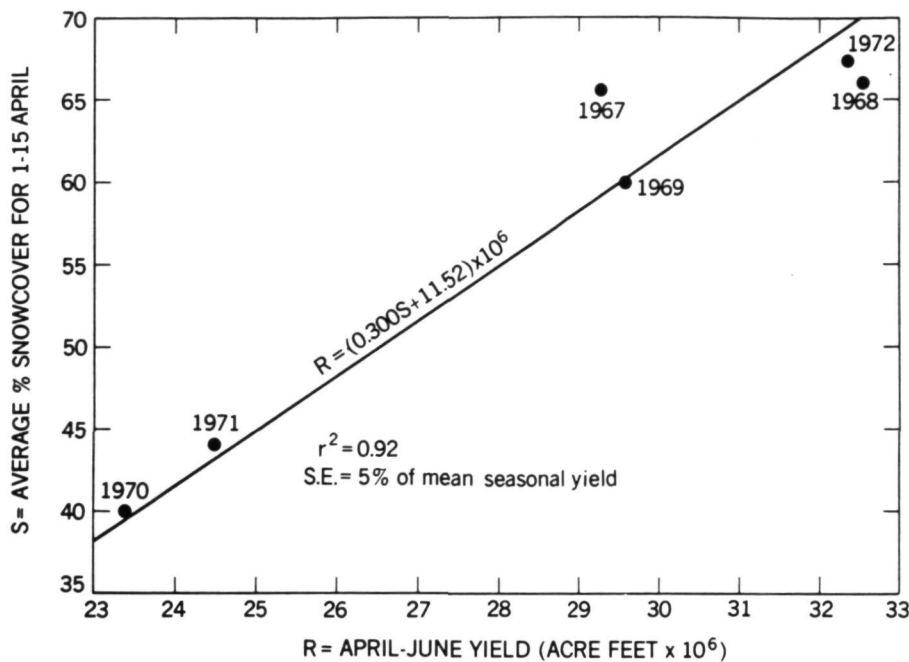


Fig. 2—Satellite-derived snowcover estimates versus measured runoff for the Indus River, 1967-1972.

As an example of the kind of snowcover changes observed during the course of a year with LANDSAT-1, Figure 4 presents four 0.6-0.7 μ m views of the Wind River Mountains during the 1972-1973 snow season. The 6 August scene shows bare rock, late-lying alpine snow, and glaciers above the tree line during minimum snowcover. The 10 December scene illustrates total snowcover over the entire area with the darker tones indicating areas of forest cover over the snowpack. The 21 May and 8 June scenes are taken during the active snowmelt season and display the kind of changes detectable from one LANDSAT-1 pass to the next. To illustrate, in the 21 May scene Bull Lake Creek and Green River are 86 and 55 percent snowcovered, respectively. Because of persistent snowmelt during the 18 day interval between satellite passes, 8 June snowcover has decreased to 58 percent for Bull Lake Creek and 27 percent for Green River. Such clear imagery was common during the melt season, and only in a few instances was a particular watershed obscured by clouds during a LANDSAT-1 overpass in 1973 and 1974.

Comparison of LANDSAT-1 images on similar dates in 1973 and 1974 indicates that generally more snowcover exists in 1974 than 1973. Stream-gage records show that more runoff occurred during the 1974 snowmelt

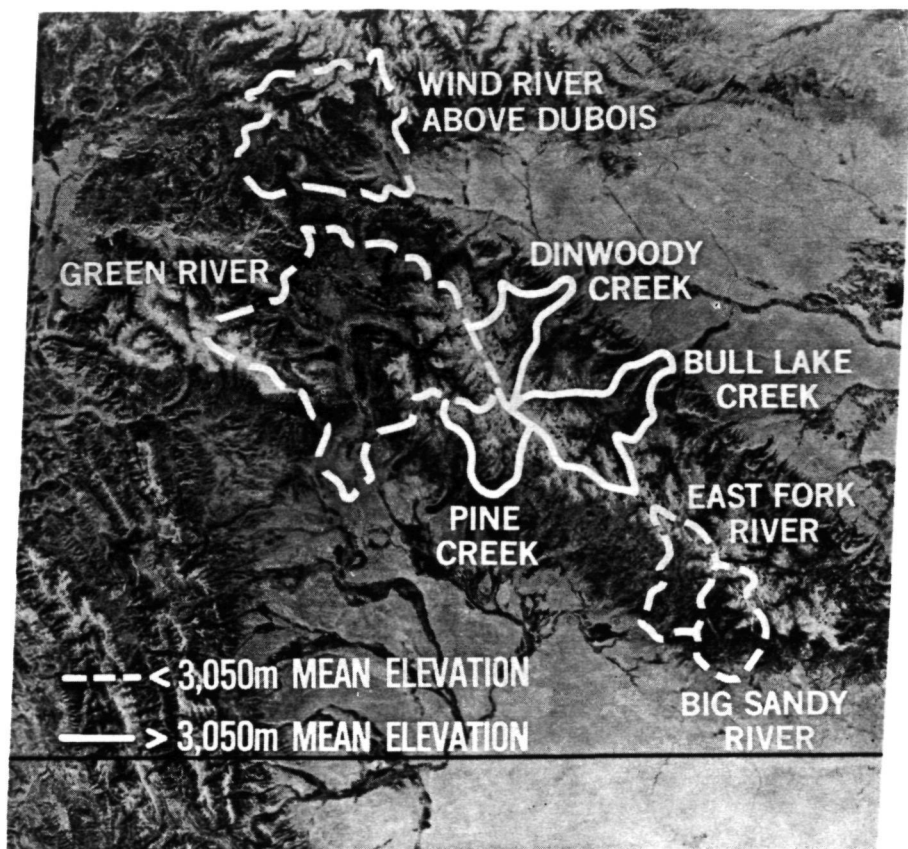


Fig. 3—LANDSAT-1 0.6-0.7 μ m view of the Wind River Mountains of Wyoming, 6 August 1972. The boundaries of the seven watersheds used in the LANDSAT-1 snowcover depletion-runoff analysis are indicated.

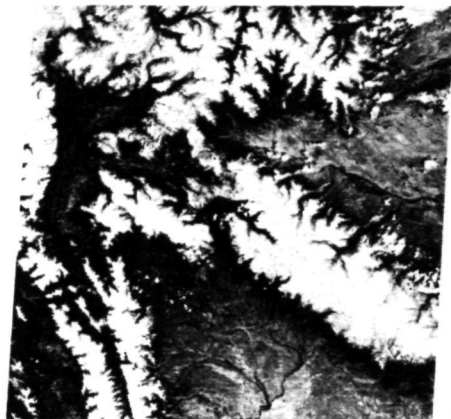
season as a direct result. This is illustrated graphically in Figure 5 showing that during the major melt period from late April to late June snowcover percentages in 1974 were in excess of those in 1973. The 18 day total flow, in cfs/mi² (m³/km²) plotted to correspond with each LANDSAT-1 pass, produces a 1974 peak considerably in excess of the 1973 value. Figure 6 shows the average snowcover depletion and runoff curves for 1973, but this time plotted on the basis of elevation. The low elevation watershed snowcover breaks off at a more rapid rate than the high elevation watersheds indicating the probability of a greater volume of snow on the higher watersheds. The resulting runoff, normalized for watershed area differences, bears out this hypothesis. A lower peak and



6 AUGUST 1972



10 DECEMBER 1972



21 MAY 1973



8 JUNE 1973

Fig. 4—Snowcover changes in northwestern Wyoming, 1972-1973.

total flow occurs on the low watersheds, and, additionally, the peak occurs two weeks earlier on the low watersheds than on the high watersheds.

Such graphical relationships are promising in that they show a positive qualitative relation between snowcover depletion and resulting runoff. A quantitative prediction of seasonal streamflow, however, is not possible using these curves. In an attempt to produce a quantitative snowcover-runoff relationship, i.e., a regression equation similar to that derived for the Indus River, the available data were treated as two different data sets based on elevation. In Figure 7 the percent snowcover on 15 May (S) is plotted against the seasonal runoff from 15 May-31 July (R) in cfs/mi^2 ($\text{m}^3/\text{sec}/\text{km}^2$) for the three high elevation watersheds for both 1973 and 1974. In order to increase the data base for a regression

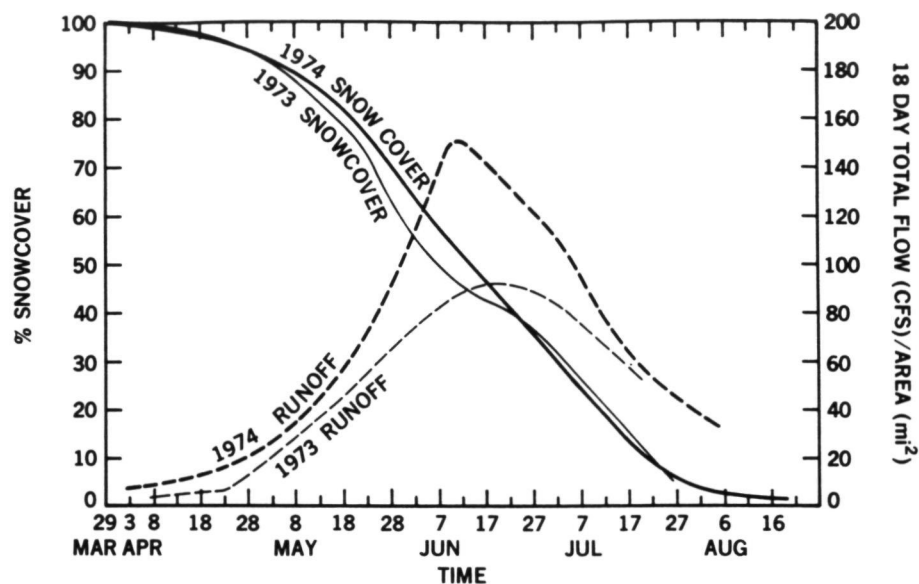


Fig. 5—Average snowcover depletion and runoff curves for seven watersheds in the Wind River Mountains of Wyoming for the 1973 and 1974 snowmelt seasons. Snowcover area obtained from LANDSAT-1 0.6-0.7 μ m observations.

analysis, the three high elevation watersheds, although possessing some differences, were assumed to be alike enough to be treated as a single watershed. Six data points were thus available for the two years and the resulting regression was $R = 30S - 2198$ with a r^2 of 0.89 significant at the one percent level and a standard error equal to 13 percent of the mean seasonal yield (15 May-31 July). For the lower elevation watersheds, the same similarity assumption was made and the data plotted in Figure 8. The equation was $R = 5.8S - 156$ with a r^2 of 0.85 significant at the one percent level and a standard error equal to 14 percent of the mean seasonal yield. Although a crude estimate of seasonal runoff could be made for nearby watersheds using these equations based on only two years of data, the real importance of such relations rests in the fact that the changes in areal snow extent as observed from space are quantitatively related to snowmelt runoff and, as a result, indirectly to the volume of water on a watershed. These data, if combined with conventionally gathered data used for streamflow forecasting, should be useful for reducing the errors associated with current prediction techniques. Because streamflow predictions are needed before the time of snowcover breakup—about 1 May in the Wind River Mountains—the satellite data could be used later in the snowmelt season to update and refine the earlier conventional predictions.

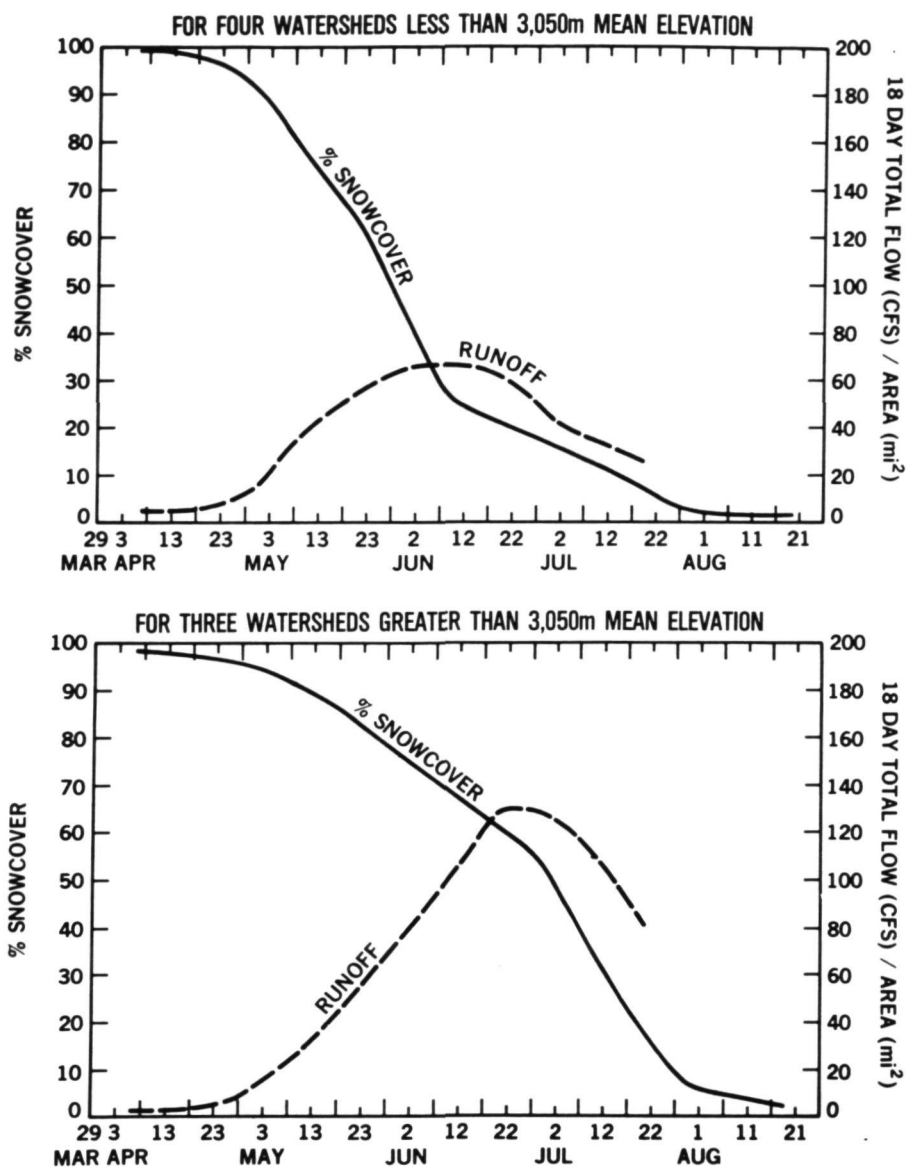


Fig. 6—1973 average snowcover depletion and runoff curves for the Wind River Mountains, separated on the basis of mean elevation. Snowcover area obtained from LANDSAT-1 0.6-0.7 μ m observations.

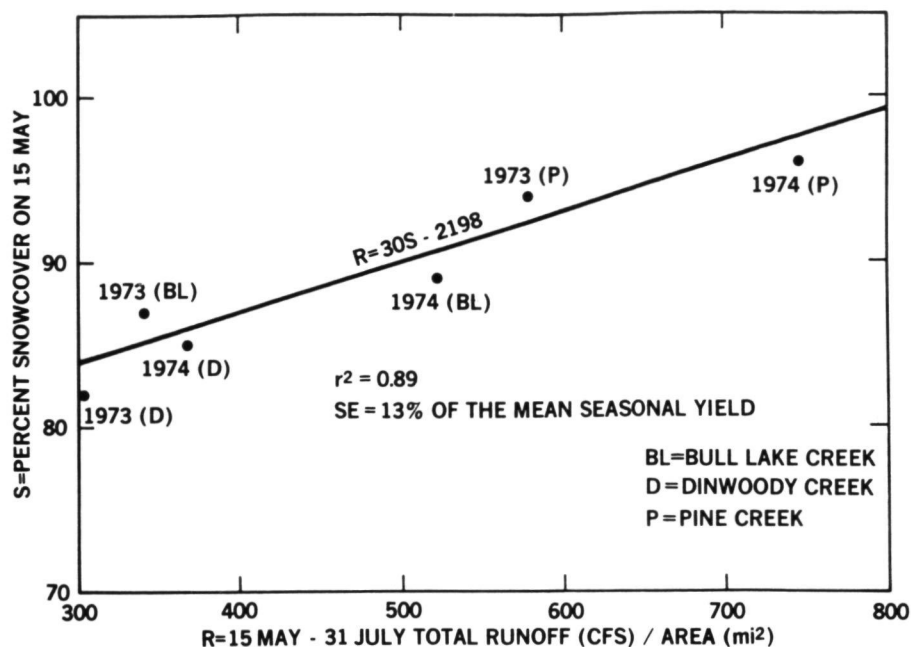


Fig. 7—LANDSAT-1 derived snowcover estimates versus measured runoff (1973 and 1974) for three watersheds greater than 3,050 m mean elevation in the Wind River Mountains, Wyoming.

The U.S. Department of Interior (1974) sponsored study has shown that such late season refinements may be worth considerable amounts of money for power generation alone. In the Southwestern United States snowpack areas snowcover breakup can be observed much sooner in the year and the satellite data should be even more useful for early runoff predictions.

Satellite snowcover data would be additionally important if they could be inserted into watershed models. The simple areal extent of snow is employed in some models now, basically for the correct application of energy balance equations, but a potentially even more useful parameter⁴ would be the area of the watershed snowpack currently or recently melting. Such data can potentially be obtained by comparing the 0.6-0.7 μ m (Band 5) and 0.8-1.1 μ m (Band 7) wavelength bands on LANDSAT-1 as indicated in Table 1. Band 5 generally is assumed to delineate the total snowcovered area whereas Band 7 consistently indicated less snowcover. This difference, as shown for the seven Wind River Mountain watersheds in Table 1, was attributed to the reduced near infrared reflectance associated with melting or refrozen previously melting snow. Such information could

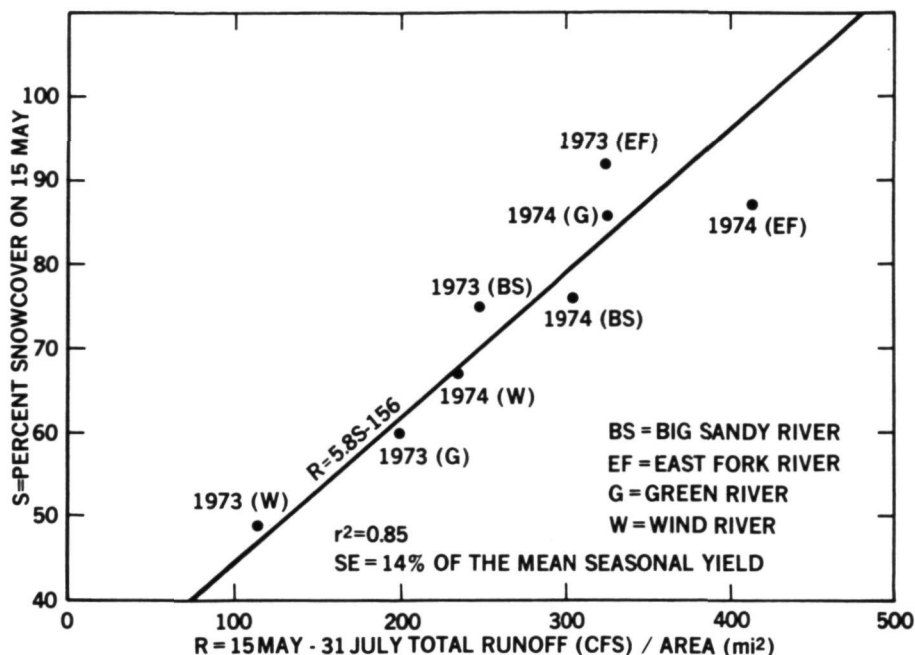


Fig. 8—LANDSAT-1 derived snowcover estimates versus measured runoff (1973 and 1974) for four watersheds less than 3,050 m mean elevation in the Wind River Mountains, Wyoming.

be invaluable to models for refining the timing aspects of predicted snowmelt runoff.

In order to assess the resolution adequacy of using LANDSAT-1 for snowcover mapping in the Wind River Mountains, high resolution (10 m) U-2 aircraft flights were flown in 1974 at the approximate time of a LANDSAT-1 overpass. Table 2 presents a comparison of the U-2 flights on 24 May and 25 June with the LANDSAT-1 overpasses on 16 May and 21 June for the high elevation watersheds. Areal extent of snow from LANDSAT-1 corresponded closely to the high resolution aircraft data, with differences no greater than 4 percent of watershed area. Analysis of the data has indicated that the area covered by snow is adequately expressed in LANDSAT-1 0.6-0.7 μ m data, and that snowcover mapping using LANDSAT-1 is much faster because it is considerably less complicated than similar mapping with the very detailed U-2 imagery. Additional advantages of the LANDSAT-1 data include the facts that no mosaicking of the small watersheds is necessary and that flight logistics problems are at a minimum.

Table 1
Wind River Mountains Multispectral Comparison of
Percent of Basin Snowcovered,
Band 5 (0.6-0.7 μ m) vs Band 7 (0.8-1.1 μ m)

1973						
	May 21		June 8		June 25-26	
	Band 5	Band 7	Band 5	Band 7	Band 5	Band 7
Bull Lake Creek	86%	85%	58%	56%	53%	46%
Dinwoody Creek	80%	78%	61%	56%	49%	43%
Pine Creek	93%	88%	80%	76%	70%	62%
Big Sandy River	71%	66%	23%	21%	19%	15%
East Fork River	91%	90%	40%	39%	24%	21%
Wind River	41%	39%	16%	11%	Cloudy	
Green River	55%	49%	27%	23%	Cloudy	
1974						
	May 16		June 2-3		June 21	
	Band 5	Band 7	Band 5	Band 7	Band 5	Band 7
Bull Lake Creek	89%	89%	79%	78%	57%	51%
Dinwoody Creek	85%	84%	76%	76%	56%	46%
Pine Creek	96%	95%	93%	90%	78%	71%
Big Sandy River	76%	73%	45%	41%	21%	18%
East Fork River	87%	83%	74%	66%	29%	25%
Wind River	67%	63%	Cloudy		23%	*
Green River	86%	85%	Cloudy		34%	31%

*Contrast in this band is not suitable for snow mapping.

Table 2
Comparison of Snow Extent Obtained From LANDSAT-1 and U-2 Sensors
Over Three High Elevation Watersheds in the
Wind River Mountains of Wyoming

Watershed		Data Source	Date	Snow Extent in Percent of Basin
1)	Bull Lake Creek	LANDSAT-1	16 May 74	89
	Bull Lake Creek	U-2	24 May 74	88
	Bull Lake Creek	LANDSAT-1	21 June 74	57
	Bull Lake Creek	U-2	25 June 74	60
2)	Dinwoody Creek	LANDSAT-1	16 May 74	85
	Dinwoody Creek	U-2	24 May 74	84
	Dinwoody Creek	LANDSAT-1	21 June 74	56
	Dinwoody Creek	U-2	25 June 74	60
3)	Pine Creek	LANDSAT-1	21 June 74	78
	Pine Creek	U-2	25 June 74	82

CONCLUSIONS

1. On large watersheds (10^5 to 10^6 km²) where the flow is relatively unimpaired by reservoirs or water withdrawals, meteorological satellite snowcover observations apparently can be used in lieu of other snowpack parameters, such as depth or volume, to predict seasonal runoff if enough years of information exist.
2. On watersheds as small as 10 km² in areas with infrequent cloud cover during the snowmelt season, LANDSAT-1 data can be used to accurately measure the extent of snowcover and monitor its change with time. It seems to be possible to quantitatively relate the percent of the basin snowcovered on a given date to a measure of seasonal runoff on the small watersheds similar in nature to that performed on the large Indus River Basin. In the United States it is necessary to develop such relations on small watersheds in order to effectively predict streamflow at points above significant water diversions.
3. Because of the quantitative relations developed here it appears that satellite observed snowcovered area could be usefully employed as an additional seasonal runoff index parameter or as an input into certain hydrologic models. The advantage of such information is that they are non hazardous, easy to obtain data requiring no access to restricted wilderness or remote areas. In the Western United States, because of the significance of water stored in the form of snow for hydroelectric power generation, irrigated agriculture, and reservoir regulation, the importance and value of more accurate runoff information provided by satellite observations is very promising.

ACKNOWLEDGMENTS

This work was partially funded by the NOAA/National Environmental Satellite Service under contract No. NA-776-74. We would like to thank Mr. M. Umar and Mr. K. Jawed of the Pakistan Water and Power Development Authority; Mr. D. J. O'Connell and Mr. J. F. Wilson of the U.S. Geological Survey, Water Resources Division, Wyoming; and Mr. G. W. Peak and Mr. G. P. Clagett of the U.S. Soil Conservation Service, Casper, Wyoming for supplying streamflow and ground snow survey data necessary for conducting this study. Additionally, we acknowledge the high altitude aircraft support provided us by the Earth Resources Aircraft Project at NASA's Ames Research Center, Moffett Field, California.

REFERENCES

- Barnes, J. C., and C. J. Bowley, Handbook of techniques for satellite snow mapping, Final Report, NAS5-21803, 95 pp., National Aeronautics and Space Administration, Goddard Space Flight Center, Greenbelt, Maryland, 1974.
- Barnes, J. C., C. J. Bowley, and D. A. Simmes, Mapping snow extent in the Salt-Verde watershed and the southern Sierra Nevada using ERTS imagery, in Proceedings of the Third ERTS-1 Symposium, NASA SP-351, vol. 1, pp. 977-993, U.S. Government Printing Office, Washington, D. C., 1974.
- Brown, A. J., Long-range goal and information needs of the coordinated snow survey program in California in Advanced Concepts and Techniques in the Study of Snow and Ice Resources, pp. 47-54, National Academy of Sciences, Washington, D.C., 1974.
- Committee on Polar Research, Polar research, a survey, 204 pp., National Research Council, National Academy of Sciences, Washington, D. C., 1970.
- Meier, M. F., Evaluation of ERTS imagery for mapping and detection of changes of snowcover on land and on glaciers, in Proceedings of the Symposium on Significant Results Obtained from ERTS-1, NASA SP-327, vol. 1, pp. 863-875, U.S. Government Printing Office, Washington, D.C., 1973.
- Rooney, J., The economic and social implications of snow and ice, in Water, Earth, and Man, pp. 389-401, edited by R. J. Chorley, Methuen and Company, Ltd., London, 1969.
- Salomonson, V. V., and N. H. MacLeod, Nimbus hydrological observations over the watersheds of the Niger and Indus Rivers in 4th Annual Proceedings, Earth Resources Review, vol. 1, pp. 5-1 to 5-11, NASA Document MSC 05937, Manned Spacecraft Center, Houston, 1972.
- U.S. Army Engineer Division, Program Description and User Manual for SSARR Model (Streamflow Synthesis and Reservoir Regulation), Program 724-K5-G0010, 188 pp., North Pacific, Portland, 1972.
- U.S. Department of Interior, Project Skywater, Bureau of Reclamation, Atmospheric Water Resources Program, 16 pp., U.S. Government Printing Office, Washington, D.C., 1970.

U. S. Department of Interior, Snow mapping and runoff forecasting:
Examination of ERTS-1 capabilities and potential benefits from an
operational ERS system, Interim Report, Contract No. 14-08-13519,
Office of Economic Analysis, Washington, D.C., 1974.

Wiesnet, D. R., and D. F. McGinnis, Snow-extent mapping and lake
ice studies using ERTS-1 MSS together with NOAA-2 VHRR, in Pro-
ceedings of the Third ERTS-1 Symposium, NASA SP-351, Vol. 1,
pp. 995-1009, U. S. Government Printing Office, Washington, D.C.,
1974.

APPLICATIONS OF SATELLITE SNOW COVER IN COMPUTERIZED SHORT-TERM STREAMFLOW FORECASTING 1/C. F. Leaf, *Fort Collins, Colorado*

ABSTRACT

A procedure is described whereby the correlation between: (a) satellite derived snow-cover depletion and (b) residual snowpack water equivalent, can be used to update computerized residual flow forecasts for the Conejos River in southern Colorado.

INTRODUCTION

In the Rocky Mountain West seasonal or total flow forecasts are generally made utilizing regressions between snow accumulation and runoff and annual surveys of peak snowpack water equivalent. Extensions of these early-spring forecasts to a short-term basis using statistical methods is extremely difficult since precipitation and meteorological conditions during the ensuing melt season vary widely from year to year.

One index of runoff, which has been found useful for improving residual flow forecasts is areal snow cover. In the United States, aerial surveillance of the snow cover was proposed more than 30 years ago. More recently the areal extent of snow has become an important parameter in the growing emphasis on applications of remote sensing in the water resource field (Rango 1975). Advanced space technology and several new satellite snow mapping procedures (Barnes and Bowley 1974, Foster and Rango 1975) promise to make satellite snow cover observations available on a dependable and routine basis. These satellite snow cover estimates used in combination with conventional snow survey data as inputs to computerized simulation models should make the problem of short-term residual volume forecasting less difficult in the very near future.

This paper shows how satellite imagery can provide key information for making residual volume streamflow forecasts in the Rio Grande basin using a computerized simulation model recently developed by the U. S. Forest Service. Mapped snow cover estimates and model output are summarized for the Conejos River, a 282-square-mile tributary of the Rio Grande in southern Colorado.

1/This study has been funded by the USDA, Soil Conservation Service, Snow Survey Unit, Denver, Colorado.

The demonstration project is one of four currently being sponsored by NASA to determine the effectiveness of satellite-derived snow-cover estimates in operational streamflow forecasting (Rango 1975).

JUSTIFICATION

THE RIO GRANDE DRAINAGE BASIN

Waters of the Rio Grande are administered under the Rio Grande Compact between three States and by an international agreement with Mexico. Accordingly, it is imperative that accurate short-term forecasting procedures be developed so that water is dispatched fairly and efficiently throughout the Basin. In Colorado, the Rio Grande provides irrigation water to the San Luis Valley. To provide maximum delivery of water to these users and still meet the Compact obligations, accurate forecasts are required on a continuing 10-day basis starting April 15 of each year (Qazi and Danielson 1973).

Conejos River

The area selected for this study is drained by the Conejos River, a key headwater tributary of the Rio Grande River. Figure 1 is a map of this basin, and Table 1 summarizes pertinent geographic characteristics of subunits selected for the simulation analysis discussed subsequently in this report. Annual water yields, corrected for Platoro Reservoir, which regulates flows from approximately 40 square miles of the drainage basin, are summarized in Table 2. These data were obtained from surface water records published by the U.S. Geological Survey. As seen in Table 2, runoff during the past 17 years has varied from a low of 7.9 inches in 1959 to a high in 1965 of 22.1 inches.

METHODS

THE SUBALPINE WATER BALANCE MODEL

In order to make the best use of satellite imagery and to provide the most flexibility for updating forecasts, it was decided to use the "Subalpine Water Balance Model" (Leaf and Brink 1973a, 1973b) to simulate flows at 10-day intervals on the Conejos River. This model simulates winter snow accumulation, the shortwave and longwave radiation balance, snowpack condition, snowmelt and subsequent runoff on as many as 25 subunits. Each subunit is described by relatively uniform slope, aspect, and forest cover. Results from each subunit are compiled into a "composite overview" of an entire drainage basin. Figure 2 is a generalized flow chart of the system.

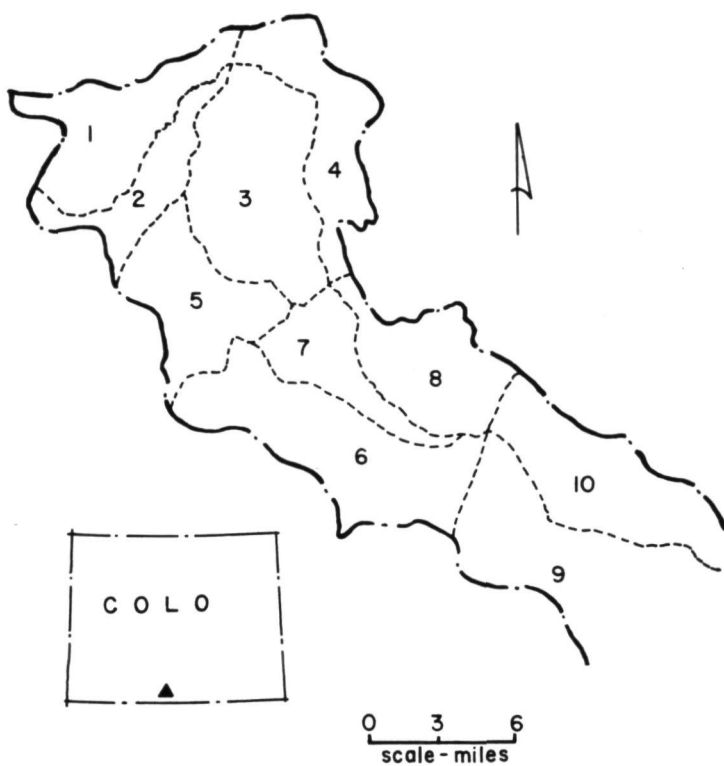


Figure 1 - Conejos River Base Map Showing Subunits (1mi.=1.61 km).

Table 1- Geographic Description of Conejos River Drainage Basin

Subunit	Area ^{1/}		Average Elev.		Average	Avg. Slope
	(mi. ²)	(km ²)	(ft.)	(m)	Aspect	(percent)
1	25.4	65.8	11,000	3,355	SE	34
2	13.5	35.0	11,500	3,507	NNW	34
3	37.5	97.1	10,500	3,202	E	28
4	30.2	78.2	10,500	3,202	SW	33
5	24.0	62.2	11,000	3,355	ESE	25
6	40.0	103.6	11,000	3,355	NNE	23
7	16.1	41.7	10,500	3,202	ENE	27
8	9.3	24.1	10,300	3,141	SW	35
9	52.7	136.5	9,400	2,867	NE	15
10	32.7	84.7	9,500	2,897	SW	15

^{1/} Total: Forest and Open

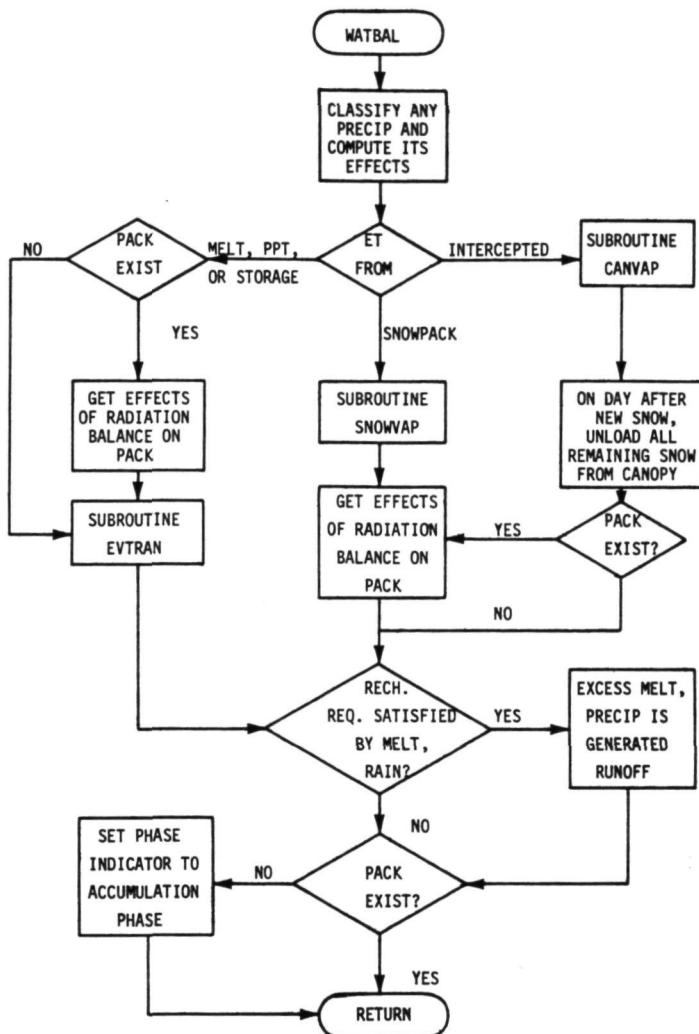


Figure 2 -Flow chart of "Subalpine Water Balance Model"(Leaf and Brink. 1973b).

Calibration of Model to Conejos River

Daily temperature extremes in each of the response units were estimated by extrapolating observed temperatures at the base station Wolf Creek Pass 1E. Because reliable long-term radiation data are not available in the Conejos drainage, short-wave radiation input to the model was generated from potential solar beam radiation adjusted for temperature and the slope/aspect characteristics of each subunit. In order to compute an index of the radiation received, potential radiation was reduced by means of a thermal factor. This factor was determined by degree-day relationships which vary according to season of the year.

Peak snowpack accumulation on the Conejos was estimated by extrapolating snow-course data published by the Soil Conservation Service. To ensure the proper snow accumulation in each response unit, base station precipitation (at Wolf Creek Pass 1E) was adjusted until the specified peak-water equivalent on each subunit was reached.

The Conejos River Basin was divided into 10 subunits as seen in Figure 1. Further division of forest and open areas resulted in 20 response units used for the simulation analysis.

RESULTS

RESIDUAL VOLUME FORECASTS (1958-1972)

Figures 3 and 4 show the comparison of simulated vs. actual residual runoff as of the first day of April, May, June, and July for 8 years. The close agreement between observed and simulated flows indicates that the model is a useful tool for continuous forecasting of short-term flows in the Conejos River for the full range of runoff observed during the past 15 years.

TEN-DAY RESIDUAL VOLUME FORECASTS (1973 and 1974)

Figure 5 summarizes observed and simulated residual flows on a 10-day basis for 1973 and 1974. Also shown in Figure 4 are satellite-derived snow cover estimates. Again, agreement is good even when residual volume forecasts are made at 10-day intervals. The superimposed snow cover estimates reveal a high correlation with simulated runoff and suggest that satellite snow cover data can provide key information for updating model input in a real forecasting situation. Just how this can be accomplished is discussed next.

INCORPORATION OF SATELLITE SNOW COVER OBSERVATIONS FOR FORECASTING

Table 3 compares mapped snow cover estimates on the Conejos River with residual water equivalent and streamflow for 1973 and 1974. In keeping with previous research, Table 3 and Figure 4 suggest that depletion vs. runoff relationships vary depending

Table 2 - Annual Runoff Corrected For Platoro Reservoir, Conejos River Basin.

Year	Runoff	Platoro Res. Change in Storage	Adjusted Runoff (in.)	Runoff (mm)
	-----inches-----			
1958	16.6	-1.02	15.6	396.2
59* ^{1/}	9.9	-1.98	7.9	200.7
60	-	-	-	-
61*	13.3	-0.27	13.0	330.2
62	16.8	+0.60	17.4	442.0
63*	8.7	-0.70	8.0	203.2
64*	10.3	+0.31	10.6	269.2
65	20.2	+1.89	22.1	561.3
66	15.8	-1.24	14.6	370.8
67	15.0	-1.08	13.9	353.1
68*	15.4	+0.55	15.9	403.9
69	17.6	-0.46	17.1	434.3
70	15.8	+0.25	16.0	406.4
71	11.7	-0.43	11.3	287.0
72*	8.0	+0.01	8.0	203.2
73*	19.7	+2.14	21.8	553.7
74*	10.7	-1.20	9.5	241.3

^{1/} * Used in simulation analysis

Table 3 - Mapped Snow Cover vs. Residual Water Equivalent and Streamflow. (Conejos River, Rio Grande Drainage Basin)

Year	Snow Cover ^{1/} (percent)	Sim. Residual Water Equiv. (in.) (mm)		Observed Residual Streamflow From Snowmelt (acre-ft) (m ³)	
<u>1973</u>					
June 22	31	3	76.2	1.379x10 ⁵	1.700x10 ⁸
<u>1974</u>					
May 12	42	4	101.6	7.015x10 ⁴	8.649x10 ⁷
May 30	18	1	25.4	5.333x10 ⁴	6.576x10 ⁷

^{1/} Personal communication with Jack Washichek, Soil Conservation Service, Denver, Colorado

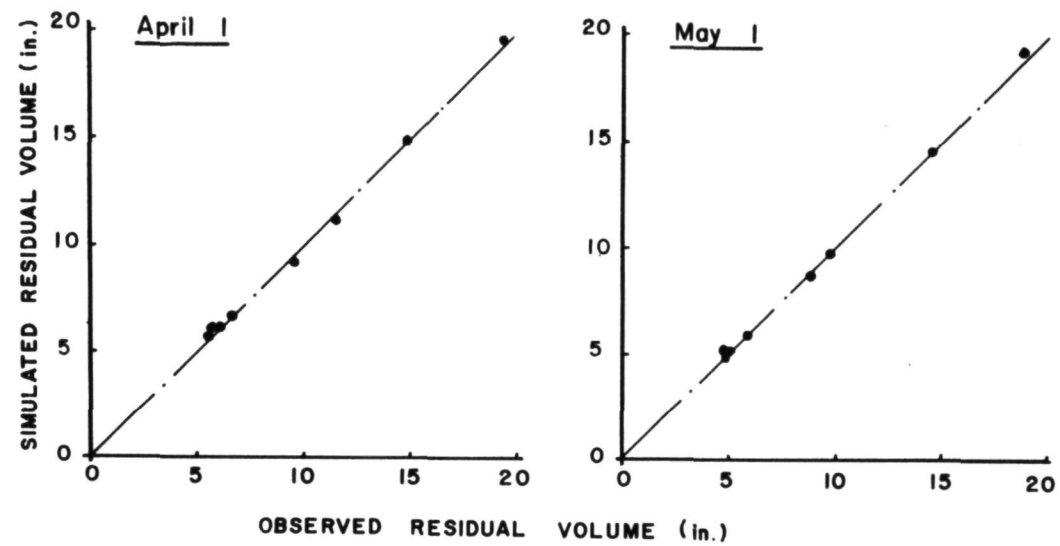


Figure 3 - Simulated vs. Observed Residual Flow Volumes, Conejos River. (1 in. = 25.4 mm)

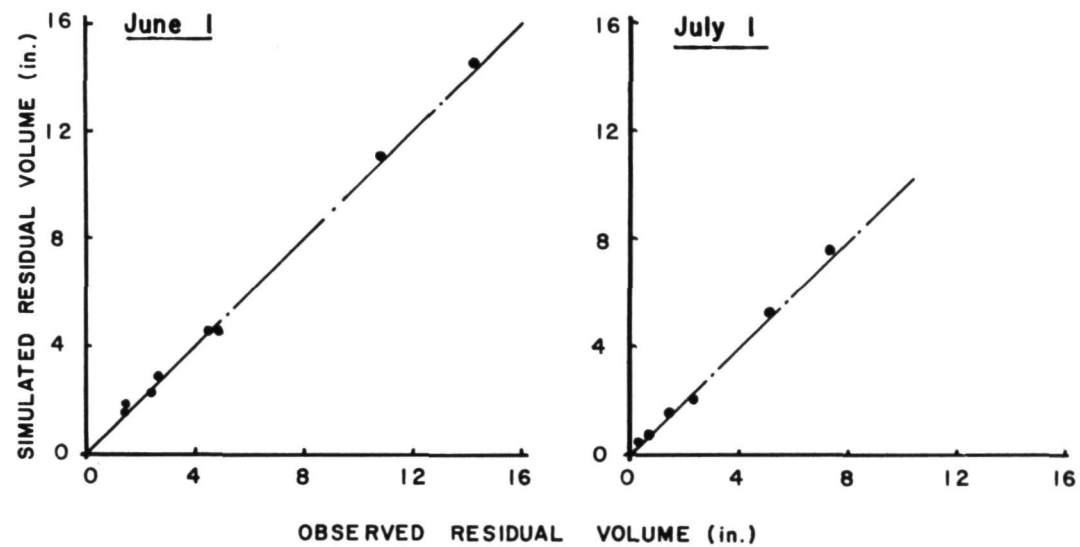


Figure 4 - Simulated vs. Observed Residual Flow Volumes, Conejos River. (1 in. = 25.4 mm)

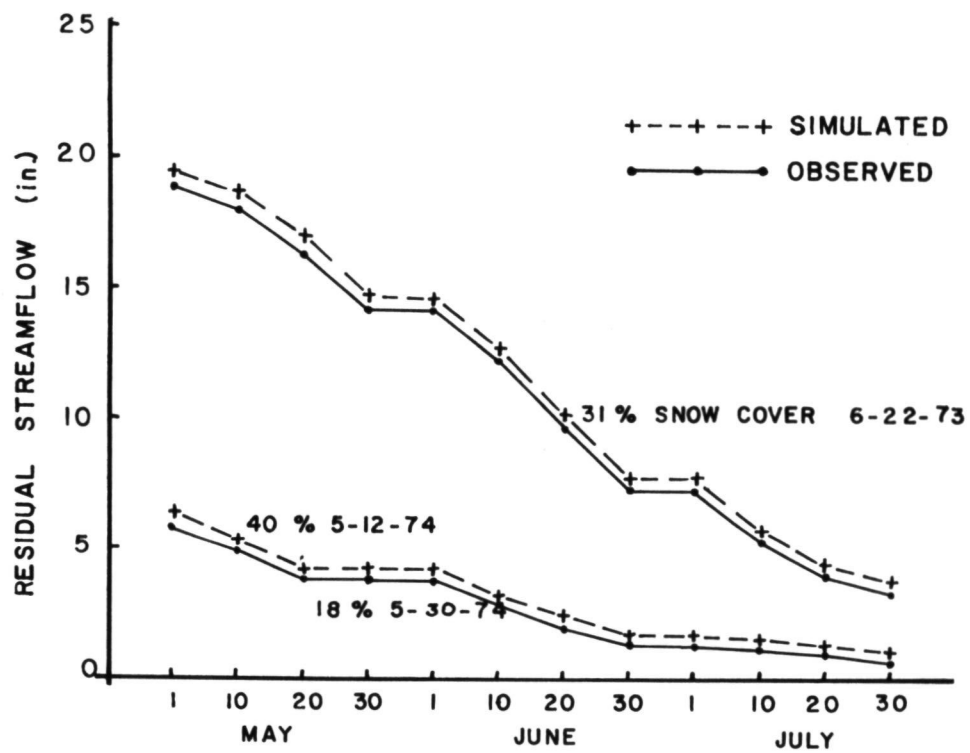


Figure 5 - Simulated vs. Observed 10-day Residual Flow Volumes For 1973 and 1974, Conejos River Basin.
 (1 in. = 25.4 mm)

on the magnitude of the snowpack and precipitation through the snowmelt season (Leaf and Haefner 1971). For example, in Table 3, 31 percent snow cover on June 22 corresponds to a residual flow of 137,900 acre-feet in 1973--a big snow year, whereas on May 12 in 1974--a low snow year--40 percent snow cover represents a residual flow of only 70,150 acre-feet. However, if one looks at residual water equivalent, one finds that a direct relationship exists between this variable and the areal extent of snow cover.

The stable correlation between snow-cover depletion and residual water equivalent is independent of precipitation input and can be utilized in combination with direct snowpack measurements through the melt season to revise model estimates of streamflow. In most areas, satellite imagery would provide the primary basis for updating streamflow forecasts so long as the drainage basin is partially snow covered. Streamflow forecasts prior to the onset of snowmelt and during those times when the watershed is completely covered with snow would rely on direct snowpack measurements.

CONCLUSIONS

Satellite snow cover data used in combination with the recently developed Subalpine Water Balance Model can provide a sound physical basis for making continuous short-term streamflow forecasts in the Upper Rio Grande Basin. Reconstitution studies of a 15-year streamflow record indicate that the model is adequate for making residual volume forecasts at time intervals as short as 10 days. A comparison of model results with mapped snow cover estimates indicates that an apparently stable relationship between satellite derived snow cover and residual water equivalent can be the primary basis for modifying short-term forecasts and ultimately delivery schedules to ensure the maximum amount of water for Colorado users while at the same time meeting Compact commitments downstream.

REFERENCES

- Barnes, J.C., and Bowley, C.J.
1974. Handbook of techniques for satellite snow mapping. ERT
Document No.0407-A, 99 p. Prepared for NASA/Goddard Space
Flight Center, Greenbelt, Maryland.
- Foster, J.L., and A. Rango.
1975. A method for improving the location of the snowline in
forested areas using satellite imagery. NASA Rep. X-910-
75-41, 8 p. Goddard Space Flight Center, Greenbelt, Mary-
land.
- Leaf, Charles F., and Glen E. Brink.
1973a. Computer simulation of snowmelt within a Colorado sub-
alpine watershed. USDA For. Serv. Res. Pap. RM-99, 22 p.
Rocky Mt. For. and Range Exp. Stn., Fort Collins, Colo.
- Leaf, Charles F., and Glen E. Brink.
1973b. Hydrologic simulation model of Colorado subalpine forest.
USDA For. Serv. Res. Pap. RM-107, 23 p. Rocky Mt. For. and
Range Exp. Stn. Fort Collins, Colo.
- Leaf, Charles F. and Arden D. Haeffner
1971. A model for updating streamflow forecasts based on areal
snow cover and a precipitation index. West. Snow Conf.
(Billings, Mont., Apr. 1967) Proc. 39:9-16.
- Qazi, Razig A. and Jeris A. Danielson.
1973. A predictive model for upper Rio-Grande index flows. Water
Resources Bulletin, Vol. 9, No. 2, p. 284-290. Amer. Water
Resources Assoc. Urbana, Ill.
- Rango, Albert.
1975. Applications of remote sensing to watershed management.
NASA Rep. X-913-75-86, (for presentation at the Symp. on
Watershed Management, ASCE, Aug. 11-13, 1975, Logan Utah),
Goddard Space Flight Center, Greenbelt, Maryland.

SIERRA NEVADA SNOW MELT FROM SMS-2

Laurence C. Breaker, *NOAA National Environmental Satellite Service, Redwood City, California 94063*; Michael C. McMillan, *NOAA National Environmental Satellite Service, Suitland, Maryland 20233*

ABSTRACT

A film loop from SMS-2 imagery shows snow melt over the Sierra Nevadas from May 10 to July 8, 1975. The sequence indicates a successful application of geostationary satellite data for monitoring dynamic hydrologic conditions.

INTRODUCTION

The National Environmental Satellite Service (NESS) has established five Satellite Field Services Stations (SFSS) to interface with field users of NESS satellite data. One of the functions of the SFSS is to provide environmental satellite data and related analyses, interpretations, and services. The support provided varies by station depending on the interests of its regional users. Since January 1975, the SFSS in Redwood City, California has participated in the NASA sponsored Snow Application Systems Verification Test (ASVT) by providing satellite imagery from the NOAA and SMS environmental satellites.

It seemed a reasonable progression, based on the effectiveness of meteorological film loops from SMS, to construct a similar registered sequence showing the time-space variations of snowfields. A film "loop" consists of a short piece of film spliced into one continuous movie, thereby allowing the same set of imagery to be seen over and over. A meteorological loop may show imagery spanning several hours but a hydrological loop showing snow melt would have to cover a period of several months.

The idea of applying time-lapse techniques to hydrological phenomena is not new. Serebreny et al, 1974, summarizes past applications of LANDSAT imagery to temporal studies.¹ For example the idea of monitoring snowline recession via sequential satellite imagery is presented. Unique in the hydrologic time-lapse sequence presented here however is the source of

data from which it has been constructed.

There are two reasons for constructing the loop. The first is to document and display the capabilities of the SMS satellites for hydrologic applications. The second reason is to show the character and rate of snowline recession in the Sierra Nevadas during this most recent snow melt season.

SATELLITE AND SATELLITE DATA

The Synchronous Meteorological Satellites (SMS) now in orbit are NASA-sponsored prototypes. Future satellites in this series will be entirely NOAA-funded and will be designated Geostationary Operational Environmental Satellites (GOES).

The SMS satellites are geostationary, their position with respect to the earth remains fixed. This occurs because the angular velocity of the satellites in their orbit is identical to that of the earth. The SMS-2 subpoint resides at the equator with a longitude of 115°W; SMS-1 is at 75°W. Both spacecraft are at an altitude of about 35,000 km.

Visible and infrared data from SMS are provided by a Visible and Infrared Spin Scan Radiometer (VISSR). Images are created through the horizontal spinning motion (100 rpm) of the satellite and by vertical internal stepping of the scan mirror after each spin. Eight identical visible sensors (0.55-0.75 μm) are aligned in a linear array so that they generate 8 scan lines per satellite rotation. This results in 1 km resolution at the satellite subpoint. In order to reduce the data volume, the visible sensor output can also be combined in sets of 2, 4, or all 8 sensors. Visible channel imagery can then be selected with 1, 2, 4, or 8 km resolution, respectively. Two identical and redundant infrared sensors (10.5-12.6 μm) provide 8 km resolution at nadir. More information on the VISSR can be found in references 2 and 3.

Although SMS-2 produces an image of almost an entire hemisphere during each scanning cycle, geographical "sectors" of limited extent are normally extracted for local use. The data stream from the satellite is sectorized by computer and the appropriate images distributed to the SFSS's. Sectors with 1 km resolution cover an area at nadir of approximately $22 \times 10^5 \text{ km}^2$ and were chosen for this study because they contain maximum spatial resolution. A sample sector is shown in Figure 1.

SMS viewing geometry produces imagery displayed in an unfamiliar cartographic projection. The display, somewhat similar to a standard orthographic meridional

↑ 21:45 25MY75 32A-H 02131 18811 SA38N115W

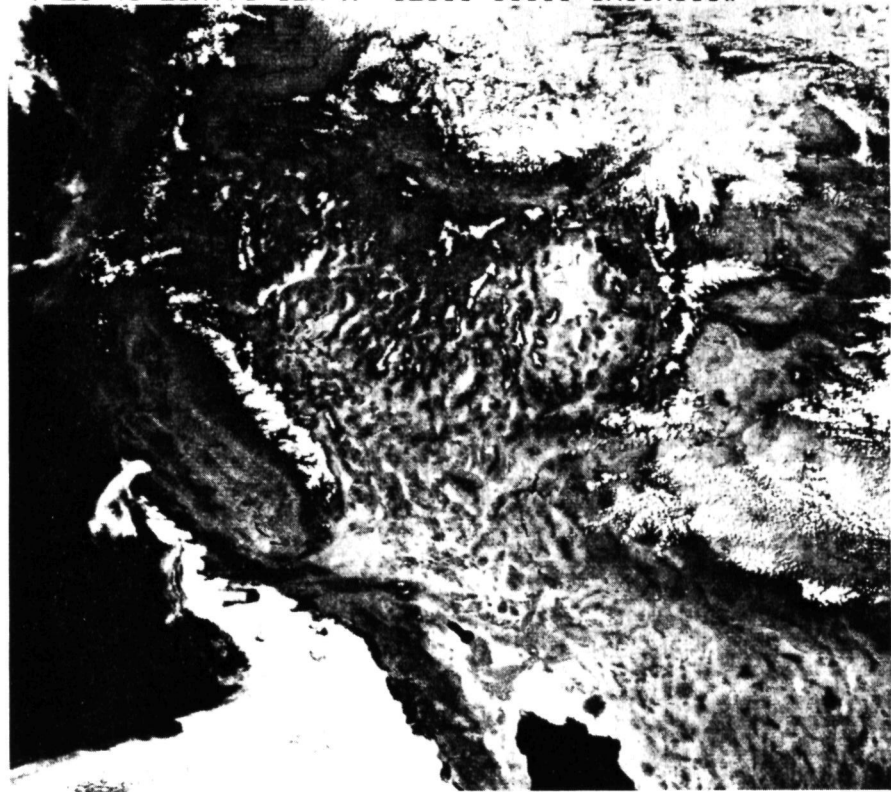


FIGURE 1 - HALF MILE VISUAL SECTOR FROM SMS-2

REPRODUCIBILITY OF THE
ORIGINAL PAGE IS POOR

projection, is identical to that produced by photographing a world globe. In this case, the camera has been replaced by the spacecraft. Related to this type of projection is a radial decrease in resolution. As the distance from the satellite subpoint increases, the earth is viewed more obliquely, such that the instantaneous field of view covers a larger area. This predictable decrease in resolution results in a value between 1 and 1.5 km for the center of the sector used in the film loop.

The quality of SMS imagery is affected by the method of transmission. The data is received from the satellite at the NESS headquarters in Suitland, Maryland. There it is sectorized and transmitted to the various SFSS's over a conditioned C-5 telephone line. There, the data are recorded photographically on 25 x 25 cm high quality negatives, from which the imagery is produced. A qualitative comparison of SMS-2 images produced at Suitland and Redwood City has indicated that a slight loss in sharpness occurs over the line. However, areal snow cover measurements from these images showed little difference.

METHOD

Area Selection

Several items were considered immediately before the data collection period. First, sector location had to be specified and was subsequently chosen to include three of the four westernmost study areas in the ASVT project, namely, the Pacific Northwest, the Sierra Nevadas, and the Salt and Verde River watersheds in Arizona. The sector chosen is centered at 38°N, 115°W as shown in Figure 1. Based on other operational requirements, it was decided that one sector per day could be allocated to the effort thus establishing the sampling frequency. Also, it was decided to request the sector at about the same time each day, 2200 GMT (Table 1). This was done to minimize day-to-day sun angle variations and to reduce sector subpoint changes due to diurnal extra-orbital motion.

It became apparent that an entire sector would provide too much information when constructing the final loop. Consequently, one of the three ASVT study areas included in the daily sector was selected for constructing the final sequence. Cloud cover during the data collection period made the choice simple. The Sierra Nevadas were completely or partially cloudfree at least 65% of the time (Table 1). Other factors also influenced our decision. First, the large areal extent

of snow in this region made its selection appealing. Second, snow can be viewed directly over much of this range because of the high percentage of unforested areas.

Loop Construction

In constructing the loop, images were pin-registered using prepunched plastic strips taped to each negative. Each negative was overlaid on a reference negative (May 11) throughout the sequence; Mono Lake was the primary geographic reference point.

A number of problems were encountered during the construction of the loop. Initially two questions arose. First, should days when clouds obscured the Sierras be included? Second, what should be done about dates during the sequence when negatives were not obtained? The first question was easily answered--yes. If cloud-cover statistics during the data collection period were to be of interest, and it was felt they would, then days with and without clouds should be included. The second problem was not serious inasmuch as only three days out of 60 were missing. It was decided to assemble the loop without the missing dates and not to fill the gaps with adjacent negatives.

The major problem in loop construction related to image-to-image brightness variations. An attempt has been made to minimize these brightness variations by first measuring individual negative densities, and then compensating photographically while exposing the negatives. This was partially successful, but could not correct for differences in contrast.

A minor problem in loop construction dealt with proper animation. Initially each image was exposed on four frames as is customarily done with meteorological loops. At a nominal film speed of 16 frames per second, each day was presented on the screen for 1/4 second. This motion, however, was too rapid and 10 frames per day were selected for the final construction.

The final product is a 16mm film loop containing 57 images over a period of 60 days. The first and last images are repeated 20 times with the intervening images repeated 10 times each. The entire loop is thus 590 frames in length, compressing two months of Sierra Nevada snow melt into about 37 seconds.

DISCUSSION

The film loop starts on May 10 and terminates on July 8, 1975. The dates are included in the upper righthand corner of each frame. In viewing the loop,

it is recommended that subareas or basins within the Sierras be selected for scrutiny. Considerable concentration is required. Cloud motion is very distracting and changes in snow cover are often not obvious.

Figure 2 illustrates major river basins of the Sierras covering the same area and in the same cartographic projection as the satellite imagery. A film loop cannot of course, be included in the text. Figure 3, however contains a selected sequence of eight images taken from the loop and illustrates the pattern of snow melt.

Over the 60 day period of the loop, a gradual recession of the dendritic snow envelope is apparent. However, during the period of the loop, significant snow accumulation occurred on at least three separate occasions, May 21-22, June 17, and June 24. New snow may be detectable following the June 17 snowfall. Unfortunately, the radiances of snow and cloud tops in the visible band are often almost identical making a distinction between the two nearly impossible. Cloud contamination was especially troublesome following the June 17 snowfall when trying to detect the presence of new snow.

The original idea for generating a snow melt film loop did not occur until the first week in May. It was indeed fortunate that snow melt was delayed this year by cooler than normal weather throughout April and into early May. Field data confirmed that maximum snow accumulation was delayed this year and occurred around the first week in May. This date for maximum accumulation was at least a month later than usual.⁴ Thus, more by good fortune than planning, we were able to capture that period when maximum snow melt occurred.

CONCLUDING REMARKS

The purpose for constructing a film loop of snow melt over the Sierra Nevadas has been to demonstrate the applicability of SMS-2 one kilometer visual-band imagery to the study of snow cover dynamics. With this time lapse sequence, the character and rate of snow line recession in the Sierra Nevadas during the 1975 snow melt season has been shown.

The Sierra Nevadas, during spring, are a subject well suited to satellite surveillance. Statistics from Table 1 indicate that the Sierra Nevadas were totally obscured by clouds only seven percent of the time and partially cloud covered one-third of the time. Cloud cover climatology indicates that this area is generally favorable for viewing from space during the spring season.⁵

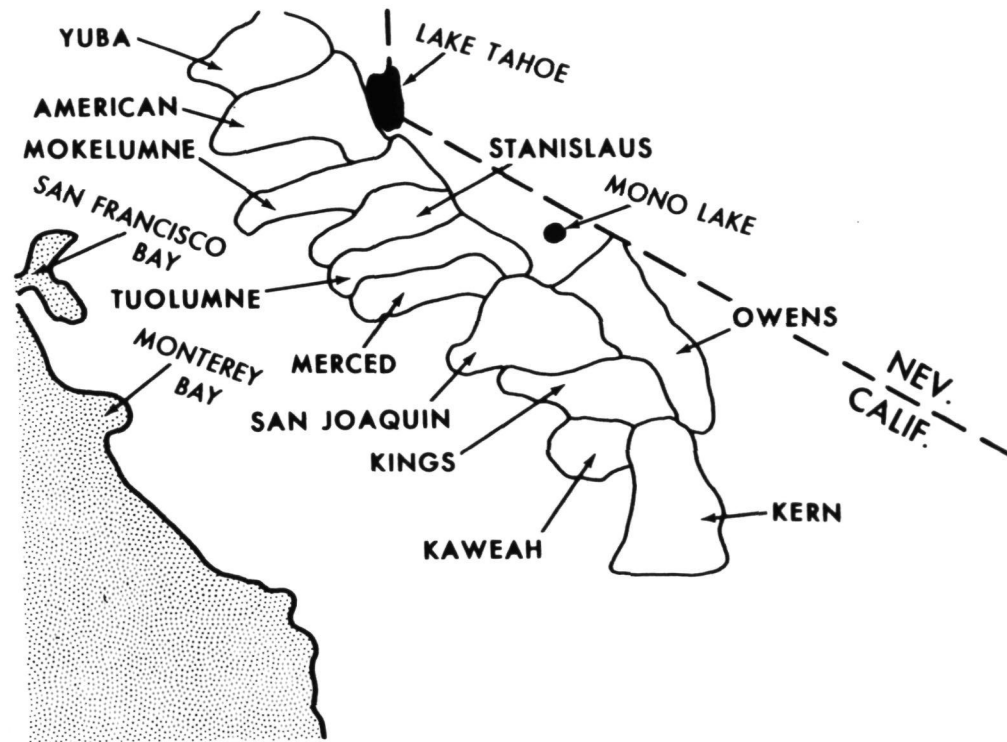


FIGURE 2 - MAJOR SIERRA NEVADA RIVER BASINS

REPRODUCIBILITY OF THE
ORIGINAL PAGE IS POOR

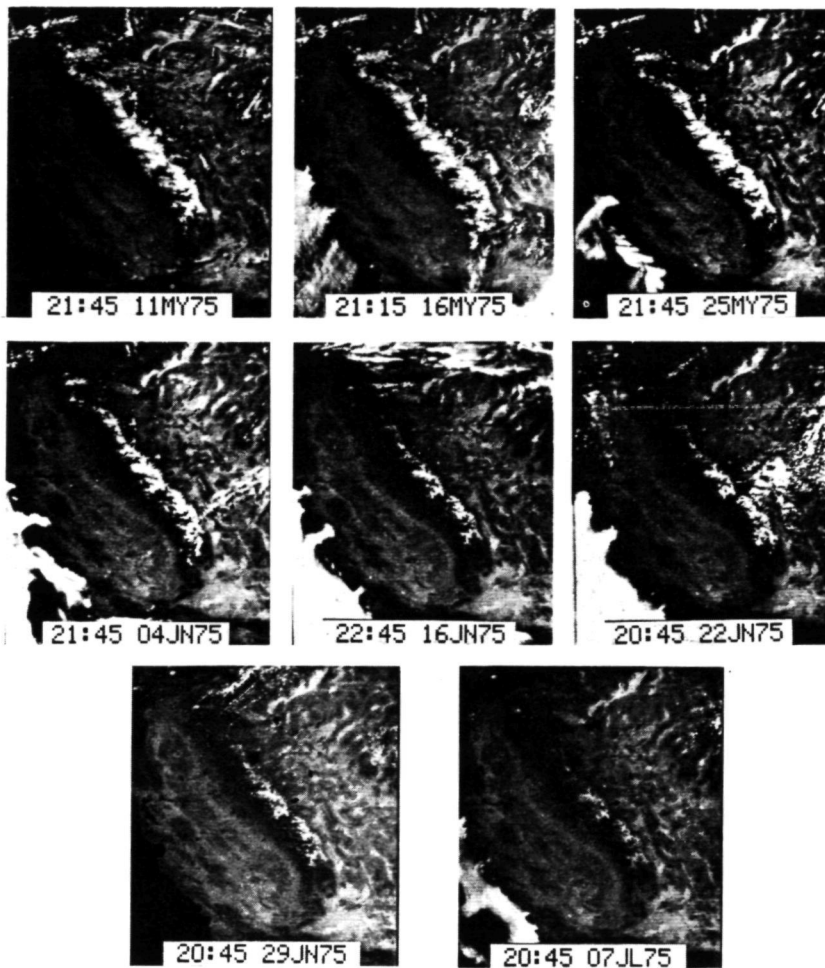


FIGURE 3 - SEQUENCE OF SMS-2 IMAGES OVER THE SIERRA NEVADAS

The SMS satellites, 1 and 2, have the ability to view the earth from a fixed vantage point as well as provide imagery every one-half hour. This combination at 1 km resolution provides the hydrologist with a unique surveillance capability. Useful applications of this capability are far more numerous than merely constructing a film loop. Several examples follow.

1. Areas having an early morning fog or mist, such as the Pacific Northwest, are difficult to snow-map with current NOAA or LANDSAT data. Cloudfree SMS imagery, however, can often be obtained in the afternoon (Schneider, 1975).⁶ In fact, imagery of a particular basin can be obtained if the area is cloudfree for only half an hour per day.

2. The daily snow melt rate may be computed. In areas of rapid snow melt, such as the Southwest, hourly snow melt rates can be determined.

3. An immediate, daily record of cloud seeding effects on both cloud shape and snowfall can be obtained.

4. Time-lapse analysis on an hourly scale can assist in snow/cloud discrimination.

5. Selection of optimum solar zenith angle for individual watersheds is possible. Basins facing west should be imaged after solar noon, for example, to minimize valley wall shadows. Similarly, the solar angle could be selected which would minimize forest shadows to assist in detecting snow in forested areas. Halverson and Smith (1974) have published tables of shadow lengths as a function of time which would be helpful.⁷

6. Middleton et al (1952) have studied snowpack reflection at various zenith angles.⁸ Their results indicate it may be possible to differentiate among snowpack surface conditions in early morning or late afternoon imagery.

ACKNOWLEDGEMENT

The authors would like to express their gratitude to Mr. Vince Leech for spending many hours in the photographic lab constructing the film loop.

REFERENCES

1. Serebreny, S.M., W.E. Evans, and E.J. Wiegman, 1974, "Study of Time-Lapse Processing for Dynamic Hydrologic Conditions." Final Report for NASA/GSFC, Stanford Research Institute, Menlo Park, Calif. 109 pp.

2. Abbott, T.M., "Visible Infrared Span-Scan Radiometer (VISSR) for a Synchronous Meteorological Spacecraft (SMS)," "Santa Barbara Research Center's VISSR Final Report, (Contract No. NAS5-21139), NASA, Goddard Space Flight Center, Greenbelt, Md., Sept. 1974.
3. Bristor, C.L., "Central Processing and Analysis of Geostationary Satellite Data," NOAA Technical Memorandum NESS 64, National Environmental Satellite Service, NOAA, U.S. Dept. of Commerce, Washington, D.C. March 1975, 155 pp.
4. Calif. Cooperative Snow Surveys, "Water Conditions in California Special Summary," June 1, 1975, State of California Dept. of Water Resources, Sacramento, Calif.
5. Miller, D.B., and R.G. Feddes, 1971. "Global Atlas of Relative Cloud Cover 1967-1970 Based on Data from Meteorological Satellites. NOAA NESS and USAF, Air Weather Service, Environmental Technical Applications Center, Washington, D.C.
6. Schneider, Stanley R., 1975, personal communication, Nat. Environmental Sat. Service, Washington D.C.
7. Halverson, Howard G. and James L. Smith, 1974. Controlling Solar Light and Heat in a Forest by Managing Shadow Sources, USDA Forest Service Res. Paper PSW-102, Pacific Southwest Forest and Range Exp. Stn.
8. Middleton, W.E. Knowles, and A.G. Mungall, 1952, The Luminous Directional Reflectance of Snow, J. Optical Soc. of Am., Vol. 42, pp 572-579.

Table 1

FILM LOOP STATISTICS

1. Number of Images

- (1) Total = 57
- (2) 3 missing over 60 day period

2. Daily Time Spread (GMT)

- (1) Total: 19:15 - 00:45 - 5-1/2 hours
- (2) Over 90% fall between 20:45 and 22:45
- (3) Mean image time \approx 2200

3. Cloud Cover

- (1) Partial Cloud Cover = 33%
- (2) Totally Obscured = 7%

**SYNOPSIS OF CURRENT SATELLITE SNOW MAPPING TECHNIQUES,
WITH EMPHASIS ON THE APPLICATION OF NEAR-INFRARED DATA**

James C. Barnes and Michael D. Smallwood, *Environmental Research & Technology, Inc., Concord, Massachusetts 01742*

ABSTRACT

The Skylab EREP S192 Multispectral Scanner data have provided for the first time an opportunity to examine the reflectance characteristics of snowcover in several spectral bands extending from the visible into the near-infrared spectral region. The analysis of the S192 imagery and digital tape data indicates a sharp drop in reflectance of snow in the near-infrared, with snow becoming essentially non-reflective in Bands 11 (1.55-1.75 μm) and 12 (2.10-2.35 μm). Two potential applications to snow mapping of measurements in the near-infrared spectral region are possible: (1) the use of a near-infrared band in conjunction with a visible band to distinguish automatically between snow and water droplet clouds; and (2) the use of one or more near-infrared bands to detect areas of melting snow.

INTRODUCTION

More than 15 years ago, in April 1960, snow could be detected in eastern Canada in the initial pictures taken by the first weather satellite, TIROS-1. Since then, as improved satellite systems have been developed, an increasing use has been made of remote sensing from space to map snowcover. Recently, a handbook of techniques for satellite snow mapping has been prepared to assist in the planning of a practical demonstration project of the application of satellite data to snow hydrology (1). In the handbook, the emphasis is on the use of NOAA VHRR (Very High Resolution Radiometer) and LANDSAT (formerly, the Earth Resources Technology Satellite) visible imagery. These data have been shown to have practical application to snow hydrology.

In addition to satellite imagery in the visible portion of the spectrum, measurements in the near-infrared spectral region may also have considerable application to snow mapping. In this paper, the results of an investigation of snow reflectance characteristics using data from the Skylab EREP (Earth Resources Experiment Package) S192 Multispectral Scanner are presented (3). The S192 Multispectral Scanner provided for the first time an opportunity to examine the spectral characteristics of snow from spacecraft altitude over the spectral range extending from the

Preceding page blank

visible to well-into the near-infrared.

S192 MULTISPECTRAL SCANNER DATA

Description of S192 Sensor

The S192 Multispectral Scanner is a 13-band radiometer with 12 of the bands being in the visible or near-infrared portion of the spectrum extending to about 2 μm (the thirteenth band is in the thermal infrared). The spectral range for each band is given in Table 1. The conical scan pattern of the S192 covers a swath of the earth's surface that is approximately 72.4 km wide; the instantaneous field-of-view (IFOV) is 79.25 meters (260 feet). A detailed description of the Multispectral Scanner is given in the Skylab Earth Resources Data Catalog (5). Both imagery and digital data from Computer Compatible Tapes were used in the data analysis.

TABLE 1.-S192 MULTISPECTRAL SCANNER SPECTRAL BANDS

<u>Band Number</u>	<u>Description</u>	<u>Spectral Range (μm)</u>
1	Violet	0.41-0.46
2	Violet-Blue	0.46-0.51
3	Blue-Green	0.52-0.56
4	Green-Yellow	0.56-0.61
5	Orange-Red	0.62-0.67
6	Red	0.68-0.76
7	Infrared	0.78-0.88
8	Infrared	0.98-1.08
9	Infrared	1.09-1.19
10	Infrared	1.20-1.30
11	Infrared	1.55-1.75
12	Infrared	2.10-2.35
13	Thermal Infrared	10.2-12.5

Data Sample

The S192 data used in this study were acquired for four test site areas: the Sierra Nevada-White Mountains are in California; the Wasatch Range in Utah; the central Arizona mountains; and a portion of the Upper Mississippi-Missouri River Basin in the north-central part of the country. Data from five EREP passes were analyzed, two from the SL-2 mission in June 1973 and three from the SL-4 mission in January-February 1974.

Meteorological data indicate the snowcover in the test site areas observed in June 1973 was quite probably in a melting condition, except perhaps at the highest elevations. In each of the test site areas observed in mid-winter, some melting could have been taking place at lower and middle elevations, or the snowpack could have been refrozen from melting that had occurred during the preceeding few days. However, the snow conditions

were more stable than in the two springtime cases. No S192 data were collected over a test site area immediately following a fresh snowfall or during a very cold period.

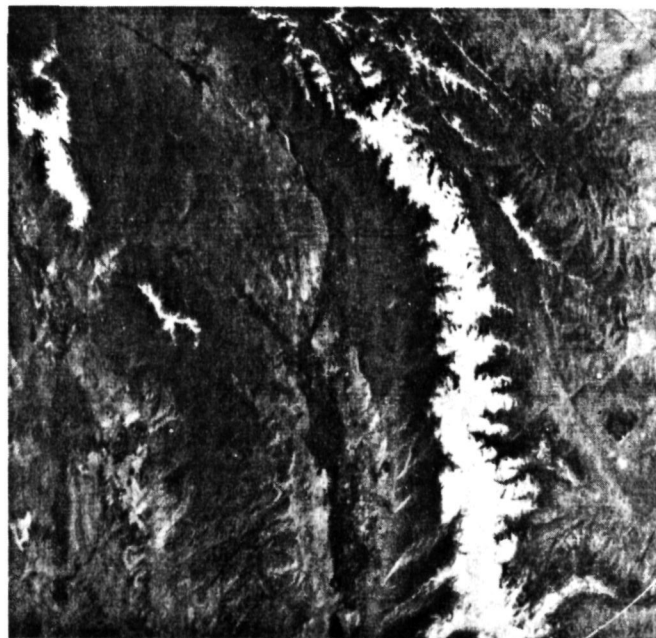
ANALYSIS OF S192 IMAGERY

The S192 imagery displays a marked drop in the reflectance of snow in the near-infrared bands. This effect is readily apparent in the imagery from the two SL-2 EREP passes, over the Sierra Nevada-White Mountain area and the Wasatch area. For the Wasatch area the S192 Band 2 and Band 11 imagery is shown in Figures 1a and 1b. Similarly, the S192 Band 3 and Band 11 imagery for the White Mountains is shown in Figures 2a and 2b. In both cases, snowcover has a high reflectance in the visible band, but appears essentially black in the near-infrared.

In Figures 2a and 2b, not only is the difference in the reflectance of the snow between the visible and near-infrared bands dramatic, but also the distinct nature of the clouds in the near-infrared spectral region. The concurrent S190A photograph indicates that cellular-type clouds, a pattern representative of cumulus (water clouds) cells, cover much of the area. Over the mountains, it is difficult to distinguish between the clouds and the snow in the visible band S192 imagery because both have essentially the same reflectance. In the Band 11 imagery, however, the clouds still appear white, whereas the snow appears essentially black; therefore, each cumulus cell is distinct, even those cells directly over the snowcovered mountains.

In the imagery from the June 1973 pass over the White Mountains, some snow can be detected in Band 9 but the extent of the snow appears less than in the visible band; the Band 9 imagery is shown in Figure 3. The apparent decrease in snow extent in the intermediate spectral bands is also observed in the data for the Utah test site area, which includes the Mt. Nebo Range and San Pitch Mountains (Figures 4a through 4f). In the visible band, the entire snowpack has a high reflectance. In Band 7, however, a slight decrease in the apparent snow extent in the Mt. Nebo Range is observed; in Bands 8, 9, and 10, the apparent snowcover successively decreases until in Band 10 the only bright area is along the highest ridge of the range; in Band 11, no snow can be detected. In the San Pitch Mountains, which are at a lower elevation, the less extensive snowcover can barely be detected in Band 7 and cannot be detected in Bands 8 through 11.

The results of the analysis of S192 imagery for the wintertime cases are essentially the same as those for the SL-2 data discussed above. In each case, snow has a high reflectance in the visible, except in areas that are forested, whereas in the Band 11 imagery, the entire snowcovered area is non-reflective. In the intermediate spectral bands, a gradual lowering of the reflectance is observed beginning with about Band 8 or 9; however, the decrease in reflectance is uniform across the snowcover, and no gradual decrease in the apparent snow extent is observed, as was the case in the data from each of the SL-2 passes.



(a) Band 2

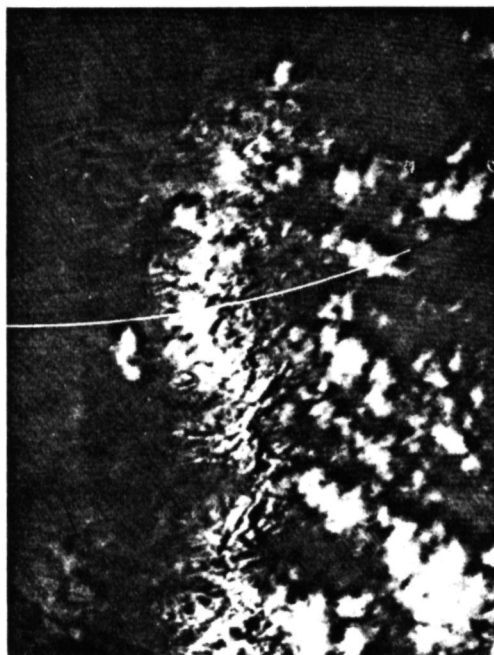


(b) Band 11

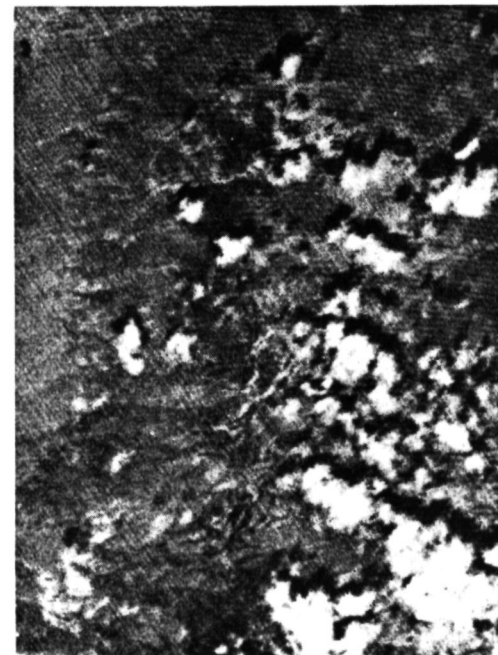
Figure 1 S192 imagery from EREP Pass 5, 5 June 1973; (a) Band 2 (0.46 - 0.51 μm), (b) Band 11 (1.55 - 1.75 μm). Area covered is the Wasatch Range in Utah. Note decreased reflectance of snow in Band 11 as compared to the Band 2 imagery.

REPRODUCIBILITY OF THE
ORIGINAL PAGE IS POOR

203

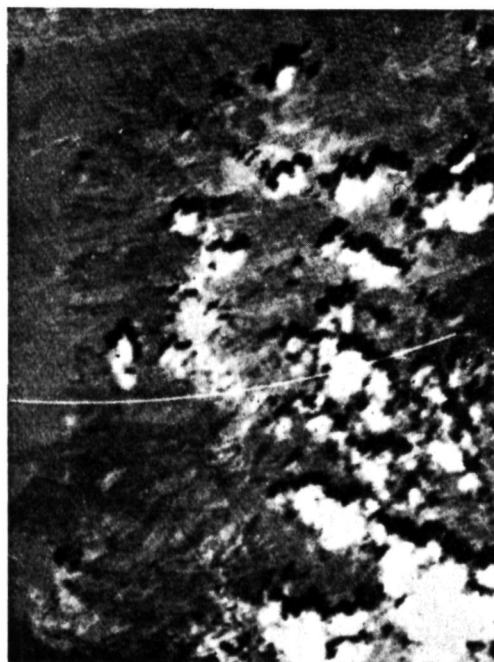


(a) Band 3

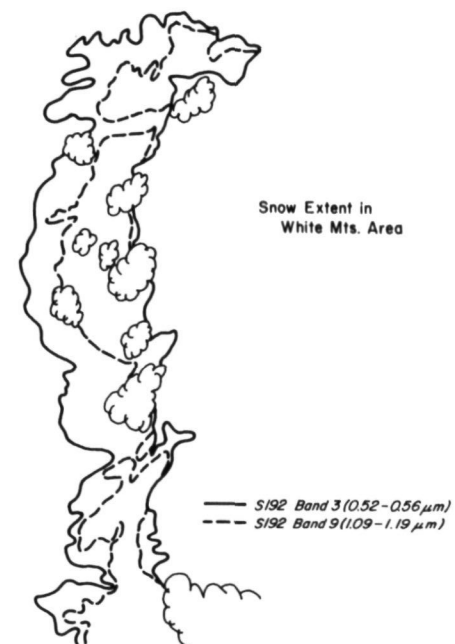


(b) Band 11

Figure 2 S192 imagery from EREP Pass 3, 3 June 1973; (a) Band 3 ($0.52 - 0.56 \mu\text{m}$), (b) Band 11 ($1.55 - 1.75 \mu\text{m}$). Area covered is the White Mountains. Because of the decreased reflectance of the snow, clouds that cannot be detected in Band 3 are distinct in Band 11.

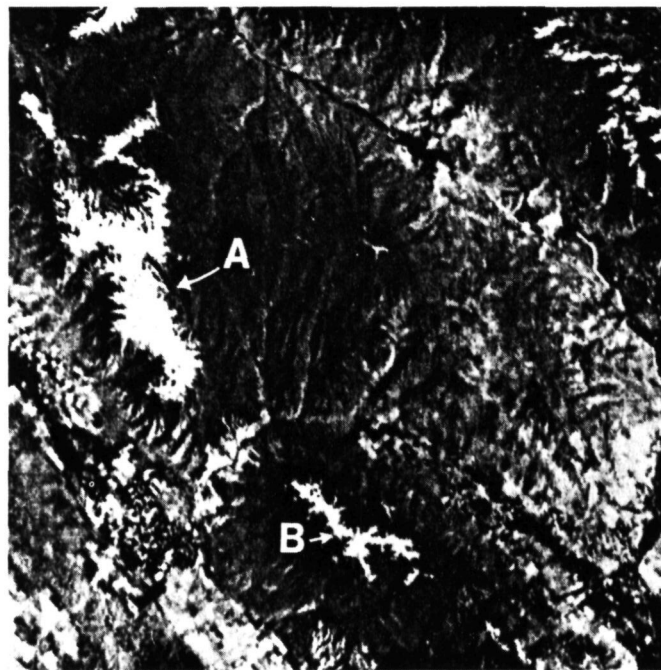


(a) Band 9

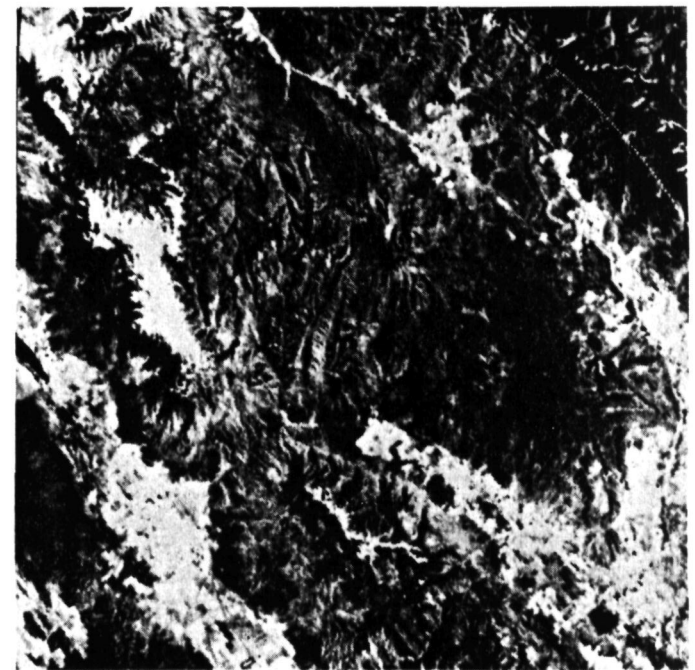


(b)

Figure 3 (a) S192 Band 9 imagery (1.09 - 1.19 μm) from EREP Pass 3, 3 June 1973; area covered is the White Mountains. Note the decrease in the apparent snow extent as compared to the visible band imagery (Figure 2a). (b) Comparative map showing relative extent of apparent snowcover mapped from S192 Band 3 (Figure 2a) and Band 9 (Figure 3a) imagery.



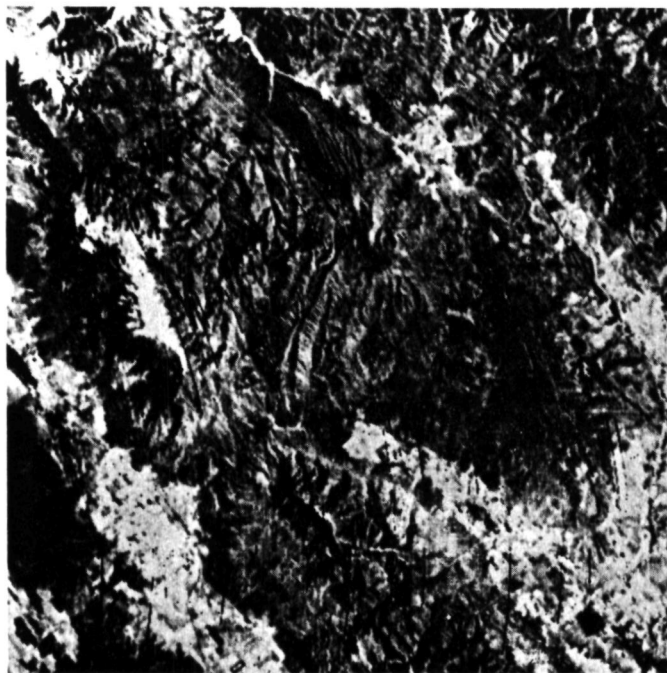
(a) Band 3



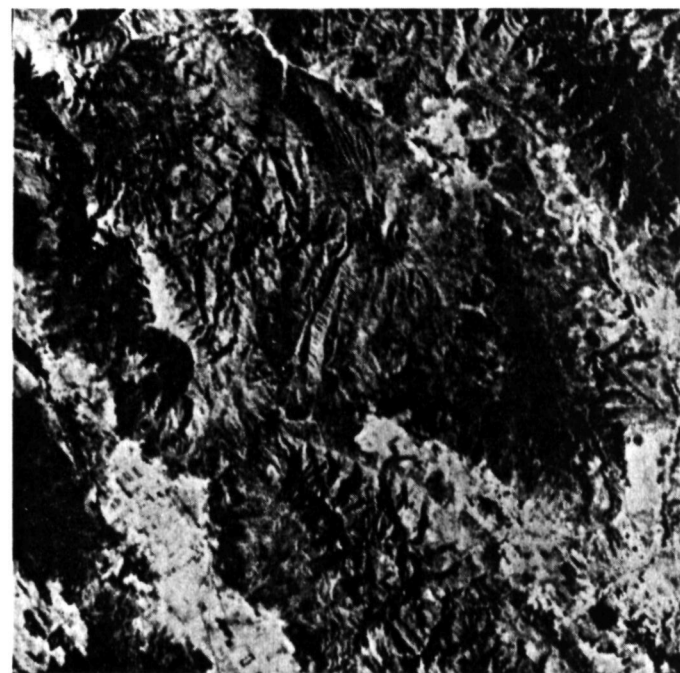
(b) Band 7

Figure 4

S192 imagery from EREP Pass 5, 5 June 1973; area covered includes the (A) Mt. Nebo Range and (B) San Pitch Mountains in Utah. (a) Band 3 (0.52 - 0.56 μm), (b) Band 7 (0.78 - 0.88 μm), (c) Band 8 (0.98 - 1.08 μm), (d) Band 9 (1.09 - 1.19 μm), (e) Band 10 (1.20 - 1.30 μm), and (f) Band 11 (1.55 - 1.75 μm). Note the gradual decrease in the extent of snowcover that maintains a high reflectance from Bands 3 through 11.

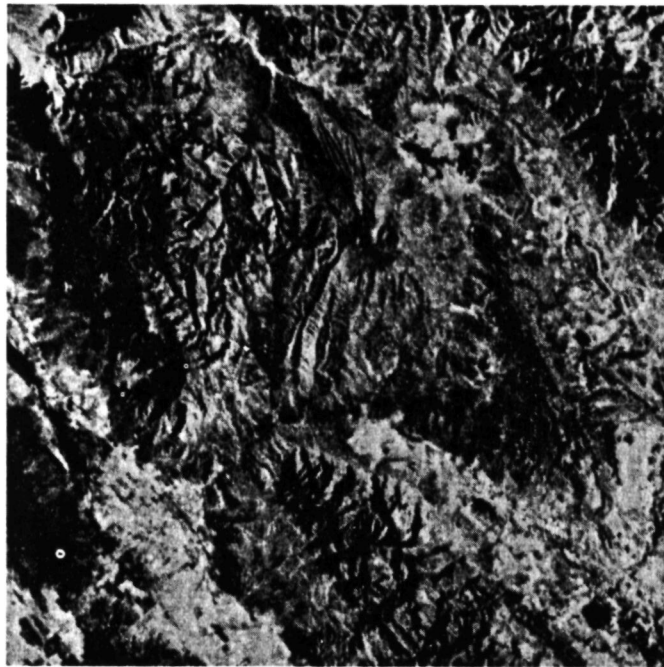


(c) Band 8

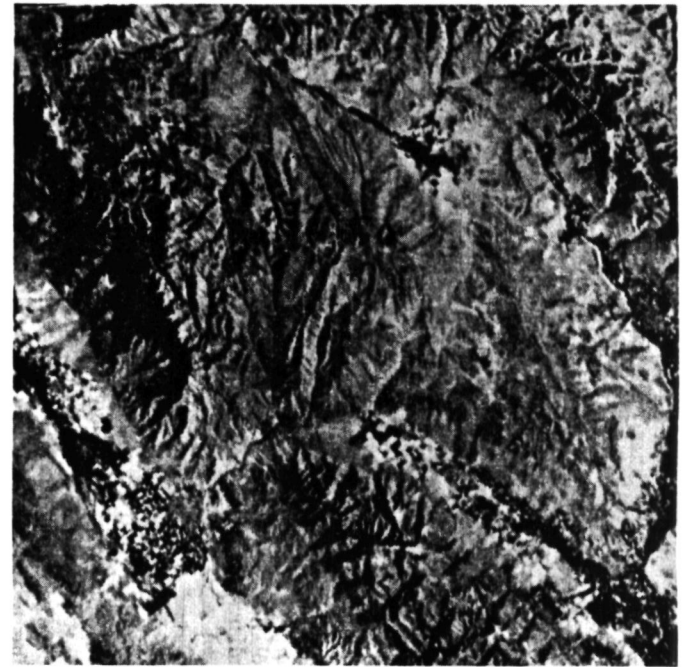


(d) Band 9

Figure 4 continued



(e) Band 10



(f) Band 11

Figure 4 continued

Data Processing Procedures

The high data rate of the S192 instrument presented some problems in working with the Computer Compatible Tapes (CCT's). Even for the rather limited time segments for which CCT's were provided, it was not feasible to perform digital count to radiance conversions for the entire data segment. The principal problem, therefore, was to devise a technique for the selection of specific data segments of only a few scanlines corresponding to the locations of known ground features.

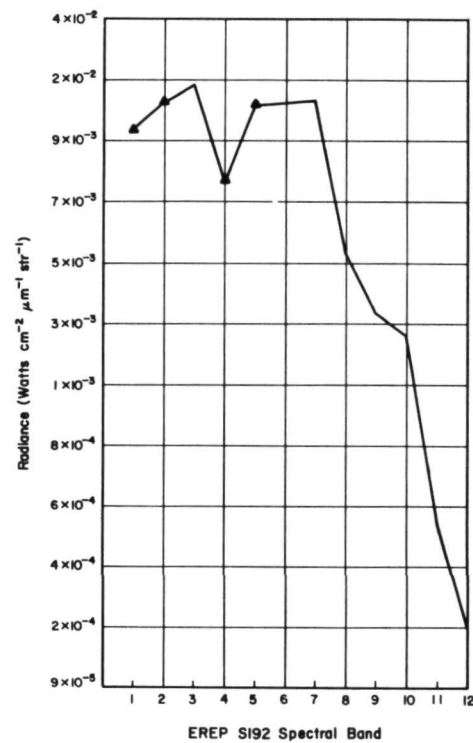
The technique devised to accomplish this task was a pre-selection procedure based on the analysis of raw channel counts. Knowing from the information on the S192 data supplied by NASA that snowcover would likely be saturated in the visible bands, a channel corresponding to one of the visible bands was selected. The CCT's were then manipulated such that each pixel in that channel that was saturated (raw data count = 255) would be printed out as a black dot and each pixel that was not saturated (raw data count < 255) would be left blank. The result produced an image-like printout where all snowcovered (non-forested) areas appear black, and, therefore, specific features could be located.

Following selection of the specific numbers of scanlines and pixels from the printout, the calibrated radiances for each required channel were computed using the appropriate conversion equation supplied with the tapes. This processing technique was found to be extremely efficient and greatly facilitated the handling of the S192 Computer Compatible Tapes.

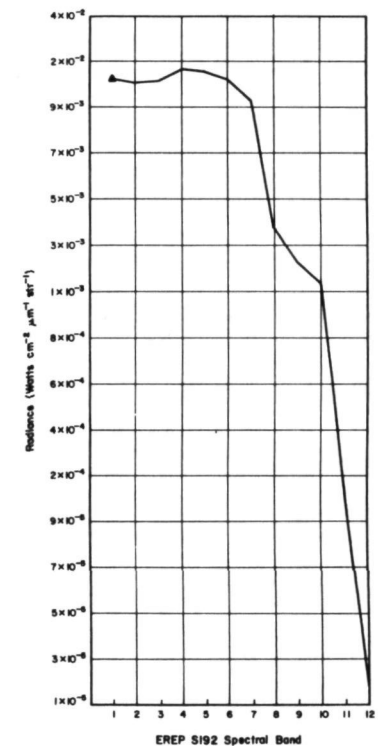
Results of Analysis

The radiance values obtained from the processing of the digitized data were analyzed for each of the four cases (digital data were not available for the June 1973 pass over the California site area). A single pixel determined to be located within a uniform snowpack was selected for each of the four test site areas. The radiance value for the pixel was averaged with the five pixels before and after it to acquire a true representation of the snow response. This process was repeated for each band, and the averaged values were then graphed. The resulting graphs of the radiance values for each spectral band are shown in Figures 5a and 5b for two of the test sites, the Wasatch and the central Arizona Mountains.

For each of the test sites, the graphs indicate saturation or near saturation values (triangles indicate saturation levels) throughout the visible portion of the spectrum followed by a significant decrease in reflectance in the near-infrared. In the interpretation of the graphs it is necessary to consider not only the curve itself, but also the curve in relation to saturation levels; in this way, a saturated value is not misinterpreted as a decrease in reflectance (such as Band 4).



(a)



(b)

Figure 5 Graph showing S192 measured radiance vs. spectral band for snowcover in (a) the Wasatch test site and (b) the central Arizona test site. Triangles indicate saturated values.

DISCUSSION OF RESULTS OF S192 DATA ANALYSIS

Comparison of SL-2 and SL-4 Data

For the five cases for which S192 data were analyzed, the overall results of the analysis of the imagery and the digital radiance values are consistent. In each case, snowcover exhibits a marked drop in reflectance in the near-infrared portion of the spectrum. Moreover, no significant difference in the reflectance characteristics of snow is apparent in the five cases examined, even though two of the cases were from the late spring and the other three from mid-winter. One difference that was observed, however, is that in both of the late spring cases the apparent extent of the snowcover gradually decreases from Band 7 through Band 11; in the winter cases, a uniform decrease in reflectance is observed with no apparent change in the detectable snow extent.

As was pointed out in the earlier discussion of the data sample, even in the winter cases no data were collected immediately following a fresh snowfall. Thus, the two spring cases were at times when the snowpack was in a general melting condition, whereas the three wintertime cases were at times when the snowpack was more stable but still consisting of somewhat aged snow that might be undergoing slight melting or had undergone melting and become refrozen.

It must also be remembered that the problem of measuring radiance values from a spacecraft platform is extremely complex. Many factors, such as the slope of the reflecting surface and especially the solar elevation angle, can influence the measurements. The solar elevation angle must be considered when attempting to compare measurements taken over different areas at different times of the year. Atmospheric attenuation must also be taken into account; however, the preliminary results of another Skylab investigation being conducted at ERT indicate that the error in determining surface reflectance for snow would be less than five percent for all spectral bands.

Comparison With Laboratory Experiments

The results of the analysis of the Skylab data are in general agreement with the results of laboratory experiments of the red and near-infrared spectral reflectance of snow (6). Since the laboratory results are in terms of the snow reflectance relative to a standard (white barium sulfate powder), it is difficult to compare these results directly with S192 measured radiances. However, graphs of the laboratory results show similar tendencies to the S192 radiances over snowcover. The S192 results indicate a decrease in snow reflectance beginning in Band 8 (0.98-1.08 μm); the laboratory experiments indicate a high reflectance in the red, with a marked decrease in reflectance from about 0.90 to 1.0 μm (a slight increase in reflectance occurs at 1.0 to 1.1 μm). Secondly, the S192 results show a slight leveling off of the drop

in snow reflectance in Band 10 (1.20-1.30 μm); the laboratory experiments show that the reflectance decreases rapidly from 1.1 to 1.5 μm with the exception that at about 1.25-1.35 μm it levels off and even makes a slight recovery. Finally, the S192 results show the lowest reflectance values to be in Bands 11 (1.55-1.75 μm) and 12 (2.10-2.35); the laboratory experiments show low reflectance values at about 1.5-1.6 μm and an even stronger depression at 1.95-2.05 μm with a very slight rise at about 2.25 μm .

In the laboratory experiments, natural aging of the snow influences both the degree and rate of change of the reflectance. In general, melting lowers the reflectance, with some recovery if the snow is refrozen. A significant difference in the reflectance curves for dry and melting snow occurs at about 1.2 -1.4 μm . The snowcover observed in the Skylab experiment had in each case aged to a certain extent.

POTENTIAL APPLICATIONS TO SNOW MAPPING

Based on the results of the analysis of S192 data, two potential applications to snow mapping of measurements in the near-infrared spectral region are possible: (1) the use of a near-infrared band in conjunction with a visible band to distinguish automatically between snow and clouds; and (2) the use of one or more near-infrared bands to detect melting snow.

The nearly complete reversal in snow reflectance between the visible bands and Bands 11 and 12 observed in each case indicates that in this portion of the near-infrared, snow surfaces are essentially non-reflective regardless of the condition of the snow. In contrast, the reflectance of clouds (water droplet) is essentially the same in each of the S192 bands, displaying no drop in the near-infrared. As a result, a technique combining two spectral bands, one in the visible and one in the near-infrared at the position of Band 11 or 12 (1.55-1.75 μm or 2.10-2.35 μm), can be used to distinguish between snow, clouds, and non-snowcovered ground. A feature having a high reflectance in the visible and a low reflectance in the near-infrared would be classified as snow; a feature having a high reflectance in both bands would be classified as cloud; and a feature having a low reflectance in the visible and a medium reflectance in the near-infrared would be classified as non-snowcovered ground. An automatic technique for distinguishing snow from clouds is of particular significance, since this has been recognized as a serious problem with regard to the eventual machine processing of satellite data for snowcover mapping.

The second potential application, that of detecting melting snow, is based on the observed behavior of snow in the intermediate bands from about Band 7 (0.78-0.88 μm) through Band 10 (1.20-1.30 μm). In an early investigation using Nimbus-3 near-infrared data (8) the observed low reflectance of snow and ice was attributed to the existence of meltwater on the snow/ice surface. In studies using LANDSAT imagery (2, 4, and 7), the near-infrared band has consistently indicated less snowcover than has

the visible band; the difference has been attributed to the reduced near-infrared reflectance associated with melting or refrozen snow.

Although the Skylab data sample was limited, the S192 film products for the spring cases (June) display snow reflectance characteristics not observed in the winter cases (January-February). In the two spring cases, the apparent snow extent decreases gradually from a maximum in the visible (Band 6) to a minimum in Band 11. This gradual decrease in the area of high reflectance is difficult to account for unless it is because the snow at the lower elevations is melting, and therefore exhibits a more rapid drop in reflectance, whereas the snow at the highest elevations is dryer or refrozen, and therefore does not exhibit a significant drop in reflectance until Band 11. In the winter cases, the snowpack is more uniform at all elevations, so does not display the gradual reduction in reflectance. It is concluded, therefore, that bands in the spectral range from about 0.8 μm to about 1.30 μm should provide the most information on the condition of the snow surface with regard to the snow being melting (wet surface) or being not melting or refrozen (dry surface).

Further study of snow reflectance characteristics is needed. The available data sample did not include a situation where snow and ice clouds are present, where the technique to distinguish between snow and water droplet clouds could be tested to determine its application to ice clouds. Also, measurements over fresh, dry snow as well as additional measurements over areas of known melting snow are needed before the relationships between reflectance and snow condition are completely understood. Nevertheless, the results of the analysis of Skylab EREP data are believed to be sufficiently conclusive to warrant careful consideration for including one or more near-infrared spectral bands on radiometers to be flown on future operational satellite systems. Measurements in the near-infrared spectral region, in combination with visible and thermal infrared measurements, have the potential for providing greatly improved information with regard to snow hydrology and thus have the potential for providing eventual significant cost savings to snow survey programs.

ACKNOWLEDGEMENTS

The investigation described in this paper was supported by NASA Johnson Space Center under Contract No. NAS 9-13305. The authors are grateful for the assistance provided throughout the study by the Technical Monitor, Mr. Larry B. York, of the Principal Investigator Office.

REFERENCES

1. Barnes, J.C., and C.J. Bowley, 1974: Handbook of Techniques for Satellite Snow Mapping, Report prepared under Contract NAS 5-21803, Environmental Research & Technology, Inc., Concord, MA, 95 pp.

2. Barnes, J.C., C.J. Bowley, and D.A. Simmes, 1974: The Application of ERTS Imagery to Mapping Snowcover in the Western United States, Final Report under Contract NAS 5-21803, Environmental Research & Technology, Inc., Concord, MA, 77 pp.
3. Barnes, J.C., M.D. Smallwood, and J.L. Cogan, 1975: Study to Develop Improved Spacecraft Methods Using Skylab/EREP Data, Final Report under Contract No. NAS 9-13305, Environmental Research & Technology, Inc., Concord, MA, 92 pp.
4. Bowley, C.J., and J.C. Barnes, 1975: The Application of ERTS Imagery to Mapping Snowcover in the Western United States, Supplemental Report under Contract NAS 5-21803, Environmental Research & Technology, Inc., Concord, MA, 43 pp.
5. NASA, 1974: Skylab Earth Resources Data Catalog, Doc. No. JSC-09016, NASA/Johnson Space Center, Houston, Texas, 359 pp.
6. O'Brien, H.W., and R.H. Munis, 1975: Red and Near-Infrared Spectral Reflectance of Snow, Research Report 332, 18 pp., U.S. Army Cold Regions Research and Engineering Laboratory, Hanover, N.H.
7. Rango, A., V.V. Salomonson, and J.L. Foster, 1975: Seasonal Streamflow Estimation Employing Satellite Snowcover Observations, Preprint X-913-75-26, NASA/Goddard Space Flight Center, 34 pp.
8. Strong, A.E., E.P. McClain, and D.F. McGinnis, 1971: "Detection of Thawing Snow and Ice Packs through the Combined Use of Visible and Near-Infrared Measurements from Earth Satellites", Monthly Weather Review 99 (11), pp. 828-830.

**COMPARISON OF DIFFERENT METHODS FOR ESTIMATING SNOWCOVER
IN FORESTED, MOUNTAINOUS BASINS USING LANDSAT (ERTS) IMAGES**

M. J. Meier, *U. S. Geological Survey, Tacoma, Washington*; W. E. Evans, *Stanford Research
Institute, Menlo Park, California*

ABSTRACT

Snow-covered areas on LANDSAT (ERTS) images of the Santiam River basin, Oregon, and other basins in Washington were measured using several operators and methods. Seven methods were used: (1) Snowline tracing followed by measurement with planimeter, (2) mean snowline altitudes determined from many locations, (3) estimates in 2.5 x 2.5 km boxes of snow-covered area with reference to snow-free images, (4) single radiance-threshold level for entire basin, (5) radiance-threshold setting locally edited by reference to altitude contours and other images, (6) two-band color-sensitive extraction locally edited as in (5), and (7) digital (spectral) pattern recognition techniques. Methods (4), (5), and (6) used the SRI Electronic Satellite Image Analysis Console (ESIAC). The seven methods are compared in regard to speed of measurement, precision, the ability to recognize snow in deep shadow or in trees, relative cost, and whether useful supplemental data (such as the distribution of snow-covered area with location or altitude) are produced. Standard errors range from about 3 to over 12 percent of the basin area depending on method and the fraction of the basin which is snow covered.

INTRODUCTION

The areal extent of snow in forested, mountainous drainage basins is difficult to measure with sensors flown in high-flying aircraft or satellites, and the cost of accurate measurements is extremely high with sensors at ground level or in low-altitude aircraft. Thus evaluation of satellite techniques for measuring snow in large, forested mountain basins is beset by both difficult (or subjective) methodologies and a general lack of accurate field data for comparison. Satellite snow measurements for drainage basins in the Cascades of Oregon and Washington are especially difficult for the basins contain large areas of virtually complete forest canopy, steep slopes with great radiance contrasts between sunlit and shadowed areas, and frequent cloud cover. Yet it is in basins such as these that the need for data

Preceding page blank

is most critical because of the importance of snowmelt forecasts for the optimal operation of a large number of hydroelectric power and irrigation reservoirs.

This paper compares snow measurements from LANDSAT (ERTS) images of basins in the Oregon and Washington Cascades using seven different measurement techniques and several operators. The measurement techniques are evaluated in terms of their usefulness for repetitive, operational programs. No absolute standard of accuracy exists; even if it had been possible to obtain complete aerial photographic coverage at the time of each satellite overpass, no measurement procedure from these photographs would be free of error. The term precision is used here when evaluating methods. A method which produces consistent, repeatable results from operator to operator, basin to basin, and image to image is said to be precise.

An important difficulty in obtaining precise readings is the subjective judgment of the area of snow obscured by forest canopy. Special attention is given to this problem. In forest openings (clear cuts, transmission-line cuts, natural openings, etc.) the existence or lack of snowcover can be observed. The snowline must then be interpolated between these openings. This interpolation is valid only if the snow observed in openings is representative of the snow in the forest. In spite of much research on this subject (e.g., Anderson and Gleason, 1959; Hoover and Leaf, 1967; Gary, 1974) it is still impossible to know how representative the snow in forest openings is. In some areas including western Oregon more snow than normal may be deposited in openings, but such snow also may melt more rapidly (Rothacher, 1965).

Attention was concentrated on the drainage basin North Santiam River above Detroit Reservoir, Oregon (1,134 km²), listed here as the Santiam Basin (Figure 1). This is a typical high Cascade basin, with heavy forest, clear cuts, steep slopes, and some high, alpine areas. It is a basin for which snow data are required for reservoir operation, and one of several basins selected in the Pacific Northwest for the Operational Applications of Satellite Snowcover Observations Program. In addition to Santiam Basin images of February 11, April 6, April 24, and May 12, 1973, and June 30, 1974, measurements were also made of images of Thunder Creek, Cascade River, and South Cascade Glacier drainage basins, all in the North Cascades of Washington.

MANUAL METHODS

LANDSAT (ERTS) band 5 (0.6 to 0.7 μ m wavelength) provided the best separation of snow from other materials, and was used in all of the three manual methods.



Fig. 1--LANDSAT (ERTS) image of Santiam Basin as of April 6, 1973. Drainage basin is indicated by the black and white line. Note the white snow showing in numerous rectangular clear cuts in the dense forest, and the grey non-snow conditions showing in other clear cuts.

Method 1: Snowline tracing and measurement with planimeter

This technique, in several variations, has been widely used and is well described elsewhere (Barnes and Bowley, 1974). The snowline and drainage basin outline can either be traced directly on an enlarged image or on a transparent overlay, or transferred to a map using a transparent, gridded overlay or an optical device such as a zoom transfer scope. The method is relatively time-consuming if the snow boundary is deeply convoluted and patchy and if the observer tries to follow the snowline carefully. Other desired information such as altitude contours or time-lapse sequences is rarely available so that snowline interpolation is

very subjective. This difficulty plus the inherent errors in measuring the area of a deeply convoluted curve make the method relatively imprecise. Standard deviations about group means of individual operator determinations using drainage basins in the North Cascades ranged from 7 to 11 percent during the melt season, and up to 32 percent in winter.

Method 2: Mean snowline altitudes determined from many locations

This technique is useful in mountainous regions because the snowpack generally varies strongly with altitude but only slightly with horizontal distance. The general technique has been used by many. In this study operators were asked to scan enlarged LANDSAT (ERTS) images (1:250,000) of the Santiam Basin for areas where the snowline was clearly defined, and then to interpolate the altitude from a transparent overlay with 152.4 m (500 ft) topographic contours. Each such determination was punched into a simple statistical routine on a pocket calculator. The operator then scanned for additional points, attempting to cover the basin uniformly, and continued until the number of points measured (as displayed on the calculator) totalled at least 20. The mean altitude and standard deviation were then calculated, and converted to equivalent area through use of an area-altitude curve.

This method is extremely fast (requiring 2-5 minutes per image), requires little expensive equipment, and is relatively precise. The standard deviation of individual operator's results from the 5-operator mean ranged from 81 to 178 m (average 126 m) in altitude, corresponding to 2.4 to 5.3 percent (average 3.8 percent) of basin area.

Method 3: Estimates in 2.5 x 2.5 km boxes with reference to a snow-free image

This technique was first exploited by Lauer and Draeger (1974), who used squares (boxes) 1.98 x 1.98 km in size. We chose 2.5 km as a convenient grid size--small enough so that major drainage basins would be adequately sampled yet large enough to contain adequate information (about 1500 resolution elements or pixels) for snowcover estimations. This box size was also convenient to index to the UTM metric grid printed on topographic maps.

Operators were provided with a 1:250,000 LANDSAT (ERTS) image, a transparent overlay showing the 2.5 x 2.5 km boxes together with some drainage information for registering to the image, a transparent overlay with topographic contours for reference, a late-summer color-IR composite image also for reference, and a set of rules for interpolating the snowline between known positions. The operator then marked the snowcover in tenths in each box, copied the result, computed the mean snow area (percent

of basin area) and some statistical parameters, and cleaned the overlay for the next measurement.

This method is not as fast as (2); careful work required at least 15-30 minutes per determination for the Santiam Basin. It is relatively precise; standard deviations of individual operator's results from the operator means ranged from 3.3 to 12.2 (average 5.9) percent of the basin area.

The method was also tested using a single color image (May 12, 1973) and two operators. Both operators measured less snow on the color image (average 11.1 percent snow) than on the black and white, band 5 image (average 14.1 percent). The information content of the color image is higher, so this suggests that the box method using a black and white enlargement may slightly bias the results. The cost and time involved in making color enlargements makes it impractical to use them in an operational program.

METHODS USING AN ELECTRONIC, INTERACTIVE ANALYZER

The Stanford Research Institute's Electronic Satellite Image Analysis Console (ESIAC) is an interactive instrument that employs television scanning, storage, and animation techniques in a manner intended to bridge the gap between traditional photo-interpretation and completely objective digital processing (Evans, 1973). It has a sequential image capability which permits rapid registration, storage and retrieval of up to several hundred TV frames. Thus time-lapse sequences can be produced, and the superposition of overlays, drainage basin maps and elevation contours can be handled efficiently. Capability for manual editing and quantitative measurement of pixel radiance is also provided. While digital tapes can be accommodated, input normally has been from film transparencies.

To make quantitative measurements of the areal extent of scene constituents with the ESIAC, the general procedure is to create a binary thematic map, or "mask", from the source imagery. This mask is maintained in revisable "scratch-pad" memory, and is displayed as a two-dimensional image that can be viewed alone or in superposition with the full-tone scene images. The binary mask may also be written on the disc file of a minicomputer in 2.5 x 2.5 km grid increments. Figure 2 shows a binary mask of the Santiam Basin (May 12, 1973) together with a computer print-out of these same data reduced so that each digit represents tenths of snowcover within each 2.5 x 2.5 km box. This procedure provides a simplified mechanism for machine storage and sorting of the data. In addition, statistical data (e.g., box-by-box means, standard deviations, and residuals) can be derived which may help to identify sources of bias from individual operators and methods.

A number of operating options are possible. Increases in

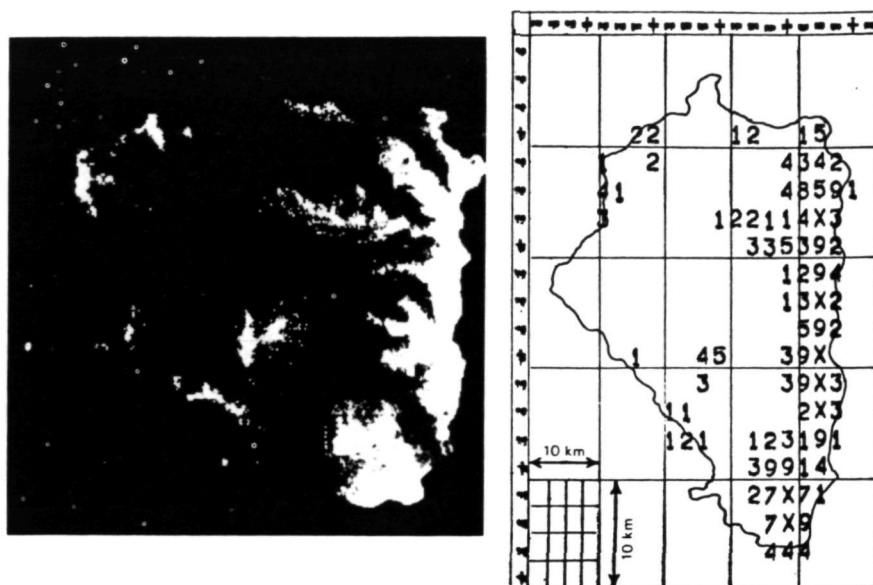


Fig. 2--(Left) Typical binary mask generated by ESIAC of the Santiam Basin, May 12, 1973 image, using a radiance-threshold locally edited by reference to altitude contours. (Right) Computer printout of the data from this mask expressed as snow-covered area (in tenths) in 2.5 x 2.5 km boxes. No snow is blank, complete snowcover indicated by X.

accuracy and precision are bought at a cost of increased set-up time, analysis time, and operator training. Three operating procedures have been studied in relation to the snow inventory problem, and will be discussed here.

Method 4: Single radiance-threshold level

This method is identical in principal to other radiance threshold or "density slicing" techniques such as use of iso-density photographic film, scanning densitometers, or certain digital computer programs. This type of processing normally is applied to data from MSS band 5 for snow measurements. All picture elements showing radiances greater than a certain threshold value chosen by the operator are classed as snow. The same threshold level is applied simultaneously to all portions of the scene. The method relies on the hope that the operator will be able to produce a mask that will yield an acceptable match to his visual interpretation of the snowpack.

This radiance procedure works well for some scenes, but in

many other scenes it is annoyingly difficult to obtain agreement among operators regarding the "best" threshold setting. The uncertainty rapidly becomes worse as the operator lowers the threshold, trying to include the low-radiance snow--regions where the response is low because of tree cover, shadowing, or patchiness. The area-above-threshold tends to be a very sensitive function of the threshold setting in the region of the "Best Visual Estimate," BVE (Figure 3).

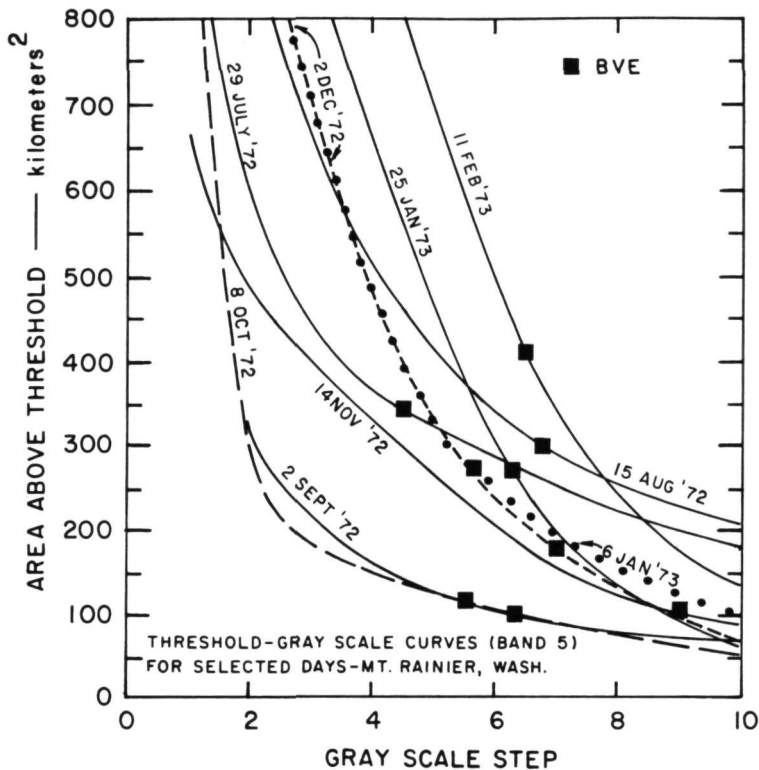


Fig. 3--Plots of radiance versus gray-scale step for several Mount Rainier, Washington, images. BVE is the best visual estimate of snow-covered area.

In addition to the operator decision problem, this high sensitivity at low radiances makes the system vulnerable to error from any of several instrumental difficulties that can cause slight differences in threshold performance for different regions of the picture. In images of late fall or early spring, when the sun angle is low and the snow extends well into the tree-covered regions, deviations of ± 30 percent of the snow-covered area are typical. Such problems are undoubtedly common to other "density slicing" techniques.

Method 5: Radiance-threshold setting locally edited by reference to altitude contours and other images

Again band 5 normally provides the source signal for the threshold circuitry. Through the use of the "scratch pad" memory it becomes possible to build up the binary snow mask in subbasin increments, each with its own threshold level rather than being constrained to accept some single compromise level. Particularly for difficult scenes, this improvement significantly reduces the inter-operator and repeat performance deviations in snowcover measurements. The effectiveness of this general approach can be further improved by always providing the operator with a good color display (even though the classification circuitry processes only one band) and by paying careful attention to details of how the various required display overlays--cursor, elevation contours, snow masks, etc.--are handled in order not to hide the subtle but important features in the image.

Assuming that the preparation of basin maps, contour overlays, and data sheets has been completed and that the operator is familiar with the region being evaluated, the incremental time required to analyze each new TV view (typically 2500 km²) is a minimum of 20 minutes. This figure includes registering two spectral bands to each other and to a previously recorded sequence, creation of a binary mask depicting the snow theme, and readout of the mask data to the computer file.

This method is the currently preferred operating procedure.

Method 6: Two-band color-sensitive thematic extractions, locally edited as in method (5)

The ESIAC operating controls permit threshold setting or "slicing" (combined upper and lower-bound thresholds) operations to be performed simultaneously in two spectral bands and on the ratio of signals from the two bands. This provides a considerable degree of freedom in making the thematic mask responsive only to scene elements that correspond to specific regions of color space, as is plotted, for example, in a diagram of radiance in band 4 versus radiance in band 7 (Figure 4). By adjusting the system to respond to a diagonal band centered on the field of snow in Figure 4, snow in shadow can be counted without accepting responses from bright sunlit trees or from silty water. On the other hand, such an algorithm completely eliminates the whole gamut of snow-tree mixtures (Figure 5). Adjustments to include the snow-tree mixtures but not the trees result in frequent responses from rock and bare ground, and the resulting masks were found usually to be only slightly different from those obtained by the much simpler process of setting high-pass thresholds on band 4 or 5 alone. Note that a single-band threshold of the visible-band-radiance signal corresponds to counting everything in Figures 4 and 5 to the right of a vertical line that defines the threshold level.

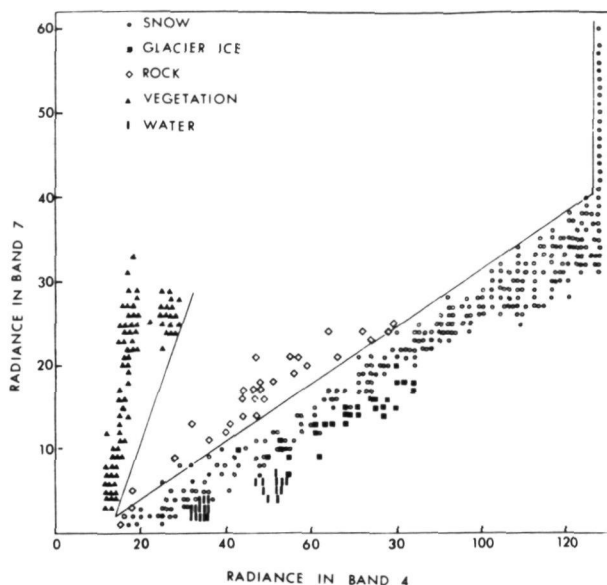


Fig. 4--Band 4/band 7, color-space plot showing five terrain types observed in the North Cascades, Washington. Note that the field of snow is clearly separated from the fields of other materials (except for glacier ice). The lines separate snow, rock, and vegetation. Each symbol represents one or more pixels.

The principal gain obtainable from operating with a tilted decision boundary instead of a vertical one lies in separating low-radiance snow--that which plots near the lower left corner of the color-space diagram--from vegetation and other materials. This separation is frequently easier to make on the basis of spatial distribution rather than spectral characteristics. An additional factor to be considered is that the low radiance corner of the diagram is a difficult region in which to work with an analog system. Signal-to-noise ratios are generally poorest, zero reference levels must be carefully watched, and photographic film is subject to "bleeding" and non-linear response.

There remains the possibility of combining bispectral classification with spatial and elevation information as was done with single-band data in method (5). It appears at this time, at least with an analog processing system, that the considerably greater attention required for both general system quality (color registration, equipment calibration, noise levels) and for adjustment of decision controls cannot be justified by expected improvements in accuracy and precision for operational snow area measurement. If the costs of digital preprocessing and input can be

tolerated, then some variant of method (6) could be come extremely attractive.

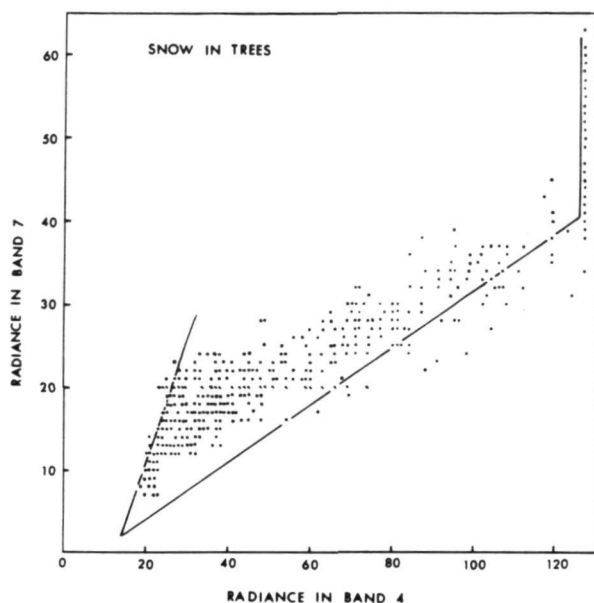


Fig. 5--Color-space plot showing snow in trees, similar to Figure 4. The lines are identical to those on Figure 4. Note that the field of snow in trees overlaps snow, vegetation, and the area between (including rock) as shown on Figure 4. Each dot represents one or more pixels.

Method 7: Digital pattern (spectral) recognition techniques

These powerful methods have been applied to snowcover measurement by Hoffer (1973) and by others. The method is most convenient when used in conjunction with an electronic console and standard pattern recognition programs. We employed only a modest computer terminal and simple two-dimensional programs to obtain a general impression of the advantages and disadvantages of the method. LANDSAT (ERTS) magnetic tapes were used of the North Cascades on May 12 and August 11, 1973.

An image denoting radiance levels of individual pixels was generated with a line printer, using characters to form an approximate grey scale. Drainage basin and training set boundaries were located on this and coded. Printouts were then obtained of two-dimensional radiance (color-space) plots for selected pairs of the 4 bands. Band 4 or 5 versus band 7 proved to be most useful for delineating the following terrain types: snow, snow and vegetation mixed, snow and rock mixed, glacier ice, water (silty and clear), rock, and vegetation (conifer forest, deciduous brush, alpine tundra). Snow could be clearly delineated

from rock, water, and vegetation (Figure 4), but snow and vegetation mixed was not always clearly separated from rock (Figure 5). Two-dimensional fields were defined and a terrain map of the South Cascade Glacier area (part of the Cascade River drainage) was produced (Figure 6). A map of the same area was produced by visual photointerpretation; the snowline in part of the area (6.2 km²) at the time of the satellite overpass was known from two cameras on the ground (Figure 7). Computer and visual recognition results are compared in Table 1. This shows a relatively high agreement in snow recognition (93.3 percent agreement,

Table 1--Summary of computer and visual recognition results for South Cascade Glacier area, for image of August 11, 1973. Numbers represent total pixels classified by each category and recognition method.

		Visual recognition						Total
		Snow	Ice	Water	Rock	Trees ¹	Tundra ²	
Computer recognition	Snow	682	20	0	47	0	2	751
	Ice	3	67	5	12	0	0	87
	Water	0	1	40	1	0	0	42
	Rock	13	5	6	269	0	54	347
	Vegetation	0	0	0	0	3	2	5
	Snow and vegetation	0	0	0	0	0	18	18
	Rock and vegetation	1	0	0	51	1	150	203
	Snow and rock	32	6	0	42	0	3	83
Total		731	99	51	422	4	229	1,536

Performance on snow: 93.3%.

Overall performance: 88.3%

1. Mature, large conifers.
2. Isolated trees, krummholz and alpine tundra intermixed with rock and soil.

equivalent to 3.2 percent error for the total area). Disagreement is attributed both to visual recognition error and to computer recognition error. In this case, with virtually no snow concealed under a forest canopy, the computer error is probably less than indicated above.



Fig. 6--Map of South Cascade Glacier area produced by computer recognition techniques. Black line is explained on Figure 7.

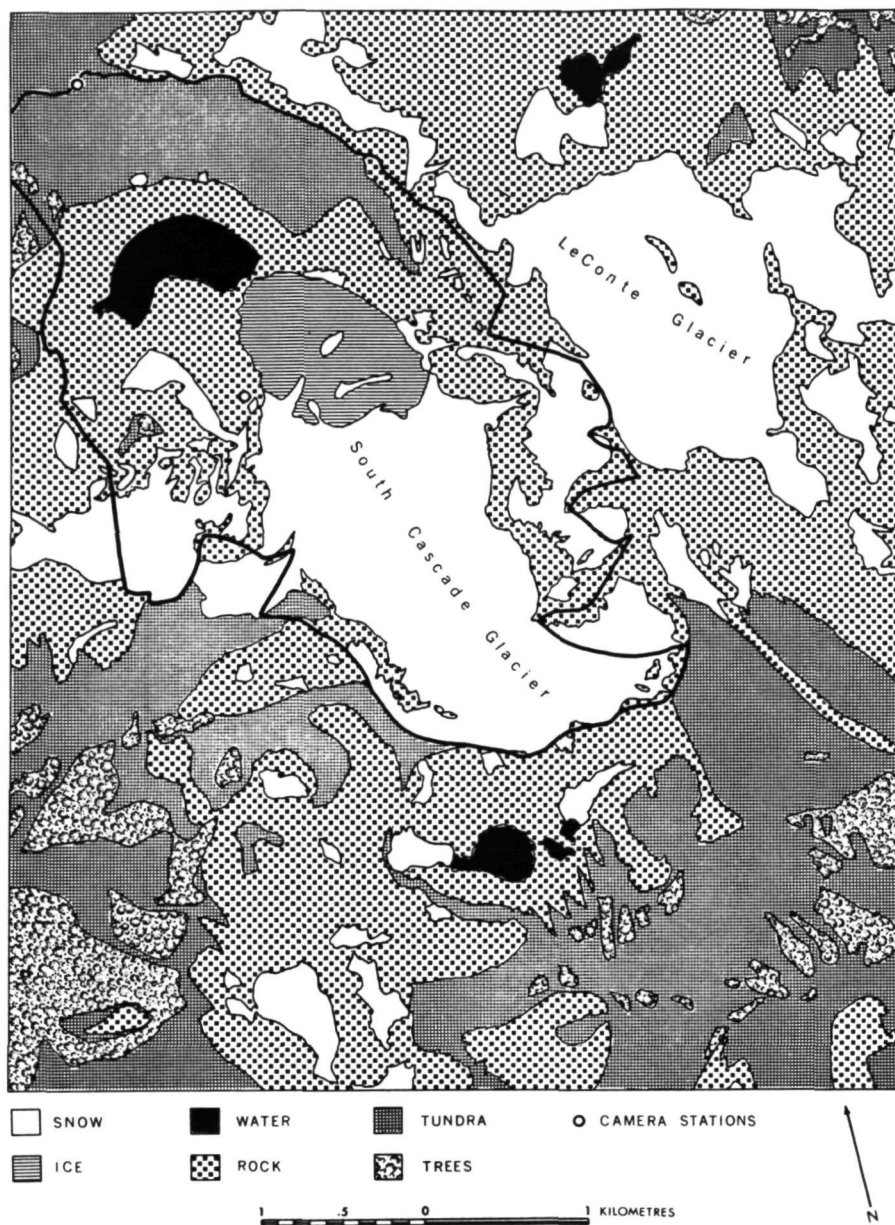


Fig. 7--Map of South Cascade Glacier produced by visual interpretation. The snowline is known only within the heavy black line, from photographs taken at two camera locations.

The program used to produce Figure 6 was then used to measure snow in the larger drainage basins of Cascade River (435 km²) and Thunder Creek (272 km²) for comparison with other methods.

COMPARISON OF METHODS

Precision

It is difficult to make other than generalized statements on the precision of different methods because of insufficient comparison data and the great flexibility inherent in each method. Also, it must be noted that for a given operator and method, the measurement error varies with the fraction of snow-covered area (Figure 8). With no snow, zero error is likely; with no snow-free ground the error also may equal or approach zero.

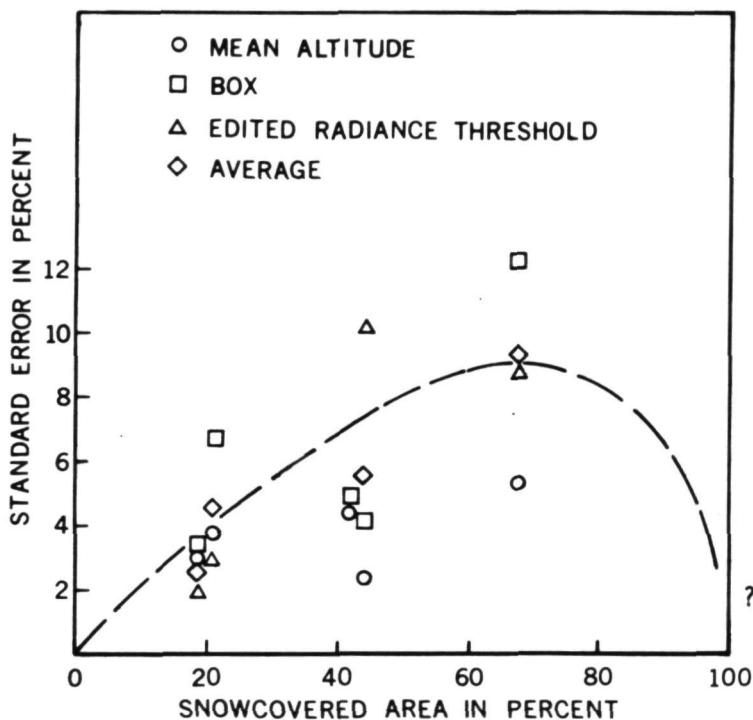


Fig. 8--Standard error for three methods as a function of snow-covered area. The dashed curve shows the probable shape of the curve, although sufficient data are not available to define it.

Results of the measurement of the five images of the Santiam Basin using three methods are shown in Table 2. The differences

Table 2--Comparison of mean altitude, box and radiance-threshold edited by altitude methods for Santiam Basin. N = number of observations (equal to or greater than the number of operators), \bar{X} = mean snowcover, in percent of basin area, S = standard deviation of individual observations from the mean for that method, in percent of basin area.

	Mean altitude			Box			Edited radiance threshold			Unweighted average	
	N	\bar{X}	S	N	\bar{X}	S	N	\bar{X}	S	\bar{X}	S
Feb. 11, 1973	5	70.7	5.3	5	65.8	12.2	4	65.3	9.4	67.3	9.0
Apr. 6, 1973	5	52.4	2.4	5	45.5	4.2	7	33.3	10.2	43.7	5.6
Apr. 24, 1973	5	45.5	4.4	5	40.2	4.9	1	41.5	-	42.4	4.6
May 12, 1973	5	23.9	3.8	9	18.4	6.7	4	19.8	2.9	20.7	4.5
June 30, 1974	5	21.8	3.0	5	19.9	3.3	4	13.9	1.9	18.5	2.7

between methods are greatest for images with large snow-covered areas, as indicated in Figure 8, as would be expected because of the greater amount of snow in the low- and middle-altitude forests. The mean-altitude method over-measures snow because small bare patches at altitudes above the snowline are not included. The differences between the mean altitude and box methods ranged from about 6 percent in early melt season to about 2 percent at the end of the melt season. Perhaps this relation could be used to adjust the results.

Box, radiance-threshold, and digital techniques are compared for the North Cascades basins in Table 3. The digital method is thought to be most precise, but it cannot detect snow under a complete forest canopy. The radiance-threshold method may under-measure snow; in the April image it may fail to recognize snow in trees, and in August it fails to recognize snow in shadow. These problems also occur with the box method but the operator has more opportunity to use judgment in extending snow into areas where it is not visible. In deep shadows (especially on the August image) the digital method also cannot distinguish all terrain types unambiguously because of overlap at low radiance ratios.

Manual and electronic analyzer methods can also be compared by reference to the individual box data. Statistical data

Table 3--Comparison of box, radiance-threshold, and digital pixel-by-pixel results for Thunder Creek and Cascade River basins, in percent of basin area. Differences in values between the two adjacent basins for the radiance method may be due to misregistration of the basin boundary masks.

	Box	Radiance threshold	Digital, pixel by pixel			
	Snow	Snow	Snow	Snow + vegetation	Snow + rock	Total snow ¹
<u>Thunder Creek</u>						
May 12	60.6	42.3	50.8	6.4	4.0	59.2
August 11	13.3	12.3	15.0	1.1	3.2	17.7
<u>Cascade River</u>						
May 12	47.3	49.3	33.3	8.2	3.7	43.4
August 11	6.9	11.9	4.9	2.1	2.5	8.2
<u>Total</u>						
May 12	52.4	46.5	40.0	7.5	3.8	49.6
August 11	9.4	12.1	8.8	1.7	2.8	11.9

1. Computed as (snow) + (snow + vegetation) + 1/2 (snow + rock).

were derived for four measurements of the image shown in Figure 2. Comparison of these statistical printouts to a gridded original image confirms the subjective impression that the deviations from the mean are largest and vary the most in the mid-elevation snow-tree-mixture regions and around the fringes of the snowpack.

Speed and cost

No quantitative results are presented here for two reasons: speed of the manual methods is extremely sensitive to requirements for precision and to operator experience, and for more sophisticated methods the set-up or preprocessing operations vary enormously in speed depending on the equipment available and whether one has already accomplished much of the task using other images of the same drainage basin. Similarly, costs depend on many factors such as availability of equipment and the cost of labor. Thus only qualitative statements will be made.

The snowline-tracing method is slow in execution and thus requires appreciable labor cost; on the other hand virtually no expensive equipment is required. The mean-altitude method is fast and little equipment is required so its cost is low. The

box method (when used to obtain high precision) is slow in execution but requires little equipment. The radiance-threshold method using an electronic analyzer is fast, but an expensive machine is involved. Edited radiance-threshold techniques require more operator and machine time and therefore are more expensive. Digital techniques are slow to average in speed depending on the equipment available for registering the image to a drainage basin boundary, and the costs are high to very high. The cost of the magnetic tapes, the cost of machine and labor for registering the image, and the computer time required for a four-dimensional pattern recognition program can be appreciable for a single measurement.

Ability to recognize snow in trees or shadow

Snow in a dense coniferous forest or in deep shadow is extremely difficult to recognize on a LANDSAT (ERTS) image either by eye or machine. Thus those methods which combine many kinds of information with interactive judgments by the operator are considered to be most efficient. An electronic analyzer utilizing either analog or digital multispectral input, with altitude contours and time-lapse sequences for editing, as well as the box technique using reference aids, can produce accurate results. Digital programs without interactive capability may be considerably less accurate. The mean-altitude method is relatively accurate. Simple radiance thresholds fail to detect snow in trees or in shadow.

Figure 9 shows a comparison of five methods plotted as percent of area snow-covered against altitude. Four of these curves were obtained by relating snowcover fraction in each box to the mean altitude of that box; this procedure is strictly correct only for very small boxes. The curve for the mean-altitude method was derived from the standard deviation of altitude obtained by an operator. Note that the curves for the radiance threshold edited by altitude and the box method have similar shapes; these are probably most nearly correct. The methods radiance-threshold and radiance-threshold edited without respect to altitude show some snow at very low altitudes and less snow at high altitudes. This is undoubtedly because snow in trees and in shadow is not detected at high altitude and bright, snow-free areas are being recorded at low altitudes.

Supplemental data produced

Most streamflow models currently in use in the west require either snow-covered area or the snowline altitude, or both, as input or as a check on calculations. All seven methods can provide these data. More sophisticated models require additional data, such as the distribution of snowcover with altitude or in subbasins. By measuring snowcover in individual boxes, either manually or through the use of a console or computer program, it

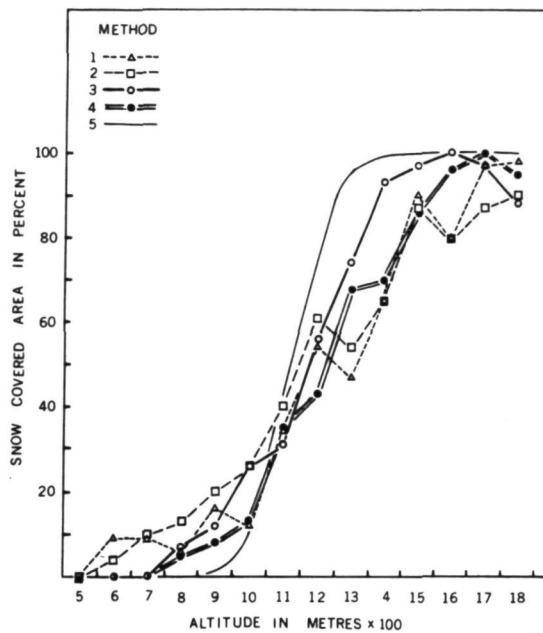


Fig. 9--Snow-covered area as a function of altitude for the Santiam Basin, April 6, 1973. These approach cumulative Gaussian distributions with standard deviation S . Method (1) used a simple radiance threshold; $S = 300$ m. Method (2) used a radiance-threshold edited without reference to altitude contours; $S = 390$ m. Method (3) used a radiance-threshold edited with reference to altitude contours; $S = 230$ m. Method (4) used box method; $S = 250$ m. Method (5) used mean-altitude method; $S = 100$ m..

is possible to provide this additional data. For instance, data can be produced showing the percent of snowcover as a function of altitude (Figure 9). These data can be used in energy-balance snowmelt models.

Summary of comparisons

Table 4 presents in summary form a qualitative comparison of the seven methods for precision, speed, cost, ability to recognize snow in trees, and supplemental data. This table represents only the views of the authors as derived mainly from the experiments on Santiam Basin images as discussed here. Other researchers using the same images or working in other areas may feel that the quality ratings should be reordered.

Several conclusions appear to be clear:

1. No method combines high precision with low costs.

Table 4--A listing of the seven methods by five important attributes. The quality distinctions given here apply only to the North Santiam, North Cascades, and similar images, as analyzed by the authors.

	Manual			Electronic, interactive analyzer			Digital computer
	(1) Plani- meter	(2) Mean alti- tude	(3) Box	(4) Radiance mask	(5) Radiance mask edited by altitude	(6) Radiance mask edited by color, altitude	(7) Pixel- by-pixel analysis
Precision	poor	average	good	poor	good	good	excellent
Speed	average	fast	average to fast	fast	average to fast	average	slow to average
Cost	average	low	average	low to average	high	high	high
Recognize snow in trees or in shadow?	fair	average	good	poor	good	excellent	good
Supplemen- tal data produced?	no	some	yes	yes	yes	yes	yes

2. The radiance-threshold method is inefficient for measuring snow in forested mountains.

3. The box method and use of a console with radiance threshold edited by altitude and other data appear to be most useful in that they are reasonably good in precision, speed, ability to recognize snow in trees or shadow, and produce supplemental data.

4. For fast inexpensive operation the mean-altitude method is probably best.

REFERENCES

- Anderson, H. W., and Gleason, C. H., 1959, Logging effects on snow, soil moisture, and water losses: Proc. West. Snow Conf., v. 27, p. 57-65.
- Barnes, J. C., and Bowley, C. J., 1974, Handbook of techniques for satellite snow mapping: Environmental Res. & Tech., Inc., Concord, MA., ERT Doc. No. 0407-A, 95 p.

- Evans, W. E., 1973, Time-lapse analysis of ERTS imagery using special electronic viewing/measuring equipment: Proc. 2nd Ann. Remote Sensing of Earth Resources Conference, Tulsa-homa, TE., Mar. 26-28, 1973, p. 883-897.
- Gary, H. L., 1974, Snow accumulation and snowmelt as influenced by a small clearing in a lodgepole pine forest: Water Res. Research, v. 10, no. 2, p. 348-353.
- Hoffer, R. M., and the LARS Staff, 1973, Techniques for computer-aided analysis of ERTS-1 data, useful in geologic, forest and water resource surveys: Lab. Applications of Remote Sensing, Purdue Univ., LARS Infor. Note 121073, 23 p.
- Hoover, M. D., and Leaf, C. F., 1967, Process and significance of interception in Colorado subalpine forest: in Forest Hydrology, Sopper, W. E., and Lull, W. W., eds., Pergamon, New York, p. 213-223.
- Lauer, D. T., and Draeger, W. C., 1974, Techniques for determining areal extent of snow in the Sierra Nevada Mountains using high altitude aircraft and spacecraft imagery: Advanced Concepts and Techniques in the Study of Snow and Ice Resources, Monterey Symposium 1973, Santeford, H. S., and Smith, J. L., compilers, Nat. Acad. Sci., Washington, D.C., p. 532-540.
- Meier, M. F., Evaluate ERTS imagery for mapping and detection of changes of snowcover on land and on glaciers: Type II Progress Report 1 July 1973 to 31 December 1973: submitted to NASA/GSFC, 6 p. (in press).
- Rothacher, Jack, 1965, Snow accumulation and melt in strip cuttings on the west slopes of the Oregon Cascades: U.S. Forest Serv. Res. Note PNW-23, 7 p.

APPROACHES TO DIGITAL SNOW MAPPING WITH LANDSAT-1 DATA

K. I. Itten, *Department of Geography, University of Zurich, CH-8006 Zurich/Switzerland*

ABSTRACT

Applying the same Landsat-1 data to three substantially different image processing systems, a snow mapping task was performed. LARSYS Ver.3, STANSORT-2 and General Electric Image-100 did all the jobs of detecting the snowline in forested mountainous terrain, and to determine the snowcovered area. While the control and accuracy achieved with LARSYS is remarkable, time and effort to perform the processing favourize the systems STANSORT and Image-100. The experiences and results demonstrate the need for a fast interactive system for operational snowmapping with multispectral satellite data.

INTRODUCTION

The great need for better information on the earth's water resources in general, and global snow cover observations in specific, call for an operational use of satellite imagery. The great amount of available satellite data leads to the question of automatization of the snowcover determination process. As an input in a runoff prediction model, the snowcovered area is the most important factor - highly linearly correlated with the runoff (Rango, Salomonson & Foster 1975).

As with Landsat 1 and 2 4-channel MSS data is available in digital form, a good base for a test in data processing is given. The problem, whether Landsat orbit and coverage characteristics are sufficient for an operational snow survey task, shall not be discussed in this paper.

Generally it is known that three main problems are observable in digital snow mapping using Landsat data.

- The differentiation between snow and clouds is often difficult given the 4 MSS bands of Landsat.

- Major interpretation problems are encountered in mountainshadow areas.
- Difficulties arise when the snowline boundary lies in forested mountainous terrain.

THE CASE STUDY

A Landsat-1 scene of 21 May 1973 of the Windriver Mountains (Wyo) was selected. Good U-2 RC-8 color aerial photography was available for part of the Bull Lake Creek watershed. Therefore that area of roughly 600 km² (230 mi²) was used as test area (see Fig. 1).

At that date no major shadow problems at snowline altitudes were observed. This specific problem is discussed in Gfeller 1975.

No clouds persisted in the test area. Therefore all effort was guided to the snowline differentiation problem in forested mountainous areas.

However it was tried to separate snow and clouds on an adjacent area with LARSYS' supervised classification (see special description under LARSYS).

To test the feasibility of digital image processing methods to classify the snowcovered areas, LARSYS Vers.3 - a non interactive statistical discriminant analysis system, and two interactive systems - STANSORT-2 with a semi supervised clustering, and General Electric Image-100 with a deterministic discriminant analysis approach were applied to the same data.

The U-2 RC-8 photography served as ground check. Training areas were determined by photointerpretation techniques. Some checking on the ground, especially for ground cover types and vegetation density, was carried out in summer 1974.

Spectral signature research on the thawing process of snow, with a Gamma Scientific ERTS-Radiometer, served as a basis for the snowmapping job.

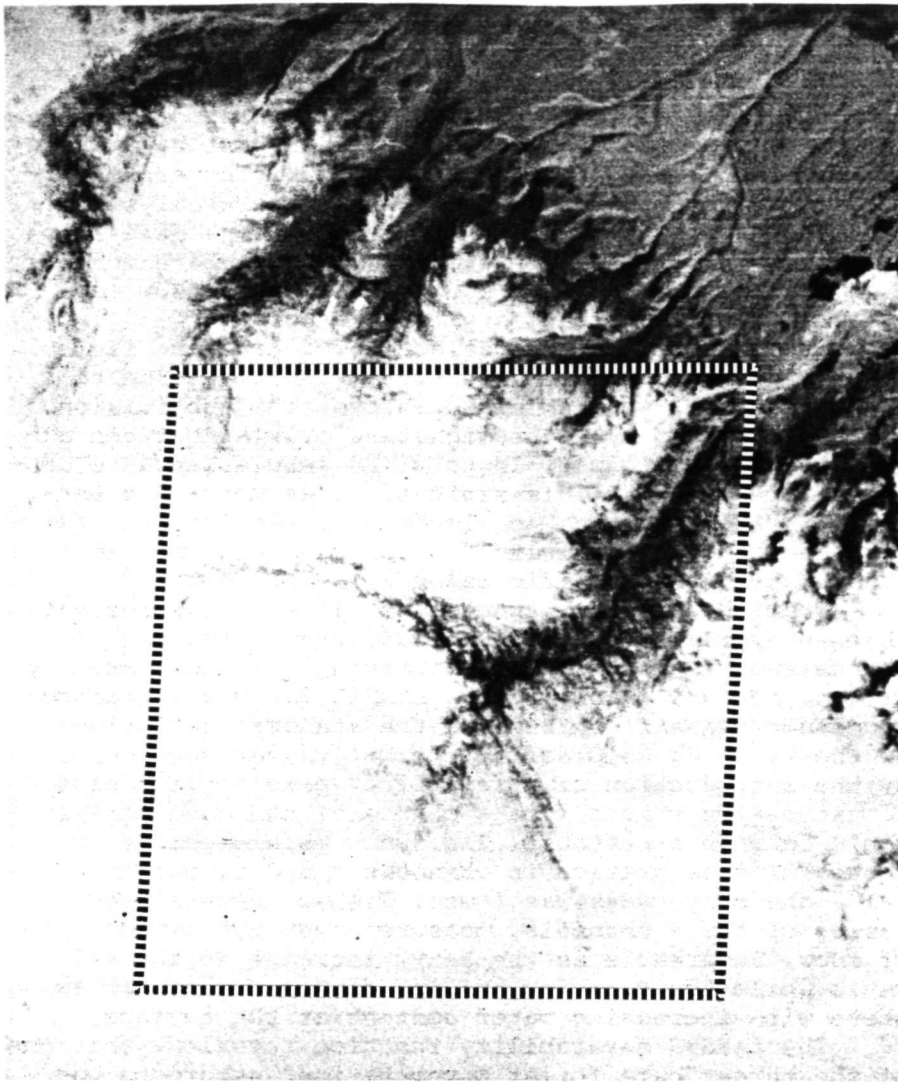


Fig. 1: Landsat-1 Channel 5 scene of the Bull Lake Creek area in the Windriver Mountains (Wyo) of 21 May 1973. The testarea for the snowcover investigation outlined. Scene ID 130217362.

REPRODUCIBILITY OF THE
ORIGINAL PAGE IS POOR

LARSYS Version 3 of Purdue University was the first system used in the investigation. Histograms showed the unique distribution of the snow pixels, and revealed also severe banding in Channel 6. Therefore this channel had to be dropped from all further analysis. Initially it was planned to divide the image data into 7 classes, namely: Water, clouds, shadows, bare forest & vegetation, forest with snow, metamorphic snow (all but dry fresh snow), and dry fresh snow.

After a very careful selection of training fields, the cluster function provided the means to assign to each class well separable subclasses. The subdivision was necessary to make the signature overlap between adjacent classes minimal. In total 28 subclasses were considered in the final classification. As mentioned earlier, in the test area no clouds were persistent, therefore the cloud class (with 7 subclasses) was not anymore important in the specific case.

From the previous spectral studies it was evident, that sunny fresh dry snow would saturate the used 3 channels of Landsat-1. This datagroup was under such conditions not acceptable to the LARSYS maximum likelihood processor/classifier, because the standard deviations of the training samples' brightness values were zero. By the introduction of a few "dirt" pixels, with close-to saturation values in all channels, the data finally could be made acceptable. The sunny metamorphic snow showed also saturation in channels 4 and 5, but in channel 7 the brightness was lower. Fig. 2 shows a plot of ratios of the 4 channels, measured over a thawing cycle of snow. Remarkable is the heavy increase in the 4/7 ratio while the snow is changing from a dry to a thawing state with increasing water content at the surface.

The LARSYS separability function revealed, that one of the three "bare forest & vegetation" subgroups was statistically not well separable from one of the ten "forest with snow" subgroups. Taking them together in the final analysis they provided an interclass which may be described as the snowline or the snow/non snow transition belt. The LARSYS classification is shown in Fig.3.

Further enlarging of the testarea to include cloud pixels as well revealed, that by direct methods, clouds could not well be distinguished from snow, given the 4 spectral channels of Landsat. However by indirect means, by an interpretation of the classification result it could be achieved. The cloud training class could be

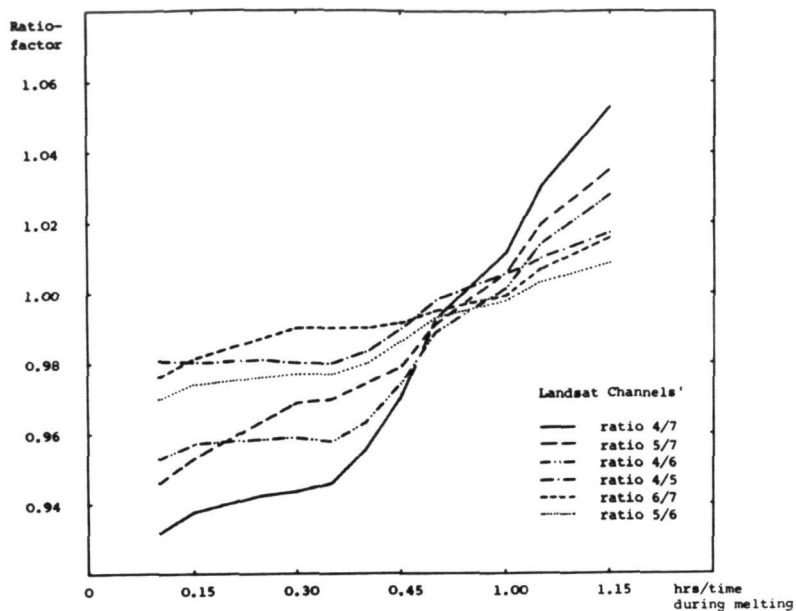


Fig. 2: Ratios of Landsat-1 channels' brightness values shown in a time sequence during melting of snow. The instrument measured, relative values were normalized and smoothed before ratioing.

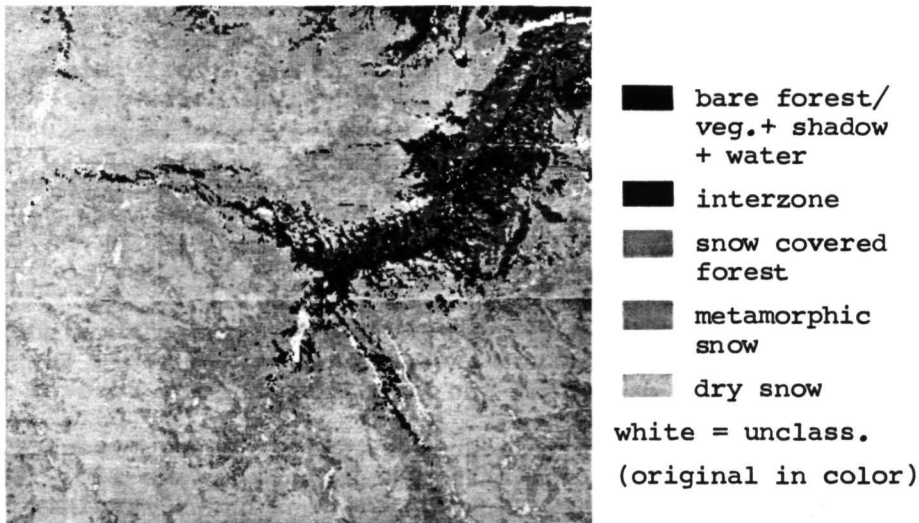


Fig. 3: LARSYS Ver.3 classification result, Bull Lake Creek test area (scene and area same as in Fig.1, distortions due to printer).

grouped into 7 subclasses, with the "metamorphic snow" we got 2, and with the "forest with snow" class 10 subgroups or subclasses. One of the cloud-subclasses (A) caused problems in distinguishing it from one "metamorphic snow" subclass (B), and another cloud subclass (C) was not well separable from a "forest with snow" subclass (D). If now in the classification a few cloud pixels of the same cloud subclass (A) were encountered alone in "metamorphic snow" area (B), they could be reinterpreted as wrong classified "metamorphic snow" pixels. Similar with the second error groups C vs. D. If however the cloud classified pixels of group A and/or C were surrounded by pixels of other cloud subclasses, they could be regarded as real cloud pixels. On an interactive system with CRT display and lightpen, these error eliminations can be achieved by pointing at problem pixels or areas and correcting them directly. While with LARSYS Vers. 3 it was quite a time consuming re-interpretation of the classification map and statistics. An automatic error correction could be made as follows: When for instance a cloud pixel is classified, all neighbouring pixels could automatically be checked for their class origin. According to the result it could then be decided, whether it is a real cloud pixel or not.

Generally it can be said about the LARSYS approach, that it uses a well supervised, stepwise, statistically proof method. Little processing knowledge is required, and the documentation and courses offered are very good. It seems not necessary to describe the LARSYS features in detail, because they are well known. Critical points are, that the whole procedure is very time consuming and therefore expensive. Mathematically there is no possibility to change algorithms in the system - one has to use the preprogrammed ones. The communication lines from external terminals to Purdue are not very reliable. Hopefully the LARSYS Vers.3 system will in the future be available to other Universities as well, to avoid the constant overloading of Purdue.

But finally it must be said, that at the end of the classification process you have gained considerable insight into your data, and you know well how you reached your result.

The overall achieved classification accuracy regarding to the training areas amounted to 92 % (see Tab. 1). The process with LARSYS Vers.3 is - good ground training data given - very accurate. But as the whole procedure is very time consuming and therefore costly, it is very questionable whether to use this approach for large area operational snow mapping at all.

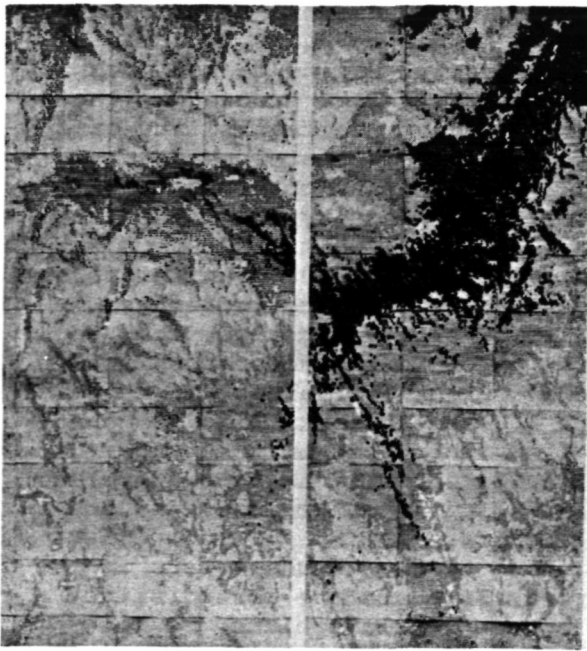
The second processing system used in the snowmapping job was STANSORT-2 developed by R.J.P.Lyon and F.R.Honey at Stanford University. Having gained much experience with the data in the LARSYS procedure, the STANSORT system was used to check the feasibility of a highly interactive semi-supervised clustering as an approach to the snow cover determination problem.

In a first step, by simple density slicing in channel 7, the dry snow pixels were detected and stored. Then an unnormalized fast cluster was used and different printouts obtained by varying the cluster tolerance levels (gates) in the STANSORT clustering algorithm. In this approach, the first pixel in the first scanline is stored with its channels' brightness values. It is named class (or clustergroup) A. Then the next pixel is checked whether its values lie within a given tolerance (gate) setting to the ones of A. If so it is assigned to class A as well; if not it is called a new class B, and so on with the following pixel...

Up to 26 classes - due to the 26 characters in the alphabeth - can be formed. If there are more distinct different groups, the spaces are left blanc. To fit those into the scheme, the tolerance setting has to be widened. If finally an acceptable or useful tolerance setting is found, these gate factors can be stored and applied over larger areas.

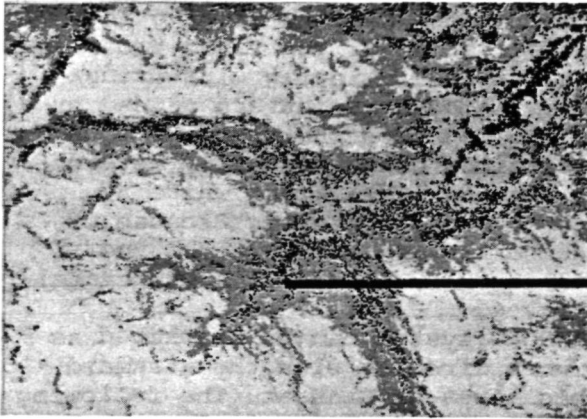
By setting in our case the upper ranges for channels 4 and 5 to exclude the saturation level, all metamorphic + dry snow areas could be extracted. The combination of this byproduct with the previous density slicing in channel 7 lead to the distinction of the first two classes. The varying results of the following clusterings were compared with the training area pattern gained by photointerpretation of the U-2 RC-8 photography. Thus the best fitting gate settings could be easily determined. This checking was done on a black and white tv screen where the cluster results appeared. Because of this interactive access to the system, we named the clustering process semi supervised. The STANSORT classification is shown in Fig. 4.

Generally the STANSORT system can be described as follows: It allows to work directly with the standard NDPF computer compatible tapes of Landsat. The following functional handling procedures can be applied to the pixel data: Smoothing, ratioing, edge detection, normalized and unnormalized clustering, removing of atmospheric effects, calibration, shadeprinting, extraction of data values, histogramming, debanding and deconvoluting. The interactive access to the PDP-10 computer



- bare forest/
veg.+ shadow
+ water
- interzone
- snow covered
forest
- metamorphic
snow
- dry snow
- white = unclass.
- (original in color)

Fig. 4: STANSORT-2 classification result, Bull Lake Creek testarea (scene and area same as in Fig.1, distortions due to printer).



- shadow +
water
- bare forest/
vegetation
- interclass
- snow covered
forest
- metamorphic
snow
- dry snow
- unclassified
- (original in color)

Fig. 5: General Electric Image-100 classification result, Bull Lake Creek testarea (scene and area same as in Fig.1, distortions due to printer).

is achieved through a keyboard, and instant control over the extremely fast operating processor is possible via a black and white CRT display. A very fast primary evaluation of test results is hereby possible, and parameter changes - as for instance the gate setting in the clustering - may be applied easily. The very fast algorithms and processor make the system comparatively inexpensive. The operation of the system can be learned quickly (1-3 hours), making it a very valuable tool for the discipline oriented user-investigator who often is not a specialist in digital image processing.

In the comparison with results obtained by the LARSYS classification, the STANSORT cluster/slicing showed almost identical distribution of the classes (see Tab. 1). The amount of time and effort however was considerably smaller than with LARSYS. On the other hand, the control and final accuracy achieved with LARSYS' supervised technique cannot be reached. Again the question is how accurate your result has to be and how much time and money that you are willing to spend.

The third and probably one of the most advanced systems in operational image processing tested was Image-100 of General Electric. The same CCT's and test area, and part of the same ground "truth" were used again. As a classification approach a parallel epiped classifier in an interactive signature mode was used. The also available more sophisticated, more precise but more time consuming classifiers were not tried, because the idea of the test was to check the feasibility to operational snowcover determination. On a color tv display which shows the test area (in any color combination of the channels), the user places a cursor around the object or ground cover class of interest to define the training area. The upper and lower limits in each spectral band of that group of training-pixels are determined. All data points in the displayed image, that spectrally fall within that parallel epiped shaped hyperspace, can be alarmed and displayed to be checked against ground data. If in the feature space there are overlapping classes, the limits or boundaries of the parallel-epipeds can be shifted to minimize the problem. For some specially distributed classes, this technique does however not give optimal results.

As normally just one to two training areas are used per class, the whole classification is statistically not that proof as with LARSYS (see Tab. 1). There, for the whole area and all classes together, 350 training areas were used. The main advantage of Image-100 is however, that a full screen of about 370 by 525 pixels of in our case 3-channel data, can be classified into 8 classes within a few seconds of computertime. The display and interactivity of the system are a great help in defining training areas. Also the color coding of an intermediate class result makes the decision process, whether to change levels or not, very easy. But the overall classification with 7 or 8 classes does not show up very well on the color display - another output medium than photography from the color screen is necessary.

The whole training and classification of the Bull Lake River test area was possible in less than 2 hours time (results see Fig. 5 and the comparison in Tab. 1). This is surely an indication that such or similar systems should be used in operational snowcover determination.

COMPARISON OF RESULTS

If we look at Tab. 1 and compare the obtained results, we might argue that LARSYS did the best job. This is sure so if we disregard the amount of time and effort spent to reach that goal. Due to system overload and non interactivity it took weeks to perform the LARSYS job. With STANSORT within about one day experiencing and classifying - but basing strongly upon the experience gained by LARSYS - almost the same could be achieved. With Image-100 the results seem to lack of precision. But comparing the two hours cost of operating the system and the little experience we had with Image-100, the result is still surprising. We are convinced that now with all the experience, we could improve the nominal Image-100 result furthermore applying the same data again.

Generally there is observable a tradeoff between the classification accuracy and the time or money needed in the three different approaches.

Tab. 1: Comparison of Classification Results
(Numbers represent areas in percent)

Cover Type	LARSYS Ver.3	STANSORT-2	GE Image-100
Dry Snow	31.8	30.8	30.9
Metamorph.Snow	22.1	22.5	21.1
Forest w.Snow	27.2	27.8	27.1
Interzone	9.4	11.2	4.6
Bare Forest/Veg.	6.2	6.0	10.4
Shadow + Water	0.4	0.2	0.2
Total Snow Covered Area	85.8	86.7	81.4
Total Area Bare of Snow	11.3	11.8	12.9
Unclassified Area	2.9	1.5	5.7
Accuracy/Testfields	92 (calc.)	90 (est.)	87 (est.)

CONCLUSIONS

Digital snow mapping is still a problem where the human interaction represents an essential factor. It has to be kept in mind, that operational snow mapping means a big number of imagery, and in most cases the requirement to cover a large area.

In this specific test an area of just 600 km² was processed, but we used 3-channel Landsat data with full pixel resolution. It is believed, that the resolution of this satellite is not needed for large area snow-mapping, and we could have been working with a bigger area by using incremental samples of the image data. But it was the aim of this project to demonstrate the substantial increase in applicability of satellite data to operational snowmapping, by connecting a multispectral approach with digital image processing techniques. As a result it is believed, that a highly interactive, specially designed system together with a skilled applications specialist can, for the future bring maximum operational use in satellite snowcover observations.

ACKNOWLEDGMENTS

The work described herein was co-sponsored by ESRO/ESA under their Fellowship Program, NASA Goddard Space Flight Center and Stanford University providing the facilities and computertime. I wish to thank all the three institutions for their support. I am very grateful to Dr.C.C.Schnetzler and the members of the Goddard Space Flight Center Earth Resources Branch for the help and advice in my project. Special thanks are extended to Prof.Dr.R.J.P.Lyon and Dr.F.R.Honey, Remote Sensing Laboratory, School of Earth Sciences, Stanford University for their support, instruction, advice in systems theory, and help in data processing.

REFERENCES

- Barnes, J.C. + Bowley, C.J. + Simmes, D.A.: The Application of ERTS Imagery to Mapping Snow Cover in the Western United States, ERT Document 0407-F, NASA Goddard Space Flight Center, Greenbelt, Md. 1974.
- Barnes, J.C. + Bowley, C.J.: Handbook of Techniques for Satellite Snow Mapping, NAS5-21803, NASA Goddard Space Flight Center, Greenbelt, Md. 1974.
- Foster, J.L. + Rango, A.: A Method for Improving the Location of the Snowline in Forested Areas Using Satellite Imagery, NASA Goddard Space Flight Center, X-910-75-41, Greenbelt, Md. 1975.
- Gfeller, R.E.: Untersuchungen zur automatischen Schneeflächenbestimmung mit Multispektralaufnahmen des Erderkundungssatelliten ERTS-1, Thesis University of Zurich, Switzerland 1975.
- Haefner, H.: Snow Survey and Vegetation Growth in High Mountains (Swiss Alps) and Additional ERTS Investigations in Switzerland, NASA-CR-142340, NTIS E75-10195, University of Zurich, Switzerland 1975.
- Hovis, W.A. + Blaine, L.R. + Forman, M.L.: Spectra of Reflected Solar Energy 0,4 to 2,4 Microns; Clouds, Snow, Fields, NASA Goddard Space Flight Center, X-652-71-215, Greenbelt, Md. 1971.
- Itten, K.I.: Application of Digital Snow Mapping with ERTS-1 Data, Using the STANSORT Image Processing System, Stanford RSL Technical Report 75-1, Stanford, Cal. 1975.

- Meier, M.F.: Evaluation of ERTS Imagery for Mapping and Detection of Changes of Snowcover on Land and on Glaciers, Proc. Symp. on Significant Results Obtained from ERTS-1, NASA Goddard Space Flight Center, NASA SP-327, Greenbelt, Md. 1973.
- O'Brien, H.W. + Munis, R.H.: Red and Near-Infrared Spectral Reflectance of Snow, USACRREL Research Report NA-869-73, Hanover, New Hampshire (Draft 1974).
- Rango, A. + Salomonson, V.V. + Foster, J.L.: Seasonal Streamflow Estimation Employing Satellite Snowcover Observations, NASA Goddard Space Flight Center, X-913-75-26, Greenbelt, Md. 1975.
- Strong, A.E. + McClain, E.P. + McGinnis, D.F.: Detection of Thawing Snow and Ice Packs Through the Combined Use of Visible and Near-Infrared Measurements from Earth Satellites, Monthly Weather Review, Vol. 99, No. 11, 1971.
- Wiesnet, D.R.: Detection of Snow Conditions in Mountainous Terrain, Proc. ERTS Symp., NASA Goddard Space Flight Center, X-650-73-10, Greenbelt, Md. 1973.
- Lindenlaub, J.C.: Guide to Multispectral Data Analysis Using LARSYS, LARS Information Note 062873, Purdue University, West Lafayette, Ind. 1973.
- Honey, F.R. + Prelat, A. + Lyon, R.J.P.: STANSORT, Stanford Remote Sensing Laboratory Pattern Recognition and Classification System, Proc. 9th Int. Symp. on Remote Sensing of Environment, Ann Arbor, Mich. 1974.
- General Electric Co.: Interactive Multispectral Image Analysis System (Image-100), Product Data Document No. 717001G, Daytona Beach, Fla. 1974.

AN ALL DIGITAL APPROACH TO SNOW AREAL MAPPING AND SNOW MODELINGV. Ralph Algazi and Minsoo Suk, *University of California, Davis***ABSTRACT**

A study has been undertaken to incorporate remote sensing data into a spatially distributed model of snowpack evolution. Preliminary results are presented on the estimation of primary parameters needed in such a model.

INTRODUCTION

In many areas of the world, as well as in California, it is necessary for the management of water resources to evaluate and predict snowmelt, an important input to hydrologic systems and models. We note that the physical basis and the mechanisms of snow ablation have been understood and modeled for a number of years [1,2]. These physically based models have been verified experimentally on a local scale using a snow lysimeter installed in the Andes Mountains in Chile by Amorocho and Espildora. They obtained good agreement between model prediction and experimental data. The same physical elements are used in the spatially lumped snow submodels of watershed hydrologic models such as the Sacramento RFC model, developed by Burnash and his associates [3,4]. However, information about the snowpack is sparse and difficult to obtain. Since the important physical parameters which determine the evolution of the snowpack vary substantially across a watershed, there are difficulties in the development, calibration and operational use of a spatially distributed, physically meaningful snow ablation model.

A number of studies on the areal mapping of snow using remote sensing have been undertaken in the last few years [5,6,7,8] which have evolved into a NASA sponsored handbook of techniques for satellite snow mapping [9]. Most of this work is directed to the estimation of the areal extent of the snowpack and attempts are now being made to incorporate such data into empirical ("rational") snowmelt runoff models.

In our work we have undertaken the incorporation of satellite into a physically based, distributed model of snowmelt to be used eventually for runoff prediction. We approached this work by the determination of the physical quantities which are of prime interest in the modeling of basin wide snowmelt. Precipitation, temperature, albedo, wind speed, relative humidity and cloud cover

The work reported is supported by NASA Grant NGL 05-003-404

Preceding page blank

are the physical parameters which determine the evolution of the snowpack. We have obtained some partial results on the determination of some of these parameters by remote sensing. Thus this paper takes the form of a progress report and outline of our work.

Because of the time scale of the dynamics of the snow ablation process we are using NOAA-3 and NOAA-4 data, which is available every day, as well as Landsat data. A very large part of our time has been spent gathering a snowmelt season, April 1975 to July 1975, of NOAA data for California and coming to grips with a number of important auxiliary data handling problems such as, radiometric correction and calibration and geometric correction. Since these problems are at the heart of the quantitative use of satellite data, we discuss briefly, in the next section, their importance in this work and the results and techniques available for their solution.

DATA GATHERING AND CORRECTION

Since the snowpack evolves quite rapidly it appeared to us from the start that we needed in our work the frequency of coverage provided by the NOAA-3 and -4 satellites. Further, at this time, only the NOAA satellites provide data in a thermal IR band as well as in a visible band. We thus proceeded to gather all usable data collected by the NOAA-3 or NOAA-4 satellites over California, both in the visible and in the thermal infrared, from April 1, 1975 to July 8, 1975. More than 20 dates are available, corresponding to more than 40 digital tapes, recorded by NOAA at 1600 bits per inch (BPI). The data had to be converted to 800 BPI before we could make use of it. The volume of data to be handled and the reformatting needed are serious limitations at this time in the quantitative use of the data from NOAA satellites. Still, the data was available very rapidly at the NOAA-NESQ satellite field receiving station in Redwood City and thus rapid access to the data for operational uses is possible.

Radiometric Calibration and Correction

Very few people, up to now, have made quantitative use of NOAA data and thus the information available on the calibration procedure and on the correction of deterministic errors in the data is fragmented and inadequate.

We have to mention first the difficulties in the calibration procedure, that is to say in the conversion of the numerical value or counts, provided on digital tape into temperature or brightness values, as recorded by the satellite. This calibration procedure contains still some uncertainties and inconsistencies which will require elucidation. Although formally calibration could be different for each scan line of the data, we have found that for an area of the size of California, the data correction is essentially constant for the whole area for any single pass of the satellite.

The limb darkening correction is a deterministic data correction for atmospheric effects. As the nadir angle of the satellite sensors varies during a scan line, the effects of the atmosphere will also change. In the thermal band the correction needed is discussed by Smith et al [10] and we used a semiempirical formula also used by Merrit and Stevenson [11]

$$\Delta T = (-26.81 + 0.107T)e^{0.00012\phi^2}$$

in which ΔT is the correction to the recorded temperature $T(^{\circ}K)$ and ϕ is the nadir angle ($^{\circ}arc$). For nadir angles of less than 30° , the angular correction is of second order. Random radiometer errors and banding or stripping errors are also present in the data. We have developed a two dimensional filtering program which substantially reduce these errors. These errors are severe only for thermal infrared data acquired by NOAA-4.

Geometric Correction

Because of the highly distorted view of the earth provided by the NOAA and to a lesser extent by the Landsat satellites, geometric correction of the data is mandatory. This geometric correction is needed for one of two purposes. The first one is in order to obtain satellite data for a ground truth station. The second one is needed to transform satellite data into map compatible data. For both purposes we have made use of a least square fitting program using biquadratic fitting polynomials. At least six ground control points are needed for this geometric correction. Because of the difficulty of locating land features on NOAA-3 or NOAA-4 images one has to use an area at least as large as the State of California in the correction procedure. At this time we have residual geometric errors of the order of 2 pixels. These residual errors result in a fundamental limitation on the fineness of the distributed model which can be developed.

ESTIMATION OF THE SNOWPACK ALBEDO

The albedo is a very important parameter to the dynamics of snowmelt. The albedo is generally quite high for new fallen snow and decreases fairly rapidly after a snow storm. The snow albedo depends primarily on the surface conditions of the snowpack. Based on an analysis of the physics of snowmelt, or on empirical observations, models have been proposed for the evolution of the albedo with time. We shall mention the albedo curves based on a study made at the Central Sierra Snow Laboratory by the Corps of Engineers [1]. These curves are shown in Figure 1. We also show in Figure 1 experimental values obtained at the Central Sierra Snow Laboratory during January 1975. The trend of the experimental curve matches well the standard curve proposed but the absolute values are significantly in error.

Several questions are of interest in the use of remote sensing for the estimation of albedo. First, we note that the albedo is the fraction of incident energy reflected by the snow.

Since satellite sensors measure the energy reflected in narrow spectral bands, it is not clear that any single band in the visible wavelength range or in the near-infrared is a good indicator of albedo. Some experimental results have been presented by O'Brien and Munis on the Red and Near-Infrared Spectral reflectance of snow [12]. Their results indicate that the spectral reflectance scales down in a fairly uniform way across the wavelength range in the near infrared but that this may not hold in the visible spectrum.

To proceed with a study of brightness values recorded by a satellite and their correlation with albedo values, we need ground truth on the albedo measured at ground stations.

To our knowledge, the only location in the Sierra Nevada where albedo is recorded is at the Central Sierra Snow Laboratory (CSSL) in Norden, California. The laboratory is in a clearing a few hundred feet wide in a forested area. Thus, the CSSL can be fairly precisely located on Landsat data but not on NOAA-3 and NOAA-4 images which have a resolution of 0.9km. A preliminary comparison of known albedo with the digital values recorded in the visible band by the NOAA-3 satellite indicate a very low correlation, if any, between the albedo and the recorded brightness. This lack of correlation may be due to the specifics of the location of the Central Sierra Snow Laboratory mentioned, with additional errors in obtaining the proper remote sensing data for the laboratory since geometric correction of the data is required. At this time, Landsat data is not available at suitable dates to allow the observation of curves such as shown in Figure 1. We are planning to use the infrequent Landsat data in a statistical correlation with albedo ground truth at CSSL. On the basis of the results of O'Brien and Munis [12], we expect that Landsat spectral band 7 may be a good indicator of albedo. We shall pursue studies with NOAA-3 data in the visible range.

Another possible use of remote sensing data in the study of albedo is to consider the spatial variation of reflectance across the snowpack as an indicator of variation in albedo. By analyzing the brightness values recorded by the NOAA-3 satellite in the visible spectrum we find in all cases that brightness covers a broad range of values across the snowpack. Since the reflectance of snow is similar for source-detector angles ranging from 0 to 30° [12], it seems that the variation in brightness in nonforested areas must be attributed mainly to differences in the evolution of snowpack with elevation, temperature, etc.

We shall proceed with our investigation by combining remote sensing data during the snow season with other data on relief and vegetation cover. Additional ground truth information on albedo is needed for continuation of our work.

ESTIMATION OF TEMPERATURE FIELDS BY REMOTE SENSING

Another important parameter which determines the evaluation of the snowpack, is the temperature. The temperature varies during the day at any specific location and also with geographic location

at any given time. One can hope to obtain by remote sensing a snapshot of the temperature field across the snowpack at the time of overflight by the satellite. Under the best of conditions, one would obtain a detailed absolute temperature field. At the least, one would like to obtain relative temperature information for portions of the watershed with different elevations and aspects. We have made use of NOAA-3 and NOAA-4 thermal infrared data which have a time of overflight of approximately 11:30 a.m. over California. On the basis of hourly temperature data obtained at the Central Sierra Snow Laboratory for January through May 1975, the daily temperature profile follows definite patterns during clear days and overcast days. Thus the knowledge of the temperature at one specific time should be adequate for a fairly accurate determination of the temperature history of the snowpack.

To assess the accuracy of the temperature recorded in the thermal IR by the NOAA-3 and NOAA-4 satellites we have used temperature data from the National Weather Service, National Climatic Center, at a number of high quality, first order stations in California and also at the station in Reno, Nevada. The data that we were able to use in our geographic area of interest was obtained at Red Bluff, Sacramento, Fresno, Reno, and Bishop. None of these stations is in a mountainous snow covered region. Data is also available at the Central Sierra Snow Laboratory but we have not made use of it up to now and we expect difficulties comparable to the ones we encountered in using the albedo data at the CSSL, because of the limited resolution of the sensors.

Using the temperature data of these first order climatic stations we have done a preliminary determination of the correlation of satellite recorded temperatures with ground truth.

The following steps are needed to carry out this work:

1. Determination of the geometric correction needed for each date. This requires ground coordinates and satellite data coordinates of seven control points and this step is a time consuming operation.
2. Transforming of climatic station coordinates into satellite data coordinates.
3. Extraction of satellite data pertinent to each climatic station.
4. Follow, for each station, the calibration procedure provided by NOAA to transform numerical values into temperatures recorded by the satellite.
5. Use the limb darkening correction outlined earlier to correct for atmospheric effects.

This procedure has been used to generate the 12 data points shown in Figure 2. The data was obtained at a total of 6 climatic stations (Mt. Shasta could be used on one date, in addition to the 5 stations mentioned earlier).

The results shown in Figure 2 call for several comments. First, two data points are not shown. They would be on the left side of the figure and give a large discrepancy between ground temperature and satellite recorded temperature, the satellite recorded temperature being very much lower. We believe that this

difference is due to the fact that the satellite was recording the temperature of the top of clouds above the station rather than the ground temperature. In one case, corresponding to Sacramento, we ascertained that clouds were actually present. Thus, these 2 data points have been discarded.

The remainder of the data points were kept and show a fair correlation between satellite recorded temperature and ground temperature (correlation coefficient = 0.67). Note however that the numerical values are significantly different for ground and satellite temperatures. It is possible that systematic errors have been made in the calibration of the data. Since empirical factors appear in the limb darkening correction, it is possible that a tuning of the calibration procedure from the range of geographic locations and temperatures of interest in this study will have to be performed. We intend to pursue the systematics of this problem by using considerably more data that we have done to date and by performing correction of the data for banding and random errors. By and large, we are encouraged by these preliminary results and believe that a usable ground temperature can be inferred from satellite data in the thermal IR.

We have also generated a number of pseudocolor images of the thermal IR data to determine whether a range of temperature could be perceived across the snowpack and whether isothermal line could be distinguished. Several such images will be shown at the workshop. Isothermal lines can be perceived readily. Variations of numerical values corresponding to approximately five degrees centigrades of temperature can also be distinguished. Thus, by the use of ground truth at one or two stations on the snowpack a usable temperature field across the snowpack could be obtained.

MONITORING THE AREAL EXTENT OF THE SNOW

Within the context of our interest in developing data for a distributed model of snowpack evolution, this specific task is not of prime importance. We anticipate that instead of being a prime input to a model, the variation of areal extent with time will be used to check that the model is working satisfactorily. We have undertaken two investigations on areal extent determination. The first one is to compare the areal extent as determined from Landsat data to the same values obtained from NOAA satellites visible data. Results showing fairly close agreement between the values obtained from the two sources of data have been reported by Wiesnet and McGinnis [6]. We are using classification algorithms and digital data rather than outlining the snowline images. We do not have yet enough comparable data from both satellite systems to derive definite conclusions.

Another related question is the determination of the snow areal extent on a daily basis (when possible) from NOAA satellite data. Since a number of data correction steps are needed in such a procedure we shall generate a "noisy" time series for snow areal extent. Since we expect, on physical grounds, a smooth

variation of snow areal extent with time we can use data filtering techniques to improve the estimate on any given date.

DISCUSSION AND CONCLUSIONS

In view of the fragmentary results presented here it is obvious that much remains to be done to develop the procedure for mapping albedo and temperature fields of the snowpack. We expect substantially more definite results on both these parameters in the coming few weeks. An interesting possibility which emerged in the course of our study is the discrimination of clouds from snow on the basis of temperature. This is a separation which is impossible to do using the visible or near infrared spectral bands. Since the information on present cloud cover is another prime parameter which determines the evolution of the snowpack, any progress on remote detection of cloud cover over snowfields would be most germane to our overall study.

Some of the problems of data correction and calibration that we have encountered are necessary to a quantitative use of remote sensing data. Some others, concerned with data gathering and conversion, should be readily amenable to solution in an operational situation. To mention a specific example the amount of NOAA satellite data needed on any watershed is quite small, a few thousand data values. At this time we have to handle and convert more than 10 million data points in order to extract the limited useful information.

With reference to the development of a distributed model of snowpack evolution we are fortunate to benefit from the cooperation of Dr. J. Amorocho of the Department of Water Science and Engineering at UC Davis. Dr. Amorocho and his associates are currently testing a local model of snowpack evolution with data acquired at the CSSL. The extension of this work to a distributed model for a watershed is a step which becomes possible with the advent of remote sensing data. Thus, significant progress on both fundamental conceptual grounds and possibly on practical grounds, runoff prediction, seem feasible.

ACKNOWLEDGEMENTS

We wish to thank many people for past, present, and future assistance: Dr. J. Amorocho at UC Davis, Dr. A. Rango at NASA, M. R. Koffler and L. Breaker at NOAA-NESS, Mr. C. Howard at the California Department of Water Resources, and finally but not least Ken Ellis for surviving, so far, in a sea of data.

REFERENCES

- [1] U.S. Army Corps. of Engineers, Snow Hydrology, 1956.
- [2] Amorocho, J. and B. Espildora. "Mathematical Simulation of the Snow Melting Processes". Water Science and Engineering Paper No. 3001, University of California, Davis, February 1966. Presented at the 15th Annual Conference Hydraulics Div. ASCE, Madison

Wisconsin, August 1966.

- [3] Burnash, R.J.C., R.L. Ferral and R.A. McGuire, "A Generalized Stream Flow Simulation Model". National Weather Service--California Department of Water Resources, March 1973.
- [4] Burnash, R.J.C., and G.H. Baird. "Approximating Snow Ablation in Mountainous Areas From Limited Data Fields". Preprint, made available by Mr. Burnash, which describe the snow submodel incorporated in the Sacramento RFC model.
- [5] J.C. Barnes, C.J. Bowley, D.A. Simmes. "The Application of ERTS-1 Imagery to Mapping Snow Cover in the Western United States, ERTS Document 0407-F, January 1974.
- [6] D.R. Wiesnet, D.F. McGinnis, Jr. "Snow Extent Mapping and Lake Ice Studies Using ERTS-1 MSS Together with NOAA-2 VHRR". Third ERTS Symposium, December 1973.
- [7] H.A. Odegaard, J. Skorve. "The Application of ERTS Imagery to Mapping Snow Cover in Norway", Final Report on ERTS-1 Contract F.418, May 1974.
- [8] Meier, M.F. "Evaluation of ERTS Imagery for Mapping and Detection of Changes of Snowcover on Land and Glaciers", NASA SP-327, pp. 863-875, 1973.
- [9] J.C. Barnes and C.J. Bowley. Handbook of Techniques for Satellite Snow Mapping, ERTS Document No. 0407-A, December 1974.
- [10] Smith, W.L., P.K. Rao, R. Koffler and W.R. Curtis. "The Determination of Sea Surface Temperature from Satellite High Resolution Infrared Window Radiation Measurements", Monthly Weather Review, 1970.
- [11] Stevenson, M.R. and F.R. Miller. "Application of Satellite Data to Study Oceanic Fronts in the Eastern Pacific: Inter-American Tropical Tuna Commission, La Jolla, California, Final Report Grant No. 04-3-158-59, May 1974.
- [12] O'Brien, H.W. and R.H. Munis. "Red and Near-Infrared Spectral Reflectance of Snow. Research Report 332, Cold Regions Research and Engineering Laboratory, Hanover, N.H., March 1975.

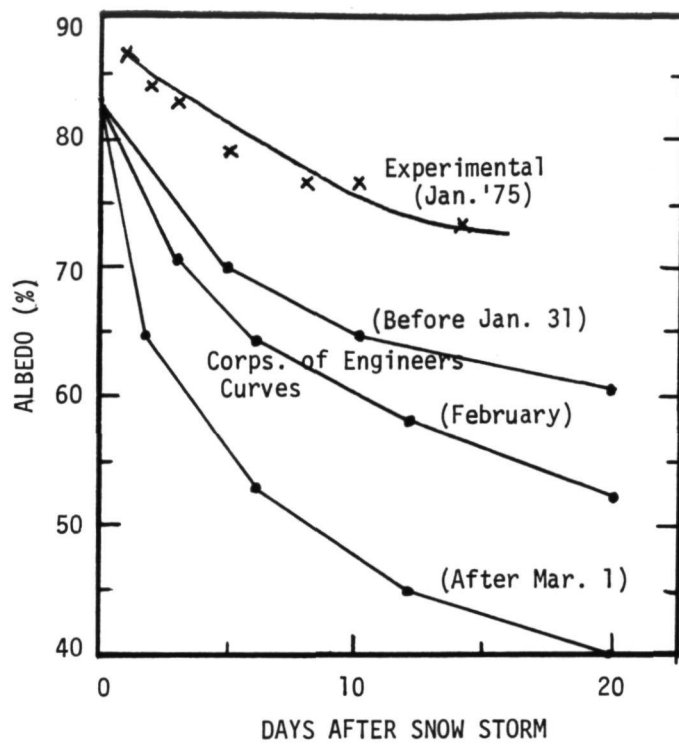


Figure 1: Evolution of Albedo

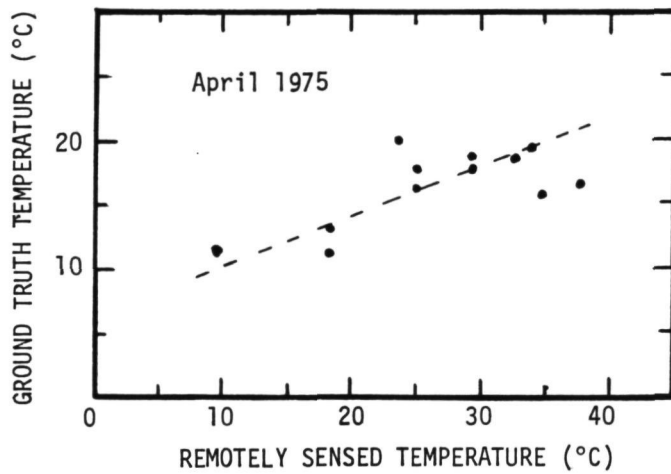


Figure 2: Correlation of Remotely Sensed and Ground Truth Temperature

**DIGITAL SNOW MAPPING TECHNIQUE USING LANDSAT DATA AND
GENERAL ELECTRIC IMAGE 100 SYSTEM**

William C. Dallam, *General Electric Company, Beltsville, Maryland*; James Foster, *Geology
Department, University of Maryland, College Park, Maryland*

ABSTRACT

The need for rapid and reliable snow mapping using LANDSAT and future satellite data has been identified. In this study a technique and procedures using General Electric IMAGE 100 system were derived for performing a snow cover analysis of small watersheds for quasi-operational application.

The study area was the Wind River Mountains of west central Wyoming. A small watershed, namely, Dinwoody Creek was selected as a test site. LANDSAT data and U-2 imagery was used in the analysis.

From a minimal snowcover LANDSAT scene, multispectral analysis was performed yielding the distribution of forest, bare rock, grassland, water and snow within the watershed. The forest and bare rock themes were saved and registered with other scenes containing greater snow cover. Likewise, elevation contours from a digitized map were stored and superimposed over the snowpack areas. Analysis of the distribution of the snowcover is facilitated by superimposing the themes and map. For any one watershed the themes (forest, bare rock and grassland) and map are constant.

Different techniques, i.e., contrast stretching, single channel slicing and multispectral signature extraction were investigated to differentiate snow types. Area measurements of the snow classes and other watershed themes were obtained. The technique and procedures derived from the study were applied to the watershed for other dates. From the receipt of the digital LANDSAT tapes, approximately three quarters of an hour have been required for a snowcover analysis.

As a result of this work, it is feasible for small watersheds to have snowcover analysis performed by digital pro-

Preceding page blank

cessing in a rapid and reliable manner. The receipt of such timely snowcover analysis by the operational agencies will aid in their management function in the control of reservoirs and in water supply forecasting.

INTRODUCTION

Several agencies participating in operational application of satellite snowcover observations are currently using photographic interpretation. In the future, the processing of satellite digital data may prove to be more economical and reliable. Hence, this study was conducted. The prime purpose of the study was to develop a technique for snowmapping by processing digital satellite data. This has been achieved by using NASA LANDSAT digital data (computer compatible tapes) as a data source, the Dinwoody watershed, Wind River, Wyoming as a test site and the General Electric IMAGE 100 multispectral analyzer as a digital processor. In using the LANDSAT data, its multispectral data provides information in four separate bands. This information when analyzed multispectrally, defines features such as forest, water, snow, grassland and rocks within the LANDSAT imagery. Through the interactive computerized system, rapid and reliable processing of the multispectral data relative to the watershed is obtained. Using the technique developed, several LANDSAT scenes containing the watershed during the snowmelt season (May-June) were analyzed providing area measurements of the snow. These area measurements and analysis time were compared with other techniques using density slicing of single bands and manual photographic interpretation.

OBJECTIVES

Briefly, the objectives of the study were:

- Show the feasibility of using a multispectral analysis technique for snowmapping using LANDSAT digital data
- Define and test a procedure for rapid and reliable snowmapping of watersheds
- Define requirements for improving processing for snowmapping multiple watersheds

STUDY AREA

The Wind River Mountain Range of west central Wyoming has been extensively snowmapped in recent years at the Goddard Space Flight Center (GSFC) (Ref. 1 & 2). Information relative to ground truth, aerial photography, LANDSAT data and analysis was

available thus making this area appropriate to be studied. Within this area, there are seven watersheds (see Figure 1). The selection of the Dinwoody Creek watershed on the northeast slope of the range was the focus of the study. The watershed has an average elevation above 10,000 feet and an area of approximately ninety-two (92) square miles. The geology (Ref. 2) in the Wind River Mountain consists of metamorphic and plutonic rocks of precambrian ages and limestone, sandstone and granitic lithologies. The climate varies with altitude, being semi-arid at the base of the mountains and alpine at the summits. Snowfall fluctuates according to elevation and topography; generally the highest elevations receive in excess of 150 inches (380cm) a year. The vegetation below 10,000 ft. (3050m) is mostly coniferous with Douglas Fir near the base and Lodgepole Pine and Western Spruce Fir forest dominating the higher slopes. Above 10,000 feet (3050m) the vegetation consists of alpine meadows and herbaceous plants and shrubs. In Figure 2, a view looking along Dinwoody Creek depicts the environment within the watershed.

DATA SOURCES

The data sources for this study consisted of four LANDSAT scenes, U-2 high altitude infrared photography (1974, 1975) and Soil Conservation Service snow survey measurements (1973, 1974, 1975). The four LANDSAT scenes are identified as:

July 27, 1974	-	ID1734-17271
May 16, 1974	-	ID1667-17283
June 21, 1974	-	ID1698-17283
May 29, 1975	-	ID5040-17145

This LANDSAT information was received in digital form on computer compatible tapes (CCTs). The information on the tape is in four multispectral ranges. These ranges are two visible bands .5-.6 μ m and .6-.7 μ m and two near infrared bands .7-.8 μ m and .8-1.1 μ m.

APPROACH

Multispectral Analysis

The General Electric IMAGE 100 multispectral image processing and analysis system was used in this study to perform the digital data processing. The prime concept of the IMAGE 100 system design is the operation of a man-machine interface.



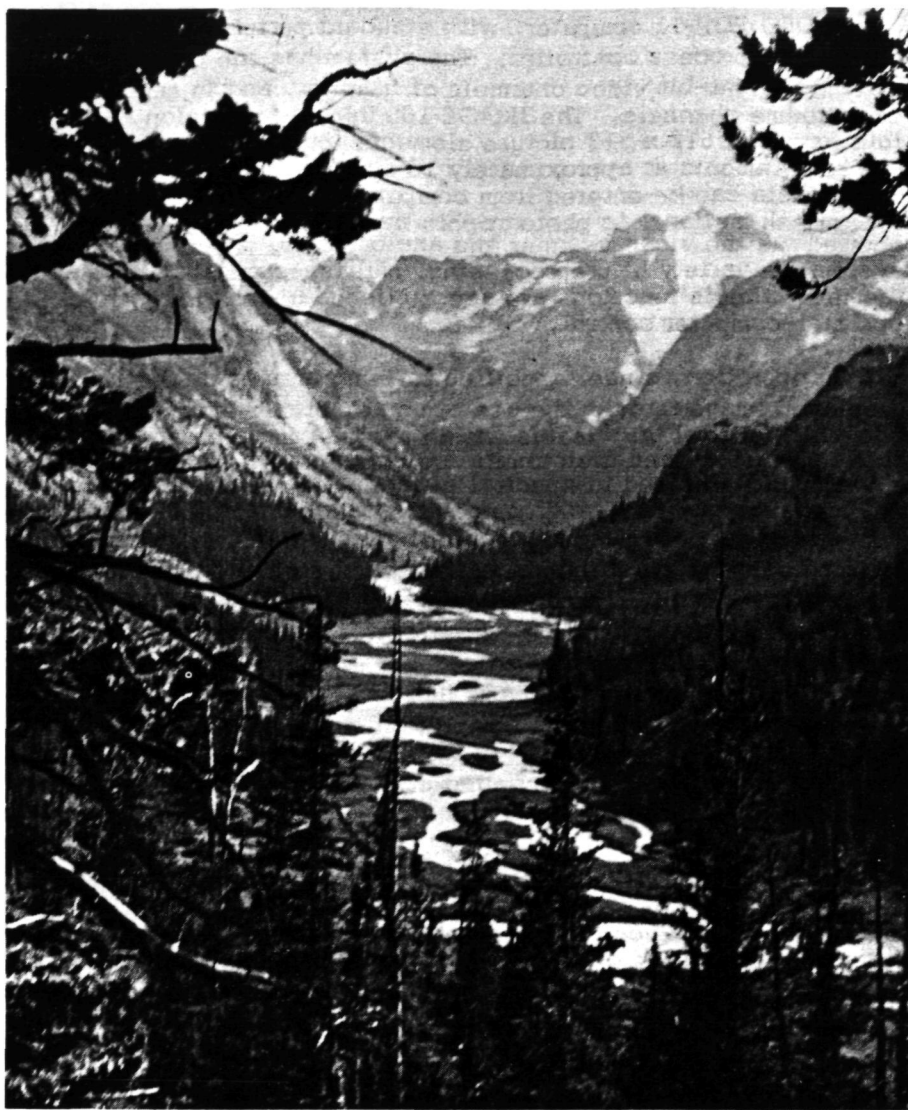
WIND RIVER MOUNTAIN, WYOMING
LANDSAT-AUG. 6, 1972 (REF. 2) WATERSHEDS

FIGURE 1.



WORKING SCENE, MINIMAL SNOWCOVER,
JULY 27, 1974, DINWOODY WATERSHED

FIGURE 4.



WIND RIVER MOUNTAIN RANGE, DINWOODY
CREEK

FIGURE 2.

REPRODUCIBILITY OF THE
ORIGINAL PAGE IS POOR

A DEC PDP-11 computer, with standard peripherals is used as the system process controller. The system has the capability of storing 4 eight-bit video channels of imagery, and in addition, eight theme channels. The IMAGE 100 uses a television compatible format of 512 x 512 picture elements (pixels) to put the storage requirements at approximately 10 million bits. LANDSAT digital data can be entered from computer compatible tapes into the refresh memory, or photographic transparency data can be entered via the video scanner and analog to digital converter subsystem. A variety of preprocessing, multispectral analysis, and theme synthesis functions are accomplished under interactive operator-computer control.

In operation, a user specified training area is delineated on the displayed image through the use of an adjustable electronic cursor. The multispectral gray levels within the training area are automatically measured and their limits are used to define a four-dimensional parallelepiped in spectral space. The entire image is scanned pixel by pixel and compared to the parallelepiped limits. All pixels which are located within the bounds defined by the training data are classified or alarmed and displayed on the monitor as a color map. If after a few iterations of the basic training and classification procedure, the operator is not satisfied with the results, other sophisticated procedures may be used. One of these is the histogram analysis. Each time the system performs a parallelepiped training, it stores complete histogram data for each of the four spectral channels. The operator can call these data to be displayed on the graphics terminal and alter any of the parallelepiped limits as defined on the histograms.

Once the classification results have been achieved, they are stored on one of the eight binary theme channels to form a thematic map. The operator can proceed to a new area by loading the refresh memory with new data. For subsequent analysis, he can rely on spectral signatures or parallelepiped limits previously derived by recalling them from storage or reentering them.

METHODOLOGY

Presently, operational snowmapping techniques require the determination of the snowline elevation of the determination of the snowcovered area of a watershed. Little emphasis has been placed upon mapping classes of snow and surface features of a watershed relative to operational snowmapping. Currently, work is being performed on the latter (Ref. 4). Knowledge of the distribution of these land use types; forests, bare rock areas, grassland, and water and shadow areas, may be useful in solving interpretation problems encountered in snowmapping. In addition,

if runoff equation or models become more refined in future years, it might be useful to know what percent of a given land use type is snowcovered.

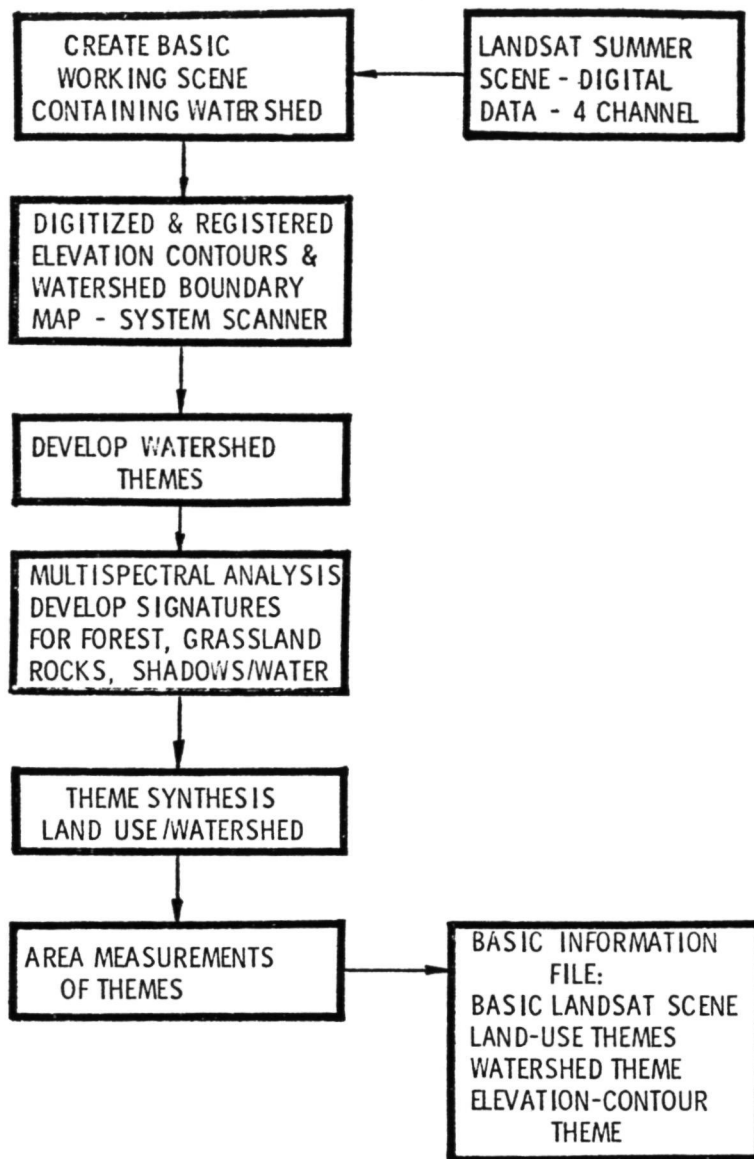
Based upon the above considerations, the technique for digital snowmapping was devised to have two parts. The first part of the technique has a permanent (basic) part and the second part an operational (quasi-operational) part. The basic part is accomplished only once for a watershed. It will remain constant and be used repetitively with the quasi-operational part for snowmapping. Items included in the basic part are digitized watershed boundary maps with elevation contours and watershed surface feature themes (forest, rocks, meadows, shadows/water). The quasi-operational procedures deals primarily with determination of snow area and the snow line.

Basic Part--In Figure 3, the basic part of the technique is schematically shown. A LANDSAT scene having a minimum of snowcover was selected for extracting multispectral signatures of surface features within the watershed. The LANDSAT data source used was dated July 27, 1974, ID1734-17271. A working scene was created using the data from LANDSAT computer compatible tapes (CCT). This working scene, Figure 4, contained the Dinwoody watershed. Elevation contours and watershed boundaries from a tracing were digitized and registered with the working scene Figure 5. This tracing was made from a 1:250,000 USGS map having contour intervals at 200 feet. Two themes were developed, the elevation contours Figure 5 and the watershed Figure 6.

Signature extraction of surface features in the watershed using multispectral analysis was performed. Signatures for forest, grassland, rocks and shadow/water were obtained, classified and assigned as themes. Extraction of the signatures was aided by information from U-2 high altitude photography. This photography assisted in selection of training areas containing surface features to be classified. Verification of the working scene classification was accomplished by comparing with the U-2 photography.

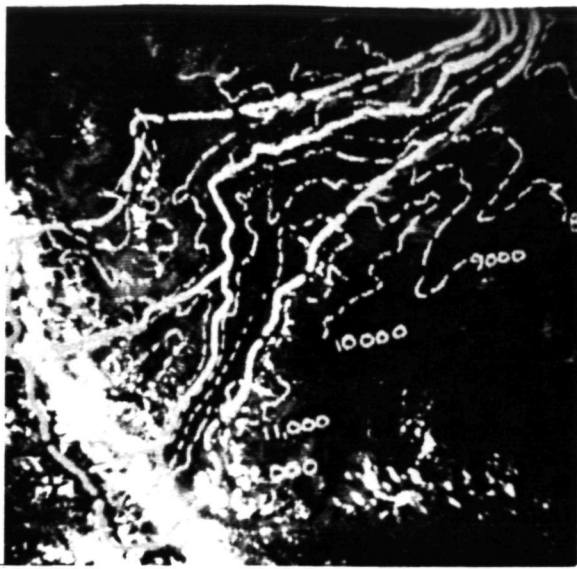
Theme synthesis provided surface feature themes relative to the watershed. Area measurements for these themes were obtained and their percentages to the watershed calculated.

A basic file consisting of four channels of LANDSAT July 27, 1974 data and one channel of themes (elevation contour/surface features/watershed) were stored on magnetic tape. This file is



BASIC INFORMATION PART

FIGURE 3



DIGITIZED ELEVATION CONTOUR AND
WATERSHED BOUNDARY, DINWOODY WATERSHED
FIGURE 5.



DINWOODY WATERSHED

FIGURE 6.

REPRODUCIBILITY OF THE
ORIGINAL PAGE IS POOR

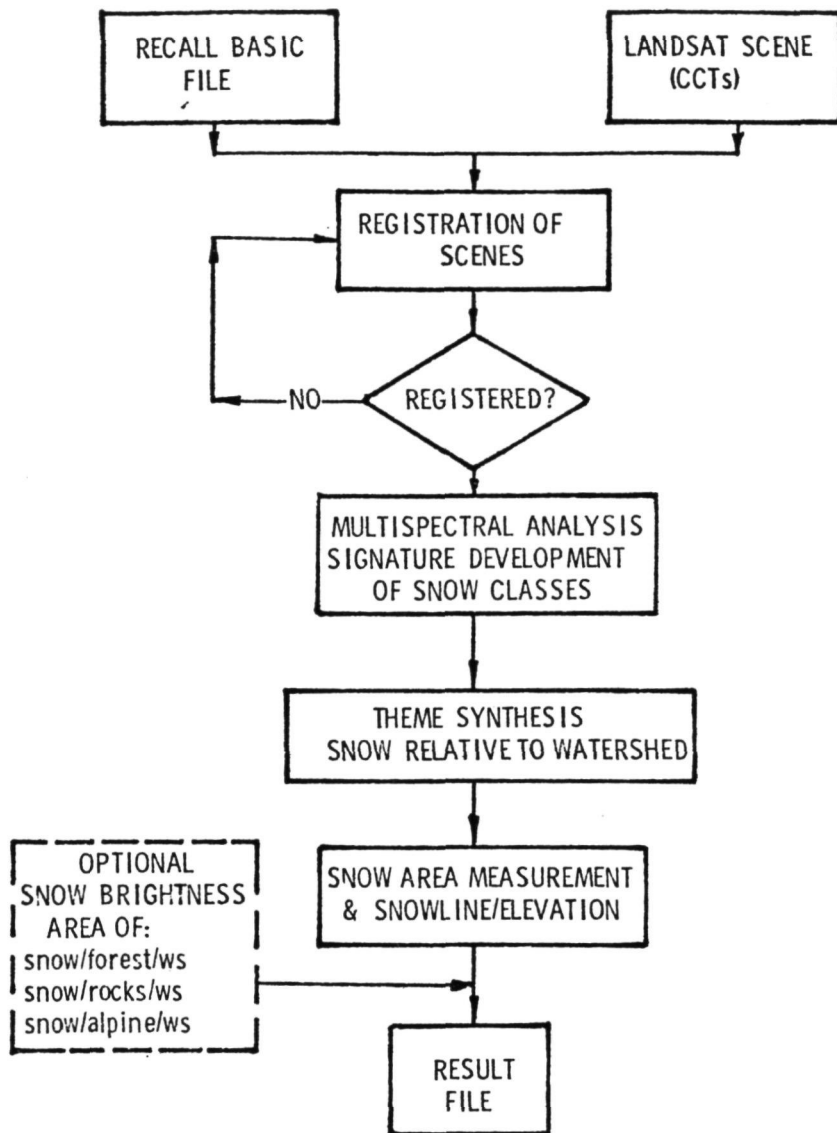
permanent, containing information constant to the watershed. This information is the reference for registration of other LANDSAT data sources and for recalling surface feature themes.

Quasi-Operational Part -- In Figure 7, the quasi-operational part of the technique is shown. Initially, the basic file information is recalled into the system. This included the original LANDSAT scene and the themes (surface features, watershed map). Registration of the two LANDSAT scenes is accomplished in an iterative mode. Registration of a single point of a working scene can be obtained by a pixel. For the complete working scene, experience has shown that registration accuracy varies from 2 to 10 pixels. Once registration is complete, All LANDSAT information for the scene to be analyzed is called into the system. Basic themes are saved. The next step is the analysis of the snowcover by multispectral analysis. The training sites were selected for areas of the snow-pack having different spectral signatures. They are located in bright or heavy snow areas, in mottled areas where the forest is concealing most of the snow, in areas where the snow is melting, and in areas where bare rock or ground is protruding through the snowcover. Classes of snow area determined from these training sites using all four channels of LANDSAT data. After the determination of the classes, the total snow class is obtained. By performing theme synthesis, snowcover classes are acquired within the watershed. As an option, snow in forested areas, snow over rocks or snow in shadows/water can be obtained. At this point, area measurements of the snow classes are obtained. Another option is selecting particular snowcover sites and obtaining brightness values of snow (in all four LANDSAT bands). If the option is not selected, a result file is made with the snow classes on magnetic tape.

Brightness values (spectral reflectance recorded by LANDSAT multispectral scanner) may be useful in discriminating snow classes along the snowline. It has been considered that snow which appeared less reflective near the snowline was indicative of "melting". In Ref. 3, it was noted that further research is required to confirm melting snow. In lieu of this, the availability of brightness values relative to characteristic of the snow may have little value but they do help in defining the snow edges.

RESULTS

- LANDSAT digital data of July 27, 1974, Figure 3, (minimal snowcover) of the Wind River Mountain Range, Wyoming was processed by the General Electric IMAGE 100 system. This processing by multispectral analysis defined the surface feature signatures such as forest, rock, grassland



SNOWMAPPING QUASI-OPERATIONAL ANALYSIS

FIGURE 7

and shadows/water within the Dinwoody watershed. Through the system scanner, an elevation contour and watershed boundary map was digitized and registered with the LANDSAT scene. Theme synthesis provided the surface features relative to the watershed. Area measurements of these surface features and the watershed are shown in Table 1.

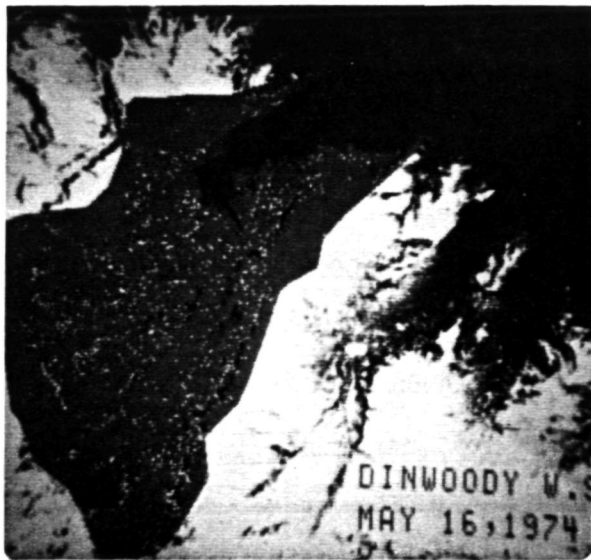
- The LANDSAT data of July 27, 1974, the surface feature themes, the elevation contour map theme and the watershed theme were used as reference for processing other LANDSAT data during the snowmelt season (May-June) for the Dinwoody watershed. Multispectral analysis of four dates of LANDSAT data has provided estimates of total snow area within the Dinwoody watershed (Figures 8, 9, and 10). Several classes of snow were obtained by the multispectral analysis. In this study, no attempt was made to correlate the physical significant of these snow classes. At this time, significance is placed on two classes of snow; the main snowpack and the snow edges. In Figure 11, classes of snow are shown. In Table 2, the snow area and percentage of snow in the watershed is shown and compared with area measurements derived by manual interpretation. The manual interpretation, is based upon mapping the snowline and measuring the area of the snow above the snowline with a planimeter.
- In Figure 5, the elevation - contour map theme is superimposed over the LANDSAT May 16, 1974 scene. This capability allows for the quick estimate of the snow line location relative to the elevation contour lines. For the LANDSAT May 16, 1974 scene, the snowline is observed between the 8000 - 10,000 foot contours and is estimated to be at 9000 feet.
- From this study, an estimate of the amount of snowcover within the watershed surface features is possible. In the case of the LANDSAT, May 16, 1974 scene, the estimate of the snowcover within forested areas in the watershed is 3511 pixels or 6.6% of the watershed. See Table 3 for other snowcover/surface feature percentages.
- A quasi-operational technique has been developed to snow map the Dinwoody watershed, Wyoming. This technique requires thirty to forty-five (30 to 45) minutes to obtain the basic information of:

DINWOODY WATERSHED
WIND RIVER MOUNTAIN RANGE, WYOMING

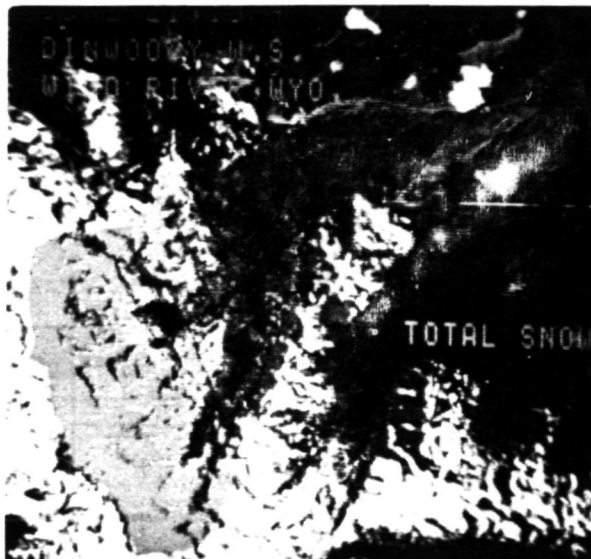
LANDSAT SCENE: JULY 27 , 1975

TABLE 1

THEMES	AREA MEASUREMENTS			PERCENT OF WATERSHED
	pixels	miles ²	kilometers ²	
WATERSHED	52650	92.5	239.6	
BARE ROCK	28031	49.2	127.5	53.2
FOREST	6213	10.9	28.3	11.8
GRASSLAND	2699	4.7	12.3	5.1
SNOW	8920	15.7	40.6	16.9
SHADOWS/WATER	1301	2.3	5.9	2.5



SNOWCOVER - MAY 16, 1974
DINWOODY WATERSHED
FIGURE 8.



SNOWCOVER - JUNE 21, 1974
DINWOODY WATERSHED
FIGURE 9.



SNOWCOVER, MAY 29, 1975 DINWOODY
WATERSHED

FIGURE 10



TWO CLASSES OF SNOW, MAY 29, 1975
DINWOODY WATERSHED

FIGURE 11

REPRODUCIBILITY OF THE
ORIGINAL PAGE IS POOR

DINWOODY WATERSHED

WIND RIVER MOUNTAIN RANGE, WYOMING

SNOW AREA MEASUREMENTS

TABLE 2

LANDSAT DATA SOURCE	TOTAL SNOW AREA MEASUREMENTS			PERCENT OF WATERSHED *	MANUAL INTERPRETATION % OF WATERSHED •
	pixels	miles ²	kilometer ²		
May 29, 1975	44155	77.6	200.9	83.9	88.
June 21, 1974	15466	27.2	70.4	29.4	52.
May 16, 1974	37484	48.3	125.1	71.2	85.
July 27, 1974	8920	15.7	40.6	16.9	

DINWOODY W. S. AREA = 52650 PIXELS

- Based on count of pixels defined multispectrally as snow.
- Interpretation based on mapping the snow line and measuring the percentage of the basin above the snow line.

DINWOODY WATERSHED
WIND RIVER MOUNTAIN RANGE, WYOMING
LANDSAT SCENE: MAY 16, 1974

TABLE 3

SNOW RELATIVE TO WATERSHED SURFACE FEATURE	AREA MEASUREMENTS			PERCENT OF SNOW COVER
	pixels	miles ²	kilometers ²	
SNOW/FOREST	3511	6.1	15.8	9.4
SNOW/ROCK	22095	38.8	100.5	58.9
SNOW/GRASSLAND	2527	4.4	11.5	6.7

TOTAL SNOW COVER: 37484 pixels

- classes of snow and snow areas/watershed
- total snow area/watershed
- snow line elevation estimate

The technique also allows for estimating the amount of snow over watershed surface features.

The Wind River Mountain Range contains several watersheds. In Figure 1, seven watersheds are shown. Applying this quasi-operational technique, an estimate of fifteen hours (15) of processing time would be required to provide basic snow information for all seven watersheds.

At the present time, General Electric, Beltsville, has implemented a bulk processing relative to LANDSAT data. This capability, with other software refinements, is estimated to reduce the processing time to approximately five (5) hours for the Wind River Mountain Range watersheds.

CONCLUSIONS

A digital snowmapping technique using LANDSAT data and the General Electric IMAGE 100 system has been implemented. This technique was tested several times on snowmapping the snow areas and snow lines of the Dinwoody watershed in the Wind River Mountain Range in Wyoming. Signatures of snow classes were rapidly determined by multispectral analysis. Area measurements of snow classes were instantaneously achieved by electronically counting the classified snow pixels. Greater detail in area measurement is obtained through the multispectral analysis rather than manual interpretation. This is because there are snow free areas within the snowpack which are too numerous and minute to measure accurately with a compensating planimeter, but these small melt areas or wind blown areas can be accounted for with the automatic planimeter function of the GE IMAGE 100 system. As compared to the manual technique, machine processing is less laborious and tedious. The average time required to process a single LANDSAT working scene to obtain snowcover and the snowline was three quarters of an hour. Repetitive processing of the Dinwoody watershed would reduce this processing time.

In addition to snow areas and snow lines, this technique has devised methods of estimating the snow distribution over watershed surface features. Presently, this distribution is not needed in operations but may prove to be of value with development of

sophisticated snowmelt models. Other possible uses of this technique is in conjunction with snow surveys. Data derived from the analysis of the snowpack may assist in location of new snow course or modifications to existing courses. Correlation studies could be performed by superimposing snow courses over working scenes and obtaining radiance values at the course locations. These radiance values and snow course measurement could be correlated.

This technique has been referred to as quasi-operational. In the true sense of an operational technique, bulk processing of LANDSAT scenes and the methods described in this paper must be incorporated into the IMAGE 100 system. The bulk processing has been implemented. Software development to expedite watershed boundary delineation and registration is required. This capability will reduce the processing time significantly; with the Wind River Mountain Range (seven watersheds) a conservative estimate of five hours will be required for acquisition of snowcover areas.

REFERENCES

- Ref. 1: Rango, A., Salomonson, V.V., and Foster, J.L.
"Seasonal Streamflow Estimation Employing Satellite
Snowcover Observation", Document X-913-75-26
Goddard Space Flight Center, Greenbelt, Maryland
pp 95
- Ref. 2: Foster, J.L. and Rango, A., "A Method for Improving
the Location of the Snow Line in Forested Areas Using
Satellite Imagery," Document X-910-75-41, Goddard
Space Flight Center, Greenbelt, Maryland, pp. 8
- Ref. 3: McGinnis, D.F., Wiesnet, D.R. and McMillan, M.C.
"Applications of LANDSAT Data for Snow Evaluation"
NASA, Earth Resources Survey Symposium, Houston,
Texas
- Ref. 4: Katibah, E.F., "Areal Extent of Snow Estimation in
the Northern Sierra Nevada Mountains Using LANDSAT
1 Imagery", NASA Earth Resources Survey Symposium,
Houston, Texas.

SNOW COVER MONITORING BY MACHINE PROCESSING OF MULTITEMPORAL LANDSAT MSS DATA

S. G. Luther, L. A. Bartolucci and R. M. Hoffer, *Laboratory for Applications of Remote Sensing, Purdue University, W. Lafayette, Indiana 47906*

ABSTRACT

LANDSAT frames were geometrically corrected and data sets from six different dates were overlaid to produce a 24 channel (six dates and four wavelength bands) data tape. Changes in the extent of the snowpack could be accurately and easily determined using a change detection technique on data which had previously been classified by the LARSYS software system.

A second phase of the analysis involved determination of the relationship between spatial resolution or data sampling frequency and accuracy of measuring the area of the snowpack.

INTRODUCTION

Climate and subsurface geology combine to make water a scarce and valuable commodity in the western United States. Most of the water supply comes from the spring and summer runoff of winter snow accumulations in the Rocky Mountains. A network of reservoirs has been constructed to conserve this resource to satisfy the water needs of urban communities and to provide water for irrigation. In addition, this water is used for generating hydroelectric power and for providing recreational facilities. The network is operated by various state and federal government agencies and private corporations.

In order to regulate these reservoirs properly, these agencies must have an estimate of both the discharge required downstream and the concomitant recharge needed from the reservoir's source, which

This research was funded by NASA Contract NAS5-21880.

in most cases is a mountain stream. The objective of this research is to investigate methods by which MSS data can be applied to the process of snow cover monitoring, thereby enabling more accurate predictions of runoff from mountain watersheds.

Since the methods to be studied may vary in time, cost and practicality of application, parameters must be established to insure that the techniques involved are economically advantageous, i.e., that similar information is provided at less cost than conventional methods or that increased cost is accompanied by additional information. To meet these objectives this analysis has purposely been kept simple and hence does not reflect the most accurate classification possible, i.e., misclassification errors in shadowed areas do occur.

Computer Aided Analysis Techniques

The Animas River watershed above Howardsville, Colorado was selected as the test site for this phase of the study because 1) it is located in the headwaters of the Colorado River, 2) it is wholly contained in the San Juan Mountain Test Site, and 3) good records exist for the gaging station at Howardsville. The watershed boundary was physically located on four USGS 7 1/2' topographic maps (see Figure 1). The boundary was defined by elevations, the stream network and the location of the gaging station in relation to the stream.

Once determined and delineated, the boundary was transferred from the map to a gray scale printout at the same scale (1/24,000), by aligning the stream networks. The watershed was then defined on the LANDSAT imagery, using a series of line and column coordinates as individual "test areas", thus providing an accurate estimation of the total area of the watershed (Figure 2).

The data for frames 1101-17203 (1 November, 1972), 1119-17204 (19 November, 1972), 1173-17202 (12 January, 1973), 1191-17204 (30 January, 1973), 1299-17205 (18 May, 1973) and 1317-17204 (5 June, 1973) were all overlaid, rotated and rescaled thereby eliminating the need for repetition of the outlining process. These frames are cloud free over the Howardsville watershed.



Figure 1. Animas River Watershed at
Howardsville, Colorado

281

REPRODUCIBILITY OF THE
ORIGINAL PAGE IS POOR

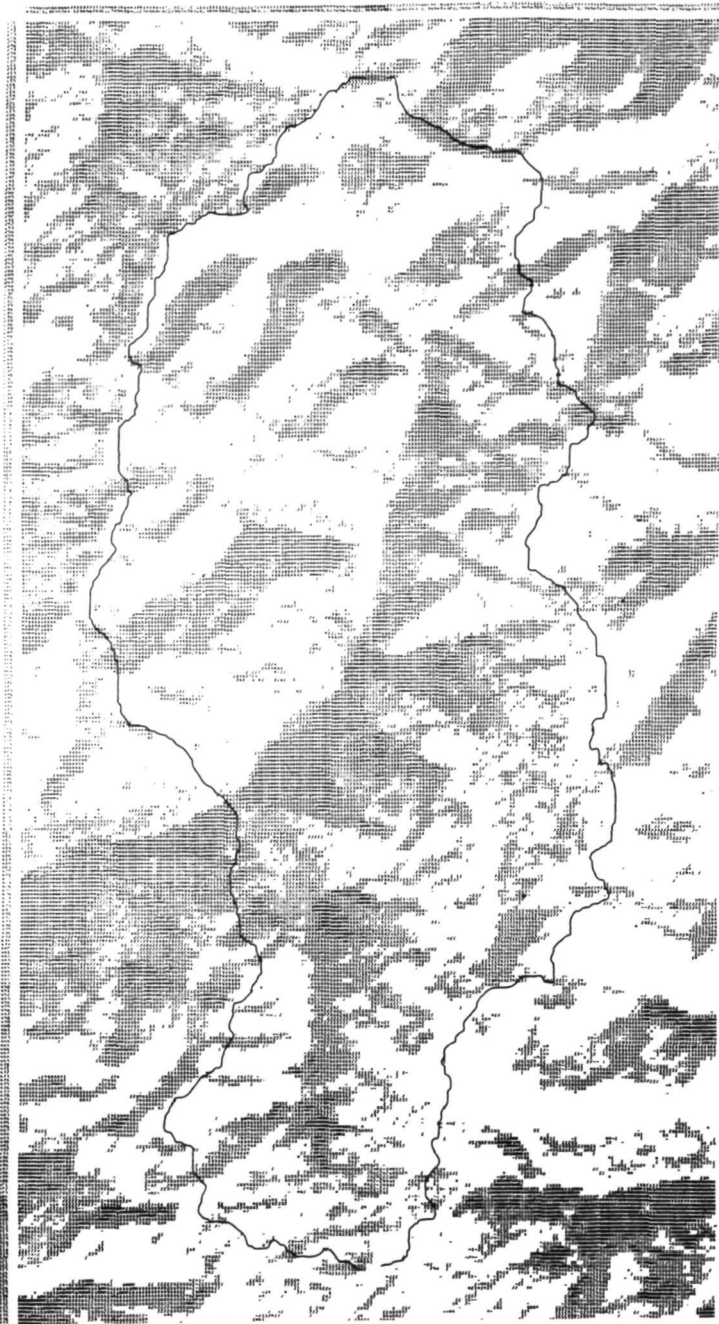


Figure 2. Location of Animas Watershed on LANDSAT Imagery

In order to ascertain the accuracy of this type of areal calculation, the relative size of a printer element must be known. Previous investigations have indicated that each LANDSAT element contains .43 hectares. Furthermore, a total of 32,405 elements was contained within the watershed, so the area was calculated to be 147 square kilometers. Since the U.S. Geological Survey had estimated the area to be 55.9 square miles (145 square kilometers) (see WSP 1925) and this coincided with an estimate obtained by planimetering the area, the error introduced by the computer tabulation and human errors in outlining the boundary was 1.5%. Band five digital display imagery for one of the frames (1119-17204) which contains the watershed is shown in Figure 3. This image consists of sixteen gray levels defined by the computer program, based on relative reflectance histograms of the area.



Figure 3. Digital Display Photograph of LANDSAT Frame 1119-17204, Band Five.

To determine the areal extent of the snow cover, two channels, (one in the visible (.6-.7 μ m) and one in the IR (.8-1.1 μ m), were used in conjunction with LARSYS. LANDSAT MSS channels four and five were generally saturated by the snow cover and the information provided by each resulted in a singular correlation matrix. This required the elimination of one of these channels in order to implement the LARSYS processor.

Two classes, "snow" and "other", were then requested from the clustering processor, to generate the statistics for these classes which are shown below in Table 1.

TABLE 1. Spectral Response of Snow

Date	LANDSAT Band	<u>Snow</u>		<u>Other</u>	
		Mean Relative Reflec- tance	Std. Dev.	Mean Relative Reflec- tance	Std. Dev.
1 Nov. 1972	5	124.73	7.01	37.29	18.21
	7	56.75	9.23	13.15	7.11
19 Nov. 1972	5	123.43	9.21	32.21	10.35
	7	54.34	10.66	18.22	6.96
12 Jan. 1973	5	121.73	11.17	31.36	10.31
	7	52.32	11.13	18.59	7.03
30 Jan. 1973	5	122.45	10.32	30.04	17.21
	7	52.70	10.78	10.34	6.72
18 May 1973	5	125.33	11.02	50.44	18.83
	7	53.50	17.42	21.12	5.50
5 June 1973	5	125.98	10.30	45.89	18.66
	7	51.72	15.26	22.30	5.90

These numbers are dimensionless and indicate the relative reflectance of each class. Note that the mean of the class snow does not vary significantly between dates and approaches the saturation level, which is 128 for band five and 64 for band seven.

Each frame was then classified separately into two classes, snow and other according to these statistics. Display maps of the classification results were obtained, along with a table showing the number of resolution elements within the watershed that were classified as snow and the percentage of snow cover (an example of this type of output is shown in Figure 4). By multiplying the number of resolution elements classified as snow by the .43 hectares represented by each resolution element or by multiplying the percentage of snow cover, the areal extent of the snowpack can be quickly and easily calculated by this computer analysis procedure.

CLASSIFICATION STUDY 325548065

CLASSIFIED

SEPT 12, 1973

CLASSIFICATION TAPE/FILE NUMBER ... 59/ 6

CHANNELS USED

CHANNEL 2	SPECTRAL BAND	0.60 TO	0.70 MICROMETERS	CALIBRATION CODE = 1	CO = 0.0
CHANNEL 4	SPECTRAL BAND	0.80 TO	1.10 MICROMETERS	CALIBRATION CODE = 1	CO = 0.0

CLASSES

	CLASS	WEIGHT		CLASS	WEIGHT
1	NS- 1/	0.000		2	NS- 2/ 0.000

TEST CLASS PERFORMANCE

GROUP	NO OF SAMPS	PCT. CORCT	NUMBER OF SAMPLES CLASSIFIED INTO	
			NS- 1/	NS- 2/
1 NS- 1/	32367	76.2	24654	7713
TOTAL	32367		24654	7713

OVERALL PERFORMANCE(24654/ 32367) = 76.2

AVERAGE PERFORMANCE BY CLASS(76.2/ 1) = 76.2

Figure 4. Snow Cover Calculation

Table 2 gives a summary of the areal fluctuations of the snowpack.

TABLE 2. Snow Acreage Fluctuations

<u>Date</u>	<u>Percent Snow Cover</u>	<u>Total Area (hectares)</u>
1 Nov. 1972	76.1	11189
19 Nov. 1972	68.3	10037
12 Jan. 1973	62.6	9203
30 Jan. 1973	65.1	10023
18 May 1973	81.0	12471
5 June 1973	87.5	13471

Figure 5 shows the last two classification results taken from the digital display. These include that portion of the area surrounding the Howardsville watershed.

The relationship between area, snowpack density and total water content of the snowpack requires much additional study. However, LANDSAT can provide accurate, rapid measurements of the areal extent of the snowpack.

Several intervening dates between January 30, 1973 and May 18, 1973 have not been included in this investigation due to cloud conditions. Thus, this study clearly indicated that LANDSAT-1 frequency of coverage can rapidly decrease from once to every 18 days to once every 36 or 54 days, a totally unacceptable condition for studying hydrological and other dynamic phenomena.

Temporal Analysis

The general technique for determining ground cover changes between two dates is known as change detection. There are at least four change detection methods; Delta Transformation, Spectral/Temporal Concurrent Classification, Spectral/Temporal Layered Classification and Post-Classification Comparison.

For this study classifications were made for the area on the various dates and then these classifications were compared. Before the classifications were attempted an overlay was made which aligned the data so a ground point could be located by the same

line and column coordinates. Channels 1-4 are the first date and channels 5-8 are the second date so that two classifications exist for the same run number, the same area, but different sets of channels.



A. May 18, 1973



B. June 5, 1973

Figure 5. Classification Results

REPRODUCIBILITY OF THE
ORIGINAL PAGE IS POOR

This program was used to analyze the snow classification results as an aid to analyzing redistribution patterns of snow within watersheds and to display the results as a third 4-class classification. Figure 6 below illustrates this process.

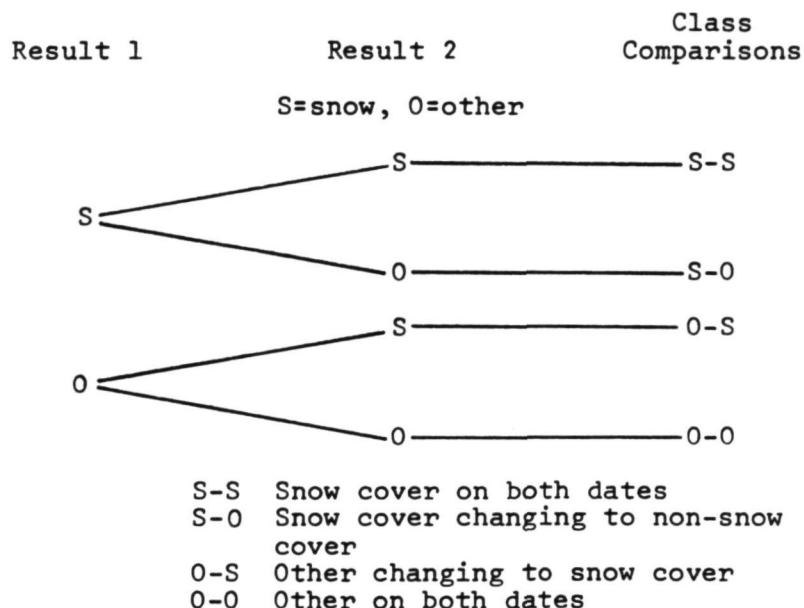


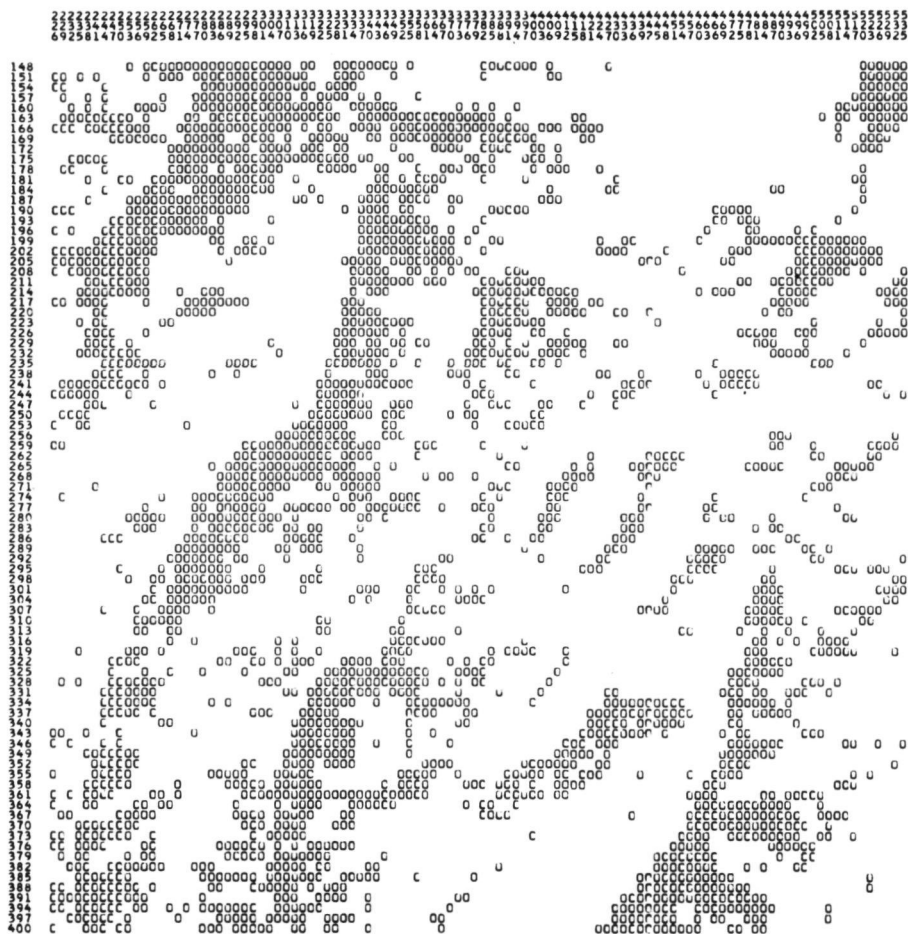
Figure 6. Flow Diagram of Post-Classification Change Detection Technique

This program, was run on the six classification results from the Animas River watershed. An example of this temporal analysis technique for a portion of the Animas watershed is shown in Figures 7, 8 and 9.

Classification Sampling Rate

The multispectral classification of enormous quantities of data gathered by earth orbiting satellites (to determine the areal extent of snow cover), requires a relatively large amount of computer CPU (Central Processing Unit) time. The purpose of this phase of the investigation was to compare the accuracy of the multispectral classification of snow cover using different data sampling rates in order to reduce the amount of computer processing time.

SYMBOL	CLASS	WEIGHT	
0	NS- 2/	0.000	Other



NUMBER OF POINTS DISPLAYED IS 9435

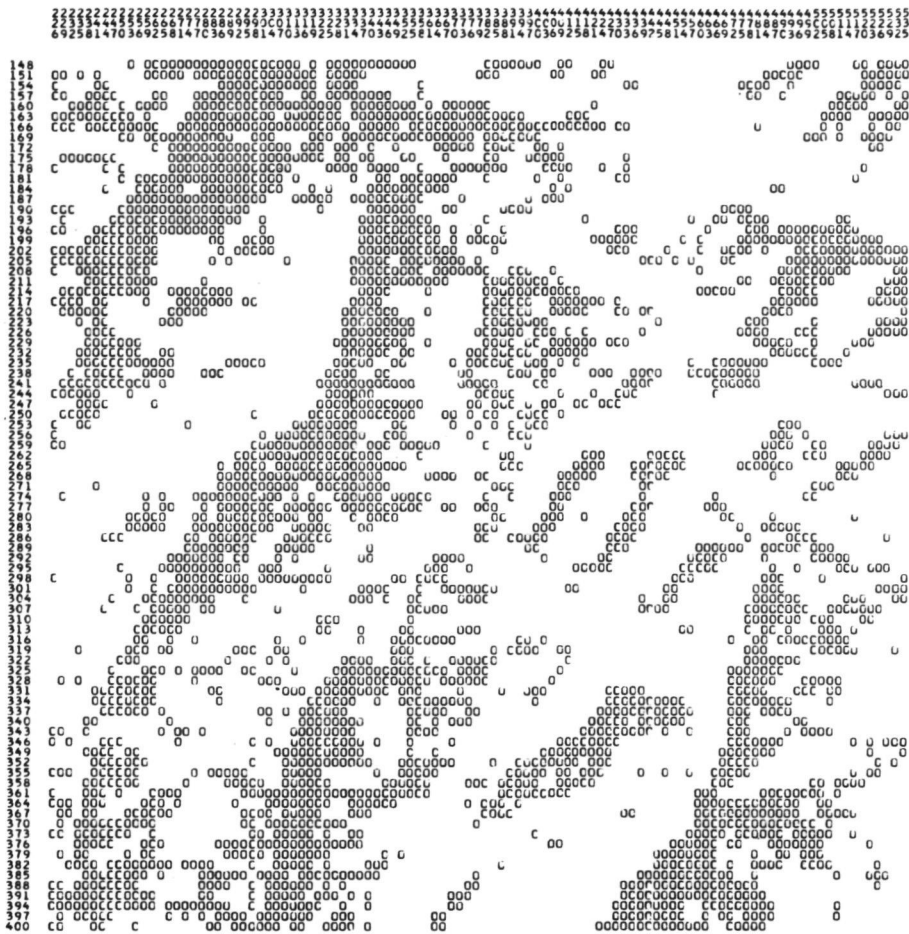
Figure 7. Snow Map for
November 1, 1973

REPRODUCIBILITY OF THE
ORIGINAL PAGE IS POOR

CLASSES

SYMBOL CLASS WEIGHT
NS- 1/ 0.000 Snow

SYMBOL CLASS WEIGHT
0 NS- 2/ 0.000 Other

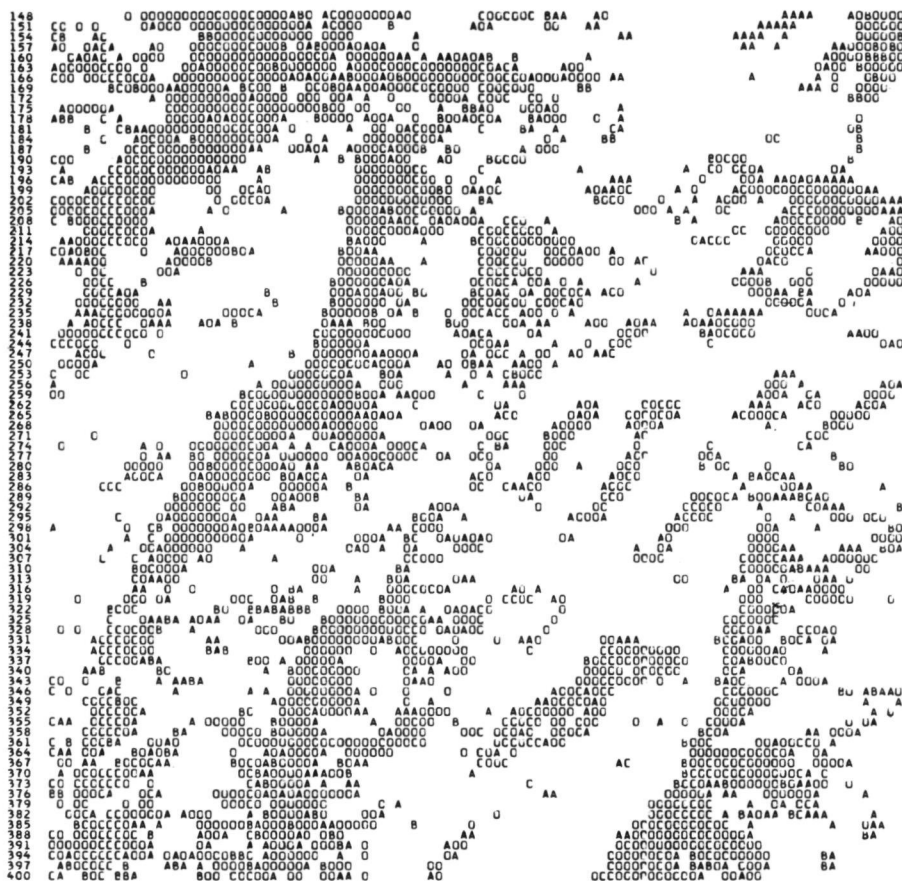


NUMBER OF POINTS DISPLAYED IS 9435

Figure 8. Snow Map for
November 19, 1973

SYMBOL	CLASS	WEIGHT
	SNO-SNO	0.000
C	OTH-OTH	0.000
A	SNO-OTH	0.000

SYMBOL	CLASS	WEIGHT
B	CTH-SNC	-.000
C	*CHANGE*	0.000

[illegible]

NUMBER OF POINTS DISPLAYED IS 9435

Figure 9. Change Detection Map
for November 1-19,
1973

REPRODUCIBILITY OF THE
ORIGINAL PAGE IS POOR

Approximately 60% of a LANDSAT-1 MSS frame (scene ID 1317-17204) was classified into four spectral classes (one snow class and three non-snow classes) using bands 5 and 6. In essence, five classifications of the area were performed each at a different data sampling rate. Then, the areal extent of the snow cover was computed for each one of the five classifications. Table 3 shows the percent of the area classified as snow cover and the corresponding CPU time used by each one of the five different data sampling rate classifications. Note in Table 3 that the difference between the area of snow for the 1x1 and 16x16 sampling rates is only 0.4 of one percent.

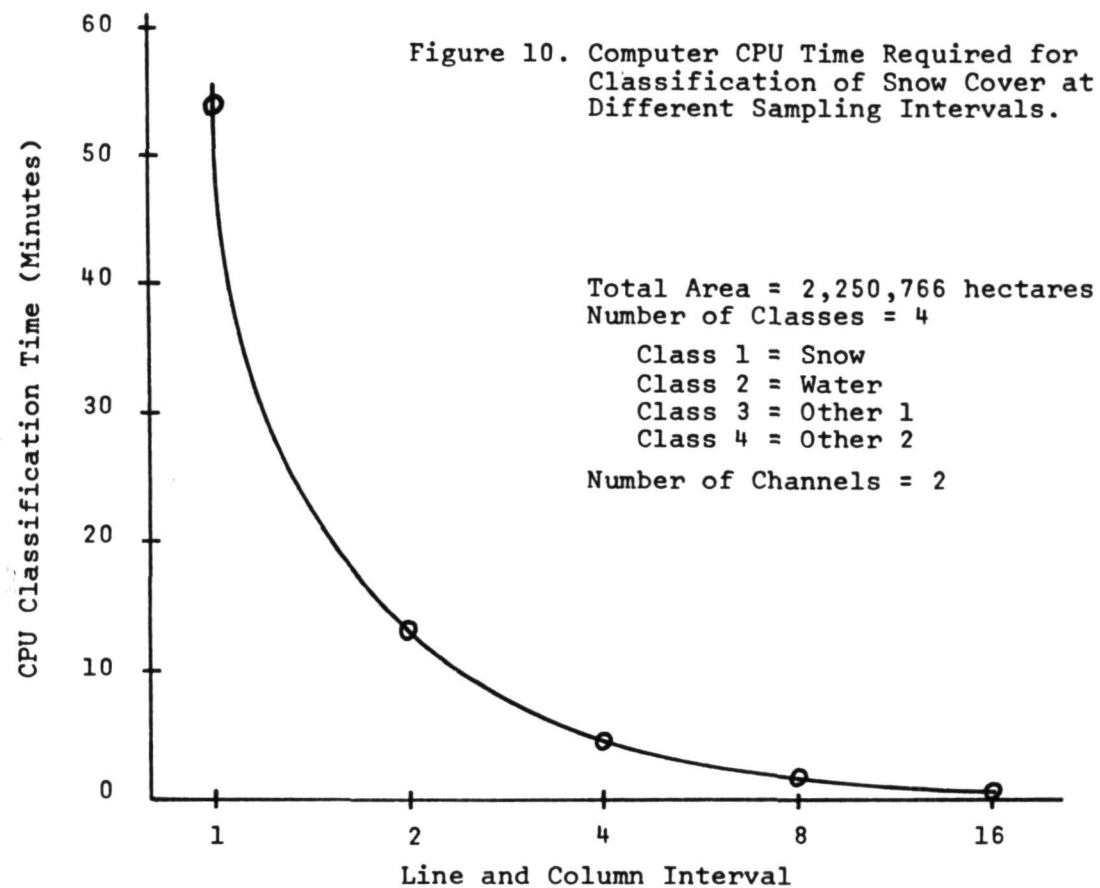
TABLE 3. Determination of Areal Extent of Snow Cover from LANDSAT MSS Data using Different Sampling Intervals

<u>Sample Interval</u>	<u>Number Data Points</u>	<u>Number of Points Classified as Snow</u>	<u>% of Area in Snow</u>	<u>Classification CPU* Time (minutes)</u>
1 x 1	4,330,561	1,385,126	31.99	54.34
2 x 2	1,083,681	345,417	31.87	13.20
4 x 4	271,441	86,433	31.84	4.21
8 x 8	68,121	21,646	31.78	1.52
16 x 16	17,161	5,422	31.60	0.65

*IBM 360 Model 67

Figure 10 shows a graph of the CPU time involved in the classification of snow cover versus the data sampling rates.

Statistical analysis of the results shown in Table 3 has indicated that the percent area of snow-cover determined by the 16x16 data sampling rate is not significantly different from the percent area covered by snow as determined by the 1x1 data sampling rate at both a 95% and 99% confidence level. In other words, the 31.60% area (in Table 3) is not statistically different from the 31.99% area, even though the sample number was decreased from over 4 million points to just over five thousand data points.



Conclusions

Six LANDSAT frames over the test site were overlaid, geometrically corrected and rescaled. The dates ranged from November 1, 1972 through June 5, 1973. Computer processing techniques were utilized to make an accurate determination of snow cover within a watershed at a scale of 1:24,000. A post-classification change detection processing technique determined and located changes in snow cover. For large geographic areas, snow cover can be accurately mapped without incurring the cost of classifying every data sample.

SNOWCOVER MAPPING BY MACHINE PROCESSING OF SKYLAB AND LANDSAT MSS DATA

L. A. Bartolucci, R. M. Hoffer and S. G. Luther, *Laboratory for Applications of Remote Sensing, Purdue University, W. Lafayette, Indiana 47906*

ABSTRACT

SKYLAB and LANDSAT MSS data were analyzed using computer-aided analysis techniques (CAAT) developed at LARS. Results indicated that the middle infrared wavelength bands of the SKYLAB S-192 scanner would allow effective discrimination between snowcover and water-droplet clouds, whereas the limited spectral response of the LANDSAT-1 or 2 scanners do not allow such spectral discrimination. In the next phase of the current investigation, five spectral classes of snowcover were defined and mapped. These classes were found to be related to differences in the proportion of snow and forest cover in the individual resolution elements. In addition, topographic data (elevation, slope, and aspect) were digitally registered onto the SKYLAB and LANDSAT data to determine their influence on snowpack characteristics. Combining these results with the digital topographic data allowed acreage estimates of the various classes of snowcover to be tabulated according to elevational zones for either the entire data set or on an individual watershed basis.

This research was funded under NASA Contract NAS9-13380.

INTRODUCTION

The water supply for much of the southwestern United States comes from snowmelt in the watersheds of the Colorado Rocky Mountains. Information on the amount of snow accumulated during the winter months is necessary for making accurate predictions of spring runoff. Leaf and Haeffner (1971) have pointed out that an important index of runoff during the snowmelt season is the areal extent of the snowcover.

For more than thirty years snow hydrologists have made innumerable attempts to correlate the areal extent of snowcover and subsequent runoff. Parshall (1941) and Potts (1944) have estimated the areal extent of snow fields for runoff forecasting using ground photography. From the late forties to date, many studies have included use of aerial photography to measure the areal extent of snowcover (Parsons and Castle, 1959; Finnegan, 1962; Leaf, 1969). However, it was not until the early 1960's that one could attain a synoptic view of large geographical areas through earth orbiting satellites. Today, a wide variety of environmental satellites are collecting an astronomic amount of data that potentially could be utilized to map the areal extent of snowcover in a repetitive mode. Wiesnet (1974) has stated that "our capacity for collecting data on snow and ice far exceeds our ability to analyze the data". Therefore, in order to keep up the pace with the existing and highly advanced data collection technology, computer-aided analysis techniques (CAAT) need to be further developed and evaluated.

The Laboratory for Applications of Remote Sensing (LARS) was organized at Purdue University in 1966 with an overall goal of applying modern computer technology and pattern recognition theory to the quantitative analysis of multispectral earth resources data. Several analysis techniques have been developed since that time and applied to a variety of disciplines. However, it was not until LANDSAT-1 MSS data became available that any of these computer-aided analysis techniques were applied to snow-hydrology studies.

The results of the work with LANDSAT-1 data indicated that the areal extent of snowcover could be obtained from these data, but that spectral variations within the snowpack area could not be reliably determined because of detector saturation problems. Another major limitation of the LANDSAT

data was the inability to discriminate between snow and clouds.

Analysis of SKYLAB S-192 multispectral scanner data indicated that the above limitations of the LANDSAT data could be overcome. The increased spectral range of the SKYLAB S-192 MSS offered significant advantages over the LANDSAT-1 data.

The purpose of this paper is to report some of the results obtained in the application of computer-analysis techniques to the SKYLAB multispectral scanner data for purposes of mapping snowcover in mountainous terrain. Two major facets of the investigation will be discussed. The first phase involves the multispectral classification of snowcover, including both snow/cloud differentiation and the definition and classification of different spectral groups of snowcover. The second major phase of the investigation consists of combining spectral data with topographic data in order to obtain a product having a greater degree of flexibility and utility than could be obtained using spectral data alone.

TEST SITE DESCRIPTION

The San Juan Mountains test site is located in a mountainous area of southwestern Colorado, containing a complex association of forest types, rangeland, alpine tundra, agricultural fields, water bodies, snow, and various man-made features. This area is fairly typical of the Rocky Mountains Region in terms of forest, water, and recreational resources.

The topography of the test site area is rugged, ranging in elevation from less than 2000 meters to over 4200 meters. Timberline in the region is at approximately 3600 meters, and extensive areas of tundra are found above this elevation. In the data set analyzed in this study, this tundra area was completely covered by snow. Below timberline, there are several different forest cover types that are distributed as a function of the topography (elevation, slope and aspect). There are many variations in stand density between and within the different forest cover types. Such stand density variations become important in interpreting the spectral characteristics of the SKYLAB S-192 MSS data for snow-cover mapping purposes, as will be discussed later.

The present study involved an unusual and particularly valuable set of data that were obtained over the test site during the SKYLAB-2 (SL-2) mission. On June 5, 1973, both SKYLAB and LANDSAT-1 data were obtained over the test site within an hour of each other, and the following day color-infrared photography was obtained from 18,288 meters (60,000 feet) by NASA's WB-57, and both photographic and multispectral scanner data were obtained from 11,186 meters (30,000 feet) by NASA's NC-130 aircraft. In addition, ground observation data were gathered throughout the week to complete the data set.

MULTISPECTRAL CLASSIFICATION OF SNOWCOVER

As previously stated, computer-aided analysis of LANDSAT multispectral scanner (MSS) data has indicated that it is possible to map and perform quantitative estimations of the areal extent of snowcover. However, cloud-cover and saturation of the LANDSAT MSS detectors limited the accuracy of the results. In most cases it was found that it was impossible to separate clouds from snow-covered areas using LANDSAT spectral information only (Hoffer and staff, 1975).

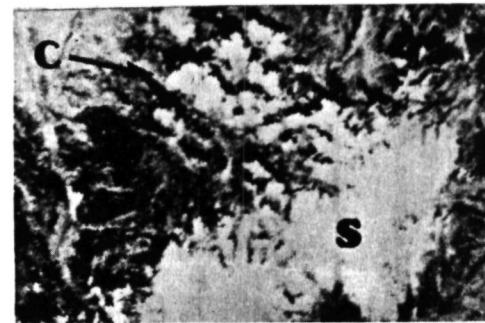
Snow and Cloud Differentiation

The problem of discriminating cloud formations from snow-covered areas was long ago identified by those researchers interpreting the early meteorological satellite images (Conover, 1964).

The extended spectral range of the SKYLAB S-192 multispectral scanner (0.41-12.5 μ m) proved to have significant advantages over the more limited spectral range of the LANDSAT MSS system (0.5-1.1 μ m). One of the advantages offered by the SKYLAB data is the ability to reliably and accurately differentiate snowcover from clouds using spectral information only. Figure 1 shows four SKYLAB-2 S-192 images representing the four different portions of the spectrum (visible, near infrared, middle infrared, and thermal infrared). A close inspection of these images shows that in the visible (0.46-0.51 μ m), near infrared (0.78-0.88 μ m), and thermal infrared (10.2-12.5 μ m) regions the clouds and snowcover have a very similar appearance, thus rendering difficult their discrimination. However, in the middle infrared (1.55-1.75 μ m) the snow appears black while the clouds still show a white appearance.



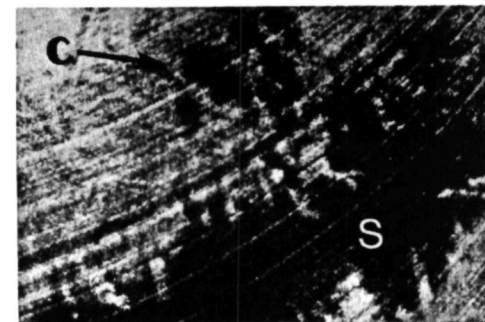
0.46-0.51 μ m (Visible)



0.78-0.88 μ m (Near IR)



1.55-1.75 μ m (Middle IR)



10.2-12.5 μ m (Thermal IR)

Figure 1. SKYLAB S-192 images representing the four major regions of the spectrum. C = clouds, S = snow.

The application of computer-aided analysis techniques to the SKYLAB-2 S-192 digital data has allowed the quantitative determination of the spectral separability and automatic discrimination between snowcover and clouds. Figure 2 shows a SKYLAB-2 S-192 image containing both snowcover and clouds, in which the rectangular outlined areas indicate the selected portions of data representing the snowcover and cloud spectral classes. The areas designated in this way were utilized to quantitatively examine the spectral characteristics of snow and clouds.

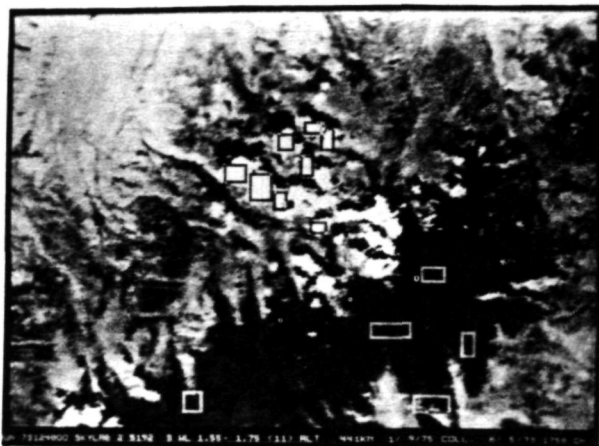


Figure 2. Middle IR wavelength imagery of the SKYLAB-2 S-192 Scanner with snow and cloud areas defined (rectangles).

The mean spectral response and corresponding standard deviation (in digital counts) for snowcover and clouds in the thirteen SKYLAB-2 S-192 wavelength bands is shown in Table 1. The digital counts range from zero to 255, where a spectral response of 255 indicates saturation of the detector. It is evident from Table 1 that the spectral responses for snowcover and clouds are very similar in channels 1 through 7, and in channel 13. It is only in channels 8 through 12 that the spectral response of the snowcover differs (in various degrees for each channel) from that of clouds. However, in order to measure accurately the degree of spectral separability between the snowcover and clouds, the LARSYS transformed divergence algorithm (Swain et al., 1971; and Swain and staff, 1972) was utilized. Figure 3 is a bar graph showing the spectral separability (based on transformed divergence values) between snowcover and clouds in the 13

SKYLAB-2 S-192 MSS bands. Values of transformed divergence greater than 1750 (the shaded area in Figure 3) indicate a reliable separability between the spectral classes in question (Swain and King, 1973).

Table 1. Mean Spectral Response and Standard Deviation for Snowcover and Clouds. SL-2 S-192 Data, 5 June 1973.

Wavelength Region	Wavelength Band (μm)	Snowcover		Clouds	
		Mean	S.D.	Mean	S.D.
Visible	0.41-0.46	255	0	254	4
Visible	0.46-0.51	250	16	248	19
Visible	0.52-0.56	229	38	229	37
Visible	0.56-0.61	255	0	254	1
Visible	0.62-0.67	254	6	254	8
Near Infrared	0.68-0.76	246	22	246	22
Near Infrared	0.78-0.88	230	38	230	35
Near Infrared	0.98-1.03	181	44	222	41
Near Infrared	1.09-1.19	165	33	228	32
Near Infrared	1.20-1.30	106	22	210	43
Middle Infrared	1.55-1.75	33	16	163	33
Middle Infrared	2.10-2.35	39	15	160	31
Thermal Infrared	10.2-12.5	67	18	61	14

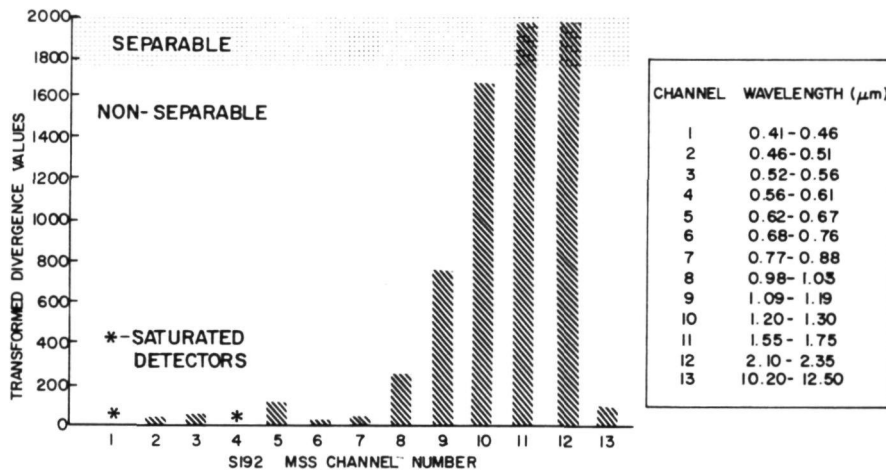


Figure 3. Spectral separability based on transformed divergence values between snowcover and clouds in the 13 SKYLAB-2 wavelength bands.

The most relevant aspect of Figure 3 is that it clearly shows that snowcover and clouds can be spectrally separated in only the two middle infrared bands (1.55-1.75 μ m and 2.10-2.35 μ m).

The data in Figure 3 shows a definite trend in the separability values as a function of wavelength. The separability between clouds and snow starts to increase in band 8 (0.98-1.03 μ m) or near IR region, and continues to increase with increasing wavelength throughout the reflective portion of the spectrum. However, in the thermal infrared band (10.2-12.5 μ m) the separability measure between the snowcover and the clouds drops sharply to a very low value. The thermal data indicates that the temperatures of the clouds and the snow are very similar. Therefore, at least for this data set, one cannot reliably discriminate snowcover from cloud formations based on their thermal response only.

The above results clearly show the advantage of obtaining multispectral scanner data in the middle infrared (1.3-3.0 μ m) portion of the spectrum for snowcover mapping applications. These results are significant in defining the appropriate wavelength bands to be included in future earth observation satellite systems.

Spectral Definition and Classification of Snowcover

An inspection of the 13 wavelength bands of SKYLAB-2 data shown in Figure 4 reveals that the areas of snowcover have a high reflectance throughout the visible wavelength bands (channels 1 through 5, from 0.41 to 0.67 μ m). On data in the near infrared wavelengths (channels 6 through 10, from 0.68 to 1.30 μ m), the areal extent of the snowpack seems to decrease in size with increase in wavelength. In the middle infrared region (channel 11, 1.55 to 1.75 μ m, and channel 12, 2.10 to 2.35 μ m), the snowcover is very low in reflectance and appears nearly black. Finally, in the thermal infrared data (channel 13, 10.2 to 12.5 μ m), the snow is relatively cold in relation to the other earth surface features, so it appears dark in tone on the imagery.

The apparent decrease in areal extent of the snowpack throughout the reflective infrared portion of the spectrum seems to be caused by two factors. First, water in liquid form has very little reflectance above 0.8 μ m, and since the snowpack was in the process of melting by June 5, particularly at the

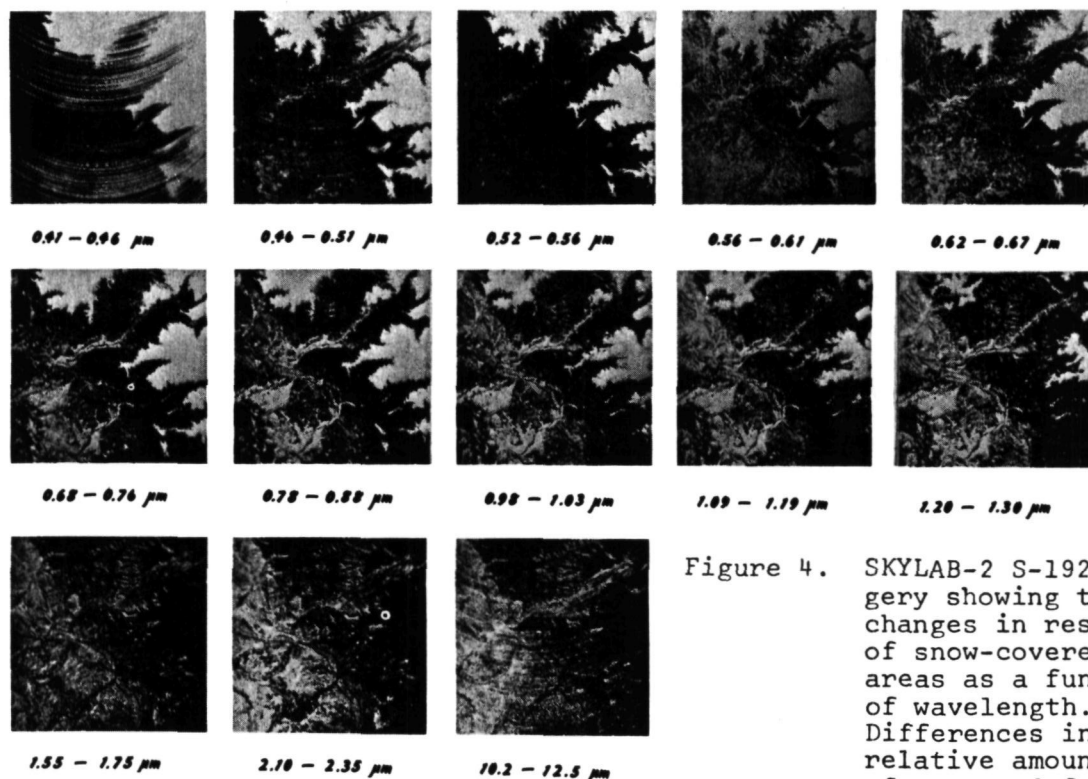


Figure 4. SKYLAB-2 S-192 imagery showing the changes in response of snow-covered areas as a function of wavelength. Differences in the relative amounts of snow and forest canopy, which are

closely associated with elevation, are a major cause for the spectral variations observed.

lower elevations, the snow crystals probably have a coating of liquid water which would cause a lower reflectance. The second and perhaps more important factor in this case is that the forest cover is denser at lower elevations, resulting in a higher proportion of forest canopy than snowcover at the lower elevations. Examination of the aerial photos (taken the day after the SKYLAB data were obtained) showed that only the tundra areas at the highest elevations had a pure snow cover, without any trees present to cause a decreased reflectance.

The computer-assisted analysis of the SKYLAB-2 S-192 MSS data for mapping snowcover involved several processing steps. The first consisted of the definition of the maximum number of spectrally separable classes or categories of snowcover present in the scene. A multispectral clustering or "non-supervised" approach was utilized for this phase of the analysis. In this case, five distinct spectral classes of snowcover could be defined. Subsequently, their statistics (means and covariance matrices) were used as training input for the computer classification of the entire data set, utilizing a "supervised" approach involving a maximum likelihood algorithm.

Figure 5 shows the snowcover map resulting from the computer classification of the SKYLAB MSS data. The five different spectral classes of snowcover are shown as different tones of white and gray. The white areas represent "snow-1" spectral class, the four gray tones represent the other four snowcover classes, and the black indicates areas having no snow cover.

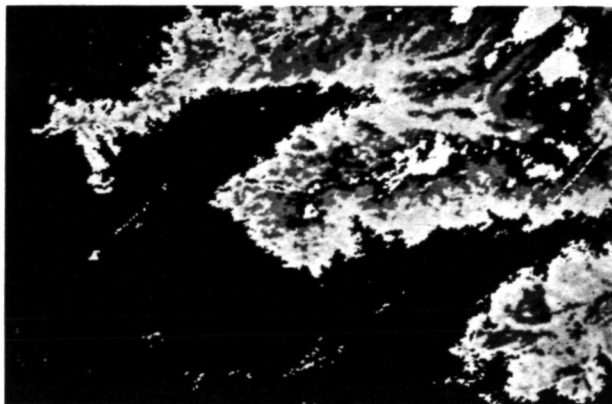


Figure 5. Multispectral classification of snowcover by computer, utilizing the SKYLAB-2 S-192 MSS data.

The five spectral classes of snowcover shown in Figure 5 are related to differences in reflectance in the individual wavelength bands in the near infrared portion of the spectrum, particularly in the 1.09-1.19 μ m and 1.20-1.30 μ m band, as indicated in Table 2.

Table 2. Mean Spectral Response of Five Snowcover Classes and a Forest Class

Band (μ m)	Spectral Classes					Forest
	Snow 1	Snow 2	Snow 3	Snow 4	Snow 5	
(0.41-0.46)	255*	255*	255*	255*	255*	205
(0.46-0.51)	255*	255*	255*	197	162	110
(0.51-0.56)	254*	252*	219	120	93	56
(0.56-0.61)	255*	255*	255*	253	251	131
(0.62-0.67)	255*	255*	255*	255*	237	72
(0.68-0.76)	255*	255*	255*	240	166	89
(0.78-0.88)	255*	255*	255*	193	148	113
(0.98-1.08)	255*	255*	194	138	108	102
(1.09-1.19)	251	196	137	104	89	92
(1.20-1.30)	185	148	98	76	68	83
(1.55-1.75)	64	61	56	54	59	72
(2.10-2.35)	19	17	14	11	13	21
(10.2-12.5)	99	100	101	105	110	124

* - Denotes detector saturation

For wavelengths from 0.41-1.08, the statistics indicated that there had been detector saturation due to the high reflectance from areas in the Snow 1 and Snow 2 classes, as well as in other spectral classes in some wavelength bands. However, in the 1.09-1.19 μ m and 1.20-1.30 μ m wavelength bands, there is a very distinct decrease in reflectance from the Snow 1 to the Snow 5 spectral class.

Comparison of the snowcover classification results with the aircraft (NC-130 and WB-57) photography taken one day after the SKYLAB-2 overpass indicated that the five different spectral classes of snowcover were closely related to the different proportions of snow and forest cover present in the individual resolution elements (pixels) of the SKYLAB-2 S-192 MSS data. The S-192 scanner integrates the reflectance from the entire area on the ground within each resolution element (approximately 0.47 hectares). Therefore, a relatively high proportion of coniferous forest cover and a relatively low proportion of snow within a single resolution element will result in a relatively low reflectance as

compared to resolution elements containing fewer trees and a larger proportion of snow.

Figure 6A shows an area of the S-192 classification map containing the five different spectral classes of snowcover. Figure 6B shows a photographic print of the same area (shown in Figure 6A) taken by NASA's WB-57 aircraft from an altitude of 18,288 meters (60,000 feet). Comparison of these two images clearly indicates that the different spectral classes of snowcover shown in Figure 6A correspond to the different proportions of snow and forest shown in Figure 6B.

The spatial distribution of the five spectral classes of snowcover shown in Figures 5 and 6A is highly correlated to the topography of the area. The "snow 1" spectral class is found at higher elevations in the areas of alpine tundra. The other four spectral classes are found at lower elevation ranges. Thus, the statistics for these spectral classes, as given in Table 2, indicate that the decreasing response values among the spectral classes (particularly well shown by the 1.09-1.19 μ m or the 1.20-1.30 μ m data) generally correspond to both decreasing elevation and increasing density of coniferous forest cover.

DIGITAL TOPOGRAPHIC DATA

To establish a more quantitative correspondence between the spectral classes of snowcover and the topography of the area, digital topographic data were overlaid onto the multispectral scanner data.

Digital tapes containing elevation data had been developed by the Defense Mapping Agency, using 1:250,000 scale U.S.G.S. topographic maps. These DMA elevation data tapes were obtained for the entire San Juan Mountains area and rescaled to match the scale of the SKYLAB and LANDSAT data tapes. From the elevation data, an interpolation procedure was developed to obtain data on slope and aspect for each resolution element. Although the interpolation procedure introduced some error into the data and there are some inherent errors in the small scale maps utilized initially in the digitization process, these errors are not significant for the type of broadscale mapping and analysis involved in this study.

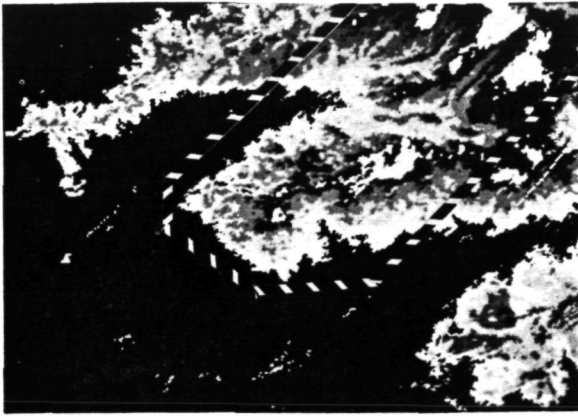


Figure 6a. Portion of the SL-2 S-192 multi-spectral classification of snow cover.

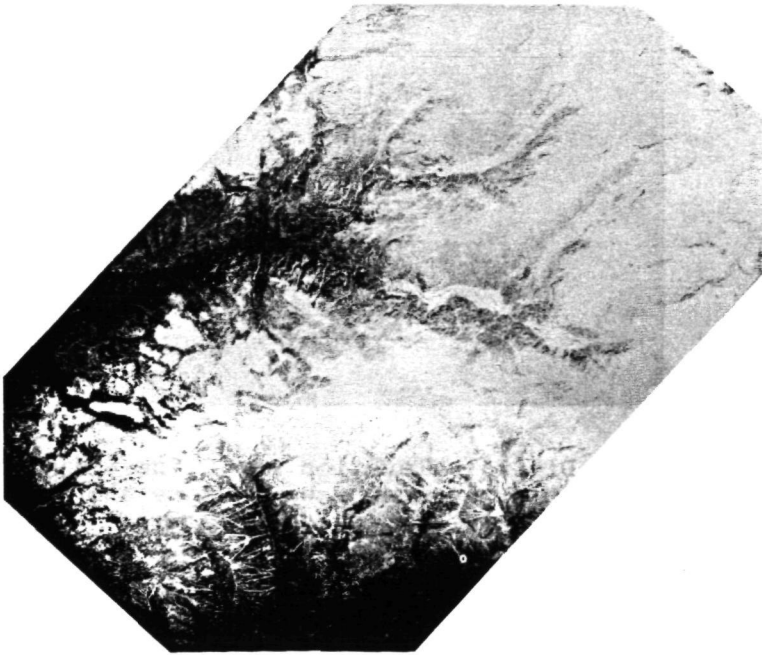


Figure 6b. WB-57 aerial photo of same area shown in Figure 6a.

REPRODUCIBILITY OF THE
ORIGINAL PAGE IS POOR

The final result of this data processing procedure (rescaling and overlay), therefore, was a single digital data tape containing 13 channels of SKYLAB MSS data, four channels of LANDSAT MSS data, and three channels of topographic data (one channel each for elevation, slope, and aspect), all geometrically correct and capable of being displayed at a 1:24,000 scale when displayed on a computer line printer. This data tape was subsequently utilized in all of the analysis sequences for the SKYLAB multispectral scanner data.

Figure 7 shows a topographic digital map of the San Juan test site, in which the different elevations are shown as different gray tones. The white tone (in Figure 7) represents elevations above 3600 meters, the darkest tone represents areas below 2000 meters, and the intermediate gray tones indicate elevation increments of 200 meters each.

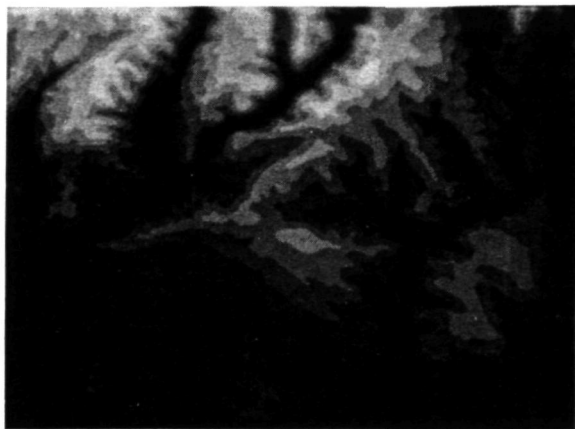


Figure 7. Digital elevation map. The white tone represents elevations above 3600 meters, the darkest tone represents areas below 2000 meters, and the intermediate gray tones indicate elevation increments of 200 meters each.

To further indicate the value of the topographic overlay data, the elevation data were combined with the results of the snowcover classification. The area of each of the five classes of snowcover was determined as a function of elevation using 100 meter elevation increments. This type of calculation can

be accomplished rapidly and effectively when an overlay of multiple data sets, such as this one, are available. These results are shown in Table 3.

Table 3. Snowpack Area (in hectares) within 100 Meter Elevation Increments

Elevation (meters)	Spectral Class of Snowcover					Total Area (hectares)
	<u>1</u>	<u>2</u>	<u>3</u>	<u>4</u>	<u>5</u>	
Above 3700	1179	2464	308	108	7	4086
3600-3700	400	1914	694	135	37	3180
3500-3600	129	1868	1858	517	61	4433
3400-3500	45	904	1858	1266	280	4353
3300-3400	13	378	1305	1417	812	3925
3200-3300	7	94	922	1258	1298	3579
3100-3200	6	22	529	793	1540	2890
3000-3100		9	213	433	1041	1893
2900-3000		1	38	188	535	752
2800-2900			4	54	289	347
2700-2800			1	13	147	181
2600-2700				1	95	96
Below 2600					79	79
<hr/>						
Totals	1779	7651	7730	6183	6221	29564

These results of applying computer-aided analysis techniques to a combined set of multispectral and topographic digital data (Table 3) reveal the tremendous potential that these techniques offer to the snow-hydrologist. The utility of being able to rapidly and accurately determine the areal extent of snowcover at different elevations becomes clear when this type of information is used in conjunction with other results such as those obtained by Caine (1975) on the relationship between the peak snow accumulation (water equivalent) and elevation in the San Juan Mountains. Caine's work demonstrated that the normals of peak accumulation in the San Juan Mountains increase with elevation in a predictable fashion. His results suggest a snow accumulation gradient of 65.5 cm of water equivalent per 1000 meter elevation increment, with a no-accumulation level at 2400 meters. Thus, the combination of accurate estimates of the areal extent of snowcover at different elevations and the predictable information on the water equivalent at the various elevations should permit a more accurate estimation of the amount of runoff to be expected during the snow melt season.

SUMMARY OF RESULTS

Computer-aided analysis of the SKYLAB-2 S-192 MSS data showed that:

(1) A reliable spectral separability between snowcover and clouds can be attained only in the middle infrared portion of the spectrum (1.55-1.75 μ m and 2.10-2.35 μ m bands).

(2) Five spectrally separable classes of snowcover were defined and mapped. These spectral classes of snowcover were primarily related to different proportions of snow and forest cover contained in the individual resolution elements of the SKYLAB-2 S-192 MSS data.

(3) For the first time, SKYLAB S-192 data were geometrically corrected and digitally overlaid onto a topographic data base from which elevation, slope and aspect data, as well as the spectral data, could be displayed at a 1:24,000 scale.

(4) The results of the spectral classification of snowcover were combined with the topographic data to obtain a table giving the area of each of the spectral classes of snowcover as a function of elevation, using 100 meter increments.

REFERENCES CITED

- Caine, N., (1975), "An Elevational Control of Peak Snowpack Variability", Water Resources Bulletin, Vol. 11, No. 3, June 1975, pp:613-621.
- Conover, J.H., (1964), "The Identification and Significance of Orographically Induced Clouds Observed by TIROS Satellites", Journal of Applied Meteorology, Vol. 3, pp:226-234.
- Finnegan, W.J., (1962), "Snow Surveying with Aerial Photography", Photogrammetric Engineering, Vol. 28, No. 5, November 1962, pp:782-790.
- Hoffer, R.M. and staff, (1975), "An Interdisciplinary Analysis of Colorado Rocky Mountain Environments Using ADP Techniques", Type III-Final Report, NAS5-21880. (in press).

- Leaf, C.F., (1969), "Aerial Photographs for Operational Streamflow Forecasting in the Colorado Rockies", Proceedings of the 37th Western Snow Conference, pp:19-28.
- Leaf, C.F., and A. D. Haeffner, (1971), "A Model for Updating Streamflow Forecasts Based on Areal Snow Cover and Precipitation Index", Proceedings of the 39th Western Snow Conference, pp:9-16.
- Parsons, W.J., and G.H. Castle, (1959), "Aerial Reconnaissance of Mountain Snow Fields for Maintaining Up-to-Date Forecasts of Snowmelt Runoff During the Melt Period", Proceedings of the 27th Western Snow Conference, pp:49-56.
- Swain, P.H., T.V. Robertson, and A.G. Wacker, (1971), "Comparison of the Divergence and B-Distance in Feature Selection", LARS Information Note 020871, LARS/Purdue University, W. Lafayette, Indiana, 12 pp.
- Swain, P.H. and staff, (1972), "Data Processing I: Advancements in Machine Analysis of Multispectral Data", LARS Information Note 012472, LARS/Purdue University, W. Lafayette, Indiana, 8 pp.
- Swain, P.H., and A.C. King, (1973), "Two Effective Feature Selection Criteria for Multispectral Remote Sensing", LARS Information Note 042673, LARS/Purdue University, W. Lafayette, Indiana, 27 pp.
- Wiesnet, D.R., (1974), "The Role of Satellites in Snow and Ice Measurements", Advanced Concepts and Techniques in the Study of Snow and Ice Resources, National Academy of Sciences, Washington, D.C., 1974, pp:447-456.

**A PROGRESS REPORT ON ESTIMATING SNOW DEPTH USING VHRR
DATA FROM NOAA ENVIRONMENTAL SATELLITES**D. F. McGinnis, Jr., *National Environmental Satellite Service, NOAA, Washington, D. C.***ABSTRACT**

The NOAA environmental satellites provide daily coverage of the Earth in the visible (0.6-0.7 μ m) and thermal (10.5-12.5 μ m) spectral bands. The ground resolution of the Very High Resolution Radiometer (VHRR) is 1 km at nadir. This improved resolution in the visible permits more detailed observations of snow features than was possible with previous operational satellites. A densitometer examination of a visible-band image from Feb. 11, 1973, which shows heavy snow cover in considerable detail over areas extending from Alabama to North Carolina, indicates that, in general, there is direct correlation between increasing brightness and increasing snow depths. A power regression analysis of greatest satellite brightness versus greatest snow depth for 201 data pairs produced a correlation coefficient of 0.86. Similar analysis of five late winter and early spring cases resulted in much lower correlations.

INTRODUCTION

The brightness of snow received as reflected radiation by visible-band sensors aboard meteorological satellites has been mentioned as a possible indicator of snow depth (Barnes and Bowley 1968, McClain 1973). Because of the much improved resolution of the Very High Resolution Radiometer (VHRR) data from the NOAA-2 environmental satellite, compared with the data available to previous investigators, a decision was made to test this hypothesis. The first opportunity for such a study occurred on Feb. 11, 1973, immediately following a heavy snow storm that struck the southeastern part of the United States.

SOUTHEAST SNOW STORM OF FEBRUARY 9-10, 1973

The winter of 1973 will be remembered well in the southeastern United States for the storm of February 9 and 10. This storm, the result of the interaction of two sharply contrasting air masses, produced record snow depths. An outbreak of very cold Arctic air entered the Northern Plains on Monday, Feb. 5, 1973. This large air mass plunged rapidly southward into Texas but made only slow progress eastward. By 1800 GMT (1300 LT) on Thursday,

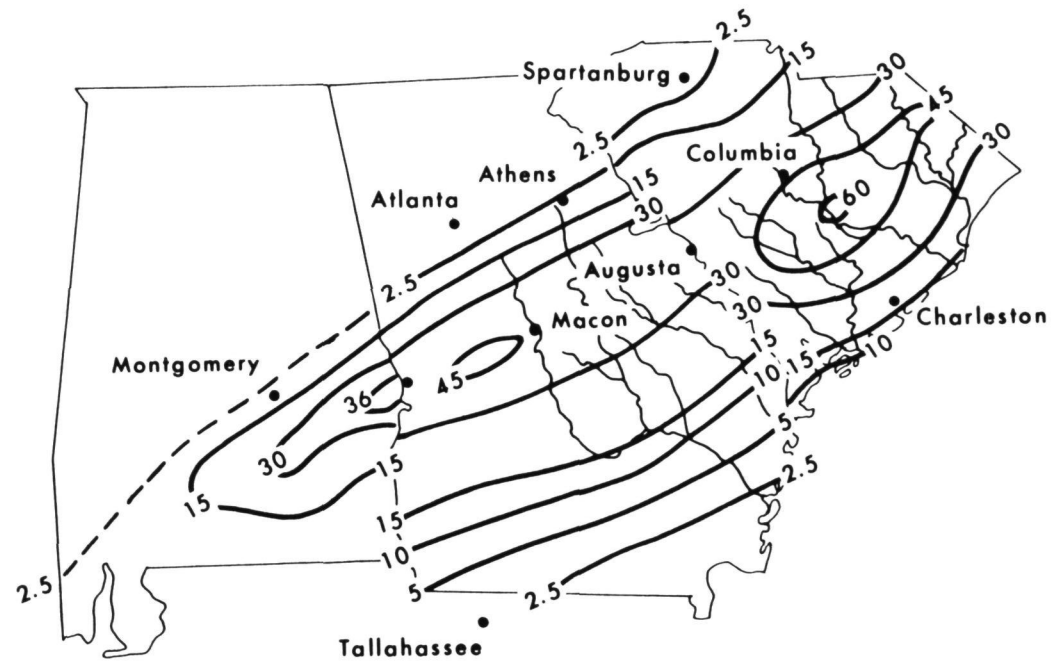
February 9, the leading edge of the cold air mass lay along the eastern slope of the Appalachian Mountains. Rain began falling in a broad band 350 km wide in the area of frontal convergence. Temperatures remained mild along the Atlantic seaboard until a developing cyclone drew in the very cold air just west of the Appalachians. The precipitation in Alabama and Georgia subsequently changed to freezing rain and sleet and then to snow during the morning and early afternoon of Friday, February 9. This snow spread into North Carolina and South Carolina as the deepening cyclonic disturbance moved northeastward into the Atlantic Ocean. Snow continued falling during most of Saturday in Georgia and the Carolinas, ending along most Carolina coastal sections after midnight. On Sunday morning, record snow depths were found on the ground at many locations in Alabama, Georgia, and the Carolinas. Figure 1 shows the total snowfall in Alabama, Georgia, and South Carolina as analyzed by the individual State climatologists from scattered point observations taken largely by untrained cooperative observers. Data and isopleths, originally in inches, were obtained from individual State climatological summaries for February 1973 (Environmental Data Service 1973). Despite inconsistent values from State to State, particularly along the Georgia-South Carolina border (where the 2.5 cm isopleth in northeastern Georgia matches the 15-cm isopleth in northwestern South Carolina) values in excess of 30 cm were reported throughout an extensive band from east-central Alabama through northeastern South Carolina. The dashed line represents the author's interpretation of the 2.5-cm isopleth in Alabama. Storm totals, because of the warm ground and settling of the snow, were somewhat greater than observations taken Sunday morning at 1200 GMT after the storm's ending. Rapid clearing followed the storm; and at approximately 1545 GMT (1045 LT) on orbit 1489, Feb. 11, 1973, the NOAA-2 satellite viewed the cloud-free but snow-covered landscape (fig. 2).

NOAA ENVIRONMENTAL SATELLITES

The NOAA Environmental satellites scan Earth in about 25 orbits every 2 days at an altitude of approximately 1500 km in a sun synchronous near-polar orbit.¹ Essentially the same area of Earth is viewed every other day, although the orbit of the satellite progresses eastward about 1° of longitude every 25 orbits. Aboard the spacecraft are various sensors (Schwalb 1972), each with its own identical backup system.

Most important of the sensors for hydrological use is the VHRR. This instrument scans Earth in both the visible (0.6-0.7 μ m) and the thermal (10.5-12.5 μ m) regions of the spectrum. The VHRR system generates analog signals that, after transmission to the readout station, are transformed into a photographic format. VHRR

¹NOAA 4, launched on Nov. 15, 1974, has been the operational satellite since Dec. 17, 1974.



— 30 — Isopleth of snow depth in centimeters

Figure 1. Total snowfall, snow storm of Feb. 9-10, 1973.

data are also available on digital tapes. With a resolution of approximately 1 km at nadir, the VHRR imagery is 4 times better in the visible and 10 times better in the thermal regions than data taken by instruments aboard NOAA 1 and earlier satellites.

One of the drawbacks of VHRR images is that panoramic distortion increases with increasing distance from the center line of the image. The image is built up through a combination of the satellite's forward motion in orbit and its VHRR scanning perpendicular to this motion. This distortion is caused, in part, by the curvature of Earth's surface and produces foreshortening of the image toward the horizon.

IMAGERY ANALYSIS

Figure 2 shows the snow-covered area as seen in the visible range by the VHRR. State boundaries have been added to point out the distortion in the image and to provide reference points for location. These boundaries were added to figure 2 by using a Zoom Transfer Scope (ZTS), an optical device used to transfer information from unrectified satellite images to base maps, and vice versa. The distortion is greatest in the eastern portion of the image. A distinct western limit of the snow is evident, as well as a highly reflective (bright) strip in the center of the snow area, corresponding generally to the deepest snows shown in figure 1. Some land features in the snow belt, such as the swampy or heavily forested areas adjacent to many rivers, contrast sharply with adjacent areas in the snow-whitened land. The more heavily forested Piedmont Plateau in the western section of the snow area is mottled in appearance and is less bright than elsewhere. The 1-km resolution of the VHRR permits easy identification of many small rivers and also enables the analyst to determine the location of the western snow edge to within 8 km when drainage features are used as local reference points.

Analysis of the recorded brightnesses takes into account the system's limitations. Each pixel (picture element) of the VHRR image covers an area of approximately 1 km² (at nadir) on the ground. The brightness value of each pixel thus represents an average response that may include dark, forested regions as well as highly reflective open fields, even when both are snow covered. Also, the VHRR visible-band sensor is not a perfect detector. Figure 3 shows that the relative response of the detector falls short of perfect (1.0) throughout the design range of 0.6 to 0.7 μ m and also senses some energy outside these limits.

The enhancement of land features by the differing reflectance of snow cover has been described. While this factor is useful for identifying and locating specific landmarks, it tends to mask the relation of snow brightness to snow depth. The aging of a snow pack is manifested in a reduction of the surface brightness--another factor to consider when attempting to relate snow brightness to snow depth. In the study of this relationship, the image was enhanced using a color densitometer. Various color schemes were tried, but none could discriminate more than three

REPRODUCIBILITY OF THE
ORIGINAL PAGE IS POOR

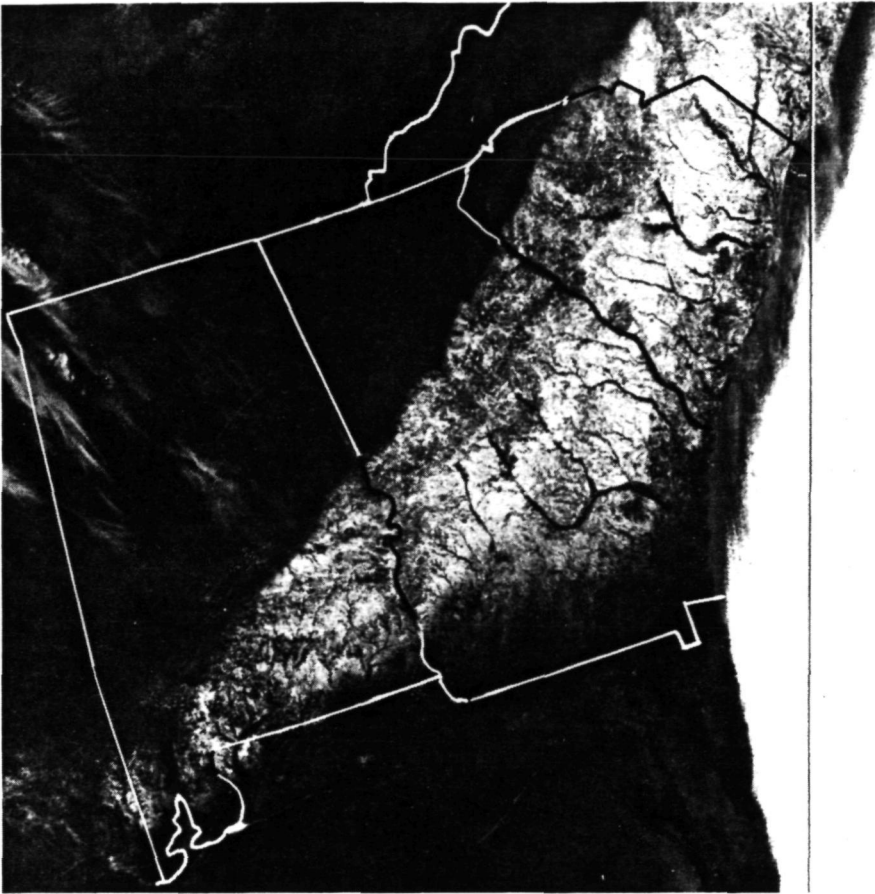


Figure 2. Portion of the NOAA-2 VHR visible (0.6-0.7μm) image taken at 1545 GMT on Sunday, Feb. 11, 1973.

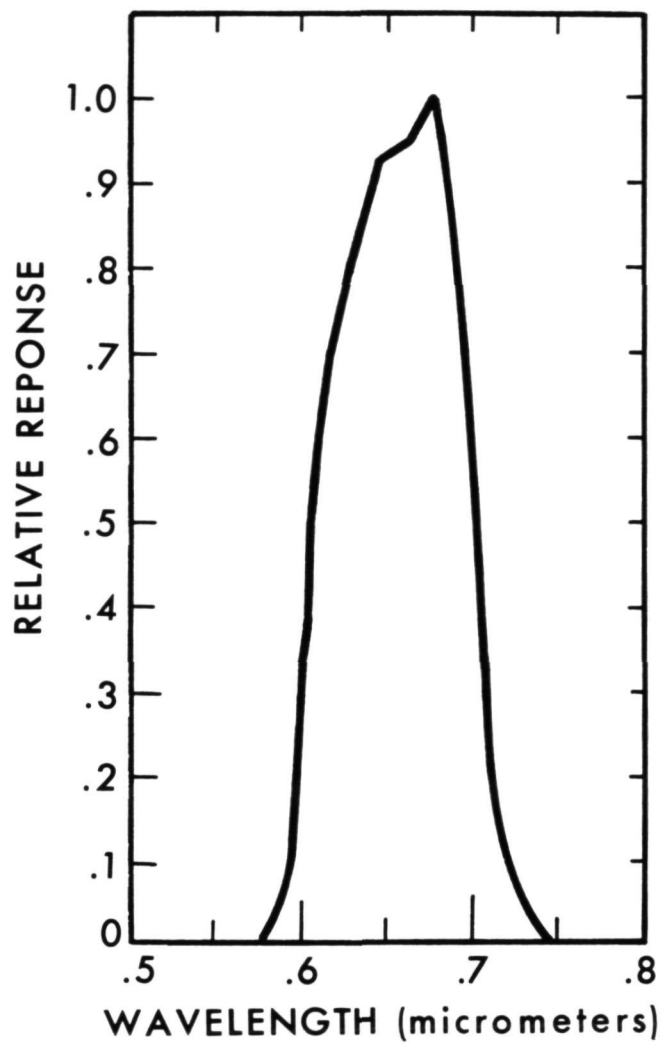


Figure 3. NOAA-2 VHRR visible relative spectral response curve (prelaunch).

ranges of depth, 0 — 8 cm, 8-30 cm, and >30 cm, which are entirely qualitative and show little improvement over earlier estimates by Barnes and Bowley (1968) using lower resolution satellite imagery. They distinguished three levels of brightness in snow-covered areas of the Great Plains: trace-2.5 cm, 2.5-10 cm, and >10 cm.

In figure 4, a north-south densitometric trace through the snow area is shown on the left; the white strip through the image is the cross section that the trace represents. The densitometer trace is a quantitative measure of changes in photographic gray scales; it was produced from a black and white photograph using a color densitometer. Brightness values are represented along the horizontal axis, with increasing values to the left. Outside the snow area, brightness values are uniformly low. Within the snow-covered area, values are higher but show several fluctuations, which are a function of varying land use. The abrupt termination of the snow along the northwest boundary of the snow area is associated with a rapid decrease in brightness. The southern boundary of the snow area is more diffuse; thus, the decrease in brightness is gradual.

DIGITAL TAPE ANALYSIS

Digital computer printouts analogous to the pictorial display were produced from the VHRR analog tapes. The analog tapes were converted into nine-track digital tapes containing every scan line generated by the VHRR. Each scan line consists of individual, partially overlapping samples, two of which cover a 1-km² field of view. These elemental pieces of information can be averaged or combined in various schemes to meet the needs of the investigator.

A computer program was adapted to accept VHRR digital data and produce, at 1-km or 4-km resolution, histograms of brightness values at preset class intervals and provide the smallest and greatest brightness values for each 32 x 32 element area. The program also contours each area using the preset class intervals, thus providing an isopleth map. The 1,024 brightness values and annotations for location are included in the program.

Using the 1-km resolution option (32 x 32 km squares), a grid of 201 VHRR squares was fitted to figure 1. Owing to the scarcity of detailed snow-depth measurements on the morning of Feb. 11, 1973, comparison of the snow brightness with ground truth necessitated substitution of snowfall totals [as provided in Environmental Data Service (1973)] for snow depth values. The greatest snow depth for each square (from fig. 1) was matched with the greatest brightness value. Various mathematical best fits were calculated for the data pairs with brightness as the dependent variable. Figure 5 shows the 201 data points and the best fitting power curve. The correlation coefficient was 0.86.

The power curve fit of the data appears more consistent with the apparent relationship of brightness to snow depth. Rather small increases in depth when the snow is only several centimeters

REPRODUCIBILITY OF THE
ORIGINAL PAGE IS POOR.

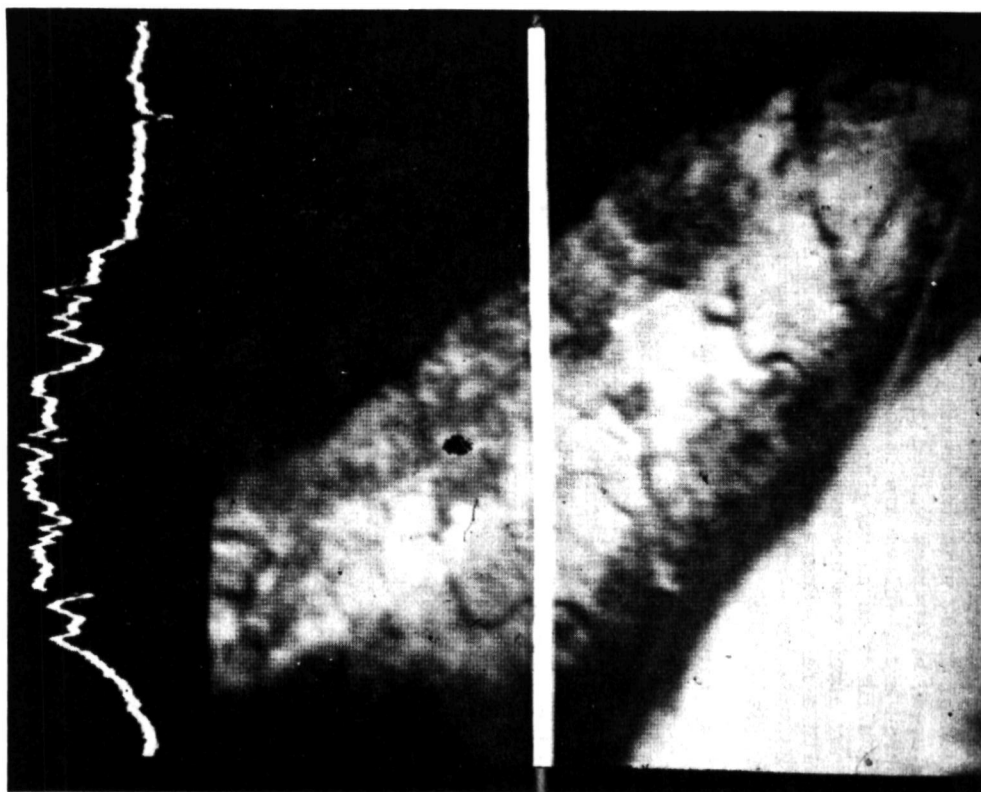


Figure 4. Densitometric trace through portion of snow-covered area in South Carolina and Georgia.

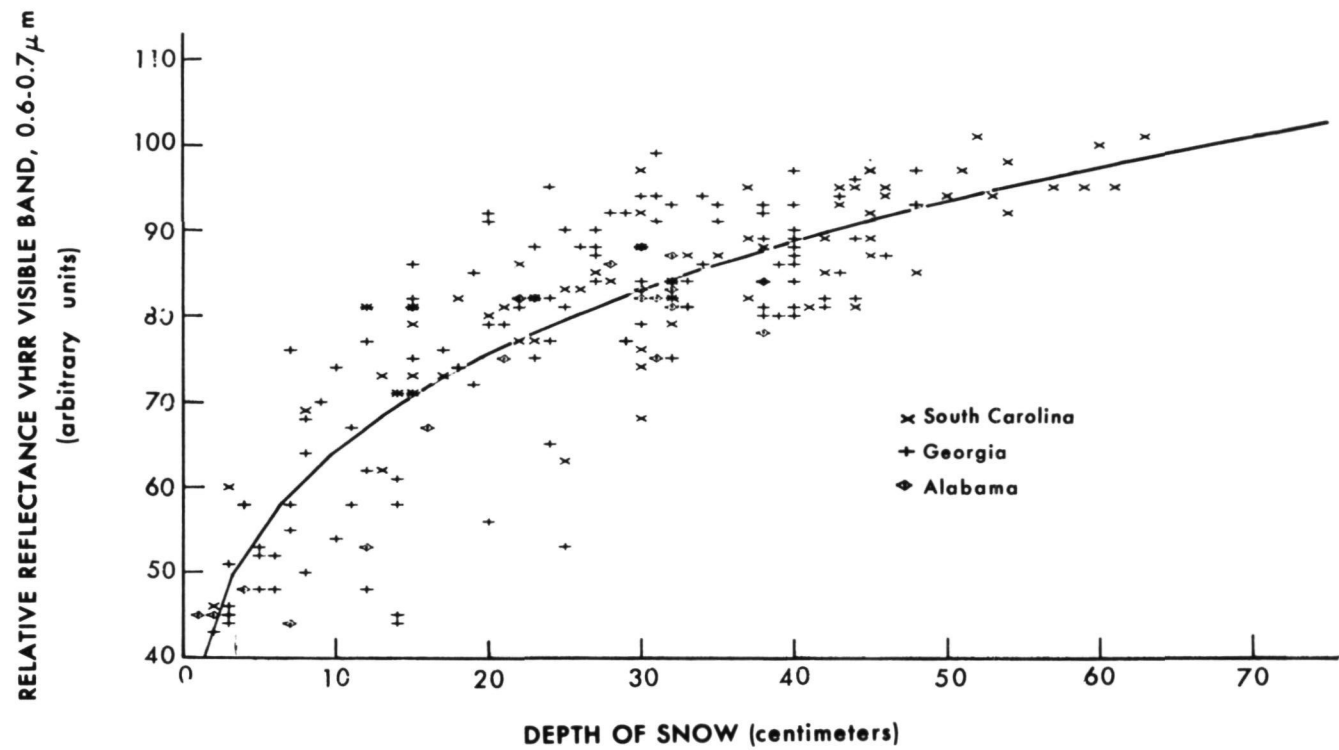


Figure 5. Relation of relative VHRR visible reflectance to depth of snow.

deep produce large increases in brightness. In this case, the snow covers more and more objects on the ground as it deepens, first individual blades of dormant grass, then small shrubs, then larger objects. Once the snow accumulates to about 25 cm, most small plants are covered, only the larger shrubs and plants (corn stalks to trees) remain visible and in most cases will remain uncovered except in some mountainous areas where extremely heavy snows occur.

Some radiation penetrating into a snow pack, if not absorbed by underlying vegetation and soil, eventually returns to the surface and contributes to the albedo. Giddings and LaChapelle (1961) demonstrated that absorption from an underlying black surface greatly reduced the albedo of aged snow until snow depths exceeded 20 cm. Thus small increases in satellite-observed brightness may be observed even when tops of vegetation are being covered with 10 to 20 cm of snow.

Regarding data discontinuities in the snow isopleths at State boundaries, the following procedure was used. When a 32-km square fell across a State boundary, the greatest depth was determined using data from the State having the greater portion of the square. Also, some error in snow-depth estimates could occur because of the misalignment or distortion of the squares fitted to figure 1. Further, most of the snow-covered area in Alabama received some sunshine late in the day on Saturday, February 10 1973, which probably melted a small amount of snow. The amount of snow remaining at the time of the satellite observation on Sunday morning, therefore, is believed to be slightly less than that indicated in figure 1. The scarcity of ground observations precluded a re-evaluation of snow depths. The effect of the Sun on the reflectivity of the snow and, thus, on the brightness recorded by the satellite also is not considered. Both of these effects caused by the Sun, however, trend in the same direction (i.e., toward decreasing values).

The curves derived from the data are for the NOAA-2 VHRR visible-sensor 1. Equivalent curves may be different for either NOAA-3 or NOAA-4 visible sensors or the other NOAA-2 VHRR visible sensor. The general relationship likely would remain, but with perhaps differing brightness limits. For this case, the lower limit of brightness (bare ground) is between 40 and 43; the upper limit of snow brightness is 101.

Five additional examples of snow cover were analyzed comparing the greatest satellite brightness with snow depth. The data examined were collected on 3/18/74, 3/24/74, 3/26/74, 4/10/74 and 4/11/74, and the locations ranged from the Midwest area eastward through New York. Correlation coefficients for various mathematical best fits ranged from 0.01 to 0.79, but principally fell between 0.40 and 0.60, with the power curve fit providing the higher correlation more frequently than the other mathematical fits as well as the highest correlation coefficient (0.79). These coefficients were much lower than those observed in the Southeast case. Temperatures remained below freezing following the first two snowfalls until after passage of the satellite on 3/18/74 and

3/24/74, while melting was occurring during the satellite overpasses, 3/26/74, 4/10/74, 4/11/74, on the later snowfalls. Since the correlation coefficients varied little for all cases analyzed, the effect of melting snow surfaces on the snow depth-snow brightness relation is not apparent.

Most critical to the analyses was the lack of snow depth measurements. The sole source of snow depths was the individual State Climatological Data summaries (NOAA 1974). The scarcity of ground observations became apparent when preparing isopleth maps of snow depths. In New York's mountainous regions much interpolation was required to produce a contoured map for comparison with satellite brightness. Snow, present in the higher elevations (as seen in satellite images), would be less or non-existent in the valleys where most observations are made. Only small variations in snow depth were noted in the Midwest. Unlike the Southeast case, no sharp gradient in snow depth existed, the satellite data being clustered at a few observed depths, for example, 2.5 cm, 5.0 cm, and 7.5 cm.

RESULTS

The improved resolution of the VHRR over previous sensors on operational satellites permits mapping of snow limits to better than a 10-km resolution, which is an improvement over the 20- to 40-km resolution reported with earlier satellites (McClain 1973). Although the radiance data received from the satellite are unrectified, the enhancement of identifiable land features by the snow permits the precise location of snow boundaries of mesoscale resolution. Color renditions of the black and white imagery by means of a color densitometer, although subjective, do permit coarse estimates of snow depths, but the improvement over estimates made from earlier, lower resolution satellite sensors is minor.

For the Southeast case a significant correlation of 0.86 was achieved when the greatest brightness value in a given 32 x 32 km square was paired with the greatest snow depth for the same square. Using the greatest brightness within a particular region is, in effect, searching for the clearings and open areas that are free of trees and other nonsnow-covered objects that lower the average brightness of the 1-km element. The same procedure, however, used on five later cases produced substantially lower correlation coefficients (0.40 to 0.60).

CONCLUSIONS

The VHRR provides a synoptic picture of snow extent not possible from point observations on the ground. The 1-km resolution of the VHRR sensors permits positioning of snow limits to within 10 km, some two to four times better than that possible with data from earlier operational satellites.

For one case, freshly fallen deep snow over an area of widely varied land use in the Southeast, snow-depth estimates

correlate well with snow brightness. The power curve relationship indicates that a rapid increase in brightness corresponds to increases in snow depths when depths are less than 25 cm; for depths exceeding 25 cm, much smaller brightness increases are encountered as depths increase.

The usefulness of satellite brightness data to estimate snow depths is apparently limited by insufficient ground observations of snow depths and limited to areas where strong gradients in snow depths occur over relatively short distances (50 km). Eighteen new cases for 1975 are presently being analyzed and it is hoped that this large sampling will enable one to define under what conditions, e.g., particular type of snow and terrain as well as necessary density of ground observations, satellite brightness can be a reliable indicator of snow depths.

ACKNOWLEDGMENTS

The author wishes to express appreciation to E. Paul McClain for initiating discussion with respect to the investigation of maximum brightness versus snow depth. Darrell Macklin and Michael McMillan are gratefully acknowledged for computations to determine correlation coefficients, as is David Forsyth for providing computer analyses.

REFERENCES

- Barnes, J.C., and Bowley, C.J., 1968, Operational Guide for Mapping Snow Cover from Satellite Photography, Allied Research Associates, Inc., Concord, Mass., 116 pp.
- Environmental Data Service, 1973, Climatological Data Alabama, Climatological Data Georgia, and Climatological Data South Carolina, Vol. 79, No. 2, National Climatic Center, National Oceanic and Atmospheric Administration, U.S. Department of Commerce, Asheville, N.C.
- Giddings, J.C., and LaChapelle, E., 1961, "Diffusion Theory Applied to Radiant Energy Distribution and Albedo of Snow," Journal of Geophysical Research, Vol. 66, No. 1, pp. 181-189.
- McClain, E. Paul, 1973, "Snow Survey from Earth Satellites--a Technical Review of Methods," WMO/IHD Report 19, WMO No. 353, World Meteorological Organization/International Hydrological Decade, Geneva, Switzerland, 42 pp.
- NOAA, 1974, Climatological Data, selected states, Nat. Oceanic and Atmospheric Administration, Vol. 79, Nos. 3 and 4, Nat. Climatic Center, Asheville, N.C.
- Schwalb, A., 1972, "Modified Version of the Improved TIROS Operational Satellite (ITOS D-G)," NOAA Technical Memorandum NESS 35, NOAA, U.S. Department of Commerce, Washington, D.C., 48 pp.

A COMPARISON OF OPERATIONAL AND LANDSAT-AIDED SNOW
WATER CONTENT ESTIMATION SYSTEMS

James M. Sharp, *Social Sciences Group*; Randall W. Thomas, *Remote Sensing Research
Program, University of California, Berkeley*

ABSTRACT

This study describes how LANDSAT imagery can be cost-effectively employed to augment an operational hydrologic model. Attention is directed toward the estimation of snow water content, a major predictor variable in the volumetric runoff forecasting model presently used by the California Department of Water Resources. A stratified double sampling scheme is supplemented with qualitative and quantitative analyses of existing operations to develop a comparison between the existing and satellite-aided approaches to snow water content estimation. Results show a decided advantage for the LANDSAT-aided approach.

1.0 INTRODUCTION

Problems in managing natural resources often reduce to problems in allocating scarce time and money resources. Technological innovations like LANDSAT, by dramatically reducing the costs of gathering information, promise to beneficially alter existing time, cost, and capability relationships in many resource management areas.

This paper describes and applies a methodology for comparing different information-gathering technologies. Although the focus here is on a particular resource (water) in a particular context (snow mapping and runoff prediction) over a particular region (the Feather River Watershed of Northern California), the approach can be generalized to cover other natural resource data acquisition situations.

The overriding objective for the work described here is "to determine if remote sensing can be cost-effectively integrated with data presently used in the California Cooperative Snow Surveys (volumetric) model to produce potentially more precise and accurate estimates of water supply" (Thomas et al., 1974).

Attention in this study is directed toward the estimation of snow water content, a major predictor variable and intermediate

* This study funded by NASA Grant NGL 05-003-404.

output of this California Cooperative Snow Surveys (CCSS) volumetric yield prediction model. Normally, snow water content estimates are developed directly from ground-based snow course measurements. Instead, this study introduces a stratified double sampling approach that relates the ground-based estimates to snow areal extent data gathered from LANDSAT-1 imagery. The resulting relationships enable low-cost remotely-sensed data to account for a large portion of basin snow water content variability.

The study's major elements are summarized below in three sections. An initial section briefly describes cost-effectiveness analysis and how it can be used. A following three-part section describes general underlying assumptions and compares the two systems in terms of their sampling designs and costs. Finally, comparative results and conclusions follow.

2.0 COST-EFFECTIVENESS ANALYSIS

Cost-effectiveness analysis is one of several techniques that attempt to apply economic rationality to public investment decision making. Benefit-cost analysis is its closest theoretical relative, although techniques used in systems analysis, operations analysis, planning, programming and budgeting systems (PPBS), and others bear strong resemblance to the cost-effectiveness approach. These techniques all share a common purpose: i.e., to make systematic and quantitative comparisons between alternative resource allocation options, using a logical sequence of steps that can be verified by others.

Traditional resource allocation processes have been a mixture of political, administrative, and professional judgement. Their purpose is typically to find a pattern of production which is most efficient, or lowest cost for a set of desired outputs. Without a price mechanism to allocate output, some other procedure is necessary.

The choice of appraisal methodology depends upon the nature of the investment and the information available. Both benefit-cost and cost-effectiveness analyses contain their own variants, advantages, and limitations. In benefit-cost analysis, every effort is made to quantify in commensurable monetary terms both the benefits and costs stemming from alternative actions. Physical outputs are projected, social values (positive and negative) are estimated for these outputs, and benefits and costs are compared over time, either on a gross annual basis or on a net benefit basis discounted to the present. A complete analysis includes not just immediate benefits and costs to the agency and its clients, but also the spillover benefits and costs to others not directly related to the action in question. The result is a ratio of benefits to costs for each

alternative action considered.

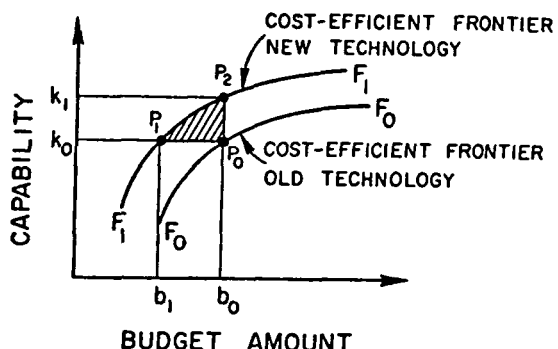
Cost-effectiveness analysis, in contrast, allows the use of multiple, non-commensurable measures on the benefit side. Economic benefits are stated in terms of cost savings. The method is specifically directed toward problems in which outputs cannot be evaluated in market prices, but where inputs can, and where the inputs are substitutable at market-developed exchange relationships. Cost-effectiveness analysis thus helps a decision-maker answer questions about how to achieve a given set of objectives at the least cost, or how to obtain the most effectiveness from a given set of resources.

Some kind of cost-effectiveness analysis is involved in any decision concerning resource allocation. In the usual case, a decision-maker relates the costs of alternative scarce resources (inputs) to specified performance standards (outputs) desired from a production process. The decision-maker may be looking for the least expensive way to meet the specifications or for a means of adjusting the specifications to fit a fixed budget. In either case, the decision-maker seeks to establish cost-capability relationships for various combinations of resource alternatives.

The system comparison type of cost-effectiveness analysis is well-suited for identifying the potential contribution of new technologies to the cost-capability relationships of existing systems. Figure 1 illustrates the effect of technological progress on the cost-capability "frontier" of an existing production system. The frontier F_0F_0 shows the maximum capability that can be expected from the present system at a given level of budget. A system producing on the frontier is defined as "cost-effective" because a decrease in cost is not possible without a decrease in capability. A technological advance would beneficially alter this relationship: the cost-efficient frontier would be pushed out to some new set of points F_1F_1 . A point P_0 on the old frontier F_0F_0 would now represent an inefficient pattern of production. A set of points in the shaded area of Figure 1 would represent an improved return, with cost-efficient points now lying on F_1F_1 between P_1 and P_2 . The effect of technological progress thus ranges between equivalent capability at a lower budget (P_1) and greater capability within the same budgetary constraints (P_2).

The foregoing model is used for assessing the effect that LANDSAT imagery would have on current snow water content estimation procedures in California. The comparative cost effectiveness framework, because it deemphasizes the quantification of benefits, is more adapted to this current stage of work than the typically more ambitious benefit-cost analysis.

FIGURE 1 - EFFECT OF A TECHNOLOGICAL ADVANCE ON A COST-CAPABILITY PRODUCTION FRONTIER



An identification and evaluation of the benefits stemming from improved hydrologic modeling will be part of the future work.

3.0 COMPARATIVE ANALYSIS

In addition to ample qualitative information, judgements about the cost-effectiveness of comparable systems usually require a resourceful use of quantitative methods. Comparative analyses, in other words, must be "custom-tailored" to the uniqueness of each case example. This section describes how we applied a cost-effectiveness analytic framework to the context of our snow survey example.

3.1 Assumptions

Real-world complications inevitably force applied cost-effectiveness analyses to deviate from their theoretical counterparts. On the cost side, the question is not one of perfection but of sufficiency. On the performance side, a balance must be struck between what we would like to measure and what can be measured with reasonable accuracy. Overriding both sides are questions concerning the comparability of different production systems.

Ideally, our own study would attempt to compare the existing DWR CCSS volumetric model with an identical model augmented with remotely-sensed snow survey information. Outputs of both models would be keyed to estimates of total water yield. Costs and accuracies would be estimated at least for the entire Feather River Basin, if not for the whole Sierra Nevada.

In reality, our study isolates those portions of the CCSS volumetric model that can be compared with LANDSAT-derived snow areal extent information developed in the University of California Remote Sensing Research Program (RSRP). An intermediate output--snow water content-- is used rather than water yield. This is nevertheless a critical step toward defining the applicability of remote sensing techniques to the possible improvement of water yield forecasts. By individually examining predictor variables such as snow water content, we may determine how precision increases that are made in predictor variable estimates can lead to precision increases in overall predictions. The analysis here thus compares the relative abilities of two systems to generate an intermediate output. Costs and accuracies for the existing model are based on published reports and interviews with DWR staff. Costs and accuracies for the LANDSAT-aided model are derived from concurrent RSRP work in the Spanish Creek Watershed, an area within the Feather River Basin.

The proposed LANDSAT-aided and the current CCSS Program snow water content estimation systems are, in fact, not identical. However, if the two systems' products are utilized similarly and are based on a concept concerning a representative quantification of the characteristics of watershed snow pack, then a common measure of relative system performance is possible. The intermediate products of both systems are designed to be utilized in water yield prediction. The error of either will affect the runoff prediction in a similar manner. Both are intended to characterize, at least in part, the general variability of the snow pack as it relates to water content.

A common statistical measure of performance is therefore implied. The often-used criterion of probability sampling, known as allowable error (AE) is appropriate here. Consequently, the CCSS snow course system must be considered as a random sample for comparison. To make this assumption and insure an equitable comparison requires that an especially favorable assumption toward the CCSS system be made. This additional assumption is that the CCSS snow courses are randomly located over the entire watershed. In fact, however, they are allocated only to the zone receiving snow that is resident on the ground for significant periods during the middle of the snow season. The result is that CCSS snow water content data will have a smaller coefficient of variation than would be expected if ground sample units were in fact allocated over the entire watershed.

3.2 Comparative Sampling Designs

3.2.1 The Current CCSS Program Snow Water Content Estimation Technique

3.2.1.1 Output

The objective of the California Cooperative Snow Survey Program's snow water content estimation technique (system) is to provide a snow water content index input to a watershed specific, multivariate regression water yield prediction model. Other predictor variables include runoff and precipitation quantities (Thomas, et al., 1974). Basin specific snow water content indices are generated monthly, February through May. January and June values may be produced as well.

The snow water content index is a statistically significant variable in prediction of monthly and April-July runoff quantities in California. This data give rise to the CCSS Program's ultimate product, the water yield forecast. Since 1929, the Department of Water Resources (DWR) has coordinated California's program of snow surveys and water supply forecasting. The stated objective of this program is to "reliably predict the State's snow-melt runoff as necessary to meet the annual operating needs of California's water using agencies." Water supply forecasts are published in DWR Bulletin 120 titled "Water Conditions in California" and issued five times a year. Four reports contain water supply forecasts based on snow conditions as of the beginning of February, March, April and May, respectively. The fifth report is distributed in December and summarizes the previous water year.

3.2.1.2 General Technique (System) Features

A watershed snow water content index is generated primarily from data gained by monthly visits to a set of snow courses distributed over the basin in question. Within a given area designated as a desirable snow course location, only certain positions presently satisfy course location criteria. These positions must be essentially open and free from extreme drift, melt, wind, and ponding (Bulletin 129, 1970). Annual measurements in the same locations provide an index to snow cover forecasting runoff.

The snow course itself consists of ten points spaced at 50 or 100 foot intervals in one or more transects. Snow depth and weight readings are taken at each point with a Mt. Rose snow sample device. The resulting average snow water content from ten points is then defined as the course snow water content value for the given sample date. Key snow courses are visited near the beginning of each month from January through May, while all snow courses are sampled on or about April 1.

Snow depth markers associated with snow courses and a growing network of experimental automatic snow sensors, provide supplemental information to the snow course networks.

3.2.1.3 Sample Size and Allocation

The current number of active snow courses in the Feather River watershed (880,000 ha), the study site in this research, is 29. However, this total number is only visited in the baseline month of April, the average date of maximum snow accumulation. Otherwise, 21 to 23 courses are visited at the beginning of each month in the February to May period. Thirteen snow courses are visited for January data.

The Feather River basin also has nine active depth marker for light aircraft observation. However, a combined total of only three aerial marker readings were made in the 1974 water year.

These snow courses are not currently allocated over a watershed (e.g., Feather River area) in a random fashion. Instead, the present CCSS Program snow course locations have evolved paralleling the development of snow hydrology sampling theory over the last fifty years (Howard 1974). For example, 30 to 40 years ago snow courses were located primarily according to site accessibility. The next twenty years saw criteria for new snow course location evolve to allow better areal and elevational snow zone sampling. Recently, locational criteria have emphasized snow zone positions with high runoff correlations. Some of these positions may not have been sampled previously.

The basic assumption of the CCSS Program's snow course allocation scheme is that the quantitative subjective allocation plan will provide data that can be correlated with water yield. As Bulletin 129 points out, snow course measurements should not be taken as an accurate measure of snow water content over a large area without careful study of both the snow course and the area of interest.

3.2.2 The LANDSAT-aided Snow Water Content Estimation System

3.2.2.1 Output

The proposed LANDSAT-aided snow water content estimation system is designed to generate an estimate of total watershed snow water content and an associated statement of precision, i.e., reliability. The estimate may then be related by regression equations directly to basin water yield for a given runoff period. Or the estimate may be used as another predictor variable in current snow survey runoff prediction equations.

3.2.2.2 General System Features

The snow water content estimation method utilized in this

study with LANDSAT information is known as a stratified double sample. Its objective is to combine snow water content information for the whole watershed, as obtained inexpensively from LANDSAT data, with that gained from a much smaller and more expensive sample of ground based snow courses. In this way, a large amount of the variability in basin snow water content is accounted for by the use of the LANDSAT data.

The desired result is that after calibration by regression of LANDSAT data on snow course data, an overall estimate of basin snow water content is possible at significantly more precise levels than available for the same cost from conventional snow course data alone. In addition, the associated gridding of LANDSAT data into an image sample unit system allows an in-place mapping of snow water content with respect to known melting environments and stream channels. Such in-place mapping is potentially very useful as an additional data type for improvement of hydrologic model accuracy.

The stratified double sampling plan is described mathematically by Thomas and Sharp (1975). The method summarized in section 3.2.2.4 generally proceeds as follows: First, black-and-white LANDSAT transparencies are obtained and transformed to a simulated infrared color composite form (Katibah, 1973). In the color combining process an image sample unit grid is randomly placed over the image so as to cover the watershed of interest. Each image sample unit is then interpreted manually as to its average snow areal extent cover class according to a snow environment-specific technique described by Draeger and Lauer (1973) and in more detail by Katibah (1975).

Snow water content is then estimated from the following first case, time specific model¹:

$$X_i = \left(\sum_{j=1}^J (M_{ij})(G_j) \right) \cdot K_i \quad \text{eq. 1}$$

where X_i = estimated snow water content for image sample unit i

M_{ij} = snow cover midclass point based on photo interpretation; expressed on a scale of 0.00 to 1.00 for image sample unit i on the j th LANDSAT snow season date,

G_j = weight assigned (0.00-1.00) to a past M_{ij} according to the date of the current estimate,

K_i = the number of times out of j that sample unit i has greater than zero percent snow cover, and

1. Investigation of more sophisticated stochastic model and physical model transforms is currently under way.

J = total number of snow season dates considered.

Image sample units utilized in this study represented 980 acre ground areas. Snow cover classes were defined as 0 percent, >0 - 20 percent, >20 - 50 percent, >50 - 98 percent, and >98 - 100 percent of ground covered by snow.

In order to insure reasonably high correlation between X_i and corresponding ground water content values, y_i , j should equal at least three. As a matter of operating procedure, one or two dates of LANDSAT imagery would be required during the early snow accumulation season after which LANDSAT snow water content estimation could proceed for a given date based on a semi-sliding two, three, or more date basis. Under certain circumstances j may only be two. For instance, an early snow season date and the mid-season date of interest may give rise to acceptable LANDSAT-ground correlations. Or, more powerfully, the first date may consist of an average April 1st snow water content map based on past year's LANDSAT data. In all cases the sample unit grids on all dates must be in common register with respect to a base date grid location (see Figure 2).

After the snow water content index for each LANDSAT image sample unit has been determined, all such units are sorted into strata according to the size of their respective snow water content index. Stratification is used to control the coefficient of variation of the overall basin water content estimate. This is accomplished by the subsequent segregation of the population of image sample units into homogeneous environmental types tending to receive, accumulate, and lose snow at similar rates (see Figure 3). Six such strata were used in the effort reported here.

The total snow water content in a given stratum was obtained from a simple linear regression equation relating image and ground data. Given the average LANDSAT-image derived snow water content index and the number of sample units in that stratum, the regression equation will predict a total

FIGURE 2

SNOW MEASUREMENTS WITHIN THE
SAMPLE UNIT GRID

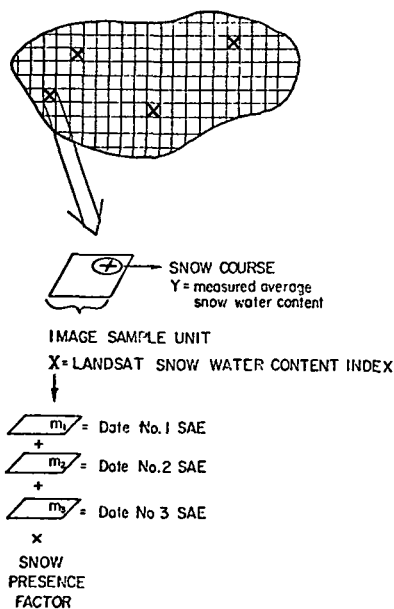
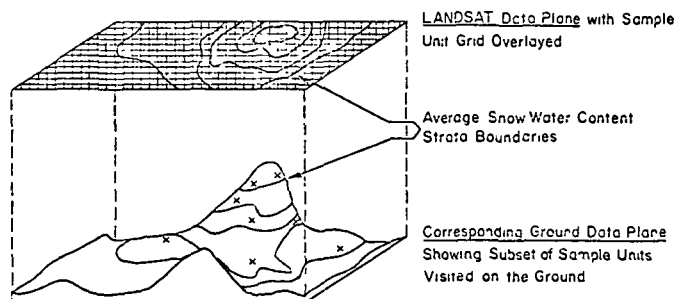


FIGURE 3

STRATIFIED DOUBLE SAMPLING FOR WATERSHED SNOW WATER CONTENT ESTIMATION



ground-based snow water content value for the stratum. The total, ground-calibrated watershed snow water content estimate is obtained by simply summing the strata estimates.

An associated estimate standard deviation may be calculated. The total snow water content estimate can then be placed in a confidence interval in which the actual basin total snow water content is said to fall a specified percentage of the time.

3.2.2.3 Sample Size and Allocation

All watershed sample units are inexpensively examined by the photointerpreter. Ground (snow course) sample sizes may be determined (Thomas and Sharp, 1975) for individual strata according to the snow survey direct cost budget for the watershed of interest and according to the following stratum specific statistics: relative stratum size, LANDSAT snow water content variability, LANDSAT to ground correlation, and LANDSAT to ground sample unit cost ratio.

Assuming the current total monthly snow survey budget of \$4,200 (see section 3.3) for the Feather River watershed, an average ground sample unit cost of \$150, an average image sample unit cost of \$0.15, and accounting for overhead costs, ground sample unit sizes were calculated for the six snow water content strata. The accumulated LANDSAT snow water content index in each stratum represented the stratum's size. Strata definitions, variances, and other statistics are given in the table below. The table in section 4.1 summarizes the image and ground sample unit sizes. A correlation coefficient of 0.80 between image and actual ground snow water content estimates, based on spring 1973 data, was used in the sample size calculations.

LANDSAT SNOW WATER CONTENT STRATUM	1	2	3	4	5	6
SNOW WATER CONTENT INDEX RANGE	0.00- <0.10	0.10- 0.35	>0.35- <1.00	1.00 <3.00	3.00- 5.00	>5.00
AVERAGE SNOW WATER CONTENT INDEX	0.00	0.18	0.78	2.05	3.96	6.18
RELATIVE ACCUMULATED SNOW WATER CONTENT INDEX	0%	3%	4%	22%	24%	47%
CV OF SNOW WATER CONTENT INDEX	0%	65%	24%	22%	11%	16%

Once stratum ground (snow course) sample sizes have been calculated for a fixed budget, the expected performance may be determined for the snow water content inventory. One standard statistical expression of performance is expected resulting allowable error (AE). This value was defined previously as the half width of an interval centered on the basin estimate in which the true basin water content value is expected to fall with given confidence probability. Calculation of the expected overall coefficient of variation (CV), selection of the confidence probability (represented by Student's-t), and use of the total snow course sample size (n) allows calculation of expected resulting AE according to the following formula.

$$AE = (t_{n_{total}-1}) \cdot (CV_{overall}) \quad \text{eq. 2}$$

If the allowable error is not low enough to satisfy snow water content estimation objectives, a larger snow survey budget is required. In this case the hypothesized larger budget level is selected and the sample size and allowable error calculation process is repeated. It should be noted that the calculation of the overall coefficient of variation would be based in part on LANDSAT data and in part on snow course data. If snow course data are not available then first year snow water content variability estimates may be based on previous LANDSAT data or supporting time coincident aircraft data alone.

After the allowable error criterion has been met, the calculated number of necessary snow courses per stratum are allocated with equal probability to image sample units within a stratum. This allocation for a given watershed may occur once during the system setup. In such a situation, sample size and AE testing should be performed for the most variable snow water content index month of the snow season. Once the snow courses were established, cost-effective basin snow water content estimation would proceed by use of the double sample regression formulae relating LANDSAT and ground data. The resulting water content estimate would then be related in combination with other

independent variables to water runoff.

For basins where established snow courses already exist, the snow courses would be classified into the appropriate strata. Under this third allocation method, additional courses could then be added, subtracted, or replaced where necessary according to an annual partial course replacement strategy.

3.2.2.4 Summary of Steps to be Used in Stratified Double Sampling for Snow Water Content Estimation

- (1) Create LANDSAT color composites with appropriate image sample unit grid over watershed(s) of interest.
- (2) Estimate snow areal extent by LANDSAT image sample unit for previous year(s) or current season snow build-up dates(s).
- (3) Estimate snow areal extent by image sample unit for LANDSAT snow season date of interest.
- (4) Transform snow areal extent data to snow water content data by LANDSAT image sample unit.
- (5) If not already performed, stratify image sample units into LANDSAT snow water content index classes. Then calculate stratum ground sample unit (snow course) sample sizes to achieve allowable error criteria for the basin snow water content estimate. Stratification and sample size calculation should be performed for the pre-snow season date combination having the most variable snow water content and/or containing the largest water runoff-related snow pack.
- (6) If not already performed for the given snow season or snow season date, allocate ground sample units to strata with equal probability within strata.
- (7) Calculate the estimate of watershed snow water content according to a summation of stratum regression relationships for LANDSAT versus ground observations.
- (8) Enter the basin snow water content estimate into statistical or physical models to predict water yield.

3.3 Comparative Costs

3.3.1 The CCSS System

3.3.1.1 CCSS Budget

An agency's budget provides an obvious starting point for

evaluating the cost of outputs produced. In the case of the snow survey and water supply forecasting activities of the DWR, we found that the entire production process has been running on an "official" annual budget of around \$300,000. About 90 percent of this amount comes from State general fund support. The remainder, about \$30,000 a year, consists of reimbursements from CCSS program cooperators.

The DWR snow surveys group has estimated that cooperators contribute services far in excess of their reimbursements. This occurs because many cooperators absorb the state survey costs along with their own snow survey efforts. The DWR estimates (very roughly) the value of these unaccounted services at around \$200,000 per year. This implies an "unofficial" snow survey annual budget in the neighborhood of \$500,000.

Program costs within the budget are allocated about 50:50 between survey support and forecast activities. The DWR's non-salary direct costs for snow survey activities in 1974/75 are budgeted at around \$28,000. This includes \$19,000 for contractors, \$4,000 for flying services and other support, and \$5,000 for sensor equipment. These costs are expected to be fully offset by contributions from cooperators. Budgets in future years are likely to contain greater outlays for sensor equipment as automatic sensors and other sophisticated measurement devices are brought into use.

3.3.1.2 Cost of Surveys

CCSS program budget information, although useful for examining the snow surveys production process as a whole, does not tell us much about the costs of producing intermediate outputs like snow density and water content measurements. Moreover, we were specifically interested in the costs of producing these outputs in our study area, the Feather River Basin, rather than for the entire state.

Estimates for the direct costs of survey work were derived from discussions with DWR snow survey personnel. Based on 1974 survey information, we determined the following average cost figures:

Aerial marker survey measurement visit \approx \$15

Snow course survey measurement visit \approx \$150

Costs of the two survey types thus differ by about a factor of ten. Aerial marker visits are relatively inexpensive because a skilled pilot can overfly and photograph many markers in a short period of time. Snow course measurement visits, because they involve detailed ground measurements, have a higher and wider range of costs. The costs of visits

appear most affected by where they are and who performs them. DWR analysts estimate the direct costs of visiting the most accessible snow courses at \$50 and \$60 each. Some courses can be reached by road or easily by snowmobile or helicopter. Remote courses accessible only by foot can represent as much as \$210 each. This would include two men at \$40 per day plus expenses plus maintenance of supply cabins.

Estimates of indirect costs are much harder to derive than direct costs. The challenge is to isolate only those indirect costs associated with the production of snow water content measurements. Indirect costs can be distinguished in the following DWR snow survey activities:

- program direction and coordination of survey work
- communication with cooperators
- preseason aerial marker and snow course setups
- measuring equipment acquisition and maintenance
- training and safety instruction sessions
- formal recording and publication of measurements

It was determined that indirect costs amounted to roughly one-third of the direct costs associated with the snow survey efforts. For the Feather River Basin in 1974, with 3 aerial marker visits and 125 snow course visits, total survey costs (C_{FRB}) were estimated as follows:

$$C_{FRB} = 1.33 (3 (\$15) + 125 (\$150))$$

$$C_{FRB} = \$25,000$$

3.3.1.3 Cost Per Survey Month

If it is assumed that direct and indirect snow survey costs accrue uniformly over the snow sampling season, it is possible to estimate how much of the annual snow survey budget is consumed in a "typical" snow survey month. April and May were considered "typical" survey months in this study. A monthly proportionality factor was derived for April and May and applied to the basin total cost budget (Thomas and Sharp, 1975). The monthly direct costs allocated to survey work were estimated to be roughly \$4,200.

3.3.2 LANDSAT-Aided System

3.3.2.1 Ground Sample Unit Costs

Since the collection of samples at snow courses is an activity common to the LANDSAT-aided and the existing snow survey

methods, it was possible to apply the same set of costs per ground sample unit to both systems. The unit costs of typical snow course measurement visits were estimated earlier at \$150. Aerial marker measurements visits do not constitute a significant portion of the snow survey budget within the Feather River Basin.

3.3.2.2 Image Sample Unit Costs

Costs per image sample unit, applicable to only the LANDSAT-aided survey system, were developed along with the sampling methodology described previously, and are derived from actual University RSRP snow survey work using 2218 image sample units in the Feather River Watershed.

The average cost for each of the 2218 image sample units was 13.6¢, of which about 10¢ went toward image interpretation and keypunching. Since most of the processed and unprocessed imagery is useful for later training and comparative analysis, an amortization factor was applied. It was assumed, for example, that two out of three dates of imagery developed for one occasion would be usable over a total of five separate occasions.

4.0 RESULTS AND CONCLUSIONS

4.1 Sample Sizes

The methodology behind sample size determination was described in section 3.2. The number of samples required were calculated for various budget levels, sample costs, and weighting options. The following table summarizes the number of image sample units (ISU's) and ground sample units (GSU's) required in each of six LANDSAT snow water content strata, given a cost per ISU of 15¢ and a cost per GSU of \$150.

LANDSAT Snow Water Content Stratum	1	2	3	4	5	6
No. of LANDSAT ISU's Examined in Watershed	503	614	205	393	220	283
No. of ISU's Visited on Ground	0	3	1	7	4	11

4.2 Performance Comparison

Use of the allowable error (AE) formulation described earlier permits a direct cost-capability comparison of the two snow water content estimation systems. For the LANDSAT-based

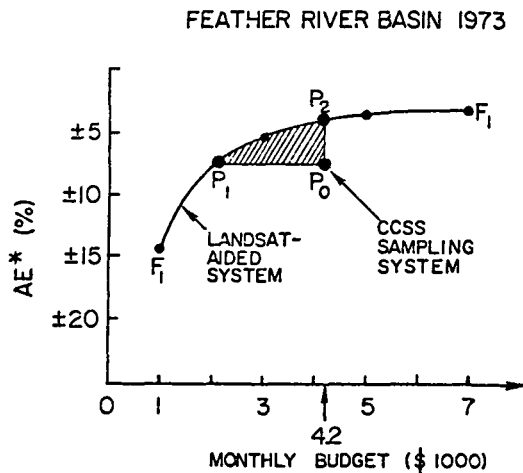
sample sizes, AE's were calculated for monthly direct cost budgets of \$1,000, \$3,000, \$4,200, \$5,000, and \$7,000 at confidence intervals ranging from 80% to 99%. For the CCSS system of snow water content estimation, AE's were calculated at four confidence intervals on a monthly direct cost budget of \$4,200. Results for the 95 percent confidence interval are shown below in Figure 4, a diagram analogous to Figure 1.

4.3 Major Conclusions

4.3.1 Cost Savings

Figure 4 permits comparison of the two production systems at many levels of effectiveness. One production possibility of the existing system is represented by point P_0 at the \$4,200 monthly direct cost budget level. Point P_1 identifies an output of similar precision and accuracy in the LANDSAT-based system. The cost advantage per snow survey month is represented by the horizontal distance between P_0 and P_1 . In this case, the LANDSAT-based system shows approximately a \$2,300 savings over the existing system of snow water content estimation. Extrapolated over the full range of survey months, this would imply a savings of around 50 percent over the existing annual snow survey budget for the Feather River Basin.

FIGURE 4 - COST-CAPABILITY COMPARISON OF SNOW WATER CONTENT SAMPLING SYSTEMS



* ALLOWABLE ERROR AT 95% LEVEL OF CONFIDENCE

4.3.2 Increased Precision

Advantages of the LANDSAT-aided system are also apparent on the capability or effectiveness side. At the \$4,200 budget level, the proposed snow water content estimation produced results approximately 1.8 times more precise than the existing system.

In general, the LANDSAT-aided system yielded relatively precise estimates of total watershed snow water content. For a \$4,200 monthly budget, this approach estimated true basin snow water content to within $\pm 3.6\%$ ninety-five times out of a hundred. The precision of basin water content estimates could be improved still further by using techniques that increase the correlation of orbital to ground snow water content estimates. Smaller image sample units, more environment-specific snow class interpretations, and automatic processing of satellite digital data are some of the more promising of these techniques.

4.3.3 Additional Abilities

The LANDSAT snow areal extent-snow water content transform presented here is only a first case model. Yet it yields correlations with ground sample data on the order of .80. More sophisticated stochastic and physical transform models now being developed should push this correlation significantly higher. The result will be greater snow water content estimation precision at the same level of budget.

The LANDSAT-to-ground correlation coefficient of .80 was achieved using satellite imagery specific to two ground survey dates plus minimal information from a third date. In an operational situation, however, detailed early-season and/or previous-snow-season LANDSAT data would be available in combination with the snow date of interest, this additional information should further increase the correlation coefficient and produce an even more cost-effective snow water content estimation.

A LANDSAT-aided snow water content estimation system offers several additional possibilities for future snow survey work:

- One byproduct of the LANDSAT-derived image sample unit data is an in-place mapping of snow water content with respect to known melting environments and stream channels. Such time- and place-specific snow melt records could be used to aid in the selection of new snow course sites or in the placement of automatic snow sensors. Snow pack and stream channel juxtaposition data could also be used in refined models of runoff timing.

- Human and automatic analysis of daily meteorological satellite data, when correlated with less frequent LANDSAT and ground data, offers the possibility of extremely frequent watershed snow water content updating.
- Hydrologic models of the future will conceivably integrate remote-sensing and meteorological data with automatic ground-based snow sensing equipment. Real-time information eventually could be generated for entire watersheds of subbasins, depending on the need to assess the impact of a major storm or a minor subdivision. The continued refinement of remote sensing-aided snow water runoff estimation procedures is likely to be a necessary input into future water resource management practices.

The foregoing conclusions suggest that remote sensing promises great potential for aiding in the snow water content estimation process. Our findings are further enhanced by the fact that snow water runoff is one of the major sources of water supply within the California Water Plan, as well as in many other parts of the world. Improved methods of identifying, monitoring, mapping, and modeling our snow water resources at this time can lead to improved methods of predicting and managing this resource in the future. LANDSAT-derived imagery, when used to augment an existing hydrologic model, thus appears to resemble a classic "technological advance" as defined in a cost-effectiveness framework.

REFERENCES

- Brown, A. J., 1974. Long-Range Goal and Information Needs of the Coordinated Snow Survey Program in California. California Cooperative Snow Surveys, California Department of Water Resources.
- California Cooperative Snow Surveys, California Department of Water Resources, 1970. Snow Survey Measurements Through 1970, Bulletin No. 129-70.
- California Cooperative Snow Surveys, California Department of Water Resources, 1971-74. Water Conditions in California, Bulletins No. 120-71, 120-72, 120-73, 120-74.
- Cochran, W. G. 1963. Sampling Techniques. Second Edition. John Wiley & Sons, Inc., New York. 413 pp.
- Dorfman, Robert, Ed., 1965. Measuring Benefits of Government Investments. The Brookings Institution. Washington, D.C.

- Goldman, Thomas A., Ed., 1968. Cost-Effectiveness Analysis: New Approaches in Decision-Making. Washington Operations Research Council. Praeger Publishers. New York.
- Howard, C., 1974. Personal communication.
- Heiss, Klaus P., 1969. Estimating the Economic Benefit of Surveying Earth's Resources. In Proceedings of Princeton University Conference on Aerospace Methods for Revealing and Evaluating Earth's Resources, September 25-26. pp. 18.1-18.13.
- Katibah, E. F. 1973. A Simple Photographic Technique for Producing Color Composites from Black-and-White Multiband Imagery with Special Reference to ERTS-1. Forestry Remote Sensing Laboratory, University of California, Berkeley. 9pp.
- Katibah, E. F., 1975. Areal Extent of Snow Estimation Using LANDSAT-1 Satellite Imagery. In an Integrated Study of Earth Resources in the State of California Using Remote Sensing Techniques (NASA Grant NGL 05-003-404), Chapter 2b. Remote Sensing Research Program, Space Sciences Laboratory, University of California, Berkeley. May.
- Kendall, M. G., Ed., 1971. Cost-Benefit Analysis. American Elsevier Publishing Company, Inc. New York.
- Lauer, Donald T., and William C. Draeger, 1973. Techniques for Determining Areal Extent of Snow in the Sierra Nevada Mountains Using High Altitude Aircraft and Spacecraft Imagery. In Advanced Concepts and Techniques in the Study of Snow and Ice Resources. National Academy of Sciences. Washington, D.C. pp. 532-540.
- Merewitz, Leonard, 1974. On the Feasibility of Benefit-Cost Analysis Applied to Remote Sensing Projects. In Annual Progress Report, May 1974, under NASA Grant NGL 05-003-404. pp. 5-40 - 5-48.
- Mishan, E. J., 1971. Cost-Benefit Analysis, An Introduction. Praeger Publishers. New York.
- Prest, A. R., and R. Turvey, 1965. Cost Benefit Analysis: A Survey. Economical Journal, 75 (December). pp. 683-735.
- Raj, Des., 1968. Sampling Theory. McGraw-Hill Book Company, San Francisco. 302 pp.
- Teitz, Michael B., 1968. Cost Effectiveness: A Systems Approach to Analysis of Urban Services. Journal of the American Institute of Planners, XXXIV (September). pp. 303-311.

Thomas, R. W. et al. 1974. Potential Value of Remote Sensing Data in Models for Estimation of Water Yield. In An Integrated Study of Earth Resources in the State of California Using Remote Sensing Techniques (NASA Grant NGL 05-003-404). Remote Sensing Research Program, Space Sciences Laboratory, University of California Berkeley. May.

Thomas, R. W. and J. M. Sharp. 1975. A Comparative Cost Effectiveness Analysis of Existing and LANDSAT-Aided Systems for Estimating Snow Water Content. In An Integrated Study of Earth Resources in the State of California Using Remote Sensing Techniques (NASA Grant NGL 05-003-404). A Remote Sensing Research Program and Social Sciences Group, Space Sciences Laboratory, University of California Berkeley. May.

Willow Run Laboratories, 1972. Design of a Study to Evaluate the Benefits and Cost of Data From the First Earth Resources Technology Satellite. Institute of Science and Technology. The University of Michigan, Ann Arbor.

RED AND NEAR-INFRARED SPECTRAL REFLECTANCE OF SNOW

Harold W. O'Brien and Richard H. Munis, *U.S. Army Cold Regions Research and Engineering Laboratory, Hanover, New Hampshire*

ABSTRACT

The spectral reflectance of snow in the range of 0.60 to 2.50 μm wavelengths was studied in a cold laboratory using natural snow and simulated preparations of snow. A white barium sulfate powder was used as the standard for comparison. The high reflectance (usually nearly 100%) of fresh natural snow in visible wavelengths declines rapidly at wavelengths longer than the visible, as the spectral absorption coefficients of ice increase. Aging snow becomes only somewhat less reflective than fresh snow in the visible region and usually retains a reflectance greater than 80%. In the near infrared, aging snow tends to become considerably less reflective than fresh snow. The rate of decline of near-infrared reflectance due to aging is strongly influenced by the history of the snow during aging. Some of the significant parameters which determine the reflectance of snow are discussed and, where possible, results are presented which illustrate the predominant influences.

INTRODUCTION

This project was initiated in response to engineering problems related to the solar energy reflected from snow covering an underlying structure. Subsequently, interest developed in the application of these studies to problems in environmental satellite technology and in military surveillance and/or camouflage activities.

Although operational environmental satellites have obtained snow data remotely, one problem facing the satellite hydrologist is that of understanding the significance of variations in the spectral reflectance of the snow cover in order to more thoroughly evaluate the remote observations. The problem becomes more complicated because when snow is melting its spectral reflectance can change drastically on a day-to-day basis.

The purpose of this program was to determine the spectral characteristics of snow in the near infrared (1.00 to 2.50 μm wavelength range) particularly with respect to changes in the spectral reflectance of snow cover during the natural aging process. More recently the scope of the project was expanded to include spectral measurements in the ultraviolet to 0.60 μm wavelength region. Only the spectral reflectance at wavelengths from 0.60 to 2.50 μm are discussed in this paper.

This investigation was conducted principally during the period January 1972 to December 1973 at the U.S. Army Cold Regions Research and Engineering Laboratory, and is discussed in more detail in Reference 1.

PROCEDURE

Spectrophotometric Methods

The physical arrangement of experimental apparatus is depicted in Figure 1. The optical configuration of

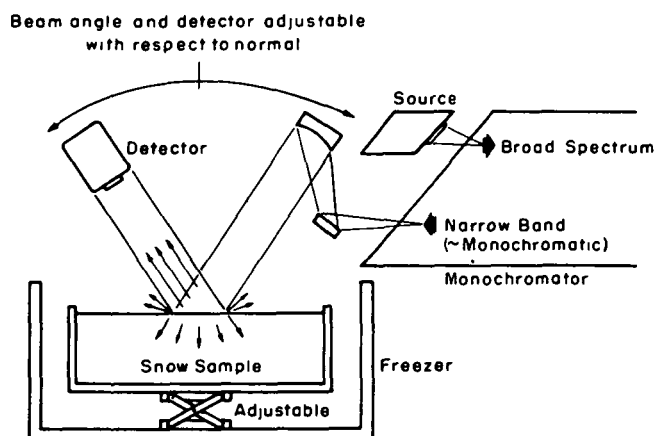


Figure 1. Instrumentation for reflectance measurements.

a Perkin-Elmer Model E-13 spectrometer was altered for utilization as a reflectometer. An open-top commercial freezer display case was used as a cold chamber to maintain snow samples during measurements. Initially the apparatus was set up in a warm laboratory with poorly controlled room temperatures. In November 1972 the equipment was moved to a cold laboratory with good temperature stabilization at 10°C.

Eastman White Reflectance Standard (Lot #201-2) was used as a standard with which to compare the snow reflectance measurements.

Spectral scans were run on the standard and on snow samples for each combination of angles of incidence and reflection desired. To eliminate the necessity of repetition of the terms and to simplify future discussion, abbreviated designations signifying an angle of incidence-hyphen-angle of reflection will be used in this paper. For example, "5°-5°" indicates an angle of incidence of 5° from normal and an equal angle of reflection; "0°-30°" indicates that the source beam was at normal incidence to the reflective surface (standard or snow) and that the reflectance was measured with the detector set at an angle of 30° to the normal. Although more measurements were made at 5°-5° and 0°-30° than at any other angles, several measurements were made at 10°-10°, 0°-15°, 0°-20°, and 0°-25°.

Preliminary tests indicated that reflectance measurements were not detectably influenced by the substrate materials (wood and/or aluminum screening on the bottom of the box) when covered with about 5 or 6 cm of snow. Therefore, all measurements were made with a minimum snow depth of 10 cm.

Snow Sampling Methods

Snow samples were collected by placing open boxes, consisting of a light wood frame covered on five sides with aluminum screen, on the ground in a reasonably level area away from the laboratory buildings and allowing snow to fall naturally into the boxes. Near the end of a fresh snowfall, a precooled, 21-ft³ home-type deep freeze cabinet was rolled, on casters, outside of the laboratory building and one or more of the snow boxes were carefully lifted and carried to the freezer. The samples were then transported in the freezer into the cold laboratory.

On subsequent days, provided there had been no precipitation in the meantime, other boxes of naturally aged snow from the same snowfall were similarly collected.

Since the investigators had no control over natural aging conditions due to weather, some snow conditions were simulated in the cold laboratory.

For some series of tests, older snow was ground in a food mill and allowed to fall loosely into regular snow sampling boxes. This milled snow appeared to simulate natural wind-drifted snow quite closely in density, hardness and texture. Generally, the temperature of the snow, whether naturally fresh or milled, was held at about -19°C during storage and measurements.

Aging of snow was simulated by taking fresh snow or milled snow and allowing various degrees of warming with the snow sample still in position for reflectance measurements. Then, sequential spectral reflectance scans were run while holding the ambient air temperature as steady as possible at each of several levels: below, near and above the freezing point.

A sample of artificial snow crust was synthesized by spraying an ice-water mist on very cold snow. Although this sample served its purpose in illustrating a point to be discussed later, it was not considered a very realistic replica of natural ice crust.

Observations were generally made of the snow density, hardness and gross particle size using usual meteorological methods. In addition, occasional Formvar replicas were made of the snow samples.

DATA ANALYSIS

The strip charts of the spectrophotometer output were digitized and corrections for drift in signal strength were formulated. Both standard and snow runs were corrected for drift and normalized to the same gain. Each snow run was then compared with the appropriate standard run by computing and plotting the ratio of snow reflectance to standard reflectance point by point throughout the portion of the spectrum covered in the run. In addition, some snow runs were compared with other snow runs by the same method (i.e., melting and refrozen snow were compared with the original cold snow samples).

Two experimental discrepancies, not prominently evident in most figures, appeared in the analyses of some samples in the form of discontinuities in the reflectance curves near $1.00\text{ }\mu\text{m}$ and again around $1.75\text{ }\mu\text{m}$. The nature of these artifacts is discussed in Reference 1.

When two or more runs were made on the same sample under essentially constant conditions, the

results were reproducible for the most part within about 1% with occasional deviations of about 3%. Greater possibilities of error occurred at the limits of each monochromator grating (1.00 μm and 2.50 μm) and especially near 2.50 μm where the signal-to-noise ratio deteriorates rapidly.

RESULTS

It is virtually impossible to separate and examine each individual factor which determines the spectral reflectance of snow. An attempt has been made here to discuss some of the significant parameters and, where possible, to present results which may be presumed to illustrate the predominant influences.

A typical example of the spectral reflectance of snow is shown in Figure 2. The overall shape of the reflectance curve is similar for all types of snow examined (except for ice-glazed snow) but the relative magnitudes of various parts of the curve vary with conditions.

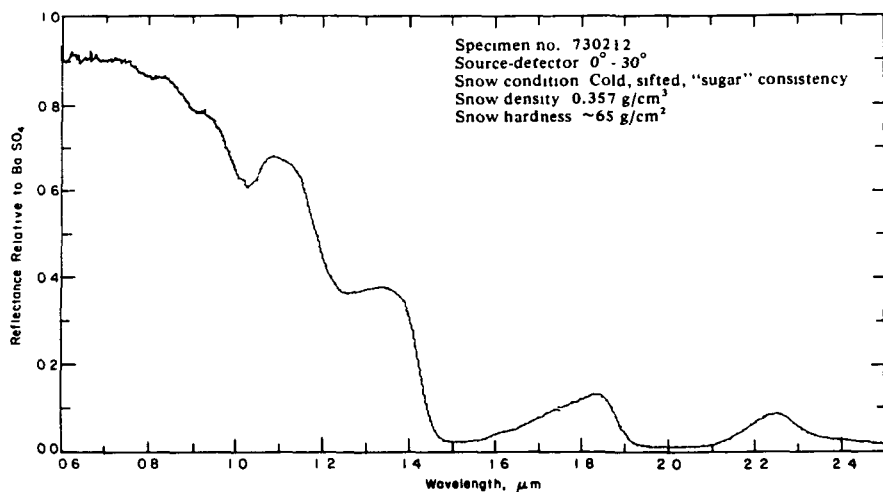


Figure 2. Typical spectral reflectance curve for snow

Changes in Snow Reflectance Related to Natural Aging

The spectral reflectance of snow in the red and near-infrared regions exhibits rather predictable changes as the snow ages naturally. The history of the snow during aging influences the degree and rate of change of reflectance with wavelength.

Figure 3 illustrates the changes in reflectance of light snow which fell during the evening of 20 January 1972. A fresh sample (curve A) was collected on the morning of the 21st. The weather was generally overcast and below freezing (about -2°C) during the time between snowfall and sample collection. The density of the fresh sample was 0.097 g/cm^3 .

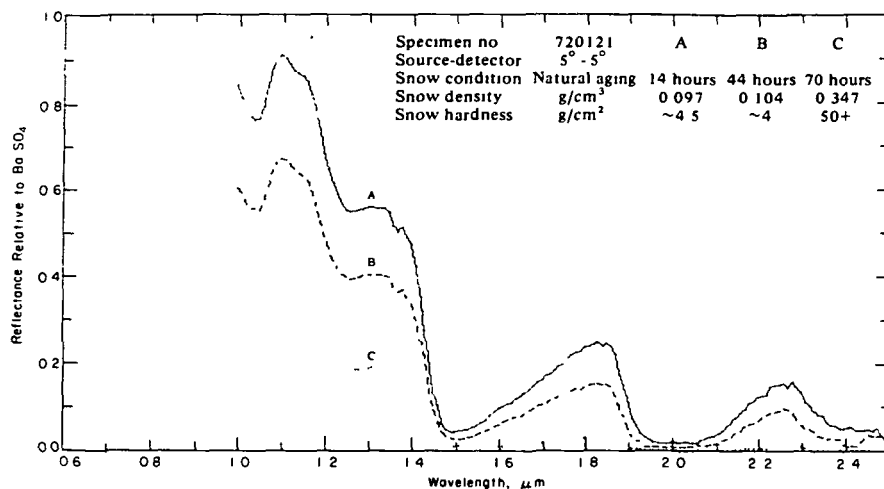


Figure 3. Changes in snow reflectance with aging.

Thirty hours later, on the afternoon of 22 January, a second sample (curve B) was retrieved from the natural snow cover remaining from the same snowfall. Although the weather was clear and cold (never above freezing and falling to -20.5°C in the night), the measured density had increased slightly to 0.104 g/cm^3 .

A third sample (curve C) was taken on the afternoon of 23 January, representing nearly three days of natural aging of the same snowfall. This time, however, the ambient air temperature had warmed to about $+7^{\circ}\text{C}$ during the last day of aging and the density of the snow cover was measured as 0.347 g/cm^3 .

Another illustration of the changes in snow reflectance with aging is shown in Figure 4. Curve A shows the reflectance of freshly fallen snow (22 Dec 1972) and curve B that of snow which had aged naturally for two days with ambient temperatures hovering above and below freezing.

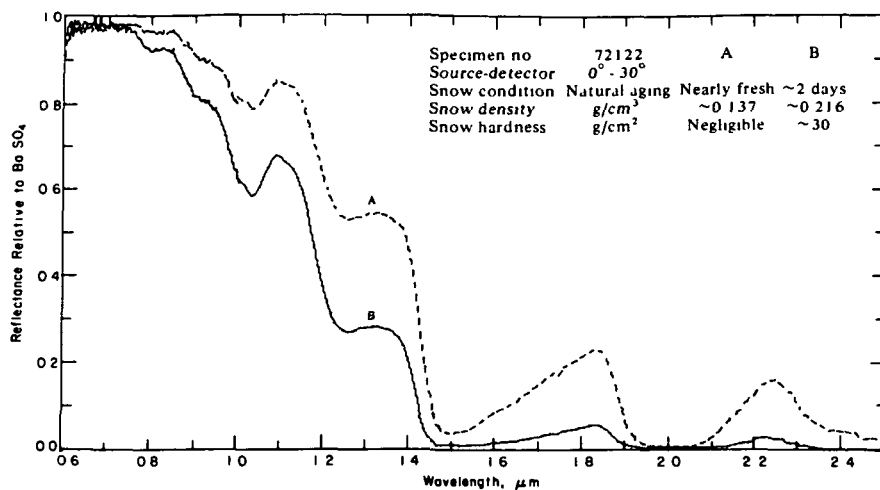


Figure 4. Changes in snow reflectance with aging.

The significance of these graphs will be more apparent after a discussion of the spectral reflectance of artificially melted and refrozen snow.

Effect of Melting and Refreezing on Snow Reflectance

Several experiments were performed to determine the effect of melting and refreezing on the spectral reflectance of snow. Since the only snow readily available at the time was somewhat aged and crusty, snow samples were prepared by sifting the old snow through a food mill. The resulting snow was very similar in appearance, texture, and physical properties to naturally windblown snow. The series of runs at 5° -5° shown in Figure 5 depicts the sequence of events which followed. The first run was made with freshly milled snow continuously cold [about -19°C (curve A)]. The ambient temperature was then raised to near melting and the snow temperature held around -1.5 to -0.5°C during the next run (curve B). The sample temperature was then returned to -19°C and the reflectance rechecked (curve C). It is obvious from the proximity of these curves that temperature changes below melting have little effect on the spectral reflectance. During the fourth run (curve D) a draft of warm air was wafted across the surface of the snow causing slight surface melting, with no visible diminution of snow volume but giving the appearance of a "glistening wet" surface. The ambient air temperature varied between +2.5°C and 10°C during the run. With

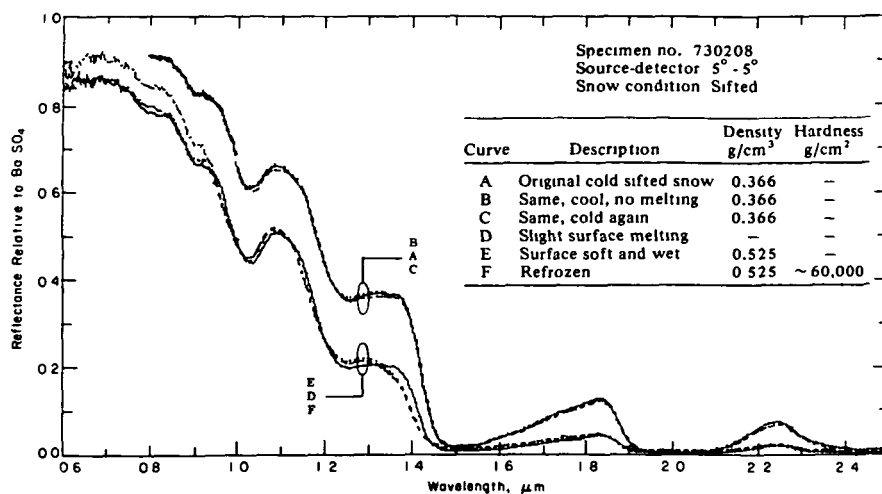


Figure 5. Effects of temperature snow reflectance.

the onset of surface melting, the near infrared reflectance decreased drastically.

By the fifth run (curve E), the surface of the snow was soft and wet to a depth of about 1/8 in. The ambient temperature was about $+6^\circ\text{C}$ without the warm air blower. The snow was then refrozen and another run (curve F) made with the ambient temperature about -5°C .

A comparison of the reflectance of cold, melting and refrozen snow are shown in Figure 6. In this case, the original cold snow was used as the reference. The ratios of the spectral reflectances of melting and refrozen snow to cold snow were then computed.

In general, melting lowers the spectral reflectance of snow. At some wavelengths, part of the reflectance lost by melting may be regained by re-freezing, particularly with source-detector angles of $0^\circ - 30^\circ$. In the spectral region from about 1.9 to 2.1 μm wavelength, the reflectance of melting and refrozen snows appears to be about the same as or greater than that of loose cold snow. This occurs in a region of high energy absorption by water, and even greater absorption by ice. Since this portion of the spectrum is one of generally low reflectance for snow, and the curves therefore represent the ratio of two relatively small numbers, caution must be observed in interpreting the significance of specific details.

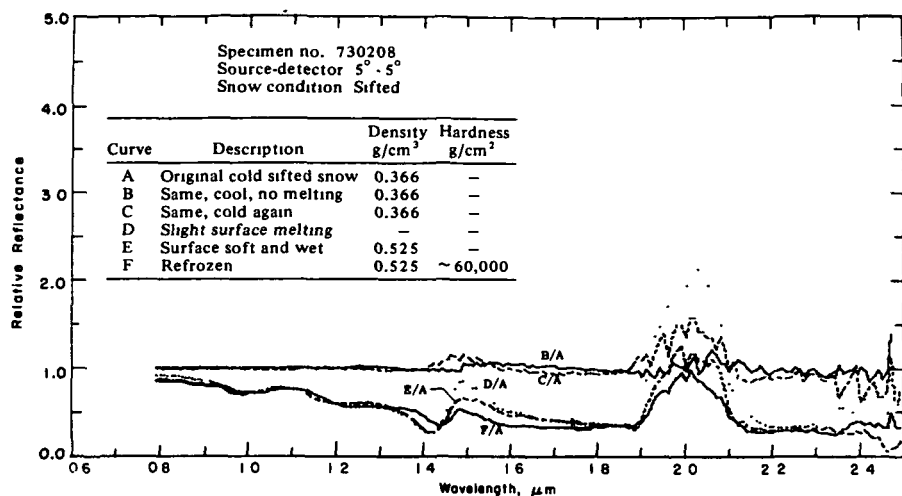


Figure 6. Ratio of curves from Figure 5.

However, there is little question that increased reflectance of slightly melting snow may occur in this region.

Reflectance of Ice-Glazed Snow

On 8 December 1972, a light snowstorm changed to freezing rain causing an extremely hard smooth ice glaze on top of the snow. A sample was taken at night at just about the time the freezing rain ended. The snow under the crust had a density of 0.148 g/cm³. The ice-glazed crust, approximately 1/4 in. thick, had a measured density of 0.903 g/cm³. The following morning the undisturbed snow cover was subjectively observed to have a very high specular reflectance in the visible range. The spectral reflectance measured in the near infrared at $5^\circ - 5^\circ$ is shown in Figure 7. In the range of wavelengths from 1.00 to 1.40 μm , the reflectance of the crust is qualitatively similar to that of other snow, particularly aged and/or refrozen samples. However, beyond 1.4 μm , the spectral reflectance of this ice crusted snow bears little resemblance to that of other snow samples studied.

Effect of Drifting and Wind-Compaction on Snow Reflectance

Approximately 8 in. of snow fell during the period of 1700 hours on 15 December and 0930 hours on 16 December 1972. A sample of this snow was collected about 2 hours after cessation of the snowstorm and

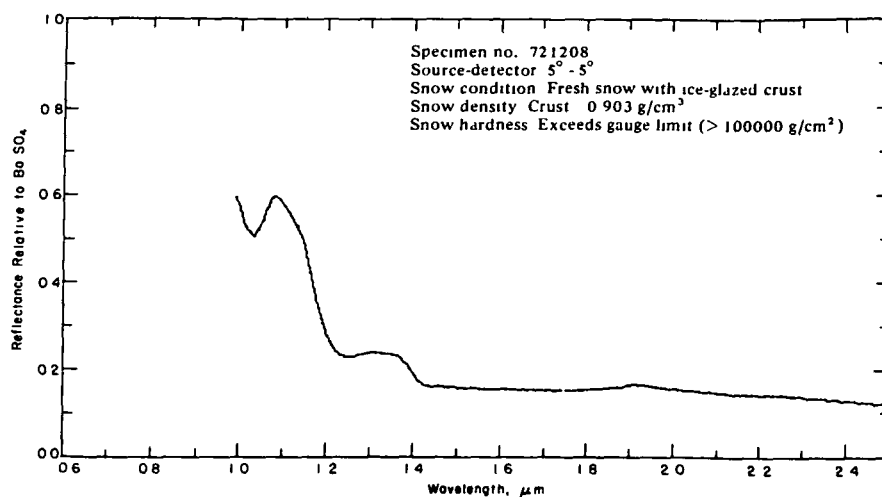


Figure 7. Reflectance of ice-glazed snow crust.

before significant wind occurred. The ambient temperature during snowfall and up to the time of collection, did not exceed -6°C . The snow density was 0.121 g/cm³ and the hardness almost negligible (<2 g/cm²). Due to equipment problems, the sample was stored in a closed deep-freeze at -19°C , for about 30 hours before reflectance measurements were made. The density and hardness remained essentially unchanged. The reflectance of this snow is shown by curve A in Figure 8. On 17

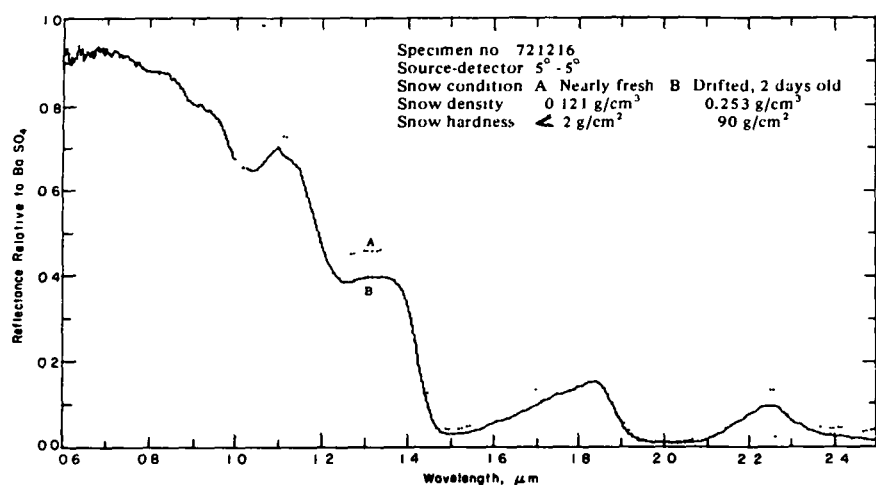


Figure 8. Effect of snow drifting on snow reflectance.

December, at about 1530 hours, another snow sample was retrieved. The weather had been cold (not above -1°C) and windy (10 to 18 knots) on the 16th and 17th of December so that the snow had drifted considerably and had compacted somewhat. The density and hardness of the drifted snow were 0.253 g/cm^3 and 90 g/cm^2 respectively. The reflectance of this drifted snow sample is shown by curve B in Figure 8.

Note that the drifted snow exhibits a lower reflectance than fresh snow. However, snow (particularly at the peaks near $1.8\text{-}\mu\text{m}$ and $2.2\text{-}\mu\text{m}$ wavelengths) retains more of its reflectance during two days of wind compaction, even with the additional aging at cold temperatures, than snow which has aged naturally and increased commensurately in density without drifting.

Snow Reflectance at Various Angles

In the present study, the reflectance curves for a given snow are generally very similar for a variety of angles, indicating agreement with the popularly held concept of near-perfect diffusivity of snow. There is, however, lack of consistency between samples in the relative magnitudes of measured reflectances at different angles. From the earlier data, many of which are not shown in the illustrations, the tentative conclusion was that the reflectance of snow seems to be about the same at 5° - 5° and 0° - 30° , with perhaps slightly greater reflectance at 0° - 30° .

On the night of 21 March 1974, a fairly heavy snowstorm occurred at Hanover, New Hampshire, presenting an opportunity to recheck the angular reflectance of a fresh snow. A fresh sample was obtained at 2100 hours. The density was 0.170 g/cm^3 and the hardness was approximately 8 g/cm^2 . Between 2100 hours and 0419 hours the following morning, spectral scans were made at several angles, as shown in Figure 9. For that particular snow, at least, the relative reflectance was greatest at 0° - 30° , decreased successively at 0° - 25° , 0° - 20° , and 0° - 15° , and was even less at 5° - 5° and 10° - 10° .

Other illustrations of snow reflectance at various angles may be seen in Figures 10a and 10b. These figures are presented in a later section because of their pertinence to another discussion.

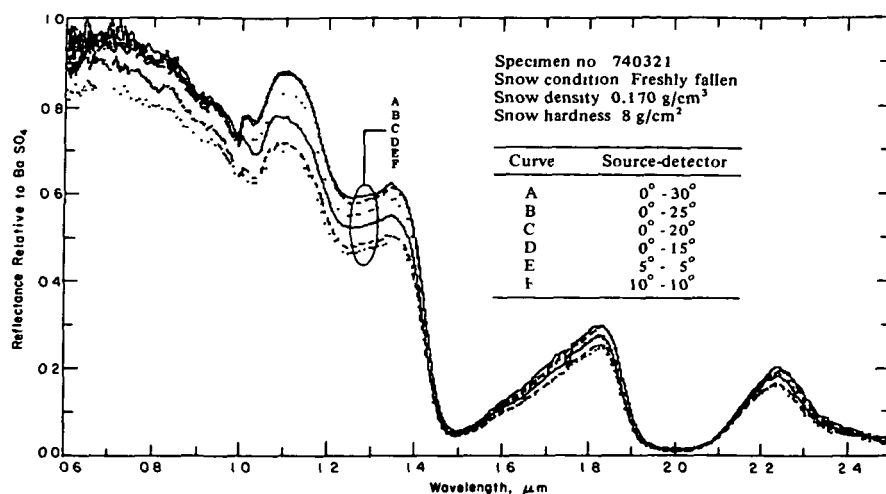


Figure 9. Comparison of angular reflectances of snow.

Relationship of Snow Reflectance to Snow Density

As previously mentioned, the reflectance of snow depends a great deal upon its history. Whatever the subsequent history of a freshly fallen snow, there is a tendency toward densification of that snow. Thus, natural aging over a period of time, even at sub-freezing temperatures, results in changes in the physical (and optical) characteristics of the snow caused by settling, sintering, and sublimation. Mechanical working of the snow, such as occurs during blowing and drifting snow, causes densification by settling and wind compaction. Melting of snow, even when slight, not only tends to increase the effective mean grain size and density by melting the smaller particles (such as dendritic branches) first but also produces free water in the snow. Densification of snow, by whatever means, is accompanied by a reduction of the reflectance of the snow - less noticeably in the visible red region but more and more significantly in the near-infrared region.

As a matter of interest, a survey was made of snows of several densities, disregarding history, and relating the reflectance at various wavelengths to the density of the snow. Wavelengths used were 1.0, 1.1, 1.3, 1.8 and 2.24 μm. In each case, the decrease in reflectance with density showed a simple correlation of about 0.8 at the 0.01 confidence level.

Dependence of Reflectance on Microstructure of Snow

Dunkle and Bevans (Reference 2) calculated the theoretical spectral reflectance (0.3 to 1.3 μm) of a snow cover "for particle sizes of 0.001, 0.01 and 0.1 in. ..." Their theory ".... indicates that, as snow ages and the snow crystals grow, the albedo should tend to decrease from the initial high values." It would therefore be anticipated that a reduction in the spectral reflectance would result from the combination of densification and increased particle size which occurs with aging. This expectation is confirmed by experimental measurements.

Although drifted snow observed immediately after being wind-blown has a greater density, due to wind compaction, than undrifted snow, the drifted snow would be expected to have a smaller size distribution and more rounded ice particles than snow which has aged by other processes due to mechanical working of the snow crystals (Reference 3). In the previous discussions of drifted snow, it was noted that drifted snow has a slightly higher reflectance, particularly at some wavelengths, than other snow samples which have otherwise "aged" to approximately the same density, thereby indicating the probable influence of the smaller particle size on the resultant reflectance.

Evidence that the spectral reflectance of snow may be preferentially affected by rather slight changes in the crystal structure of the snow may be inferred from Figures 10a and 10b. The reflectance of a freshly fallen snow (composed predominantly of spatial dendritic crystals with plate-like branches) is shown in Figure 10a. Figure 10b shows the reflectance of the same snow after slight aging was revealed microscopically by some loss of crystal detail. From a comparison of the two figures, it appears that, although the reflectance decreased at all angles, the diffuse reflectance deteriorated considerably more than did the specular component.

SUMMARY

Many factors influence the red and near-infrared spectral reflectance of snow. The principal parameters affecting the spectral reflectance, particularly in a natural meteorological environment, are so interrelated as to defy precise definition of the role of individual factors.

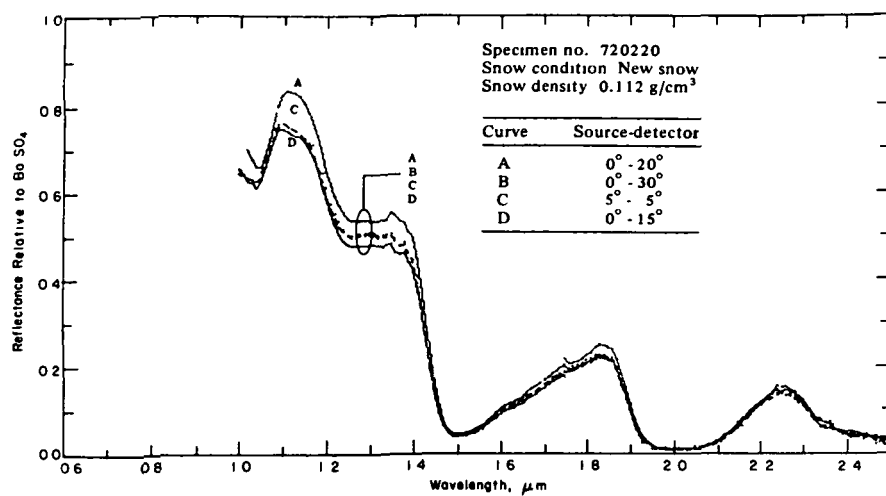


Figure 10a. Comparison of angular reflectances of snow.

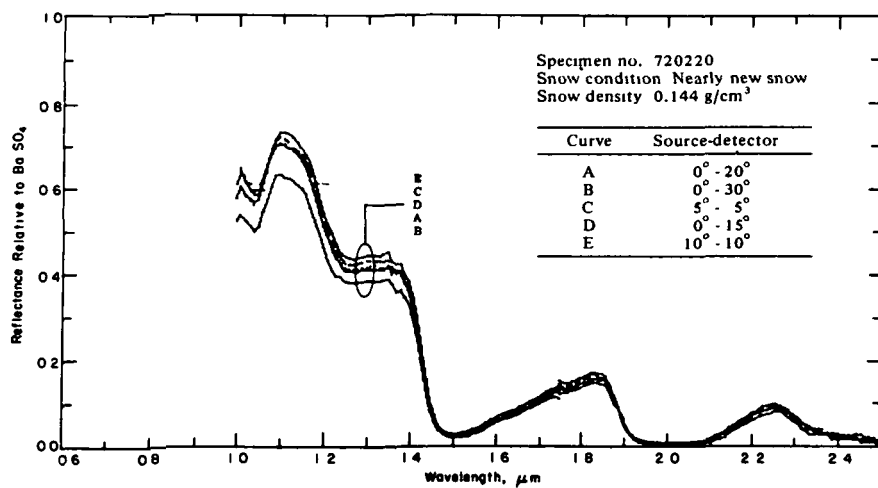


Figure 10b. Comparison of angular reflectances of snow.

Because of the polydisperse crystal shapes, sizes, and orientations which occur in a natural fresh snowfall, together with the innumerable possible sequences of natural aging to which the snow may be subjected, it is much simpler (and perhaps as valuable from a practical standpoint) to formulate some general conclusions concerning the spectral reflectance of fresh snow and the reflectance changes that take place during several types of natural aging.

1. Fresh snow has a very high reflectance in the visible red region. The spectral reflectance falls off sharply in the near-infrared wavelengths and is strongly related, inversely, to the spectral absorption coefficients of ice (Fig. 3, curve A).

2. Snow which has aged under cold conditions, with normal settling and densification, shows a slight decrease in red reflectance and moderate decreases in infrared reflectance (Fig. 3, curve B).

3. Snow which has drifted under cold conditions, and become densified to some degree by wind-compaction, also exhibits a slight decrease in red reflectance and moderate decreases in infrared reflectance (Fig. 15). However, compared with cold aged snow which has not been wind-blown but which has achieved equivalent densification by natural settling, the drifted snow tends to have a slightly higher reflectance, particularly near 1.8- μm and 2.2- μm wavelengths (compare Fig. 3 and 8).

4. Snow which is even slightly melting, when compared with nearly fresh cold snow, has a distinctly lower reflectance in the red region and an even more pronounced decrease in infrared reflectance generally. There is an exception, however, in that the reflectance may stay nearly the same as that of fresh snow (or even increase slightly) in the 1.9 to 2.0- μm wavelength region (Fig. 5,6).

5. Refreezing of snow which has previously been exposed to melting temperatures has a relatively minor effect, resulting in a reflectance curve generally resembling that of the melting snow. Refreezing may, however, cause an increase of reflectance relative to that of melting snow at wavelengths near 1.4 μm and 2.1 μm (Fig. 6,5).

6. The specular reflectance of ice-glazed crust is spectrally similar to that of refrozen snow in the 1.00 to 1.40- μ m range. The ice glaze reflects fairly uniformly from 1.00 to 2.50 μ m with gradual diminution of reflectance and just the suggestion of a minor peak in reflectance around 1.9 μ m (Fig. 7). Unfortunately, the diffuse component of reflection from the ice-glazed crust was not studied.

7. Measurements of snow reflectance at various angles indicate that for light fresh snows, with the source normal to the snow surface, the spectral reflectance generally increases slightly with increasing detector angles between 15 and 30°. The reflectance at 5° -5° and 10° -10° is slightly less (Fig. 9-10b). For aging snow, results are erratic, presumably due to the variety of microstructural changes involved in the aging process.

8. The red and infrared spectral reflectance has a significant inverse correlation to snow density. Since densification is the result of many of the natural aging phenomena, it is probable that this correlation is the result of many concomitant influences.

REFERENCES

1. O'Brien, H.W. and R.H. Munis (1975) Red and near-infrared reflectance of snow. U.S. Army Cold Regions Research and Engineering Laboratory (USACRREL) Research Report 332. (ADA007732).
2. Dunkle, R.V. and J.T. Bevens (1956) An approximate analysis of the solar reflectance and transmittance of a snow cover. Journal of Meteorology, vol. 13, April, p. 212-216.
3. Middleton, W.E. Knowles and A.G. Mungall (1952) The luminous directional reflectance of snow. Journal of the Optical Society of America, vol. 42, no. 8, p. 572-579.

REMOTE SENSING OF SNOWPACK DENSITY USING SHORTWAVE RADIATION

Michael C. McMillan, *NOAA, National Environmental Satellite Service, Washington, D. C. 20233*; James L. Smith, *USDA Forest Service, Pacific Southwest Forest and Range Experiment Station, Berkeley, California 94701*

ABSTRACT

Albedo or satellite radiance measurements can be used to estimate average snowpack density by means of a multiple linear equation. The in situ data equation predicted density with a correlation (r^2) of 0.79 and a standard error of 0.027 gm cm^{-3} . The data from LANDSAT-1 were not as significant in a similar equation, possibly because of the large field of view.

INTRODUCTION

Current research on remote sensing of snowpack parameters, other than of areal extent, is largely centered in the microwave and gamma-ray portions of the electromagnetic spectrum. It appears possible, however, to use measurements in the shortwave region to estimate snowpack density statistically. In situ measurements at the Central Sierra Snow Laboratory and remote observations from the LANDSAT-1 spacecraft show the possibility of estimating average snowpack density with albedo or radiance measurements, respectively.

Snow courses and related instruments are the current source of snow water equivalent data used in streamflow and flood prediction equations. Snow water equivalent may be remotely obtained from pressure pillows (Beaumont, 1965) and from the horizontal-type radioisotope snow gage (Peck, 1972). Depth, density, and water equivalent may be obtained from a profiling nuclear snow gage (Smith, Halverson, and Jones, 1972). Only a limited number of these remotely-operated snow sensors can be deployed in an area because of the high cost of installation and operation.

To meet the increasing demands on the snow water resource requires more accurate streamflow estimates than those now being obtained through conventional snow survey methods. Streamflow estimates can be improved by increasing the sampling frequency temporally and spatially at a more reasonable cost than that associated with remote operation of snow sensors. This paper suggests a method for accomplishing this task. The method is based upon measurement of snow albedo from either aircraft-mounted or spacecraft-mounted radiometers, and the relation of these readings to point estimates of snowpack average density at certain sites. The necessary additional data would be obtained

from the already established network of hydrometeorological stations where such data as temperature, precipitation, and snow depth, density, and water equivalent are currently monitored, or from a small number of new instrumented sites.

SELECTED LITERATURE REVIEW

The use of albedo measurements to monitor the physical condition of snow has been suggested in several previous studies. In 1956, Dunkle and Bevens wrote that their analysis of the reflectance and transmittance of snow would be of value in correlating albedo measurements with the physical characteristics of snow. Mil'kis (1956) published equations and resulting nomograms for finding snowpack density and albedo knowing elevation and date. Although Mil'kis emphasized that the density was given merely to characterize the state of the snow, his equations could be combined to estimate density knowing albedo. Giddings and LaChapelle (1961) found reflectance depends on the area of ice-to-air interface per unit volume of snow. They suggested "the possibility of following metamorphic changes in snow by optical methods without disturbing the naturally occurring processes." Experiments on the extinction coefficients of visible light ($.4-.7\mu\text{m}$) through snow as a function of density, grain size, and wavelength are presented in Mellor, 1965. One of his conclusions was remote sensing might be used to detect subtle differences within the snowpack since the magnitude and wavelength of reflectance vary with snow type. Bergen (1970, 1971) also found a relation between the extinction coefficient and snow density and grain size. His experiments with CdS cells ($.45-.90\mu\text{m}$) settled within the snowpack agree with the correlation between transparency of snow and its air permeability and density suggested by the model of Dunkle and Bevens (1956). In 1974, Bohren and Barkstrom published a study on the theoretical optical properties of snow. Their calculations indicate very little (less than 5%) reflection takes place at an ice grain's surface; most radiation is internally transmitted. Hence, the results of remote observations of the snowpack would be dependent upon the snow's internal structure. Bohren and Barkstrom's calculations also indicate albedo under diffuse illumination should be independent of density and proportional to the square root of grain size. Snowpack remote sensing using shortwave radiation from spacecraft, however, is restricted to the non-diffuse condition of cloud-free weather. Further, an empirical relationship should exist between grain size and density since the two are related. Recently, O'Brien and Munis (1975) studied the spectral reflectance of snow from 0.6 to $2.5\mu\text{m}$. Their measurements indicate a reduction in the reflectance results from the combination of densification and increased particle size that occurs with aging. In addition, O'Brien and Munis related various snow sample densities at wavelengths of 1.0 , 1.1 , 1.3 , 1.8 , and $2.4\mu\text{m}$ to their corresponding reflectances. They reported, "In each case, the decrease in reflectance with density showed about a 0.8 correlation at the

METHOD

In Situ Study

The relationship between albedo and snowpack density was investigated at the Central Sierra Snow Laboratory at Soda Springs, California. The Laboratory is a field station of the U.S. Forest Service, Pacific Southwest Forest and Range Experiment Station, and is located just to the west of the crest of the Sierra Nevadas at an elevation of 2100 m.

Measurements were compiled for the 1969-1970 through 1971-1972 snow seasons. For the three seasons, 553 pairs of average density and concurrent snow albedo measurements were taken. Some days during each season were excluded. These included days on which storms were in progress, days following precipitation events of less than 7 mm water equivalent, and days when snow density measurements were not taken.

The dependent variable, average snowpack density, was measured with the isotopic profiling snow gage (Smith, Halverson, and Jones, 1972). Average snowpack density is the average of 1 cm incremental densities from the soil surface to the snow-air interface. Density determinations by this method have a standard error near $.01 \text{ gm cm}^{-3}$.

Snow surface albedo measurements were taken with two pyrhelimeters (0.3-4.0 μm) situated 1 m above the snow surface, one mounted in the normal position and the second inverted. Decimal albedo determinations were made at half-hour intervals for three hours before or after the snow density measurements.

Developing a relationship to predict average snowpack density requires some information beyond albedo. Additional variables included the date of measurement, number of days since the last storm, and the type of precipitation in the last storm.

The rate of new snow densification and the density of the existing snowpack vary throughout the snow season. Late season snowpacks are denser than early season packs and new snow metamorphosis proceeds faster in late season. The date was expressed in the equations as solar declination, the angular displacement of the Sun north (+) or south (-) of the celestial equator. Solar declination can be found in annual tables provided in several Naval Observatory publications (1975a or 1975b).

The type of precipitation affects the average density of the resulting snowpack. Winter precipitation may not be snow-fall; it may be all rain or rain-and-snow mixed. A rain-on-snow event results in a rapid decrease in albedo and a rapid increase in density. Storms were coded into three groups: snow only, mixed snow and rain, and rain only. The precipitation type was then assigned the value 0, 0.5, or 1.0, respectively.

The several variables which appeared important were

combined into a functional expression

$$RHO = f(A, SD, D, R)$$

in which

RHO = average snowpack density (decimal)
A = albedo (decimal)
SD = solar declination (degrees)
D = days since cessation of storm (integer)
R = proportion of rain to snow in last storm
(0, 0.5, 1.0)

For a more complete description of the initial study as well as a study on areal snowpack variation, see Halverson and Smith (in process).

Cloud cover can significantly affect the shortwave radiation balance over snow (Ambach, 1974). The diffuse radiation normally present under overcast skies becomes even more uniform when over a snow surface (Fritz, 1955). To investigate the influence of cloudiness on the albedo correlation, the data were divided into three sets. The classification was based on average daily cloud cover as reported by the nearby Blue Canyon weather service office (NOAA, 1972). Days on which 0 to 2 tenths cloud cover were reported were considered clear days, 3 to 7 tenths were considered partly cloudy, and 8 to 10 tenths cloud cover days were classified as overcast.

LANDSAT Study

Regression methods were also applied to the spacecraft data (McMillan, 1975). Terrestrial radiance values over snow courses in the American River Basin, California, were obtained from the multispectral scanner subsystem (MSS) onboard the LANDSAT-1 satellite. Data from MSS band 7 (0.8-1.1 μ m) were chosen to avoid the problem of saturation of the sensor. A description of the satellite sensors and orbital parameters can be found in General Electric Corporation, 1972.

Digital radiance data from the MSS were obtained from LANDSAT computer tapes in unrectified, contoured 32 by 32 pixel arrays. These arrays were combined into a large map of the study area. Topographic maps (1:24,000 scale), with snow-course locations indicated, were optically enlarged, superimposed, and registered over the data arrays. The highest pixel value corresponding to the snow course location was recorded.

A variable to normalize the satellite radiance values for differing irradiance levels was needed. The potential solar insolation at each snow course was computed using the method of Frank and Lee (1966). Slope and aspect data were determined from the topographic maps.

Snowpack density is affected by temperature (Corps of Engineers, 1950). The sum of average daily air temperature above freezing since snowfall was included as a variable in this study,

and was computed from data given in the monthly Climatological Data Summaries (NOAA, 1973). Data from the Tahoe Valley airport weather station, located near the snow courses, were used.

Snowpack density measurements were provided by the California Cooperative Snow Survey. Data from eight snow courses in the southeastern portion of the American River Basin were used. Only those locations and dates having a minimum of 60 cm of snow were considered. Table 1 lists the snow courses and their elevations.

Since density measurements were normally taken during the first part of the month and the spacecraft has an 18-day revisit cycle, the density had to be adjusted to the date of satellite overpass. This was accomplished by interpolation weighted according to the daily average temperature.

Data from four satellite passes were obtained. The dates of these passes, covering the snowmelt period, were March 16, April 3 and 21, and May 9, 1973. Light, scattered cumulus clouds on April 21, prevented data retrieval from some snow courses.

Snowpack density is known to vary with elevation. High elevation snowpacks densify at a slower rate than low elevation snowpacks. A term representing snow-course elevation was included in the equation. These values also acted as a counter, having the same value per snow course on different dates.

These variables were combined into a functional expression

$$\text{RHO} = f(\text{RAD}, \text{SD}, \text{DEG}, \text{I}, \text{E})$$

in which the undefined terms are

RAD = satellite radiance (integer)

DEG = sum of average daily air temperature above
freezing since snowfall (degrees, F)

I = potential solar insolation (decimal)

E = snow course elevation (meters)

RESULTS

The analyses were performed using a stepwise linear regression (IBM, 1970), a statistical technique for analyzing a relationship between a dependent variable and a set of independent variables. The criterion of importance is based on the reduction of sum of squares. In the equations that follow, the independent variables are listed in their order of importance. Regression coefficients and their significance for all equations are given in Tables 2 through 6.

In Situ Study

Initial graphical analysis showed albedo to be a predictor of average snowpack density, but the relationship was not linear. The square of albedo showed a better fit, and it was adopted for future analysis.

The equation using in situ data for all cloud conditions

is:

$$\begin{aligned} \text{RHO} = & .00323\text{SD} + .00193\text{D} + .0279\text{R} \\ & - .0756\text{A}^2 + .412 + \text{error}. \end{aligned} \quad (1)$$

The multiple correlation coefficient (r^2) is 0.79, with a standard error of estimate of 0.027 gm cm^{-3} , for 548 degrees of freedom.

The equation using in situ data for overcast conditions is:

$$\begin{aligned} \text{RHO} = & .00325\text{SD} - .123\text{A}^2 + .0334\text{R} \\ & + .00145\text{D} + .436 + \text{error}. \end{aligned} \quad (2)$$

The multiple correlation coefficient is 0.79, with a standard error of estimate of 0.031 gm cm^{-3} , for 159 degrees freedom.

LANDSAT Study

Potential insolation term, I, was not significant in reducing the sum of squares. Although there is a slight dependence of density on snow course slope and aspect, this term may be more important in future equations by combining with satellite radiance in a suitable algorithm.

The equation using remote data is:

$$\begin{aligned} \text{RHO} = & .00125\text{DEG} + .00243\text{SD} + (2.93 \times 10^{-6})\text{E} \\ & - (2.96 \times 10^{-6})\text{RAD} + .339 + \text{error}. \end{aligned}$$

The multiple correlation coefficient is 0.92, with a standard error of estimate of 0.016 gm cm^{-3} , for 23 degrees of freedom.

The computed t-values indicated each variable in the in situ study was significant above the 99 percent level (t_D greater than $t_{.01}$). This means there is less than 1 chance in 100 that any variable could be dropped from the equation because it is not significantly different from zero. The t-values associated with the LANDSAT variables indicate significance at varying levels of confidence. Variables other than satellite radiance were significant at the 75 to 95 percent level. The radiance t-value fell slightly below the 60 percentile.

DISCUSSION

An empirical relationship among average snowpack density, albedo, and various other site and storm variables does exist. The average snowpack density can be estimated from albedo measurements when general site and storm information are available. Snow albedo can be measured from aircraft (Bauer and Dutton, 1962). Because of cost, 1 or 2 samples would be measured rather than the traditional 10 points on a snow course. Similarly, Leaf and Kovner (1972) recommend fewer sample points per snow course, 1 or 2 versus 10, and a greater distribution of snow sampling areas within a watershed. Increasing the number of snow courses is difficult and costly when it increases foot travel or telemetered

equipment, but is relatively easy to do when the information can be obtained remotely from aircraft or spacecraft.

Equation 1 is mainly a predictive equation, the date and days since snowfall reducing the majority of the sum of squares. Under overcast conditions (equation 2), the albedo term is more significant than during either partly cloudy or clear conditions. On the basis of these equations, it would appear aircraft-borne radiometers should be flown under the diffuse conditions of overcast skies to maximize the contribution of the albedo term.

The results of the satellite data regression (equation 3) were mixed. Although the correlation and standard error were favorable, the satellite radiance term was significant at only the 60 percent level. This low significance could result from several factors. The instantaneous field of view of the MSS is 0.64 ha (1.6 acres). Undoubtedly, the area covered by each pixel integrated snow and non-snow objects (vegetation, shadows) which decreased the radiance from the true snow value. Also, if a concerted effort were made to obtain snow course data on the date of satellite overpass, the error associated with the snow course density interpolation could be removed.

The launch of the next satellite in the LANDSAT-series (LANDSAT-C) will enable satellite data to be obtained with one-quarter the field of view of present LANDSATs. A Return Beam Vidicon camera system onboard this future satellite will have an instantaneous field of view of only 0.16 ha (0.4 acres). This should decrease the possibility of viewing snow and non-snow objects simultaneously.

There is an error associated with the predicted variable in any linear regression technique. The standard error in this study ranged from 0.016 gm cm^{-3} (1.6 percent density) to 0.031 gm cm^{-3} (3.1 percent density). According to Work et al. (1956), the slotted Federal Sampler overmeasures water equivalent by 7 to 12 percent. Although it is difficult to convert errors in snow water equivalent to errors in density because of the influence of depth, it appears that snow density measurements are high by about 0.040 gm cm^{-3} . An additional source of error is present with snow tube data; the Federal Sampler always overestimates density, so the errors are not normally distributed about the true snow density. In contrast, average density estimates based on the discussed equations are better distributed around the true snow density.

CONCLUDING REMARKS

Using albedo and general site and storm information to estimate average snowpack density shows promise as an alternative to establishment of additional conventional snow survey courses in supplying data for water supply forecasting. Errors associated with this statistical method are equivalent to those from the traditional snow survey measurement. Areal water equivalent can be more accurately estimated by this method since measurements are taken in more sections of the watershed.

The results of the in situ study at the Central Sierra Snow

Laboratory suggest the immediate application of aircraft-mounted radiometers to obtain albedo data for use in estimating average snowpack density. The results of the LANDSAT study, however, are not as acceptable for immediate use in the Sierra Nevadas. Satellite data may be applicable, though, in the broad flat regions of the Midwest. Similarly, data from the visible channel of the NOAA-series environmental satellites may be useful in equations for major river basins of the Midwest or Canadian Plains.

The regression equations presented are empirical relationships. Coefficients may need re-evaluation if they are applied to areas where the snow maturation process is different from that near the American River Basin, California.

REFERENCES

- Ambach, W., 1974, The Influence of Cloudiness on the Net Radiation Balance of a Snow Surface with High Albedo, J. of Glaciology, Vol. 13, no. 67, pp. 73-84.
- Bauer, Kenneth G. and John A. Dutton, 1962, Albedo Variations Measured from an Airplane over Several Types of Surface, J. of Geophys. Res., Vol. 67, no. 6, pp. 2367-2376.
- Beaumont, R.T., 1965, Mount Hood Pressure Pillow Snow Gage, J. Applied Meteo., Vol. 4, no. 5, pp. 626-631.
- Bergen, James D., 1970, A Possible Relation between Grain Size, Density, and Light Attenuation in Natural Snow Cover, J. of Glaciology, Vol. 9, no. 55, pp. 154-156.
- Bergen, James D., 1971, The Relation of Snow Transparency to Density and Air Permeability in a Natural Snow Cover, J. of Geophys. Res., Vol. 76, no. 30, pp. 7385-7388.
- Bohren, Craig F. and Bruce R. Barkstrom, 1974, Theory of the Optical Properties of Snow, J. of Geophys. Res., Vol. 79, no. 30, pp. 4527-4535.
- Corps of Engineers, 1950, Albedo of the Snow Surface as Related to Weathering Factors and Stage of the Season, Corps of Eng.-Weather Bureau Cooperative Snow Invest. Res. Note PSDGC 206-50, San Francisco, Calif., 25 pp.
- Dunkle, Robert V. and J.T. Bevans, 1956, An Approximate Analysis of the Solar Reflectance and Transmittance of a Snowcover, J. of Meteo., Vol. 1, no. 2, pp. 212-216.
- Frank, Ernest C. and Richard Lee, 1966, Potential Solar Beam Irradiation on Slopes, USDA Forest Service Res. Paper RM-18, Fort Collins, Colo., 116 pp.
- Fritz, Sigmund, 1955, Illuminance and Luminance under Overcast Skies, J. Optical Soc. America, Vol. 45, no. 10, pp. 820-825.
- General Electric Corp., 1972, Data Users Handbook, NASA-Goddard Space Flight Center, Doc. no. 71SD4249, Greenbelt, Maryland, 225 pp.
- Giddings, J.C. and E. LaChapelle, 1961, Diffusion Theory Applied to Radiant Energy Distribution and Albedo of Snow, J. of Geophys. Res., Vol. 66, no. 1, pp. 181-189.
- Halverson, Howard G. and James L. Smith, in process, Snowpack Density Estimation by Non-Contact Methods, USDA Forest Service, Berkeley, Calif., 20 pp. To appear in Water Resources Res.

IBM, 1970, System/360 Scientific Subroutine Package Version III, Programmer's Manual GH 20-0205-4, Fifth Edition, White Plains, New York, 454 pp.

Leaf, Charles F. and Jacob L. Kovner, 1972, Sampling Requirements for Areal Water Equivalent Estimations in Forested Subalpine Watersheds, Water Resources Res., Vol. 8, pp. 713-716.

McMillan, Michael C., 1975, Preliminary Snowpack Density Observations from Landsat-1, abs., EOS, Transactions AGU, Vol. 56, no. 6, p. 359.

Mellor, Malcolm, 1965, Optical Measurements on Snow, US Army Cold Regions Res. and Eng. Lab., Res. Report 169, Hanover, New Hampshire, 19 pp.

Mil'kis, B.E., 1956, Calculating the Albedo and the Density of Thawing Snowbeds, translated from Russian, 13 pp. Available from: Clearinghouse for Federal Scientific and Technical Information (NTIS), Springfield, Va., Acc. no. TT 65-50029.

NOAA, 1972, Local Climatological Data, Blue Canyon WSO, Nat. Oceanic and Atmos. Admin. (various months in 1969 through 1972), Nat. Climatic Center, Asheville, North Carolina.

NOAA, 1973, Climatological Data, California, Nat. Oceanic and Atmos. Admin., Vol. 77, nos. 4-6, Nat. Climatic Center, Asheville, North Carolina.

O'Brien, Harold W. and Richard H. Munis, 1975, Red and Near-Infrared Spectral Reflectance of Snow, US Army Cold Regions Res. and Eng. Lab., Res. Report 332, Hanover, New Hampshire, 18 pp.

Peck, Eugene L., 1972, Methods of Measuring Snow Cover, Snowmelt, and Streamflow under Winter Conditions, Proceedings Symposium-The Role of Snow and Ice in Hydrology, IAHS-AISH Pub. No. 107 Vol. 1, pp. 582-597, WMO, Geneva, Switzerland.

Smith, James L., Howard G. Halverson, and Ronald A. Jones, 1972, Development of a Radioactive Isotope Profiling Snow Gage, U.S. Atomic Energy Comm., 86 pp. Available from: NTIS, Springfield, Va., Acc. no. TID 25987.

U.S. Naval Observatory, 1975a, The American Ephemeris and Nautical Almanac, U.S. Government Printing Office, Washington, D.C., 520 pp.

U.S. Naval Observatory, 1975b, The Air Almanac, U.S. Government Printing Office, Washington, D.C., 490 pp.

Work, R.A., Homer J. Stockwell, T.G. Freeman, and R.T. Beaumont,
1965, Accuracy of Field Snow Surveys, Western United States
including Alaska, US Army Cold Regions Res. and Eng. Lab., Tech.
Rep. 163, Hanover, New Hampshire, 43 pp.

TABLE 1

Snow Courses used in LANDSAT Study

Snow Courses	Elevation (m)
Alpha	2320
Echo Summit	2270
Lake Audrain	2230
Darrington	2160
Wrights Lake	2100
Phillips	2070
Lyons Creek	2040
Tamarack Flat	2000

TABLE 2

Linear Regression Coefficients and t-Values
All Cloud Conditions

Variable	Value	t_b	$t_{.01}$
SD	.00323	24.57	2.58
D	.00193	11.03	2.58
R	.0279	9.50	2.58
A ²	-.0756	-7.57	2.58
intercept	.412		

degrees of freedom = 548 $r^2 = 0.79$ standard error of estimate = 0.027 gm cm^{-3}

TABLE 3

Linear Regression Coefficients and t-Values
Clear Conditions (0/10-2/10)

Variable	Value	t_b	$t_{.01}$
SD	.00321	12.02	2.58
D	.00254	7.95	2.58
R	.0257	4.67	2.58
A ²	-.0617	-3.31	2.58
intercept	.401		

degrees of freedom = 218 $r^2 = 0.75$ standard error of estimate = 0.028 gm cm^{-3}

TABLE 4

Linear Regression Coefficients and t-Values
Partly Cloudy Conditions (3/10-7/10)

Variable	Value	t_b	$t_{.01}$
SD	.00330	17.42	2.60
D	.00162	6.32	2.60
R	.0239	5.92	2.60
A^2	-.0412	-2.89	2.60
intercept	.402		

degrees of freedom = 161 $r^2 = 0.84$

standard error of estimate = 0.022 gm cm^{-3}

TABLE 5

Linear Regression Coefficients and t-Values
Overcast Conditions (8/10-10/10)

Variable	Value	t_b	$t_{.01}$
SD	.00325	12.67	2.60
A^2	-.123	-6.63	2.60
R	.0334	5.48	2.60
D	.00145	4.01	2.60
intercept	.436		

degrees of freedom = 159 $r^2 = .79$

standard error of estimate = 0.031 gm cm^{-3}

TABLE 6

Linear Regression Coefficients and t-Values
LANDSAT Study

Variable	Value	t_b		
DEG	1.25×10^{-3}	2.23	$t_{.05} =$	2.07
SD	2.43×10^{-3}	1.25	$t_{.20} =$	1.32
E	2.93×10^{-6}	1.13	$t_{.30} =$	0.86
RAD	-2.96×10^{-6}	0.49	$t_{.40} =$	0.53
intercept	.339			

degrees of freedom = 23 $r^2 = .92$

standard error of estimate = 0.016 gm cm^{-3}

SNOW WETNESS MEASUREMENTS FOR MELT FORECASTING

William I. Linlor, *Ames Research Center, NASA, Moffett Field, California*; Fred D. Clapp, *Consultant, University of California, Berkeley, California*; Mark F. Meier, *U. S. Geological Survey, USDI, Tacoma, Washington*; James L. Smith, *U. S. Forest Service, USDA, Berkeley, California*

ABSTRACT

A microwave technique for directly measuring snow pack wetness in remote installations is described. The technique, which uses satellite telemetry for data gathering, is based on the attenuation of a microwave beam in transmission through snow.

INTRODUCTION

The water-equivalent of snowpacks represents an important resource. In California, for example, the Sierra Nevada snowpack provides more than half of the total water supply and about one-third of the electric energy. For the western United States in 1972, Federal Power Commission records show that a total of 1.7×10^{11} kWhr of electricity were generated by hydroelectric stations. A barrel of oil burned in the best central station produces 650 kWhr, so the hydroelectric energy is equivalent to 2.62×10^8 barrels of oil. At a cost of \$10 per barrel, this represents \$2.62 billion. Efficient operation of hydroelectric installations requires maximum head consistent with avoidance of spilling water if sudden inflows should occur. Effective management of water resources for power generation, irrigation, domestic use, and many other applications including flood control, is evidently dependent on adequate knowledge on a timely basis of the snowpack characteristics.

The amount of stored water is obtained from snow course sample measurements of depth and weight, with additional information from automatic instrumentation such as pressure pillows and gamma-ray density profilers. However, the time of snowpack melting and related water discharge rates involves ripening and wetness of snow; at present, this information is obtained indirectly from such quantities as heat input factors and temperature index measurements.

The purpose of this paper is to summarize water runoff forecasting under snowmelt conditions, and to discuss the importance of including measurement information of snow wetness. For background and convenient reference, brief reviews are given regarding the water-holding capacity of snow, present-day methods for measuring snow wetness, and the electromagnetic systems under development. The discussion of snowmelt runoff forecasting techniques

is necessarily quite simplified and contains no new information for the snow hydrologist; however, the review may be helpful to remote-sensing specialists who do not ordinarily come in contact with the problems of the operational water management specialists. An authoritative source of information regarding detailed aspects of water forecasting under snowmelt conditions is the monumental work, "Snow Hydrology," prepared by the U.S. Army Corps of Engineers (1956).

Although a standard nomenclature is emerging in snow hydrology literature, terms such as "water content" have varying meanings in current papers. To avoid possible ambiguity, definitions of terms for this paper are given in Appendix A. Two terms should be particularly identified: "water-equivalent" means the amount of water that would be obtained from the complete melting of a given volume of snow, regardless of whether the snow is initially dry or wet; "water-content" means the amount of liquid-phase water present in the snow, also known as "wetness."

WATER-HOLDING CAPACITY OF SNOW

Dry snow consists of ice crystals and air. The density of newly-fallen snow may be 0.1 gram/cm^3 or less; during the winter and spring months a variety of processes occur, producing snow density up to about 0.4 to 0.6 grams/cm^3 . It has generally been assumed that snow density must reach about 0.4 grams/cm^3 before melt water can begin to drain from the snowpack (Kittredge, 1948, and Bertle, 1965). However, as pointed out by Smith (1974) this is not always true. At the Central Sierra Snow Laboratory (CSSL) melt water has been observed to flow through the pack all winter long in most years, with density in various layers ranging from 0.2 to 0.7 grams/cm^3 .

Various values have been reported regarding the water-holding capacity of snow. Because of the importance of determining this quantity, and the divergence of views expressed in the literature, direct quotations from recognized authorities are given in Appendix B for convenient reference.

Snow Hydrology (1956) expresses the opinion that ripe snow has a liquid-water-holding capacity between 2 to 5 percent by weight, with the qualification that the lack of information on the capacity of snow to retain liquid water against gravity, as a function of some index of the stage of metamorphism, constitutes a major gap in knowledge of the storage effect of snow on runoff. The point is stressed that at times the snowpack may be similar to a vast "sponge," but that at other times the storage potential may become very small. At any given time the actual condition of the snow must be determined in order to evaluate the storage capacity.

A laboratory experiment by Garstka and co-workers has been reported by Bertle (1965) in which runoff from an artificially-wetted snow sample did not occur until the added-water reached 83 percent by weight, relative to the original dry snow.

According to Smith (1974), water-holding capacities for snow-packs from natural and simulated rain have been studied with the

profiling snow gage at CSSL. Density increases from water uptake and retention against the pull of gravity ranged from 0.03 gram/cm³ for matured snow, to over 0.20 gram/cm³; increase was directly related to the original density and wetness of the snow. Other studies by Smith et al. (1969) show that the amount of retained water in the normally isothermal (0° C) snowpacks of the Sierra Nevada appears to be related to a pore space function: the greater the density, the less the pore space size, and the greater the amount of water that can be held. Such results obtained at CSSL indicate that naturally occurring snowpacks can at times have a stored liquid-phase water as high as 30 to 40 percent by weight.

In recent review paper de Quervain (1972) reports that some authors have the opinion that liquid-phase water ranging from 1 to 6 percent is usually found in equilibrium with snow. However, de Quervain (1948) believes that a more realistic range is 5 to 25 percent, and Moskalev (1966) finds the upper limit to be as high as 55 percent. Wakahama (1968) reports snow layers with 20 to 30 percent liquid-phase water.

The importance of direct measurements of stored liquid-phase water, (water content) of the snowpack becomes evident from the foregoing information. Snowmelt water or rain on snow may be produced by sunny or stormy weather; in either event, when such water is present within the snowpack, accurate forecasts of the runoff rate are not possible unless the state of the snow wetness is known. If as much as 10 to 40 percent by weight is involved, it represents a major factor in the runoff rate, and may in such an event predominate over all other factors.

Those portions of the snowpack having essentially horizontal ice lenses may temporarily hold liquid water by ponding. Such a situation is unstable in the sense that an additional load can cause failure of the ice lenses or detention layers, resulting in rapid discharge of the ponded water. The additional load may be produced by rapid increase in melt water, or by a brief but intense rainfall.

An apparent example of the "triggering" action implied by the preceding paragraph was experienced at Bull Run, Oregon in December 1964. With a snowpack about 60 in. deep, a rainfall of about 2 in. was recorded, and hydrograph records from similar storms showed that the runoff should have occurred within 8 hr. Instead, it appeared to be delayed 24 hr. Subsequent rainfall apparently required only a few hours for its runoff to occur, based on the observed flow records. The peak streamflow was about twice the value expected from the rainfall intensity pattern. This episode is reported by Hydrocomp, Inc. (1974) with the statement: "It appears that Bull Run experienced a phenomenon of liquid water storage in the snowpack followed by a sudden release. The snowpack apparently collapsed much more rapidly than rates of snowmelt from heat balance would predict. Many other reports of this phenomenon are found in the literature."

The purpose of this paper as previously mentioned is a discussion of water runoff forecasting under snowmelt conditions, aided by direct measurement information of snow wetness. We shall review and summarize four basic procedures, although in any operational situation these may be combined in various ways depending on the requirements for the forecast:

1. Historical normal
2. Index method
3. Water-balance method
4. Hydrologic models

An important distinction must be made between seasonal or annual runoff forecasts versus short-term runoff forecasts. The former is important in agricultural planning, irrigation schedules, filling and lowering of large reservoirs, and similar activities for which the time scale is months or longer. The short-term runoff forecasts are important in flood forecasting, reservoir operation for power production, and other applications for which the time scale is a few days. The latter situation is of primary interest in this paper.

Historical Normal

Historical records provide the simplest (and least dependable) basis for water runoff forecasting. For example, the forecast for a selected time interval in the future is likely to be similar to the average runoff for the same time interval during the past 10 years (or more). Some idea of the expected range within which the actual runoff value will occur can also be obtained from the distribution of historical values. These approximate statements can of course be refined by statistical treatment for more precise expressions involving probability values.

Index Method

The index method is based on correlations of historical records of runoff with indexes of important determinants of runoff for the area under consideration. An adequate number of years for the measurements is essential to establish the relationships, known as regression functions. The forecasting procedures may be based on combinations of statistical and graphical correlations, relating the means and deviations of the measured index values with the actual subsequent runoff.

The index method of forecasting has been used for many years by the California Cooperative Snow Survey Program. Brown (1974) states: "Each major river basin whose runoff is to be forecasted has several discrete 'points' in the form of snow courses, where several months each winter the water equivalent of the snowpack at that location is measured. After several years a statistical relationship is built up which relates the water equivalent at that point and the other points in the basin at any given time of

measurement to the runoff to be expected from that basin. Thus, the collective measurements of water equivalent at several snow courses within and adjacent to a basin provide an 'index' to the anticipated April-July runoff. The actual forecasting procedures take into account other factors, in addition to the water equivalent of the snow, such as antecedent precipitation and cumulative runoff from the beginning of the Water Year up to the date of the forecast. Precipitation in future of the forecast is assumed to be equal to the historical normal for those months in the forecast period beyond the date of the forecast."

For the index method of forecasting, determinants in addition to the water equivalent provide useful information. These include, for example: (1) area of snow cover; (2) accumulated heat supply, such as degree-days, to be discussed later; and (3) low-elevation winter streamflow. A graphical method of determining the effect of several variables on runoff is the "coaxial method" described by Linsley et al. (1949). Multi-variable statistical procedures can also be employed.

We suggest that measurement of snow wetness at selected sites should receive consideration as one of the determinants, particularly in areas where melt or rain-on-snow events may occur throughout the snow season. Because of expected rapid changes in wetness levels, automatically operated instrumentation in remote stations appears to be desirable.

Water-Balance Method

Runoff forecasting with the water-balance method consists of evaluating each of the major components of an input-output equation and summing them algebraically. If all factors are evaluated correctly, the total input to a basin must equal the total output. Water input to a selected basin is represented by total snow accumulation plus total rainfall during the time interval of interest. For that same time interval the water output includes losses, storage, and runoff for the basin. The losses may occur by evaporation, sublimation, transpiration, and similar effects; the storage includes the change in snowpack water equivalent, which can be either positive or negative, and ground-water storage including soil moisture. Basin runoff includes mainly streamflow. If water flow in underground channels is appreciable, it must also be included (by measurement or estimate), as a part of the basin runoff.

The distinguishing feature of this procedure is that index values are not used, but rather the effect of each major factor on runoff is evaluated separately, in accordance with its actual value. Because of the large amount of data input that is required, the water-balance method is useful mainly for highly instrumented, relatively small basins. The value of the water-balance method is the assurance that all major factors have been properly assessed — otherwise the input-output equation would not add algebraically to zero. Although historical data are used in the development of the method, the forecast of runoff is based upon an appraisal of each

component for the time interval desired, rather than upon the effect produced by a given set of conditions in past years.

As suggested for the index method, measurement of snow wetness should receive consideration in the water-balance method as one of the contributing factors. For example, an increase in snow wetness may account for storing rainfall input; a decrease in snow wetness may produce a (runoff) output. Changes in snow wetness, alternatively, may have no effect on input or output, but instead may represent the integrated effect of heat exchange with the surroundings. Field measurement data are necessary to evaluate the relationship between snow wetness and basin water balance. Such measurements should be made automatically, repetitively in time, without impairing the snowpack, over representative areas of the basin.

Hydrologic Models

Simply stated, a hydrologic model represents a technique for mathematical simulation of physical processes or relationships. Modern computer technology makes practical the accompanying extensive numerical calculations. The mathematical model can include all of the techniques so far discussed: historical relationships, index data, or actual input-output information can be utilized, together with meteorological predictions. If some of the information has elements of uncertainty, the numerical values supplied to the mathematical model can be altered in successive runs to demonstrate the net effect.

The hydrological model can simulate daily, weekly, or seasonal flow from a basin or watershed, utilizing a host of hydrologic and meteorologic parameters. Reservoir storage and maximum-efficiency hydroelectric power generation can be scheduled on the basis of predicted stream flows, with the constraint that flood-risk situations must be avoided.

Snow wetness data can readily be included in a hydrologic model. The snowpack water equivalent represents a special type of reservoir storage, a component of which is the wetness that can act either in a positive (storage) or negative (release) fashion.

SNOWMELT RUNOFF RATE

The snowpack water equivalent represents the major portion of the annual water supply in many western U.S. watersheds. A review of the snowmelt process is useful in regard to understanding snow wetness and its measurement.

The rate of snowmelt runoff is dependent on the rate of heat supply. For snow at 0°C , 80 cal/cm^2 must be absorbed for each centimeter of liquid water produced, which can be recognized as being the latent heat of fusion of ice. The sources for such heat include net radiation absorbed, conduction and convection of heat from the ambient air, condensation of water vapor, heat supplied by rainfall, and conduction from the underlying earth.

A convenient resume of the theoretical aspects of heat input to a snowpack is given by Gray (1970, pp. 9.2-9.12). An extensive treatment is given in Snow Hydrology (1956, Chap. 5). To indicate the type of analysis that is necessary, an illustrative example is given in this paper of radiant energy interchange between the snowpack and its surroundings.

The amount of solar radiation effective in producing energy input to the snow is dependent on the reflectivity, or albedo, of the snow. For new snow almost 90 percent of the incident radiation is reflected; however, as the snow matures, its albedo can drop to 50 percent or less. The intensity of solar radiation above the earth's atmosphere perpendicular to a square centimeter is 0.14 W. For a "reasonably clear day" in March at 40° north latitude, the energy incident on a horizontal square meter during a 24-hr day is about 3.3 kWhr (Hildebrandt et al., 1972). Converting this into snowmelt equivalent, assuming an albedo of 50 percent, the liquid water produced is about 2 cm. Snow radiates in "black-body" fashion; the outgoing long-wave radiation at 0° C during 24 hr is equivalent to about 8.4 cm of (negative) melt. The atmosphere intercepts and re-radiates a portion back to the snow, the amount depending on the air temperature, atmospheric vapor pressure, and extent and type of cloud cover. With clear sky, and 0° C temperature for dewpoint, air, and snow, the net loss of heat by the snow during a 24-hr day caused by long-wave radiation is equivalent to about 2 cm of water (Linsley et al., 1958). Local conditions such as snow albedo and prevailing cloud cover represent significant factors in determining the radiative heat exchange of the snowpack. Other considerations exist in addition, such as variations in elevation, slope, aspect, forest cover, snow density and wetness, etc.

For rain-on-snow conditions, the heat interchange relations are complicated. Snow Hydrology (1956, page 326) states: "The computation of snowmelt during periods of significant rainfall is a problem quite different from the computation of melt during non-rain periods. Because of the generally overcast conditions, solar radiation has but a minor role in the melt scheme; longwave radiation losses are small, and at times there is even a net heat gain from this source. Because of the turbulent conditions which usually accompany rainstorms, convection and condensation melts are relatively large. In addition, fairly high vapor pressures result from the high relative humidities encountered in this situation, tending further to increase condensation melt."

It is evident that a heat-balance equation for predicting snowmelt is quite complicated; it would be of little point in this paper to consider the various heat-interchange processes in detail. Ideally, extensive instrumentation would be desired to provide field data for an operational heat balance analysis. This is not always necessary, because often the major heat balance terms can be estimated or found from correlations; that is, long-wave radiation exchange can be correlated with forest cover and cloudiness. The results do not replace instrumentation, but can be superior to degree-day calculations, which are discussed next.

Index factors for snowmelt rate are often useful. An index based on temperature has been given the name "degree-day" method. A degree-day is defined as a departure of one degree in mean daily temperature above freezing. A day whose mean temperature is 42° F thus has 10 degree-days. (Engineering units are employed, to avoid conversion from values given in the literature.) The term degree-day-factor (DDF) is defined to be equal to the inches of water melted from the snow per degree-day. The DDF varies with local conditions of weather, time of day, month, snow condition, altitude, etc. Index temperatures can be chosen to be maximum rather than mean values for a day, and base values can be chosen other than 32° F. As illustrative values, the DDF at the Central Sierra Snow Laboratory has been found to vary from 0.07 at the minimum melt station to 0.13 at the maximum melt station. These are averages for several years. Individual values for within-year periods exhibit a wide range of values.

It should be noted that these DDF values are obtained by correlating degree-days with measured changes in snowpack water equivalent. However, water content of the snowpack affects the results. For example, if the snowpack is initially dry, absorbed heat causes a certain amount of melting which we assume is retained by the snowpack. The water content is increased, but no change in water equivalent can be measured. For these conditions the incorrect conclusion could be made based on gravimetric data that the snowpack did not absorb heat. Thus it is evident that measurement of water equivalent or local runoff with lysimeters does not necessarily correspond to heat absorption or loss by the snowpack. Only under the condition that no changes in snow wetness occur does the measurement of water equivalent yield information regarding heat absorption.

Clearly a system to measure snow wetness directly, preferably a depth profile, would provide important information for snowpack water runoff predictions, because the wetness is the integrated result of the effects of temperature, radiation, local wind, etc., which produce heat transfer to the snowpack.

PRESENT-DAY INSTRUMENTATION FOR SNOW WETNESS MEASUREMENT

This section presents a summary of current instrumentation for measurement of snow wetness, and field tests of performance. The subsequent section describes systems under development.

Existing methods for obtaining snow wetness are based on three effects: calorimetric, centrifugal, and capacitive. The calorimetric method (Radok et al., 1956, and Yosida, 1966) is based on the temperature change of a heat reservoir necessary to melt (or freeze) a known quantity of wet snow. Hot water can be used for the melting process, or chilled gasoline for the freezing process. The centrifugal method (Langham, 1973) involves rotating a sample of wet snow to extract the water. The capacitive method (Ambach, 1966) yields the net dielectric constant of snow mixed with water, the latter contributing a relatively large dipole moment.

A comparative study of these three techniques was performed by Edgerton and Sakamoto (1970). They used a freezing calorimeter and two hot-water calorimeters; two centrifuges having 35 cm³ and 500 cm³ containers; and a capacitance meter designed by Ambach and Howorka (1966). A site on South Cascade Glacier, Washington, was selected because typically the snow cover on glaciers is relatively homogeneous, and thus allow a reasonably critical evaluation of the techniques.

The tests were performed on 7 and 8 August 1969 with snow grain sizes ranging from 0.5 mm to 1.5 mm; snow density was 0.52 gm/cm³ on 7 August and 0.57 on 8 August. Results are given in Table 1 and plotted in Fig. 1; snow wetness is given in percent by weight versus time.

TABLE 1.- SNOW WETNESS MEASUREMENTS IN PERCENT BY WEIGHT*

Date	Calorimeters					
	Freezing		Sakamoto		Combination (Yosida)	
	Avg.	Range	Avg.	Range	Avg.	Range
7 Aug. 1969	11.2	8.0-14.7	15.4	12.1-28.2	28.7	23.3-37.8
8 Aug. 1969	5.8	4.1- 7.9	9.3	3.7-28.0	15.7	7.3-22.7

Date	Centrifuge				Capacitive	
	500 cc		35 cc		Ambach	
	Avg.	Range	Avg.	Range	Avg.	Range
7 Aug. 1969	9.3	7.9-10.9	7.5	6.4-8.7	9.2	7.1-14.0
8 Aug. 1969	2.3	1.4- 4.7	---	---	0.6	0.0- 1.5

*Data from Edgerton and Sakamoto, 1970.

Edgerton and Sakamoto state: "Large variations in snow wetness were indicated by all techniques on consecutive measurements, and a comparison of results obtained with different instruments shows even larger differences between them. . . . This suggests that instrument accuracies are not sufficiently high and/or large natural variations of snow wetness within the snowpack exist."

The development of the density-profiling gage (Smith and Halverson, 1969, and Smith et al., 1972) has made possible accurate measurements of snowpack density profiles, and determination of changes that occur. Since the snow properties can be measured at the time of deposition, and regularly thereafter, the retention of any rain that may occur can be measured by changes in the density profile. Smith (1974) states: "Utilizing the water holding data so generated, and working with snow density profiles taken prior to rainstorms Smith et al., 1969, were able to successfully predict the amount of water snowpacks at CSSL could retain from rain-on-snow storms before water began draining from the snowpacks."

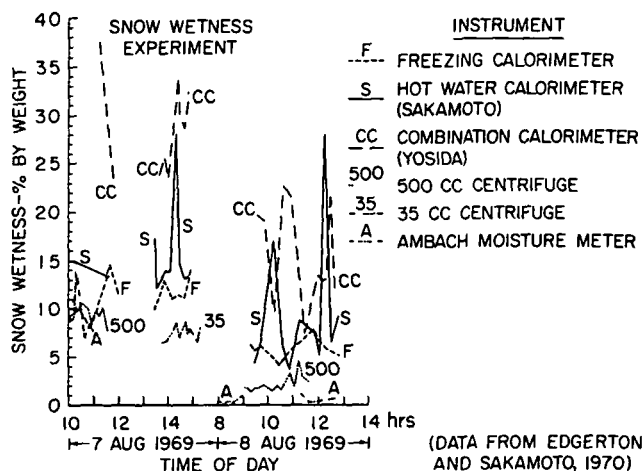


Fig. 1-Comparison of snow wetness instruments

SYSTEMS UNDER DEVELOPMENT FOR SNOW WETNESS MEASUREMENT

Three electrical methods for measuring snow wetness are being developed, for which descriptions have been given by Linlor and Smith (1974), Linlor et al. (1974) and Linlor et al. (1975):

1. Change in capacitance of a sample before and after freezing
2. "Quality factor" of a sample in a high-frequency field
3. Attenuation of a microwave beam in transmission through snow

These methods have been tested with natural snow at the Central Sierra Snow Laboratory, yielding results in accordance with theoretical predictions. Calibration of the systems requires elaborate procedures that are presently being developed. Our investigations have been expedited by the use of a host medium, foam polyurethane, whose properties can be readily controlled and are reproducible. Weight of a sample before and after adding water yields the volume percent wetness. Results can be expected to serve as a guide to the behavior of wet snow, because the basic interaction involves the liquid phase water rather than the host substance.

The capacitance of a given test unit is proportional to the net dielectric constant of the medium between the electrodes. For

dry snow — a mixture of air and ice — the factors that affect the net dielectric constant include (1) the individual dielectric constants of the air and the ice, (2) the relative proportions of each, (3) the temperature, (4) the oscillation frequency at which the measurements are made, and (5) the "form factor" (also called the "formzahl"), which depends on the shapes and orientations of the individual crystals of snow.

For wet snow, the situation is more complicated, even though the temperature is not a variable, being essentially 0° C. The dielectric constant of pure water at 0° C is 87.7, but when the water is in contact with snow crystals, intramolecular forces can affect the dipole moment of the water molecules. Nevertheless, the dielectric constant of snow is greatly increased by the presence of liquid-phase water, and this fact has been the basis for previous methods of determining snow wetness by Gerdel (1954) and Ambach and Denoth (1972).

The relative dielectric constant k^* has real and imaginary components k' and k'' , the latter also being known as the "loss factor." The ratio k'/k'' is known as the "quality factor" or Q .

$$k^* = k' + k'' \quad (1)$$

$$Q = k'/k'' \quad (2)$$

Change in Capacitance upon Freezing

The change in capacitance of a sample before and after freezing is directly related to the amount of moisture initially present. Since the effects of form factor and density are unchanged in both measurements, the net contribution vanishes in the subtraction process. Let C_0 represent the capacitance of the empty unit (only air being present), C_1 the capacitance of the unit having wet snow, and C_2 the capacitance of the unit after freezing:

$$C_1/C_0 - C_2/C_0 = A W \quad (3)$$

where A is a proportionality factor, and W is the volume percent wetness (defined to be equal to 100 times the grams of water per cm^3 of wet snow). The value of A must be determined by calibration tests.

Specimens of foam polyurethane having known wetness were placed between the plates of a capacitor for measurement of the change in dielectric constant with wetness, at a range of frequencies. Results are shown in Fig. 2, where the increase in the real part of the dielectric constant (k') is plotted versus wetness at selected frequencies.

Quality-Factor Dependence on Wetness

The dependence of the intrinsic quality-factor Q_s of a snow sample on wetness is shown in Fig. 3. Water was added to

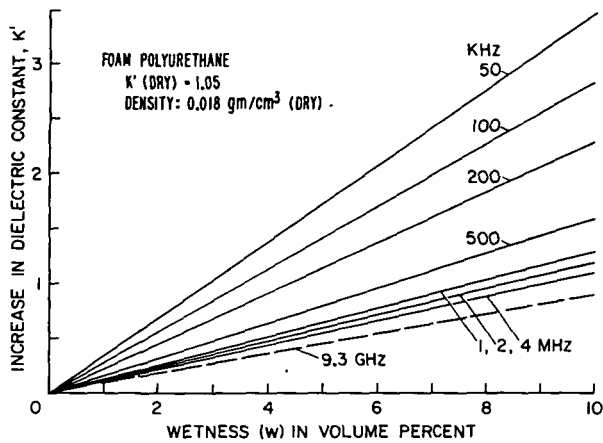


Fig. 2-Dependence of dielectric constant on wetness

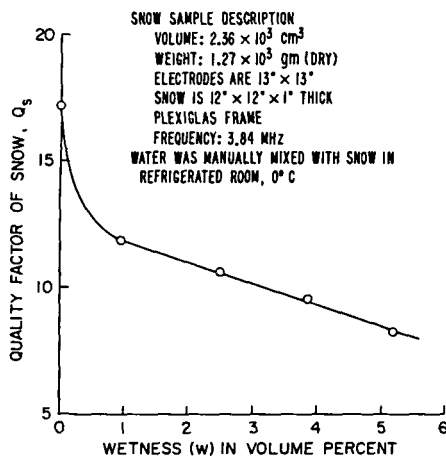


Fig. 3-Quality factor of snow capacitor versus wetness

initially-dry snow and manually mixed with it in a refrigerated room. The intrinsic quality factor is given by:

$$Q_s = \frac{Q_1 Q_2 (C_1 - C_2)}{C_1 (Q_1 - Q_2)} \quad (4)$$

For the Q-meter and associated coaxial leads, let the initial readings be designated C_1 and Q_1 , where C_1 includes the lead capacitance plus the dial-indicated capacitance. Next with the snow capacitor connected to the Q-meter, let the readings be designated as C_2 and Q_2 ; C_1 minus C_2 represents the capacitance of the snow capacitor, and Q_s represents the quality factor associated with the snow.

Microwave Beam Attenuation

Measurement of snow wetness by the attenuation of a microwave beam can be accomplished in a variety of alternative configurations. The basic interaction is the absorption of microwaves by liquid-phase water, in the frequency range of 10^9 to 10^{10} Hz. The wetness of a sample can be obtained by placing it in a beam of known intensity, and measuring the transmission. The average wetness of a snowpack can be obtained by placing a transmitter on a tower and a properly-packaged receiver on the earth beneath the snow, and measuring the transmission. A profile of the wetness of a snowpack can be obtained by placing the transmitter in a vertical tube, with a receiver in another vertical tube spaced about a meter away; with these units moving in synchronism vertically, a transmitted horizontal beam traverses the snowpack, and its attenuation at successive levels yields the wetness profile.

Transmitters were constructed to operate at the frequencies of 1.83, 2.73, 5.00, and 8.00 GHz. Tests in an anechoic chamber yielded the results shown in Table 2. The received power levels are relative to an arbitrary level; at -60 dB the receivers reached the noise level. Thus at the distance of 100 cm between source and receiver the dynamic range was about 30 dB or greater for all frequencies.

TABLE 2.- RELATIVE POWER AT RECEIVERS

Frequency, GHz	Relative power at receivers, dB	
	Distance, 50 cm	Distance, 100 cm
1.83	-17.1	-23.4
2.73	-21.4	-26.3
5.00	-23.5	-30.7
8.00	-24.8	-30.5

To measure the effect of wetness, transmission tests were performed on samples of foam polyurethane. At a selected

frequency, transmission levels were measured through interposed layers of foam polyurethane, each having approximately the same wetness. The transmission test results for foam polyurethane with an average wetness of 8.5 volume percent are given in Fig. 4. At 5.00 and 8.00 GHz the data points fall reasonably well on the straight lines that are expected for exponential attenuation. At 1.83 and 2.73 GHz the data points exhibit oscillations with regard to the exponential attenuation lines. Such oscillations are expected on the basis of theory, produced by interference effects at the front and back surfaces of the foam polyurethane stack. Refinement of the experimental technique to remove the interference effects is possible, but adequate information can be obtained from the straight lines that are fitted to the data points.

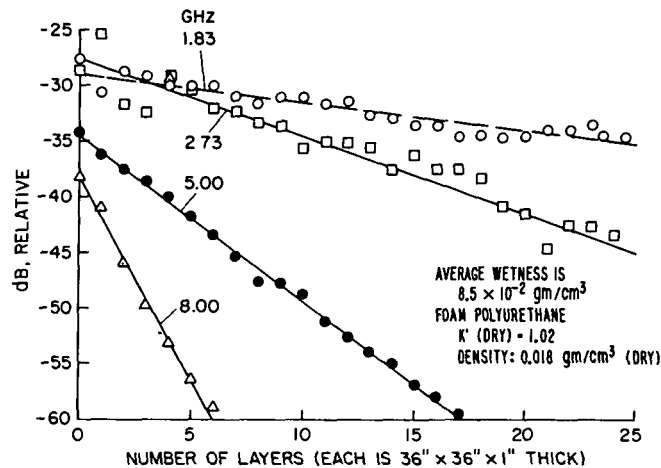


Fig. 4-Microwave beam intensity versus thickness of wet foam polyurethane

Tests were run at 8.00 GHz for other values of wetness, with the results given in Table 3. If the absorption coefficient is proportional to the wetness, then the absorption per unit of electrical length (equal to the physical length multiplied by the square root of the dielectric constant) divided by the volume percent wetness should be a constant for a selected frequency. Our measured values for the absorption in decibels divided by the electrical length in centimeters and volume percent wetness are:

TABLE 3.- ABSORPTIVITY DEPENDENCE ON FREQUENCY

Frequency, GHz	Wetness, vol. %	Dielectric constant k'	dB/cm	dB/cm % $\sqrt{k'}$
1.83	8.5	1.78	0.101	0.0089
2.73	8.5	1.78	0.276	0.0243
5.00	8.5	1.78	0.587	0.0517
8.00	8.5	1.78	1.444	0.1272
8.00	4.8	1.45	0.722	0.1248
8.00	10.5	2.01	1.693	0.1139
8.00	12.0	2.32	2.150	0.1176

0.125, 0.127, 0.114, and 0.118 for the respective volume percent wetness values of 4.8, 8.5, 10.5, and 12.0. These four absorptivities have an average value of 0.121 and a standard deviation of ± 0.006 .

To obtain the electrical length, a measurement of the dielectric constant k' is necessary. This was done by measuring the phase shift produced by the wet foam polyurethane. The signal from a microwave source operating at 9.3 GHz was divided into two legs, one of which had transmitting and receiving apertures; the other (comparison) leg had a calibrated phase shifting unit and a variable attenuator. The signal in the comparison leg was adjusted in phase and amplitude so as to essentially cancel the signal from the other leg; that is, a phase difference of 180° was obtained. As each layer of the wet foam polyurethane was inserted into the transmitter-receiver leg, the change in phase and attenuation in the comparison leg, necessary to preserve the 180° relationship, was measured. The phase shift is a measure of the electrical length of the inserted foam polyurethane layers, and because the physical length is known, the dielectric constant k' can be calculated.

Results are shown in Fig. 5 for the dielectric constant, as a function of wetness in volume percent, for a frequency of 9.3 GHz. Six samples were tested at a variety of wetness values; the straight lines were fitted to the data points.

The data given in Table 3 have been plotted in Fig. 6, showing the attenuation per unit electrical length and per unit volume percent wetness, for the four frequencies. A theoretical curve for pure water, based on data published by Peter Ray (1972), is also shown, for which the abscissa is given at the top of the page.

Preliminary tests using microwave equipment were made at the Central Sierra Snow Laboratory. On 29 January 1975 the snow was about 65 cm deep and was below freezing, so it could be characterized as being dry. Two receiver distances were employed with each of the four transmitters: 223 cm and 798 cm. No measurable absorption was observed at any of the four frequencies. Some "ducting" effects on the transmitted signal were noted, as well as the expected multi-path interference effects.

Another set of measurements was taken at CSSL during the week of 17 March 1975; the snow was about 250 cm deep. Multi-path interference effects were noted; however, between the snow depth

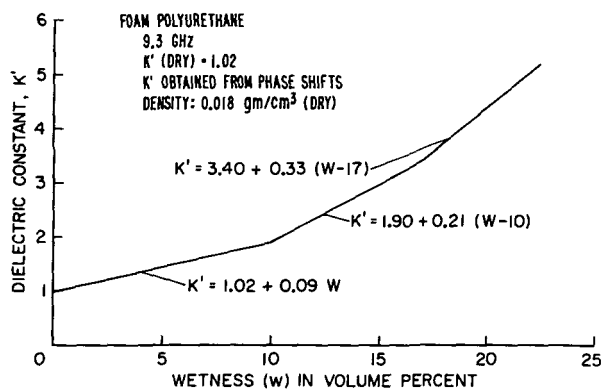


Fig. 5-Phase shift produced by wetness

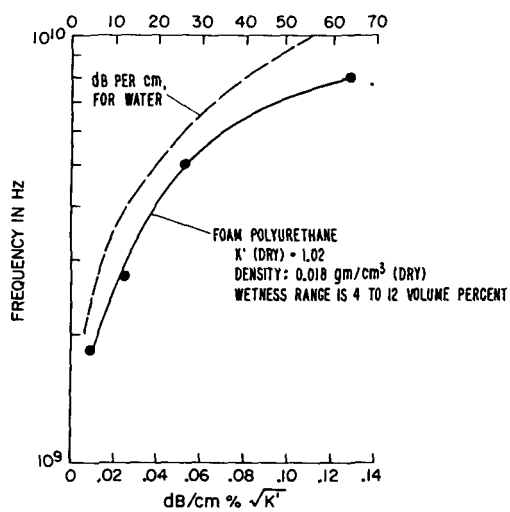


Fig. 6-Absorptivity versus frequency for wet foam polyurethane

levels of 125 cm to 175 cm a wet layer was evident. If the assumption is made that the wet snow is similar to wet foam polyurethane in absorption characteristics, this snow layer had an average wetness of about 1 percent by volume. For the average snow density of about 0.35 gm/cm^3 , this is equivalent to about 3 percent wetness by weight.

A third set of measurements was made in late May 1975 at CSSL, when the snow was actively melting, having a depth of about 170 cm. These data are being analyzed; results to date are in agreement with theoretical predictions. Phase shifts are evident, caused by density gradients in the snowpack producing "fading" that is similar to attenuation, but this effect is being removed on the basis of pattern structure (variation with depth).

Although our experience with in situ measurements of snowpack wetness with microwave systems is in the initial stages, the results are very encouraging. The planned program for the immediate future includes (1) tests of snowpacks, under natural conditions, with circularly-polarized antennas (to discriminate against reflections) and automatic profiling; (2) comparison of attenuation of microwave beams with dielectric constant measurements and with quality-factor of snow samples; and (3) comparison of electrical measurements with density-profiling gage data. Calibration of the systems on an absolute basis will be investigated. As soon as possible the systems will be coordinated with measurements involving passive microwave systems.

Theoretical studies are being made to determine the suitability of an active electromagnetic remote-sensing system to measure snowpack wetness from an airplane or helicopter. Descriptions have been published (Linlor, 1974; Linlor and Jiracek, 1975; and Linlor, 1975), based on snowpack layers whose electrical properties were determined by field measurements. The proposed airborne system is a multi-frequency sounder; that is, a transmitter sends a sequence of pulses of stepped frequencies, and the reflections are measured by a sensitive receiver. The combination of snowpack and earth interact with the electromagnetic wave so as to modify the characteristics of the reflected signals. The variation of the reflected intensity with frequency provides the desired information.

The presence of wetness in the snow greatly affects the reflected signal characteristics. A frequency can be selected so that the skin depth is approximately one-half of the snowpack thickness, so that earth roughness is immaterial. Analyses are being made to determine the applicability of this approach in a practical system.

Passive microwave systems in airplanes or satellites can provide important information regarding snowpack areal coverage and water equivalent (Meier, 1972). Such methods make use of the natural radiation from observed objects. The characteristics of this radiation are determined by the emittance, transmittance, reflectance, and temperature of the object (that is, snowpack). Meier (1972) points out that passive microwave systems can determine the areal coverage of snow in mountainous regions despite the presence of cloud cover. Mapping of the snow-covered area may be

unnecessary because the radiometric data provide integrated measurements, yielding the fraction of the land that is snow covered. The total mass of the snow and its wetness may perhaps be obtained by the use of several carefully selected frequencies, viewing angles, and polarizations. Because wetness affects the measurements strongly, ground truth instrumentation is necessary for proper interpretation of the passive microwave data. The methods described in this paper can provide such needed information.

DISCUSSION AND CONCLUSIONS

Water runoff forecasting under snowmelt conditions is difficult because the amount of liquid water that is already present or that may still be stored in the snowpack is not known in general. A review of the literature regarding water-holding capacity of snow shows wide divergence of estimates.

Present-day instrumentation apparently is not adequately accurate, or else considerable differences in snow wetness occur on successive days at the same site under conditions where uniformity would be expected. Also, available techniques are difficult to automate.

Three new approaches to the problem of measuring snow wetness have been discussed, of which the microwave absorption method can be operated entirely automatically in remote installations, thus permitting repetitive measurements of a snowpack to determine how its wetness changes with time.

Density and wetness profiles of the snowpack can be obtained simultaneously over essentially the same path by combining a microwave and radioactive source in a vertical tube, with another vertical tube about a meter away containing microwave and gamma-ray detectors. When both density and liquid-water profiles are available, the condition of the snowpack can be accurately determined and, combined with meteorological information, useful predictions can be made regarding the melting and water discharge rates from snowpacks. Satellite telemetry can be used for data gathering.

The elements of water runoff forecasting were briefly reviewed. It was pointed out that in-situ measurement of snow wetness can be included in all of the forecasting methods: historical, index, water-balance, and hydrologic model. For each percent increase in utilization of water runoff, the annual hydroelectric energy value is about \$30 million, in the western United States.

Passive microwave systems hold great promise for satellite-based synoptic measurements of snow areal coverage and depth; however, the measurements are affected by the presence of liquid-phase water in the snow. The snow wetness techniques described in this paper can provide ground truth for the development of such passive systems.

ACKNOWLEDGEMENTS

We appreciate the interest and help of Ron Jones and Jim Bergman during the field tests at the Central Sierra Snow Laboratory. We thank Drs. Edgerton and Sakamoto (1970) for permission to use their Fig. 1 to show the comparative performance of wetness instruments under field conditions.

APPENDIX A - DEFINITION OF TERMS

Water exists in the solid, liquid, or vapor forms; in this paper the liquid phase is meant whenever the term "water" is used alone.

"Water-equivalent" means the amount of water that would be obtained from the complete melting of a given volume of snow. It can be expressed as centimeters (or inches) of water, assuming that the cross-sectional area is constant. It is also measured by the weight of a given volume of snow, such as a Mount Rose sampling tube.

"Water-content" means the amount of water (liquid-phase) present in the snow (also referred to as the "wetness"). "Liquid-water" is used interchangeably with water-content. Two sets of units are used alternatively:

- (a) grams of water per gram of dry snow,
- (b) grams of water per cubic centimeter.

Multiplication of each of these quantities by 100 gives, respectively, the percent wetness based on weight, and the percent wetness based on volume. Quantity (b) is evidently equal to quantity (a) multiplied by the dry-snow density in g/cm^3 . As a numerical illustration, consider a cubic centimeter having 0.4 g of dry snow to which is added 0.1 g of liquid water. With the assumption for convenience, though not valid in actuality, that the total volume of wet snow remains constant at 1 cm^3 , the percent wetness by weight is (a) = 25; the percent wetness by volume (b) = 10.

"Localized-water" refers to water molecules that have an energetically significant binding to the snow (that is, ice) crystals, and remain attached until final melting of the crystal, assuming that no freezing intervenes. Such molecules contribute to the complex dielectric constant of the snow, but not as much as would an equal number of molecules of pure water in the absence of a host medium. Localized-water is also known as "hygroscopic-water," or water held by adsorption.

"Capillary-water" is held by surface tension forces in the capillary spaces of the snow. The pull of gravity is insufficient to overcome the attraction of the snow and water molecules. If the density of the snow changes, or if metamorphic processes occur, such that the capillary spaces become modified, the water-retention capability of the snow is correspondingly modified. For dry snow, the water-retention capability is dependent on density and crystal shapes.

"Free-water" is defined in Snow Hydrology (1956, p. 144):

"Free-water includes only that water permanently held within the

snowpack; that is, water held by adsorption and capillarity. It does not include water in the process of percolating through the pack or water impounded in the pack as the result of poor drainage conditions." We suggest that the hydrology term "retention storage" is applicable for free-water storage. Our definition of water-content (or liquid-water or wetness) includes free-water (retention storage) and water in transit (detention storage).

APPENDIX B — REFERENCE QUOTATIONS REGARDING SNOW WETNESS

The following direct quotations give the opinions of recognized authorities regarding water-holding capacity of snow.

Snow Hydrology (1956, p. 303)

"Experiments on liquid-water-holding capacity of snow are limited . . . between 2 to 5 percent by weight is recommended for the liquid-water-holding capacity of snow. Additional observations are required to establish the relationship between snow density and liquid-water-holding capacity. The lack of information on the capacity of the snow to retain liquid water against gravity, as a function of some index of the stage of metamorphism, constitutes a major gap in knowledge of the storage effect of the snow on runoff. . . . It is pointed out that the liquid-water-holding capacity of snow, as discussed in the preceding paragraphs, represents conditions where free drainage of the snowpack is assured. In flat areas, horizontal drainage through channels is impeded by the lack of sufficient slope. Thus, portions of the snowpack in foothills and flat lands may hold liquid water far in excess of that for mountainous areas where free drainage is rapid."

Snow Hydrology (1956, p. 313)

"The effect of varying snowpack conditions on runoff from either rainfall or snowmelt is one of the basic considerations of snow hydrology. Divergent opinions exist as to the storage effect of the snowpack. They range from considering the snowpack to be a vast "sponge" capable of retaining large quantities of liquid water, to the assumption that storage in the snowpack is negligible in any basin study. Actually, there are times when either viewpoint may be correct, and there is no generalization which is universally applicable. The important consideration is that the actual snowpack condition be evaluated in order to properly assess its immediate storage potential."

de Quervain (1972, p. 209)

"Wet snow crystals are coated with a thin layer of water, and in re-entrant angles at contacting grains, water pockets are found. To what extent this water will remain as equilibrium water content and represent a free water-holding capacity has not been unanimously agreed on. Some authors accept only free water in the order of 1 to 6 percent as being in equilibrium (Gerdel, 1954 and Snow Hydrology, 1956), whereas

others assume a wider range from 5 to 25 percent (de Quervain, 1948) or even up to 55 percent (Moskalev, 1966). Wakahama (1968) reports snow layers with 20 to 30 percent water without referring to a state of equilibrium.

"Equilibrium water content, whatever its range, depends on snow density, grain size, and grain shape in a complex manner. The specific inner surface of snow, specific number of grain contacts, and pore width are important. Snow with fine grains holds more water than that with coarse grains; therefore, high equilibrium water content is related to new snow, snow of felt-like structure, and fine granular material, whereas low values are found in metamorphic coarse old snow. An optimum dry density for maximum storage obviously exists.

"In addition to equilibrium water, a considerable amount of free water may exist in a transient state during and following a melting period or a rainstorm."

Hydrologic reaction of snowpacks to rainfall is discussed in Snow Hydrology (1956, p. 323)

"In rain-on-snow situations, the effects of the snowpack are twofold: (1) to add an increment of melt water to the rainfall and (2) to store and detain, in varying degrees, the melt and rain water generated. It is the latter effect that makes the reconstitution of rain-on-snow floods most complex. Rain falling on a snowpack may be stored by the pack or pass through without depletion, depending on the condition of the pack. A considerable quantity of rain water may be stored by a dry, sub-freezing, snowpack. Moreover, a deep snowpack that has previously experienced little or no melt or rainfall of consequence may add an additional increment of storage by virtue of its delaying effect upon runoff. Impenetrable ice planes within the snowpack may give a large horizontal component to the flow of water through the pack itself (along the ice planes seeking a pervious area). Then too, water may be perched above such impenetrable layers. . . . From the foregoing discussion, one important fact stands out: the condition of the snowpack has a dominant effect upon the initial basin discharge of rain-on-snow event. Because of this, rain-on-snow floods are difficult to synthesize; some knowledge of the initial condition of the snowpack is mandatory."

REFERENCES

1. Ambach, W. and F. Howorka (1966). Avalanche activity and free water content of snow at Obergurgl. International Symposium on Scientific Aspects of Snow and Ice Avalanches, April 5-10, 1965, Davos, Switzerland.
2. Ambach, W. and A. Denoth (1972). Studies on the Dielectric Properties of Snow, Zeitschrift fur Gletscherkunde und Glazialgeologie, Bd. VIII, Heft 1-2, S. 113-123.
3. Army Corps of Engineers (1956). "Snow Hydrology" Portland, Oregon.

4. Bertle, F. A. (1965). Snow compaction method for the analysis of runoff from rain on snow. Proc. Western Snow Conf., Colorado Springs, Colorado, April 20-22, 1965.
5. Brown, A. J. (1974). Long-range goal and information needs of the coordinated snow survey program in California. Advanced Concepts and Techniques in the Study of Snow and Ice Resources, National Academy of Sciences, Washington, D.C.
6. de Quervain, M. R. (1946). Zur Temperaturdynamik der Schneedecke. Int. Ber. Eidg. Inst. F. Schnee u. Lawinenforschung, Weissfluhjoch/Davos, No. 25.
7. de Quervain, M. R. (1972). Snow structure, heat, and mass flux through snow. Int. Symp. on Role of Snow and Ice in Hydrology, Unesco-WMO, Banff, Canada, Sept. 6-20, 1972.
8. Edgerton, A. T. and S. Sakamoto (1970). Microwave radiometric investigations of snowpacks. Interim Report No. 2 for USGS, Aerojet-General Corp., El Monte, Calif.
9. Gerdel, R. W. (1954). The transmission of water through snow. Transactions, Amer. Geophys. Union, vol. 35, no. 3, pp. 475-485.
10. Gray, D. M. (1970). Principles of hydrology. Secretariat, Canadian National Comm. for Int. Hydrol. Decade, Ottawa, Canada.
11. Hildebrandt, A. F., G. M. Haas, W. R. Jenkins, and J. P. Colaco (1972). Large-scale concentration and conversion of solar energy. Transactions, Amer. Geophys. Union, vol. 53, no. 7, pp. 684-692.
12. Hydrocomp, Inc. (1974). Simulation network newsletter, vol. 6, no. 4, May 15, 1974, Palo Alto, Calif.
13. Kittredge, J. (1948). Forest influences. McGraw-Hill Book Co.
14. Langham, E. J. (1973). The occurrence and movement of liquid water in the snowpack. Advanced Concepts and Techniques in the Study of Snow and Ice Resources, National Academy of Sciences, Washington, D.C.
15. Linlor, W. I. (1974). Remote sensing and snowpack management. J. AWWA, Sept. 1974, pp. 553-558.
16. Linlor, W. I. and J. L. Smith (1974). Electronic measurements of snow sample wetness. Advanced Concepts and Techniques in the Study of Snow and Ice Resources, National Academy of Sciences, Washington, D. C.
17. Linlor, W. I., M. F. Meier, and J. L. Smith (1974). Microwave profiling of snowpack free-water content. Advanced Concepts and Techniques in the Study of Snow and Ice Resources, National Academy of Sciences, Washington, D.C.
18. Linlor, W. I. (1975). Multilayered models for electromagnetic reflection amplitudes. NASA Technical Report TR R-438.
19. Linlor, W. I., J. L. Smith, M. F. Meier, F. D. Clapp, and D. Angelakos (1975). Measurement of snowpack wetness. Proc. 43rd Annual Meeting, Western Snow Conf. April 23-25, 1975, San Diego, Calif.
20. Linlor, W. I. and G. R. Jiracek (1975). Electromagnetic reflection from multilayered snow models. J. of Glaciology (in press).

21. Linsley, R. K., M. A. Kohler, and J. L. H. Paulhus (1949). Applied hydrology, McGraw-Hill, New York.
22. Linsley, R. K., M. A. Kohler, and J. L. H. Paulhus (1958). Hydrology for engineers, McGraw-Hill, New York.
23. Meier, M. F. (1972). Measurement of snow cover using passive microwave radiation. Int. Symp. on Role of Snow and Ice in Hydrology, Unesco-WMO, Banff, Canada, Sept. 6-20, 1972.
24. Meier, M. F. (1973). New ways to monitor the mass and areal extent of snowcover. Proc. Intl. Symp. Earth Survey Problems, COSPAR.
25. Moskalev, Y. D. (1966). Voznidnoveniye i Dvizheniye Lavin. (Avalanche Mechanics.) Hydromet. Publ. House, Leningrad, USSR.
26. Radok, U. (1956). Note on the free water content of Australian snow. Meteorology Dept., Univ. of Melbourne, Australia.
27. Ray, P. (1972). Broadband complex refractive indices of ice and water. Applied Optics, vol. 11, no. 8, pp. 1836-1843.
28. Smith, J. L. and H. C. Halverson (1969). Hydrology of snow profiles obtained with the profiling snow gage. Proc. 37th Annual Meeting, Western Snow Conf. Salt Lake City, Utah.
29. Smith, J. L., H. G. Halverson, and R. A. Jones (1972). Central Sierra snow gage: a guide to fabrication and operation. TID-25986, Division of Isotopes Development, U.S. Atomic Energy Commission.
30. Smith, J. L. (1974). Hydrology of warm snowpacks and their effects upon water delivery. Advanced Concepts and Techniques in the Study of Snow and Ice Resources, National Academy of Sciences, Washington, D.C.
31. Wakahama, G. (1968). Infiltration of melt water into snow cover. Low Temp. Sci. Ser. A, vol. 26, pp. 54-85.
32. Yosida, Z. (1966). Free water content of wet snow. Proc. Intl. Conf. on Low Temp. Sci. Hokkaido Univ., Sapporo, Japan.

MICROWAVE EMISSION FROM DRY AND WET SNOW

T. C. Chang and P. Gloersen, *Goddard Space Flight Center, Greenbelt, Maryland*

ABSTRACT

A microscopic model has been developed to study the microwave emission from snow. In this model the individual snow particles are considered to be the scattering centers. Mie scattering theory for spherical particles is then used to compute the volume scattering and extinction coefficients of the closely packed scattering spheres, which are assumed not to interact coherently. The results of the computations show significant volume scattering effects in the microwave region which result in low observed emissivities from cold, dry snow. In the case of wet snow, the microwave emissivities are increased considerably, in agreement with earlier experimental observations in which the brightness temperatures have increased significantly at the onset of melting.

I. INTRODUCTION

Recently, satellite detection of melting snow and melting ice by using a combination of visible and near infrared data has achieved some success (Strong, et al., 1971). The utility of this technique is limited by frequent cloud cover over areas of interest. The Electrically Scanned Microwave Radiometers (ESMR) on board the NIMBUS 5 and 6 satellites provides an additional ability to sense through the cloudy sky. Therefore, it is needed to develop an applicable analytical model for explanation of the microwave emission from snow.

A microwave model has been developed to study the microwave emission from snow and glacier ice (Chang, et al., 1975). It was assumed that the snow field or snow cover consists of closely packed scattering spheres which do not interact coherently. Comparing with the macroscopic multilayer or variable dielectric model, this method in addition provides the scattering processes in the radiative transfer equation. Since each individual snow grain is considered as a scattering center, the Mie scattering theory (Stratton, 1941) was utilized to compute the scattering cross-sections. In this paper, the particular signature of melting snow is studied.

II. THEORETICAL APPROACH

The rigorous solution for the diffraction of a plane monochromatic wave by a homogeneous dielectric sphere was first obtained by Mie (1908). The more detailed development of the theory can be found in the literature (Stratton, 1941; Van de Hulst, 1957).

Consider a uniform dielectric sphere of radius r and the complex index of refraction n in the presence of a linearly polarized plane wave with wavelength λ and electric field vector E_i . The electric field E observed at a distance $R \gg r$ from the sphere is the vector sum of incident field and scattered field. It can be expressed as:

$$E = E_i + \bar{S} E_i \frac{e^{ikR}}{ikR} \quad (1)$$

where k is the propagation constant $2\pi/\lambda$ and \bar{S} is the scattering matrix. The solution takes the form of an expansion in spherical wave functions with complex scattering coefficients a_m and b_m determined by the boundary and the angular dependence of each multipole. The extinction cross-sections for spherical ice particles with refractive index $n = 1.78 + i 0.0024$, which corresponds to the values in the centimeter wavelength range of pure water ice at 0°C (Sweeny and Colbeck, 1974) is calculated for several wavelengths and particle radii. The results of the calculations are shown in Figure 1.

In order to develop the model for the case of melting ice sphere, it is assumed that the sphere consists of a central core of ice and a surrounding shell of water. The solution of scattering of electromagnetic waves from these concentric spheres has been solved by Aden and Kerker (1951). In this study the thickness of the water layer is set to be one tenth of the radius of the sphere. The index of refraction for water is calculated according to the results of Lane and Saxton (1952). The extinction cross-section for water coated ice particle with refraction index of $n = 1.78 + i 0.0024$ for ice cover, several wavelengths and particle radii are shown in Figure 2.

The Rayleigh-Jeans approximation for the intensity of thermal radiation from a blackbody is applicable at microwave frequencies and at temperatures typical of the earth surface and its atmosphere; thus the radiative transfer equation (Chandrasekhar, 1950), with axial symmetry, may be written as:

$$\begin{aligned} \cos \theta \frac{dT_B(\theta)}{dX} + \gamma_{ABS}(T_B(\theta) - T(X)) \\ = \frac{\gamma_{SCA}}{2} \int_0^\pi T_B(\theta_s) F(\theta, \theta_s) \sin \theta_s d\theta_s - \gamma_{SCA} T_B(\theta) \end{aligned} \quad (2)$$

$$n_{ice} = 1.78 + i0.0024$$

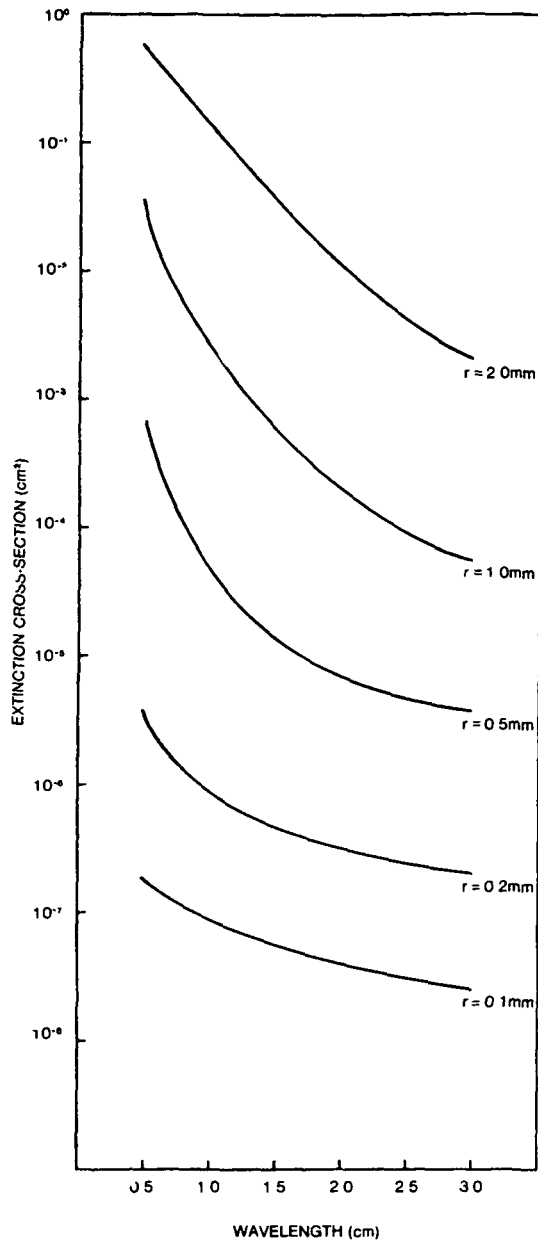


Fig. 1—Extinction cross-section as a function of microwave wavelength for several snow particle radii.

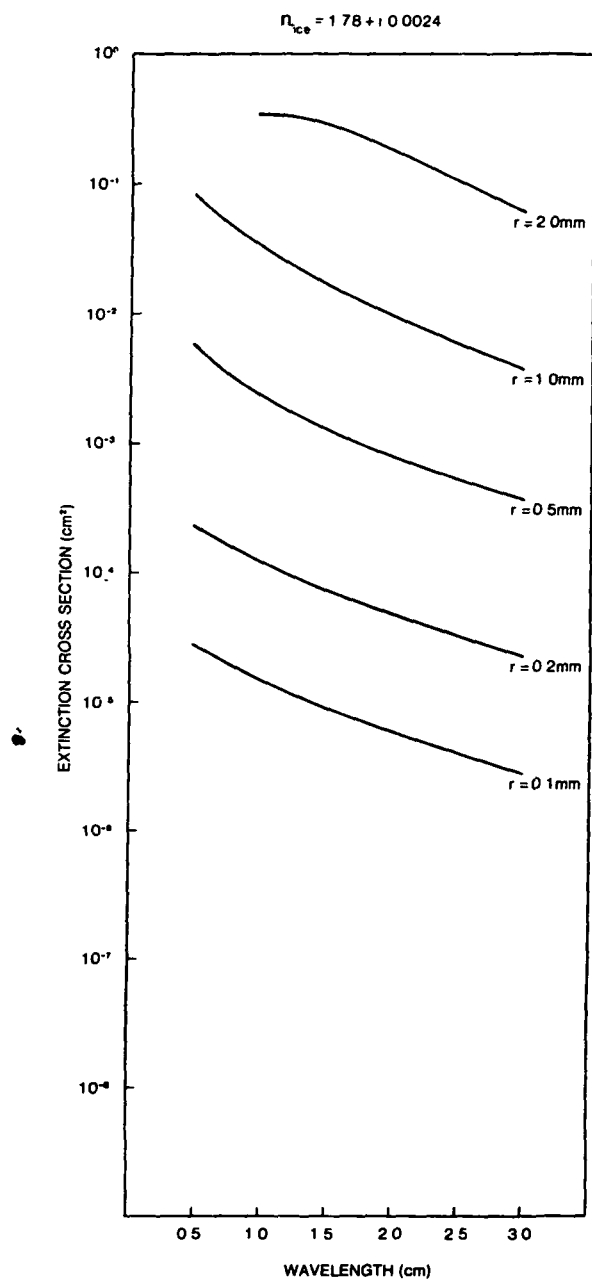


Fig. 2—Extinction cross-section as a function of microwave wavelength for several wet snow particle radii.

For a non-scattering medium, the left-hand side of the equation would be equated to zero; the right-hand side represents the angular distribution of radiation resulting from the scattering. To solve this equation the snow layer is first divided into a number of smaller layers. An initial estimate is then made of the brightness temperature for the upwelling radiance from the lower boundary. This upwelling component is then scattered by the medium of next small layer and the radiance redistributed according to the scattering phase function. The upwelling brightness temperature can then be calculated from the bottom layer upward order. The downwelling components are then similarly calculated from the top most layer downward. The reflected downwelling radiance from the bottom underlying surface attribute to non-neglectable amount of radiance in the microwave observation, it is necessary to take into account the effect of the reflecting surface. Unfortunately, then is little data or theory available to help in determining this surface effect, so approximations are used. The simplest approximation is to assume a specular surface. On the other hand, the surface can be assumed infinitely rough and apply the Lambertian approximation (Peake, et al., 1966). The reflected radiances are then added to the upwelling radiance and the process is repeated until a satisfactory convergence is obtained. The method of solution is a variation of the Gauss-Seidal interaction (Hildebrand, 1946).

III. COMPUTATIONAL RESULTS

To illustrate the scattering effects on the upwelling microwave brightness temperature, a simplified snow field model is constructed. A layer of uniformly sized spheres (the snow cover) is situated on top of the earth. The earth surface is assumed to be a Lambertian surface with index of reflection of $1.75 + i 0.03$ for dry soil surface and $3.0 + i 0.1$ for wet soil surface. The particle density $N(r)$ for different particle radius r is represented analytically as

$$N(r) = \left(\frac{1}{2r} \right)^3 \quad (3)$$

The particle density corresponds to a typical moderately packed snow with mass density $(4/3 \pi r^3 N(r) \rho)$ of 470 kg/m^3 . The physical temperature for the snow layer is assumed to be uniform at 273°K .

To demonstrate the effect of snow melting in the field, the model is chosen to be a snow particle coated with a thin layer of water. The thickness of the water layer is one tenth of the radius of the snow particle. A set of brightness are then calculated by using the formula derived in Section II. The results for dry and wet snow layer at wavelength of 1.55 cm are displayed in Figures 3, 4, and 5.

When the particle size parameter $\alpha \equiv 2\pi r/\lambda$ is small, the calculated extinction cross-section for the melting snow particle is approximately

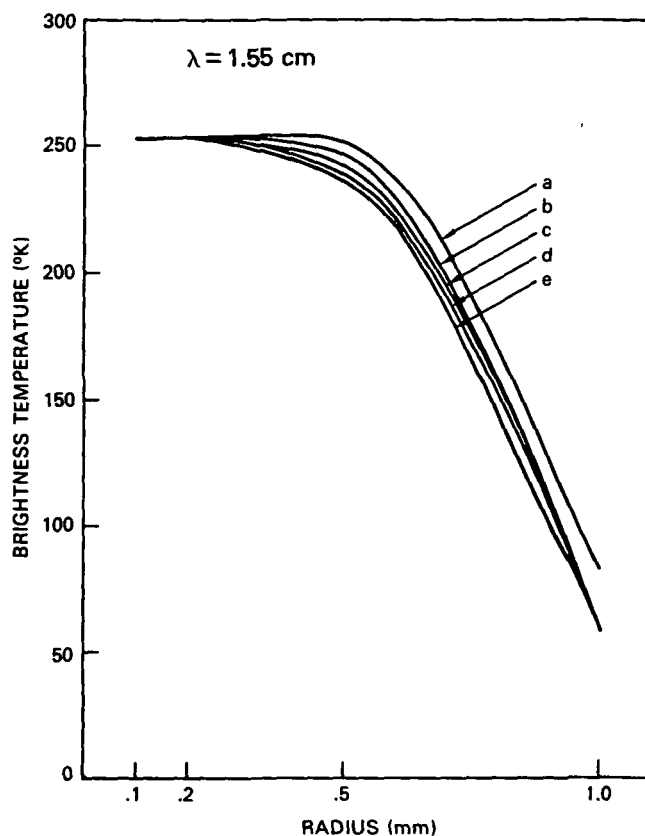


Fig. 3—Surface brightness temperature as a function of snow particle radius. The thicknesses of the snow layer are: (a) 10 cm, (b) 50 cm, (c) 1 m, (d) 2 m and (e) 5 m.

two orders of magnitude larger than that of dry snow particle. The increase of σ_{SCA} the scattering cross-section for melting snow particle is not as fast as σ_{EXT} the extinction cross-section, therefore the ratio $\sigma_{SCA}/\sigma_{EXT}$ decreases for the melting snow particle as compared to the dry snow particle. Since less radiance is scattered by the snow particle; the upwelling brightness temperature becomes higher for melting snow temperature becomes higher for melting snow (Edgerton, et al., 1971; Gloersen, et al., 1974).

IV. CONCLUSIONS

A microscopic model, consisting of the individual snow particles as the scattering centers for Mie scattering, has been used to explain

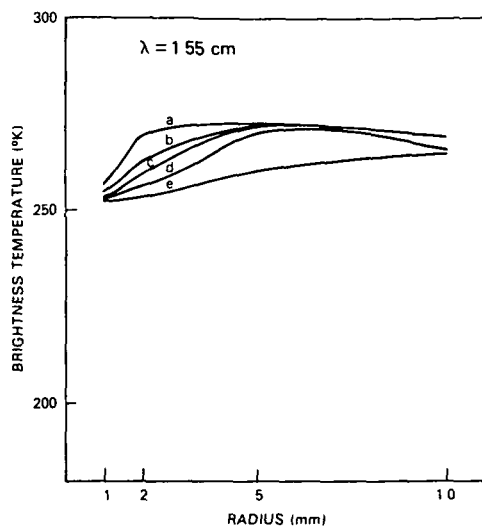


Fig. 4—Surface brightness temperature as a function of wet snow particle radius on dry earth surface. The thicknesses of the snow layer are: (a) 10 cm, (b) 50 cm, (c) 1 m, (d) 2 m and (e) 5 m.

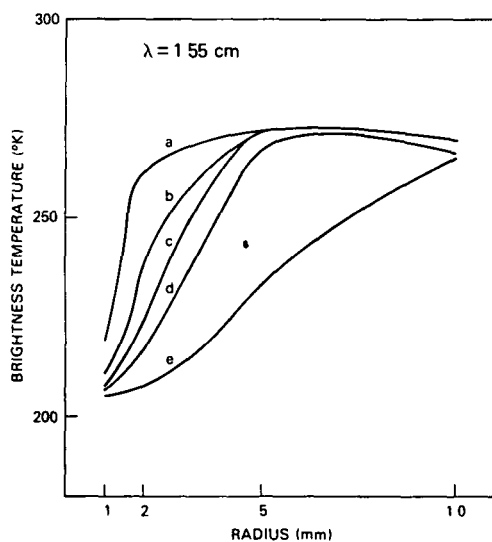


Fig. 5—Surface brightness temperature as a function of wet snow particle radius on wet earth surface. The thicknesses of the snow layer are: (a) 10 cm, (b) 50 cm, (c) 1 m, (d) 2 m and (e) 5 m.

qualitatively the brightness temperatures over dry and wet snowfields. The computational results show that scattering from the individual snow particles is a dominant factor in the measured upwelling brightness temperature in the case of dry snow. When the snow thickness is larger than the penetration depth, the earth surface, whether dry or wet, will not contribute to the upwelling brightness temperature. For wet snow layers of 50 cm or more, the brightness temperatures approach the physical temperature of the snow layer. The distinction between these two signatures may be used to detect the dry and wet snow cover.

REFERENCES

- Aden, A. L. and M. Kerker, "Scattering of Electromagnetic Waves from Two Concentric Spheres," *Journal of Applied Physics*, Vol. 22, pp. 1242-1246, (1951).
- Chandrasekhar, S., *Radiative Transfer*. Claredon, Oxford, (1950).
- Chang, T. C., P. Gloersen, T. Schmugge, T. T. Wilheit and H. J. Zwally, "Microwave Emission from Snow and Glacier Ice," NASA/GSFC Preprint, X-910-75-36, (1975).
- Edgerton, A. T., A. Stogryn and G. Poe, "Microwave Radiometric Investigations of Snowpack," Final Report No. 1285 R-4 for U.S.G.S. Contract No. 14-08-001-11828, Aerojet General Corp., El Monte, California, (1971).
- Gloersen, P., T. T. Wilheit, T. C. Chang, W. Nordberg, and W. J. Campbell, "Microwave Maps of the Polar Ice of the Earth," *Bul. Am. Met. Soc.*, Vol. 12, p. 1442, (1974).
- Heldebrand, F. B., *Introduction to Numerical Analysis*. Chapter 10, McGraw-Hill, New York, (1956).
- Lane, J. A. and J. A. Saxton, "Dielectric Dispersion in Pure Polar Liquids at Very High Radio-frequencies, I. Measurements on Water, Methyl and Ethyl Alcohols," *Proc. Royal Society*, Vol. 213, pp. 400-408, (1952).
- Peake, W. H., R. L. Riegler, and C. A. Shultz, "The Mutual Interpretation of Active and Passive Microwave Sensor Outputs," *Proc. 4th Symp. on Remote Sensing of Environment*, Univ. of Michigan, (1966).
- Stratton, J. A., *Electromagnetic Theory*. McGraw-Hill, New York, pp. 563-573, (1941).

Strong, A. E., E. P. McClain, and D. F. McGinnis, "Detection of Thawing Snow and Ice Packs Through Combined Use of Visible and Near-Infrared Measurements from Earth Satellites," Monthly Weather Review, Vol. 99, pp. 828-830, (1971).

Sweeny, B. D., and S. C. Colbeck, "Measurements of the Dielectric Properties of Wet Snow Using a Microwave Technique," U.S. Army, Corps of Engineers CRREL, (1974).

Van de Hulst, Light Scattering by Small Particles, John Wiley, New York, (1957).

APPLICATION OF BAYESIAN DECISION THEORY TO AIRBORNE
GAMMA SNOW MEASUREMENT

Vernon C. Bissell, *National Weather Service, River Forecast Center, Portland,
Oregon 97209**

ABSTRACT

Measured values of several variables are incorporated into the calculation of snow water equivalent as "measured" from an aircraft by snow attenuation of terrestrial gamma radiation. Bayesian decision theory provides a "best" snow water equivalent measurement by taking into account the uncertainties in the individual measurement variables and "filtering" information about the measurement variables through prior notions of what the calculated variable (water equivalent) should be. Generalizations of principles involved in the application are presented in subsequent discussion.

INTRODUCTION

The importance of snow measurements for both water supply forecasting and for flood forecasting is well established. In the case of flood forecasting, the assessment of flood potential based on the water equivalent of snow on the ground provides a lead time for productive action which is not enjoyed during rainfall-caused floods. For example, during the record floods of the spring of 1969 in the upper Mississippi and middle Missouri River drainages, an estimated 137 million dollars in savings was realized through preventive action based on river forecasts. An estimated additional 97 million dollars savings was realized through the proper use of flood control structures based on forecasts [Mondschein, 1971]. Since snow water equivalent is the primary data input to the forecast procedure, the importance of good snow measurements is readily seen.

One very recent snow measurement method, the airborne gamma survey, appears to have great potential in plains areas such as the north-central United States. This method overcomes the difficulties of nonrepresentative sample points and sparseness of samples now encountered in utilizing a ground-based point measurement network. Airborne measurements of gamma radiation coming from the soil in an area provide an excellent indication of the

*Concepts presented in this paper were developed primarily while the author was on the staff of the Hydrologic Research Laboratory, NOAA, National Weather Service, Silver Spring, Maryland 20910.

Preceding page blank

amount of snow water shielding the airborne gamma radiation detector from the radiation flux emanating from the ground. Either the flux in the entire energy range ("total count" method), or the flux within a particular energy range ("spectral peak" method) can be used. The use of natural background radiation to measure snow water equivalent was first proposed in the Soviet Union [Kogan *et al.*, 1965]. Dimitriev *et al.* [1972] reported that operational airborne gamma snow surveys are now conducted over several million square kilometers of the U.S.S.R., mainly in regions where the ground hydrometeorological network is extremely sparse. Research in the method has been conducted in the United States since 1969 [Peck *et al.*, 1971; Burson and Fritzsche, 1972; Bissell, 1974; Larsen, 1975].

AIRBORNE GAMMA SNOW MEASUREMENT METHOD

The total gamma radiation near the surface of the earth is dominated by flux of terrestrial origin. As seen in Figure 1, beyond an altitude of about 1500 meters radiation of cosmic origin begins to dominate. The spectral composition of terrestrial gamma radiation flux is shown in Figure 2. Prominent peaks in the spectrum indicate the presence of ^{40}K (1.46 MeV), ^{214}Bi (1.76 MeV, 2.20 MeV), and ^{208}Tl (2.62 MeV) in the lithosphere and, unfortunately, perhaps in the atmosphere as well. Radiation of atmospheric origin is unfortunate because it is a noise source in airborne gamma surveys. The isotope ^{214}Bi is a subsequent decay product of the radioactive noble gas radon which, with a half-life of 3.6 days, can range far into the atmosphere from its origin uranium in the earth's crust. Consequently, much of the ^{214}Bi decay radiation measured during snow surveys may not have been subjected to the hazard of attenuation by snow cover and is therefore noise in the desired radiation signal. The isotope ^{208}Tl is similarly the decay product of a noble radioactive gas (thoron), but is found in the atmosphere in only small quantities due to thoron's much shorter half-life (57 seconds). The primary snow measurement peaks are the ^{40}K spectral peak at 1.46 MeV and the ^{208}Tl spectral peak at 2.62 MeV. The radiation of atmospheric origin is of sufficient magnitude that the usefulness of the "total count" method is considerably reduced. The ^{40}K spectral peak also has an atmospheric contribution to due Compton-scattering of 1.76 and 2.20 MeV photons down to the lower 1.46 MeV energy range, but a correction can be applied to "strip out" this effect by keying on the magnitude of the 1.76 MeV ^{214}Bi peak. Both the ^{40}K and ^{208}Tl peaks have cosmic components which can be "stripped out" by keying on the magnitude of the purely cosmic portion of the spectrum above 3 MeV. Another significant effect which can enter in is the variable attenuation of radiation within the soil itself due to changing soil moisture, and a correction is also applied for this effect based on measured, estimated, or simulated soil moisture.

The airborne "measured" value of water equivalent is given by the inverse of the relationship expressing the attenuation of

soil-originating spectral peak count rates as a function of water equivalent. An exponential form of this relation is given in equations (1) and (2):

$$R_K(W) = \frac{R_O^{(K)}}{1+KS} \exp(-\alpha_K W) \quad (1)$$

$$R_{Tl}(W) = \frac{R_O^{(Tl)}}{1+KS} \exp(-\alpha_{Tl} W) \quad (2)$$

where W = effective water equivalent, including air blanket (g/cm^2);
 α_K = attenuation coefficient of ^{40}K 1.46 MeV gamma rays in water (cm^2/g);
 α_{Tl} = attenuation coefficient of ^{208}Tl 2.62 MeV gamma rays in water (cm^2/g);
 S = soil moisture (fraction of dry weight);
 K = ratio of gamma attenuation cross section in water to cross section in air, taken to be unity;
 $R_O^{(K)}$ = expected value of count rate in ^{40}K decay in soil, with $W=0$ and $S=0$ (counts/second);
 $R_O^{(Tl)}$ = expected value of count rate in ^{208}Tl spectral peak due only to ^{208}Tl decay in soil with $W=0$ and $S=0$ (counts/second);

The "stripping" equations (3) and (4) express the "pure" count rates R_K and R_{Tl} as the actual spectral peak count rates obtained minus counts from noise sources:

$$R_K(W) = C_K - B_K + \beta_{BK} (C_B - B_B) + \beta_{CK} C_C \quad (3)$$

$$R_{Tl}(W) = C_{Tl} - B_{Tl} + \beta_{CT} C_C \quad (4)$$

where C_K = expected count rate in ^{40}K spectral peak window;
 B_K = expected value of aircraft background count rate contribution in ^{40}K spectral peak window;
 C_B = expected value of count rate in ^{214}Bi spectral peak window;
 B_B = expected value of aircraft background count rate contribution in ^{214}Bi (1.76 MeV) spectral peak window;
 C_{Tl} = expected count rate in ^{208}Tl spectral peak window;
 B_{Tl} = expected value of aircraft background count rate contribution in ^{208}Tl spectral peak window;
 C_C = expected value of count rate in cosmic (high energy) spectral window;
 $\beta_{BK}, \beta_{CK}, \beta_{CT}$ = "stripping" coefficients, generally negative.

Airborne water equivalent measurements are obtained by estimating C_K, C_B, C_{Tl} , and C_C by the computed count rates $N_K/t, N_B/t, N_{Tl}/t$, and N_C/t ,

where N_K = counts in ^{40}K peak during time t ;
 N_B = counts in 1.76 MeV ^{214}Bi peak during time t ;

N_{Tl} = counts in ^{208}Tl peak during time t ;
 N_C = counts in cosmic window during time t .

A linear combination of the ^{40}K and ^{208}Tl spectral peak measurements of a 15 cm. water equivalent will have an accuracy of somewhere near one centimeter water equivalent [Bissell, 1974].

Operational use of the gamma snow measurements would require some quality control on the water equivalent calculation. Since automated calculations would be desirable, some mechanism which would automatically impose a constraint of "reasonableness" on the final calculated water equivalent would be in order. This is one area in which Bayesian decision theory seems to fit nicely.

APPLICATION OF BAYESIAN DECISION THEORY

Bayesian decision theory departs from classical statistics in that the distinction between parameters and random variables is not quite so sharp. It is recognized that initial parameter values may not actually be the true values, and some prior, or *a priori*, distribution for parameter values is allowed.

Bayesian decision theory departs from classical estimation theory in that prior knowledge is allowed to play a role in the final decision. The difference between classical estimation theory and Bayesian decision theory is given in Figure 3. It is by introducing the prior distribution of the parameters that the "reasonableness" constraint is imposed. A large variance on this distribution would allow the sample values a greater weight in the final estimate. A very small variance in the *a priori* distribution would cause the estimation function to virtually ignore an outrageous sample.

In the case at hand, the random variables are the count values received in individual spectral windows. In vector form this is

$$\underline{N} = \begin{bmatrix} N_K \\ N_B \\ N_{Tl} \\ N_C \end{bmatrix} \quad (5)$$

The main parameter to be estimated is water equivalent, but other parameters must enter in as well because of their effect on \underline{EN} . The expected values of the elements of \underline{N} are given by

$$\begin{aligned} EN_K &= C_K t \\ &= t \{ R_K(W) + B_K - \beta_{BK}(C_B - B_B) - \beta_{CK}C_C \} \\ &= t \{ R_O^{(K)} \frac{\exp(-\alpha_K W)}{1+KS} + B_K - \beta_{BK} \frac{R_O^{(B)} \exp(-\alpha_B W)}{1+KS} + B_B + G \} \\ &\quad - \beta_{CK}C_C \end{aligned} \quad (6)$$

where G = rate of airborne radon contribution to ^{214}Bi peak count;

$R_O^{(B)}$ = expected value of count rate in ^{214}Bi spectral peak due only to ^{214}Bi decay in soil, with $W=0$, $S=0$;

α_B = attenuation coefficient of 1.76 MeV ^{214}Bi gamma rays in water.

$$EN_B = C_B t = t \{ R_0^{(B)} \frac{\exp(-\alpha_B W)}{1+KS} + B_B + G \} \quad (7)$$

$$EN_{T1} = C_{T1} t = t \{ R_0^{(T1)} \frac{\exp(-\alpha_{T1} W)}{1+KS} + B_{T1} - \beta_{CT} C_C \} \quad (8)$$

$$EN_C = C_C t \quad (9)$$

Looking at equations (6) through (9), the items W (water equivalent), S (soil moisture), G (representing the magnitude of ^{214}Bi concentration in the atmosphere), and C_C (cosmic flux) are the parameters. Thus the parameter vector is given by

$$\underline{Q} = \begin{bmatrix} W \\ S \\ G \\ C_C \end{bmatrix} \quad (10)$$

Now considering \underline{Q} itself as a random variable, the desired result is to develop a posterior distribution for \underline{Q} after the sample results are in [Lindgren, 1968, p. 234]. Let $f(\underline{n} | \underline{Q})$ be the conditional distribution of \underline{N} , and $g(\underline{Q})$ be the *a priori* distribution of \underline{Q} . The joint distribution of \underline{N} and \underline{Q} is

$$f(\underline{n}, \underline{Q}) = f(\underline{n} | \underline{Q}) g(\underline{Q}) \quad (11)$$

The marginal (or absolute) distribution of \underline{N} is given by

$$h_N(\underline{n}) = \int f(\underline{n} | \underline{Q}) g(\underline{Q}) d\underline{Q} \quad (12)$$

and finally the posterior density of \underline{Q} conditioned on the observation $\underline{N}=\underline{n}$ is

$$h(\underline{Q} | \underline{N}) = f(\underline{n} | \underline{Q}) g(\underline{Q}) / h_N(\underline{n}) \quad (13)$$

If the loss function is taken to be $(W-\hat{W})^2$, then the Bayes risk (the posterior expected value of the loss function) is

$$E_h[W-\hat{W}(\underline{N})]^2 = \text{Bayes Risk} \quad (14)$$

If we use the posterior expected value of W as the estimate of W,

$$\hat{W} = E_h(W) = \int W h(\underline{Q} | \underline{N}) d\underline{Q} \quad (15)$$

then this value minimizes the Bayes risk since the Bayes risk written above is a second moment, and the smallest second moment is that taken about the mean of a distribution [Lindgren, 1968, p. 239]. Hence \hat{W} is the Bayes estimate of the water equivalent.

With the above background development, now for some simplification. With a little (not unreasonable) bending, the problem can be fit into a multivariate normal framework, within which calculation of conditional means (i.e. the Bayes estimate - equation (5) - when a quadratic loss function - equation (4) is selected) is relatively simple. First it must be recognized that equations (6) through (9) express conditional means of \underline{N} given \underline{Q} . Assume that \underline{Q} is multivariate normal. Analysis of the individual elements of \underline{Q} indicates that this is a reasonable assumption, with perhaps the normality of G falling the most in question. Also, W is an effective water equivalent which includes both the

air blanket and water blanket. Thus even for values of zero snow water equivalent, W is not bumping up against a physical boundary which would disallow negative values.

Let the *a priori* (marginal) distribution of $\underline{\theta}$ be

$$\underline{\theta} \sim N(\underline{\theta}^*, \Sigma_{\theta}) \quad (16)$$

where

$$\underline{\theta}^* = \begin{bmatrix} W^* \\ S^* \\ G^* \\ C^* \end{bmatrix}$$

and where Σ_{θ} is known beforehand. Now (following Anderson, 1958, p. 28) let's put the random vector \underline{N} and the parameter vector $\underline{\theta}$ together into a single augmented vector:

$$\underline{X} = \begin{bmatrix} \underline{X}(1) \\ \dots \\ \underline{X}(2) \end{bmatrix} = \begin{bmatrix} \underline{\theta} \\ \dots \\ \underline{N} \end{bmatrix} \quad (17)$$

If \underline{X} is multivariate normal, its distribution is designated as

$$f(\underline{X}) \sim N(\underline{\mu}, \Sigma) \quad (18)$$

where

$$\underline{\mu} = \begin{bmatrix} \underline{\mu}(1) \\ \dots \\ \underline{\mu}(2) \end{bmatrix}, \quad \Sigma = \begin{bmatrix} \Sigma_{11} & \vdots & \Sigma_{12} \\ \vdots & \ddots & \vdots \\ \Sigma_{21} & \vdots & \Sigma_{22} \end{bmatrix}$$

From (16),

$$\underline{\mu}^{(1)} = \underline{\theta}^* \quad (19)$$

and

$$\Sigma_{11} = \Sigma_{\theta} \quad (20)$$

When the distribution (18) is completely specified, calculation of the posterior expected value of $\underline{\theta}$ (our final goal) is a simple matter. First we must determine $\underline{\mu}^{(2)}$, Σ_{12} (which is the transpose of Σ_{21}) and Σ_{22} . These are determined by looking at the

conditional mean and covariance of \underline{N} based on \underline{Q} . Continuing to follow the notation of Anderson,

$$E(\underline{x}^{(2)} | \underline{x}^{(1)}) = \underline{\mu}^{(2)} + \underline{\Sigma}_{21} \underline{\Sigma}_{11}^{-1} (\underline{x}^{(1)} - \underline{\mu}^{(1)}) = \underline{v}(\underline{x}^{(1)}) \quad (21)$$

and

$$\begin{aligned} E\{[\underline{x}^{(2)} - \underline{v}(\underline{x}^{(1)})][\underline{x}^{(2)} - \underline{v}(\underline{x}^{(1)})]^T\} \\ = \underline{\Sigma}_{22} - \underline{\Sigma}_{21} \underline{\Sigma}_{11}^{-1} \underline{\Sigma}_{12} \stackrel{\text{def}}{=} \underline{\Sigma}_{22.1} \end{aligned} \quad (22)$$

Let's see if we can identify some of the terms in (21) and (22) to be something known. First, recognize that equations (6), (7), (8) and (9) express conditional expectations. Assume that our prior knowledge of W and S is good enough that a first order expansion can be made about the prior expected values W^* and S^* . Then the exponential terms in equations (6), (7), and (8) may be expanded. For example,

$$\frac{R_0^{(K)} \exp(-\alpha_K W)}{1+KS} \approx \frac{R_0^{(K)} \exp(-\alpha_K W^*)}{1+KS^*} \left[1 + \alpha_K (W - W^*) - \frac{K(S - S^*)}{1+KS^*} \right] \quad (23)$$

Thus by incorporating the linear expansions, adding and subtracting a few terms in the right places, and rearranging, we get

$$E(\underline{N} | \underline{Q})_{4 \times 1} = \underline{A}_{4 \times 4} (\underline{Q} - \underline{Q}^*)_{4 \times 1} + \underline{N}_{4 \times 1}^* \quad (24)$$

where the matrix \underline{A} and vector \underline{N}^* are constants. Comparing (24) and (21) we get the identification

$$\underline{\mu}^{(2)} = \underline{N}^* \quad (25)$$

and

$$\underline{\Sigma}_{21} \underline{\Sigma}_{11}^{-1} = \underline{A} \quad (26)$$

Therefore

$$\underline{\Sigma}_{21} = \underline{A} \underline{\Sigma}_{11} = \underline{A} \underline{\Sigma}_{\underline{Q}} \quad (27)$$

The elements of $\underline{\Sigma}_{22.1}$ of equation (22) are determined by physical reasoning. The matrix $\underline{\Sigma}_{22.1}$ gives the covariance of the counts vector once \underline{Q} is specified. But once \underline{Q} is specified, the variability in the elements N_1 is due only to the random nature of nuclear counting. The nature of nuclear counting produces a Poisson random variable which, for sufficiently large expected values, is very

well approximated by a normal distribution. This condition is satisfied in gamma snow surveys. Since the Poisson distribution has variance equal to the mean, we take the diagonal elements of $\Sigma_{22,1}$ to be the elements of the conditional mean vector of equation (21). Also, randomness of nuclear counting in one spectral window is independent of nuclear counting in another window during the same time. Thus the off-diagonal elements of $\Sigma_{22,1}$ will be zero, and

$$\Sigma_{22,1} = \begin{bmatrix} v_1(\underline{x}^{(1)}) & 0 & 0 & 0 \\ 0 & v_2(\underline{x}^{(1)}) & 0 & 0 \\ 0 & 0 & v_3(\underline{x}^{(1)}) & 0 \\ 0 & 0 & 0 & v_4(\underline{x}^{(1)}) \end{bmatrix} \quad (28)$$

Physical reasoning requires that the diagonal elements of $\Sigma_{22,1}$ be positive. If the calculated values are not positive in any particular situation, a different method of computing water equivalent should be used. Finally then Σ_{22} is computed from equation (22) as

$$\begin{aligned} \Sigma_{22} &= \Sigma_{22,1} + \Sigma_{21} \Sigma_{11}^{-1} \Sigma_{12} \\ &= \Sigma_{22,1} + \underline{A} \Sigma_{11}^{-1} \underline{A}^T \end{aligned} \quad (29)$$

It should be noted that Σ_{22} must be a positive definite matrix in order to be a marginal covariance matrix for \underline{N} . Since $\Sigma_{22,1}$ is positive definite (diagonal, with positive elements), and since Σ_{11} is p.d. (by definition of marginal covariance matrix) it is sufficient to have matrix \underline{A} with at least as many columns q as rows p , and be of rank p . This means that to compute Σ_{22} in this fashion we must have at least as many parameter values (we have four) as count values (also 4), which condition is satisfied (Anderson, 1958, Appendix A, Theorem 1). The rank of the matrix \underline{A} would have to be checked in each separate situation.

Now to write the answer. The Bayes estimate of water equivalent under a quadratic loss function is the posterior expected value or, identically, the conditional mean based on the observed sample:

$$\begin{aligned} \hat{\underline{\theta}} &= \begin{bmatrix} \hat{W} \\ \hat{S} \\ \hat{G} \\ \hat{C}_C \end{bmatrix} = E(\underline{x}^{(1)} | \underline{x}^{(2)}) = \underline{\mu}^{(1)} + \Sigma_{12} \Sigma_{22}^{-1} (\underline{x}^{(2)} - \underline{\mu}^{(2)}) \\ &= \underline{\theta}^* + \Sigma_{\underline{\theta}} \underline{A}^T [\Sigma_{22,1} + \underline{A} \Sigma_{\underline{\theta}} \underline{A}^T]^{-1} (\underline{y} - \underline{N}^*) \end{aligned} \quad (30)$$

which is seen simply to be a regression function on the count values. It is noted that not only is the posterior estimate of water equivalent given, but posterior estimates of soil moisture, atmospheric ^{214}Bi concentrations, and mean cosmic flux are given as well. Furthermore, the posterior covariance is given by a matrix $\Sigma_{11,2}$ computed by exchanging indices in equation (22). Thus the first element in the first row of $\Sigma_{11,2}$ is the posterior variance of the water equivalent measurement \hat{W} .

THE KEY TO THE PROBLEM - ENCODING PRIOR KNOWLEDGE

Looking back at the final product (equation (30)) of the previous section, it is seen that two major inputs were necessary: (1) the matrix A which is a linearized version of the physical laws relating random variables and parameters, and (2) the vector Q^* and matrix Σ_Q which quantify the description of prior knowledge. The whole key to the Bayesian approach is having enough prior knowledge to make all the gyrations worthwhile. In the present application, the question is "where do we get our prior information?" The present formulation of the National Weather Service's Snow Accumulation and Ablation Model (Anderson, 1973) will provide hydrological simulation of snow cover water equivalent W . Periodic ground measurements by cooperative observers where available assist in keeping the simulation "on track". It is anticipated that an associated soil moisture model will produce estimates of soil moisture S under the snow cover for input to the airborne gamma snow measurements. Development of the covariance matrix Σ_Q first of all requires special calibrations over a period of time to quantify the performance of the hydrological simulations in updating previous measurements. The airborne ^{214}Bi concentrations certainly follow physical laws, but the inability to model these adequately means that in general some kind of a mean ^{214}Bi level G^* will have to be used in conjunction with a large "ignorance factor" (entry on the diagonal of Σ_Q) for G . The cosmic flux is reasonably well defined as a function of season and barometric pressure.

The most important point to be made in this paper is found in the above paragraph - the usefulness of simulation of physical processes to provide information which may be helpful in interpreting signals received in the remote sensing process. This principle would seem to go beyond the airborne gamma snow survey application and extend to other remote observations of hydrological variables as well. The continuing effort to wring more and more information from remote sensing imagery would seem to require more and more sophistication as more and more automated interpretation processes are applied. A critical consideration is that progress must be made on a coordinated front so that remote sensing products are useful to the simulation practitioner and, similarly, that simulation results are available and useful to the remote sensing interpretation process.

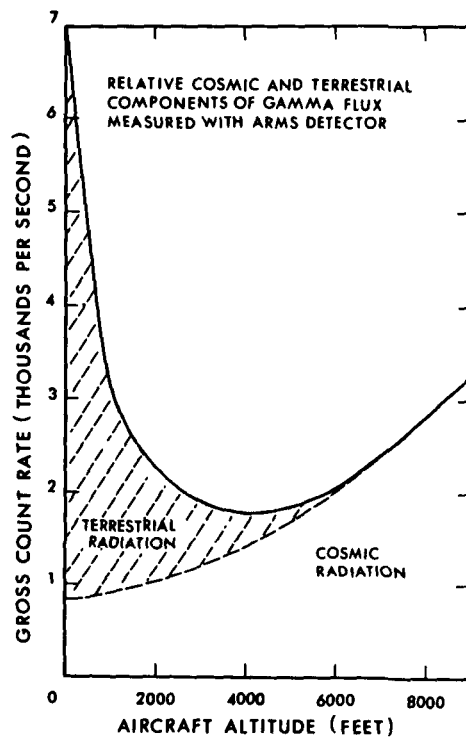


Figure 1. Relative contribution of terrestrial and cosmic gamma flux with altitude.

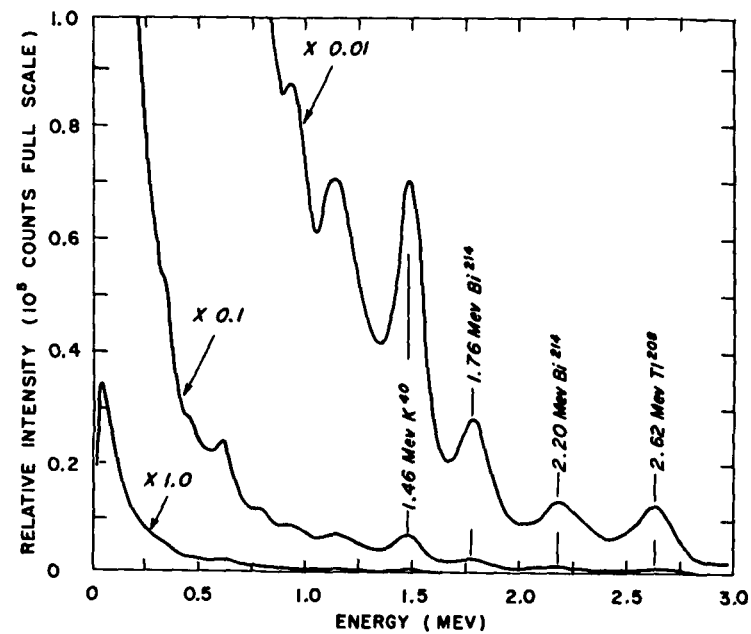


Figure 2. Spectral composition of terrestrial gamma radiation flux.

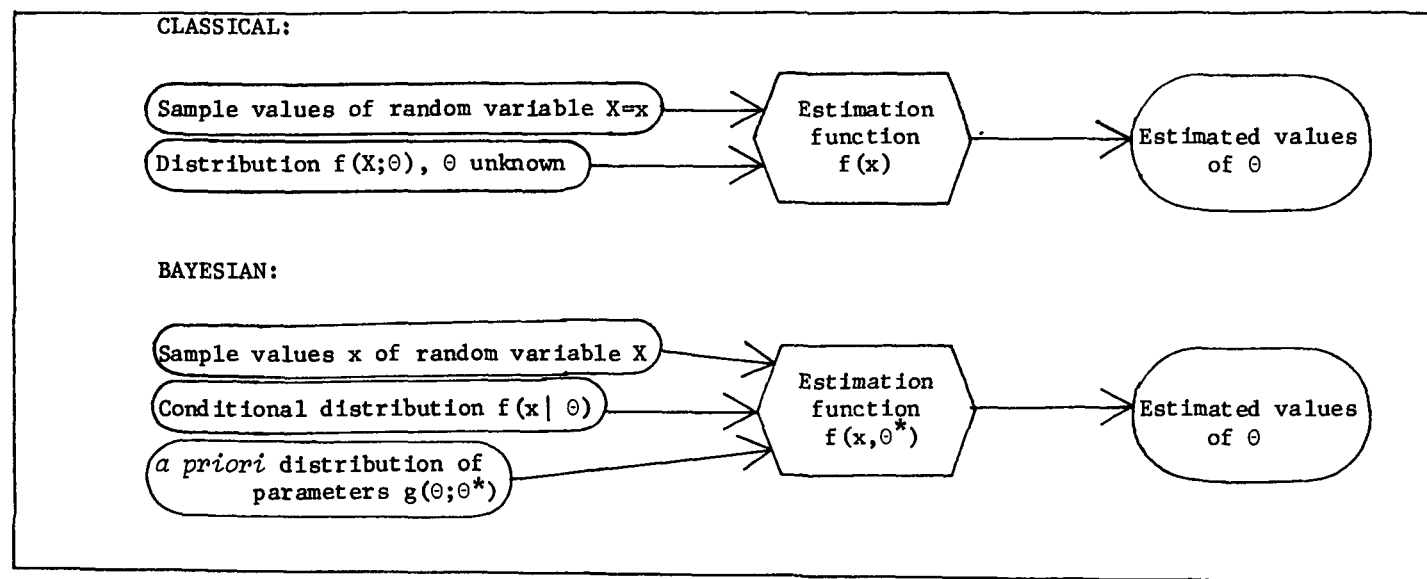


Figure 3. Classical estimation versus Bayesian decision theory to determine value of parameter θ .

REFERENCES

- Anderson, E. A., "National Weather Service River Forecast System: Snow Accumulation and Ablation Model", Tech. Memo. NWS HYDRO-17, U.S. Dept. of Commerce, NOAA, National Weather Service, Silver Spring, Maryland, November, 1973.
- Anderson, T.W., An Introduction to Multivariate Analysis, John Wiley and Sons, New York, 1958.
- Bissell, V.C., "Natural Gamma Spectral Peak Method for Snow Measurement from Aircraft", Proceedings of the Interdisciplinary Symposium on Advanced Concepts and Techniques in the Study of Snow and Ice Resources, pp. 614-623, U.S. National Academy of Sciences-National Research Council, Washington, D.C., 1974.
- Burson, Z.G., and A.E. Fritzsche, "Snow Gaging by Airborne Radiological Surveys- Status Through September 1972", EGG-1183-1565, E G & G, Inc., Las Vegas, Nevada, 1972.
- Kogan, R.M., M.V. Nikiforov, Sh.D. Fridman, V.P. Chirkov, and A.F. Yakovlev, "Determination of Water Equivalent of Snow Cover by Method of Aerial Gamma Survey", Soviet Hydrology, No. 2, 1965.
- Larsen, L.W., "An Application of the Aerial Gamma Monitoring Technique for Measuring Snow Cover Water Equivalent on the Great Plains", Proc. of Symposium on Snow Management on the Great Plains, Great Plains Agricultural Council Pub. #73, Agric. Exp. Station, U. of Nebraska, Lincoln, 1975.
- Lindgren, B.W., Statistical Theory, Second Ed., MacMillan, London, 1968.
- Mondschein, H.F., "Forecasting the Spring 1969 Midwest Snowmelt Floods", U.S. Dept. of Commerce, NOAA Tech. Memo. NWS CR-40, National Weather Service Central Region, Kansas City, Mo., 1971.
- Peck, E.L., V.C. Bissell, E.B. Jones, and D.L. Burge, "Evaluation of Snow Water Equivalent by Airborne Measurement of Passive Terrestrial Gamma Radiation", Water Resources Research, Vol. 7, No. 5, pp. 1151-1159, 1971.

**SUMMARY OF THE OPERATIONAL APPLICATIONS OF SATELLITE
SNOWCOVER OBSERVATIONS WORKING SESSION - AUGUST 20, 1975**

V. V. Salomonson and A. Rango, *NASA/Goddard Space Flight Center, Greenbelt,
Maryland*

INTRODUCTION

Following two days of excellent formal paper presentations and constructive discussions, a working session dealing primarily with problems, techniques for analysis, possible solutions, and recommendations for future work pertaining directly to the Snow ASVT study areas was held. This session, chaired by V. V. Salomonson, treated in greater detail some of the points brought out in the discussions during the previous two days. Various techniques for reducing the satellite data to a form useable by the operational agencies were covered in mini-presentations and discussions by the operational satellite-snow interpretive personnel. These mini-presentations were followed by open discussion and actual manipulation of data by those present in the audience.

Similar mini-presentations were made by operational agency stream-flow forecasters on how satellite-derived snow data could be incorporated into runoff forecasting methods, potential influence on management decisions, and eventual transfer to completely operational use. A general discussion dealing with the directions that the snow ASVT should take as a result of the previous presentations and discussions concluded the working session.

It was apparent throughout the conference that no specific data reduction technique or application of the data could be applied in all the Snow ASVT study areas. The greatest contrast between applicable techniques and their relationship to the available water resource existed between arid, vegetation sparse, relatively cloud-free Arizona and the humid, densely vegetated, cloud covered Northwest. Straight-forward analysis techniques and data application were employed in Arizona. In the Northwest, however, more sophisticated analysis is required in order to extract meaningful information. The evaluation of the data by the four differing areas should provide an adequate range of results for other water agencies to decide whether or not to adopt the new remote sensing snow mapping technology.

In order that the major approaches and problems could be addressed in an orderly fashion, the working session was structured into three main areas. These areas were: photointerpretation techniques, digital techniques, and management/implementation considerations. Within the

discussion and presentations on the first two areas the objective was to bring together as much information as possible as to the speed, costs, accuracy and precision, equipment, and training associated with the various approaches. The following paragraphs summarize the information gathered during the working session.

PHOTOINTERPRETATION TECHNIQUES

The key participants in this session of the workshop were the following:

1. James Foster — University of Maryland
2. Tony Mikesell — U.S. Soil Conservation Service
3. Roderick L. Hall — Sierra Hydrotech
4. A. Gerald Thompson — University of Wyoming
5. Stanley Schneider — NOAA/National Environmental Satellite Service (NESS)

It appeared that there was a clear preference for the 9 inch, approximately 1:1 million scale LANDSAT images for snow mapping. In the black and white image format, the 0.6-0.7 μ m images were preferred. The most information, however, was observed on the color composites with the cost of producing the color composites being the major drawback to their use.

Equipment for photointerpretation was relatively modest. Light tables, planimeters, and standard office supplies are needed as basic tools. If funds do not permit the direct purchase of color composites, diaso processing equipment can be used very successfully. In order to most expeditiously transfer or superimpose data from the images onto topographic maps, the Bausch and Lomb Zoom Transfer Scope was generally recognized as a highly desirable tool. In order to preserve the images, A. Gerald Thompson described the use of protective glass plates. More durable materials for the preservation of thematic maps of snow-cover were also recommended, particularly if a lot of handling of the data was to be expected.

The procedures for extracting relevant information basically involved locating snowlines and measuring the area or percentage of a watershed covered by snow. Some skill and/or ingenuity in locating snowlines in forested areas, distinguishing between snow and clouds, and recognizing the presence or absence of snow in shadows was very commonly noted as being necessary. In the case of locating snowlines in forested areas techniques such as using clearcut areas, powerline swaths, or overall

increased reflectance-grey tones in the images were described. Over-exposure of LANDSAT imagery so as to enhance snow in forests was one exemplary technique described by J. Foster of the University of Maryland.

False-color composites generally were quite helpful in distinguishing bare rock from high-altitude snow-covered areas, particularly when summer scenes were compared to winter scenes. Furthermore, the false-color, red tone typically associated with vegetation permitted snow-cover in the trees versus trees with no snowcover beneath the foliage to be more readily distinguishable. The diazo process provided most investigators with the opportunity to produce images that met their individual preferences and, at the same time, were relatively inexpensive as contrasted against purchasing color composites from the normal Data Centers.

For measuring snowcovered area there were basically three approaches that seemed to stand out. One approach consisted of determining the mean snowline altitude and converting it to an equivalent area using a watershed area-altitude curve. A second method consisted of simply locating the snowline and planimetering the snowcovered area and presenting the information as a percent of basin covered. The third method consisted of using a grid or regular array of boxes overlaying the watershed area. The boxes typically cover an area of approximately four km². It was recommended that 1:250,000 enlargements of LANDSAT images be used. The analyst then simply estimates the snowcover in each box in tenths and performs the appropriate summations to get the total watershed area covered by snow.

In terms of precision and accuracy the box or grid method was recognized to be the most preferable by the end of the workshop. Not only was a rather high degree of precision provided, but ancillary statistics could be derived and the format for data gathering provided degrees of freedom for partitioning according to altitude zones or for input into numerical runoff prediction schemes. The major disadvantage was the time it takes to perform the analysis. For minimum equipment, relative speed, and a sustained, consistent level of accuracy and precision, the mean snowline altitude-equivalent area method seems preferable. Of course, the costs in all the photointerpretation methods are relatively low, but of the methods proposed, the simple planimetering of snow-covered area is the least expensive.

The level of training required for snowmapping using photointerpretation is relatively low. The most training comes in using equipment or materials that facilitate the analysis. For example the use of the Diazo process or the Zoom Transfer Scope requires some instruction. Furthermore, the pitfalls of snowcover photointerpretation when forested areas, shadows, and clouds exist requires instruction and experience in order that they be avoided.

The LANDSAT data, while having high spatial resolution and cartographic fidelity that made it attractive, often was not available frequently enough to observe rapid snowcover changes. NOAA/VHRR data provides

data every day at 1km resolution, but in a non-cartographic format. The Zoom Transfer Scope is definitely needed when using VHRR data in order to facilitate snowmapping and some considerable skill is needed to superimpose the image on a map. As a result of the relatively low spatial resolution and the mapping difficulty, many investigators in the study areas were not using this approach. Mr. Stan Schneider of NOAA/NESS described how he uses the VHRR data to map snowcover and spent a considerable amount of time instructing many individuals on the use of the Zoom Transfer Scope.

It was clear that most of the ASVT study areas were using photo-interpretation methods, and the workshop served to provide all the study areas with techniques or approaches for improving their snowcover mapping procedures and the evaluation of satellite snowcover data.

DIGITAL PROCESSING

Although the use of digital, feature recognition approaches was obviously not being used by most of the study areas, it was recognized as a definite possibility for the future as more experience and sophistication was developed in the use of LANDSAT data. In order that a variety of approaches could be explored, five individuals presented results representing major approaches employing digital data. They were:

1. William E. Evans — Stanford Research Institute
2. Klaus Itten — University of Zurich, Switzerland
3. Stephen G. Luther and Luis A. Bartolucci — Purdue University
4. William C. Dallam — General Electric Company

In addition, Dr. Mark Meier, U.S. Geological Survey, made a short presentation describing an intercomparison study of various methods that he had tested.

Several different procedures were described in the digital processing areas. The use of supervised and unsupervised classification techniques were described. Furthermore, the well-known or commonly employed classification programs were described including LARSYS from Purdue University, STANSORT from Stanford University, and the parallel-piped approach used by the General Electric Image 100 configuration. The discussion and presentations brought out tradeoffs among the methods associated with diagnostic and statistical information, speed, classification accuracy, and cost.

Among the advantages of digital processing that became apparent was the fact that the digital classification methods are reproducible and

quantitative. Furthermore, more classes of snowcovered area can be provided due to the advantage of multispectral classification over the ability of the photointerpreter to reliably separate classes of snow. Because of the difficulty of mapping snow within trees, in shadows, and in partially cloud-covered areas, the overall accuracy of digital techniques, however, seems to presently stand at about the same level as that of the photointerpretation techniques. Methods of getting around these problems were described along with methods of digitally superimposing elevation contours on snowcover information using digital contour information obtainable from the Defense Mapping Agency.

The equipment necessary to utilize computer-oriented digital snowcover mapping approaches is, relative to the photointerpretation approach, quite costly and complex. Furthermore, there is a certain amount of computer programming training and data processing skill necessary to implement these techniques. In many cases the computer equipment and programming skills may already exist within the larger water resources management agencies, but these skills and equipment may be devoted to other tasks. In order to justify the acquisition of new equipment and personnel or the reallocation of existing resources to the job of snowmapping, it would seem that the use of satellite snowcover data and the desire for greater precision and information content will have to increase considerably to the point where these actions can be justified more explicitly than presently possible.

MANAGEMENT/IMPLEMENTATION CONSIDERATIONS

A panel of experienced and knowledgeable individuals were convened to discuss the various tactics and challenges to be faced and overcome if satellite snowcover information is to eventually be operationally implemented. This panel also served as a nucleus for offering suggestions as to the next steps to be taken in the ASVT. The participants were:

1. Jack F. Hannaford — Sierra Hydrotech
2. Fred A. Limpert — Bonneville Power Administration
3. Ronald E. Moreland — U.S. Soil Conservation Service
4. Donald R. Wiesnet — NOAA/NESS
5. Charles H. Howard — California Department of Water Resources
6. Gary J. Freeman — Pacific Gas and Electric Company
7. Ed Kirdar — Salt River Project

The panel noted that the problems in snowmapping are distinctly different in each of the study areas. For instance, in the Northwest the snowcover is persistent, but obscuring cloudcover for satellite observations is frequent. On the other hand in Arizona, cloud-free observations are readily available, but the snowcover comes and goes so rapidly that LANDSAT observations may not observe significant snowstorm events. In both cases it seemed desirable to supplement LANDSAT data with NOAA/VHRR observations.

Because snowcover-runoff relations are necessarily empirical, several years of data will be necessary to substantiate relationships that may be developed. Therefore, it is absolutely mandatory in order for the ASVT to be successful that it be continued for its designed period; namely, four years. It was also noted that, wherever they exist, aircraft data taken in previous years should be utilized to extend the years of record used in building snowcover versus runoff relationships. Where aircraft data have been used in the past, some mechanisms already exist that can make use of the satellite data. For instance, Sierra Hydrotech has used aircraft snowcover observations in the Southern Sierras to build snowcover-runoff relationships that they hope to improve and extend using LANDSAT data. The Bonneville Power Administration has used aircraft data in their SSARR model. With the LANDSAT data available, they hope to be able to inject snowcover data more frequently into the model as a check and adjustment factor for the snowcover estimation and prediction subroutines.

One key item that needs to be improved is the speed of data delivery. Examples of the Canadian "Quick Look" system were made available and seemed quite appropriate for ASVT needs. The use of this system would provide the essential step forward in meeting data delivery goals.

Overall, the promise of the satellite snowcover observations appears quite high after one year of study and evaluation. As already mentioned, all the agencies directly concerned were quite clear in indicating that more years of observation must be acquired and evaluated before complete implementation of procedures using these data can be validated and justified. Simple demonstration of performance within existing budgetary and manpower constraints is basically needed. However, sufficient promise has been seen by some of the agencies to indicate that written support and backing could be provided to NASA and other U.S. Government Agencies, if needed, in order to insure that the Snowmapping ASVT effort can continue.

OPERATIONAL APPLICATIONS OF SATELLITE
SNOWCOVER OBSERVATIONS

NASA/GODDARD SPACE FLIGHT CENTER
UNIVERSITY OF NEVADA, RENO

SOUTH LAKE TAHOE, CALIFORNIA
AUGUST 18-20, 1975

FINAL ROSTER OF PARTICIPANTS

WORKSHOP DIRECTOR

Albert Rango
Research Hydrologist
NASA/Goddard Space Flight Center
Code 913
Greenbelt, MD 20771

PROGRAM COORDINATOR

Marjorie Cutler
Conferences and Institutes
General University Extension
University of Nevada, Reno

ALGAZI, V. RALPH
Professor
Dept. of Electrical Eng.
University of California
Davis, California 95616

ANDERSON, JOHN L.
Program Manager
Code NS, NASA
600 Independence Ave.
Washington, D. C. 20546

AVERA, HARMON Q.
Sales Manager
441 Cienaga Dr.
Fullerton, CA 92635

BAIRD, GAYLEN H.
Meteorologist
U.S. Bureau of Reclamation
7680 Sierra Dr.
Roseville, CA 95678

BALDWIN, JAMES A.
Research Assistant
Statistics Dept.
University of California
Riverside, CA 92502

BARNES, JAMES C.
Manager Geophysical
Studies Sect.
Environmental Research
& Tech. Inc.
696 Virginia Rd
Concord, MA 01742

BARTOLUCCI, LUIS A.
Research Instructor
LARS/Purdue
1220 Potter Dr.
W. Lafayette, IN 47906

BAUER, DON J.
Project Meteorologist
Environment Canada
30 Campus Dr.
Saskatoon, Canada S7N 041

BELLAMY, ROBERT E.
Hydraulic Engineer
2507 Estrella Ave.
Loveland, CO 80537

BISSELL, VERN
Lead Hydrologist/
Computer Systems
River Forecast Center
Portland, OR 97209

BONNER, WILLIAM J.
Senior Physicist
Bureau of Land Mgt.
Bldg. 50 D-140
Denver Federal Center
Denver, CO 80125

BROWN, ALVIN J.
Coordinator
CA Cooperative Snow
Surveys
2836 Kerria Way
Sacramento, CA 95821

BURNS, JOSEPH I.
Vice President
Murray Burns and Kienlen
600 Forum Bldg.
1107 9th St.
Sacramento, CA 95814

CARR CHRISTOPHER
Assistant Engineer
Route 1 Box 1978
Meadow Vista, CA 95722

CHANG, ALFRED T.C.
Hydrologist
Goddard Space Flight
Center Code 913
Greenbelt, MD 20771

CLAPP, FRED D.
Consulting Engineer
21 Queensbrook PI
Orinda, CA 94563

BREAKER, LAURENCE C.
Oceanographer
NOAA/NESS 660 Price Ave.
Redwood City, CA 94063

CLORETY, BARNEY
Hydrographer
SMUD P. O. Box 15830
Sacramento, CA 95813

COX, LLOYD M.
Hydrologist
ARS-USDA
P. O. Box 2700
Boise, ID 83701

CRAIG, ROBERT N. Satellite Hydrologist Room 1724 601 E. 12th St. Kansas City, MO 64106	GORDON, FREDERICK, JR. Technical Manager NASA/GSFC 12203 Tilbury Lane Bowie, MD 20715	KAHLE, ANNE Supervisor Earth Applications & Climatology Group 183-501 Jet Propulsion Lab 4800 Oak Grove Dr. Pasadena, CA 91103
DALLAM, WILLIAM C. Earth Resources Analyst General Electric Co 13622 Colefair Dr. Silver Spring, MD 20904	HALL, RODERICK L Partner, Sierra Hydrotech P. O. Box 169 Placerville, CA 95667	KATIBAH, EDWIN F. Assistant Specialist University of California 260 Space Sciences Lab Berkeley, CA 94720
DANIELSON, JERIS A. Deputy State Engineer 1854 Sheeman St., Rm 300 Denver, CO 80203	HANNAFORD, JACK F. Partner Sierra Hydrotech P. O. Box 169 Placerville, CA 95667	KERBES, RICHARD Canadian Wildlife Service 2721 Highway 31 Ottawa, Ontario Canada K1A0H3
DAVIES, NEIL J. Student - Employee Lawrence Livermore Laboratory P. O. Box 808 Livermore, CA 94550	HANSON, BRADFORD C. Research Scientist University of Kansas Center for Research Inc. Remote Sensing Lab. 2291 Irving Hill Rd. Lawrence, KA 66044	KHORRAM, SIAMAK Staff Research Associate RSRP, Space Sciences Lab (Rm. 260) University of California Berkeley, CA 94720
DUFFIN, RICHARD Grad. Student UNR Renewable Natural Resources Reno, NV 89507	HOWARD, CHARLES H. Associate Engineer California Dept. of Water Resources 1416 9th St., Rm 550 Sacramento, CA 95814	KIRDAR, ED Senior Engineer P. O. Box 1980 Phoenix, AZ 85001
DUNCAN, WALTER W. Assistant Chief Hydrologist Corps. of Engineers 2364 Gallant Fox Court Reston, VA 22091	ITTEN, KLAUS I. Doctor of Philosophy Dept. of Geography University of Zurich Bluemlisalpstr. 10 CH-8006 Zurich, Switzerland	KOLAR, SCOTT H. Doctoral Student, Geography Dept. Oregon State University 1781 Sylvan St. Eugene, OR 97403
ECKERMAN, JEROME Research Physicist 11817 Huntingridge Ct. Potomac, MD 20854	JENSEN, GENE Science Teacher 935 Fairway Dr. Bakersfield, CA 93309	LAHEY, JAMES F. Professor - Geography Dept. Oregon State University Corvallis, OR 97330
EVANS, WILLIAM E. Staff Scientist, SRI 333 Ravenswood Ave. Menlo Park, CA 94025	JOHNSON, JIMMY T. Hydrologic Tech Corps of Engineers 650 Capitol Mall Sacramento, CA 95824	LEAF, CHARLES F. Hydrologist 4412 E. Mulberry - 113 Ft. Collins, CO 80521
FFOLLIOTT, PETER F. Associate Professor University of Arizona Tucson, AZ 85721	JOHNSTON, J. RONALD Hydraulic Engineer 2638 South Flower Ct. Lakewood, CO 80227	LEAKE, ROBERT E. JR. Watermaster Kings River Water Assoc. 4888 East Jensen Fresno, CA 93725
FOSTER, JAMES Faculty Research Assistant University of Maryland 320 Vierling Drive Silver Spring, MD 20904	JONES, JAMES R. Asst. Research Coordinator P. O. Box 14287 So. Lake Tahoe, CA 95702	LEAVESLEY, GEORGE H. Hydrologist Colorado Dist. WRD Denver Federal Center Lakewood, CO 80225
FREEMAN, GARY J. Hydrologist Pacific Gas & Electric Co. Hydro Generation, Room 3027 77 Beale St. San Francisco, CA 94106		

LIMPERT, FRED A.
Head Hydrology Section – BPA
5590 S. W. Chestnut Ave.
Beaverton, OR 97005

LINLOR, WILLIAM I.
Staff Scientist
NASA/Ames Research Center
Moffett Field, CA 94040

LINSLEY, RAY K.
Hydrocomp, Inc.
1502 Page Mill Rd.
Palo Alto, CA 94304

LOIJENS, H. S.
Hydrologist
Glaciology Division
Environment Canada
Ottawa, Ontario, Canada
K1A 0E7

LUTHER, STEPHEN G.
Project Manager
LARS/Purdue
S. Lafayette, IN 47906

MAIRS, JOHN W.
Environmental Remote Sensing
Applications Laboratory (ERSAL)
Oregon State University
Corvallis, OR 97331

MCFADIN, FLOYD P.
Water Resources Engineer Assoc.
7445 E. Parkway
Sacramento, CA 95823

MCGINNIS, DAVID F. JR.
Hydrologist
NOAA/NESS
Rm. 3312 Stop D.F.O.B. No. 4
Washington, D.C. 20233

MCMILLAN, MICHAEL C.
Research Hydrologist
NOAA/NESS
F.O.B. – 4 Stop D
Washington, D.C. 20233

MEIER, MARK F.
Project Chief – Glaciology
Dept. of the Interior
USGS – 1305 Tacoma Ave. So.
Room 300
Tacoma, WA 98402

MEISNER, DOUGLAS
Graduate Research Assistant
SUNY Coll. Envir. Sci. & For
Syracuse, NY 13210

MIKESELL, TONY
Engineering Aide
P. O. Box 17107
Denver, CO 80217

MILLER, HARLAN J.
Hydraulic Engineer
P. O. Box 515
Pueblo, CO 81002

MOORE, HAROLD D.
Geologist
Gregory Geoscience LTD
1750 Courtwood Cr.
Ottawa, Canada, Ont. K2C2B5

MORELAND, RONALD E.
Snow Survey Supervisor
Soil Conservation Service
P. O. Box 4850
Reno, NV 89505

O'BRIEN, HAROLD W.
Research Physicist
US Army CRREL
Hanover, NH 03755

ONDRECHEN, WILLIAM
Hydrologist
Idaho Dept. of Water Resources
Statehouse
Boise, ID 83720

PETERSON, NED R.
Field Activities Engineer
Snow Surveys Branch
Dept. of Water Resources
P. O. Box 388
Sacramento, CA 95802

PUTNAM, MARTIN
Research Assistant
ECON, Inc.
419 N. Harrison St.
Princeton, NJ 0854

RANGO, ALBERT
Research Hydrologist
NASA/Goddard Space Flight Center
Code 913
Greenbelt, MD 20771

RIDD, MERRILL K.
Director
Center for Remote Sensing
& Cartography
Dept. of Geography
University of Utah
Salt Lake City, UT 84112

ROSENFELD, CHARLES I.
Assistant Professor of Geography
Oregon State University
Corvallis, OR 97331

RUSSELL, HAROLD
Engineer – Mgr.
Buena Vista Water Storage Dist.
P. O. Box 756
Buttonwillow, CA 93206

SALOMONSON, VINCENT V.
Head Hydrology &
Oceanography
Code 913
Greenbelt, MD 20771

SCHNEIDER, STANLEY RE.
Hydrologist
3921 Patrick Henry Dr.
Falls Church, VA 22044

SCHUMANN, HERBERT H.
Hydrologist – US
Geological Survey
Suite 1880 Valley
Bank Center
Phoenix, AZ

SEIBERT, RICHARD D.
Research Hydrologist
Instructor of Water
Resources
University of Alaska
Fairbanks, AK 99701

SEREBRENY, SIDNEY M.
Staff Scientist
Stanford Research
Institute
Menlo Park, CA 94306

SHARP, JAMES M.
Space Sciences Laborator
University of California
Berkeley, CA 94720

SHERRETS, RAYMOND E.
Senior Engineering Tech.
6201 "S" St.
P. O. Box 15830
Sacramento, CA 95813

SIMONS, W.D.
Hydrologist
345 Middlefield Rd.
Menlo Park, CA 94025

SOHN, ROBERT I.
Project Manager
4800 Oak Grove Dr.
Pasadena, CA 90402

STADLER, JAMES
Civil Engineer
Boswell Co.
P. O. Box 877
Corcoran, CA 93212

SUK, MINSOO
Dept. of Elect. Eng.
University of California
Davis, CA 95616

TAYLOR, JEFF L.
General Mgr.
Kings River Conservation
Dist.
4886 East Jensen
Fresno, CA 93725

THOMAS, BILLY J.
Hydraulic Engineer
210 Custom House
Portland, OR 97209

THOMAS, RANDY
RSRP Technical Services
Branch Manager
260 Space Sciences Lab.
Remote Sensing Research Program
University of California
Berkeley, CA 94720

THOMSON, K.P. B.
Head Applications
Development
Canada Centre for
Remote Sensing
717 Belfast Rd
Ottawa, Ontario, Canada
K1A 0E4

THOMPSON, A. GERALD
Staff Scientist WRRI
Box 3067 University Station
Laramie, WY 82070

THOMPSON, VERNON
Hydraulic Engineer
US Army Corps Engs.
Walla Walla, WA 99362

THORLEY, GENE A.
Scientist EROS Program
1925 Newton Plaza East
Reston, VA 22091

TSOU, PETER
Engineer
Jet Propulsion Laboratories
4800 Oakgrove Dr.
Pasadena, CA 91103

VAN DEN BERG, MAX E
Hydraulic Engineer
Regional Hydromet Coordinator
Bureau of Reclamation,
PN Region
Boise, ID 83724

WALTERMEYER, SCOTT
Hydrologic Technician
405 N. 1150 W
Vernal, UT 84078

WARSKOW, BILL
Lead Watershed Specialist
Salt River Project
P. O. Box 1980
Phoenix, AZ 85001

WASHICHEK, JACK H.
Snow Survey Supervisor
P. O. Box 17107
Denver, CO 80217

WIESNET, DONALD R.
Sr. Res. Hydrol
NOAA/NESS
S-33 FOB No. 4 (Stop D)
Washington, D.C. 20233